(2)

The University of New Mexico

Mechanical Engineering Department

APPLICATION OF THE WAVY MECHANICAL FACE SEAL
TO SUBMARINE SEAL DESIGN

BY

A. O. LEBECK, L. A. YOUNG, Y. M. HONG,
P. KANAS, AND K. SAMPAYAN

SUMMARY REPORT ME-129(84)ONR-233-1

PREPARED FOR THE OFFICE OF NAVAL RESEARCH UNDER
CONTRACT NUMBER ONR-N-00014-83-K-0304

JULY 1984

Re: Summary Report ME-129(84)ONR-233-1 dated July 1984

This report was originally released on a restricted basis to the sponsors in 1984. By agreement with ONR, public release was delayed pending patent applications. The report herein is a corrected version of the original 1984 report.

***

APPLICATION OF THE WAVY MECHANICAL FACE SEAL
TO SUBMARINE SEAL DESIGN

by

A. O. Lebeck
Professor of Mechanical Engineering,

L. A. Young
Staff Engineer,

and

Y. M. Hong, P. Kanas, K. Sampayan
Research Assistants

The University of New Mexico
Department of Mechanical Engineering
and
Bureau of Engineering Research
Albuquerque, New Mexico 87131

Summary Report ME-129(84)ONR-233-1

July 1984

Prepared for the Office of Naval Research under
Contract Number ONR-N-00014-83-K-0304

SECURITY CLASSIFICATION OF THIS PAGE (When Data Entered)

REPORT DOCUMENTATION PAGE

READ INSTRUCTIONS BEFORE COMPLETING FORM

1. REPORT NUMBER

2. GOVT ACCESSION NO.

3. RECIPIENT'S CATALOG NUMBER

4. TITLE (and Subtitle)

APPLICATION OF THE WAVY MECHANICAL FACE SEAL TO SUBMARINE SEAL DESIGN

5. TYPE OF REPORT & PERIOD COVERED

Summary Report
Aug. 1, 1982-Jun. 30, 1984

6. PERFORMING ORG. REPORT NUMBER

ME-129(84)ONR-233-1

7. AUTHOR(s)

A. O. Lebeck, L. A. Young, Y. M. Hong, P. Kanas, and K. Sampayan

8. CONTRACT OR GRANT NUMBER(s)

ONR-N-00014-83-K-0304

9. PERFORMING ORGANIZATION NAME AND ADDRESS

The University of New Mexico
Albuquerque, New Mexico 87131

10. PROGRAM ELEMENT, PROJECT, TASK AREA & WORK UNIT NUMBERS

11. CONTROLLING OFFICE NAME AND ADDRESS

Director, Power Program
Dept. of the Navy-Office of Naval Research
Arlington, Virginia 22217

12. REPORT DATE

July 1984

13. NUMBER OF PAGES

14. MONITORING AGENCY NAME & ADDRESS (if different from Controlling Office)

15. SECURITY CLASS. (of this report)

15a. DECLASSIFICATION/DOWNGRADING SCHEDULE

16. DISTRIBUTION STATEMENT (of this Report)

[redacted]

17. DISTRIBUTION STATEMENT (of the abstract entered in Block 20, if different from Report)

18. SUPPLEMENTARY NOTES

19. KEY WORDS (Continue on reverse side if necessary and identify by block number)

Mechanical Seals, Seals, Face Seals, Lubrication, Wear, Friction, Waviness

20. ABSTRACT (Continue on reverse side if necessary and identify by block number)

This report details two years of work on the development of a long life submarine seal. In the first portion of the report, three different long life designs based on the waviness concept are described. Design details and test results are given. The conclusions reached are that the first design gives long life but is too complicated. The second design is much simpler but still gives long life. The third design is very simple but life may be compromised. Even so, the fixed wave (third design) appears to be the best way to apply the

DD FORM 1 JAN 73 1473 EDITION OF 1 NOV 65 IS OBSOLETE

SECURITY CLASSIFICATION OF THIS PAGE (When Data Entered)

waviness principle. A new type of grinding apparatus was designed to produce the wave.

Details of seal ring deflection calculations are given. A ring finite element and ring deflection program are given. A contact model is presented. Deflection studies on actual submarine seal rings are presented, and it is shown how present designs are sensitive to lock ring groove waviness. Experimental verification is provided for the contact model. Work on a nonlinear joint model is described.

Experiments to validate the existence of microasperity lubrication in water are described and dismissed. A unique apparatus was constructed. Experiments suggest microasperities do not cause a large hydrodynamic load support in water.

Several seal analysis programs are described. These programs are very useful for evaluating seal designs. One of the programs provides for a fully automated heat transfer analysis of seal pairs.

Finally, new concepts in squeeze seals and bearings are described. Some numerical results are given showing how in some cases the squeeze seal is the same as at present but in other cases it is different.

A summary and detailed conclusion chapter is given at the end of the report.

APPLICATION OF RESEARCH TO THE NEEDS OF THE U.S. NAVY

Mechanical face seals are used in numerous applications in Naval machinery. These applications range from propeller shaft seals to boiler feed pump seals. In such equipment the mechanical seal plays a vital role. When such seals fail, repair is costly both in terms of lost time and direct costs, so any improvement in seal life and reliability would be of significant benefit.

As more advanced equipment is designed, it is sometimes difficult to achieve desired performance in more severe service environments with the present state of the art of seal design. Thus, an improvement in seal technology would serve this important application.

One objective of the research herein is to further the understanding of mechanical face seal lubrication phenomena. Another objective is to develop the capability of designing contacting face seals having a longer life, greater reliability, and for extreme environments. The immediate objective herein is to apply the knowledge gained to the design of a small scale submarine type seal having exceptionally long life and high reliability.

TABLE OF CONTENTS

		Page
CHAPTER 1	INTRODUCTION	1
	Mechanical Face Seals	1
	Seal Lubrication	2
	Background	4
	Submarine Seals	7
	Wavy Seals	11
CHAPTER 2	NINE WAVE SEAL--FIRST DESIGN AND RELATED TESTS	15
	Seal Design (Review)	15
	Initial Test Results	18
	2000 Hour Test	26
	Performance During Test	26
	Post Test Analysis	33
	Conclusions on First Nine Wave Design	37
	500 Hours Flat Face Test	39
	Integral Force Transducer Design and Test	43
CHAPTER 3	NINE WAVE SEAL--SECOND DESIGN	51
	Criteria	51
	Initial Configuration	52
	Seal Ring Design Solution	54
	Bending Stiffness	56
	Buckling	58
	Torsion of a Composite Section	60
	All Carbon Seal Design	67
	Warping Analysis	67
	Design Solution	75
	Predicted Performance	75
	Strength Analysis and Test	80
	Other Calculations	83
	Final Design	84
	Young's Modulus Tests	88
	2000 Hour Test Results	91
	Performance During Test	91
	Post Test Analysis	95
	Comparison to Theory	98
	Split Ring Design	101
	Conclusions on Second Design	108
CHAPTER 4	NINE WAVE SEAL--THIRD DESIGN	111
	Design Approach	114
	Advantages	114
	Limitations	114
	Wavy Seals	115
	Seal Design	117

TABLE OF CONTENTS (continued)

	Page
Expected Performance	118
Waviness Grinding Apparatus	118
Flexure Design	120
Waviness Profile Results	125
100 Hour Test Results	129
Conclusions on Third Design	132
CHAPTER 5 SEAL RING DEFLECTION	133
Ring Finite Element	133
Comparison to Other Results	142
Single Ring Deflection by Formulas	148
Single Ring Deflections by FEM	148
Simple Seal Contact Model	150
Two Ring Contact Model	154
Theory	155
Method	165
Experiments and Checks	168
Two Ring Contact Model Studies--Submarine Seal	172
Seal Gap Caused by Bolted Joints	175
Conformability of Primary Ring to a Wave	180
Lock Ring Groove Studies	181
Face Offset	186
Two Ring Contact Model--Magnetic Seal	188
Nonlinear Joint Model	192
CHAPTER 6 MICROASPERITY LUBRICATION	199
Background	199
Theory	200
Microasperity Lubrication	202
Test of Hypothesis	210
Experimental Apparatus	213
Hydrostatic Bearing Design	220
Support System	229
Hydrostatic Bearing Tests and Calibration	231
Experimental Procedure	233
Test Results	234
CHAPTER 7 SEAL ANALYSIS	243
Role of Automated Analysis of Seals	243
Geometrical Considerations	244
Method	244
Section Properties Program	248
Mesh Generation	249
Heat Transfer	250
Other Programs	251

TABLE OF CONTENTS (contined)

Page

CHAPTER 8 SQUEEZE SEALS/BEARINGS. 253
Introduction. 253
Rigid Body Squeeze Seals/Bearings 257
Governing Equations. 257
Equations for Conventional and Squeeze Wavy Seals with No Cavitation. 261
Equations for Conventional and Squeeze Wavy Seals with Cavitation 262
Comparison Between Conventional and Rigid Squeeze Wavy Bearings/Seals 265
a) Complete film conditions occur throughout the bearing. 265
b) Cavitation occurs somewhere in the fluid film. 266
i) One-Dimensional Case. 266
ii) Two-Dimensional Case. 274

Deformable Body Squeeze Sliding Bearings/Seals. 278
Deflection of an Infinite Plate Resting on an Elastic Foundation. 283
Governing Equation of the Squeeze Wavy Bearing with Variable Stiffness 285
Numerical Results. 287
Conclusion 288

CHAPTER 9 SUMMARY AND CONCLUSIONS 291

REFERENCES 299

APPENDIX A--FINITE DIFFERENCE SOLUTION TO THE TORSION PROBLEM OF A COMPOSITE CROSS SECTION A-1

APPENDIX B--SINGLE RING DEFLECTION PROGRAM B-1

APPENDIX C--TWO RING DEFLECTION PROGRAM. C-1

APPENDIX D--SECTION PROPERTIES PROGRAM D-1

APPENDIX E--MESH GENERATING PROGRAM. E-1

APPENDIX F--HEAT TRANSFER ANALYSIS F-1

LIST OF FIGURES

Figure		Page
1-1	Mechanical Face Seal	3
1-2	Moving Waviness Concept	8
1-3	Wavy-Tilt Seal Face	13
2-1	Nine Wave Seal Assembly--First Design	16
2-2	Nine Wave Seal--Isometric View	17
2-3	Predicted Performance--Torque	19
2-4	Predicted Performance--Leakage	20
2-5	Test #118--Nine Wave Seal, 100% Pressure, 40% Speed	22
2-6	Test #119--Nine Wave Seal, 100% Pressure, Variable Speed	23
2-7	Test #120--Nine Wave Seal, Variable Pressure and Speed	24
2-8	Test #121--Nine Wave Seal, Variable Pressure and Speed	25
2-9	Test #122--Nine Wave Seal, 2000 Hour Test, Initial Operation	28
2-10	Test #122--Nine Wave Seal, 2000 Hour Test, Final Operation	29
2-11	Final Radial Surface Profile of Carbon, 2000 Hour Test	35
2-12	Test #123--500 Hour Flat Face Test, Variable Conditions	41
2-13	Integral Force Transducer	45
2-14	Integral Force Transducer Test Setup	46
2-15	Integral Force Transducer, Force Test Results	48
3-1	Initial Nine Wave Seal Configuration--Design 2	53
3-2	Composite Seal Ring Geometry	55
3-3	Finite Element Mesh of Composite Seal Ring	57

LIST OF FIGURES (continued)

Figure		Page
3-4	Torsion of Composite Section	61
3-5	Normal Shear Stress Component	63
3-6	All Carbon Seal Design	68
3-7	3-D Finite Element Configuration	71
3-8	Predicted Torque	77
3-9	Predicted Leakage	78
3-10	Predicted Worn Face Shape	79
3-11	Finite Element Configuration	81
3-12	Strength Test Apparatus	82
3-13	Nine Wave Seal Assembly--Second Design	85
3-14	Test Setup for Youngs Modulus Experiments	89
3-15	Test #129, 167-335 Hours	92
3-16	Test #129, 1679-1847 Hours	93
3-17	Test #129, 383-431 Hours	94
3-18	Test #129, 2063-2111 Hours	96
3-19	Preload Ring	103
3-20	Modified Preload Ring	105
3-21	Split Ring Seal	106
4-1	Wavy-Tilt-Dam Seal Face	112
4-2	Wavy-Tilt-Dam Seal	113
4-3	Effect of Radial Offset	116
4-4	Grinding Apparatus--Schematic	121
4-5	Grinding Apparatus	122
4-6	Flexure Mounts	123

LIST OF FIGURES (continued)

Figure		Page
4-7	Waviness in Steel Ring--First Run	126
4-8	Waviness in Steel Ring--Second Run	127
4-9	Waviness in WC Ring	128
4-10	Test #130, 500 psi, 1800 rpm, Nine Wave Tungsten Carbide	130
5-1	Loads on a Ring	135
5-2	Ring Geometry and Definitions	136
5-3	Ring Finite Element	137
5-4	Check Problem 1	143
5-5	Check Problem 2	144
5-6	Test Ring	146
5-7	Flattening Load Distribution	152
5-8	Contact of Two Rings	156
5-9	Contact Model	158
5-10	One Element of Contact Model	159
5-11	Two Contacting Rings with Eccentric Load	170
5-12	Submarine Shaft Seal	173
5-13	Seal Ring Face Flatness	174
5-14	Seal Gap Due to Joints	179
5-15	Conformability of Seals with Different Support Stiffness	182
5-16	Effect of 2nd Harmonic Wave in Lock Ring Groove	184
5-17	Effect of Shim in Lock Ring Groove	185
5-18	Effect of Groove Face Offset	187
5-19	Magnetic Seal	189

LIST OF FIGURES (continued)

Figure		Page
5-20	Surface Profiles and Seal Gap	190
5-21	Comparison of Experimental Theoretical Leakage	191
5-22	Finite Element Mesh	194
5-23	Moment-Rotation Curve	195
5-24	Joint Test Apparatus	197
6-1	Asperity Pressure Distributions Predicted by Classical Lubrication Theory	203
6-2	Truncated Asperity Pressure Distribution	204
6-3	Experimental Results from Hamilton, et al. [9]	206
6-4	Asperity Geometry from Hamilton, et al. [49]	207
6-5	Zero Load Support	211
6-6	Load Support versus Ambient Pressure from Hamilton [49]	212
6-7	Load Support versus Ambient Pressure from Kistler [3]	214
6-8	Friction and Wear Test Apparatus	215
6-9	Point Load Design	217
6-10	Hydrostatic Bearing Support	219
6-11	Hydrostatic Bearing Piston	221
6-12	Bearing Misalignment and Moment Generated	222
6-13	Hydrostatic Bearing Piston	223
6-14	Hydrostatic Bearing Cup	224
6-15	Hydrostatic Bearing Assembly	227
6-16	Torsional Spring Model	228
6-17	Water System Plumbing System	225
6-18	Friction Test Support System	230

LIST OF FIGURES (continued)

Figure		Page
6-19	Friction Torque versus Speed (Early Tests)	235
6-20	Friction Torque versus Time	237
6-21	First Torque versus Ambient Pressure (High Speed)	238
6-22	Friction Torque versus Ambient Pressure--Low Pressure	239
6-23	Friction Torque versus Speed (Low Speed)	240
7-1	Seal Ring Cross Section Definition	245
7-2	Coarse Mesh Generation	247
8-1	Squeeze Seal/Bearing	254
8-2	Conventional Wavy Seal/Bearing	255
8-3	Elastic Foundation Squeeze Seal/Bearing	256
8-4	Finite Difference Symbol Definition	260
8-5	Comparison of Pressure with Cavitation	272
8-6	Effect of Mesh Size on Squeeze Seal Load Support	273
8-7	Control Volume in Cylindrical Coordinates	275
8-8	Effect of Mesh Size--Two-Dimensional Case	279
8-9	Wavy-Squeeze-Deformable Journal Bearing	281
8-10	Wavy-Squeeze-Deformable Problem	282
8-11	Plastic Foundation	284
8-12	Wavy-Squeeze-Deformable Seal Load Support	289
8-13	Condition of Maximum and Minimum Load Support	290

LIST OF TABLES

Table		Page
2-1	Simulation Submarine Operation Weekly Test Cycle	27
2-2	Zero Shift of Torque Transducer	32
2-3	Wear Measurements--2000 Hour Wavy Test	36
2-4	Wear Measurements--500 Hour Parallel Face Test	42
2-5	Tests of Epoxy Force Transducers	47
3-1	Composite Section Stiffness	66
3-2	Warping Function Calculation	73
3-3	Solid Carbon Seal Design	76
3-4	Nine-Wave Amplitude Study	87
3-5	Young's Modulus Results for P658RC Carbon	90
3-6	Wear Results (2000 hours)	97
3-7	One Week Average Torque Values	99
3-8	Comparison of Experimental and Theoretical Results--Design 2	100
3-9	Weekly Average Leak Rate	102
4-1	Seal Performance (Static)	119
4-2	Carbon Wear Measurements -- Test # 130	131
5-1	Experimental Results	147
5-2	Ring Deflection	149
5-3	Two Contacting Rings with Eccentric Load	171
5-4	Significance of Seal Gap	176
5-5	Submarine Seal Conformability Studies	177

LIST OF TABLES (continued)

Table		Page
8-1	Distribution of Film Thickness Over One Wave of a Seal Face	267
8-2	Pressure Distribution for a Conventional Wavy Seal Under Full Film Conditions	268
8-3	Pressure Distribution for a Squeeze Wavy Seal Under Full Film Conditions	269

LIST OF SYMBOLS

a	Ring cross sectional area - m^2
$A = \frac{EJ_x}{GJ_\theta}$	Stiffness ratio - dimensionless
$B = \frac{r_o^2 - r_b^2}{r_o^2 - r_i^2}$	Balance ratio for an outside pressurized seal
E	Youngs modulus - N/m^2
F	Force - N
{F}	Load matrix
G	Shear modulus - N/m^2
h	Nominal film thickness - m
h_n	Amplitude of the nth harmonic - m
I_x, I_y, I_{xy}	Moments of inertia based on straight beam theory
$J_x = \int_A \frac{y^2}{1 - x/r_c} dA$	Moment of inertia about x axis for circular ring cross section - m^4
$J_y = \int_A \frac{y^2}{1 - x/r_c} dA$	Moment of inertia about y axis for circular ring cross section - m^4
$J_{xy} = \int_A \frac{x^2}{1 - x/r_c} dA$	Product of inertia for a circular ring
J_θ	Torsional stiffness constant for ring cross section - m^4
k_F, k_S	Spring constants representing face contact and support contact
K	Stiffness matrix
{K}	Stiffness matrix for two ring model support contact

$[K_R]$	Individual ring stiffness matrix
m_x, m_y , m_θ	Distributed moments on seal ring $N \cdot m/m$
M_x, M_y, M_θ	Ring moments - $N \cdot m$
n	Number of the harmonic or number of waves around seal face or normal direction
N	Number of nodes
N_θ	Ring normal force - N
p	Fluid pressure - N/m^2
p_c	Cavity pressure - N/m^2
p_i	Seal inside pressure - N/m^2
p_m	Pressure at asperity contact--equals compressive strength - N/m^2
p_o	Seal outside pressure - N/m^2
p_s	Shear strength of asperities - N/m^2
p_{sp}	Spring pressure on face - N/m^2
Q	Total leakage for the seal - m^3/s
r	Radial coordinate
r, θ, z	Seal coordinates
r_b	Seal balance radius - m
r_c, R_c	Radius to centroid of seal ring - m
r_f	Friction radius - m
r_i	Inside radius of seal - m
r_o	Outside radius of seal - m

R	Radius to centroid of seal ring - m
t	time - s
T_q	Seal friction torque - N · m
u, v, w, ϕ	Ring displacements
u, v, w	Displacements in torsion problem
U	Velocity - m/s
v	Ring centroid displacement - m
V_x, V_y	Ring shear forces - N
x, y, θ	Ring coordinates
x, y, z	Coordinate in torsion problem
W	Total load support - N
W^*	Required load support - N
δ	Displacements
$[\delta]$	Displacement matrix
δ_{FO}, δ_{SO}	Initial gap between springs and mating surface for face and support
Δ	Net deflection at the face
η	Vicosity - N · s/m^2
θ	Angular coordinate or flow variable
θ_1, θ_2	Angular coordinates of end nodes of ring element
ψ	Stress functions or angle of twist about y axis
ρ	Density - kg/m^3
Γ^*	Warping constant - m^6
ϕ	Rotation of seal ring about its centroid
ω	Angular speed

ν	Poisson's ratio

<u>Subscripts</u>

e	Refers to one element
P, M	Refers of primary and mating rings of seal
F, S	Refers to face contact and support contact
1, 2	Refers to nodes at ends of element

CHAPTER 1

INTRODUCTION

Mechanical Face Seals

Applications of face seals range from boiler water feed pumps to compressors, to petrochemical process pumps, to propeller shafts. In many applications the reliability of the mechanical seal is of the greatest importance to the reliability of the equipment itself.

Mechanical face seal technology has been steadily improving over the past several decades. However, there still remain demands for seal performance which have not been met. One such application of note is the submarine propeller shaft.

Such demands on a particular technology can often be satisfied by first improving the technology. In the case of mechanical face seals, the main barrier to advancement has been that the mechanics of seal operation are not well enough understood to be able to reasonably anticipate seal performance as a function design parameters.

During the past eight years of this research program, much has been learned about controlling the hydrostatic and hydrodynamic mechanisms which enhance face seal operation. In this present work, this knowledge is applied to the design of an improved small scale submarine shaft seal. Theory, design, and test results are presented. The results show promise that significant improvements in submarine shaft seal design are possible, and the application of such designs could greatly increase the length of trouble-free shaft seal service.

Seal Lubrication

As background, the mechanical face seal consists basically of two annular rings which rotate relative to each other and which are pressed together by spring and fluid pressures (see Figure 1-1). In conventional seals, the surfaces that rub together are generally manufactured as flat as possible initially so as to minimize leakage. The effective gap between the faces is ideally quite small (order of 1 μm) so that leakage flow across the faces will be quite small. The difficulty in designing a mechanical seal is in maintaining the gap at a very low value while at the same time providing a definite lubricant film between the faces.

The load that must be supported at the faces of a mechanical seal is due primarily to loading caused by the sealed pressure. The load support at the faces is derived from fluid pressure and mechanical pressure. If the fluid pressure at the faces is large enough to support all of the load, then there will be no contact and no adhesive wear.[1] If none of the load is supported by fluid pressure, the load must be carried by mechanical contact, and the wear rate will be large.

In practice, conventional seals often operate at one of two extremes. At one extreme, a large gap will be created by hydrostatic or hydrodynamic pressure or distortion, all of the load will be supported by fluid pressure, and the seal will leak a lot and wear very

[1] There may still be abrasive or corrosive wear even if the sufaces do not touch.

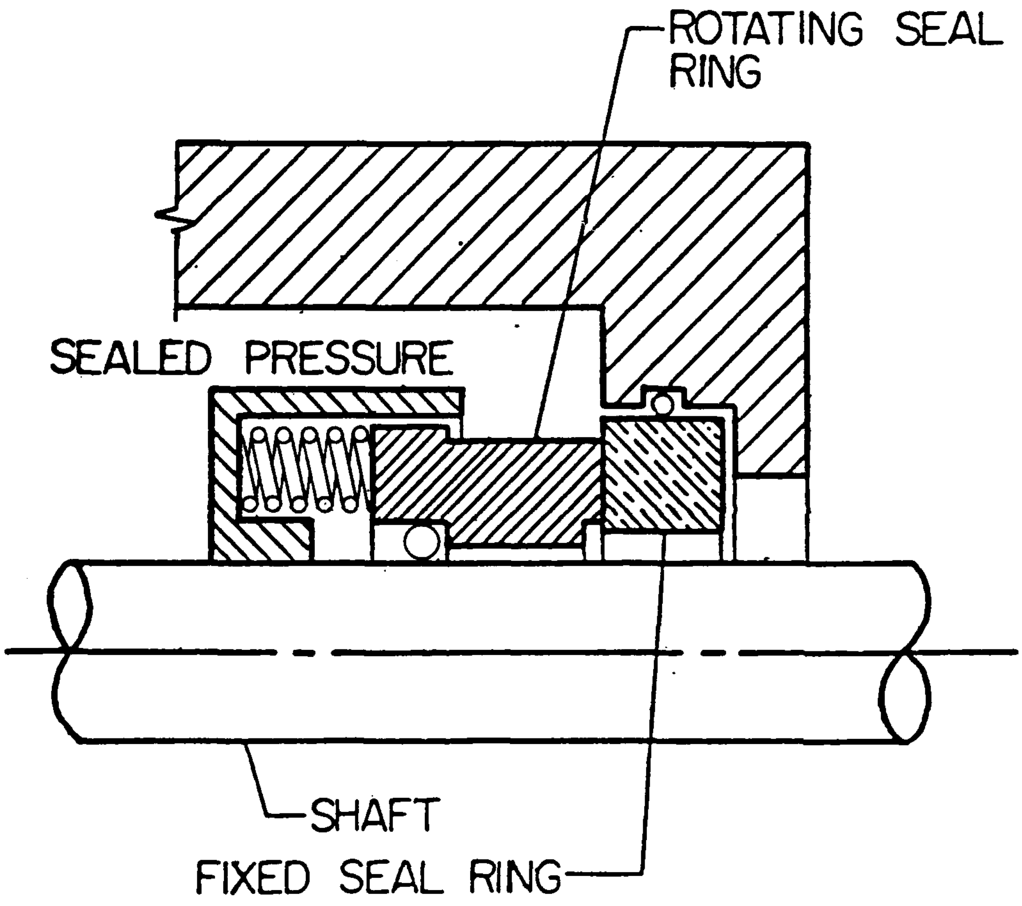

Figure 1-1. Mechanical Face Seal.

little. At the opposite extreme, the gap will close completely. Leakage will be low but only a fraction of the load will be carried by fluid pressure, and wear and heat generation will increase.

Based on the above, it can be concluded that an effective seal should operate between these two extremes--having both adequate fluid pressure load support and low leakage. The seal should operate so that it just touches to minimize leakage but such that the load is carried by fluid pressure. To do this requires that any fluid pressure generation mechanism used to provide load support to the seal must be very carefully controlled. At present in commercial seals, this is left in part to chance and sometimes seals operate at one of the undesirable extremes mentioned.

In this research program, attention has been devoted toward studying the effects of waviness as a source of controlled hydrodynamic and hydrostatic load support. Waviness was selected because it is controllable. In this present work, waviness has been applied as the basis for the design of an improved small scale submarine shaft seal.

Background

ONR-sponsored research on mechanical seals had been conducted for five years prior to the beginning of the submarine seal design phase described herein. The work being reported now evolved from various discoveries over this initial five year period, and the past work must be reviewed to better understand the nature of the current work.

As a starting point for this Navy research program, the effects of waviness on seal performance were modeled in some detail. In the first

annual report for this project, Reference [1], this general problem was solved using a one-dimensional theory. In the second annual report, [2], the much more complex two-dimensional solution to the above problem was solved. The effects of waviness, roughness, asperity contact, wear, cavitation, and elastic deflection were included in this model. Using this model, predictions were made for the relative wear rate, friction, and leakage as a function of roughness, waviness, speed, size, pressure, viscosity, and material.

A number of conclusions were reached based on these first two annual reports:

1) The effect of roughness on hydrodynamic lubrication are not completely understood. Certain fundamental questions remain concerning the roughness model used.

2) As to the potential of utilizing hydrodynamic effects caused by parallel face waviness to advantage by design, the results show that wear rate and friction can be greatly reduced while maintaining leakage at acceptable levels.

3) While a comparison of predicted results to experimental results given in the literature is generally good, data contained in the literature is incomplete, so more complete experimental data are needed for comparison.

4) In low viscosity or heavily loaded applications where some touching is expected to occur, waviness will wear away with time and any benefit derived will be lost unless something is done to counteract this effect.

5) Based upon data for some commercial seals and using the model, it was determined that there was insufficient accidently caused waviness to produce significant hydrodynamic effects in water. One cannot generalize to say that such effects do not occur in commercial seals. However, using the model the question can be answered on a case by case basis.

Item 1) was treated extensively in the third annual report [3]. Even after this analysis certain fundamental questions remain concerning how to deal with roughness in lubrication problems. However, this thorough analysis led to conclusions allowing certain simplifying assumptions discussed in the fourth annual report [4].

Item 2) was also treated extensively in the third annual report [3]. A methodology for the design of a wavy face seal was developed and applied. Theoretical results showed large reduction in friction and wear rate compared to conventional designs whereas leakage could be controlled.

Concerning Item 3), the second and third annual reports [2,3] describe a test apparatus designed to test the wavy seal theory. This apparatus has been in operation for more than five years and many tests have been conducted. These test results are reported in the fourth and fifth annual reports [4,5].

Early in the test program it was observed that the type of waviness which can be practically applied is not of the radially parallel type. Waviness generally consists of alternating tilt plus radially parallel waviness. Based on these considerations, a new model for

predicting performance was developed and appears in the fourth annual report [4].

Concerning Item 4) above, a solution to this problem was first proposed in the first annual report [1]. It was proposed to move the waviness slowly around the seal so that whatever wear occurred would be uniformly distributed. Then the shape of the wave would be preserved and tests using a constant wave could be made. The concept is illustrated in Figure 1-2. This concept was incorporated into the test apparatus and is described in detail in References [2] and [3]. In the fifth annual report [5], a new concept to move the waviness with no internal moving parts is described in detail.

In the fifth annual report [5], additional experimental results using waviness are presented, the wavy seal model is further improved, and theory and experiment are compared. The results using a new concept, that of a self-generating seal profile, are reported. Results from tests of the effects of radial taper and high temperature environment are also reported and compared to theory.

Both the theoretical and experimental basis for applying waviness to a mechanical seal to reduce friction and wear were well established during these first five years.

Submarine Seals

Starting in December 1980, under joint NAVSEA-ONR sponsorship, a three-year submarine seal program was initiated. The general objectives of the three-year effort were:

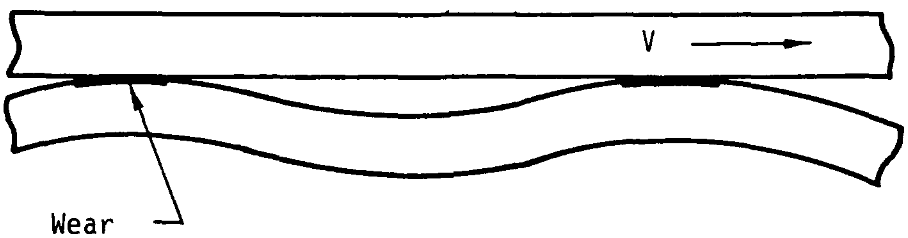

Distorted Ring

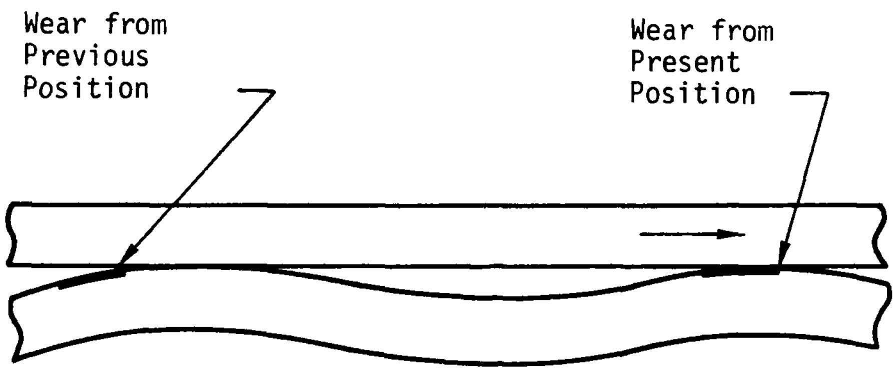

Distorted Ring after Wave Has Moved

Figure 1-2. Moving Waviness Concept.

1) to conduct further experiments using moving waviness to further the understanding of this concept.

2) to refine mathematical models already developed so as to be able to better predict performance.

3) to demonstrate in a practical way the use of the concept of moving waviness to reduce friction and wear in mechanical seals.

4) to undertake the development needed to be able to demonstrate the applicability of the concept to submarine shaft seals and to design a full scale long life seal.

5) to explore other uses of the waviness concept such as for gas seals and to create better methods by which the concept can be applied.

From these objectives, the following specific tasks were defined:

1) Design, fabricate, and test a nine wave optimum seal. Nine waves are needed to minimize changes in tilt with changes in pressure and speed.

2) Operate the seal or an extended period of time under simulated submarine operating conditions including seawater and changing speed, pressure, and alignment.

3) Evaluate compliancy of existing and proposed submarine seals.

4) Conduct friction and wear tests on carbon and hard face materials.

5) Seek alternate methods of applying moving waviness.

6) Perform analysis of a moving wave gas seal.

In the most recent annual report [6] the progress made on these items is reviewed in detail. Preliminary nine wave test results were reported. Modifications to the test apparatus, design methods and problems and seal deflection calculations were discussed. Details of the progress on all of the above items are contained in this current annual report.

It became clear during the three year period that more work was needed on the development of the wavy seal particularly in the simplification of the waviness mechanism itself. In addition, other submarine seal related problems were identified. Thus this led to a proposal for a fourth year of submarine seal development work, the specific objectives of which were:

1) Complete a long term test of a split wavy seal.
2) Make a preliminary squeeze seal design.
3) Perform a final design and fabricate a new waviness drive mechanism.
4) Evaluate seal conformability.
5) Evaluate the effect of dirt on a wavy seal.
6) Make a face width study for parallel face seals.
7) Perform a review of recent submarine seal designs.
8) Make a preliminary full scale design.

Considerable progress has been made on these items in addition to the previous list and is reported herein. In particular a wavy seal design which eliminates the need for a waviness drive is proposed and preliminary test results suggest that an ideal wavy seal design may be in hand.

This entire research program spans a number of years. Thus, the entirety of the technical work is reported in six previous annual reports [1-6], this report, sixteen published papers [7-22], and seven master's theses [23-29].

Wavy Face Seal

The concept of waviness is that the film thickness varies in some fashion circumferentially around the seal. Generally speaking, film thickness may vary radially as well as tangentially.

$$h = h(r, \theta) \; . \tag{1-1}$$

In the present work interest is focused upon film thickness shapes of the following functional form

$$h = h_0 + f(r) \cos n\theta \; . \tag{1-2}$$

At any particular radius r the film shape is periodic with n waves around the seal and is therefore wavy. However, film shape can also vary in some general manner with r.

If $f(r) = \text{const}$ then the faces are always radially parallel. This component of film thickness variation is commonly termed waviness. If $f(r) \neq \text{const}$, then the faces are not in general radially parallel. $f(r)$ is referred to as tilt. Thus, the film thickness shapes of interest are combinations of waviness and tilt. Since at any radius the film thickness is wavy, the combination of waviness and tilt defined above will also be called a wavy film shape.

The reason for choosing film shapes as described by Equation (1-2) as a subject for study is that these shapes can conveniently be generated by planned mechanical distortions in a seal ring, and the shapes also include common modes of unplanned distortion found in operating seals. For example, generally seals undergo a uniform tilt due to pressure and thermal deformation. When rings are loaded by any non-axisymmetrical load they become wavy as described by Equation (1-2).

Now, for the sake of illustration, assume a seal has a wavy film thickness shape given by Equation (1-2) where f(r) is a piecewise linear function of r. This gives a shape as shown in Figure 1-3 where for each of the n periods a flat mating seal ring will touch all across at the high points and is radially convergent π/n radians away. At any radius, the seal is wavy circumferentially. The waviness enhances hydrodynamic effects and the radial convergence enhances hydrostatic effects. The region where contact is uniform acts as a sealing dam.

It is this shape which previous research has shown has the greatest potential to reduce friction and wear while holding leakage at very low levels. This is the film shape used for the design of the small scale submarine seal.

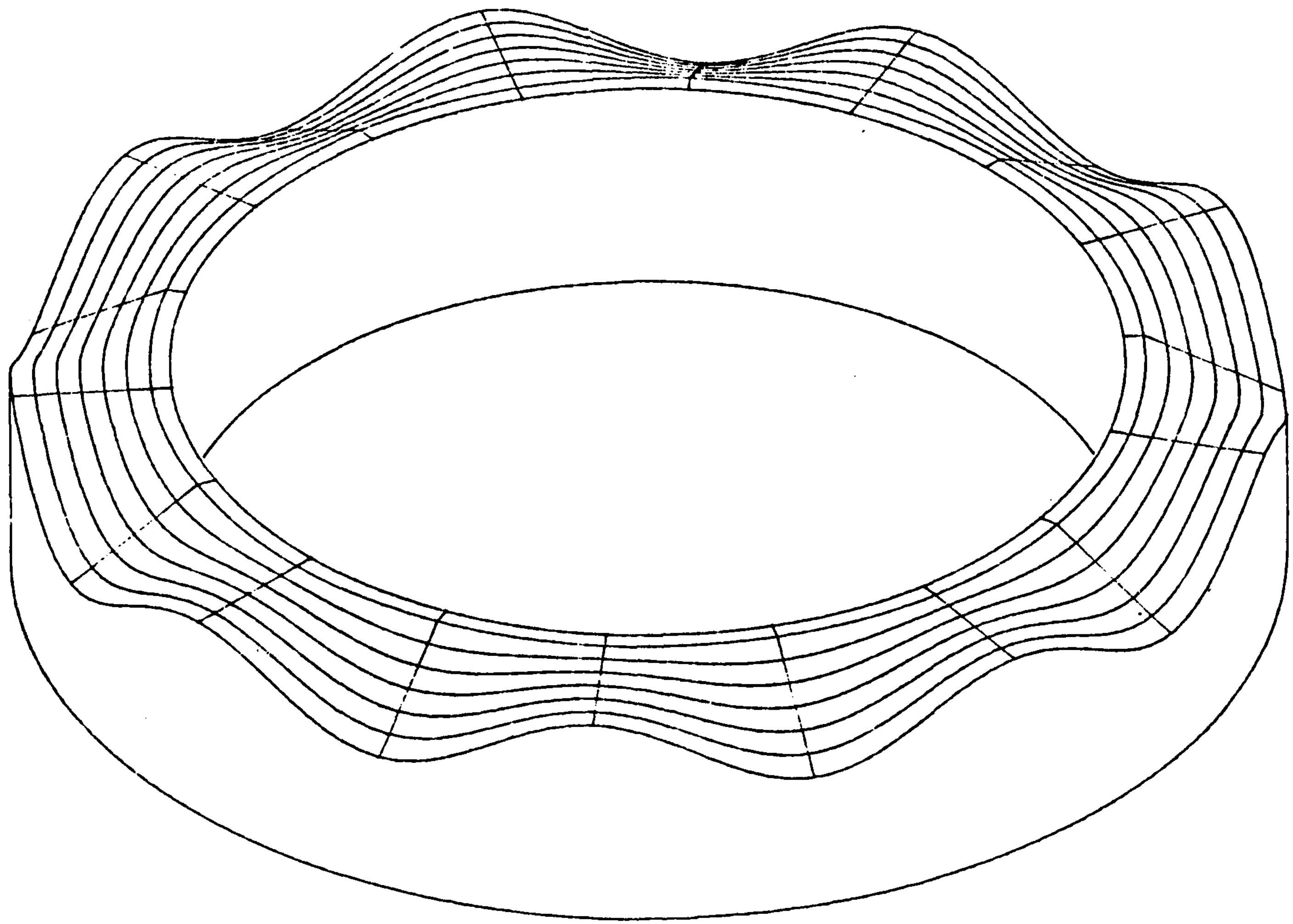

Figure 1-3. Wavy-Tilt Seal Face.
(Patent Pending)

CHAPTER 2

MOVING NINE WAVE SEAL--FIRST DESIGN AND RELATED TESTS

Seal Design Review

The details of the first nine moving wave seal design are given in a previous report [6]. A brief review of the principles of operation will be given here.

Figure 2-1 shows the assembly drawing of the first nine wave seal. Starting at the left, one of three sinusoidally varying pressures generated by the waviness drive unit [5] is directed into two of six pressure channels (1) in the waviness cylinder (2). The pressurized fluid then passes through the pressure coupler (3) and is ported to one of three circumferential chambers on the left end of the waviness adapter (4). Eighteen smaller passages, connected to each of the three circumferential channels, terminate at pressure pockets (5) located on the inside and outside diameters of the waviness adapter (4). The 54 pressure pockets (three sets of eighteen) apply a waviness pressure to the 54 fingers of the nine wave seal (6).

Figure 2-2 shows a modified isometric cross section of the nine wave seal. The pads shown are labeled (1), (2), or (3) depending on which of the three sinusoidally varying pressures is connected to the pad. The load on the outer pads is directed radially outward and on the inner pads radially inward. With this configuration, three sets of nine waves, each set spaced 13-1/3 degrees from the other, can be elastically imposed on the face of the carbon insert. As discussed

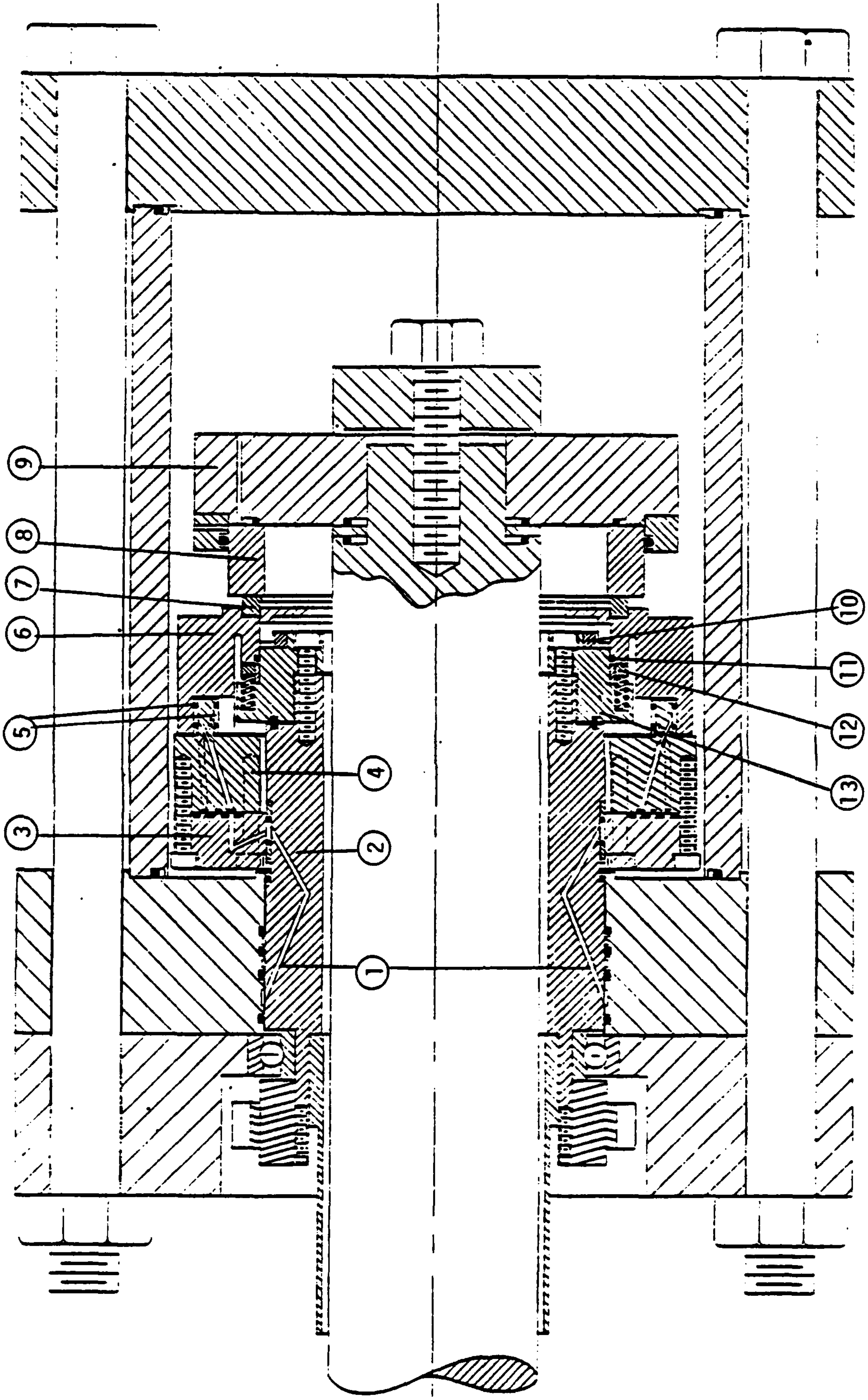

Figure 2-1. Nine-Wave Seal Assembly View.

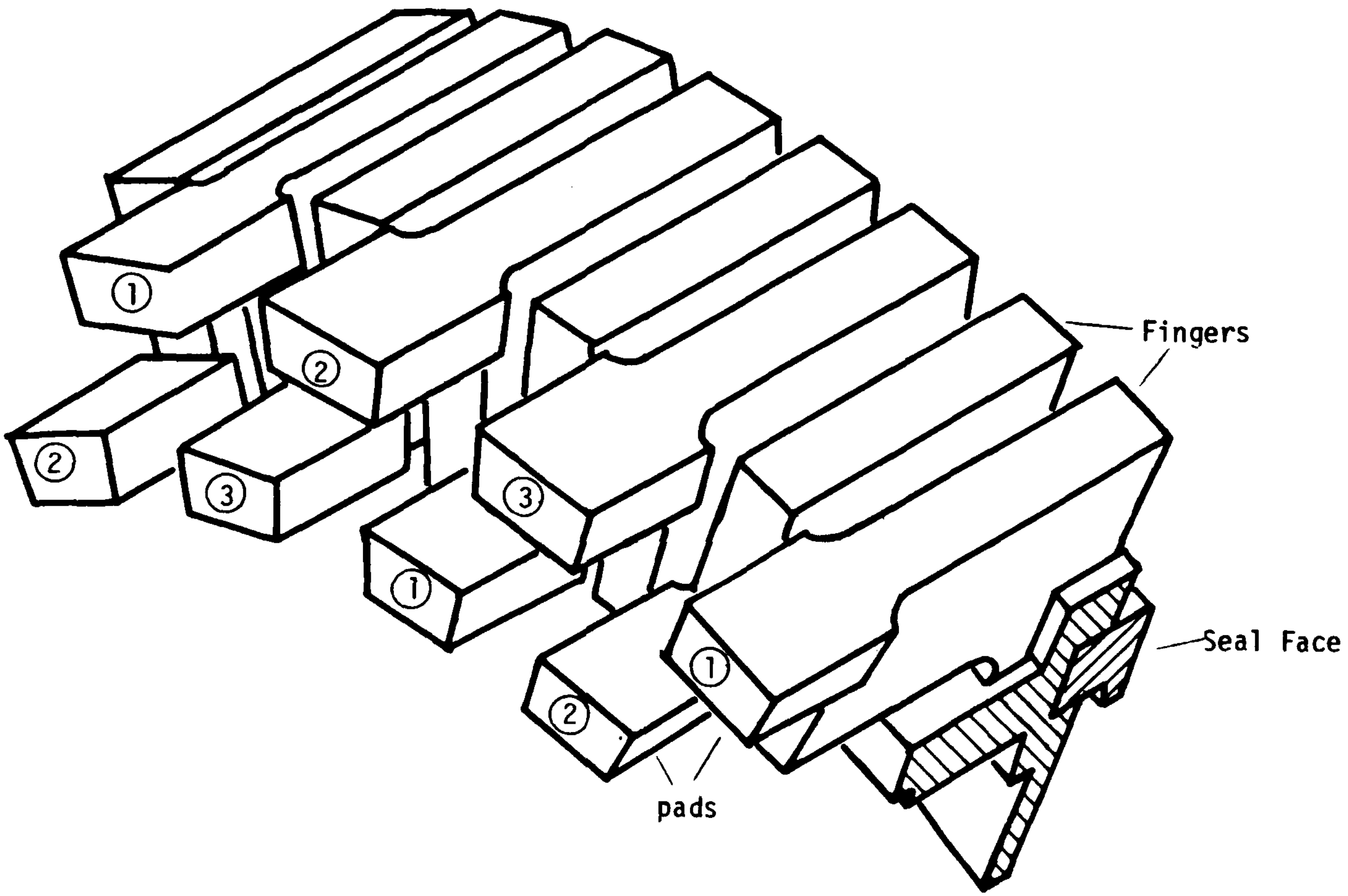

Figure 2-2. Nine-Wave Seal - Modified Isometric Cross Section.

previously [5], by sinusoidally varying the three separate pressures with time, the result is one set of nine waves which moves circumferentially around the seal with time.

The carbon insert (7) in pure carbon P 658 RC material epoxied into the carrier ring using 3M 1838 B/A adhesive. The seat or mating ring (8) is made of silicon carbide. The secondary seal (11) is located at the left end of the seal on the inside diameter. Springs (13) provide preload through the spring seat. Balance ratio is 1.0.

Based on seal modeling reported earlier [5], performance of this seal was predicted as shown in Figures 2-3 and 2-4. A very low wear rate was also predicted.

Initial Test Results

Several initial tests were conducted during which several problems were encountered and resolved. The details are reported in Reference [6]. Based on these early tests, the following changes were made.

1) The cross sectional area of the seal was reduced to reduce stiffness and obtain more waviness.

2) The epoxy bond thickness was reduced so that the wave would be more effectively transferred from the carrier to the carbon.

3) The pressure pad design was modified to use smaller O-rings with miniature pistons.

After these changes were made, performance was much improved, however, there was still some concern over the significant radial taper which had been observed (1500 μm/m convergent).

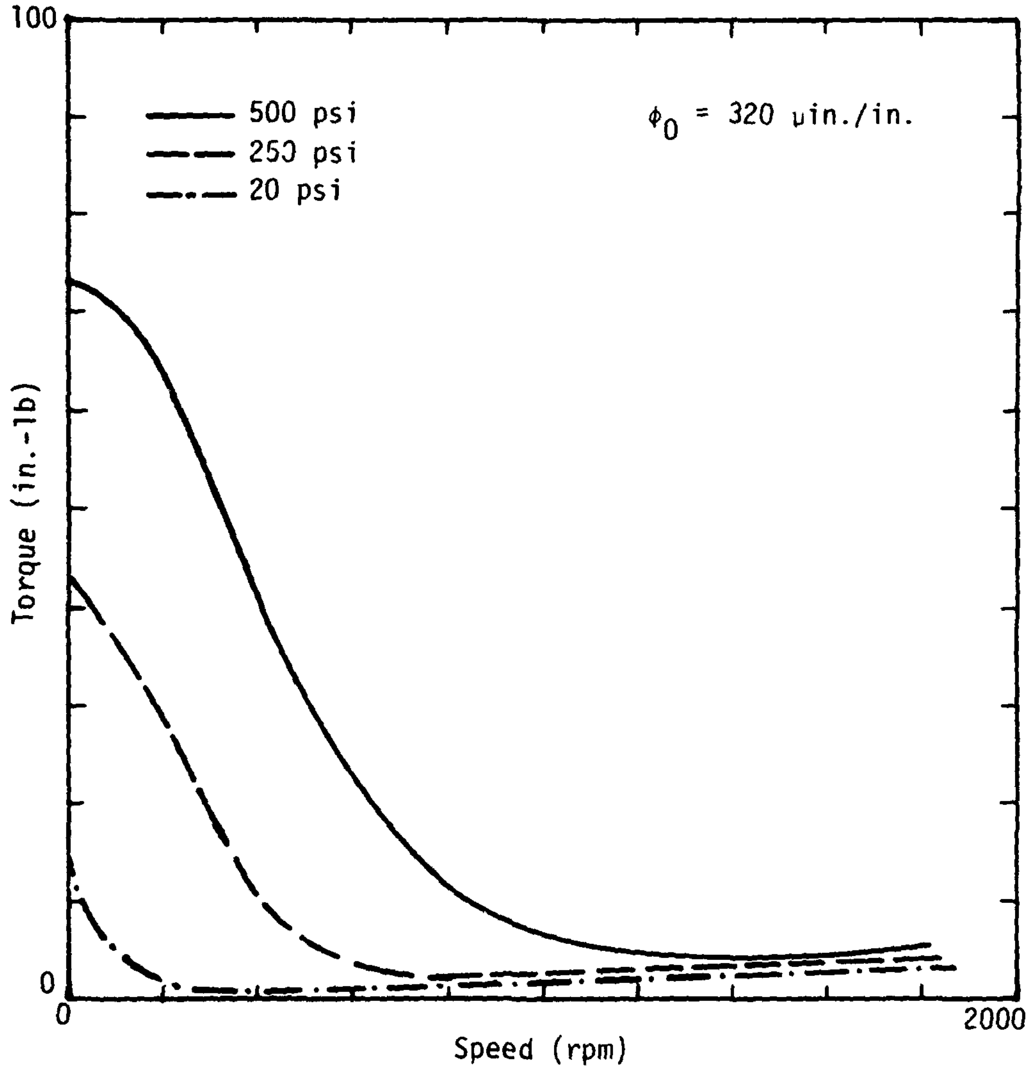

Figure 2-3. Predicted Performance - Torque.

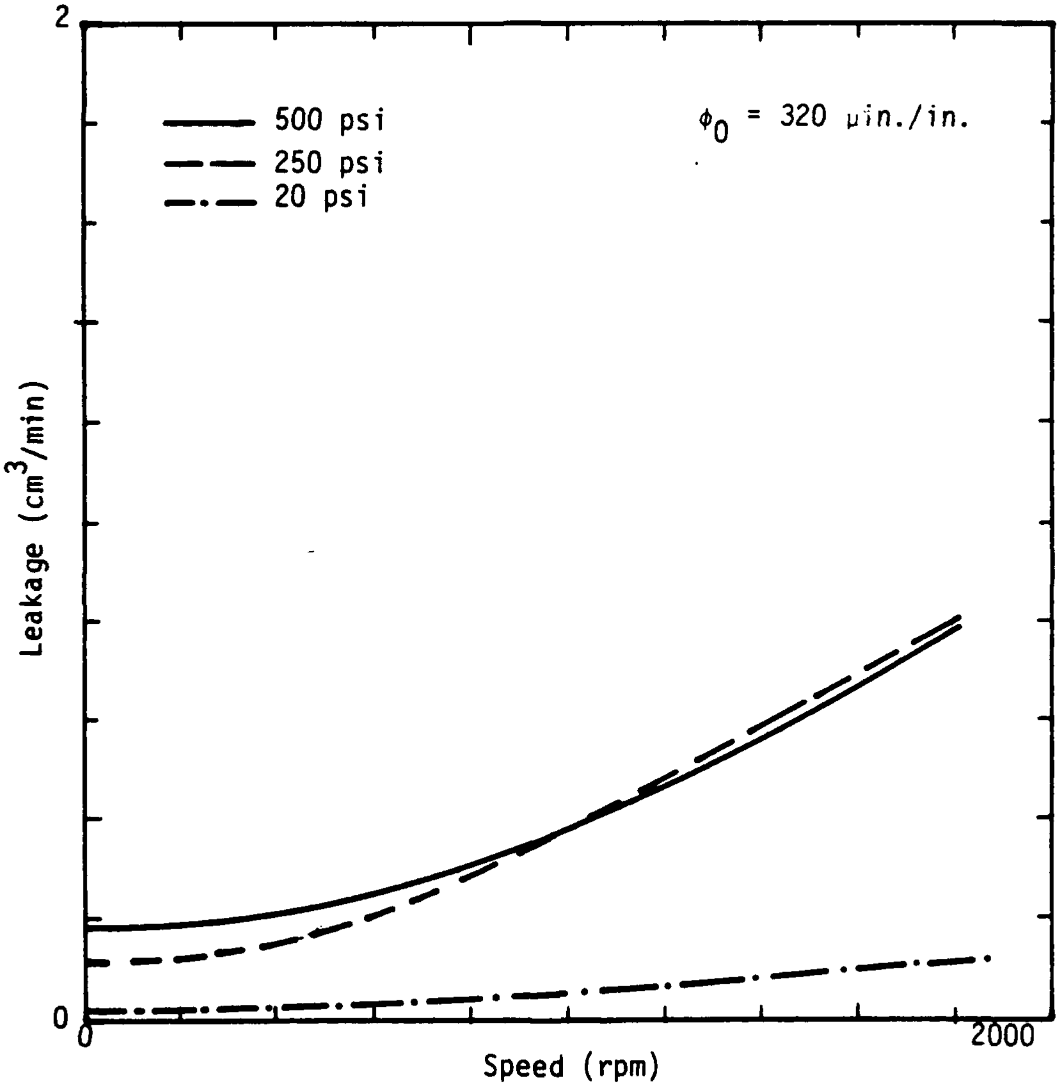

Figure 2-4. Predicted Performance - Leakage.

To determine the possible cause of such a taper several independent tests were run. These were:

1) Lap a convergent taper into the seal and test under 100 percent water pressure at low rpm (Test No. 118, Figure 2-5).

2) Check for possible creep at end of test.

3) Lap the seal flat and assemble the waviness adapter and check for induced radial taper.

4) Apply 750 psi to all pads and again check for any induced radial taper.

The results of Test 1 above showed that little if any of the rotation was being caused by pressure induced moments (low speed eliminated thermally caused rotation) as designed. Also, the same radial surface profiles revealed no creep of the carbon insert. Tests 3 and 4 above showed that the pressure adapter and the pressure applied to it does not cause the problem. While the cause is still being investigated, it is pointed out that this taper does not appear to effect the waviness operation. The seal faces are touching all over their surfaces during the test as required.

Tests Nos. 119, 120, and 121 (Figures 2-6 through 2-8) were run to check for software and hardware bugs. These tests were the first to incorporate the full range of variable condition control of the test machine by the computer. Also Test No. 121 was run particularly to check the operation of the combination O-ring-piston pad method of sealing the hydraulic oil. After 168 hours of operation no oil leaks were detected and the test was stopped. With previous hardware and

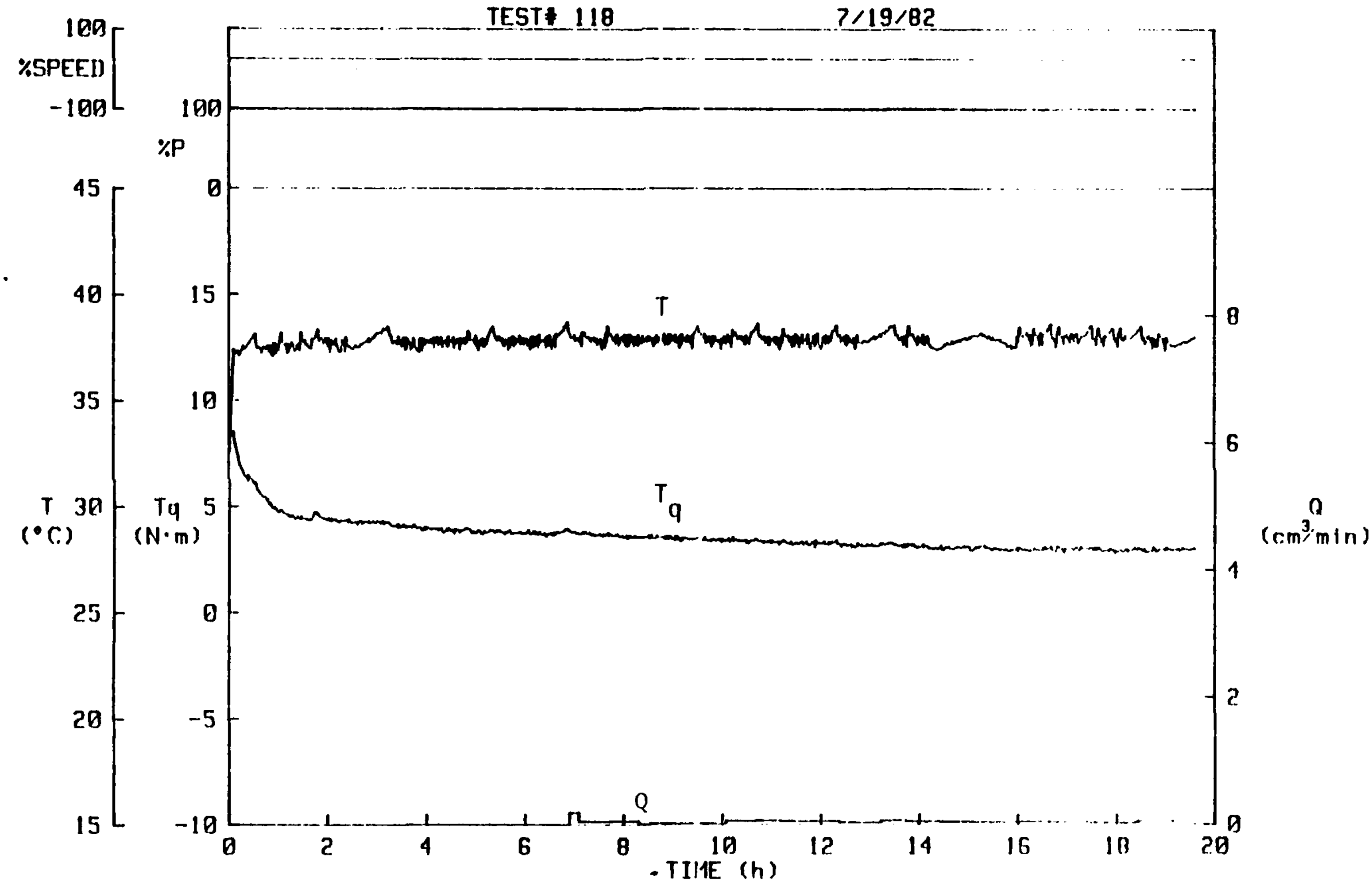

Figure 2-5. Test #118--Nine-wave Seal, 100% Pressure, 40% Speed.

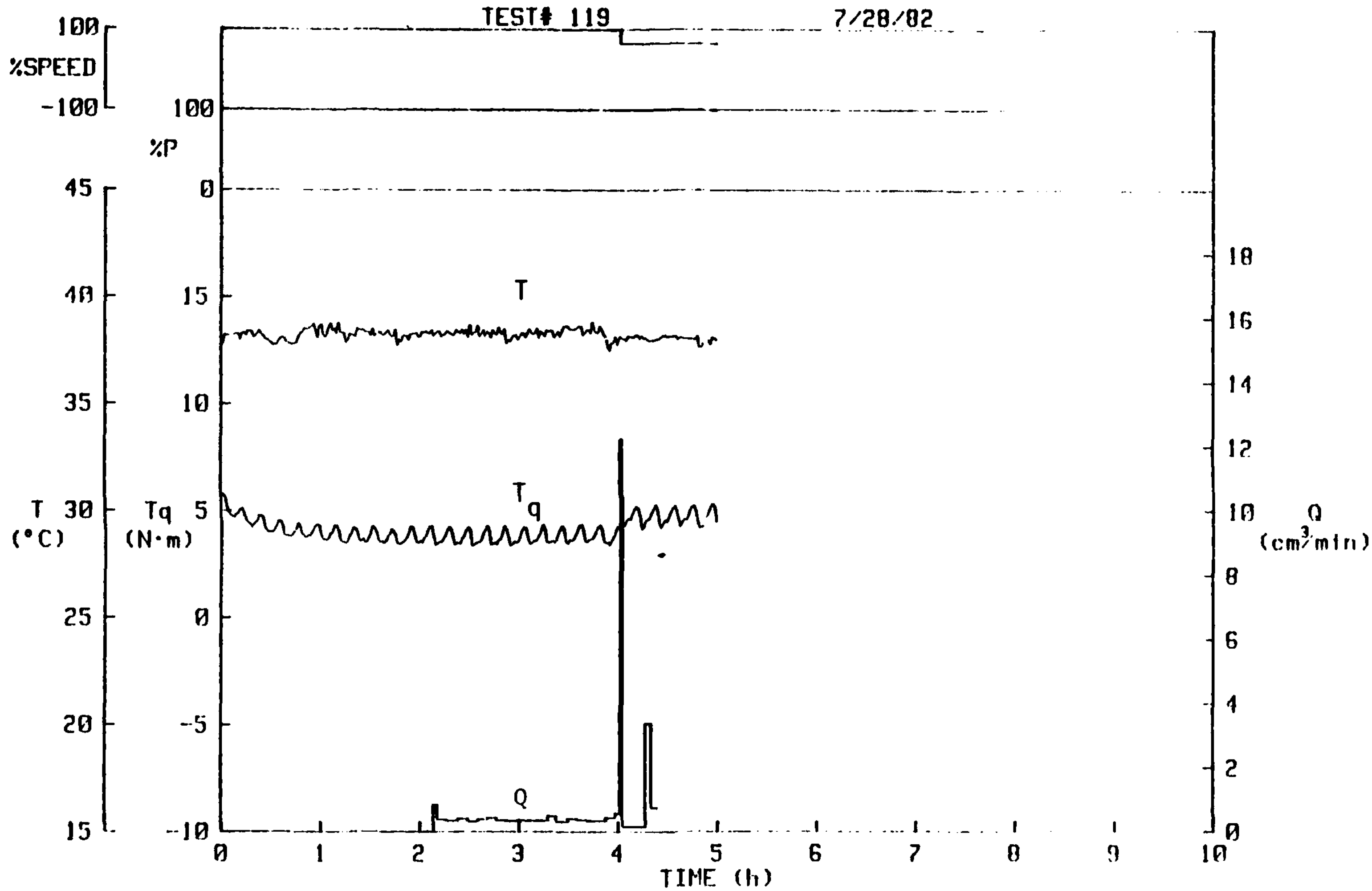

Figure 2-6. Test #119--Nine-wave Seal, 100% Pressure, Variable Speed.

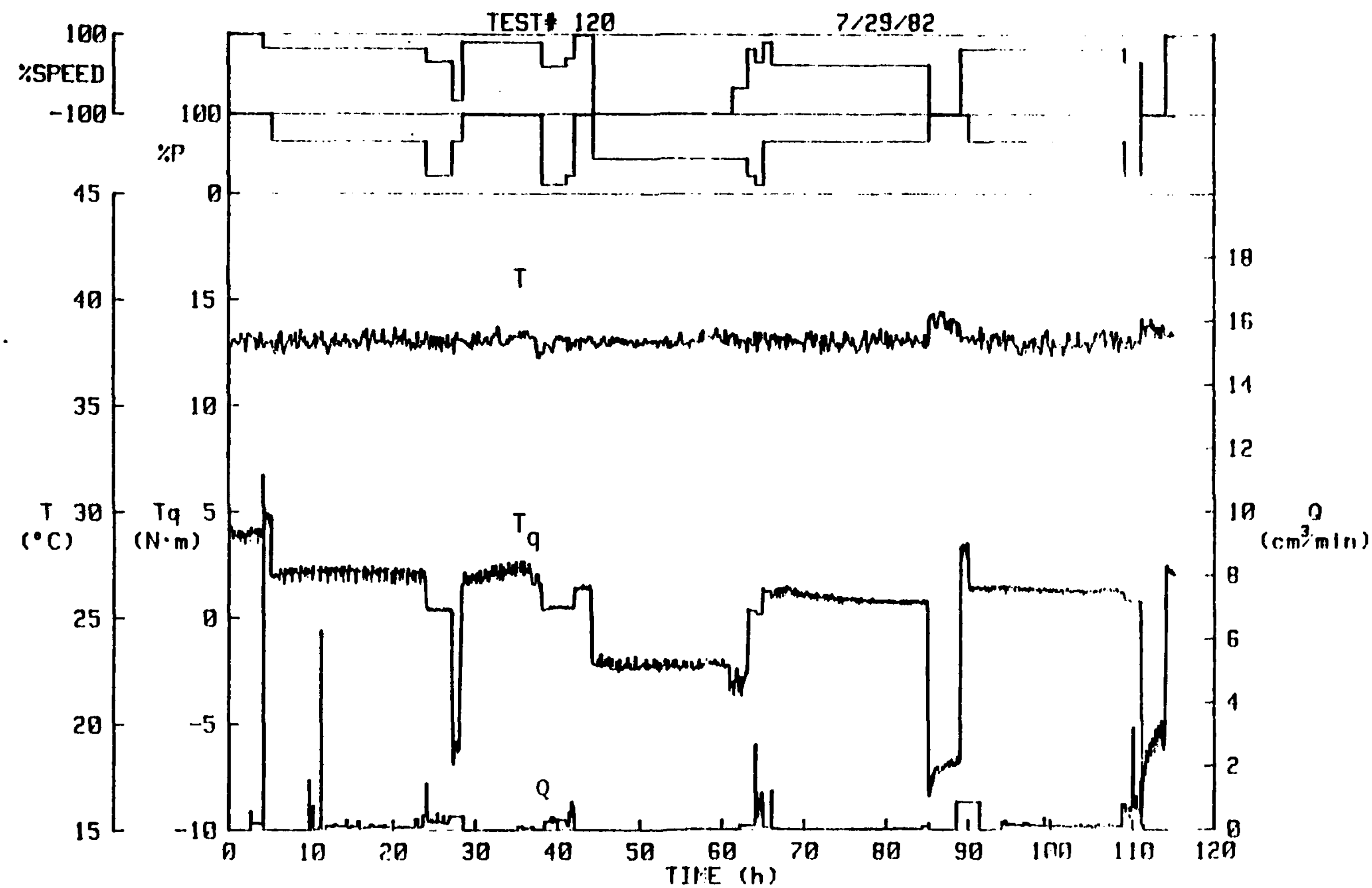

Figure 2-7. Test #120--Nine-wave Seal, Variable Pressure and Speed.

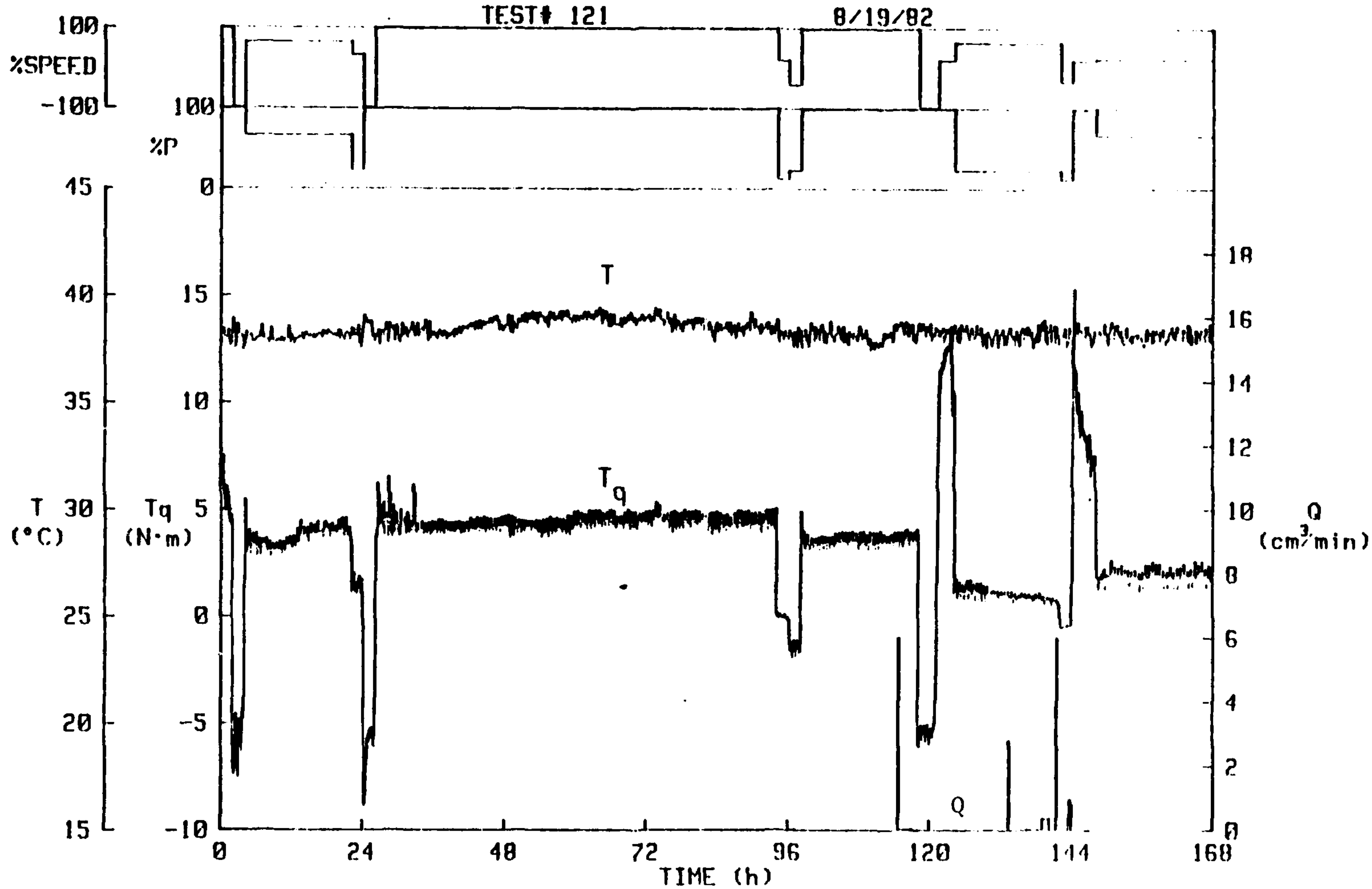

Figure 2-8. Test #121--Nine-wave Seal, Variable Pressure and Speed.

software problems cleared up, the apparatus and seal were ready for the first 2000 hour test.

2000 Hour Test

The seal test period of 2000 hours is similar to Navy seal tests. During the test, pressure, speed, and alignment are varied according to schedule shown in Table 2-1. The cycle period is one week and the summary results shown represent one week of operation. Synthetic seawater maintained at 38°C was the test fluid.

The test apparatus and the variations of operating conditions were all controlled by a computer. Data was recorded and safe operation was assured using the same computer. Details of this system have been reported previously [6].

Performance During Test

Figures 2-9 and 2-10 show seal operation for one week near the start of the test and near the end of the test. The figures show the speed changes and the pressure changes. Seal temperature (taken behind the carbon face), drive torque, and leakage are recorded.

A comparison of the two figures shows that the seal performance becomes much more stable with increased operating time. As an example one of the large changes in torque occurs at 49.5 hours into the weekly schedule (216.5 hours on Figure 2-5). Up to that time torque has been running at near zero under conditions of 7 percent pressure and 14 percent speed for 17 hours. Then within 1.5 hours the pressure changes from 7 to 50 percent and then to 100 percent, the speed remaining at 14

TABLE 2-1

Simulated Submarine Operation Weekly Test Cycle

Hour	Day	% Speed	% Pressure	Tilt & Offset Position
0	1	33	100	1
6.5		-100		
7.5		100		
24	2	33	100	3
31		14	7	1
48	3	14	50	2
49.5			100	3
54		-33		
55.5		100		
72	4	14	100	3
79.5		100	50	2
96	5	Var.	Var.	Var.
102		100	100	3
120	6	100	100	3
144	7	100	100	3
168				

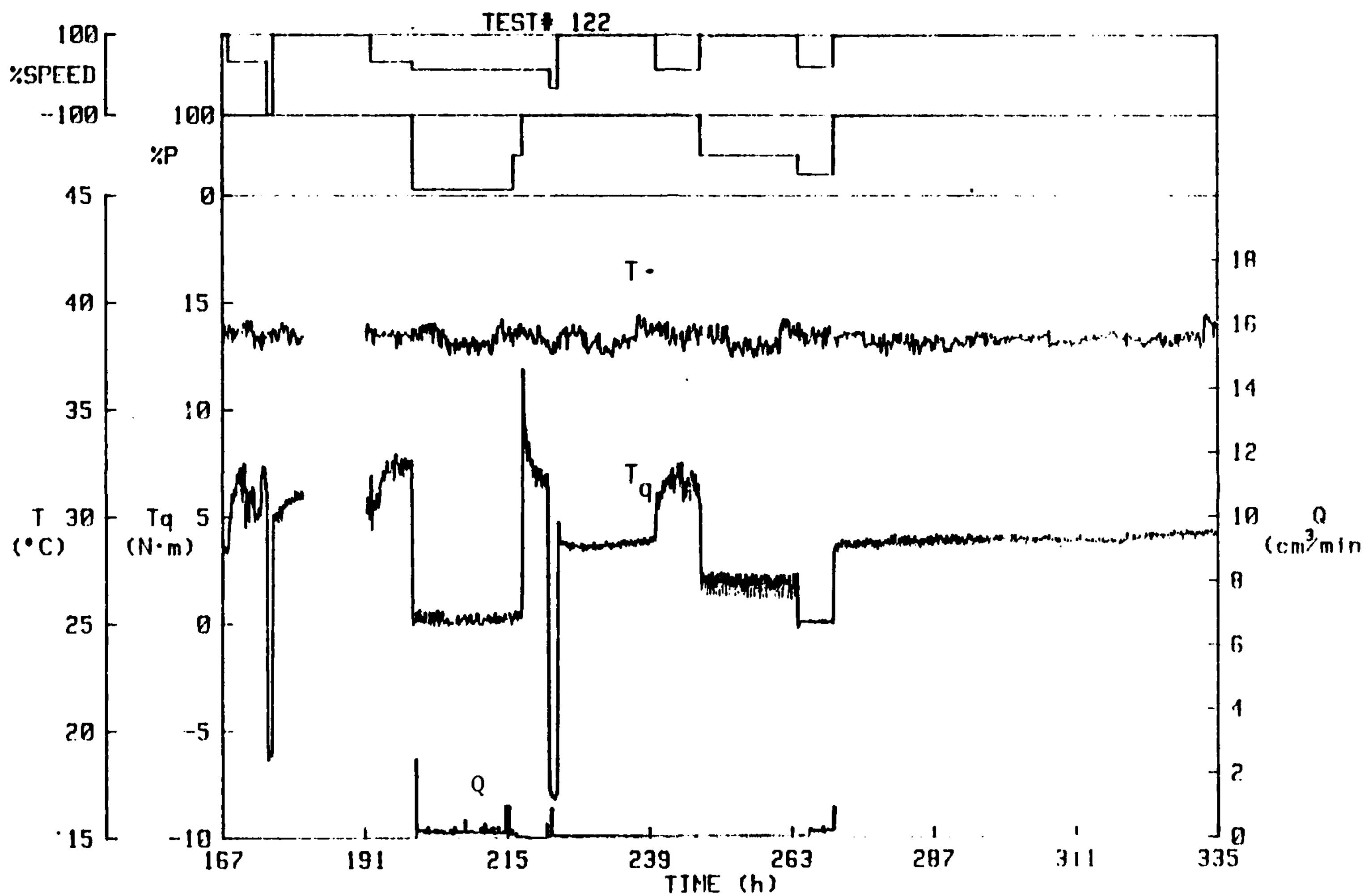

Figure 2-9. Test #122--Nine-wave Seal, 2000-hour Test (initial operation).

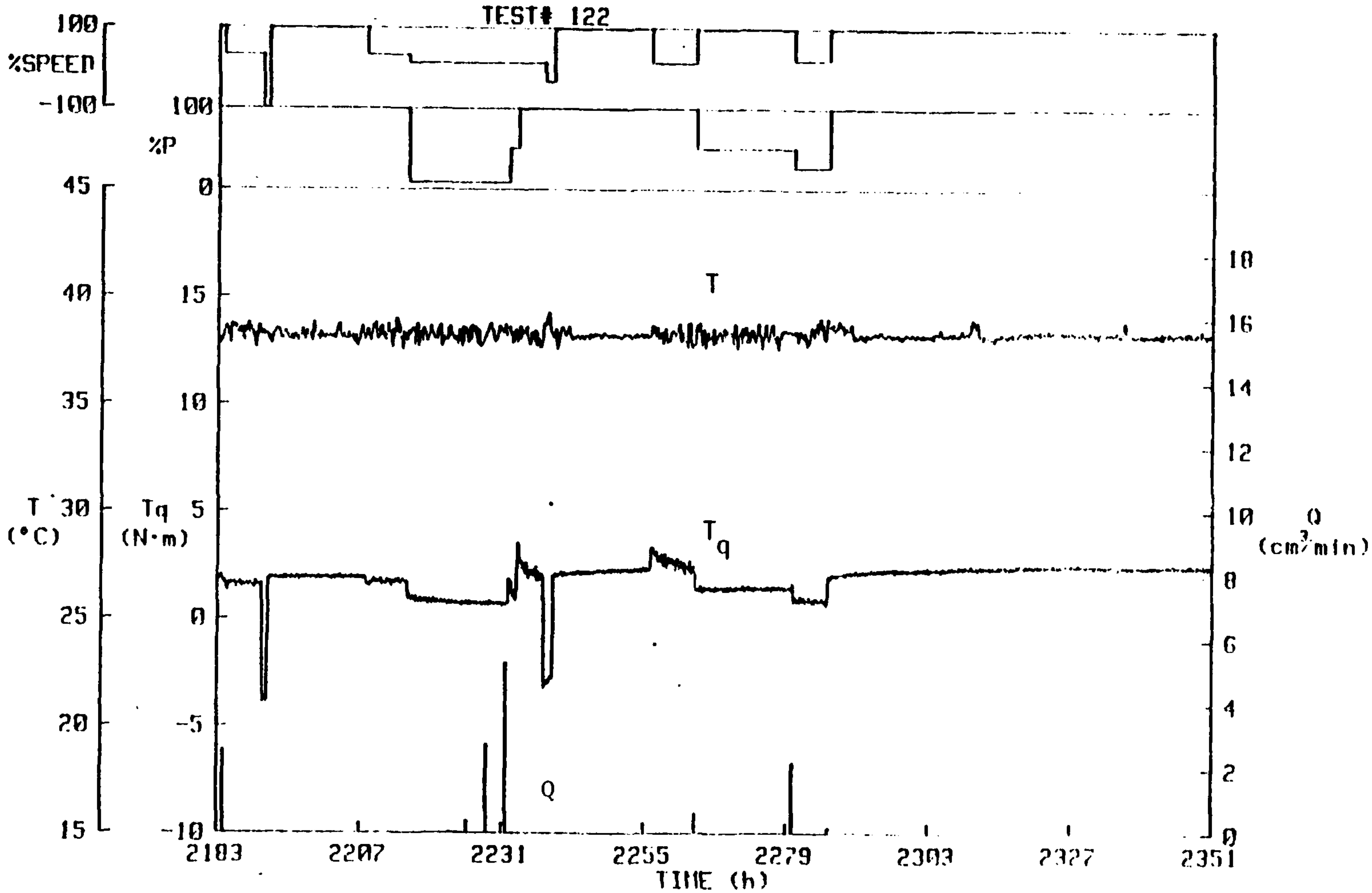

Figure 2-10. Test #122--Nine-wave Seal, 2000-hour Test (final operation)

percent. When the pressure goes from 50 to 100 percent the torque jumps to almost 13 N · m and then starts to fall rapidly. Figure 2-10 shows that this effect is greatly reduced. One possibility for this sudden increase might be that some change in the face profile is occurring causing additional wear momentarily and therefore resulting in a temporary increase in friction. This effect is lessened as the test proceeds possibly because the seal wears to some equilibrium face profile which minimizes these abrupt changes in performance.

Another anomaly in the data is shown by the torque output when there is a direction reverse. Two reversals take place during the weekly program, one at 6.5 hours relative to the weekly schedule (173.5 hours on Figure 2-9 and 2189.5 hours on Figure 2-10) and the other at 54 hours (221 hours on Figure 2-9 and 2237 hours on Figure 2-10). The first direction reversal goes from -100 percent speed to +100 percent speed at 100 percent pressure. On Figure 2-9 the average torque changes from approximately -6 N · m to +4 N · m. The second direction reversal is from -33 percent speed to +33 percent speed at 100 percent pressure. On Figure 2-9, the average torque changes from approximately -8 N · m to +3 N · m.

Figure 2-10 shows that these differences have greatly minimized as indeed they should. The apparent explanation for the anomaly early in the test is that some change in distortion occurs when the direction is reversed which causes some localized hard contact of the faces and higher friction. Evidently this wears away with time and does not appear to degrade performance in the long run.

During the length of the test, the torque transducer was re-zeroed nine times. This was done under zero water pressure by the motor in both the forward and reverse directions and sampling the torque and then averaging the results. These results are shown in Table 2-2. As stated in Reference [6], the torque transducer is sensitive to bearing housing temperature. A temperature increase in the bearing housing causes a torque shift of 0.109 ($T_{housing}$ - $T_{reference}$) in.-lb/°F. Table 2-2 shows the amount of shift due to temperature effects and the zero shift not attributed to the bearing housing temperature change. The fact that the zero shifted during this long term test might explain some of the differences between torques in the forward and reverse directions at a particular point in time. However, by re-zeroing periodically the uncertainty caused by this error was minimized.

The other measured quantity which changes considerably is that of leakage. At the beginning of the test, Figure 2-9, the leakage was approximately 500 cm^3 for the whole week which gave a weekly average of 0.05 cm^3/min. By the end of the test, Figure 2-10, the leakage had dropped to approximately 42 cm^3 for the weekly cycle or an average of 0.004 cm^3/min, a reduction of an order of magnitude. Again, this behavior can be attributed to the seal wearing into a more favorable equilibrium profile.

The leakage data often shows spikes which means that there are spurts of leakage flow being discharged from the test apparatus. There is little doubt that the seal itself does not leak in this fashion; it leaks more steadily. This erratic leakage flow is thought to be caused by some type of trapping, surface tension and wetting mechanism inside

TABLE 2-2

Zero Shift of Torque Transducer

Time (hr)	Zero (N·m)	Temperature (°C)	Zero Shift Attributable to Temperature Change (N·m)	Zero Shift not Attributable to Temperature Change (N·m)
0	33.98	22.04		
29	35.53	25.39	+ .07	+ 1.48
72	34.17	39.67	+ .32	- 1.71
264	33.97	35.71	- .09	- .11
674	34.05	22.28	- .3	+ .38
703	34.72	30.27	+ .18	+ .49
1543	36.81	31.23	+ .02	+ 2.07
1879	37.17	30.85	- .01	+ .37
2047	37.06	28.98	- .04	- .07

the apparatus. Corrosion may also play a role in trapping the leakage flow. Of course, when the speed is changed, a spurt of leakage is expected because the retention of leakage by centrifugal effects changes.

The test was operated a total of 2046 hours. Figure 2-10 shows a larger number because the test was shut down for a period during which the operators were unavailable.

Post Test Analysis

The following observations were made on disassembly:

1) The top portions of the pressure coupler and waviness adapter were coated with a light oil film. The waviness drive was started up and run for 3 hours to see if any oil would leak from the O-rings of the waviness adapter. No oil leaks were detected. Thus, there must have been a small leak at some point during the test.
2) The seal face temperature thermocouple was slightly worn due to rubbing contact with the pressure vessel.
3) Rust deposits were found on the threaded ends of the bolts used on the spring seat.
4) Considerable amounts of mineral deposits (white scale) were found on the inner portion of the seal where $p = 0$ psi.
5) The seal face was polished with some mineral deposits on the inside diameter edge.
6) The Delrin spacer used with the spring retainer experienced enough swelling to make removal difficult.

7) The waviness cylinder could not be rotated fully to Position No. 1 or No. 3. This had become a problem during the last 500 hours of operation such that the full extent of misalignment could not be achieved (see misalignment mechanism described in [6]).

8) The small O-rings on the pressure adapter received about a 0.002 in. permanent set.

9) Some chipping was noticed on the outer edge of the K_TSi-C seat.

10) Steel end plates showed considerable rust and corrosion on bottom half of the inside surface.

11) The worm gear had severe rust deposits on the lower 25 percent of it.

12) The inside diameter of the torque transducer at the front end (end plate side) showed signs of galvanic corrosion.

13) The bearing which fits over the waviness cylinder was removed from the end plate and disassembled. The bearing was locked due to rust and corrosion between the balls and races.

14) The waviness cylinder and other seal parts showed no corrosion.

The carbon ring was measured for wear and radial taper. Figure 2-11 shows a typical radial surface profile showing the unexplained radial taper (which averages 2700 µm/m). The profile also shows that contact occurred across the entire face.

Table 2-3 shows a summary of the wear values taken at five different locations around the seal. The technique for making wear

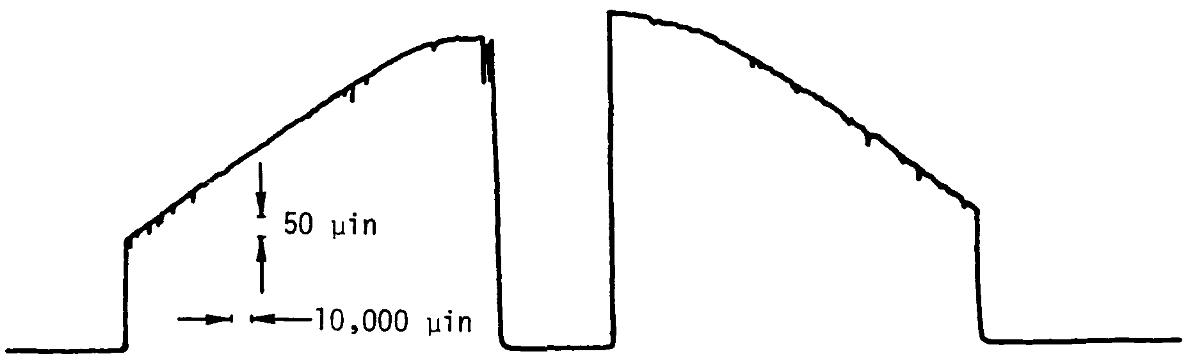

Figure 2-11. Final Radial Surface Profile of Carbon, 2000-hour Test.

TABLE 2-3

Wear Measurements

2000 Hour Wavy Test

Comparison to 8/18/81 Traces--Test #122

Location[1]	Original Nose Height (μin)	Final Nose Height (μin)	Wear (μin)
1-6[2]	3925	3700	225
4-5[2]	3900	3050	850
2	3950	2750	1200[3]
4	3800	3100	700
6	4000	3650	350
		Average excluding Location 2	530 μin 13.5 μm

[1]Because of deposits on wear track, not all locations could be measured.

[2]Designates a trace taken midway between the given locations.

[3]Questionable value because of deposits.

measurements is to initially grind a very shallow and narrow offset (0.004 in.) at the seal ID. The original height of the face relative to this offset is determined using a profilometer as shown in Table 2-3. Then, after the test is completed, the same measurements are made and compared.

One problem using this method is that sometimes unusual deposits form in the offset, invalidating the wear references. This problem was taken into account in compiling the data in Table 2-3. The wear on the Si-C ring was just a few microinches.

Concerning the general character of the test results compared to prediction (see previous figures) torque values are somewhat higher and leakage values are lower. It was concluded that given the problem in applying the waves as discussed that the wave amplitude is not as large as the values used in the calculation and that further comparison would not be too meaningful. However, a detailed comparison is made for design 2 in Chapter 3.

Conclusions on First Nine Wave Design

1. The moving wave concept works in actual operation. That is a moving wave was imposed which caused low friction and wear while maintaining low leakage. Earlier tests and later tests using the same seal in a parallel face mode show that drive torque is several times higher in the absence of waviness.

2. This first nine wave seal design is very difficult to make. Its design requires many intricate cuts and small holes to be made in relatively hard to machine Inconel 625.

3. The hydraulic drive for the pressures for the moving wave, while being a relatively simple device, does add a layer of complexity to the seal design. A digitally controlled device might in fact be simpler than the mechanical device used.

4. The use of the oil hydraulic system to drive the wave can be accomplished reliably on a 2000 hour test. However, as discussed in the previous report [6], the utmost care in O-ring seal design must be used to eliminate O-ring wear and leakage. There is some question as to the long term (10 years) reliability of a device such as this although hydraulic system of other types in known applications do operate reliably for many years.

5. While wear and friction were quite low, they were expected to be lower. The reason for this is that the actual design value of wavy tilt could not in fact be imposed on the seal. Just over one half of the design values was available because of the limitation of the mechanism as discussed previously [6].

6. The corrosive problems mentioned previously were all related to a design change which allowed leakage to flow on occasion into the gear mechanism of the waviness cylinder drive--a region not designed for water contamination. This corrosion also caused the binding in turning the waviness drive being used as the misalignment mechanism. This problem was readily overcome for future tests by redesigning the leakage flow path.

7. The seal and support system were made using inconel, 316 stainless and monel. Concerning corrosion on the seal and supporting parts, there was no detectable (to the eye) corrosion of surfaces nor

galvanic corrosion between mating parts (except the screws noted). The electrical insulation method of mounting the parts made of different metals apparently was adequate.

8. The bond between the carbon and its support or holder is very critical. Early experiments show that a thick (0.010 in.) epoxy bond will permit the wave which is imposed on the carrier to simply be flattened out after it reaches the carbon. A very thin bond, which has a much greater stiffness, was used to solve this problem.

9. After an initial wear in, performance becomes consistent from week to week. There was no degradation of performance over the course of the test. The seal had lower friction and lower leakage during its last week of operation than during the first week.

10. The total wear was low and could be expected to meet ten year life objectives. Projecting the average wear of 530 μin. to 150000 hours of continuous operation gives a total wear of 0.040 in., well within what can be allowed for in a seal design.

11. The radial taper source has still not been identified. Some type of distortion which has not been duplicated in bench tests is occurring in the actual seal installation itself. Some of the wear is being caused by this behavior. In the test, however, once beyond this wear in period, the radial taper does not appear to be affecting the results.

500 Hour Flat Face Test

Test No. 123 was run using the nine-wave seal but without any waviness, a flat face test. The conditions of operation were the same

as for the 2000 hour test so that the performance could be compared for the two. Figure 2-12 shows a sample weekly plot for the flat face test. Comparing the performance at 100 percent conditions reveals that the torque in the flat face test was nearly four times higher than in the waving test (approximately 9 N · m to approximately 2 N · m). Thirteen times during the test the test machine was shut down by the control system because of excessive horsepower demands due to high friction. Torques as high as 46 N · m were recorded. Test No. 123 was actually operated for a total of 420 hours and then stopped.

Wear measurements were taken for the flat face test so that a comparison could be made with the wavy test. Final profiles showed an average wear of 117 μin. (3 μm) for the 420 hours of operation (Table 2-4). Adjusting this to the 2046 hours for the wavy test would give a wear of 570 μin. (14.5 μm). This is essentially the same; however, the comparison is not really valid.

The 100 percent pressure and speed conditions did not represent the proper fraction of the total time of operation because of the high amount of down time at 100 percent conditions. The actual time operated at 100 percent conditions was 186 hours of the 420 whereas it should have been 317 of the 420. From this information, the wear rate could have been as much as two times higher had the test run properly.

In conclusion, the wavy seal has a much lower drive torque and probably a lower wear rate. Leakage of the parallel face seal is lower although the wavy seal leakage is also quite low. Probably the most important but hard to evaluate difference is that the flat face seal has torque spikes (none are shown in Figure 2-12, but they do occur).

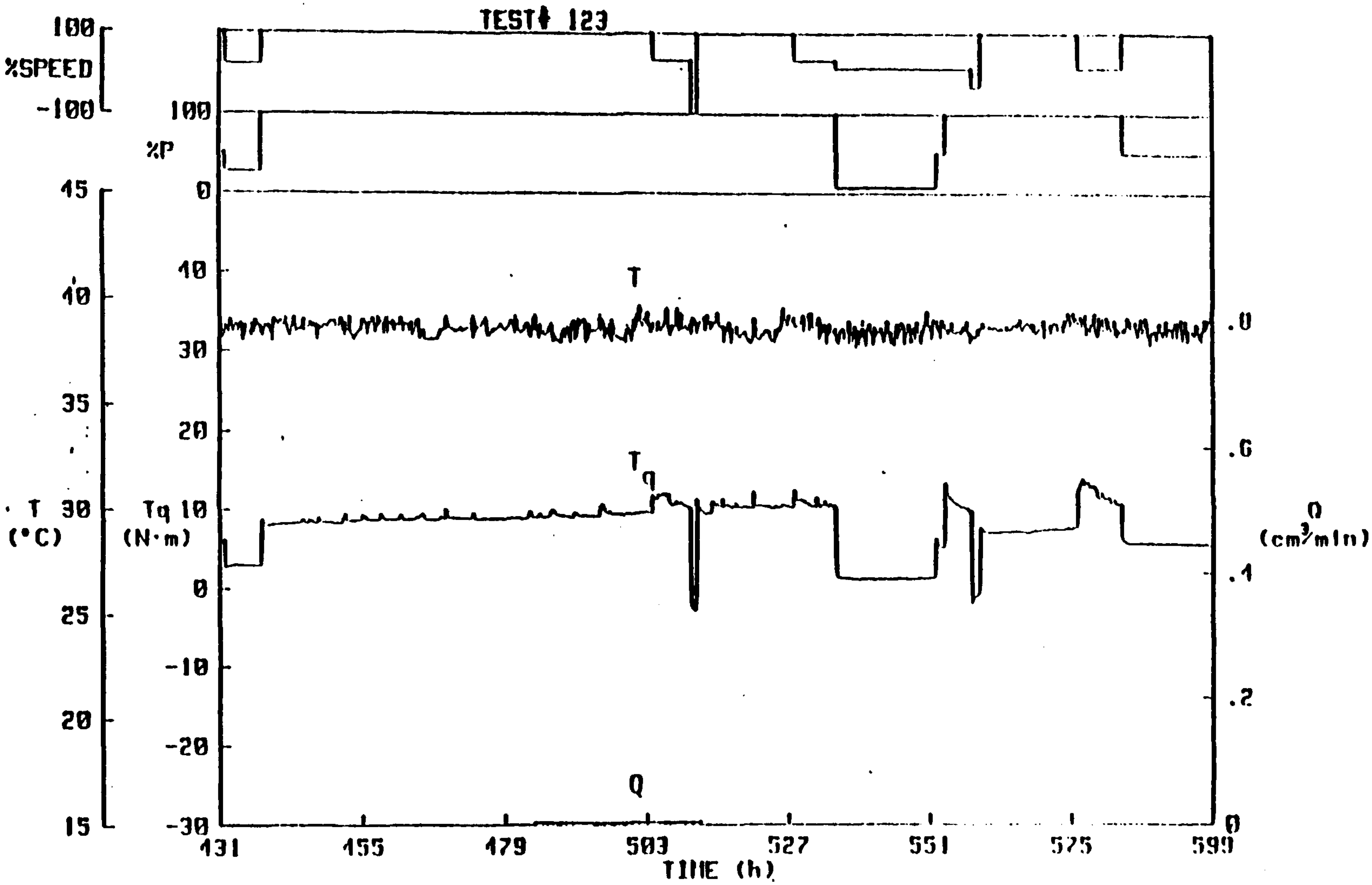

Figure 2-12. Test #123--500 Hour, Flat Face Test, Variable Conditions.

TABLE 2-4

Wear Measurements--500 Hour Parallel Face Test

Loccation	Wear (μin)
#1	200
#4	150
#3	200
#6	50
#2	0
#5	100
Average	117 μin

The wavy seal does not. It is thought that the torque spike is caused by divergence and pinching off fluid pressure load support across the film--thus high friction. High average torque and torque spikes represent potential problems in that they cause high mechanical loads on the system, larger thermal loads, and the possibility of causing thermal instability. Consistent nonsticking drive torque is preferable.

The wear results above may be interpreted as suggesting that at this level of PV service the carbon-Si-C wearing pair may give adequate seal life. In many industrial applications where face wear is the limiting factor this is the case. However, for higher PV and for cases where extremely long life is of interest, then reduction of face friction and mechanical contact, such as by using a wavy seal, is very important.

Integral Force Transducer Design and Test

After evaluating the previous design, many alternatives for a simpler design were considered. As part of this evaluation, it became clear that a different type of force t:ansducer should be considered which might make implementation of other types of wavy seal design much simpler. The criterion for the force transducer were:

1) Must convert pressure to force proportionally and consistently.

2) Must be absolutely reliable, i.e., no leaks or blowouts permitted.

3) Must be salt water compatible.

4) Must be easy and low cost to fabricate.

5) Force must be relatively insensitive to clearance (otherwise a serious tolerance problem and other uncontrollables result).

6) Must allow force to consistently go back to zero.

7) Must allow for easy manifolding of pressure.

To meet these needs, the idea shown in Figure 2-13 was developed. The cylindrical steel shell is for the purpose of testing the concept. The epoxy could be formed around many transducers and their tubes in any holder as needed. The idea is that pressure will cause fluid to flow from the tube into the porous metal. The porous metal is contained on all sides but the diaphragm side by epoxy. Since the diaphragm is thin, the fluid will raise it until it touches a mating part as shown in Figure 2-14. Then the fluid will become pressurized behind the diaphragm and apply the needed force.

The epoxy casing and diaphragm make the device corrosion proof. The tubing connections will all be encased in epoxy so that manifolding can be performed using simple soldered connections. Cost would be low once initial fixtures were fabricated.

Several such devices were fabricated as shown in Figure 2-13 and tested as shown in Figure 2-14. The results are shown in Table 2-5 and Figure 2-15. Figure 2-15 shows the measured force for one cycle of pressure. Force is clearly linearly proportional to pressure. Test 1 was the first successful transducer. Tests 2, 3, and 4 show how this transducer operated with increasing clearance. As expected the force decreases with increasing clearance. For the 0.5 in. diam. unit the

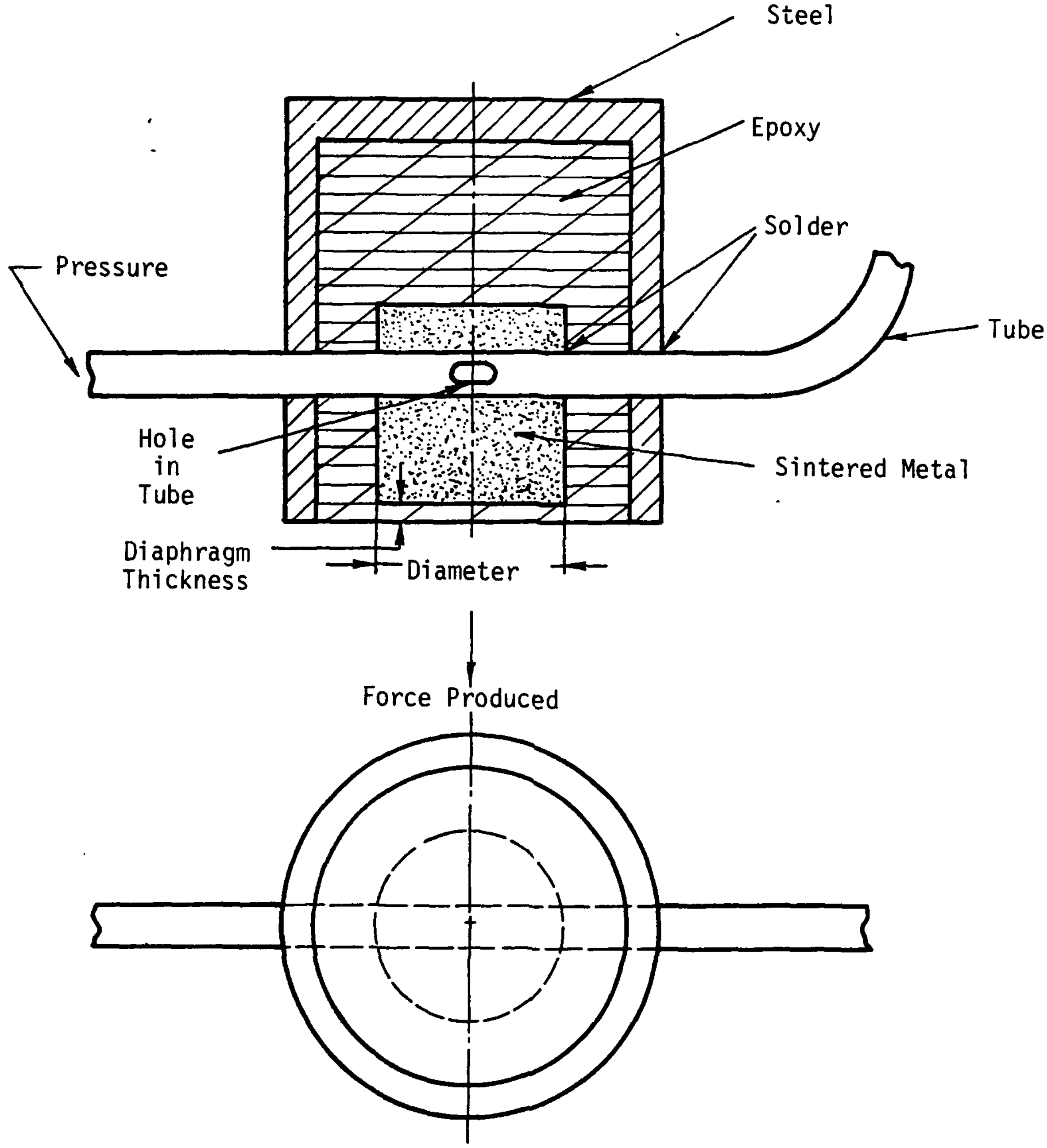

Figure 2-13. Integral Force Transducer.

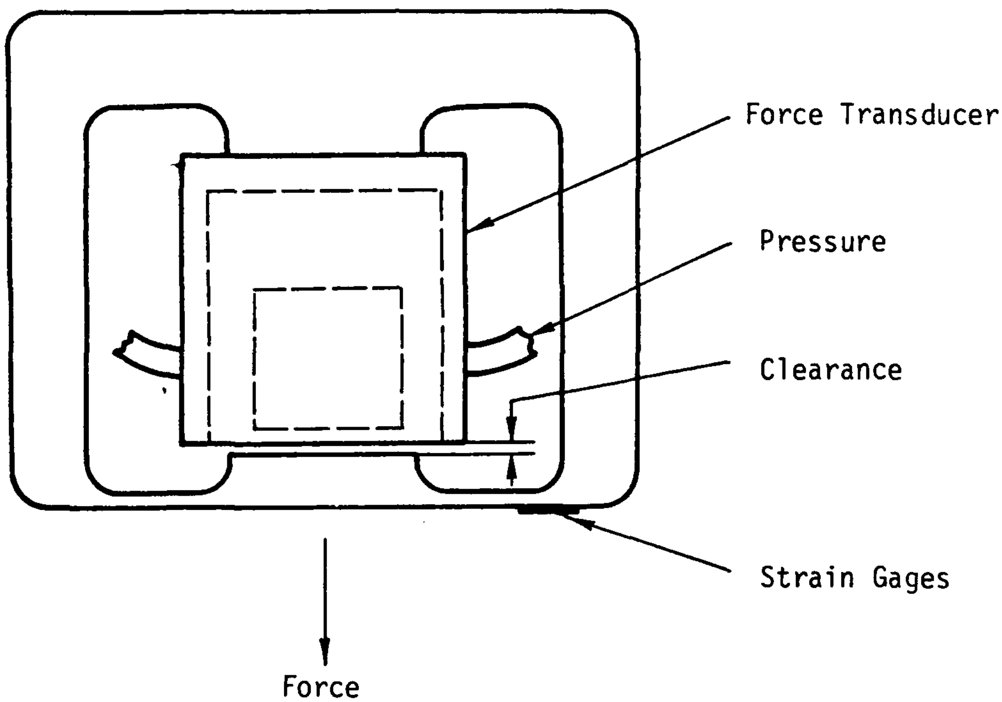

Fugyre 2-14. Integral Force Transducer Test Setup.

TABLE 2-5

Tests of Epoxy Force Transducers

Test	Element	Diaphragm	Clearance
1	0.5 in dia. sintered	0.021 in	.0 in
2	0.5 in dia. sintered	0.021	.0013
3	0.5 in dia sintered	0.021	.0024
4	0.5 in dia. sintered	0.021	.0046
5*	0.5 in dia. sintered	0.021	.0046
6	0.25 in dia. sintered		.0
7	0.25 in dia. sintered		.0015
8	0.25 in dia. sintered		.0030

*Run for two hours

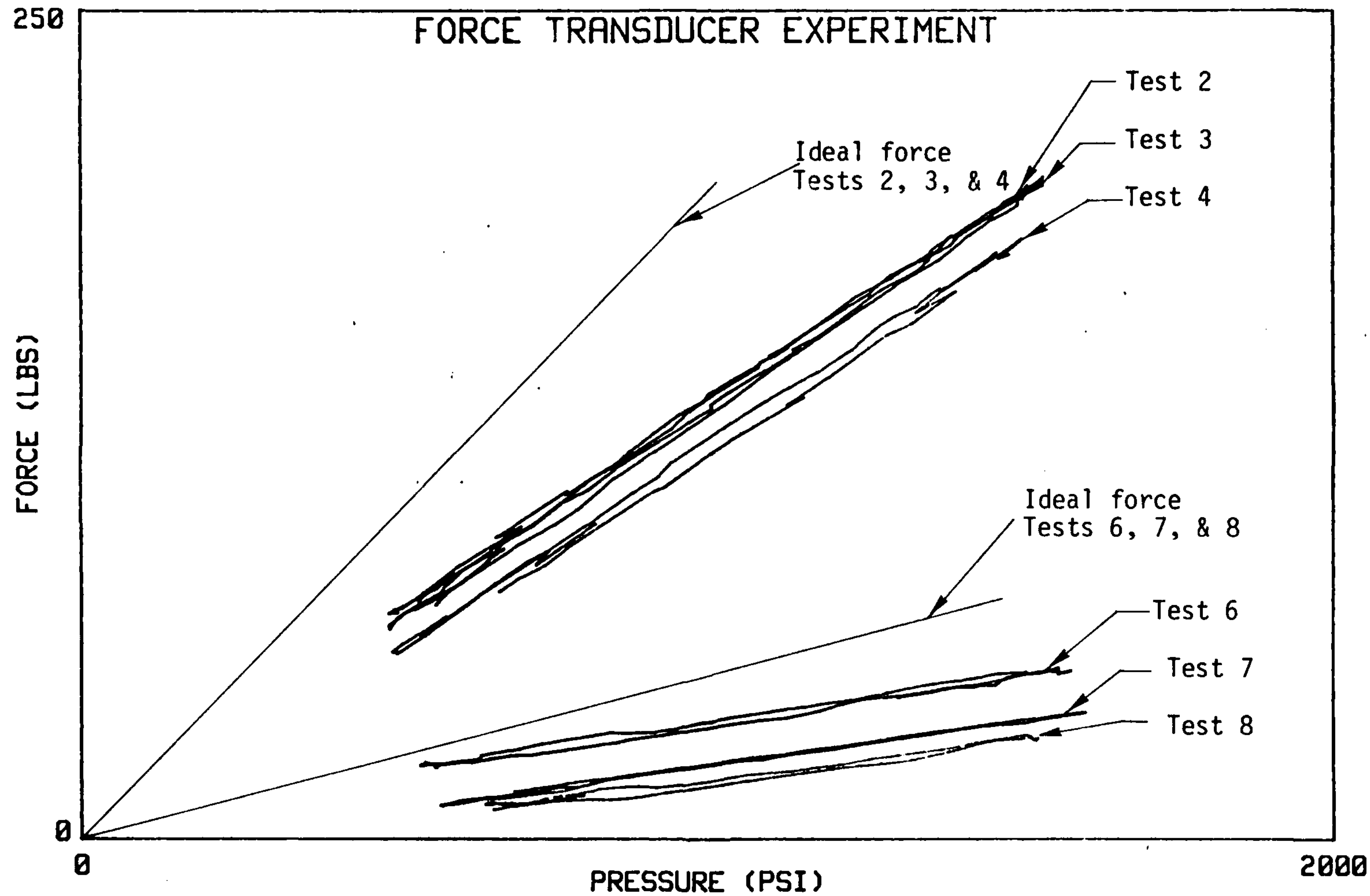

Figure 2-15. Integral Force Transducer--Force Test Results.

percent reduction would be considered acceptable for a seal design. From Tests 6, 7, and 8, for the 0.25 in. diam. transducers, the percent reduction is much larger, indicating that a thinner diaphragm should be used to decrease the sensitivity. Test 5 (not shown) was cycled for a period of two hours to evaluate endurance of the device. The comparison of the actual force produced to the ideal force shows that the epoxy diaphragm is holding back a substantial fraction of the pressure load.

While force performance above was considered to be satisfactory for the initial attempts to create such a device, the reliability of the device came into question. Two of the devices ruptured on first use and one ruptured after being used in multiple tests. While some of these problems were related to fabrication technique, it became clear that epoxy may not be the most reliable material for a pressure containment application. A material with more reliable strength and flow characteristics was needed.

At this point the study was ended as it was decided to use traditional O-rings with pistons for the next design. The logic was that O-rings with proper piston were known to be reliable, and while not being necessarily the best force transducer from a fabrication standpoint, could be applied with greater expediency than finding and developing the proper candidate material for the integral force transducer. Even so, the integral force transducer work is encouraging should some application warrant further development.

CHAPTER 3

NINE WAVE SEAL--SECOND DESIGN

Criteria

Even though the performance of the first nine wave seal design was reasonably good, it was decided that performance should be somewhat better if full waviness could be applied and, to make the wavy seal practical, a simpler, more reliable means of applying the wave must be designed which can be more easily fabricated. Thus, the overriding criteria were simplicity, fabricability, and reliability.

The specific criteria for the design of a wavy seal are as given previously [6]. They are:

1) Very low wear--10 year life.
2) Moderate to low leakage--leakage consistent over time.
3) Low friction to ensure low thermal distortion.
4) Operation in the 500 psi, 1800 rpm at 4 in. mean diameter range.
5) Operation in seawater.
6) Seal components themselves must be reliable to be compatible with 1) above.

To design a wavy seal, additional criteria must be satisfied for proper operation.

1) The seal rings must be of a zero-moment design, i.e., no rotation of the rings due to changes in the sealed pressure should occur.

This eliminates the need for the seal rings to wear to a new profile at each operating pressure.

2) Nine waves must be imposed on the seal. Reference [6] shows the need for nine waves so as to increase the relative tilt stiffness of the seal and thereby maintain a face profile which is relatively unaffected by operating conditions. Thus, different operating conditions do not wear new profiles on the seal.

3) Application of the waviness forces must be made to the zero pressure side of the seal. This eliminates the need to compensate for the effect of sealed pressure on the applied waviness force.

4) The centroid of the cross section must be optimally located to provide a continuous sealing dam around the seal to give both minimum leakage and maximum load support.

5) Stiffness of the seal ring is to be minimized. This will ensure compliance of the seal ring with the mating ring at lower harmonics and also makes application of waviness easier.

Initial Configurature

Figure 3-1 shows the initial basic configuration used in the design analysis. There are 54 pistons located circumferentially around the inside diameter of the metal ring. Three sets (18 pistons per set) are pressurized with a sinusoidally varying hydraulic pressure. The 18 pistons per set are divided up so that there are nine pistons acting to the left of the centroid and nine pistons acting to the right. This produces one set of nine waves. The three sets of 18 pistons are connected as in the previous design to provide nine moving waves. The

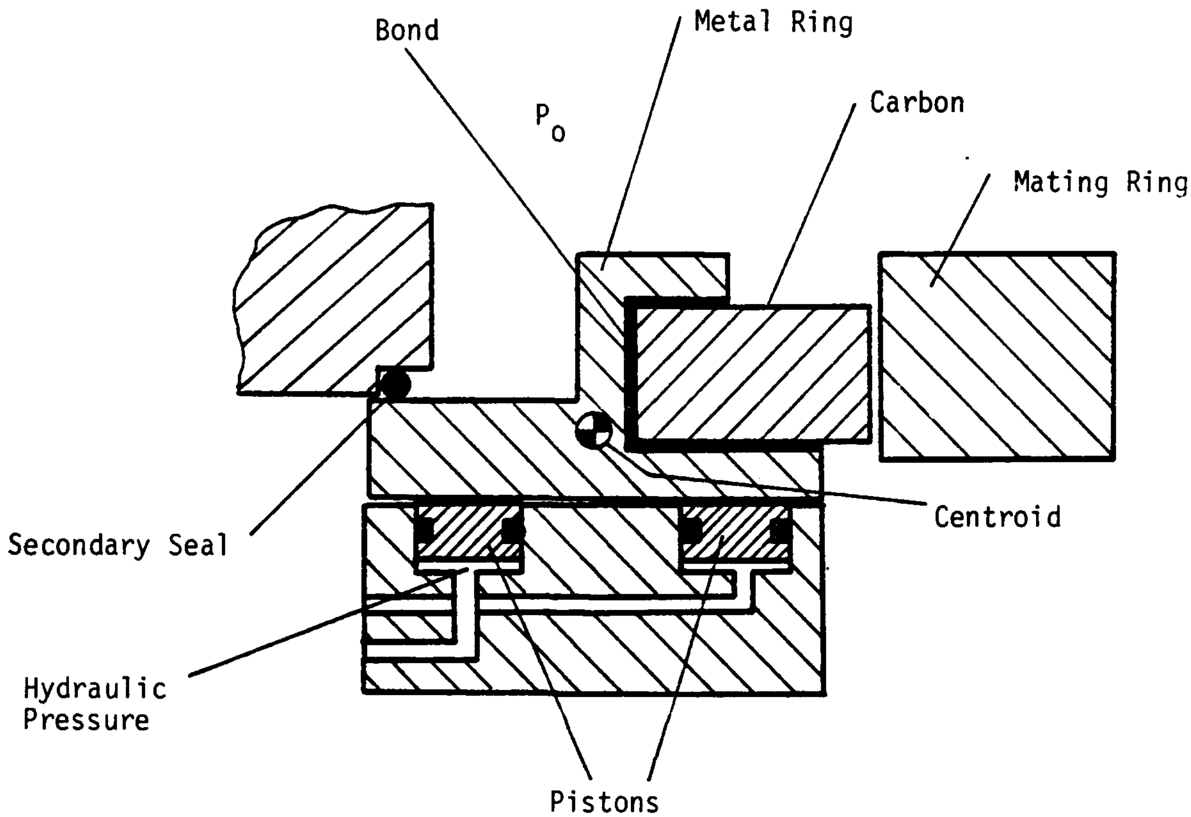

Figure 3-1. Initial Nine-Wave Seal Configuration - Design 2.

carbon is bonded as before into the metal ring which is made of Inconel 625. Inconel 625 was chosen for its excellent corrosion resistance in salt water.

The configuration shown avoids some of the problems associated with the previous design. The pistons are considered to be a more reliable method of applying the forces with no leakage. Manifolding of the pressure can be accomplished with small diameter tubing (see detailed descriptions later). The entire force mechanism is located on the leakage or zero pressure side of the seal so that the mechanism is not affected by operating pressure. On the other hand this arrangement does cause a high hoop stress as discussed later.

Seal Ring Design Solution

Figure 3-2 shows the details of the seal ring. The fixed parameters are essentially the same as for the previous design [6]. The method of solution is identical except for the location of the pressure force that produces the waviness and the method of zeroing out rotation due to sealed pressure. In this new design obtaining a zero moment can be easily achieved by adjusting the secondary seal position.

In addition to meeting the previous criteria, it was decided for this new design that the product GJ_θ (torsional stiffness) must be about ten times lower than for the previous design. This condition was imposed to ensure that the needed wave could be produced at a reasonable hydraulic pressure and moment arm. Due to this requirement, the metal part became quite thin. This means that even though $E_{carbon} \ll E_{metal}$, the carbon in conjunction with the metal tends to stiffen it up

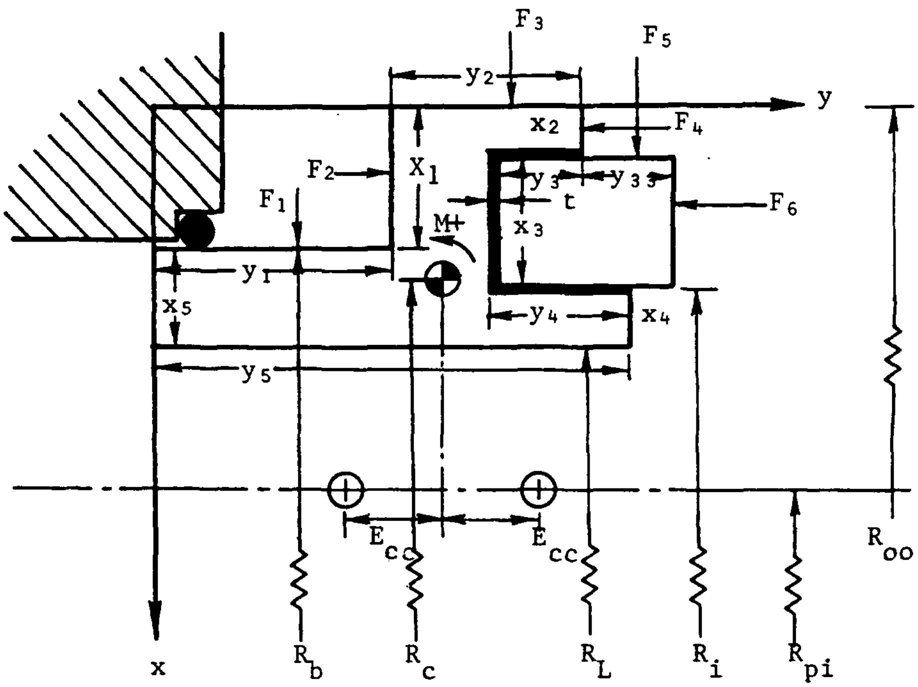

Figure 3-2. Composite Seal Ring Geometry.

and one cannot use the metal only as a basis for computing section properties.

Bending Stiffness

To get an estimate of the stiffening effect of the carbon, the cross section shown in Figure 3-3 was analyzed using a FEM program. The cross section shown is typical of those analyzed as having potential for the final design. The ring was analyzed in bending as produced by a moment about the circumferential axis uniformly distributed around the ring. The metal and the carbon were considered to be perfectly bonded at the interface.

Based on the rotation of the cross section in the plane of the figure as predicted by the FEM program, the equivalent stiffness of the composite ring was computed using the formula for twist (bending) of a ring due to a uniform moment about its circumferential axis.

$$\phi = \frac{m_\theta r_c^2}{EI_x} . \qquad (3\text{-}1)$$

The FEM prediction is:

$$(EI_x)_{\text{equivalent}} = 5.8 \cdot 10^4 \text{ lb in.}^2 . \qquad (3\text{-}2)$$

Based on the metal only

$$EI_x = 2.3 \cdot 10^4 \text{ lb in.}^2 . \qquad (3\text{-}3)$$

The conclusion is that the composite section is about twice as stiff in bending than as predicted by considering the metal only. This

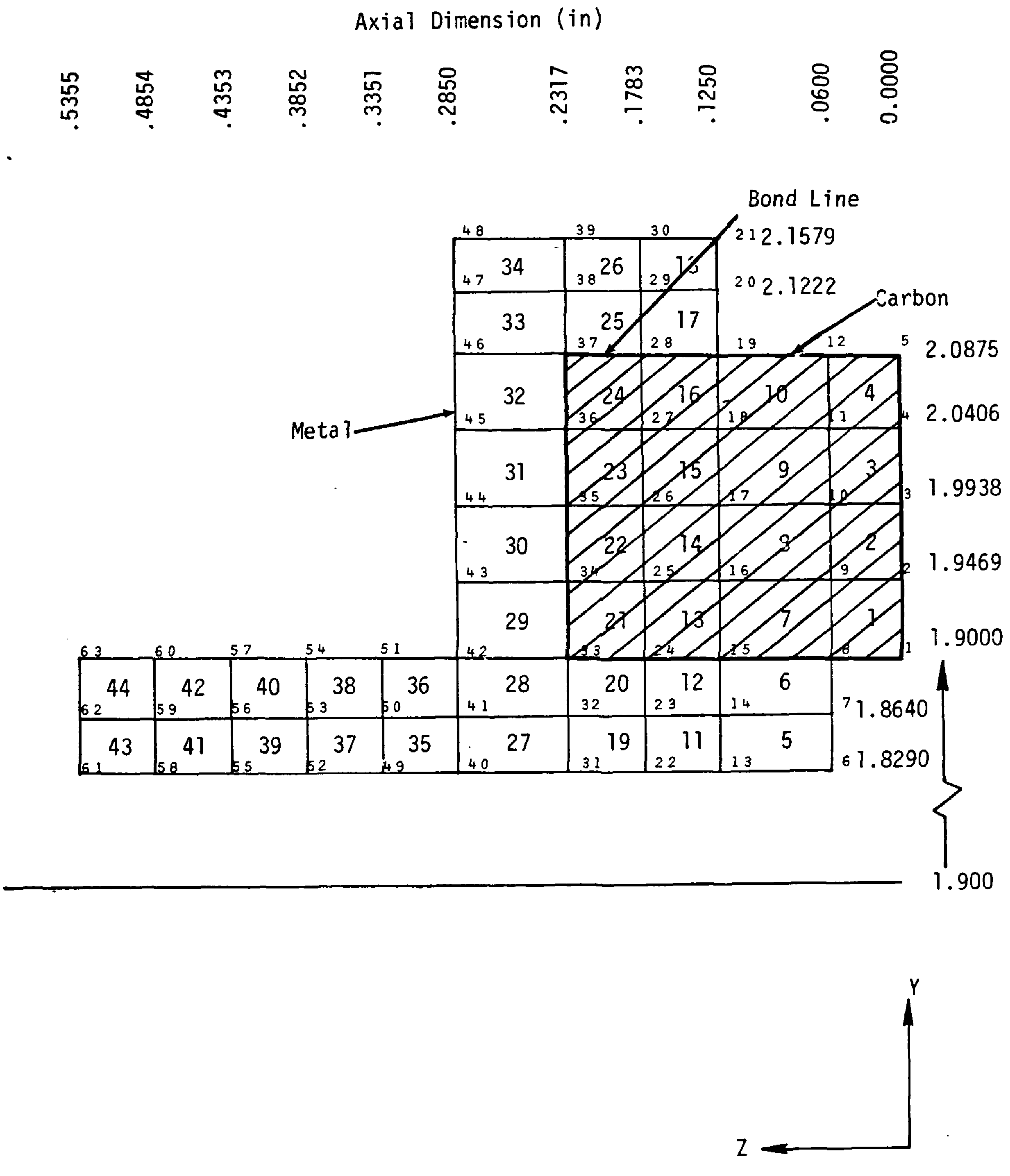

Figure 3-3. Finite Element Mesh of Composite Seal Ring.

added stiffness is particularly important when calculating out of plane buckling or conformability of the ring and was taken into account in the design.

Buckling

For rings of small cross section under external pressure, buckling of the ring must considered. Such a ring can buckle in the plane of the seal face or it can possibly buckle out of the plane. The second case, while unlikely, appears to be the more limiting case for the type of ring of interest so has been used as a design criterion.

Williams [30] treats the non-symmetrical cross section ring buckling problem and shows that for out of plane buckling the critical radial load can be predicted using the following equation.

$$C_1\bar{p}^3 + C_2\bar{p}^2 + C_3\bar{p} + C_4 = 0 \ , \tag{3-4}$$

where

$$C_1 = \frac{2\nu}{n^2(1 - \nu)^3} \ , \tag{3-5}$$

$$C_2 = \frac{1}{(1 - \nu)^2}\left\{2\nu\ \bar{I}_y + \frac{1}{n^2}\left[1 + n^2\ \frac{GJ_\theta}{\bar{E}I_x} + 2\nu\left(n^2 + \frac{GJ_\theta}{\bar{E}I_x}\right)\right]\right\} \tag{3-6}$$

$$C_3 = \frac{1}{(1 - \nu)} \left[(n^2 - 1)^2 \frac{GJ_\theta}{n^2 \bar{E} I_x} + \left(\bar{I}_y - \bar{I}_{xy}^2\right) (1 + 2\nu\, n^2) \right.$$

$$\left. + \bar{I}_y \frac{GJ_\theta}{\bar{E} I_x} (n^2 + 2\nu) \right] , \tag{3-7}$$

$$C_4 = \left(\bar{I}_y - \bar{I}_{xy}^2\right) (n^2 - 1)^2 \frac{GJ_\theta}{\bar{E} I_x} , \tag{3-8}$$

and,

$$\bar{E} = \lambda + 2G , \tag{3-9}$$

$$\lambda = \frac{\nu E}{(1 + \nu)(1 - 2\nu)} , \tag{3-10}$$

$$\bar{p} = \frac{u_o \; a \; r_c}{I_x} , \tag{3-11}$$

$$p_{crit} = \frac{\bar{p} \; \bar{E} \; I_x}{r_c^3} , \tag{3-12}$$

$$\bar{I}_{xy} = \frac{I_{xy}}{I_x} , \tag{3-13}$$

$$\bar{I}_y = \frac{I_y}{I_x} . \tag{3-14}$$

The lowest buckling mode, n=2, was used as a basis for design calculations.

Torsion of a Composite Section

The formula for tilt waviness shows that that torsional stiffness GJ_θ is the most important stiffness parameters at high values of n (n=9 for the present case).

$$\phi = \frac{m_{\theta_o}}{EI_x} \frac{r_c^2(1 + An^2)}{(n^2 - 1)^2} \rightarrow \frac{m_{\theta_o} r_c^2 n^2}{GJ_\theta(n^2 - 1)^2} \quad \text{for large n} .$$

One expects that the effect of the carbon will be to stiffen the section of interest torsionally in spite of its low shear modulus. To evaluate this case, some new theory was developed for the composite cross section case.

Referring to Figure 3-4, Timoshenko [31] reasons that pure torsion causes a rotational displacement where the displaceme are given by

$$u = -\theta zy , \qquad v = \theta zx \tag{3-16}$$

where θ is the rate of twist. It can be reasoned the same form of displacement applies to a composite section as shown having zero slip at the boundaries. Warping of the cross section is defined by the use of a warping function ψ so that

$$w = \theta\psi(x,y) \tag{3-17}$$

and this same equation applies. Then, by definition, since normal stresses are assumed to be negligibly small in the torsion problem,

$$\gamma_{xz} = \frac{\partial w}{\partial x} + \frac{\partial u}{\partial z} = \theta \left(\frac{\partial \psi}{\partial x} - y\right) , \tag{3-18}$$

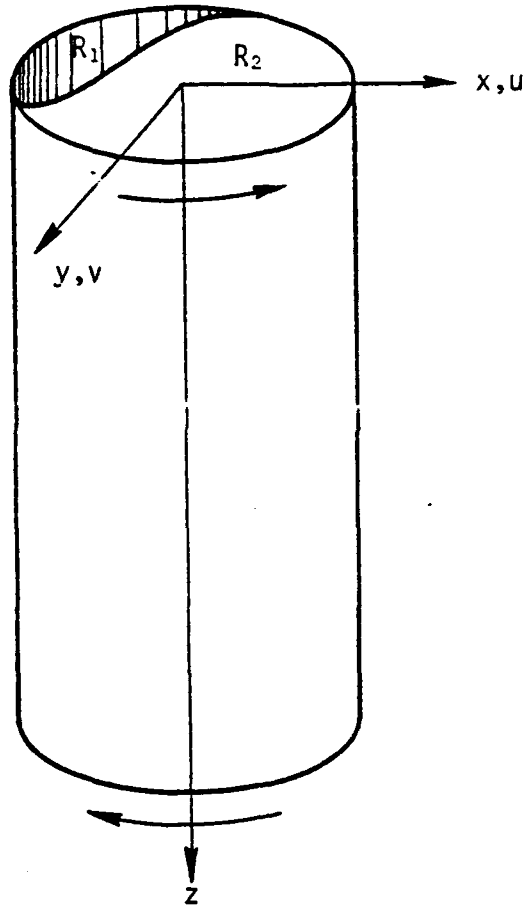

Figure 3-4. Torsion of a Composite Section.

$$\gamma_{yz} = \frac{\partial w}{\partial y} + \frac{\partial v}{\partial z} = \theta \left(\frac{\partial \psi}{\partial y} + x \right) \tag{3-19}$$

and using stress strain relationships

$$\tau_{xz} = G\theta \left(\frac{\partial \psi}{\partial x} - y \right) , \tag{3-20}$$

$$\tau_{yz} = G\psi \left(\frac{\partial \psi}{\partial y} + x \right) . \tag{3-21}$$

Equations (3-18) through (3-21) are valid for R_1 and R_2 separately. Using equilibrium and equations (3-20 and 3-21)

$$\frac{\partial^2 \psi}{\partial x^2} + \frac{\partial^2 \psi}{\partial y^2} = 0 \tag{3-22}$$

within each region.

Referring to Figure 3-5 for the development of the boundary conditions and noting the clockwise convention for moving around the section, we have for the shear stress acting normal to a boundary:

$$\tau_n = \tau_{yz} \cos \alpha + \tau_{xz} \sin \alpha \tag{3-23}$$

where

$$\sin \alpha = - \frac{\Delta y}{\Delta s} , \qquad \cos \alpha = \frac{\Delta x}{-\Delta s} . \tag{3-24}$$

so

$$\tau_n = -\tau_{yz} \frac{dx}{ds} + \tau_{xz} \frac{dy}{ds} \tag{3-25}$$

or substituting Equation (3-20 and 3-21), we have

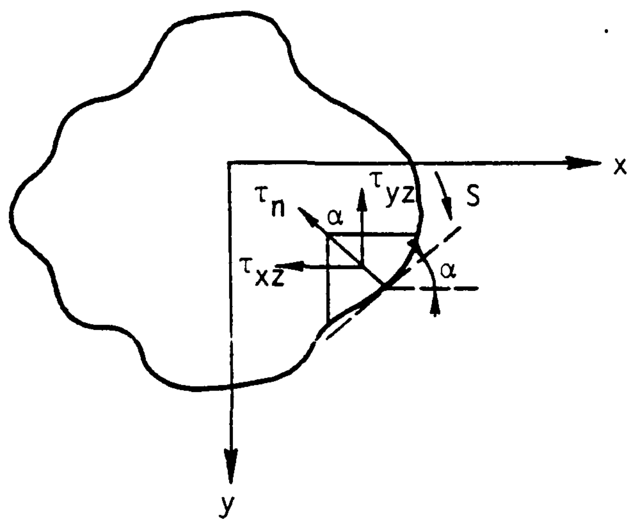

Figure 3-5. Normal Shear Stress Component.

$$\tau_n = G\theta \left(\frac{\partial\psi}{\partial y} + x\right) \frac{dx}{ds} + G\theta \left(\frac{\partial\psi}{\partial x} - y\right) \frac{dy}{ds} . \tag{3-26}$$

On a free boundary

$$\tau_n = 0 \tag{3-27}$$

and on a common boundary between regions

$$\tau_{n\,1} = G_1\theta \left(\frac{\partial\psi_1}{\partial y} + x\right) \frac{dx}{ds} + G_1\theta \left(\frac{\partial\psi_1}{\partial x} - y\right) \frac{dy}{ds} , \tag{3-28}$$

$$\tau_{n\,2} = G_2\theta \left(\frac{\partial\psi_2}{\partial y} + x\right) \frac{dx}{ds} + G_2\theta \left(\frac{\partial\psi_2}{\partial x} - y\right) \frac{dy}{ds} . \tag{3-29}$$

The normal shear stresses must transfer across the boundary. Therefore, since θ is the same for both regions,

$$\left\{G_1 \left(\frac{\partial\psi_1}{\partial y} + x\right) - G_2 \left(\frac{\partial\psi_2}{\partial y} + x\right)\right\} \frac{dx}{ds}$$

$$+ \left\{G_1 \left(\frac{\partial\psi_1}{\partial x} - y\right) + G_2 \left(\frac{\partial\psi_2}{\partial x} - y\right)\right\} \frac{dy}{ds} = 0 . \tag{3-30}$$

So the problem is reduced to finding a function ψ that satisfies both Equation (3-22) and the boundary conditions of Equation (3-30) and (3-27).

Once ψ is found the torsional stiffness is found by taking the moment of the shear stress. This gives the equivalent stiffness as

$$GJ_\theta = \sum_{i=1}^{n} \left(\iint_{R_i} G_i \left(x \frac{\partial \psi_i}{\partial y} + x^2 \right) dx\, dy \right.$$

$$\left. - \iint_{R_i} G_i \left(y \frac{\partial \psi_i}{\partial x} - y^2 \right) dy\, dx \right) , \qquad (3\text{-}31)$$

where the summation is over the n regions. Appendix A contains the finite difference solution to this problem and some examples.

The above method was incorporated into the seal design program so that the proper stiffness GJ_θ would be used to predict waviness. Table 3-1 shows the effect of the carbon composite on the stiffness for one of the seal ring designs very close in size to that shown in Figure 3-3. The actual torsional stiffness is four times larger than that based on the metal alone.

After repeated attempts to vary proportions on this design it was concluded that no satisfactory composite section could be designed. The main problem was that for designs where torsional stiffness was low enough such that waviness could be applied, the metal part engaging the secondary seal (Figure 3-2) was too thin to transmit the load from the pistons to the ring without bending. Or, in many otherwise satisfactory designs, the required forces were larger than available. The problem comes about because making the seal long enough to provide moment arm space causes the stiffness to be too high for the forces available when the part is made of metal.

TABLE 3-1

Composite Section Stiffness

	$\bar{x}$	$\bar{y}$	$G^* J_\theta$	Moment Arm Needed
Metal Only	.2184 in	.2790 in	1446 lb in^2	.1680 in
Composite Section	.2193	.2795	4242	.4386

All Carbon Seal Design

The solution to the above problem is to make the entire ring out of low modulus carbon. Thus the ring does not get too stiff for the size needed to accommodate the force application.

Figure 3-6 shows the configuration of the all carbon seal design. It is essentially the same shape as before. This change not only reduces the stiffness, and therefore the needed moment arm, but also eases design, fabrication, and assembly problems. The design computer program for the previous configuration was modified slightly to accommodate this all carbon configuration and design proceded accordingly.

Warping Analysis

One additional area that must be considered is the effect of warping on the stiffness of the cross section. Warping is the nonuniform z direction displacement which accompanies torsion. Oden [32] shows that warping can induce stresses in the section that will have the effect of increasing the torsional stiffness. This occurs when warping is constrained as it is in the alternating torsion of a wavy ring.

Equations for waviness where warping is significant will now be derived. Warping makes the following change in the stress resultant-displacement equations:

$$M_\theta = \frac{GJ_\theta}{R_c}(\phi' + \bar{v}') - \frac{E\Gamma^*}{R_c^3}(\phi''' + \bar{v}''') , \qquad (3\text{-}32)$$

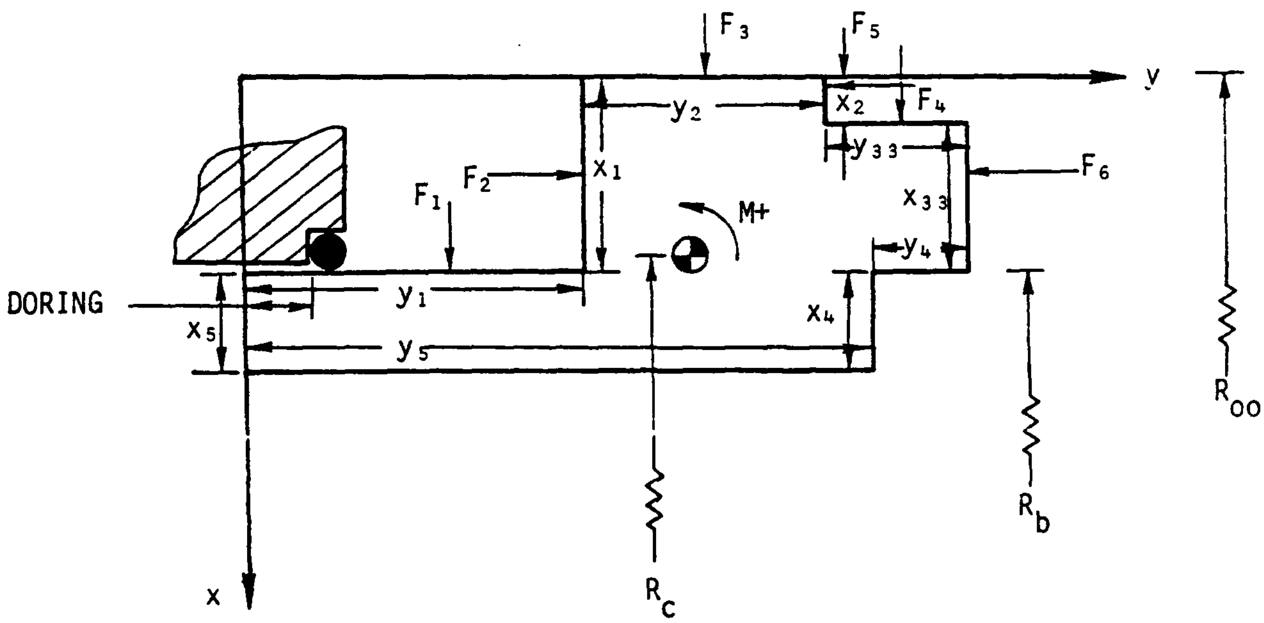

Figure 3-6. All Carbon Seal Design

where Γ^* is the warping constant and all other ring equations remain the same [33].

The equilibrium equations are [34]

$$M_\theta - M_x + m_\theta R_c = 0 \text{ ,} \tag{3-33}$$

$$M_x'' + M_\theta' = 0 \text{ .} \tag{3-34}$$

Using the previous equation for M_x and M_θ from [33] gives:

$$(\phi'' - \bar{v}'''') + \frac{1}{A}(\phi'' + \bar{v}'') - \frac{1}{B}(\phi'''' + \bar{v}'''') = 0 \tag{3-35}$$

and

$$\frac{1}{A}(\phi'' + \bar{v}'''') - \frac{1}{B}(\phi'''' + \bar{v}'''') - (\phi - \bar{v}'') + \frac{m_\theta R_c^2}{EJ_x} = 0 \text{ ,} \tag{3-36}$$

where

$$A = \frac{EJ_x}{GJ_\theta} \quad \text{and} \quad B = \frac{J_x R_c^2}{\Gamma^*} \text{ .} \tag{3-37}$$

Assuming that

$$m_\theta = m_{\theta o} \cos n\theta \tag{3-38}$$

it follows that

$$\phi = \phi_o \cos n\theta \quad \text{and} \quad \bar{v} = \bar{v}_o \cos n\theta \text{ .} \tag{3-39}$$

Substitutior gives

$$\phi_o = \frac{m_{\theta_o} R_c^2}{EJ_x} \frac{1}{\left(\frac{n^2}{A} + \frac{n^4}{B} + 1\right) - \frac{\left(1 + \frac{1}{A} + \frac{n^2}{B}\right)}{\left(n^2 + \frac{1}{A} + \frac{n^2}{B}\right)} \left\{\frac{n^2}{A} + \frac{n^4}{B} + n^2\right\}} \tag{3-40}$$

and

$$v_o = \frac{m_{\theta_o} R_c^3}{EJ_x} \frac{1}{\left(\frac{n^2}{A} + \frac{n^4}{B} + 1\right) - \frac{\left(n^2 + \frac{1}{A} + \frac{n^2}{B}\right)}{\left(1 + \frac{1}{A} + \frac{n^2}{B}\right)} \left\{\frac{n^2}{A} + \frac{n^4}{B} + n^2\right\}} . \tag{3-41}$$

Equations (3-40) and (3-41) are the modified form used in the design program to predict waviness considering warping.

It now becomes necessary to determine Γ^* for the particular cross section in question. This was accomplished by again using a finite element program and using three-dimensional solid elements (eight node brick). The section considered was a bar of exact cross section and length equal to that of one half wave (of nine waves) around the seal (see Figure 3-7). A moment was applied to the end of the bar and the resultant twist was calculated. In this calculation the z displacements at both ends were not constrained, only x and y. Next, the z displacements were constrained and the angles of twist again calculated. This simulates the symmetry conditions where warping must go to

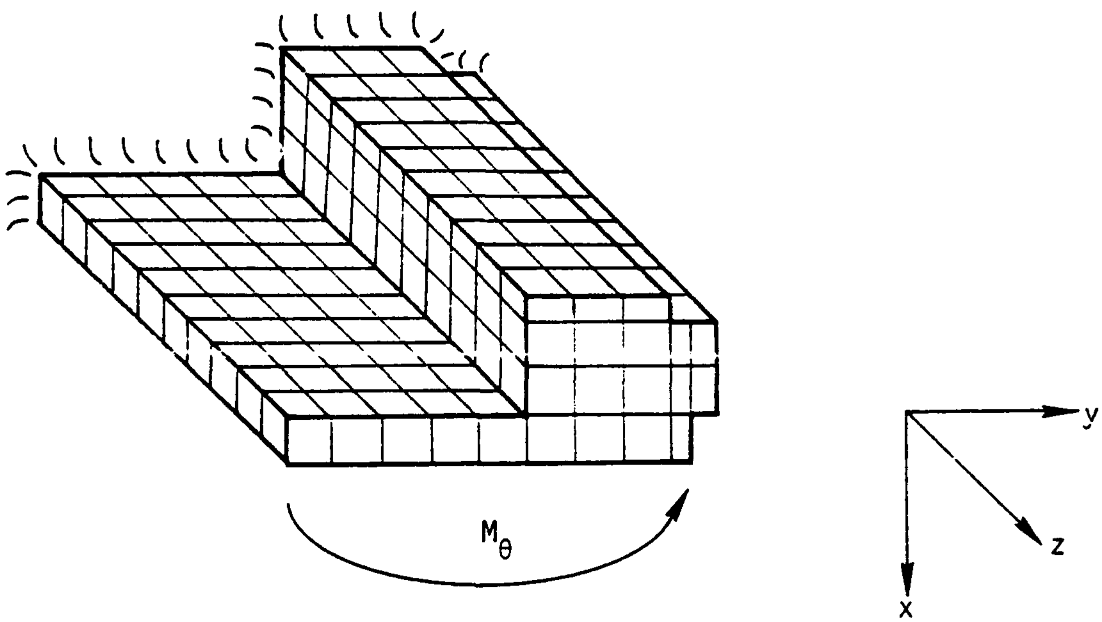

Figure 3-7. 3-D Finite Element Configuration.

zero in the alternating twist. Table 3-2 shows the results for a cross section very close in dimensions to the final solid carbon design.

Now the straight bar version of Equation (3-32) is:

$$E\Gamma^*\phi''' - GJ_\theta \, \phi' + M_\theta = 0 \, . \tag{3-42}$$

For M_θ constant solving for ϕ gives

$$\phi = C_1 e^{rx} + C_2 e^{-rx} + \frac{M_\theta x}{GJ_\theta} + C_3 \, , \tag{3-43}$$

where

$$r = \sqrt{\frac{GJ_\theta}{E\Gamma^*}} \, . \tag{3-44}$$

The boundary conditions are

$$\phi(0) = 0 \, ,$$

$$\phi'(0) = 0 \, ,$$

$$\phi'(\ell) = 0 \, , \tag{3-45}$$

where $\phi' = 0$ again simulates the symmetry conditions. The final solution is

$$\phi = -\frac{M_\theta}{rGJ_\theta}\left[\frac{(e^{-r\ell} - 1)}{(1 - e^{-2r\ell})} + 1\right] e^{rx} - \frac{M_\theta}{rGJ_\theta}\,\frac{(e^{-r\ell} - 1)}{(1 - e^{-2r\ell})}\, e^{-rx}$$

$$+ \frac{M_\theta x}{GJ_\theta} + \frac{M_\theta}{rGJ_\theta}\left[\frac{2(e^{-r\ell} - 1)}{(1 - e^{-2r\ell})} + 1\right] . \tag{3-46}$$

Dividing through by $M_\theta \ell / G_\theta$ and evaluating at $x = \ell$ gives,

TABLE 3-2

Warping Function Calculation

	twist (in/in)	$G\ J_{\theta}$ (lb-in^2)
Z Deflections Unconstrained	.002703	3575
Z Deflections Constrained	.001742	--

$$\frac{\phi(\ell)}{\frac{M_\theta \ell}{GJ_\theta}} = -\frac{1}{r\ell}\left(\frac{(e^{-r\ell}-1)}{(1-e^{-2r\ell})}+1\right)e^{r\ell} - \frac{1}{r\ell}\left(\frac{(e^{-r\ell}-1)}{(1-e^{-2r\ell})}\right)e^{-r\ell} + 1$$

$$+\frac{1}{r\ell}\left[\frac{2(e^{-r\ell}-1)}{(1-e^{-2r\ell})}+1\right] . \qquad (3\text{-}47)$$

The left-hand side is the ratio of twist for the condition of the z displacements constrained to the condition of the z displacements unconstrained. Going back to Table 3-2 and using those values we have for the problem of interest

$$\frac{\phi(\ell)}{\frac{M_\theta \ell}{GJ_\theta}} = 0.644596 \ . \qquad (3\text{-}48)$$

Now, letting ℓ = 0.543 in., the length of the bar section, and using a root finding technique to solve Equation (3-47) for r for the condition of Equation (3-48) we get

$$r = 10.286/\text{in.} \qquad (3\text{-}49)$$

Then, using Equation (3-44) and section properties determined later we have

$$\Gamma^* = 1.0144 \times 10^{-5} \text{ in.}^6 \qquad (3\text{-}50)$$

and Equation (3-37) gives

$$B = 3097 \ . \qquad (3\text{-}51)$$

Design Solution

Using the above information in the design program and the criteria discussed, final satisfactory design dimensions were found and are shown in Table 3-3.

Predicted Performance

Previously developed computer programs [5] were used to predict the performance of the new design. Figures 3-8 and 3-9 show these results. The friction torque is high at lower speeds but drops very quickly for increasing rpm. Even at zero speed the friction is less than half as much as would be expected with no waviness. The decreased torque at higher speed is due to hydrodynamic effects which result in 100 percent fluid pressure load support at the higher speed.

Figure 3-9 shows that leakage is quite small, less than 1.5 cc/min up to 1800 rpm for all cases. A slightly larger value of ϕ_0 was used for this design compared to the first design (400 as compared to 320) so that sufficient wave would be available for hydrodynamic effects. Leakage is increased by about one-half a cubic centimeter per minute at the worst case compared to the previous design.

Figure 3-10 shows the comparison of the worn profile shapes for the extremes of operating conditions. As can be seen, the profile changes very little and as a result additional wear is minimized as the operating conditions are changed. This is as expected using nine waves.

TABLE 3-3

Solid Carbon Seal Design
(Ref. Fig. 3-6)

ϕ_o	$= 400 \times 10^{-6}$ in/in		
d	= .316 in		
x_1	= .2345 in	y_1	= .4200 in
x_2	= .0470 in	y_2	= .2600 in
x_3	= .1875 in	y_3	= .2100 in
x_4	= .0900 in	y_4	= .0600 in
x_5	=.0900 in	y_5	= .8300 in
R_{Pi}	= 1.8100 in		
R_b	= 1.900 in		
R_{oo}	= 2.1345 in		
R_c	= 1.9427 in		
DORING	= .2026 in		
$\bar{x}$	= .1918 in		
$\bar{y}$	= .5453 in		
I_x	= .0083085 in^4		
I_y	= .0014610 in^4		
$G\ J_\theta$	= 3183 $lb\text{-}in^2$		
J_θ	= .002546 $lb\text{-}in^2$		
A	= 7.83		
v	$= 5.687 \times 10^{-6}$ in		
e_{cc}	= .2053 in		

Critical buckling pressure = 1007 lb/in

Pressure caused rotation = 1.1×10^{-9} in/in

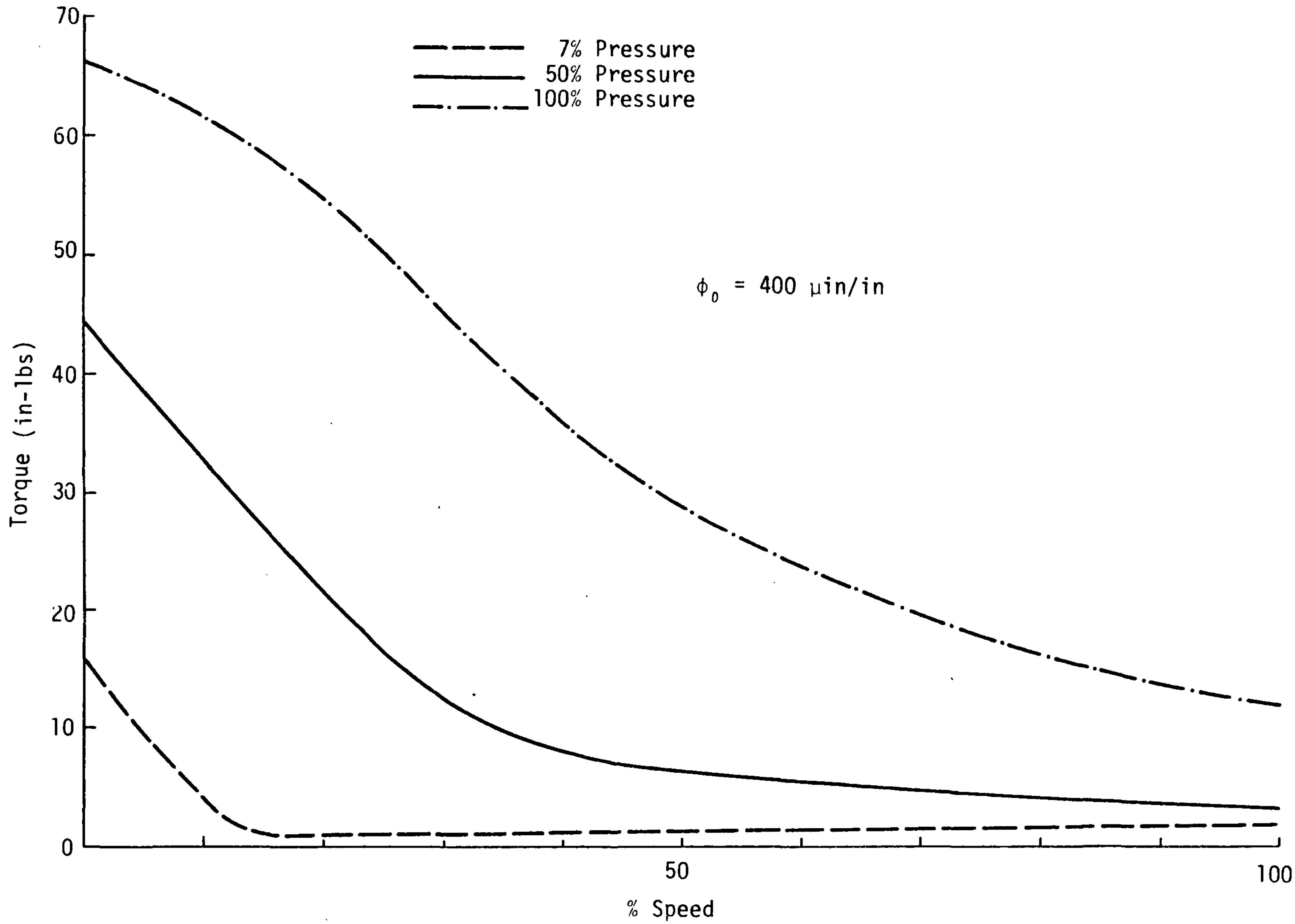

Figure 3-8. Predicted Torque

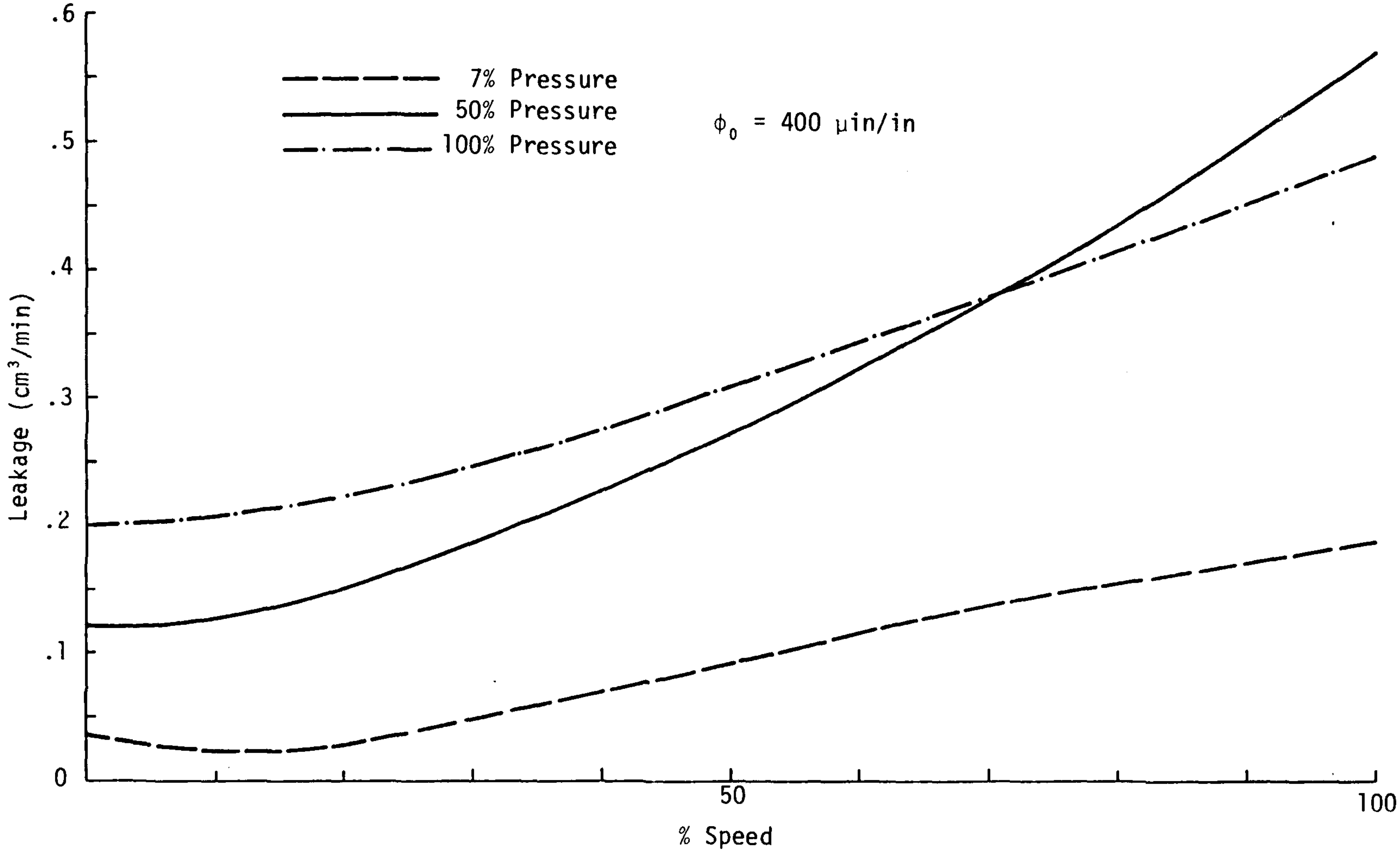

Figure 3-9. Predicted Leakage.

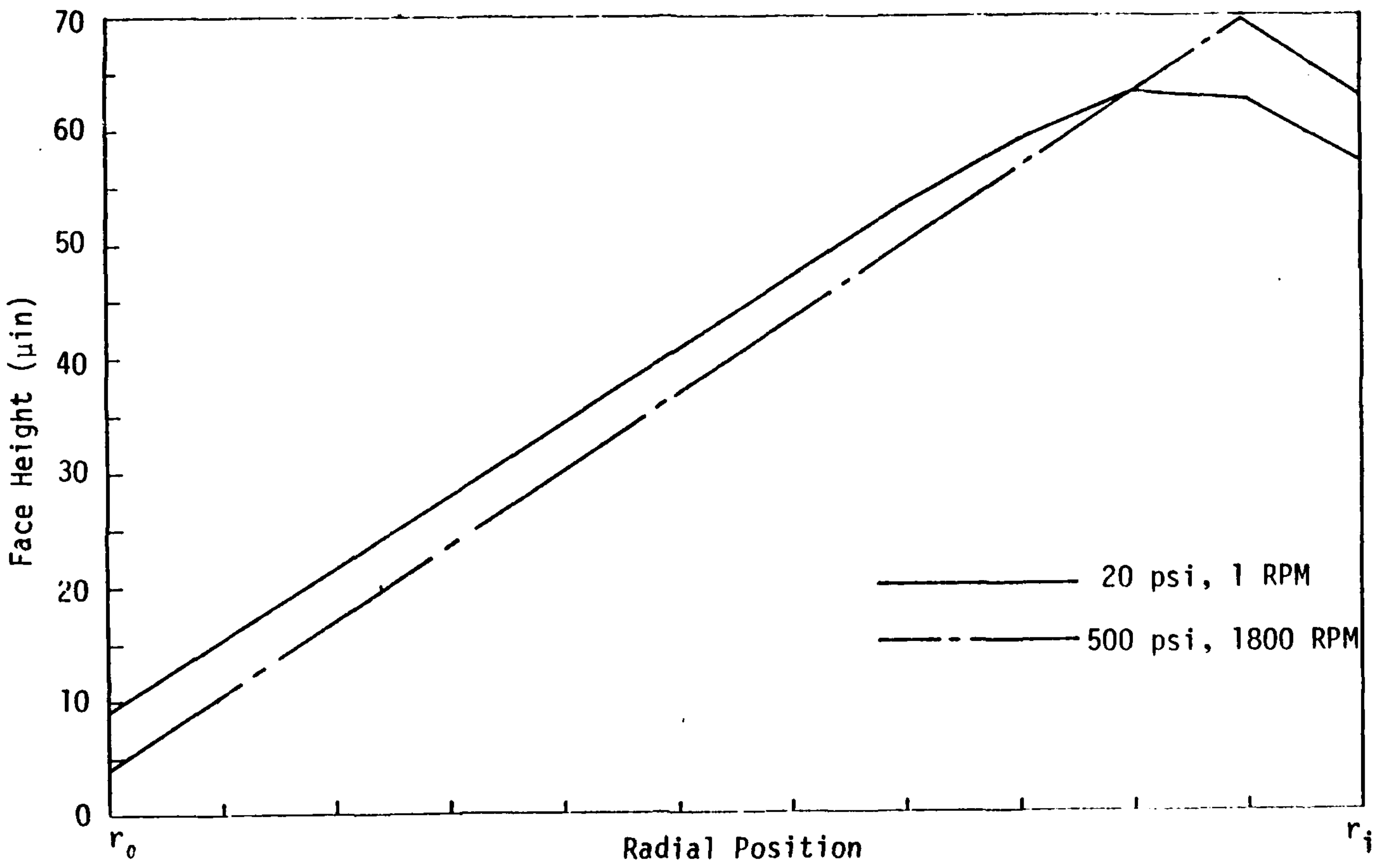

Figure 3-10. Predicted Worn Face Shape.

Strength Analysis and Test

Because of the reduced cross section of this all carbon design, a primary concern becomes the strength of the carbon in relation to the waviness loads applied as shown in Figure 3-11. Each piston produces a maximum load of 86 lb distributed as shown but of course at discrete intervals around the seal ring. The carbon was modeled by finite elements as shown using an assumption of axisymmetric loading to get a first approximation. It was found that the maximum tensile stress is about 4000 psi on element No. 8 in Figure 3-11. The tensile strength is only 8000 psi.

Given that the approximate solution was not considered conservative because the concentrated loads had to be distributed to obtain the axisymmetry needed for solution, other methods to calculate the maximum stress were tried but none were considered accurate enough to be relied upon. The problem is clearly a 3-D stress analysis problem, the modeling for which is very cumbersome. Thus, it was decided that the only reliable way to assess the adequacy of the strength of the part was by actual test.

Figure 3-12 shows a cross section of the test set up. The carbon shown was machined out of an existing carbon ring to similar dimensions and the same cross sectional area as the new design. Pressurized oil was slowly introduced into the test fixture and the pressure monitored by computer and pressure transducer. Failure was localized at the point of application and occurred at a load of 177 lb. The maximum

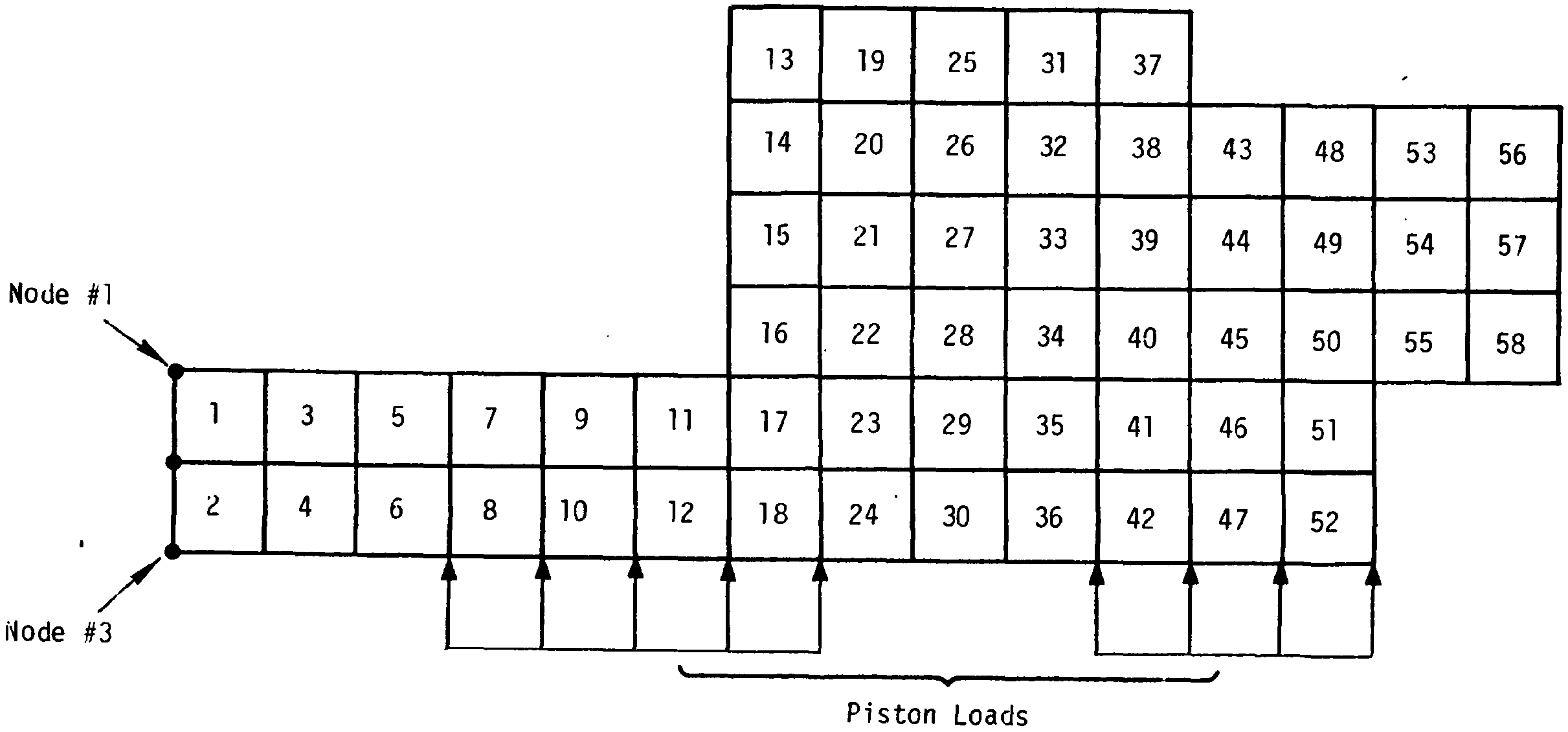

Figure 3-11. Finite Element Configuration.

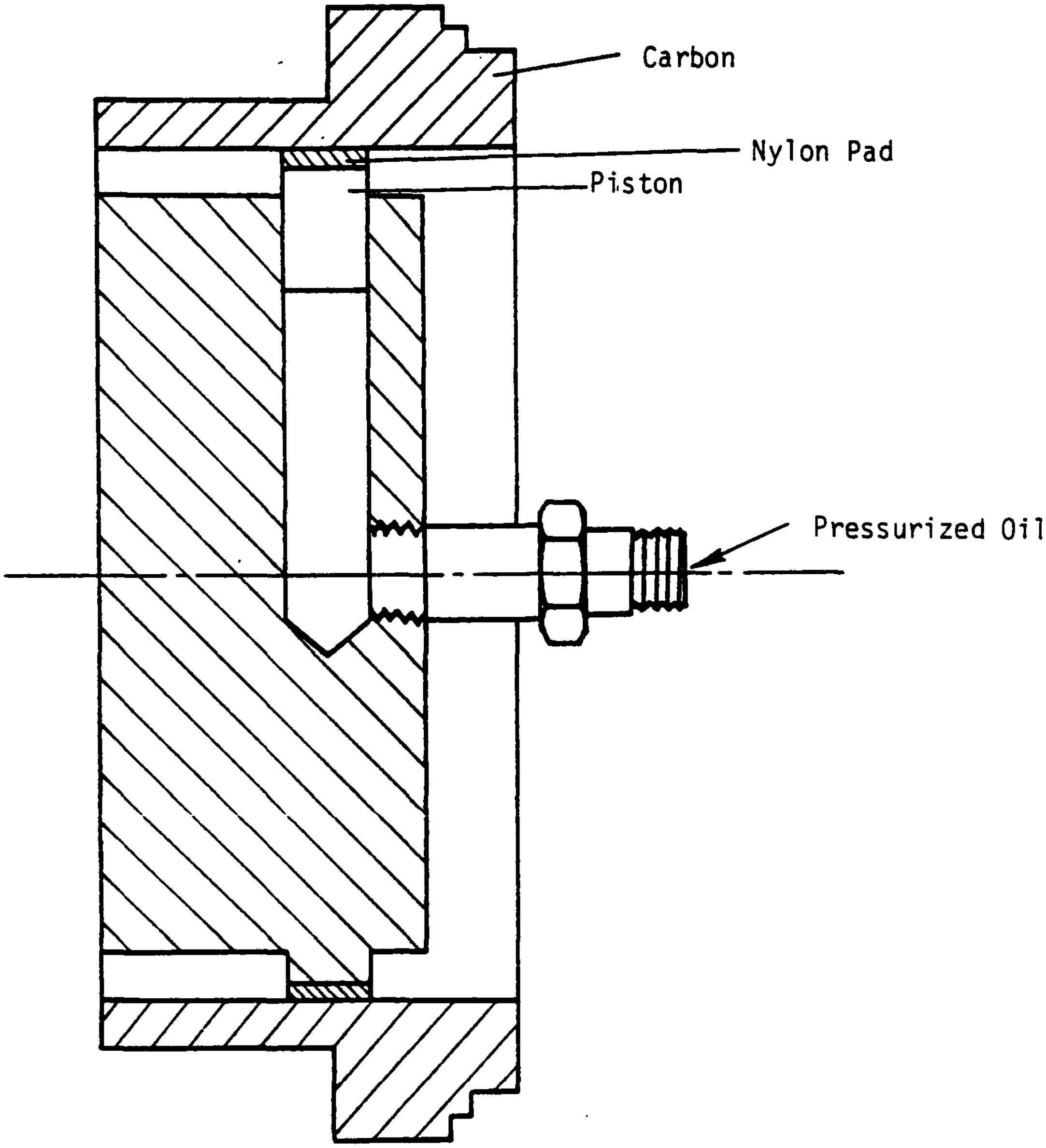

Figure 3-12. Destructive Test Set-up.

design piston load, as stated before is 86 lb. This indicates a safety factor of 2.05.

The question of fatigue strength also had to be addressed. Paxton [35] states that the terminal fatigue strength of most carbon is thought to be between 45 and 85 percent of the original tensile strength. Thus for the present design, the safety factor could be as low as 1.0 but most likely higher. It was decided since no specific fatigue data was available, the design would be considered acceptable on a prototype basis.

Other Calculations

Many other design calculations were made but will not be presented in detail here. However, the subject areas were:

1) O-ring friction on spring seat.
2) Stresses in waviness inducer.
3) Piston stresses.
4) Pressure caused rotation of spring seat.
5) Buckling of spring seat.
6) Hoop stress caused by piston load and band clamp stress for split design.

Concerning the last item, it was decided early on that the carbon had to be clamped at its OD with a metal band so as to place a large enough compressive stress on the carbon to overcome the tensile stress caused by the piston loads. This would allow the design to be split in half and simply be clamped together.

Final Design

Figure 3-13 shows the assembly view of the seal. Starting at the left, one of three sinusoidally varying pressures is directed through two (180° apart) pressure channels in the waviness cylinder (1). It was desired that the existing waviness cylinder be used since it already had the necessary tilt and offset machined into it. This waviness cylinder was therefore modified so that it could be used with the present design. One of the modifications was the addition of three drilled and tapped holes (2) (one of which is shown). These intersect the pressure channels in the waviness cylinder. The pressure is then directed through one of three swagelok fittings (14) to one of three 1/16 in. monel inlet tubes (13) which delivers the pressure to the waviness inducer (9) and terminating at a set of 18 pressure pistons (11) via connecting tubing (12). The pressure induces a force through the pressure piston (11) to a delrin spacer (10) which causes a counterclockwise moment (in this particular cross-section) to the all-carbon seal (7). The seal is a pure carbon P658RC carbon. The seal is driven by the drive ring (5) through the drive ring adapter (6). This arrangement allows for the carbon to "float" and therefore take its alignment from the face of the rotating secondary seat (8) which is a carborundum KT® silicon carbide. Both primary and secondary rings are of zero moment design, i.e., no rotation of the rings under water pressure. Preload is provided by the springs housed in the spring retainer (3) through the spring seat (4). The design of the spring seat is such that the secondary O-ring seal (15) moves with the carbon ring with

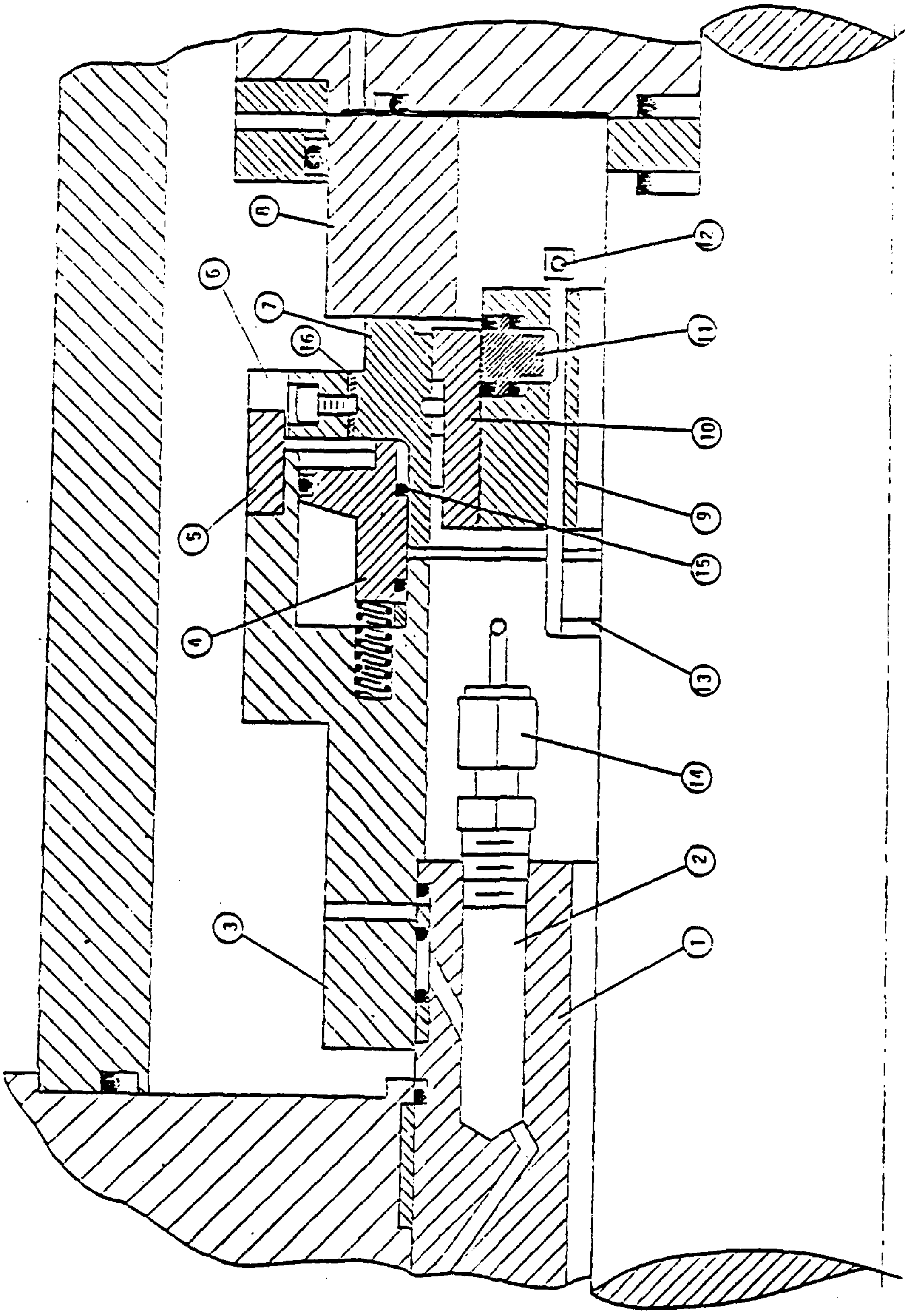

Figure 3-13. Nine-wave Seal Assembly View, Second Design.

wear so the pressure balance is relatively uneffected. The clamp band (16) produces a radial preload to the carbon ring (7) for the case when the carbon will be split.

Waviness of the new seal was measured external to the test rig by the use of the waviness inducer and the addition of a fixture that would hold pressure on 18 of the 54 pistons. Pressurizing 18 pistons gives one complete set of nine waves. The apparatus was placed on the precision rotary table and axial displacement traces near the OD of the carbon face were taken with the stylus of a surface analyzer. The signal was digitized by a computer and a Fourier analysis of waviness components was made. Table 3-4 shows the results of the waviness measurements.

The results show that the first waviness measurements were considerably lower than the 60 μin. design value. It was determined that the original Delrin band, which transmits the load from the piston of the waviness inducer to the inside diameter of the seal ring, was absorbing the wave by distributing the load over a much larger area than the area of the pistons. This was checked by making 18 individual Delrin pads which fit on the pistons, making each piston independent of any other and concentrating the load at the point of application. Results showed a dramatic increase in the harmonic waviness.

Since the original Delrin band was by design, necessary for waviness inducer-carbon seal alignment, the band was modified. This modification was accomplished by machining 54 pad locations leaving only 0.020 in. of material between pads on the inside diameter. This allowed for more individual freedom of movement for each piston and

TABLE 3-4

Nine-Wave Amplitude Study

Waviness Amplitude Near Seal O.D.

Date	h_9	P_{test}	h_9* @ 750 psi	Conditions
6/14	51	750	51	Carbon wo band, {improved pad alignment / modified delrin spacers}
6/13	46	650	53	Carbon wo/band, {improved pad alignment / modified delrin spacers}
6/10	44	1100	30	Carbon w/band, modified delrin spacers
6/9	68	1100	46	Carbon wo/band, modified delrin spacers
6/8	24	1100	16	Carbon wo/band
6/8	13	1100	9	Carbon w/band

*Equivalent to actual test pressure.

less absorption by the ring as a whole. The waviness results are shown in Table 3-4.

Secondly it was found that the metal clamp band greatly stiffened the seal ring torsionally (Table 3-4). For the purpose of these and subsequent tests it was removed with the question of how to put it in place for the split ring without stiffening the ring being left unanswered.

Afte these two modifications were made, the measured waviness started to approach the calculated waviness although it was still considered somewhat low. Further explanations were sought.

Young's Modulus Tests

An experiment was set up to check the value of Young's modulus for P658RC carbon. The test apparatus is shown in Figure 3-14. Three carbon beams were machined out of a carbon seal ring and then ground to size. The beams were simply supported by two 3/32 in. diameter dowel pins. The load was applied at midpoint through another 3/32 in. diameter dowel pin and the resultant deflection measured by a 0.0001 in. indicator at that point. Simple beam theory was then used to calculate the value for E. The results are given in Table 3-5.

From these results it was concluded that the value of $E = 3.0 \cdot 10^6$ psi used in design was reasonably close to the measured result. It was decided that an ample wave was available for test.

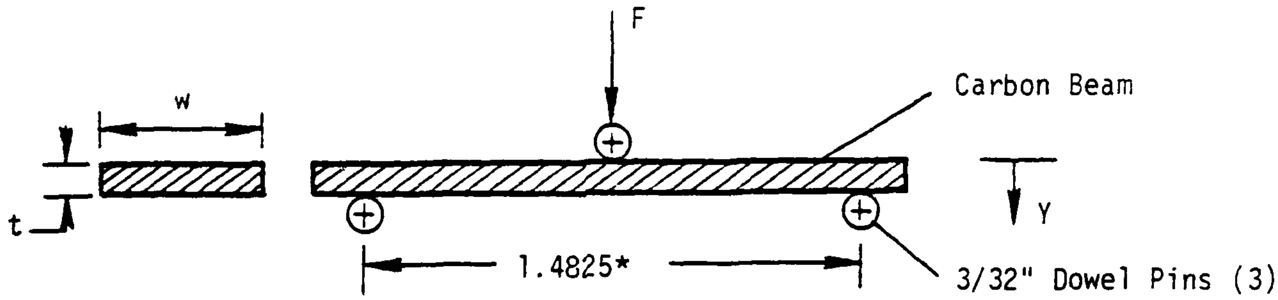

*Measured by profilometer.

Figure 3-14. Test Setup for Young's Modulus Experiments.

TABLE 3-5

YOUNG'S MODULUS RESULTS

FOR P658RC CARBON

Beam #	w (in)	t (in)	I (in^4)	F/y (lb/in)	E (lb/in^2)
1	.3824	.0602	6.9522×10^{-6}	327.2	3.19×10^{6}
2	.3825	.0602	6.9540×10^{-6}	323.3	3.15×10^{6}
3	.3826	.0602	6.9559×10^{-6}	323.9	3.16×10^{6}

2000 Hour Test Results

Performance During Test

Figures 3-15 and 3-16 show the performance of the seal one week after start and then eight weeks later. Each plot is for one complete weekly cycle. These are presented so as to compare the initial and final operation. The performance is much the same on the average. The torque fluctuations are somewhat higher, at the 14 percent speed and 100 percent pressure conditions, at the beginning than at the end of the test. The 100 percent speed and pressure conditions show a torque which is quite the same throughout the test, averaging about 2 N·m both in the forward and reverse directions. The total leakage during the second week of operation (Figure 3-15) was 253 cc, which resulted in an average leakage rate of 0.025 cc/min. Figure 3-16 has a total leakage for the week of 321 cc, which is a leakage rate of 0.032 cc/min. The spikes are the result of leakage getting trapped because of surface tension within the leakage path and then suddenly flowing.

One problem encountered during the test is illustrated by Figure 3-17. The torque readings became erratic as a result of insufficient waviness. This was caused by a clogged oil supply line filter to the waviness generator. The filter was cleaned and replaced at about 412 hours into the test. This eliminated the erratic behavior. This problem occurred a few more times during the test and in each case the filter was replaced with a new one.

One problem occurred during the test. The time of its first occurrence is not exactly known, but it became more pronounced toward the end of the test. Figure 3-18 shows uniform large fluctuations in

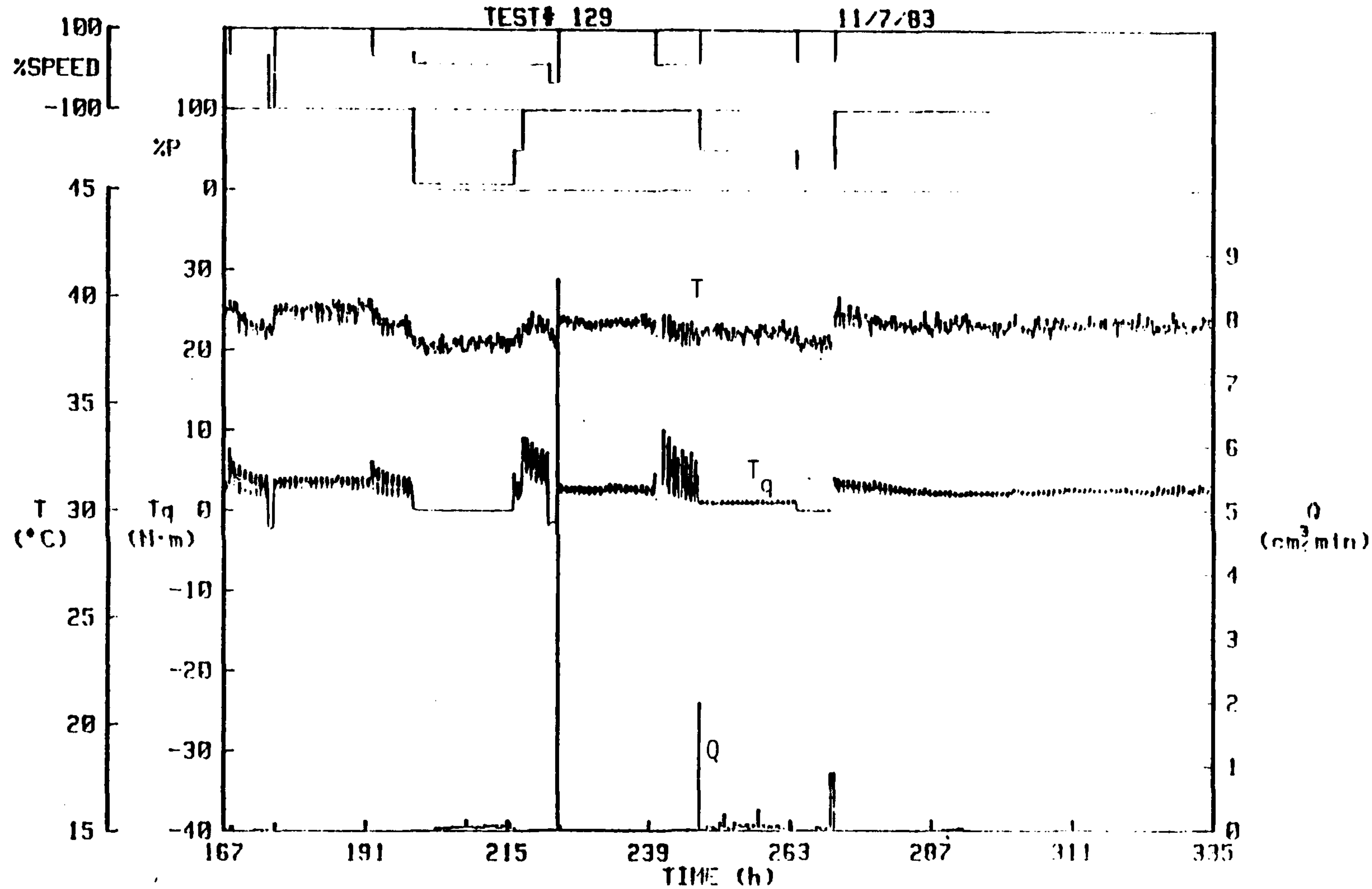

Figure 3-15. Test #129--167-335 Hours.

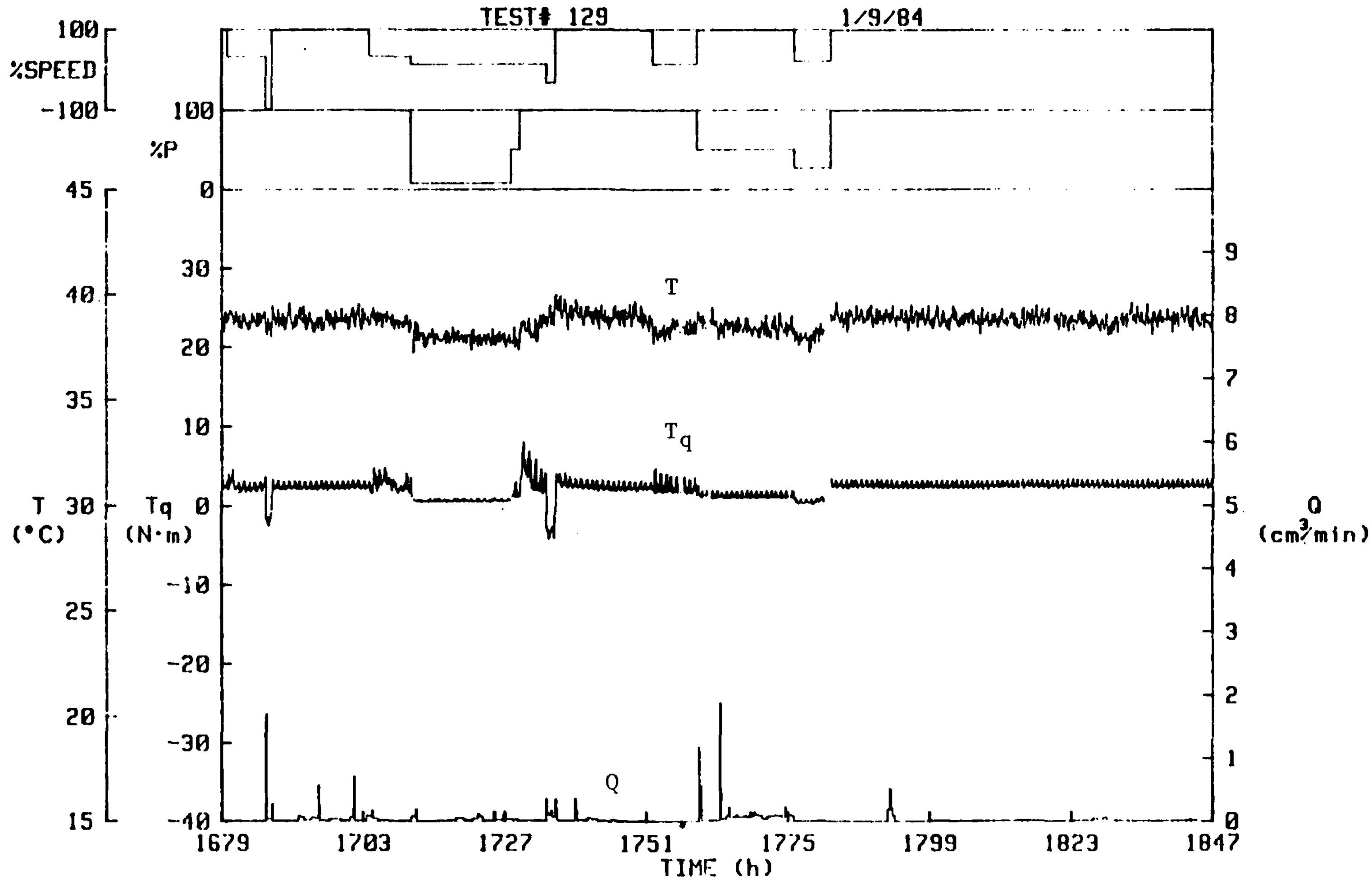

Figure 3-16. Test #129--1679-1847 Hours.

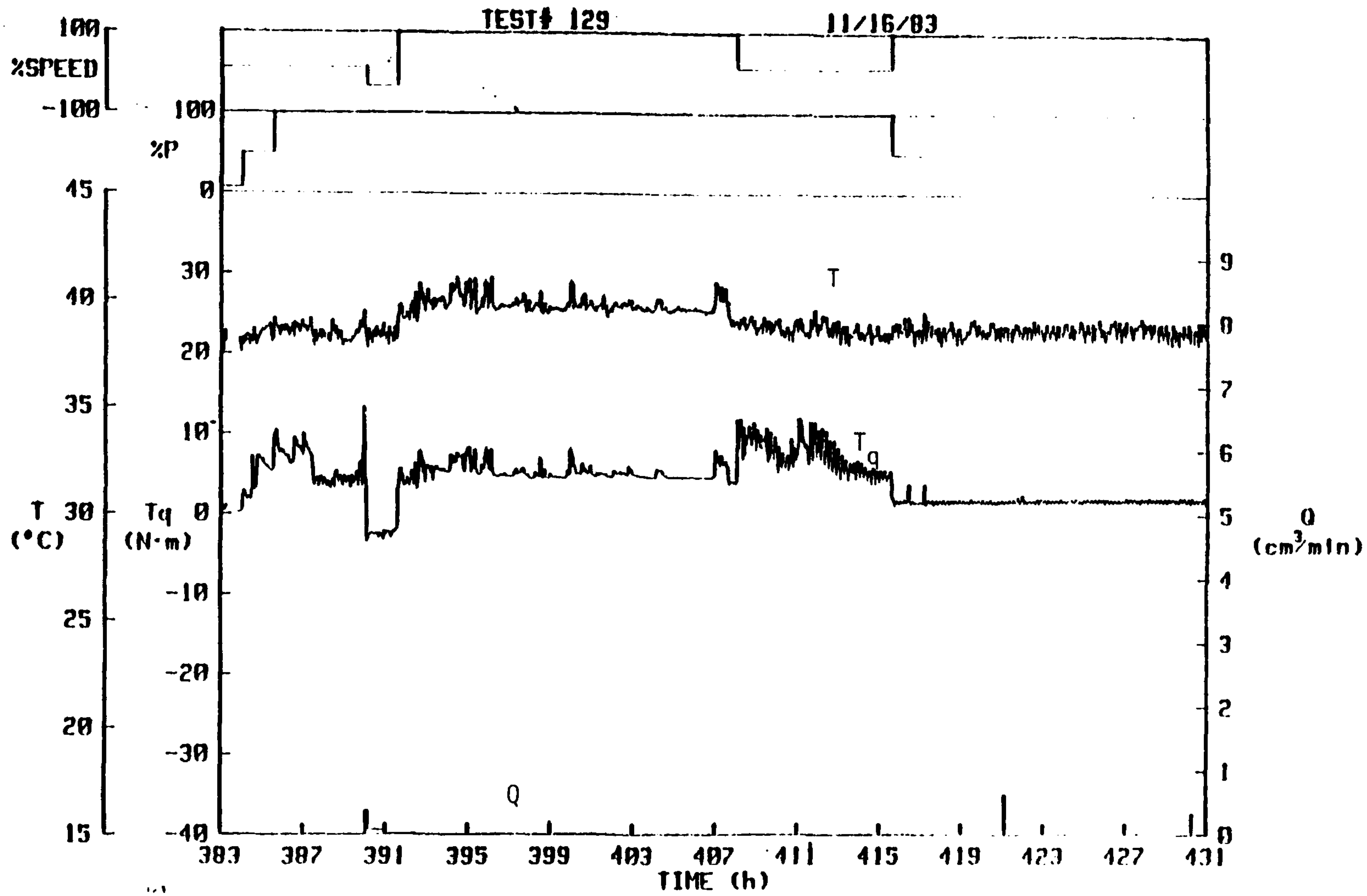

Figure 3-17. Test #129--383-431 Hours.

torque at the different operating conditions. On disassembly it was observed that the seal thermocouple was severely bent due to some relative motion between the carbon seal and the spring retainer. The reason for this angular displacement is due to the fact that the seal slipped in its silicon rubber bond. As a result, some small angular rotation of the carbon resulted causing the thermocouple to bind and ultimately become severely bent. This introduced a component of force which coupled with the movement of the wave around the seal, caused the fluctuations observed in Figure 3-18.

Silicon rubber bonding material was used so as to allow for the differential rates of thermal expansion for the carbon and the monel drive ring and also to be able to withstand the forces needed to drive the seal. The rubber adhered very well to the carbon but the bond was poor with the monel.

Post Test Analysis

Disassembly also showed that five springs behind the spring seat were bent due to the rotation of the carbon as stated above. One of these springs was broken. The epoxy case covering tubes in the waviness inducer had a slight bulge in it indicating some seepage of oil from the tubes inside. Because of the design, however, the oil could not contaminate the sealed fluid since the waviness mechanism is on the zero pressure side.

Radial profiles of the carbon showed a divergent taper of -763 μm/m average, this being the result of pressure caused rotation of the seal. Table 3-6 shows the wear results. The average wear for the 2000

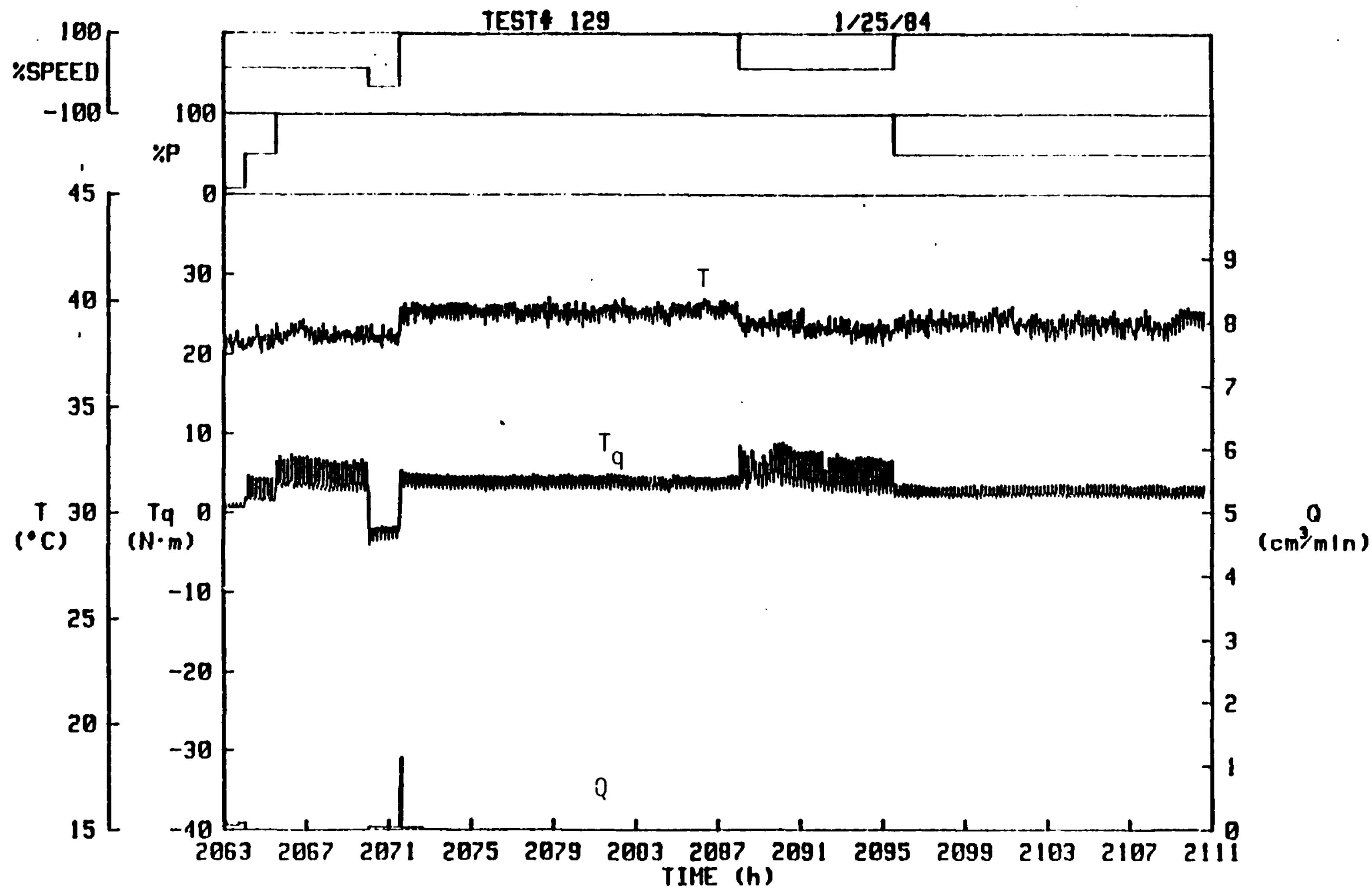

Figure 3-18. Test #129--2063-2111 Hours.

TABLE 3-6

Wear Results (2000 hours)

Position	Initial Wear Groove Depth (μin)	Final Wear Groove Depth (μin)	Wear (μin)
1	2800	2500	300
2	2860	2500	360
3	2240	1880	360
4	2520	2120	400
		Average	355

hour test was 355 μin. Radial traces of the K_TSiC seat showed wear of about 15 to 20 μin.

Comparison to Theory

Using a numerical model of wavy seal operation developed previously [5], performance was predicted for the various operating conditions in the 2000 hour test as shown in Figures 3-8 and 3-9. For the experimental results, six weeks of operation were used to establish average values at the different operating conditions. These values are given in Table 3-7. The results show a wide variation sometimes even though the apparatus was rezeroed weekly. These results are compared in Table 2-4 for drive torque only.

The table shows that there is a good relationship between predicted and experimental torque, although under some conditions agreement is not as close as desired. Perhaps most importantly is that the reduction of friction with increasing speed shown by the theoretical data is followed by the experimental data although the experiment does not show as strong a relationship. This agreement verifies the predicted operation of hydrodynamic effects in water. In earlier tests, face geometry could change with speed. In this test, the nine waves have a very high stiffness and remain constant and geometry does not change with speed. The other very encouraging result in Table 3-8 is that the speed effects are symmetrical. This indicates that some type of torque caused geometry change is not really influencing the results and more importantly, that the average torque values are reliable because they repeat in the opposite direction.

TABLE 3-7

One Week Average Torque Values
Test 129 (N · m)

Speed % / Pressure %	671 to 839	839 1007	1007 1175	1571 1679	1679 1847	2015 2183 hrs
	Week					
14/7	0.42	0.61	0.77	0.96	0.65	0.70
14/50	2.55	7.93	1.36	1.98	1.58	2.22
14/100	7.19	7.60	2.36	2.95	2.92	4.42
33/100	5.20	3.58	3.25	3.16	2.63	3.58
100/50	1.05	1.23	1.22	1.70	1.28	2.51
100/100	2.91	2.95	2.45	2.66	2.53	4.33
-33/100	-5.05	-4.76	-2.91	-2.51	-3.34	-2.50
-100/100	-2.39	-3.11	-2.80	-5.25	-1.73	-2.33

TABLE 3-8

Comparison of Experimental and Theoretical Results--Design 2
Torque* (N · m)

Experimental† / Theory	% Speed -100	-33	14	33	100
7	** / -.3	** / -.1	.7 / .2	** / .1	** / .3
50	** / -.4	** / -1.2	2.9 / 3.2	** / 1.2	1.5 / .4
100	-2.9 / -1.4	-3.5 / -4.7	4.6 / 6.7	3.6 / 4.7	3.0 / 1.4

*Leakage was not compared because of erratic rates caused by collection passages.

**Conditions not run experimentally.

†Based on six weeks data from Test #129.

With regard to leakage, the model was used to predict a weekly average rate of 0.4 cc/min. The average measured weekly for the week of operation shown in Table 3-9 was 0.028 cc/min. Thus leakage does not agree well at all. The experimental result of course is favorable since it is lower than predicted. However, it is known that the model is weak in predicting leakage. Previous work [16] showed that in contact problems like this one actual leakage is very hard to predict to better than an order of magnitude.

Split Ring Design

To meet ultimate submarine needs, it is necessary to be able to design a split seal. Thus as part of this program, a small scale prototype wavy split seal was to be investigated.Thus, a design had to be made that would allow the carbon to be split (two places, 180° apart) and then clamped and still be able to transmit the wave-causing moments across the split. The first iteration for this design was to make a preload ring that would be pressed over the OD of the carbon ring. This preload ring would have to be able to apply a compressive load of 250 lb/in. radially at the centroid in order to offset the effect of the loads generated outward by the waviness inducer. Figure 3-19 shows the configuration of the band designed. The band has a slight taper ground into it as does the carbon, which allows for ease of press.

A three-dimensional SAPIV finite element analysis was then made on the carbon cross section without the band. Results showed a stiffness, GJ_θ, of 3527 lb-in^2. The design program used calculated a GJ_θ of 3183

TABLE 3-9

Weekly Average Leak Rate*
Test 129

Week	167 to 335	1679 hrs to 1847 hrs	Predicted
Leakage	0.025 cc/min	0.032	0.4

*Based on total leakage for the week.

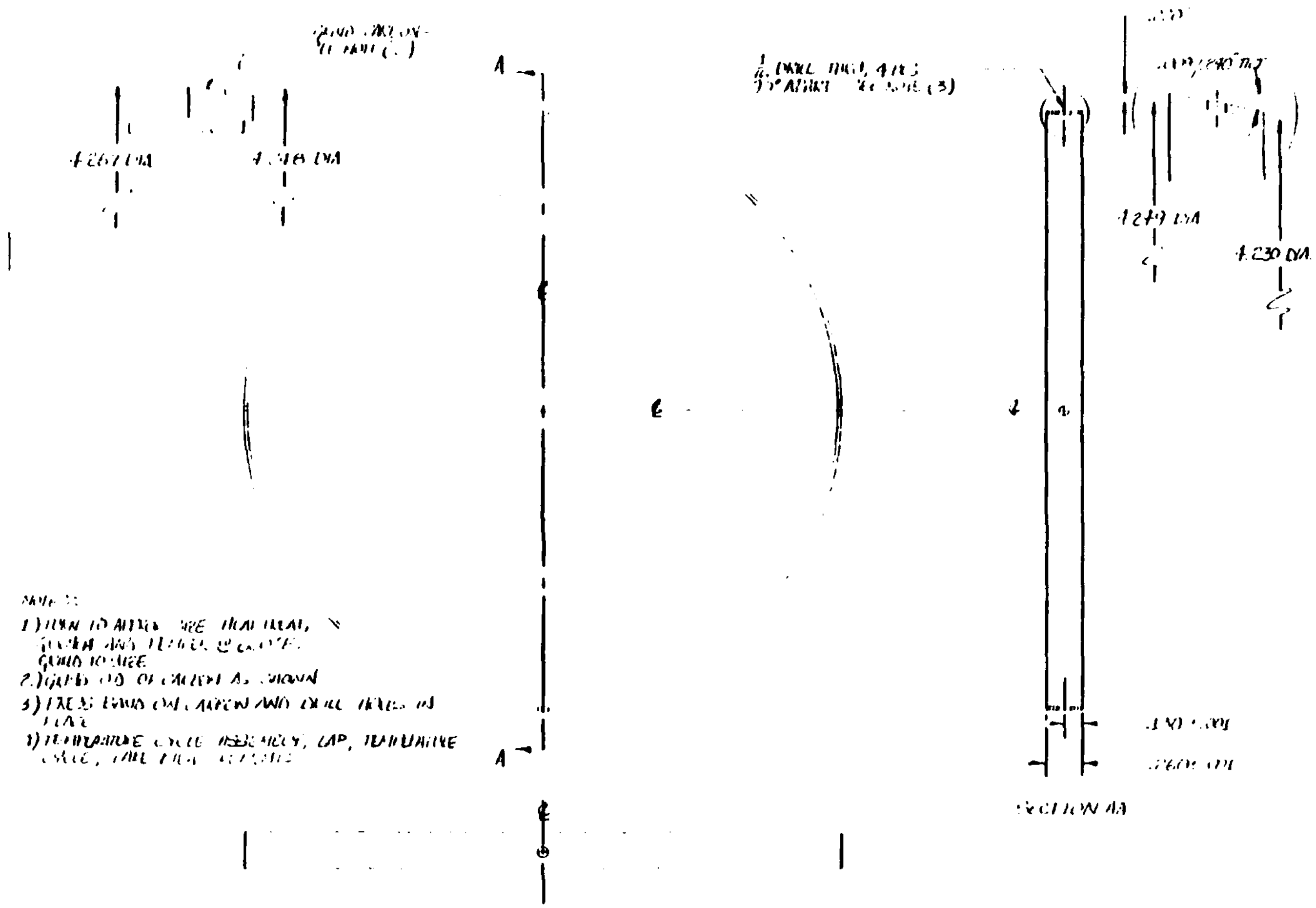

Figure 3-19. Pre-load Ring.

lb-in.^{2}, which is within 10 percent. It was therefore felt that the design program was satisfactory in its method of solution.

The next step was to re-run the three-dimensional SAPIV program with the inclusion of the preload ring. The resultant GJ_θ was 4368 lb-in.^{2}, a 24 percent increase. The band (Figure 3-11) was then made and pressed on a new carbon seal. The measured ninth harmonic waviness of the carbon without the preload ring was 50 μin. With the preload ring on the carbon, the ninth harmonic waviness was measured at 32 μin. a 36 percent reduction. The SAPIV finite element program predicted a 20 percent decrease in waviness with the addition of the band. From these results it was determined that the design method was sufficiently valid to serve as a useful tool.

From the preceding results, a new preload ring would need to be designed which would not restrict so much of the wave. Again, the three-dimensional SAPIV program was used and the design shown in Figure 3-20 was the result. This particular ring would only give a 12 percent increase in the stiffness, which would result in a reduction of ninth harmonic waviness from 50 μin. to only 44 μin.

The split seal itself, as shown in Figure 3-21, is to be machined out of two existing carbon seals. Internal moments are to be carried across the split sections by means of eight stainless steel dowel pins. These dowel pins were sized based on an analysis of the internal moment generated due to the induced waviness.

Referring back to Equation (3-32) the internal moment is given by

$$M_\theta = \frac{GJ_\theta}{R} (\phi' + \bar{v}') - \frac{E\Gamma^*}{R^3} (\phi''' + \bar{v}''') \quad (3\text{-}52)$$

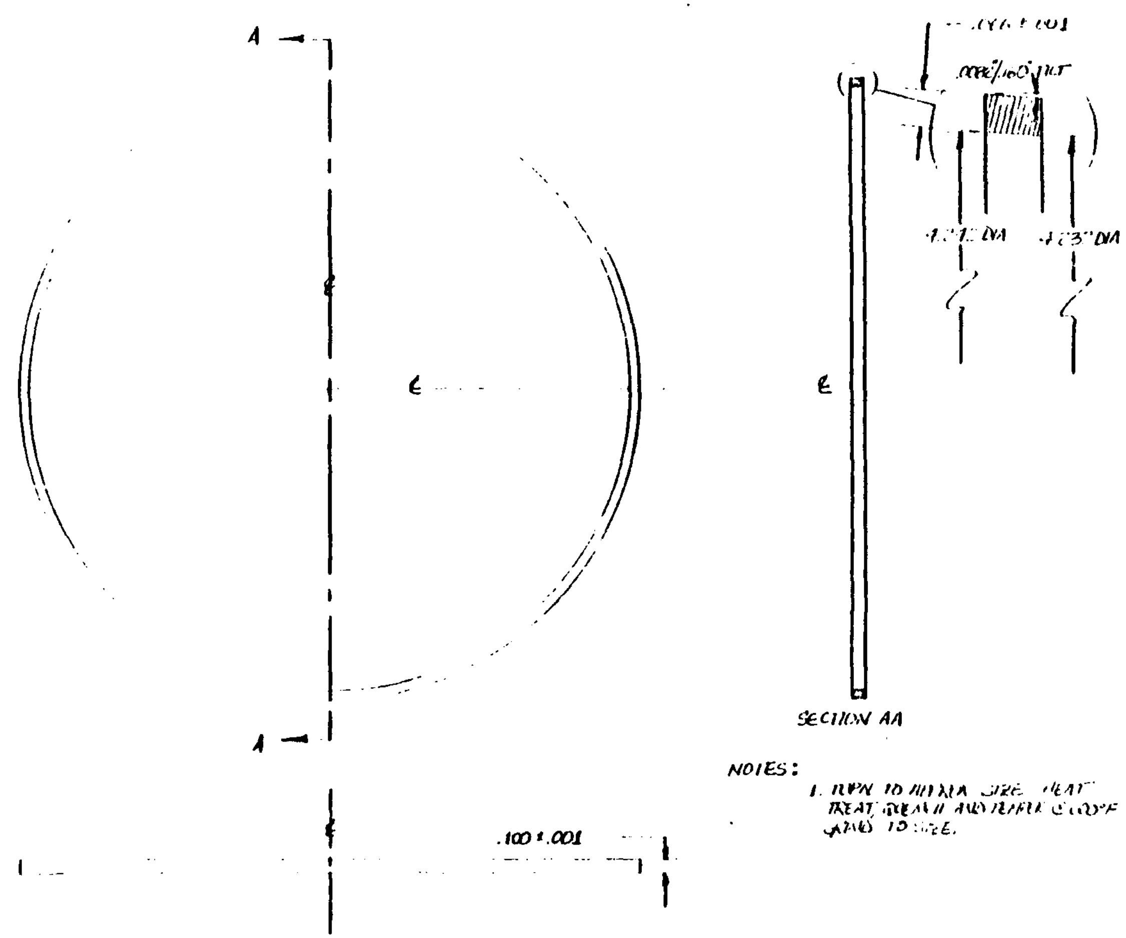

Figure 3-20. Modified Pre-load Ring.

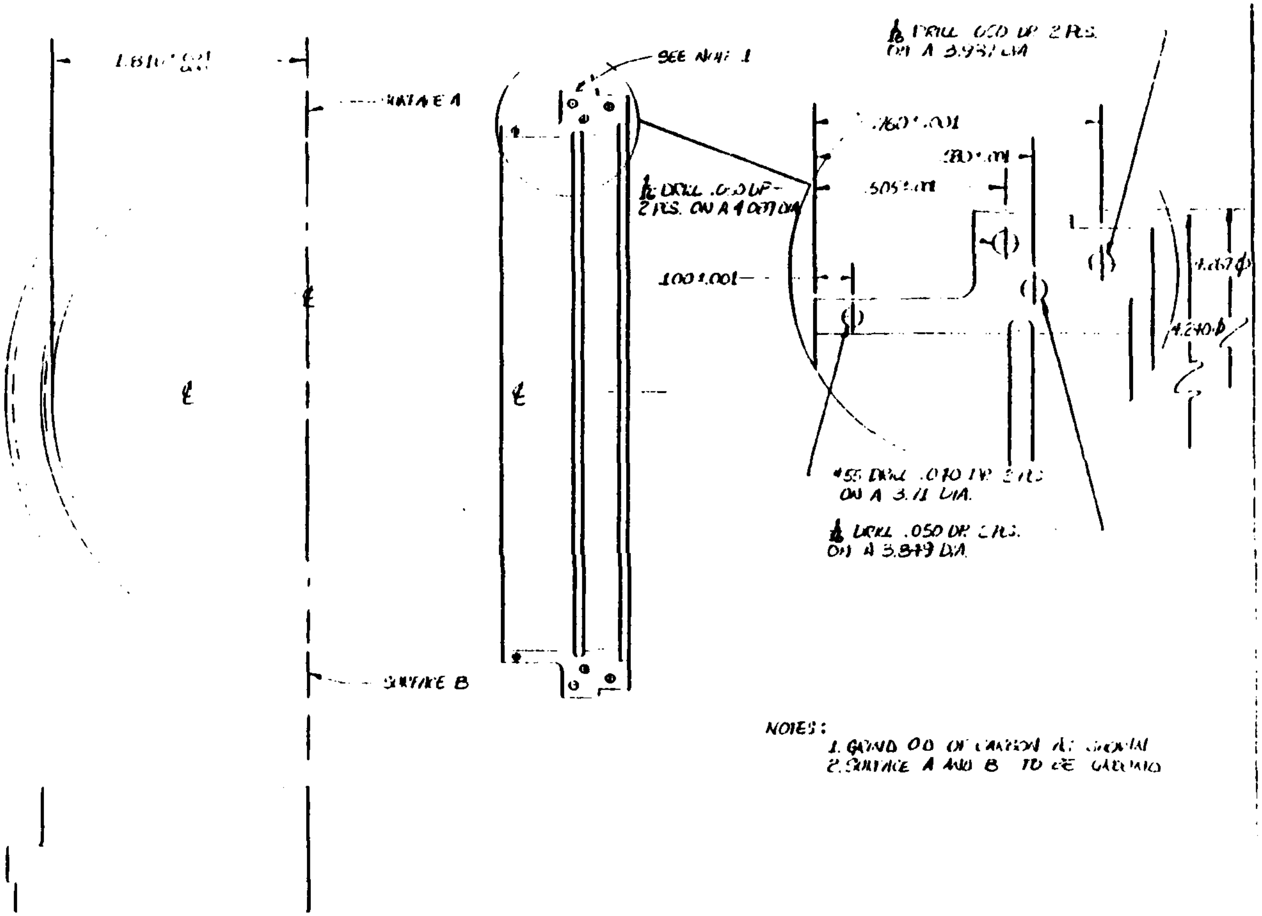

Figure 3-21. Split Ring Seal.

Considering warping gives,

$$\bar{v} = -\frac{m_{\theta_o} R^2}{EJ_x} C_1 \cos(n\theta) , \tag{3-53}$$

$$\bar{v}' = n \frac{m_{\theta_o} R^2}{EJ_x} C_1 \sin(n\theta) , \tag{3-54}$$

$$\bar{v}''' = -n^3 \frac{m_{\theta_o} R^2}{EJ_x} C_1 \sin(n\theta) , \tag{3-55}$$

and

$$\phi = \frac{m_{\theta_o} R^2}{EJ_x} C_2 \cos(n\theta) , \tag{3-56}$$

$$\phi' = -n \frac{m_{\theta_o} R^2}{EJx} C_2 \sin(n\theta) , \tag{3-57}$$

$$\phi''' = n^3 \frac{m_{\theta_o} R^2}{EJ_x} C_2 \sin(n\theta) , \tag{3-58}$$

where

$$C_1 = \frac{\frac{1}{A} + \frac{n^2}{B} + 1}{\frac{(n^2 - 1)^2}{A} + \frac{n^2}{B} (n^2 - 1)^2} \tag{3-59}$$

$$C_2 = \frac{\frac{n^2}{A} + \frac{n^4}{B} + n^4}{\left(\frac{n^2}{A} + \frac{n^4}{B} + n^4\right)\left(\frac{n^2}{A} + \frac{n^4}{B} + 1\right) - \left(\frac{n^2}{A} + \frac{n^4}{B} + n^2\right)^2} . \qquad (3\text{-}60)$$

Substitution of (3-54), (3-55), (3-57), and (3-58) into (3-52) gives

$$M_\theta = \frac{GJ_\theta}{R} \frac{nm_{\theta_o} R^2}{EJ_x} \Big[[-C_2 \sin(n\theta) + C_1 \sin(n\theta)$$

$$- \frac{E\Gamma^*}{R^3} \frac{n^3 m_{\theta_e} R^2}{EJ_x} [C_2 \sin(n\theta) - C_1 \sin(n\theta)] \Big] . \qquad (3\text{-}53)$$

Using the previous design data for the solid ring, the internal moment is

$$M_\theta = -7.65 \text{ in.-lb} . \qquad (3\text{-}54)$$

The dowels were sized to handle this moment.

Conclusions on Second Design

In many ways the performance of the second design was similar to that of the first design. Torque and leakage values were similar. Wear was significantly lower amounting to 355 μin. Since some taper did wear into this seal, it is expected that much of this wear took place early in the test, so the long term wear rate would be even better than on this test.

Theory predicts somewhat different values for friction torque than found experimentally but the hydrodynamic effect is nonetheless displayed. Leakage values are significantly lower than predictions. This is an advantage to seal operation but shows a significant weakness in the model.

An improvement is needed in the drive arrangement to get a positive engagement or improve the bond of the adhesive. Some improvements in oil plumbing reliability need to be made as there was one seep in the system.

Except for the problems mentioned the seal itself performed very well. At the wear rate measured, the wearing faces could be designed to meet a 150,000 hour life objective. The concept from the standpoint of wear reduction works very well. The question now becomes: would the waviness force applicator be sufficiently reliable? Certainly no significant problem was encountered in the 2000 hour test. The piston arrangement appears to be reliable. However, the O-rings and their associated plumbing introduces an element of chance failure or shortened life due to wear out which cannot be quantified. It can only be stated that the design would be more reliable absent these elements. Thus, while the test and the design were both very successful, there is still a need to find a simple more reliable means to impose a wave.

CHAPTER 4

NINE WAVE SEAL--THIRD DESIGN

Early in the wavy seal investigation it became clear that a simple means of imposing a moving wave was essential to the ultimate success of the idea. While it was proven early in the test program that a moving wave would provide low friction and low wear along with low leakage, the greatest difficulties in designing, fabricating, and operating the wavy seal have been with the waviness causing device itself.

While a remedy to this problem has been sought all along, during the present contract period an extra effort was made to find a much simpler waviness device. To this end, the ideas explained in Chapter 8 on squeeze seals and bearings were conceived and analyzed. One of the conclusions as explained in Chapter 8 was that the squeeze seal (when the wave moves at shaft speed) is equivalent to the current wavy seal and therefore offers no advantage of further reduced wear. However, the squeeze seal does offer the possibility of facilitating the application of the wave. In fact, it happens that the squeeze seal as originally conceived is equivalent to forming the wave fixed in the hard face and rubbing against a flat soft face. This becomes then the basis for the third nine wave design.

The design is shown in Figures 4-1 and 4-2. The wave as shown in Figure 4-1 is ground into the hard face. The wave is similar to that used in present wavy seal designs just described in the previous chapters. Nine waves are again used so that the carbon does not

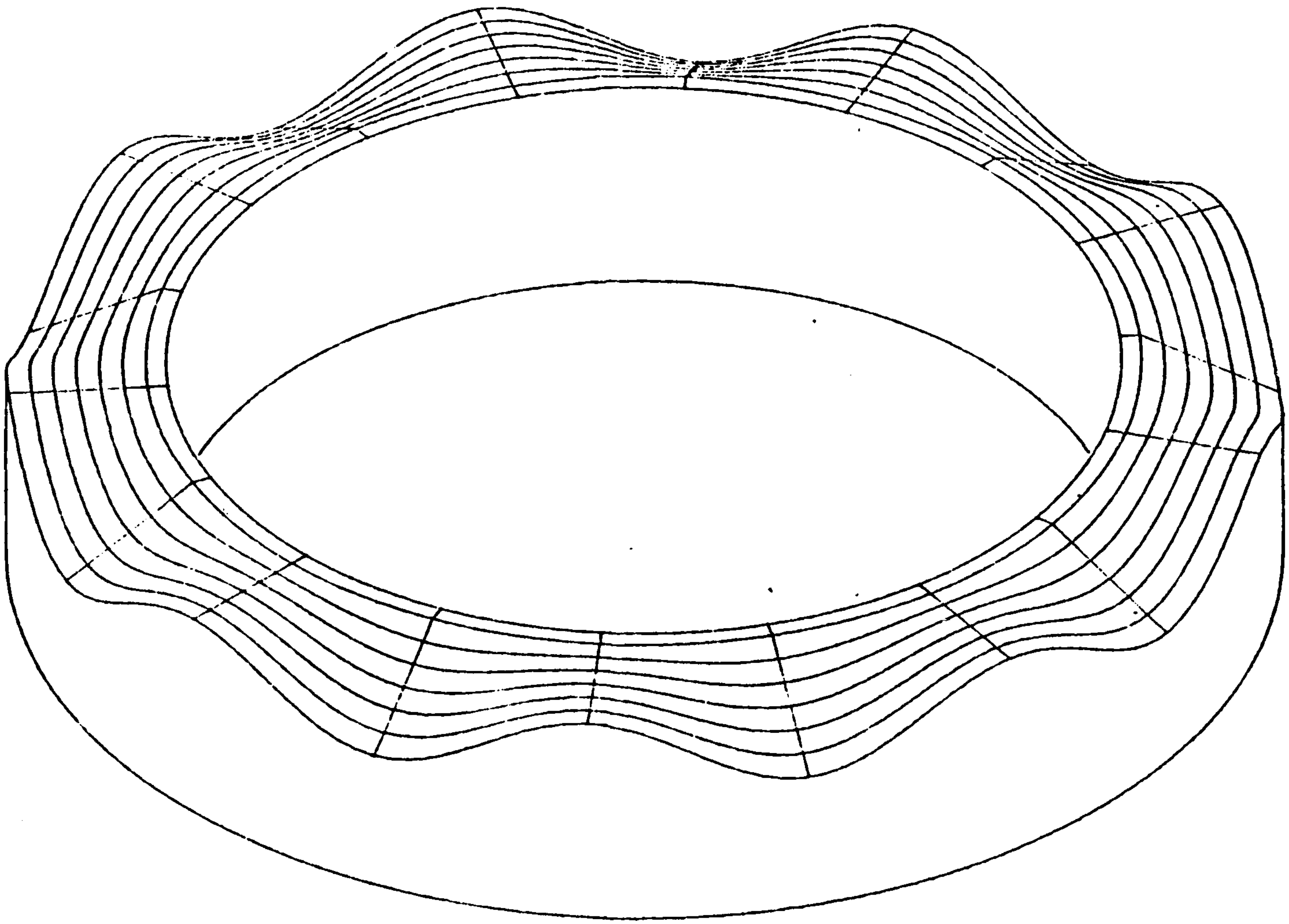

Figure 4-1. Wavy-Tilt-Dam Seal Face.
(Patent Pending)

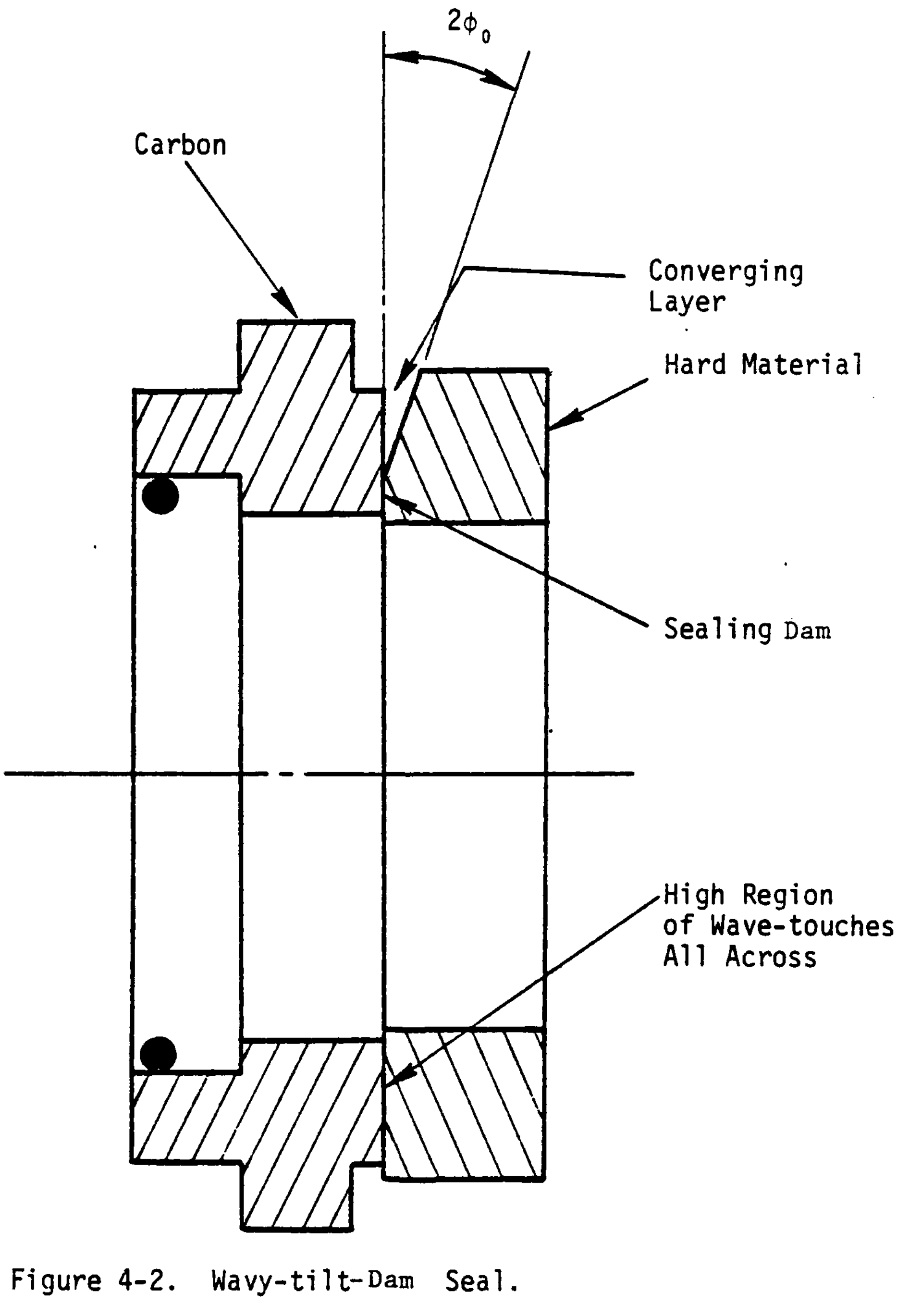

Figure 4-2. Wavy-tilt-Dam Seal.

significantly flatten out and thus eliminate the desired wave. The wavy-tilt design is used in order to obtain hydrostatic lift from the radial taper and hydrodynamic lift from the wavy part. The wavy tilt stops at some radius beyond which the seal face remains flat. This flat portion is the sealing dam and serves to minimize leakage flow.

In this design the carbon face is everywhere wiped by the high spots of the wave on the hard face. Thus the carbon must wear uniformly. The high spots on the wave do wear unevenly; that is, unlike design 2, wear is not spread out all across the hard face. However, the localized wear effect is on the hard face, not the carbon. The hard face is not wiped all over. Operation of the seal is identical to design 2.

Advantages

Compared to the moving wave, this seal design, once the parts are made, is as simple as current seals. No waviness drive is needed. Reliability should be very high. Because of the fact that with the present wavy design wear on the hard face is insignificant, it is expected that the same will hold true for this design. The carbon will wear slowly (same as at present). The hard face will wear very slowly such that the wave is preserved for the entire life of the seal. Long life and low leakage are expected just like for the current wavy seal.

Limitations

There is some difficulty in grinding the shape shown in Figure 4-1 into the hard face. While it is easy to deform carbon elastically to

get a wavy surface, this technique will not work for the high modulus hard face material.

The fact that the hard face is not wiped everywhere may allow debris or corrosion to build up in the low spots of the hard face. Also in some applications wear of the hard face presents an unknown factor. There is some evidence that hard face materials such as silicon carbide when lightly loaded (as in the case here) will experience only a few microinches of wear in a thousand hours. For applications where this is true for the fixed wave seal, then wear of the wave will present no problem. Experiments will answer the wear question as well as the corrosion buildup question.

One other limitation of this design is that special features must be incorporated so that radial misalignment can be accommodated. Figure 4-3 shows that with the normal seal design, a gap could result due to radial misalignment. The solution to this problem requires that the carbon and the hard face both be made wider as shown. The complications of solving the problem this way or using other approaches have not been evaluated as yet.

Wavy Seals

Wavy seals have been experimented with and proposed for use previously by other investigators [36,37]. The obvious question to be raised is why the wavy seal did not become a routine practice and what is different about the present proposal. First, the type of wave used and proposed here is a wavy tilt. The wavy tilt offers a sealing dam as well as hydrostatic support and hydrodynamic support. This type of

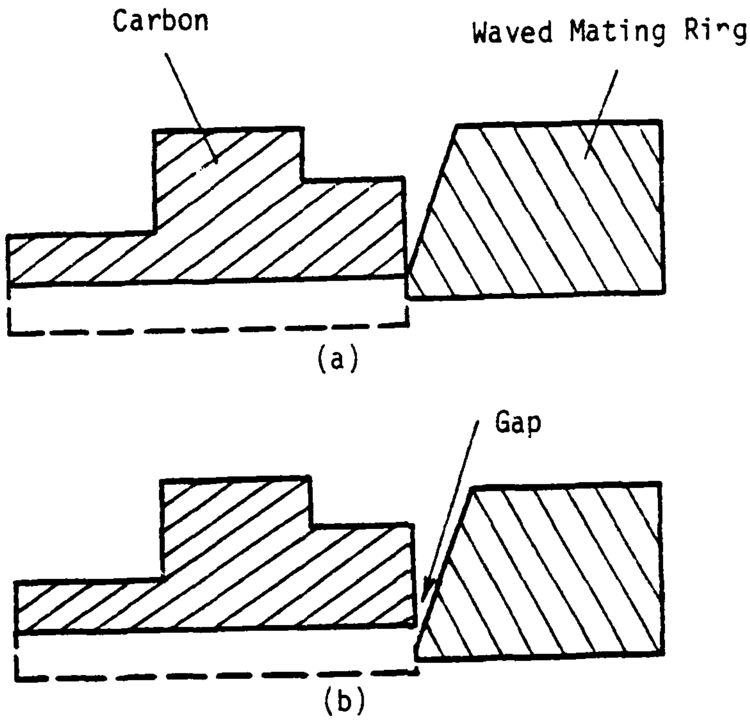

Figure 4-3. Effect of Contact Radius and Offset on Leakage.

(a) Properly Aligned Seals
(b) Result of Radial Offset

wave, as far as is known, has never been used before. Simply lapping a radially parallel wave into a seal may cause excessive leakage if the seal is stiff or nothing may happen if the seal is compliant [22]. Secondly, no consideration has been given previously to the relationship between stiffness and waviness. Early work in this project showed [4,5] that waves can be easily flattened out. It also showed that seal rings also tilt as they deform. Thus, imposing a wave on a seal ring without careful consideration of the deflection and net waviness may easily lead to undesirable contact geometries or unknown geometries. Deflection has been carefully considered in these designs. Thus in summary, the present work represents the first series of work where the wave shape has been carefully controlled, both in its creation and in operation, so that the desired effects will likely occur. Thus, the idea being proposed here, while not new as a general concept, is novel when considered carefully in detail, and it is these details which make the difference between successful operation and poor performance.

Seal Design

The third design is the result of only three modifications to the second design as shown in Figure 3-13. The first is the removal of the waviness inducer and spacer. This was done since the waviness is not imposed on the carbon for this design. The second modification was made on the method of driving the carbon. As pointed out before, the carbon rotated relative to the drive ring adapter in test no. 130, as a result of too much tangential load, due to friction torque of the seal, for the strength of the adhesive used. To eliminate this problem, four

#2-56 socket head cap screws were recessed into the carbon 0.05 inches to provide the additional drive capability along with the silicone adhesive.

The third modification was that of putting the desired wave on the hard mating face of the seal assembly. The technique for doing so is explained later, the performance for such a design follows.

Expected Performance

Seal performance is expected to be like that described in Chapters 2 and 3 for designs 1 and 2. However, some additional consideration was given to static (low speed) performance. Table 4-1 shows the static performance of the seal at various wave tilts. ϕ_o is the tilt amplitude on the mating hard face and ϕ_{net} is the resulting tilt due to the conformability of the carbon. As can be seen, not a lot of friction reduction is gained by raising ϕ_m above 500 μin./in. The leakage does, on the other hand, increase quite rapidly. This tradeoff was the basis for the selection of ϕ_o = 500 μm/in. for the new design. Previous designs used a slightly lower waviness.

Waviness Grinding Apparatus

The procedure for putting the wave on the mating face is by means of grinding. Since the desired wave is of a special case, i.e., tilted in the radial direction, waved in circumferential direction, and having a circumferential strip of constant height at some given radial location, a unique method of grinding had to be devised.

TABLE 4-1

Seal Performance (Static)

n = 9 Speed= 1 RPM
P_o = 500 psi

Φ_o (μin/in)	Φ_{net} (μin/in)	Q (cm^3/min)	T_q (in-lb)	μ	% fluid pressure load support
50	20	.09	120.6	.049	50
80	43	.10	113.9	.046	53
100	63	.11	106.0	.043	56
500	475	.33	68.6	.028	72
1000	967	.62	62.4	.025	74
1500	1461	1.07	59.7	.024	76
2000	1960	1.66	57.5	.023	77

Figures 4-4 and 4-5 show the grinding apparatus. The seal ring is mounted in a fixture and very precisely rotated about x-x in a lathe. The cam shown also rotates with the ring. The grinding wheel and its driver and the cam follower are all mounted to a plate which pivots about the axis y-y. The plate is flexure mounted as shown later so is actually very stiff relative to the base. However forces in the z direction produced by the cam follower and spring cause the plate to rotate (on its flexure mounts) about axis y-y. Therefore as the seal ring and cam turn about axis x-x, the cam follower causes the grinding wheel and plate assembly to oscillate about axis y-y. With the grinding wheel running about axis z-z, this action causes the wave of Figure 4-1 to be ground into the seal ring. The cam used has nine waves to produce the nine wave seal ring. Axis y-y is located at the sealing dam radius so that the waviness at that radius is zero.

Flexure Design

The flexure support system was chosen over bearings because of its high stiffness, zero looseness, and simplicity. The plate rotates only ±500 µm/m. Figure 4-6 shows the approximate pattern of flexure beams used to mount the plate. Point 0 is the pivot point whose location is assured by the four surrounding flexures. Flexures 5 and 6 provide additional stiffness to the mount.

Referring to Figure 4-6 summing moments about "0" give:

$$\sum M_0 = F_0R_0 = F_1R_1 + F_2R_1 + F_3R_1 + F_4R_1 + F_5R_2 + F_6R_2 \qquad (4\text{-}1)$$

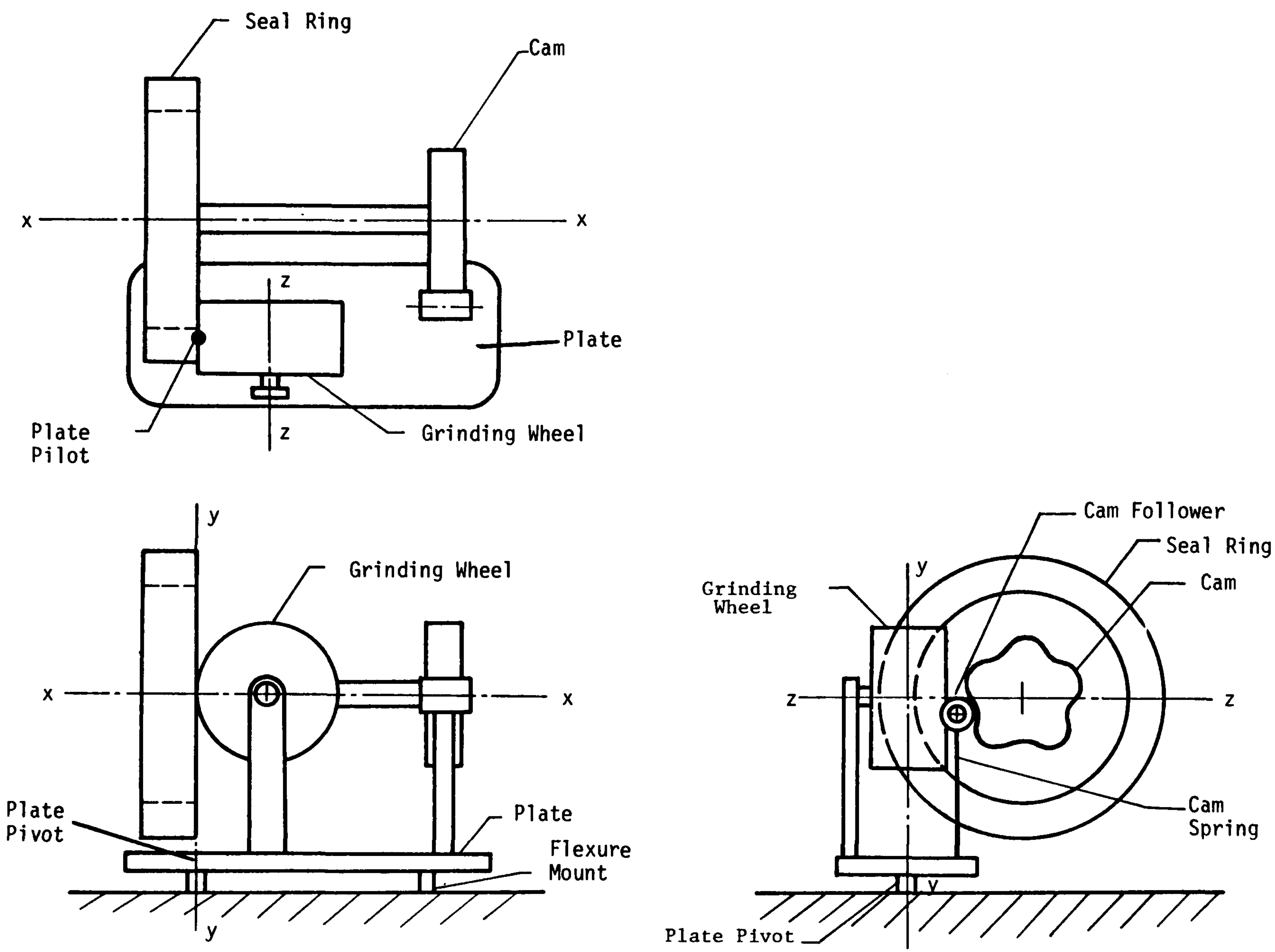

Figure 4-4. Grinding Apparatus Schematic.

(Patent Pending)

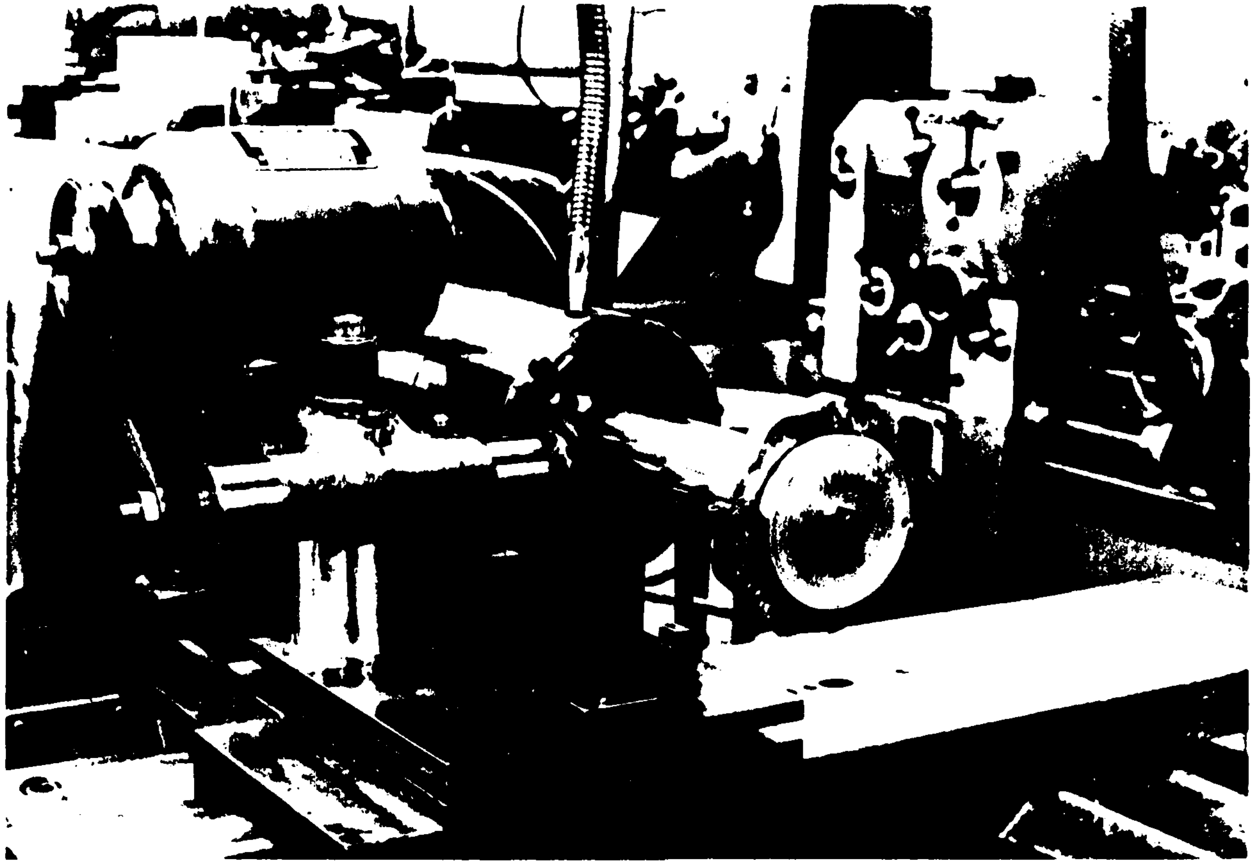

Figure 4-5. Grinding Apparatus.
(Patent Pending)

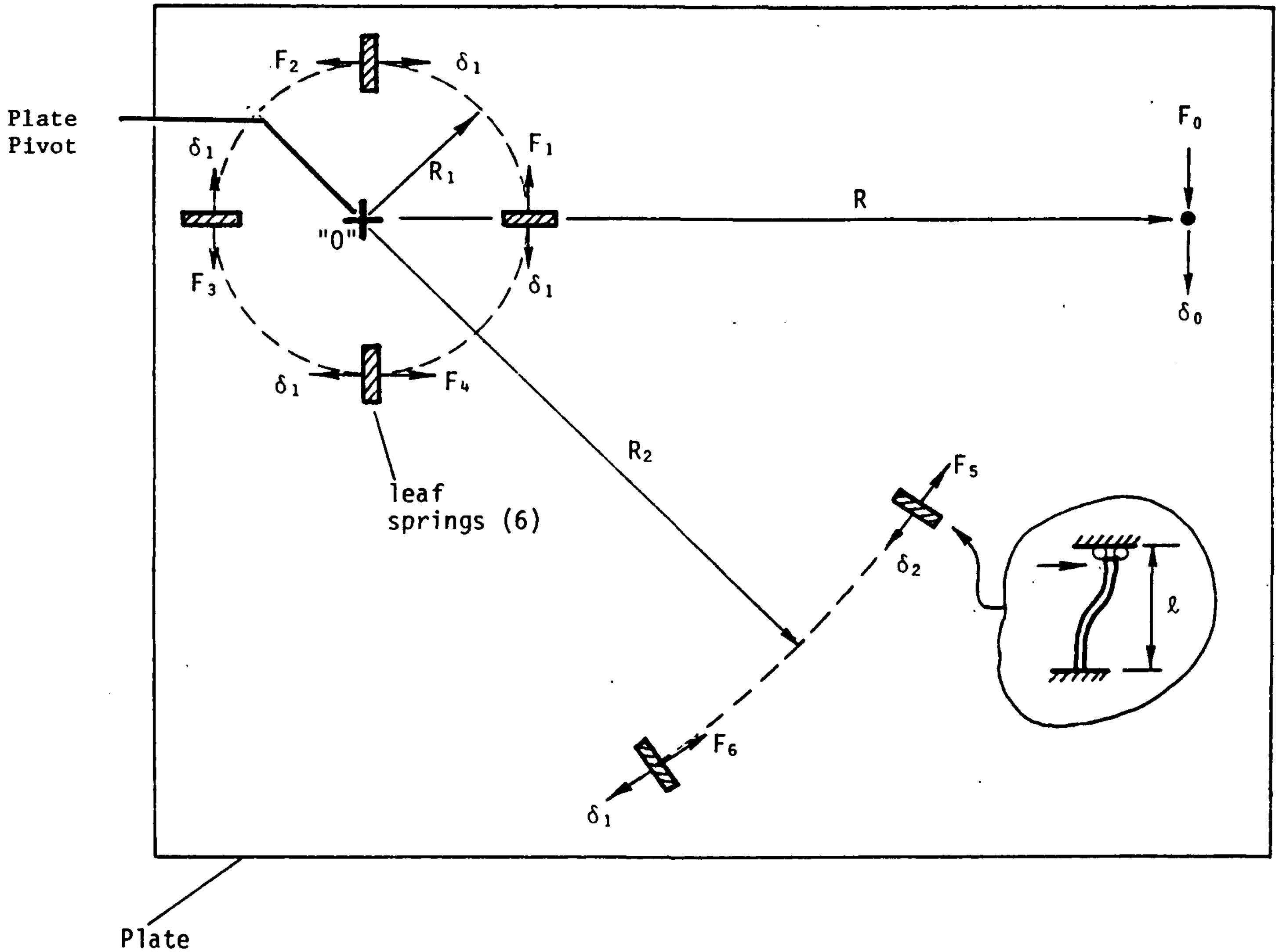

Figure 4-6. Flexure Mounts

(Patent Pending)

where

$$F = k\delta \tag{4-2}$$

and

$$\delta = R\theta \tag{4-3}$$

which gives

$$F = kR\theta \ . \tag{4-4}$$

Substituting (4-4) into (4-1) and assuming that all leaf springs have the same stiffness gives,

$$F_0 R_0 = 4kR_1^2\theta + 2kR_2^2\theta \ . \tag{4-5}$$

Now,

$$F_0 R_0 = k_T R_0^2 \theta \tag{4-6}$$

where k_T is the total effective spring constant of the system. Substitution of (4-6) into (4-5) gives

$$k_T = k \left[\frac{4R_1^2}{R_0^2} + \frac{2R_2^2}{R_0^2} \right] \tag{4-7}$$

The spring constant, k, for a beam fixed on one end and guided at the other end is [38],

$$k = \frac{12\ EI}{\ell^3}. \tag{4-8}$$

The cam was designed to cause a 0.150 inch amplitude cam follower displacement. The stiffness was designed using the above relationships

so that the corresponding force produced by the cam follower spring produced the ±500 μm/m rotation needed.

Waviness Profile Results

To test the grinding apparatus, a seal ring was machined out of 1018 steel to the dimensions of an existing seal ring. A 2 inch diameter, 60 grit, silicon carbide wheel was used for the grinding. The steel ring was then ground and a polar plot of waviness at the seal carbon outside radius (r_o) was taken. These results are shown in Figure 4-7. A Fourier analyses showed a ninth harmonic waviness of only 41 μin. It was desired that a 75-100 μin. (based on 500 μin./in.) wave be produced. The discrepancy was found to be due to the effect of stiffness of the connection between the upper grinding mount plate and the grinder itself. Some flexing was occurring at this connection and as a result the deflection of the grinding wheel was less than expected.

To correct for this, a calculation was made to re-size the input spring of the cam follower mechanism, making it stiffer. The steel ring was again ground and the resultant waviness plot is shown in Figure 4-8. The ninth harmonic waviness increased to 141 μin. From these results it was concluded that the waviness grinding apparatus was indeed operating as designed and the next step was to grind a tungsten carbide for actual testing.

Grinding a tungsten carbide ring was done using a 2 inch diameter, 320 grit, diamond impregnated wheel. The results of this grinding is shown in Figure 4-9. The amplitude of the ninth harmonic wave is 134

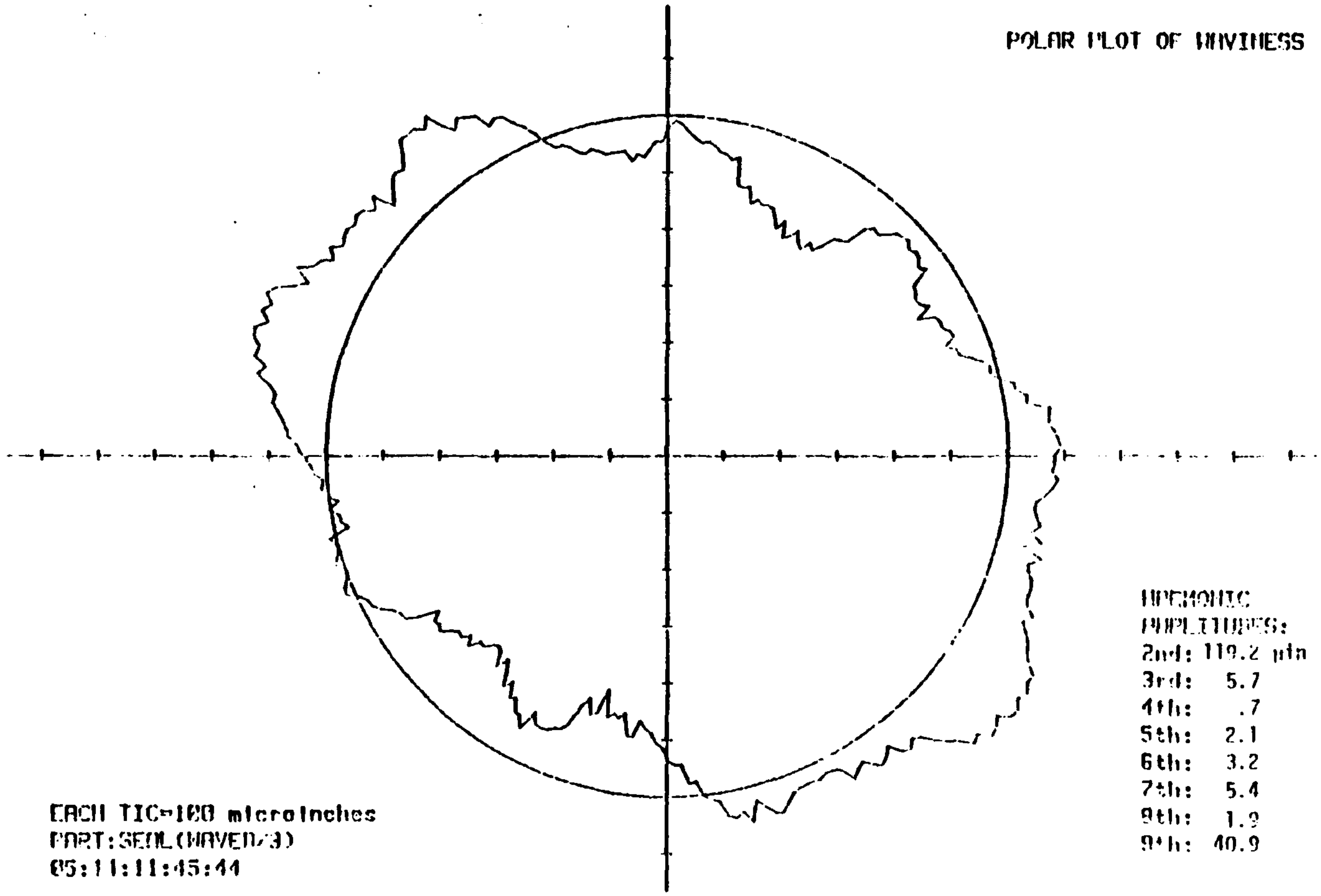

Figure 4-7. Waviness in Steel Ring--First Run.

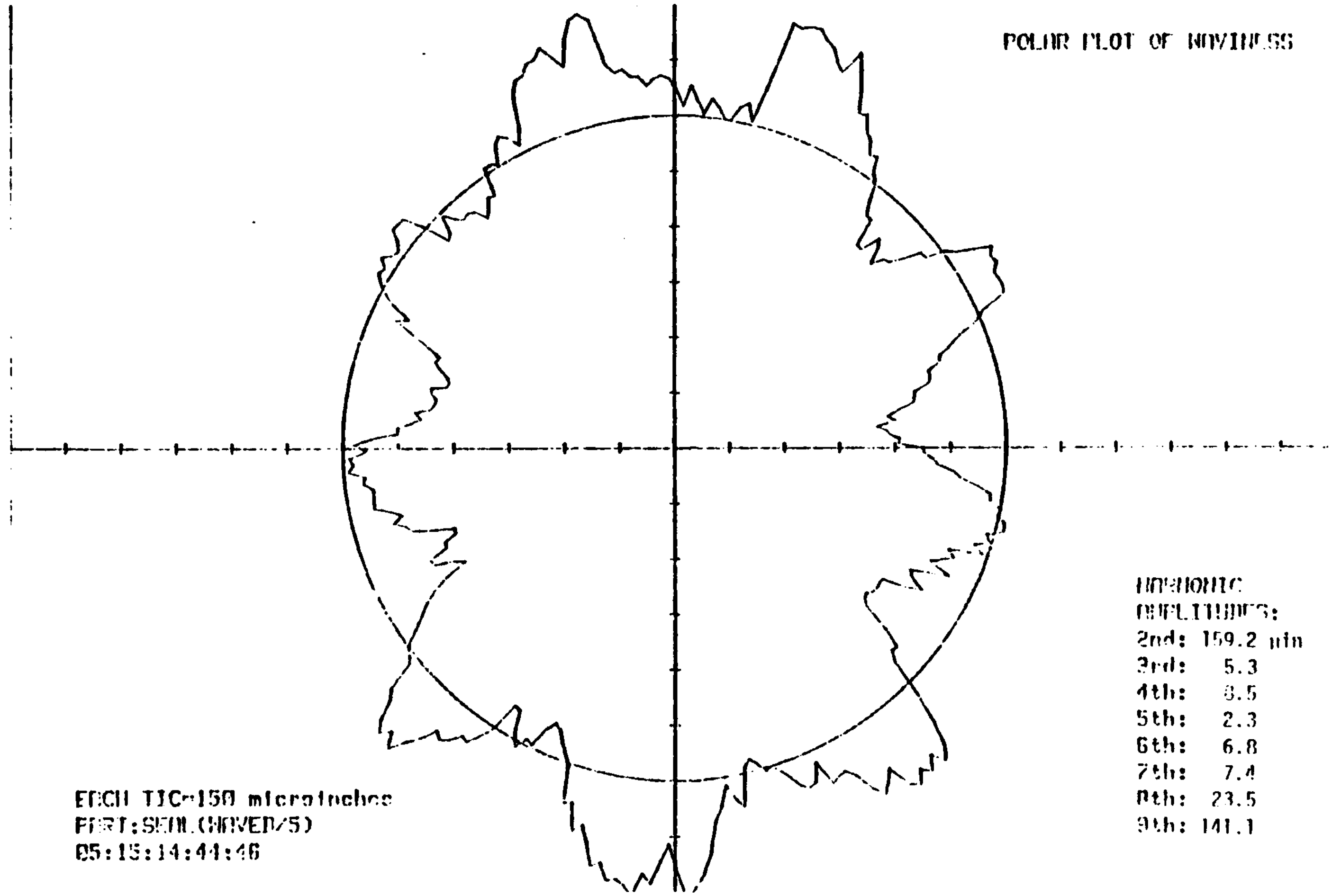

Figure 4-8. Waviness in Steel Ring--Second Run.

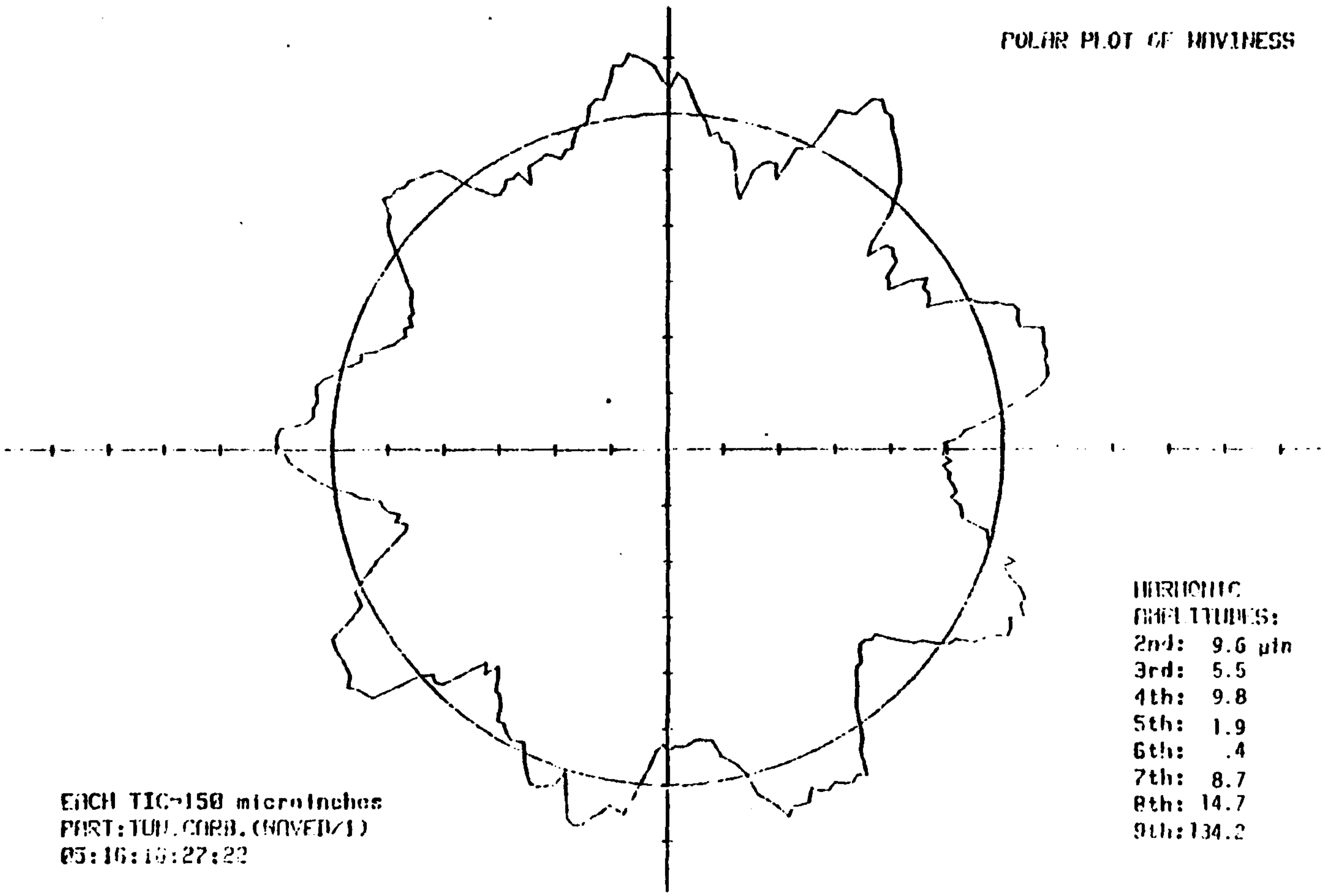

Figure 4-9. Waviness in w-c Ring.

μin., very close to that measured on the steel ring, which is good indication of repeatability. This tungsten carbide was used for the first 100 hour test.

100 Hour Test Results

Test No. 130 was the first 100 hour test run using the new concept of a wavy mating seal ring. The tungsten carbide ring had a wave 134 μin. amplitude at r_o. Figure 4-10 shows the performance during the test. The gap between approximately 62 hours and 112 hours was caused by a shutdown. The torque was, for the most part, unmeasurable, indicating nearly zero throughout the test. The leakage had some erratic behavior at the start, due to surface tension effects within the leakage collection passage. The average leakage for the approximate 100 hours of operation was about 3 cm^3/min.

Wear measurements were taken at four locations around the face of the carbon and compared to those taken before the test. Table 4-2 shows the results. The average wear was about 263 μin. It is believed that the wear occurred during the first few minutes of zeroing and test operation because the faces did not directly conform to each other at the start. Once the seal was in full operation, hydrodynamic effects lifts the faces apart, as evidenced by the low torque readings, and very little if any touching occurred.

Traces of the tungsten carbide face before and after the test showed no signs of wear.

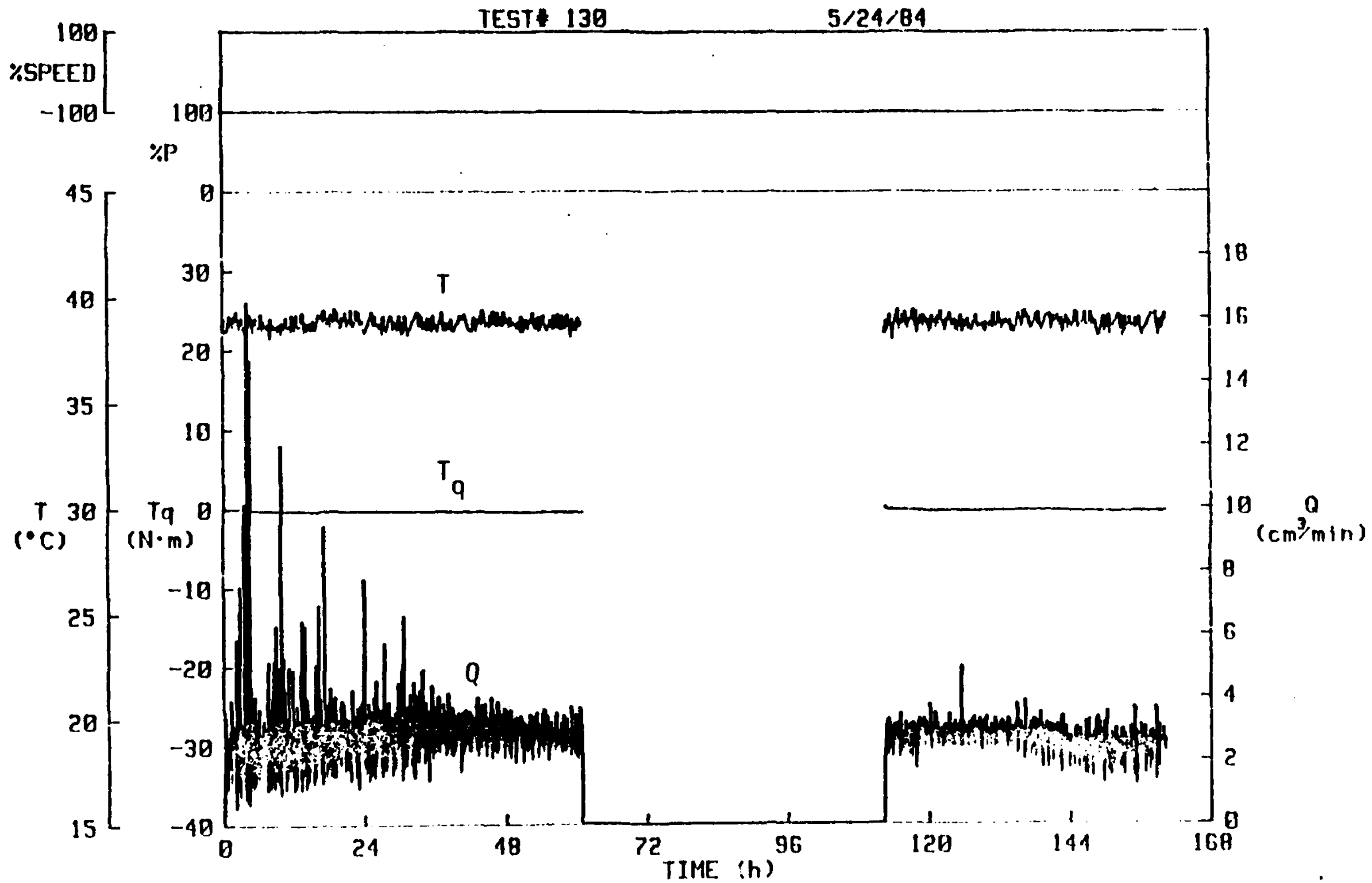

Figure 4-10. Test #130, 500 psi, 1800 RPM, Nine-wave Tungsten Carbide.

TABLE 4-2

Carbon Wear Measurements
Test # 130

Location	Wear
#1	200
#2	400
#3	250
#4	200

Average =263 μin

Conclusions on Third Design

The first test using a fixed wave showed promising results. The wave was too large and needs to be reduced to lower the leakage rate. The surface roughness on the w-c was too large and there is concern that plowing wear will occur when the waviness is reduced. At the time of this writing short term tests are being made using other seal materials and waviness levels in anticipation of making a long term 2000 test. Thus, while results so far look very promising, too little experimental information is available to make final conclusions at this time.

CHAPTER 5

SEAL RING DEFLECTION

In the early days of seal design, seal ring deflection was essentially ignored. Seal rings were lapped flat and presumed to stay that way during operation. Now it is recognized that seal rings may undergo many different types of deflections, some causing excessive leakage and others allowing the seal to operate more effectively.

In this chapter no comprehensive review of seal deflection will be made; the subject would occupy several chapters of a book. Instead the more recent developments obtained under this research program will be presented in depth. These developments focus primarily on the prediction of whether or not seal rings will flatten out against each other in operation so as to minimize leakage. Theory is developed, tools are established, and many calculations on real seals are made and presented. It is thought that given these methods, much insight into the problem of seal leakage as related to deflection can be obtained, and such leakage can be minimized by well founded design changes.

Ring Finite Element

It was determined earlier in this investigation that a ring finite element was needed in which in-plane and out-of-plane forces and deflections are coupled by a non-zero product of inertia term. Such a finite element would serve as a basis for solving all types of ring deflection problems including a special class of two ring contact

problems. A survey of the literature indicated that the development of an element of this type had not been published.

Thus, such a ring finite element was derived and published in a previous report [6], thesis [28], and paper [19]. The ring FEM will be briefly described here so that subsequent developments in this report are more clear. Figure 5-1 shows a ring with all of the possible types of loading shown. Figure 5-2 shows a segment of the ring and all of the internal and external moments and forces acting on it. Figure 5-2 serves as a basis for writing six equations of equilibrium for the ring segment. Using these equations and stress resultant-displacement relationships [34,39] allows one to derive the generalized relationship between the stress resultants and the displacements for an arbitrary segment of the ring--the stiffness matrix in the finite element method. Figure 5-3 shows the element, the end forces and moments, and the displacements. The generalized displacement and force vectors are given by

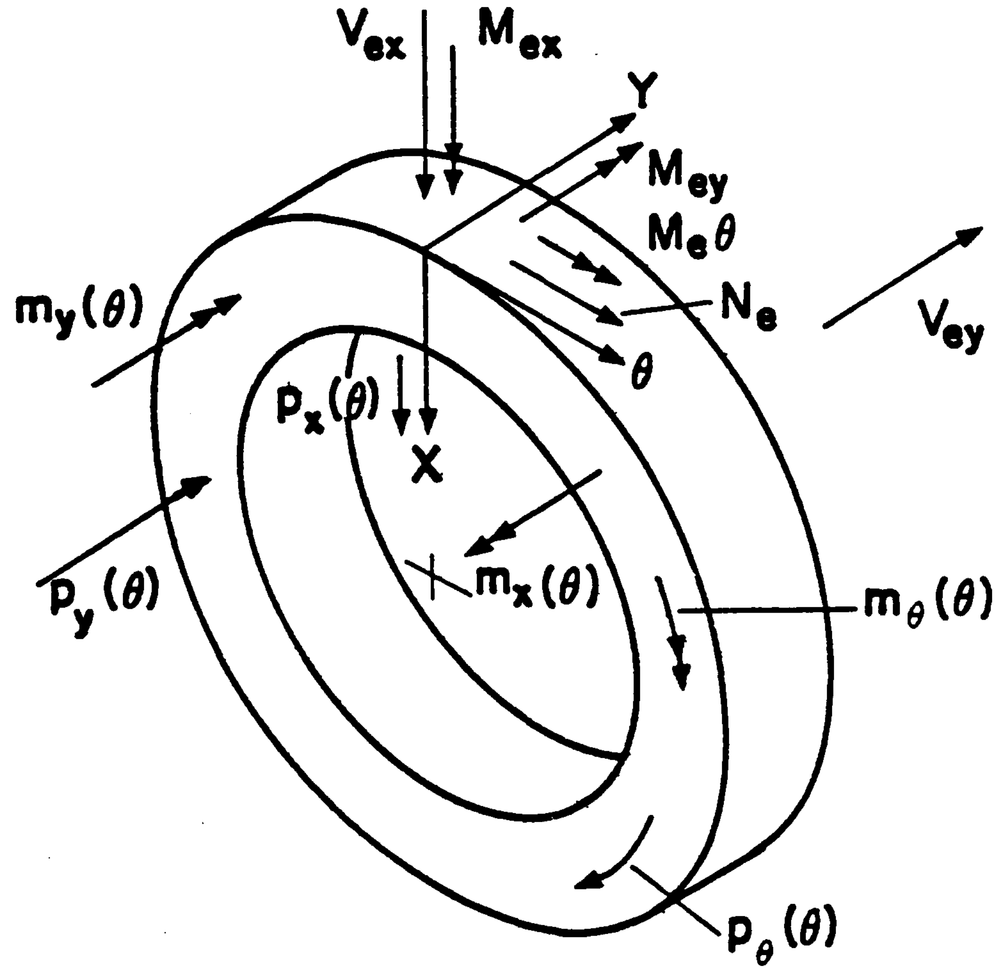

Figure 5-1. Loads on a Ring.

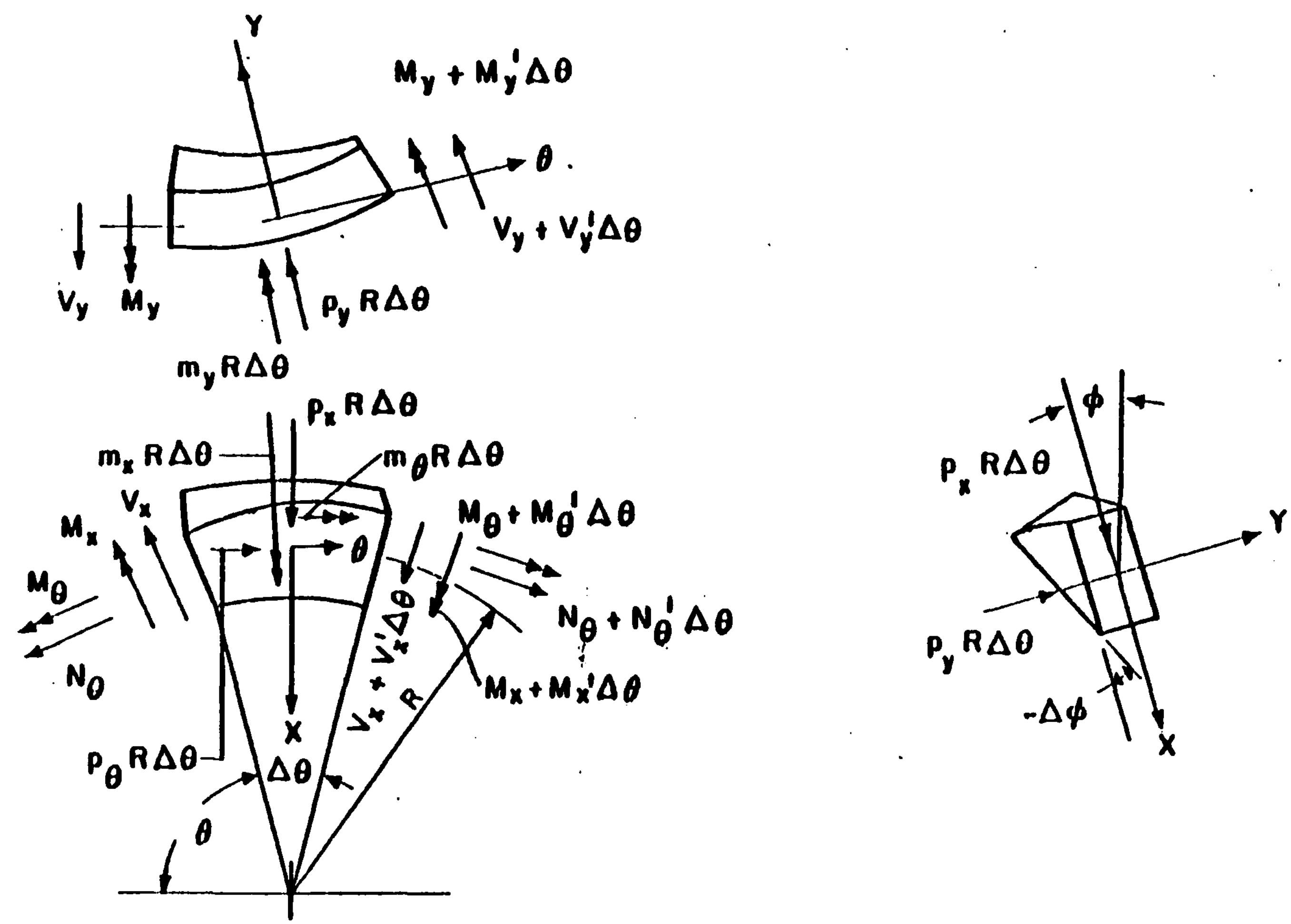

Figure 5-2. Ring Geometry and Definition.

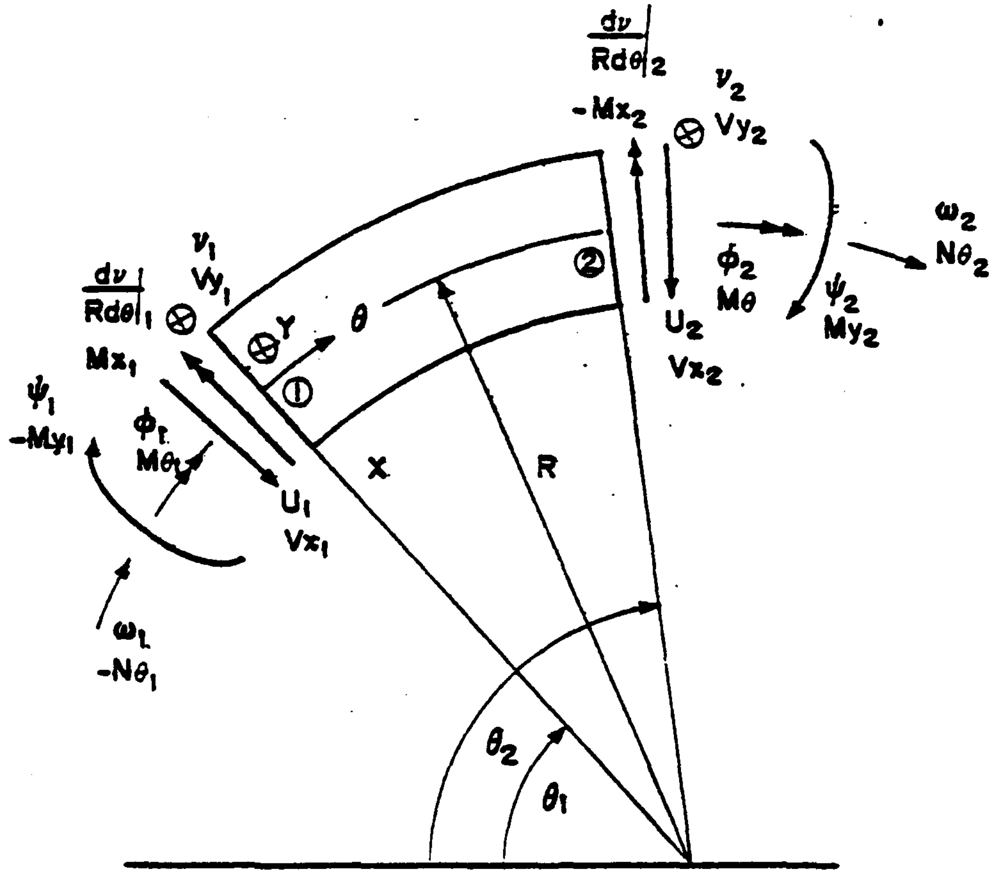

Figure 5-3. Ring Finite Element.

$$[\delta] = \begin{bmatrix} u_1 \\ v_1 \\ w_1 \\ \frac{v_1'}{R} \\ \psi_1 \\ \phi_1 \\ u_2 \\ v_2 \\ w_2 \\ \frac{v_2'}{R} \\ \psi_2 \\ \phi_2 \end{bmatrix} \qquad (5-1) \qquad\qquad [F] = \begin{bmatrix} -V_{x_1} \\ -V_{y_1} \\ -N_{\theta_1} \\ M_{x_1} \\ -M_{y_1} \\ -M_{\theta_1} \\ V_{x_2} \\ V_{y_2} \\ N_{\theta_2} \\ -M_{x_2} \\ M_{y_2} \\ M_{\theta_2} \end{bmatrix} \qquad (5-2)$$

The stiffness matrix [K] is defined by the relationship between forces and displacements:

$$[F] = [K]\,[\delta]\ . \qquad (5-5)$$

The previous work provided two essential matrix equations shown on the next two pages. Equations [5-4] and [5-5] relate the force and deflection vectors to section properties and the arbitrary constants of the solution to the differential equations. Repeating

$$[A]\,[G] = [\delta]\ , \qquad (5-3)$$

$$\frac{EJ_x}{R^2}\,[D]\,[G] = [F]\ . \qquad (5-4)$$

$$
[A]\,[G] = [\delta]
$$

$$
\begin{bmatrix}
0 & 0 & -Q\theta_1\cos\theta_1 & Q\theta_1\sin\theta_1 & -P\theta_1\sin\theta_1 & -P\theta_1\cos\theta_1 & P & -Q\theta_1\cos\theta_1 & Q\theta_1\sin\theta_1 & P\sin\theta_1 & P\cos\theta_1 & 0 \\
1 & \theta_1 & \sin\theta_1 & \cos\theta_1 & \theta_1\sin\theta_1 & \theta_1\cos\theta_1 & 0 & 0 & 0 & 0 & 0 & 0 \\
0 & 0 & -Q(\cos\theta_1 + \theta_1\sin\theta_1) & Q(\sin\theta_1 - \theta_1\cos\theta_1) & -P(\sin\theta_1 - \theta_1\cos\theta_1) & -P(\cos\theta_1 + \theta_1\sin\theta_1) & S\theta_1 & -Q(\cos\theta_1 + \theta_1\sin\theta_1) & Q(\sin\theta_1 - \theta_1\cos\theta_1) & -P\cos\theta_1 & P\sin\theta_1 & 1 \\
0 & \frac{1}{R} & \frac{1}{R}\cos\theta_1 & -\frac{1}{R}\sin\theta_1 & \frac{1}{R}(\theta_1\cos\theta_1 + \sin\theta_1) & \frac{1}{R}(-\theta_1\sin\theta_1 + \cos\theta_1) & 0 & 0 & 0 & 0 & 0 & 0 \\
0 & 0 & -\frac{2}{R}Q\cos\theta_1 & \frac{2}{R}Q\sin\theta_1 & -\frac{2}{R}P\sin\theta_1 & -\frac{2}{R}P\cos\theta_1 & \frac{S}{R}\theta_1 & -\frac{2}{R}Q\cos\theta_1 & \frac{2}{R}Q\sin\theta_1 & 0 & 0 & \frac{1}{R} \\
0 & 0 & 0 & 0 & -\frac{1}{R}\theta_1\sin\theta_1 & -\frac{1}{R}\theta_1\cos\theta_1 & \frac{1}{R} & \frac{1}{R}\sin\theta_1 & \frac{1}{R}\cos\theta_1 & 0 & 0 & 0 \\
0 & 0 & -Q\theta_2\cos\theta_2 & Q\theta_2\sin\theta_2 & -P\theta_2\sin\theta_2 & -P\theta_2\cos\theta_2 & P & -Q\theta_2\cos\theta_2 & Q\theta_2\sin\theta_2 & P\sin\theta_2 & P\cos\theta_2 & 0 \\
1 & \theta_2 & \sin\theta_2 & \cos\theta_2 & \theta_2\sin\theta_2 & \theta_2\cos\theta_2 & 0 & 0 & 0 & 0 & 0 & 0 \\
0 & 0 & -Q(\cos\theta_2 + \theta_2\sin\theta_2) & Q(\sin\theta_2 - \theta_2\cos\theta_2) & -P(\sin\theta_2 - \theta_2\cos\theta_2) & -P(\cos\theta_2 + \theta_2\sin\theta_2) & S\theta_2 & -Q(\cos\theta_2 + \theta_2\sin\theta_2) & Q(\sin\theta_2 - \theta_2\cos\theta_2) & -P\cos\theta_2 & P\sin\theta_2 & 1 \\
0 & \frac{1}{R} & \frac{1}{R}\cos\theta_2 & -\frac{1}{R}\sin\theta_2 & \frac{1}{R}(\theta_2\cos\theta_2 + \sin\theta_2) & \frac{1}{R}(-\theta_2\sin\theta_2 + \cos\theta_2) & 0 & 0 & 0 & 0 & 0 & 0 \\
0 & 0 & -\frac{2}{R}Q\cos\theta_2 & \frac{2}{R}Q\sin\theta_2 & -\frac{2}{R}P\sin\theta_2 & -\frac{2}{R}P\cos\theta_2 & \frac{S}{R}\theta_2 & -\frac{2}{R}Q\cos\theta_2 & \frac{2}{R}Q\sin\theta_2 & 0 & 0 & \frac{1}{R} \\
0 & 0 & 0 & 0 & -\frac{1}{R}\theta_2\sin\theta_2 & -\frac{1}{R}\theta_2\cos\theta_2 & \frac{1}{R} & \frac{1}{R}\sin\theta_2 & \frac{1}{R}\cos\theta_2 & 0 & 0 & 0
\end{bmatrix}
\begin{bmatrix} G_1 \\ G_2 \\ G_3 \\ G_4 \\ G_5 \\ G_6 \\ G_7 \\ G_8 \\ G_9 \\ G_{10} \\ G_{11} \\ G_{12} \end{bmatrix}
=
\begin{bmatrix} u_1 \\ v_1 \\ w_1 \\ \frac{1}{R}\frac{dv}{d\eta}\Big|_1 \\ \psi_1 \\ \phi_1 \\ u_2 \\ v_2 \\ w_2 \\ \frac{1}{R}\frac{dv}{d\eta}\Big|_2 \\ \psi_2 \\ \phi_2 \end{bmatrix}
$$

$$
P = \frac{J_x}{J_{xy}}, \quad Q = \frac{1}{2}\frac{J_x}{J_{xy}}\left(1 + \frac{1}{\lambda}\right), \quad S = \left(1 + \frac{J_y}{aR^2}\right)\frac{J_x}{J_{xy}} - \frac{J_{xy}}{aR^2}
$$

Equation (5-3)

$$
\frac{EJ_x}{R^2}
\underbrace{\begin{bmatrix}
0 & 0 & \frac{V}{R}\cos\theta_1 & -\frac{V}{R}\sin\theta_1 & \frac{2U}{R}\sin\theta_1 & \frac{2U}{R}\cos\theta_1 & 0 & \frac{V}{R}\cos\theta_1 & -\frac{V}{R}\sin\theta_1 & 0 & 0 & 0 \\
0 & -\frac{1}{R\Lambda} & 0 & 0 & 0 & 0 & 0 & 0 & 0 & 0 & 0 & 0 \\
0 & 0 & \frac{V}{R}\sin\theta_1 & \frac{V}{R}\cos\theta_1 & -\frac{2U}{R}\cos\theta_1 & \frac{2U}{R}\sin\theta_1 & 0 & \frac{V}{R}\sin\theta_1 & \frac{V}{R}\cos\theta_1 & 0 & 0 & 0 \\
0 & 0 & -\frac{1}{\Lambda}\sin\theta_1 & -\frac{1}{\Lambda}\cos\theta_1 & 0 & 0 & 0 & -\frac{1}{\Lambda}\sin\theta_1 & -\frac{1}{\Lambda}\cos\theta_1 & 0 & 0 & 0 \\
0 & 0 & -V\sin\theta_1 & -V\cos\theta_1 & 2U\cos\theta_1 & -2U\sin\theta_1 & -U & -V\sin\theta_1 & -V\cos\theta_1 & 0 & 0 & 0 \\
0 & -\frac{1}{\Lambda} & -\frac{1}{\Lambda}\cos\theta_1 & \frac{1}{\Lambda}\sin\theta_1 & 0 & 0 & 0 & -\frac{1}{\Lambda}\cos\theta_1 & \frac{1}{\Lambda}\sin\theta_1 & 0 & 0 & 0 \\
0 & 0 & -\frac{V}{R}\cos\theta_2 & \frac{V}{R}\sin\theta_2 & -\frac{2U}{R}\cos\theta_2 & -\frac{2U}{R}\cos\theta_2 & 0 & -\frac{V}{R}\cos\theta_2 & \frac{V}{R}\sin\theta_2 & 0 & 0 & 0 \\
0 & \frac{1}{R\Lambda} & 0 & 0 & 0 & 0 & 0 & 0 & 0 & 0 & 0 & 0 \\
0 & 0 & -\frac{V}{R}\sin\theta_2 & -\frac{V}{R}\cos\theta_2 & \frac{2U}{R}\cos\theta_2 & -\frac{2U}{R}\sin\theta_2 & 0 & -\frac{V}{R}\sin\theta_2 & -\frac{V}{R}\cos\theta_2 & 0 & 0 & 0 \\
0 & 0 & \frac{1}{\Lambda}\sin\theta_2 & \frac{1}{\Lambda}\cos\theta_2 & 0 & 0 & 0 & \frac{1}{\Lambda}\sin\theta_2 & \frac{1}{\Lambda}\cos\theta_2 & 0 & 0 & 0 \\
0 & 0 & V\sin\theta_2 & V\cos\theta_2 & -2U\cos\theta_2 & 2U\sin\theta_2 & U & V\sin\theta_2 & V\cos\theta_2 & 0 & 0 & 0 \\
0 & \frac{1}{\Lambda} & \frac{1}{\Lambda}\cos\theta_2 & -\frac{1}{\Lambda}\sin\theta_2 & 0 & 0 & 0 & \frac{1}{\Lambda}\cos\theta_2 & -\frac{1}{\Lambda}\sin\theta_2 & 0 & 0 & 0
\end{bmatrix}}_{[D]}
\underbrace{\begin{bmatrix} G_1 \\ G_2 \\ G_3 \\ G_4 \\ G_5 \\ G_6 \\ G_7 \\ G_8 \\ G_9 \\ G_{10} \\ G_{11} \\ G_{12} \end{bmatrix}}_{[G]}
=
\underbrace{\begin{bmatrix} -V_{x1} \\ -V_{y1} \\ -N_{\theta1} \\ M_{x1} \\ -M_{y1} \\ -M_{\theta1} \\ V_{x2} \\ V_{y2} \\ N_{\theta2} \\ -M_{x2} \\ M_{y2} \\ M_{\theta2} \end{bmatrix}}_{[\Gamma]}
$$

$$U = \frac{J_x}{J_{xy}} - \frac{J_{xy}}{J_x}\,, \qquad V = \frac{J_x}{J_{xy}}\left(1 + \frac{1}{\Lambda}\right) - \frac{J_{xy}}{J_x}$$

Equation (5-4)

Given (5-5) above Equations (5-4) and (5-5) may be solved to give

$$[K] = \frac{EJ_x}{R^2} [D] [A]^{-1} . \tag{5-6}$$

Then the stiffness matrix for the coupled ring problem is readily evaluated as the product of known matrix D and the inverse of known matrix A. It is useful to observe that if $\theta_2 - \theta_1$ is constant and the section properties are constant, [K] is constant--a very useful property when assembling a global stiffness matrix.

If $J_{xy} = 0$ the above equations may not be used directly to solve for K. However one may numerically allow $J_{xy} \rightarrow 0$ to get a satisfactory result. Also, when $J_{xy} = 0$ one actually gets two uncoupled cases, and these have been solved exactly and are presented in References [6], [19], and [28].

The element derived is readily assembled into a closed circular ring or a segment of a ring. Elements of various sizes ($\theta_2 - \theta_1$) can be used as needed. Assembly is straightforward in that no coordinate transformations are needed. Also, just as in common straight beam elements, the element derived is the exact solution to the governing equations. Thus, if no distributed loads are present, then the element size can be as large as possible while still accommodating concentrated loads. If distributed loads are present, then element size must be made relatively small to give a good approximation. On two examples for distributed load cases, it was found that 40 elements gives deflection results within a few percent of that predicted by exact theory.

Beyond these points, assembly is straightforward and needs no further discussion.

Comparison to Other Results

Solutions to two coupled problems were found in the literature and have been used to check the accuracy of the derived element.

The first check is based on earlier analytical work by Lebeck [34]. The problem is shown in Figure 5-4. A circular ring is subjected to two tangential concentrated loads. These are equilibrated by a distributed tangential load. For $J_{xy} \neq 0$, an out-of-plane deflection v is produced by this loading. For a completely arbitrary selection of section properties and using 36 elements, the deflection was found using the element derived. The deflection was compared to that found analytically and given in Reference [34]. Agreement was exact to four significant places. Since both the previous solution and the present solution are based on the same equations, this agreement verifies the correctness of the derivations of the element only, not the beam theory used.

A second check problem was taken from the work of Meck [40]. Using the energy method, Meck derives the equation for the three-dimensional displacement of the end of a curved nonsymmetrical beam (other end fixed) caused by completely arbitrary loading. The problem is shown in Figure 5-5. Using the coupled finite element given and arbitrary section properties, a solution was found for all displacements u, v, w, ψ, v', ϕ for each of the loads shown. Agreement with Meck's solution

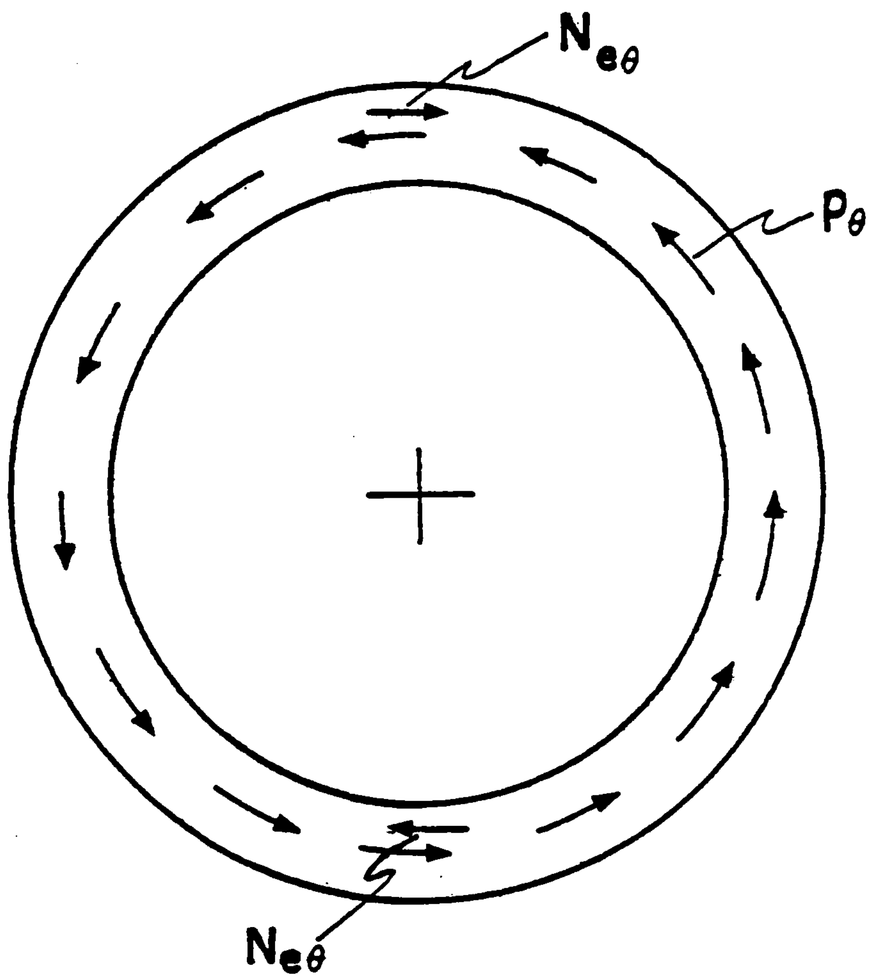

Figure 5-4. Check Problem 1.

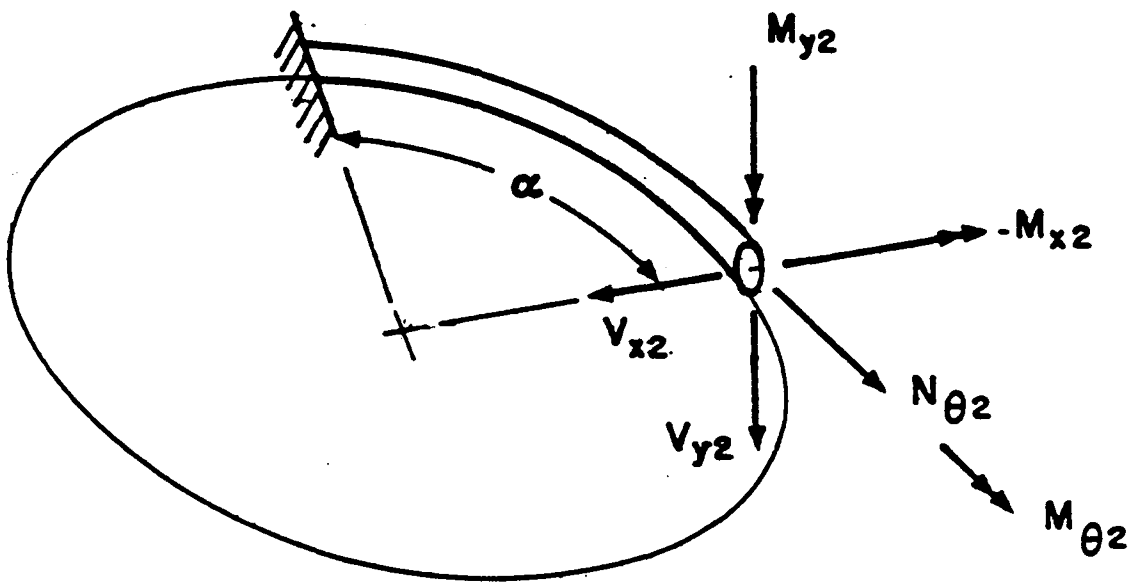

Figure 5-5. Check Problem 2.

was excellent thus verifying the correctness of the beam theory used relative to other beam theory as well as the finite element itself.

A third check was made experimentally using the aluminum ring shown in Figure 5-6. The ring was loaded by two radial loads through the centroid. Before loading and after loading measurements of deflection were made at locations 1, 2, and 3 perpendicular to the surface using a precision rotary table and precision displacement transducer. Data was analyzed to pick out on the second harmonic net distortions in each case. The experimental results are shown in Table 5-1. The results show clearly how an out-of-plane deflection is produced by the in-plane load.

The theoretical results shown were obtained using an 8 element assembly and finding the second harmonic component of the various displacements. Agreement on the in-plane deflections is reasonable. The out-of-plane deflection error is larger. There are numerous sources of error when comparing this experiment to theory. First, the shear center does not coincide with the centroid as is assumed in the theory. Second, exact material properties for the particular alloys used were not measured. Third, only an approximate formula was used to find J_θ. Fourth, the measurements themselves are good only to a few percent. Thus, without considerable refinement in theory and experiment, one probably has as good an agreement as can be expected; and the experiment does generally verify the coupling described by the theory.

The coupled ring finite element will now be used in various developments.

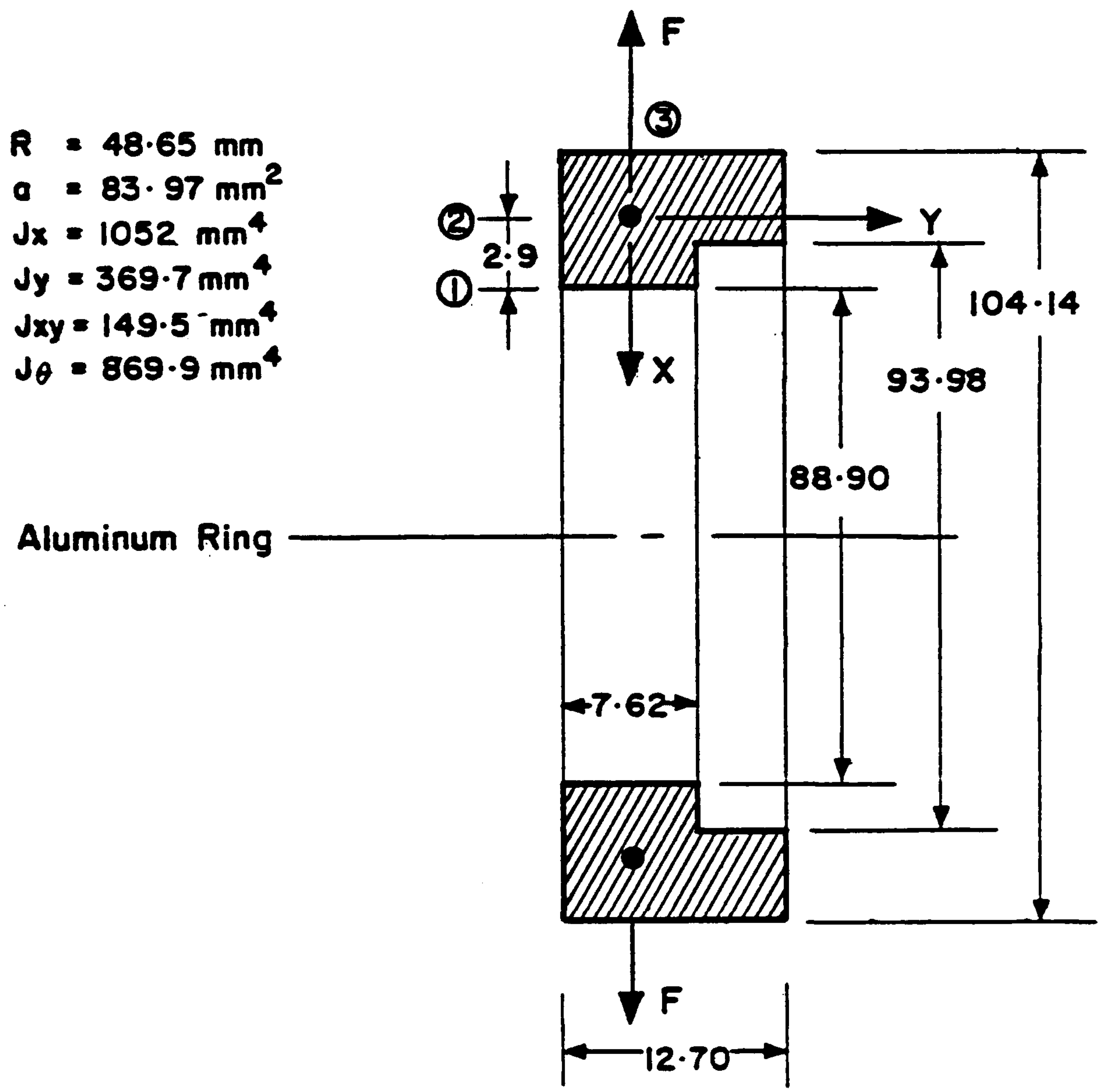

Figure 5-6. Test Ring.

TABLE 5-1

Experimental Results

111 N Radial Load - 2nd Harmonic Amplitudes

Location	1	2	3	2 - 1
Experiment	6.27 μm	6.63 μm	41.48 μm	0.36 μm
Theory	4.90	5.21	36.93	0.31
% Error	22	21	11	14

Single Ring Deflection by Formulas

While finite element methods are acknowledged as being accurate and capable of handling complex problems, many times it is useful to be able to calculate ring deflection for seals using easily available formulas. Many formulas have been derived during the early period of this seal research and are presented in Reference [34] and [39]. Since that time several additional useful formulas have been derived and the formulas have been checked using the FEM program described in the next section.

The complete set of formulas available at present is presented here. These cases are those which have been found to be useful for seal ring calculations. Particular note of equilibrium loads must be made. They were chosen to most closely represent what will happen as faces touch together in a seal. The deflection formulas for v only (out of plane of the face) deflections are given in Table 5-2. ϕ is also important but such formulas are not available at this time.

Single Ring Deflections by FEM

The ring element described in the first section of this chapter was used as a basis for writing a general ring finite element program. The program is described in detail in Appendix B. The program is set up for equal element size with constant section properties but can be readily modified to deal with variable elements so that a non-axisymmetric ring as well as non-axisymmetric loads can be considered. The program calculates the Fourier series coefficients of the primary deflections in recognition of the importance of these deflections for

TABLE 5-2

Ring Deflection

Type Load	Equilibrium Load	Waviness	Equation for displacement
Two equal and opposite moments $M_{e\theta}$ located 180° apart[1]	None required	$\begin{bmatrix} v_2 \\ v_4 \\ v_6 \end{bmatrix} = \begin{bmatrix} 0.0707 \\ 0.0028 \\ 0.0005 \end{bmatrix} \frac{M_{e\theta}R^2}{EJ_x}(1 + A)$	$v = \frac{M_{e\theta}R^2}{EJ_x}(1 + A)\left[\sin\theta + (\frac{\pi}{2} - \theta)(\cos\theta)\right]$ $0 \le \theta \le \pi$
Two equal and opposite moments M_{ex} located 180° apart[1]	None required	$\begin{array}{cccc} A = 2 & 4 & 6 & 8 \end{array}$ $\begin{bmatrix} v_2 \\ v_4 \\ v_6 \end{bmatrix} = \begin{bmatrix} 0.212 & 0.283 & 0.354 & 0.424 \\ 0.013 & 0.014 & 0.016 & 0.017 \\ 0.003 & 0.003 & 0.004 & 0.004 \end{bmatrix} \frac{M_{ex}R^2}{EJ_x}$	$v = \frac{M_{ex}R^2}{EJ_x}\left[A(\frac{\theta}{\pi} - \frac{1}{2}) + \frac{1}{2}A\cos\theta + \frac{1}{4}(A + 1)(\theta - \frac{\pi}{2})\sin\theta\right]$ $0 \le \theta \le \pi$
Single $M_{e\theta}$[1]	Sinusoidal varying pressure p_y around face	$\begin{bmatrix} v_2 \\ v_3 \\ v_4 \\ v_5 \end{bmatrix} = \begin{bmatrix} 0.0354 \\ 0.0050 \\ 0.0014 \\ 0.0006 \end{bmatrix} \frac{M_{e\theta}R^2}{EJ_x}(1 + A)$	$v = \frac{M_{e\theta}R^2}{EJ_x}(1 + A)\left[-\frac{1}{8\pi}\theta^2\cos\theta + \frac{\pi}{16} - \frac{1}{4}\sin\theta - \frac{\pi}{16}\cos\theta + \frac{1}{4\pi}\theta\sin\theta + \frac{1}{4}\theta\cos\theta\right]$ $0 \le \theta \le 2\pi$
Single M_{ex}[1]	Sinusoidal varying pressure p_y around face	$\begin{array}{cccc} A = 2 & 4 & 6 & 8 \end{array}$ $\begin{bmatrix} v_2 \\ v_3 \\ v_4 \\ v_5 \end{bmatrix} = \begin{bmatrix} 0.106 & 0.141 & 0.177 & 0.212 \\ 0.018 & 0.022 & 0.025 & 0.028 \\ 0.006 & 0.007 & 0.008 & 0.008 \\ 0.003 & 0.003 & 0.003 & 0.004 \end{bmatrix} \frac{M_{ex}R^2}{EJ_x}$	$v = \frac{M_{ex}R^2}{EJ_x}\left[-\frac{1 + A}{8}\theta^2\sin\theta - \frac{A}{2} + \frac{A}{2\pi}\theta + \frac{A}{2}\cos\theta + \frac{(1 + A)}{4}\theta\sin\theta - \frac{A}{2\pi}\theta\cos\theta\right]$ $0 \le \theta \le 2\pi$
Single V_{ey}[1]	Sinusoidal varying plus a constant pressure p_y at face	$\begin{bmatrix} v_2 \\ v_3 \\ v_4 \\ v_5 \end{bmatrix} = \begin{bmatrix} 0.0532 & 0.0707 & 0.0884 & 0.1060 \\ 0.0061 & 0.0072 & 0.0083 & 0.0094 \\ 0.0016 & 0.0018 & 0.0020 & 0.0021 \\ 0.0006 & 0.0006 & 0.0007 & 0.0007 \end{bmatrix} \frac{V_{ey}R^3}{EJ_x}$	$v = \frac{V_{ey}R^3}{EJ_x}\left[-\frac{(A + 1)}{8\pi}\theta^2\cos\theta - \frac{A}{4\pi}\theta^2 + \frac{A}{2}\theta + \frac{3A + 1}{4\pi}\theta\sin\theta + \frac{A + 1}{4}\theta\cos\theta - \frac{(A - 1)\pi}{16} - \frac{(3A + 1)}{4}\sin\theta + \frac{(A - 1)\pi}{16}\cos\theta\right]$ $0 \le \theta \le 2\pi$
n Forces V_{ey} located $\alpha = 2\pi/n$ apart[1]	Uniform face load p_y	$\begin{bmatrix} v_2 \\ v_3 \\ v_4 \\ v_5 \\ v_6 \end{bmatrix} = \begin{bmatrix} 0.0531 & 0.0707 & 0.0884 & 0.1061 \\ 0.0061 & 0.0072 & 0.0083 & 0.0094 \\ 0.0016 & 0.0018 & 0.0019 & 0.0021 \\ 0.0006 & 0.0006 & 0.0007 & 0.0007 \\ 0.0003 & 0.0003 & 0.0003 & 0.0003 \end{bmatrix}^3 \frac{n V_{ey}R^3}{EJ_x}$	$v = \frac{V_{ey}R^3}{EJ_x}\left[\frac{A}{2}\theta(\frac{\theta}{\alpha} - 1) + \frac{\frac{A + 1}{4}(6\sin\alpha + 2\alpha) - \sin\alpha}{2(\cos\alpha - 1)}(1 - \cos\theta) - \frac{3A + 1}{4}\sin\theta - \frac{A + 1}{4}\frac{\sin\alpha}{\cos\alpha - 1}\theta\sin\theta - \frac{A + 1}{4}\theta\cos\theta\right]$ $0 \le \theta \le \alpha$

TABLE 5-2 (Cont.)

Ring Deflection

Face pressure of n waves of amplitude p_{yo}[1]	None required	$\begin{bmatrix} v_2 \\ v_3 \\ v_4 \\ v_5 \\ v_6 \end{bmatrix} = \begin{array}{cccc} A = 2 & 4 & 6 & 8 \\ \hline \end{array} \begin{bmatrix} 0.1667 & 0.2222 & 0.2778 & 0.3333 \\ 0.0191 & 0.0226 & 0.0260 & 0.0295 \\ 0.0050 & 0.0056 & 0.0061 & 0.0067 \\ 0.0019 & 0.0020 & 0.0022 & 0.0023 \\ 0.0009 & 0.0009 & 0.0010 & 0.0010 \end{bmatrix}$ [4]	$v = \frac{p_{yo}R^4}{EJ_x}\left[\frac{A + n^2}{n^2(n^2-1)^2}\right]\cos n\theta$ $0 \leq \theta \leq 2\pi$
Two equal and opposite loads V_{ex} located 180° apart[2]	None required	$\begin{bmatrix} v_2 \\ v_4 \\ v_6 \end{bmatrix} \begin{bmatrix} 0.0707 \\ 0.0028 \\ 0.0005 \end{bmatrix} \frac{V_{ex}R^3J_{xy}}{E(J_xJ_y - J_{xy}^2)}$	$v = \frac{V_{ex}R^3J_{xy}}{4E(J_xJ_y - J_{xy}^2)}\left(-\theta\cos\theta - \frac{\pi}{2} + \sin\theta + \frac{\pi}{2}\cos\theta\right)$ $0 \leq \theta \leq \frac{\pi}{2}$
Two tangential loads $N_{e\theta}$ located 180° apart[2]	Uniform tangential friction p_θ at face	$\begin{bmatrix} v_2 \\ v_4 \\ v_6 \end{bmatrix} \begin{bmatrix} 0.0354 \\ 0.0007 \\ 0.0000 \end{bmatrix} \frac{N_{e\theta}R^3J_{xy}}{E(J_xJ_y - J_{xy}^2)}$	$v = \frac{N_{e\theta}R^3J_{xy}}{E(J_xJ_y - J_{xy}^2)}\left(-\frac{\theta}{\pi} + \frac{1}{2} - \frac{1}{4}\theta\sin\theta + \frac{\pi}{8}\sin\theta - \frac{1}{2}\cos\theta\right)$ $0 \leq \theta \leq \pi$
Two moments M_{ey} located 180° apart[2]	Uniform tangential friction p_θ at face	$\begin{bmatrix} v_2 \\ v_4 \\ v_6 \end{bmatrix} \begin{bmatrix} 0.106 \\ 0.011 \\ 0.003 \end{bmatrix} \frac{M_{ey}R^2J_{xy}}{E(J_xJ_y - J_{xy}^2)}$	$v = \frac{M_{ey}R^2J_{xy}}{E(J_xJ_y - J_{xy}^2)}\left[\frac{\theta}{\pi} + \frac{1}{2}(\cos\theta - 1)\right]$ $0 \leq \theta \leq \pi$

[1] $J_{xy} = 0$.

[2] $J_{xy} \neq 0$.

[3] These are the fundamental harmonics only, e.g., v_4 is not the fourth harmonic resulting from two loads, but in the fourth harmonic resulting from 4 loads.

[4] Only the fundamental harmonic exists here.

seal analysis. It is generally useful for all types of ring deflection problems and has served as a basis for the more complex contact problems discussed later. The program was used to check the Fourier series coefficients of the previous section.

Footnote 1 in the table denotes all cases where the assumption of $J_{xy} = 0$ has been used to simplify the derivation. These formulas are valid even if $J_{xy} \neq 0$ for a first approximation of deflection. The last three cases (footnote 2) were derived specifically for coupled problems where $J_{xy} \neq 0$ couples the in-plane deflection to the out-of-plane deflection or waviness.

In addition to the formulas for deflection the tables provide Fourier series coefficients for each case. The series terms are either all even or all odd depending on the loading case. These data show at a glance the magnitude of the wave caused by a disturbance. The first harmonic is not shown since it represents tilt of the ring which has no meaning in a seal since seals are self-aligning.

Formulas for n - V_{ey} and n waves of p_{yo} are used to study the flattenability or conformability of seal rings. This subject is discussed in detail later in this report.

Simple Seal Contact Model

Seal performance is dramatically affected when the waviness/stiffness combination is such that the faces do not contact all around and leakage gaps develop. Prediction of such gaps in the general case is a complex problem as will be discussed in detail in the next section.

Very useful but simple models of seal contact can also be developed. On the basis of simple harmonic waviness, two formulas given in Table 5-2 can be used to estimate flattenability of a ring in face contact. There are at least two reasonable assumptions which might be made as to how the net flattening load is distributed. For seal rings where waviness is fairly large, the load might be considered as being concentrated at n points equally spaced as shown in Figure 5-7 for n = 2. In this case the individual loads are given by

$$V_{ey} = \frac{F_{net}}{n} . \tag{5-7}$$

Case b in Figure 5-7 shows the net flattening load distributed continuously and sinusoidally. It is readily shown that the maximum amplitude the sine wave can have while maintaining zero or greater contact pressure all around the seal is

$$P_{amplitude} = \frac{F_{net}}{2\pi R} . \tag{5-8}$$

Both of these distributions serve to make useful calculations. The discrete load case gives the maximum flattening which can occur. It is used to compute the net wave in a case where contact will remain at n points even after the wave has been flattened somewhat. On the other hand, case b represents a load which causes the maximum possible waviness for a given net load while still maintaining contact all around the seal. That is, case b can be used to calculate the maximum wave amplitude allowable before some separation of the rings occurs.

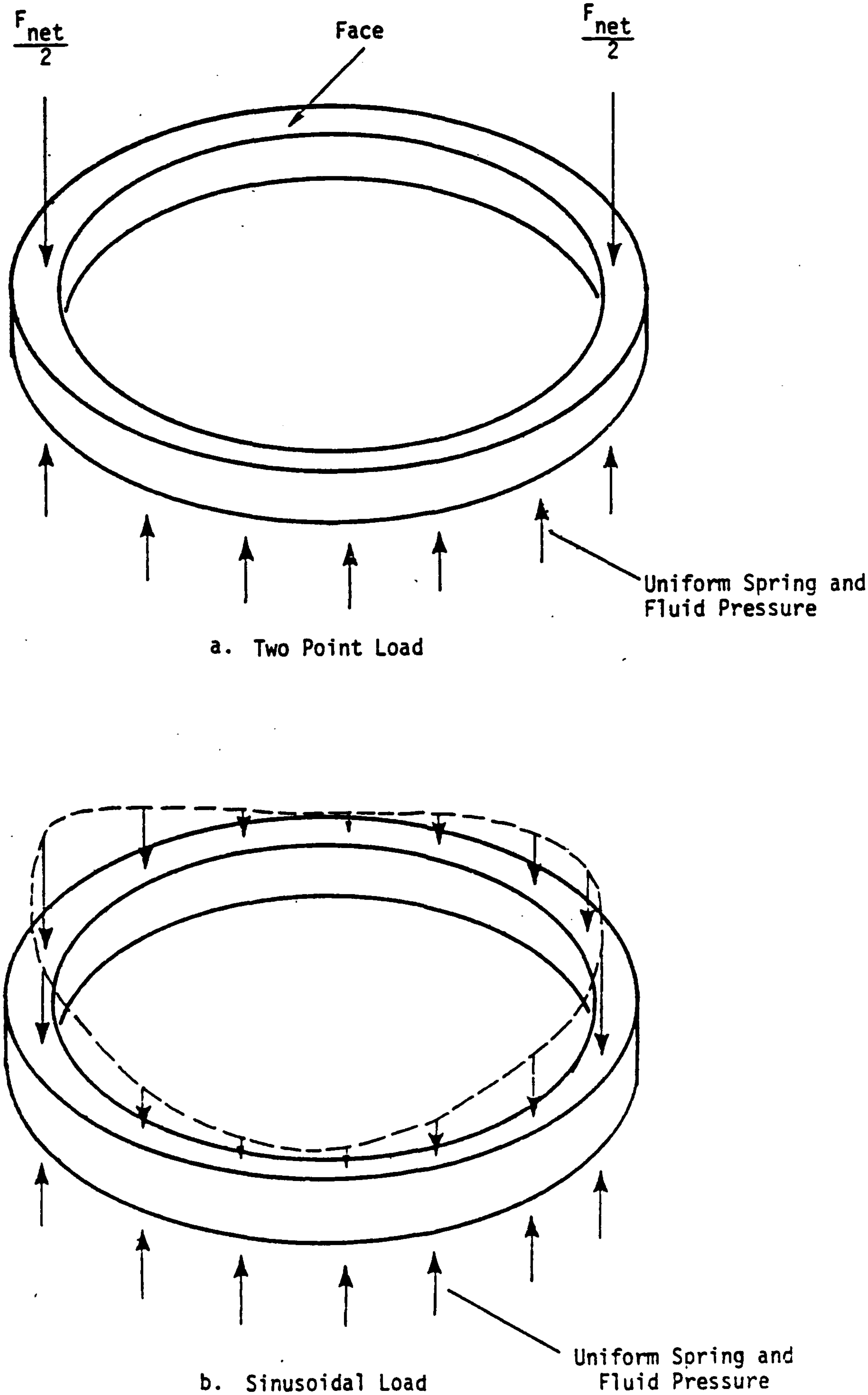

Figure 5-7. Flattening Load Distribution.

Deflection formulas have been derived for both cases using the methods for ring deflection developed in Reference [39]. For case a in Figure 4, there are n equally spaced concentrated loads V_{ey}, balanced by a uniformly distributed load. Case b in Figure 5-7 is for a sinusoidal load balanced by a uniform load. Both cases are given in Table 5-2.

Before the flattening calculations can be made, the net load in the above formulas must be considered. Only a fraction of the total load at the seal faces can act to flatten the seal faces. Assuming for the sake of simplification that the seal faces are neither significantly divergent or convergent or that such effects as caused by face taper average out to zero, the hydrostatic fluid pressure distribution across the face is linear and remains so regardless of film thickness. Therefore with respect to hydrostatic fluid pressure load support of the faces, the seal has no axial stiffness, and given the previous assumption, no circumferential variations in the hydrostatic fluid pressure load support can occur in spite of changes in film thickness. Therefore, the hydrostatic fluid pressure load support does not help to flatten out the seal faces. Only the mechanical or hydrodynamic part of the load support (that which must be provided to support the total load) can flatten a wave. To express this load in terms of a formula for an outside pressurized seal with zero inside pressure, the total load on the seal faces is

$$F_{total} = \pi(r_o^2 - r_i^2)\,(Bp_o + p_s)\ . \tag{5-9}$$

The hydrostatic load support is 1/2 p_o average. After subtracting,

$$F_{net} = \pi(r_o^2 - r_i^2)\ ((B - 0.5)\ p_o + p_s)\ . \tag{5-10}$$

Using the above formulas and Table 5-2, one can assess the flattenability of seal rings. Detailed studies using these simple formulas have been carried out in References [22], [41], and [42].

Two Ring Contact Model

For simple rings with constant cross sectional properties, no splits, and simple harmonic deflections, the face loading distribution required for continuous contact is relatively easily obtained as just shown. However, for more realistic conditions related to the cross section properties and more complex distortions, finding the correct distribution of face loading and seal gap becomes a very difficult problem. This development is presented in detail in Reference [21] and it will be summarized here.

The state of the art of predicting face loading in complex cases is illustrated by a report by Noell, Rippel, and Niemkiewicz of the Franklin Institute [43]. An evaluation of out-of-plane seal distortion caused by the nonuniformity of the joints in a split seal was made using finite elements applied to the rings and faces comprising the seal assembly. It is shown how a nonuniform cross section near the joints causes out-of-flatness of the faces. In the report the contact between the seal faces is modeled by springs where tensile stresses across the faces are allowed. Since such stresses cannot occur in

reality, the computed results do not predict how much and where the faces separate. Thus, the utility of the work to date is limited.

Theory

To define the problem of interest, one is trying to find the resultant gap, as a function of angular position, formed between two rings of arbitrary face profile and arbitrary geometry in a tangential direction, as they are loaded one upon the other by an arbitrary load. The variation in sealing gap results from two sources: 1) non-axisymmetric initial displacement (waviness) and 2) non-axisymmetric deflection due to non-axisymmetric loads (including face contact) or non-axisymmetric section properties. The loads arise from the contact itself, spring loads, hydrostatic loads, and drive force loads.

The problem can best be illustrated by looking at a projection of the circumferential centroidal axes of two rings as shown in Figure 5-8. Waviness of the surface may arise from production processes themselves or other types of distortion and creep. It is assumed that the centroidal axes initially have no distortion. As the two seal rings are brought together by the closing load, contact is initially established at three points. As the load is increased the contact points become regions and there may be any number of such regions. If the load is large enough and the waviness is not too steep, the gap may close around the entire seal and the contact pressure will be circumferentially variable. Alternatively, if the load is not large enough, regions of a seal gap will exist as shown in Figure 5-8.

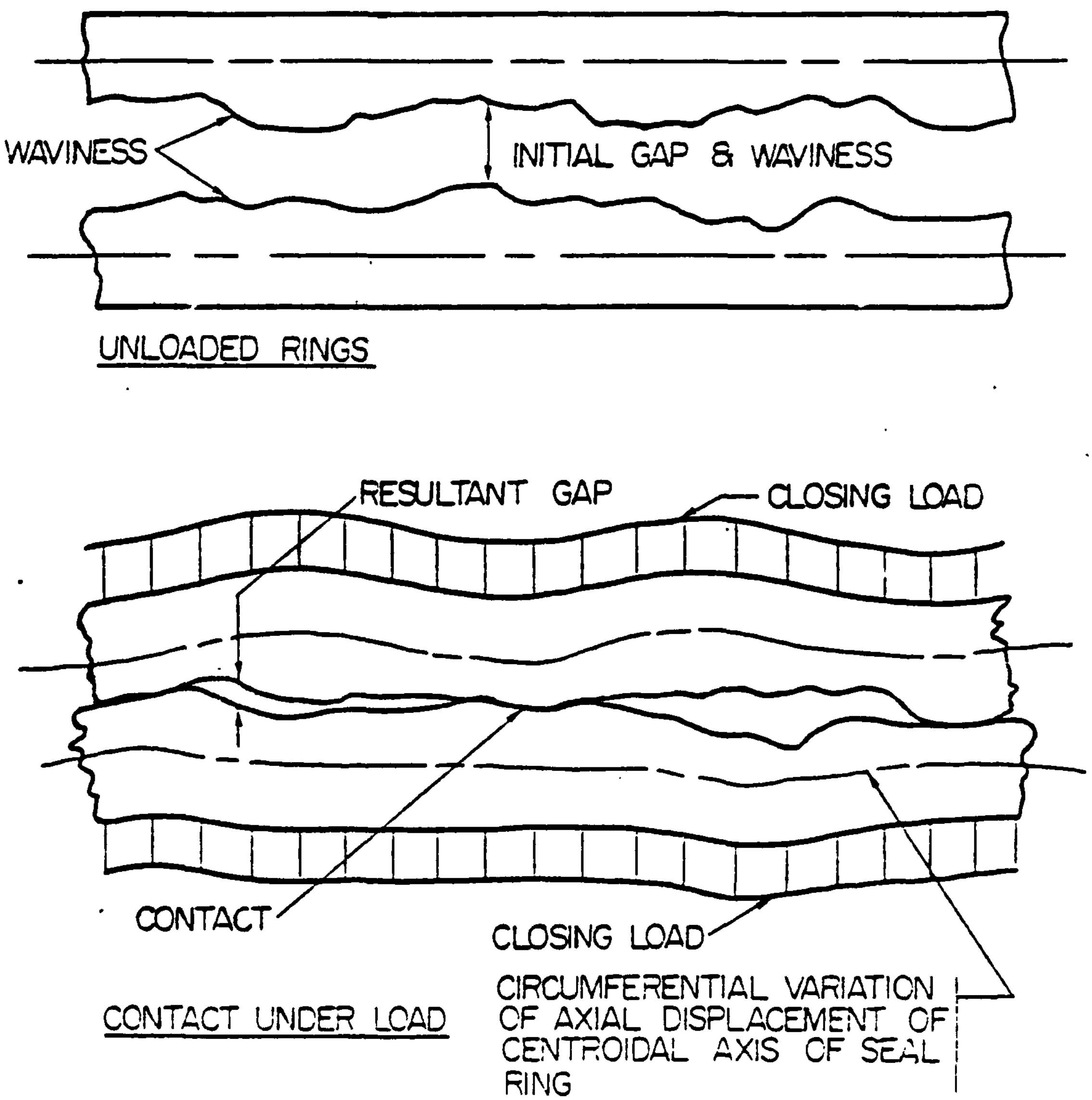

Figure 5-8. Contact of Two Rings.

There are two major features needed in the model to predict such contact/gaps. First, one needs a very general tool to predict deflections in arbitrarily loaded variable cross section rings. Second, as the two rings are brought together to contact, the pressure distribution must be predicted. The ring finite element described previously has been used to take care of the first feature. The second feature represents a specific type of contact problem. Such contact problems have been treated previously using finite element methods. These models are put together here to find the needed solutions.

The contact model assumes that contact can be represented by a system of linear springs as shown in Figure 5-9. Each spring represents localized deformation of the faces of the seal rings. If face deformation of the seal ring relative to its centroid is significant compared to the deformation of the centroidal axis itself (as it might be if one ring is carbon) then the values of k can be chosen based on an estimate of this stiffness. If the relative deformation is small then the k values may be chosen accordingly and they will not really influence the results as long as they are not chosen so large as to numerically dominate the stiffness matrix and cause errors.

Contact is defined as when the spring touches and is compressed. A gap results if the spring cannot touch due to either initial or elastic deformation due to load. Mathematically, when touching cannot occur, the spring constant is set to zero.

Figure 5-10 shows how the ring and contact models are combined. The figure represents the plane of one node in the finite element technique to be described. Note that each of the ring cross sections can

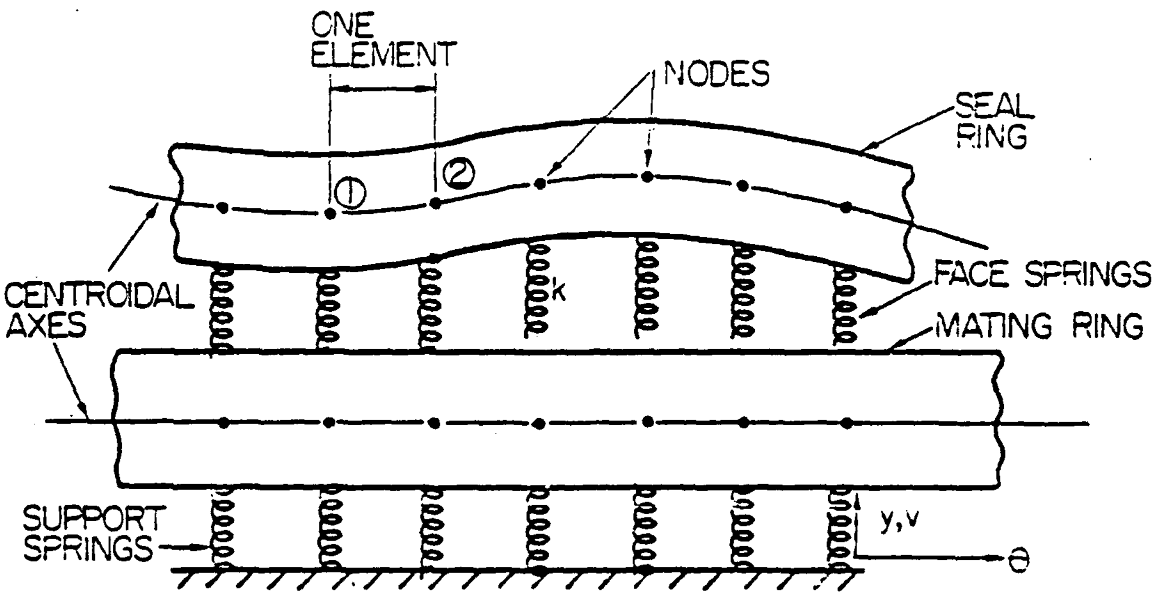

Figure 5-9. Contact model.

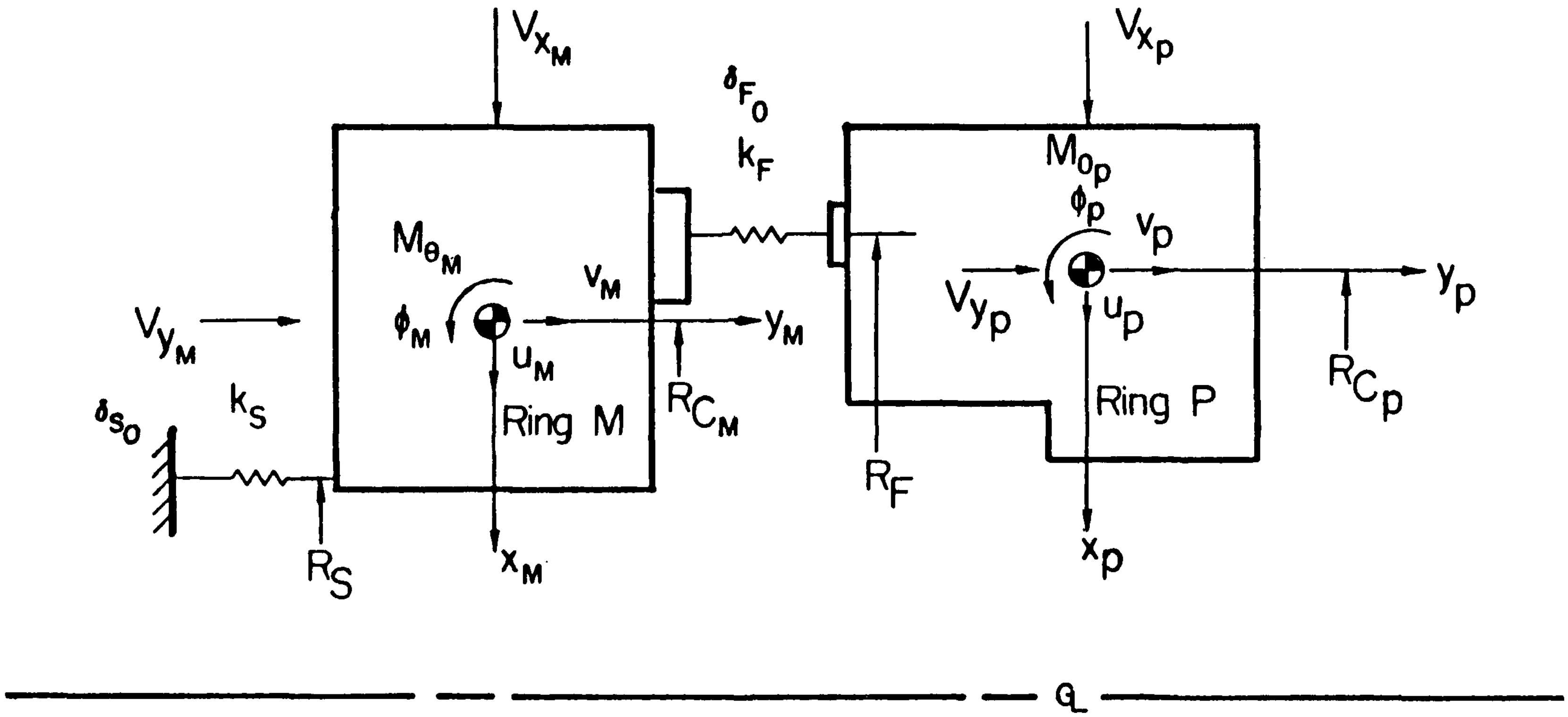

Figure 5-10. One Element of Contact Model.

be loaded by concentrated forces and moments. These are used to represent various external loadings. In an actual seal assembly these forces and moments would arise from fluid pressure, spring pressure, and possibly some drive force components. The contact of the two faces is represented by springs k_F which have initial deflection δ_{FO} (to later account for initial waviness). The left-hand ring is anchored by a series of springs k_S (with initial deflection δ_{SO}) which can be chosen to represent a very conformable support like an O-ring by making k_S small or a very rigid support such as a machined shoulder with an initial waviness on it by providing δ_{SO} and making k_S large.

To formulate the two ring deflection problem as a finite element problem, one must find the total energy of the system. The strain energy arises from that in the two rings, the face contact springs and the support springs. The potential energy is that due to the applied loads. Two ring finite elements plus two one-half face springs and two one-half support springs will be defined as one element in this combined problem (see Figure 5-10). It is readily shown that the strain energy plus the potential energy for such an element is given by

$$U_e = \frac{1}{2} [\delta_p]^T [K_{RP}] [\delta_p] + \frac{1}{2} [\delta_M]^T [K_{RM}] [\delta_M]$$

$$+ \frac{1}{2} \frac{k_{F1}}{2} [v_{M1} - v_{P1} - \phi_{M1}(R_F - R_{CM}) + \phi_{P1}(R_F - R_{CP}) - \delta_{FO1}]^2$$

$$+ \frac{1}{2} \frac{k_{F2}}{2} [v_{M2} - v_{P2} - \phi_{M2}(R_F - R_{CM}) + \phi_{P2}(R_F - R_{CP}) - \delta_{FO2}]^2$$

$$+ \frac{1}{2} \frac{k_{S1}}{2} [-v_{M1} - \phi_{M1}(R_{CM} - R_S) - \delta_{SO1}]^2$$

$$+ \frac{1}{2} \frac{k_{S2}}{2} [-v_{M2} - \phi_{M2}(R_{CM} - R_S) - \delta_{SO2}]^2$$

$$- [\delta_P]^T [F_P] - [\delta_M]^T [F_M] \, . \tag{5-11}$$

The matrices $[K_{RP}]$ and $[K_{RM}]$ are as defined by Equation (5-6) for the two different rings. $[\delta_P]$ and $[\delta_M]$ are defined by Equation (5-1) and represent a total of 24 displacements associated with each of these elements. The four expressions with the k coefficient are recognized as being the potential energy of the springs.

Equation (5-17) can be rewritten in the following form

$$U_e = \frac{1}{2} [\delta_e]^T [K_e] [\delta_e] - [\delta_e]^T [F_e] - [C_e] \tag{5-12}$$

where $[F_e]$ includes initial deflection terms as well as loads and $[C_e]$ is a constant due to initial deflection. Subscript e indicates that the matrices are for one element. For the above form, Equations (5-13) and (5-14) (next page) give δ_e and F_e.

The stiffness matrix $[K_e]$ is somewhat cumbersome but can be represented as follows:

$$
[\delta_e] = \begin{bmatrix} u_{P1} \\ v_{P1} \\ w_{P1} \\ \left.\frac{1}{R}\frac{dv}{d\theta}\right|_{P1} \\ \psi_{P1} \\ \phi_{P1} \\ u_{M1} \\ v_{M1} \\ w_{M1} \\ \left.\frac{1}{R}\frac{dv}{d\theta}\right|_{M1} \\ \psi_{M1} \\ \phi_{M1} \\ u_{P2} \\ v_{P2} \\ w_{P2} \\ \left.\frac{1}{R}\frac{dv}{d\theta}\right|_{P2} \\ \psi_{P2} \\ \phi_{P2} \\ u_{M2} \\ v_{M2} \\ w_{M2} \\ \left.\frac{1}{R}\frac{dv}{d\theta}\right|_{M2} \\ \psi_{M2} \\ \phi_{M2} \end{bmatrix} \tag{5-13}
$$

$$
[F_e] = \begin{bmatrix} -V_{x_{P1}} \\ -V_{y_{P1}} + \frac{k_{F1}\,\delta_{F01}}{2} \\ -N_{\theta_{P1}} \\ M_{x_{P1}} \\ -M_{y_{P1}} \\ -M_{\theta_{P1}} - \frac{k_{F1}\,\delta_{F01}}{2}(R_F - R_{CP}) \\ -V_{x_{M1}} \\ -V_{y_{M1}} - \frac{k_{F1}\,\delta_{F01}}{2} + \frac{k_{S1}\,\delta_{S01}}{2} \\ -N_{\theta_{M1}} \\ M_{x_{M1}} \\ -M_{y_{M1}} \\ -M_{\theta_{M1}} + \frac{k_{F1}\,\delta_{F01}}{2}(R_F - R_{CM}) + \frac{k_{S1}\,\delta_{S01}}{2}(R_{CM} - R_S) \\ V_{x_{P2}} \\ V_{y_{P2}} + \frac{k_{F2}\,\delta_{F02}}{2} \\ N_{\theta_{P2}} \\ -M_{x_{P2}} \\ M_{y_{P2}} \\ M_{\theta_{P2}} - \frac{k_{F2}\,\delta_{F02}}{2}(R_F - R_{CP}) \\ V_{x_{M2}} \\ V_{y_{M2}} - \frac{k_{F2}\,\delta_{F02}}{2} + \frac{k_{S2}\,\delta_{S02}}{2} \\ N_{\theta_{M2}} \\ -M_{x_{M2}} \\ M_{y_{M2}} \\ M_{\theta_{M2}} + \frac{k_{F2}\,\delta_{F02}}{2}(R_F - R_{CM}) + \frac{k_{S2}\,\delta_{S02}}{2}(R_{CM} - R_S) \end{bmatrix} \tag{5-14}
$$

$$
\left[\begin{array}{c:c:c:c}
\begin{matrix} K_{RP1,1} & & \\ & \ddots & \\ & & K_{RP6,6} \end{matrix} & 0 & \begin{matrix} K_{RP1,7} & & \\ & \ddots & \\ & & K_{RP6,12} \end{matrix} & 0 \\
\hdashline
0 & \begin{matrix} K_{RM1,1} & & \\ & \ddots & \\ & & K_{RM6,6} \end{matrix} & 0 & \begin{matrix} K_{RM1,7} & & \\ & \ddots & \\ & & K_{RM6,12} \end{matrix} \\
\hdashline
\begin{matrix} K_{RP7,1} & & \\ & \ddots & \\ & & K_{RP12,6} \end{matrix} & 0 & \begin{matrix} K_{RP7,7} & & \\ & \ddots & \\ & & K_{RP12,12} \end{matrix} & 0 \\
\hdashline
0 & \begin{matrix} K_{RM7,1} & & \\ & \ddots & \\ & & K_{RM12,6} \end{matrix} & 0 & \begin{matrix} K_{RM7,7} & & \\ & \ddots & \\ & & K_{RM12,12} \end{matrix}
\end{array}\right]
\tag{5-15}
$$

Each nonzero 6 x 6 submatrix is taken from part of the appropriate 12 x 12 ring stiffness matrix defined by Equation (5-6). One 12 x 12 is defined for ring P and one for ring M. The elements of the P ring stiffness matrix and the M ring stiffness matrix must have the same length θ to properly combine above.

The coupling terms which derive from Equation (5-11) must now be added to the 24 x 24 stiffness matrix. Since these terms are sparse, they are summarized by Equation (5-16) (next page) as additions to the stiffness matrix above.

Thus

$$[K_e] = [\text{Eq. (5-15)}] + [\text{Eq. (5-16)}] \ . \tag{5-17}$$

$$
\begin{array}{c|cccccccc|}
I,J & 2 & 6 & 8 & 12 & 14 & 18 & 20 & 24 \\
\hline
2 & \frac{k_{F1}}{2} & -\frac{k_{F1}}{2}(R_F - R_{CP}) & -\frac{k_{F1}}{2} & \frac{k_{F1}}{2}(R_F - R_{CM}) & 0 & 0 & 0 & 0 \\
6 & -\frac{k_{F1}}{2}(R_F - R_{CP}) & \frac{k_{F1}}{2}(R_F - R_{CP})^2 & \frac{k_{F1}}{2}(R_F - R_{CP}) & \begin{array}{l} -\frac{k_{F1}}{2}(R_F - R_{CM}) \\ \times (R_F - R_{CP}) \end{array} & 0 & 0 & 0 & 0 \\
8 & -\frac{k_{F1}}{2} & \frac{k_{F1}}{2}(R_F - R_{CP}) & \frac{k_{F1} + k_{S1}}{2} & \begin{array}{l} -\frac{k_{F1}}{2}(R_F - R_{CM}) \\ +\frac{k_{S1}}{2}(R_{CM} - R_S) \end{array} & 0 & 0 & 0 & 0 \\
12 & \frac{k_{F1}}{2}(R_F - R_{CM}) & \begin{array}{l} -\frac{k_{F1}}{2}(R_F - R_{CP}) \\ \times (R_F - R_{CP}) \end{array} & \begin{array}{l} -\frac{k_{F1}}{2}(R_F - R_{CM}) \\ +\frac{k_{S1}}{2}(R_{CM} - R_S) \end{array} & \begin{array}{l} \frac{k_{F1}}{2}(R_F - R_{CM})^2 \\ +\frac{k_{S1}}{2}(R_{CM} - R_S)^2 \end{array} & 0 & 0 & 0 & 0 \\
14 & 0 & 0 & 0 & 0 & \frac{k_{F2}}{2} & -\frac{k_{F2}}{2}(R_F - R_{CP}) & -\frac{k_{F2}}{2} & \frac{k_{F2}}{2}(R_F - R_{CM}) \\
18 & 0 & 0 & 0 & 0 & -\frac{k_{F2}}{2}(R_F - R_{CP}) & \frac{k_{F2}}{2}(R_F - R_{CP})^2 & \frac{k_{F2}}{2}(R_F - R_{CP}) & \begin{array}{l} -\frac{k_{F2}}{2}(R_F - R_{CM}) \\ \times (R_F - R_{CP}) \end{array} \\
20 & 0 & 0 & 0 & 0 & -\frac{k_{F2}}{2} & \frac{k_{F2}}{2}(R_F - R_{CP}) & \frac{k_{F2} + k_{S2}}{2} & \begin{array}{l} -\frac{k_{F2}}{2}(R_F - R_{CM}) \\ +\frac{k_{S2}}{2}(R_{CM} - R_S) \end{array} \\
24 & 0 & 0 & 0 & 0 & \frac{k_{F2}}{2}(R_F - R_{CM}) & \begin{array}{l} -\frac{k_{F2}}{2}(R_F - R_{CP}) \\ \times (R_F - R_{CP}) \end{array} & \begin{array}{l} -\frac{k_{F2}}{2}(R_F - R_{CM}) \\ +\frac{k_{S2}}{2}(R_{CM} - R_S) \end{array} & \begin{array}{l} \frac{k_{F2}}{2}(R_F - R_{CM})^2 \\ +\frac{k_{S2}}{2}(R_{CM} - R_S)^2 \end{array}
\end{array}
$$

Equation (5-16)

It must be recognized that the moments and forces will combine in assembly such that the total term at each node is equivalent to the external load at each node.

Using conventional summation techniques to assemble the elements and the principle of minimum potential energy, it can be shown that

$$\left(\sum_{e=1}^{N} [K_e] \right) [\delta] = \sum_{e=1}^{N} [F_e] \tag{5-18}$$

defines the linear problem to be solved. $[\delta]$ represents the equilibrium displacements and becomes a matrix of 12 N unknowns for a ring with N nodes and N elements. To minimize bandwidth, $[K_e]$ was assembled around the ring using an alternating numbering scheme.

Boundary conditions must be supplied for Equation (5-18) to prevent rigid body motion. For the system as shown in Figure 5-10, the needed boundary conditions are

$$\begin{aligned} u_{M1} &= 0 \qquad & u_{P1} &= 0 \\ w_{M1} &= 0 \qquad & w_{P1} &= 0 \\ w_{MN/2} &= 0 \qquad & w_{PN/2} &= 0 \end{aligned} \tag{5-19}$$

These constraints keep the rings from rotating about their own axes and eliminate rigid body motion in the θ-x plane.

Method

Before considering solutions to the above set of equations, it is important to summarize the assumptions in this model. They are:

1) Ring finite elements are used, so the seal parts must be able to be suitably modeled as such. Ring finite elements give only translation of the centroid and rotation of the cross section.

2) The ring finite element derivation assumes a compact section where the effects of warping and shear center offset are negligible. Small deflection theory is used. Deflections due to shear are neglected.

3) Seal face taper is not accounted for in the contact model. Contact is assumed to occur only at the mean face radius. Thus the analysis is most accurate for narrow-faced seals or where face taper deflection (ϕ in the model) is small relative to face axial translation (v in the model).

4) Contact is represented by a linear spring model which represents deformation of the surface relative to centroid. The model is one dimensional.

The method of solution used for the above problem is as follows:

1) Evaluate ring stiffness matrices K_p and K_M for actual sections using Equation (5-6).

2) Define all other input including the face springs , the support springs k_{Si}, and external loads [F].

3) Assume at least three points on the faces touch. Such points were found by an iterative scheme to pick the three most likely points of contact under zero load pushing the rings together. Place springs k_{Fi} at these points with all other face springs set to zero. Depending on the type of support,

similar initial conditions can be established for the k_{Si}. For the cases studied the k_{Si} were all set to the same value thus representing a uniform support of the seal ring. Given the assumed contact and the waviness of the surface, then the δ_{FO_i} and δ_{SO_i} can be calculated and input.

4) The external load [F] is divided into M increments so that one increment of load is given by

$$\frac{1}{m} [F] . \tag{5-20}$$

One such increment is input as the load vector on the right-hand side of Equation (5-18).

5) The element stiffness matrices $[k_e]$ are constructed. Note this requires adding appropriate terms from the two ring stiffness matrices from Equation (5-6) in the form of Equations (5-15) and (5-16). The element stiffness matrices, Equation (5-17), require complete information concerning k_{Fi}, k_{Si}, δ_{FO_i}, δ_{SO_i}. Thus, the element stiffness matrices must be reconstructed each time the k_{Fi} and k_{Si} are changed.

6) Assemble the element stiffness matrices as in Equation (5-18). Use assembly rules to minimize bandwidth and store in compact form.

7) Solve Equations (5-18) using Gauss elimination.

8) Examine the deflection at each point on the face:

$$\Delta_i = v_{Mi} - v_{Pi} - \phi_{Mi}(R_F - R_{CM}) + \phi_{Pi}(R_F - R_{CP}) . \tag{5-21}$$

Then

$$\text{if} \quad \Delta_i \geq \delta_{F0i} \qquad k_{Fi} = k_F \, , \tag{5-22}$$

$$\text{if} \quad \Delta_i < \delta_{F0i} \qquad k_{Fi} = 0 \, . \tag{5-23}$$

A similar procedure is followed for the support. This step places springs in place only where contact is occurring.

9) Add another increment to the load and repeat steps 4) through 8) m times.

10) Repeat steps 5) through 8) again without adding any more load (the full load is already applied). If the contact conditions, Equations (5-22) and (5-23), are the same at each node, a correct solution is obtained. If such cannot be achieved, increasing the value of m will usually achieve a satisfactory solution.

The use of the increment of load was found to be essential to obtain a converged, consistent solution. Other approaches were tried with no success.

The final result is the complete set of displacements (5-13) at each node. In addition one also gets the seal gap h.

$$\text{if} \quad \Delta_i < \delta_{F0i} \, , \quad \text{then} \quad h_i = \delta_{F0i} - \Delta_i \, , \tag{5-24}$$

$$\text{if} \quad \Delta_i > \delta_{F0i} \, , \quad \text{then} \quad h_i = 0 \, . \tag{5-25}$$

Experimental Checks

The algorithm detailing steps 1) through 10) has been checked in several ways. By a suitable choice of constraints one may solve any

individual ring problem. Several such problems were solved thus verifying the ring stiffness matrix and the assembly of matrices. Several problems were also solved to check out the spring support system. Again, these checks verified the modeling. The model has also been applied to two experimental situations, one a contrived seal-like configuration, discussed below, the other, a real face seal for which data was available discussed in a later section.

Figure 5-11 shows the details of two aluminum rings and a loading arrangement designed to cause the rings to separate at the contact face. The moment arm is attached at node 1 as shown. As the load is applied the faces separate starting at node 1. Additional load causes the separation to move around the ring. Separation will also occur at node 5.

Table 5-3 gives the details of the section properties for the tests. Using the computer program developed and using only eight nodes, the resulting gap was predicted and is shown in Table 5-3. Experimental results are shown in Table 5-3 for comparison. Considering the numerous assumptions in the model and the experimental error, agreement is considered good. Of particular note is the fact that theory and experiment agree that node 5 just barely lifts off at the given load. Thus, this test result provides some direct confirmation of the validity of the model.

The model is now applied to some important and practical problems. The numerical model itself is described in detail in Appendix C.

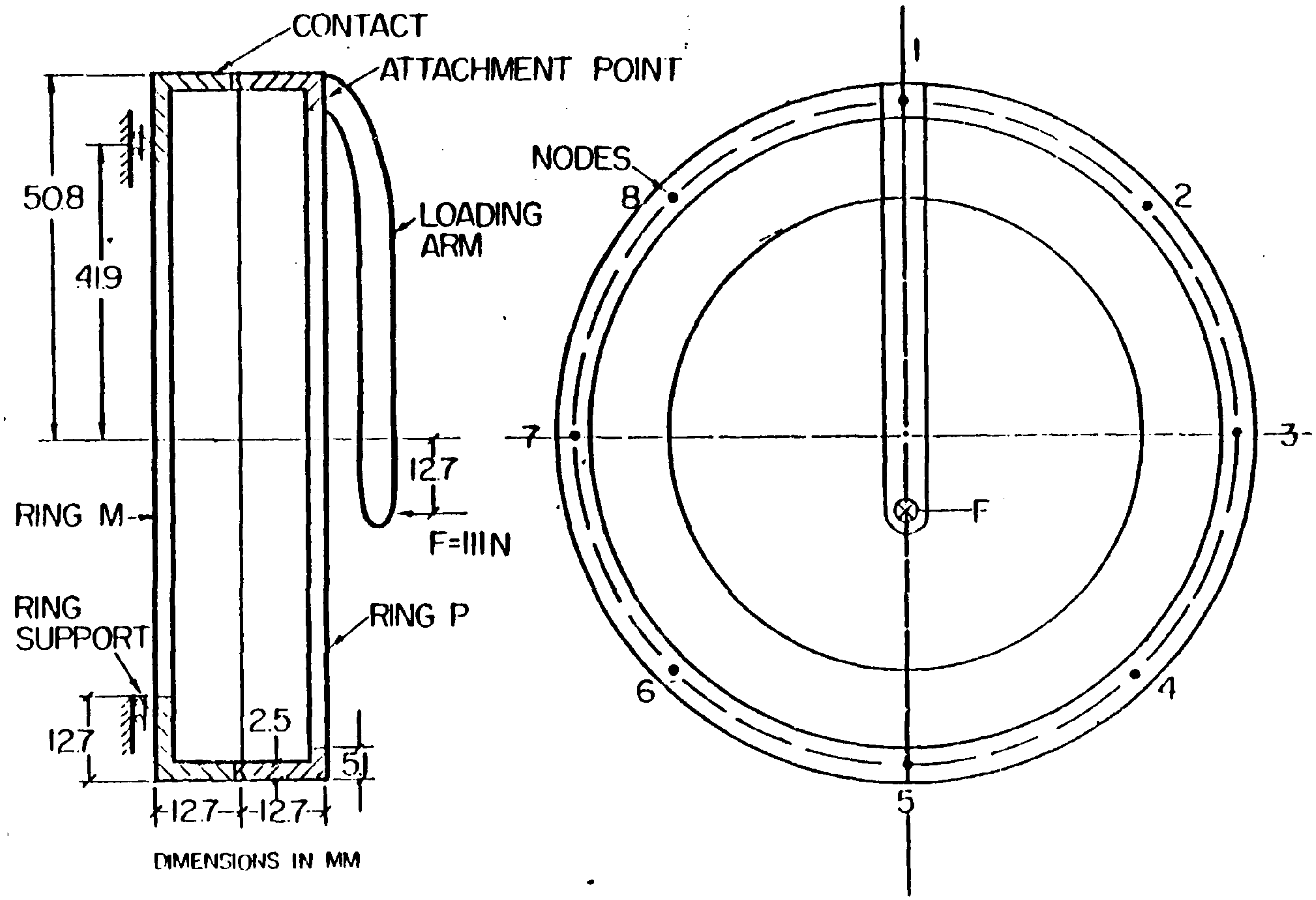

Figure 5-11. Two Contacting Rings with Eccentric Load.

TABLE 5-3

Two Contacting Rings with Eccentric Load

Section Properties (aluminum)		
	Ring M	Ring P
R_c	48.0 mm	50.4 mm
a	58.1 mm^2	38.7 mm^2
J_x	8.03×10^3 mm^4	5.77×10^2 mm^4
J_y	8.85×10^3 mm^4	5.66×10^1 mm^4
J_{xy}	4.87×10^2 mm^4	7.18×10^1 mm^4
J_θ	1.25×10^2 mm^4	8.33×10^1 mm^4

Results

Node	Predicted Gap (mm)	Measured Gap (mm)
1	0.65	0.51
2	0.29	0.20
3	0.0	0.0
4	C.0	0.0
5	0.04	0.04
6	0.0	0.0
7	0.0	0.0
8	0.29	0.20

Two Ring Contact Model Studies--Submarine Seal

A representative submarine seal is shown in Figure 5-12. The primary ring floats but does not rotate. It contains a carbon insert wearing element. Axial hydrostatic pressure and spring pressure load the primary face onto the mating ring face. The radial hydrostatic pressure causes a tilt which causes a divergence of the seal as well as a compressive hoop stress and radial deformation. The primary ring seals against the mating ring which also has a wear insert. The mating ring rotates with the shaft sleeve. The radial pressure creates a divergent rotation in the mating ring as well. The axial pressure load is far greater than that applied by the primary ring so that the mating ring is forced to contact the edge of the lock ring groove. This means that the mating ring will, under large pressure, tend to take on the shape of the locking groove.

Both the primary and secondary rings are made of monel (recent designs use Inconel 625). Both rings are split as shown. The two halves are bolted together using a taper pin and a bolt. Thus the cross section is reduced on both rings in two regions.

Section properties for 688 class submarine seals are shown to give some idea of the size of the seal rings and the cross section. The J_θ values used are not exact but taken from an approximate formula. I values have been used instead of J values. The figure shows how the bolt or pin cutout reduces the section properties (at the point of maximum cutout).

To illustrate the importance of seal gap and leakage in a submarine seal, Figure 5-13 shows the profile of an unloaded primary ring

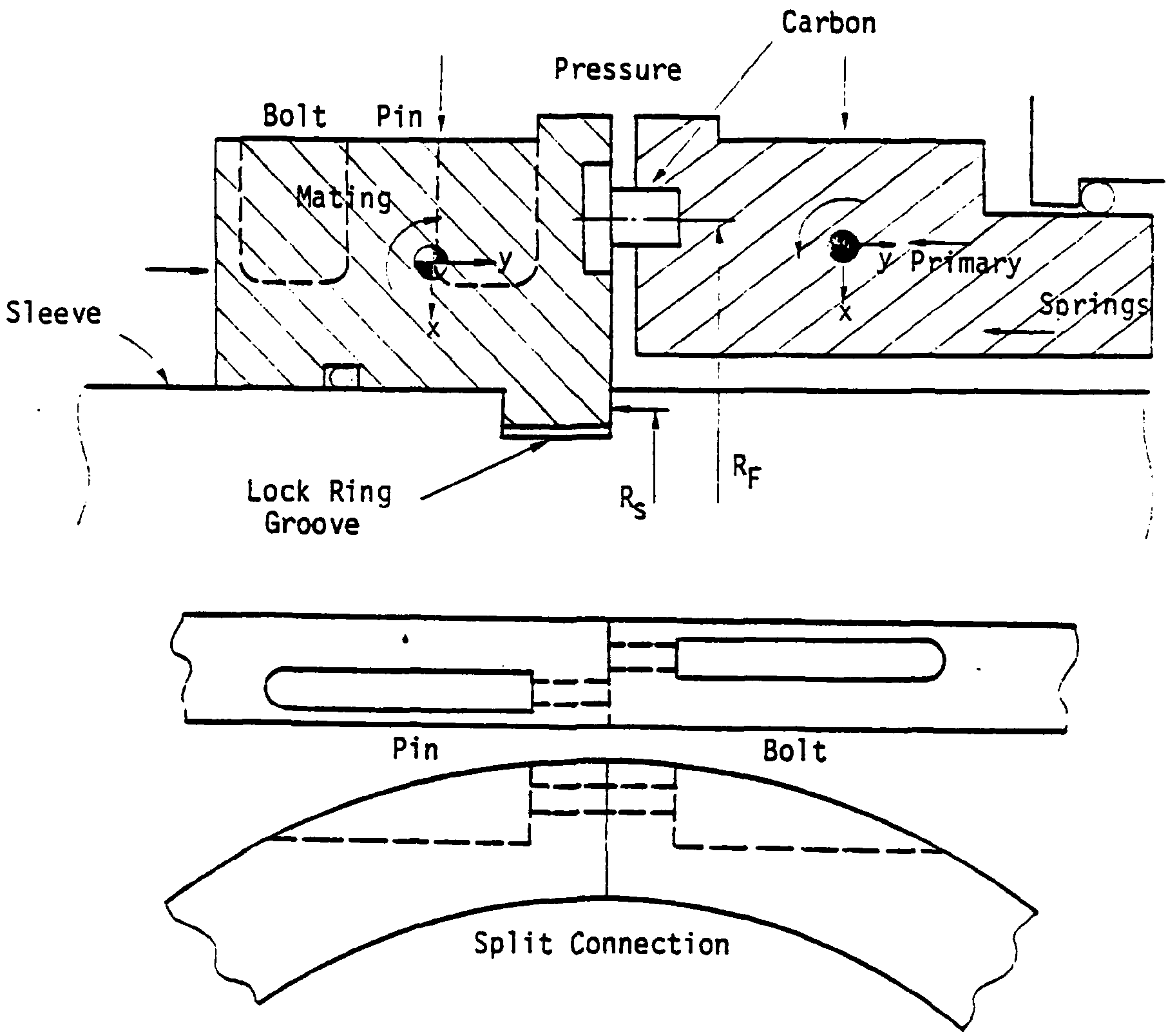

Section Properties

Mating	Mating at Pin Cutout	Mating at Bolt Cutout	Primary
R = 13.08	13.808	13.808	R = 13.844 in
I_x = 14.15	12.92	10.91	I_x = 38.18 in^4
I_y = 9.76	7.31	7.31	I_y = 6.70 in^4
J_θ = 24.40	8.11	9.00	J_θ = 21.45 in^4
I_{xy} = 1.73	2.93	-0.33	I_{xy} = 2.99 in^4
a = 11.52	9.00	9.00	a = 13.30 in^2

Figure 5-12. Submarine Shaft Seal.

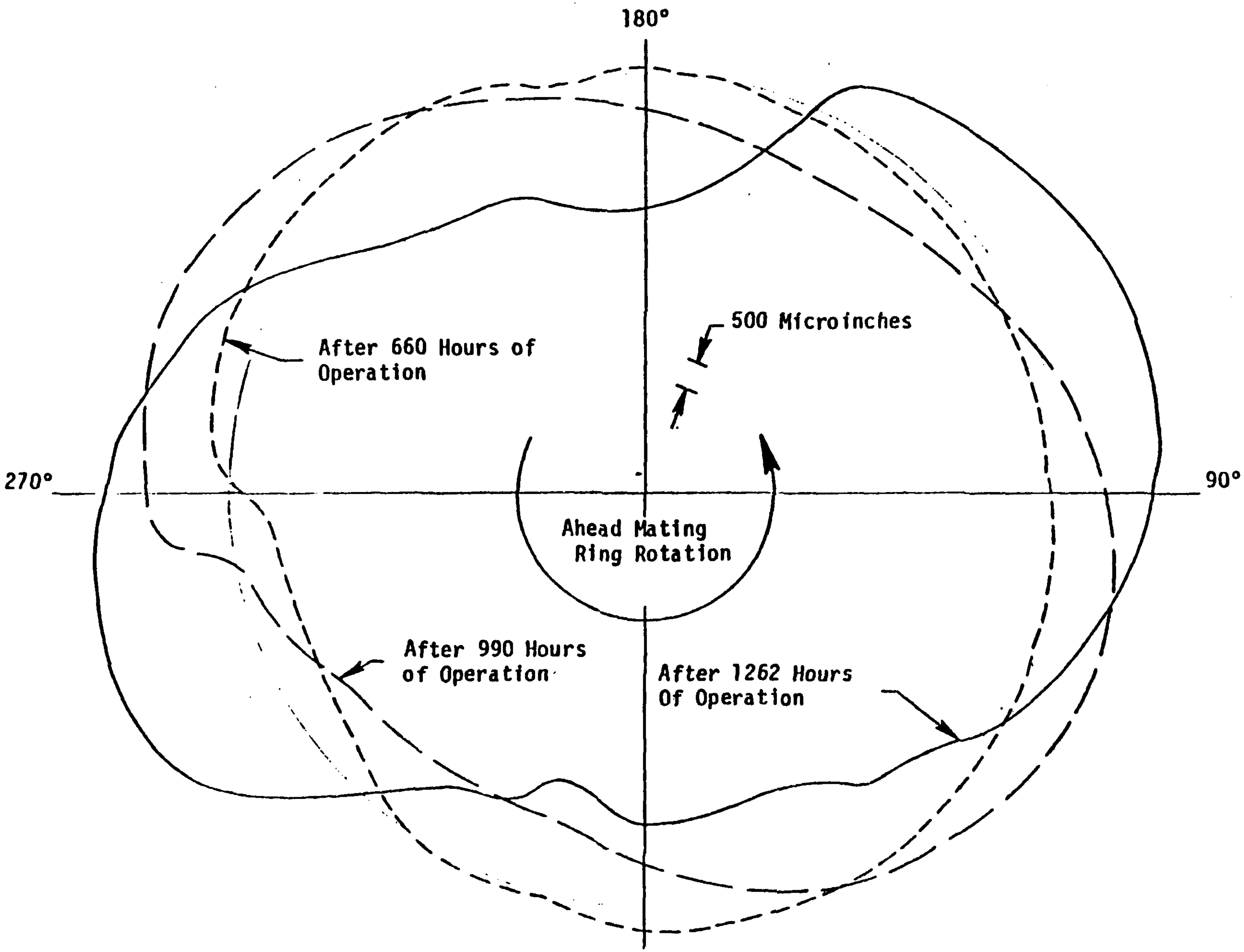

Figure 5-13. Seal Ring Face Flatness.

that develops after a period of operation. This seal was leaking badly (10 GPM). Table 5-4 shows that high leakage would be expected from this seal unless the gap shown in Figure 5-13 closes up on contact with the opposing face.

The two ring contact model is ideally suited to study such problems in submarine seals. Several different kinds of studies have been made using the program to try to assess submarine seal characteristics in regard to waviness and conformability. Table 5-5 summarizes the results of these studies which are now discussed in detail.

Seal Gap Caused by Bolted Joints

The bolted joints in a seal causes a non-axisymmetric stiffness. This variable stiffness coupled with the large moment associated with the radial hydrostatic component of pressure load can cause the faces to go out of flat. This condition was assessed using the two ring program for the seal described in Figure 5-12. A number of assumptions were made for this analysis.

1) Primary ring in perfectly flat and axisymmetric effects are eliminated for this analysis.
2) Mating ring is perfectly flat before loading. Reduced sections due to bolt/pin cutouts are included.
3) Mating ring is modeled in two ways: with joint as stiff as ring itself (assuming a large preload and a perfect joint) and assuming that the bolts are just snugged tight and stretch elastically as the joint comes open.
4) Lock ring groove is perfectly flat.

TABLE 5-4

Significance of Seal Gap

Q* (gpm)	Q mℓ/min	h_{avg} (μin)	h_2 equivalent (μin)
10.0	37850	882	650
1.0	3785	409	301
0.1	378	190	140
0.01	38	88	65
0.001	4	41	30

*For 688 size and 100 percent pressures at 60°F

TABLE 5-5

Submarine Seal Conformability Studies

	Study	Case	Cube mean of face* Gap (μin)	Results
1	Effect of seal ring cutout and bolted joint (688 mating ring)	Tight joint	0	Does not open
		Loose joint	111	Seal opens due to moment on joint
2	Conformability of maximum flattenable waviness (688 primary)	h_2 = 795 μin	0	Waviness was completely flattened.
3	Effect of lock ring groove stiffness on mating ring conformability (688)	h_2 = 1590 μin		
		KS = 10 x KF	122	Leakage = 112 ml/min
		KS = KF	91	Leakage = 46 ml/min
		KS = 0.1 x KF	1	Leakage = 0 ml/min
4	Effect of a 0.001" offset in seal face	Present design	100	Gap =15° (3.62") 60 ml/min
		Backfit design	99	Gap = 10° (2.41")
5	Effect of shim in lock ring groove (Trident)	2" x 0.003" shim	186	Leakage = 460 ml/min (Experimental = 150 ml/min [43])
		2" x 0.006" shim	529	Leakage = 10,900 ml/min)(Experimental = 5000 ml/min [43])
6	Effect of 2nd harmonic wave in lock ring groove (Trident)	500 μin amplitude	0	No gaps in face
		650 μin amplitude	1	Gaps just barely develop
		1000 μin amplitude	83	Large gaps in face

*The cube mean rather than the simple average is the proper value of h to use when estimating the leakage.

5) Face stiffness is based on face carbon. Support stiffness is taken as 10X face stiffness to represent a very rigid (metal on metal) support.

6) A variable node spacing is used to account for the joints and the cutouts.

7) The mating ring does not separate from the lock ring groove (later studies show it does and this causes even more gap than predicted here at the faces).

Using the stiff joint assumption the seal does not open under load although the face loading does become variable because of the non-axisymmetry. If the bolts are just tightened, the faces do separate. This occurs because the large moment opens the joint slightly and distorts it out of flat. Because of the high rigidity of the rings, this distortion cannot be flattened back out by the deflection of the rings. Figure 5-14 shows the actual gap which results. The negative deflection portion represents the axial deflection of the carbon insert. Table 5-5 shows that the effective gap is 111 μin., enough to cause a significant leak.

Now the actual joint does not correspond to either of these extremes. The preload on the bolts is high but not high enough to insure that the seal joint will behave the same way as the parent material. Loose joints are also not realistic. In fact, it is thought that the stiffness characteristics of a joint such as this are non-linear because the fraction of the joint separated increases with

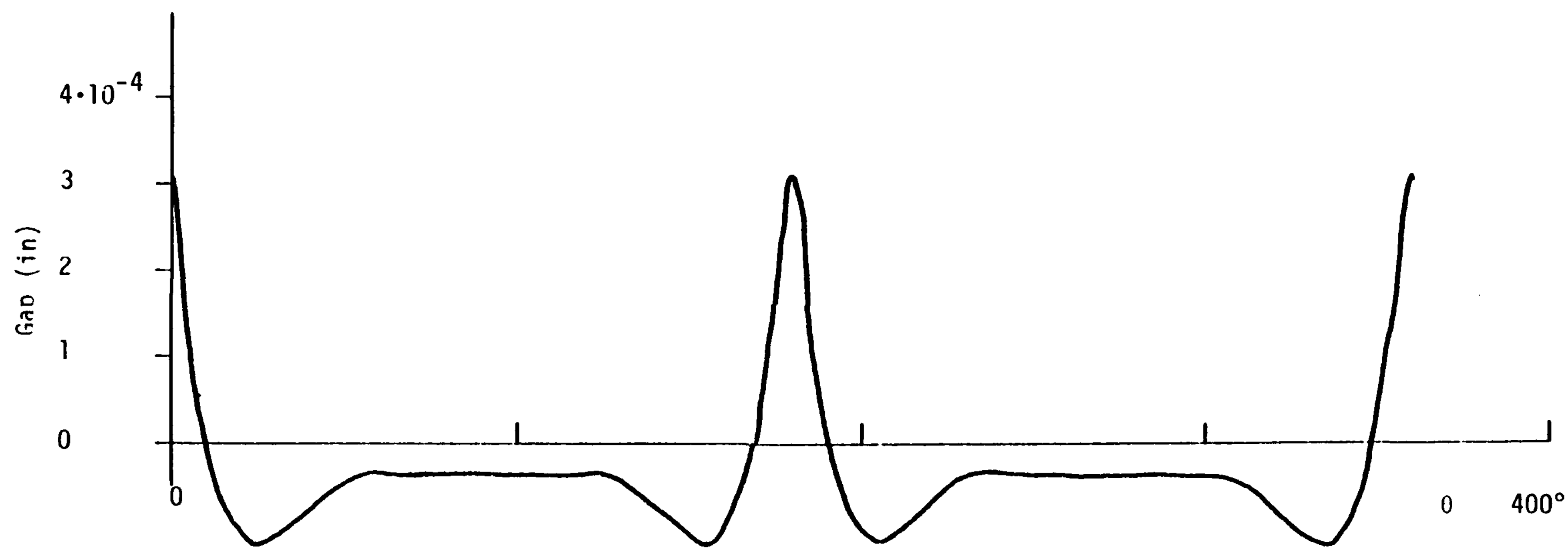

Figure 5-14. Seal Gap due to Joints.

increasing load. Thus a more accurate joint model is needed to accurately predict seal gap resulting from such non-axisymmetric effects. This subject is discussed in detail in a later section of this report.

The results presented here must be taken as a first estimate of the effects of non-axisymmetric stiffness on a seal. The important thing that these preliminary results show is that the joints in concert with the large moment tend to cause the seal to open, and this may in fact, at the very least, aggravate seal leakage problems. The most effective remedy is to eliminate the large moment on the ring. This will eliminate a large fraction of the out of flatness caused by joints.

Conformability of Primary Ring to a Wave

A second harmonic wave of 795 μin. amplitude was introduced on the face of the primary ring (see Table 5-5). Both rings were modeled axisymmetrically. The mating ring was made infinitely stiff. The results from the contact model showed that the seal faces just touched all around. The contact pressure dropped to zero at two points indicating that the seal faces were just about to separate. This case was run to verify the program result using a simple formula prediction as described previously. Reference [42] details these formula predictions, this one being for the 688 at 88 percent balance. (A simple study showed that the maximum flattenable waviness for the mating ring was 1270 μin., however the mating ring is stiffened by the lock ring groove.)

The significance of second harmonic waviness flattenability is discussed in detail in Reference [22]. Maximum flattenable second harmonic waviness serves as an indicator of the relative conformability of seals. It is known that seals that leak a lot often have a worn in waviness much greater than that which can be flattened out--thus the high leakage. The relative conformability serves as a good guide for designing seals with adequate conformability, but there are many other complications to the conformability question as the next few studies will show.

Lock Ring Groove Studies

The mating ring in current submarine seals is held in place on the shaft sleeve by a lock ring which fits a groove in the sleeve as shown in Figure 5-12. Pressure caused forces on the ring press the mating ring onto the face of the groove. There are two consequences. First the mating ring tends to take the shape of the groove, i.e., groove waviness is reflected in the mating ring. Second, the groove acts to stiffen the mating so that its conformability is not fully utilized. These effects are studied here.

Table 5-5, study 3, shows the stiffening effect of the lock ring groove. A 1590 μin. amplitudal wave is imposed on the seal faces. According to the maximum flattenable wave for the primary plus the mating ring, this amount of wave should be easily flattened out. The first case of study 3 shows that with a rigid lock ring groove (the actual case) a gap develops large enough to cause significant leakage (Figure 5-15). Thus the groove acts to stiffen the mating ring so that

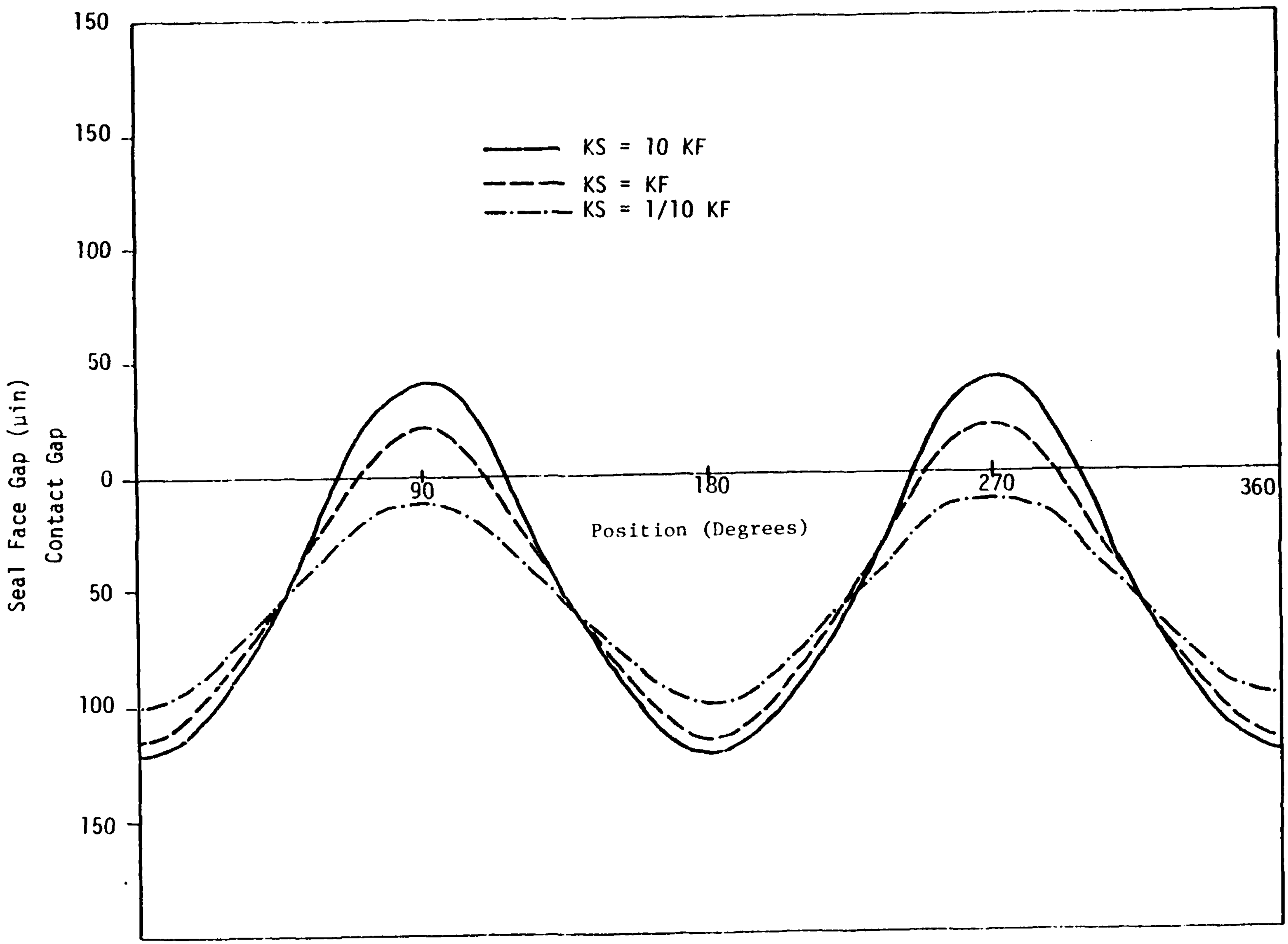

Figure 5-15. Conformability of Seals with Differing Support Stiffnesses.

it does not readily conform to the mating ring in the presence of a wave on the faces.

If the groove itself is allowed to be compliant such as by allowing the ring to press against a rubber cushion instead of metal, case 3 of study 3 shows that the face gap disappears (Figure 5-15). Thus this study shows that the lock ring groove reduces the conformability of the seal. Little is gained by having the mating ring be compliant.

The solution to the problem is to allow the mating ring to become nearly free floating so that it is not forced to take a shape from some other part. Such designs have to be tried and do show an improvement [43].

Study 6 in Table 5-5 shows that effect of putting a second harmonic wave directly into a lock ring groove. This study assumes the faces as originally flat and the rings are axisymmetric. As the amplitude of the lock ring waviness gets to around 0.001 in., the seal opens and cannot be closed any longer by the conformability of the faces. Figure 5-16 shows the results.

The solution to this problem is the same as above. The pressure load on the mating ring must be relieved so that the mating ring does not take its shape from another part.

Study 5 shows the effect of placing a 2 in. long shim in an otherwise flat lock ring groove. The model shows that the seal opens and this indicates in another way the previous point that seal leakage may be caused by lock ring out of flatness. Figure 5-17 shows these results. Interestingly this case was also run as a physical experiment

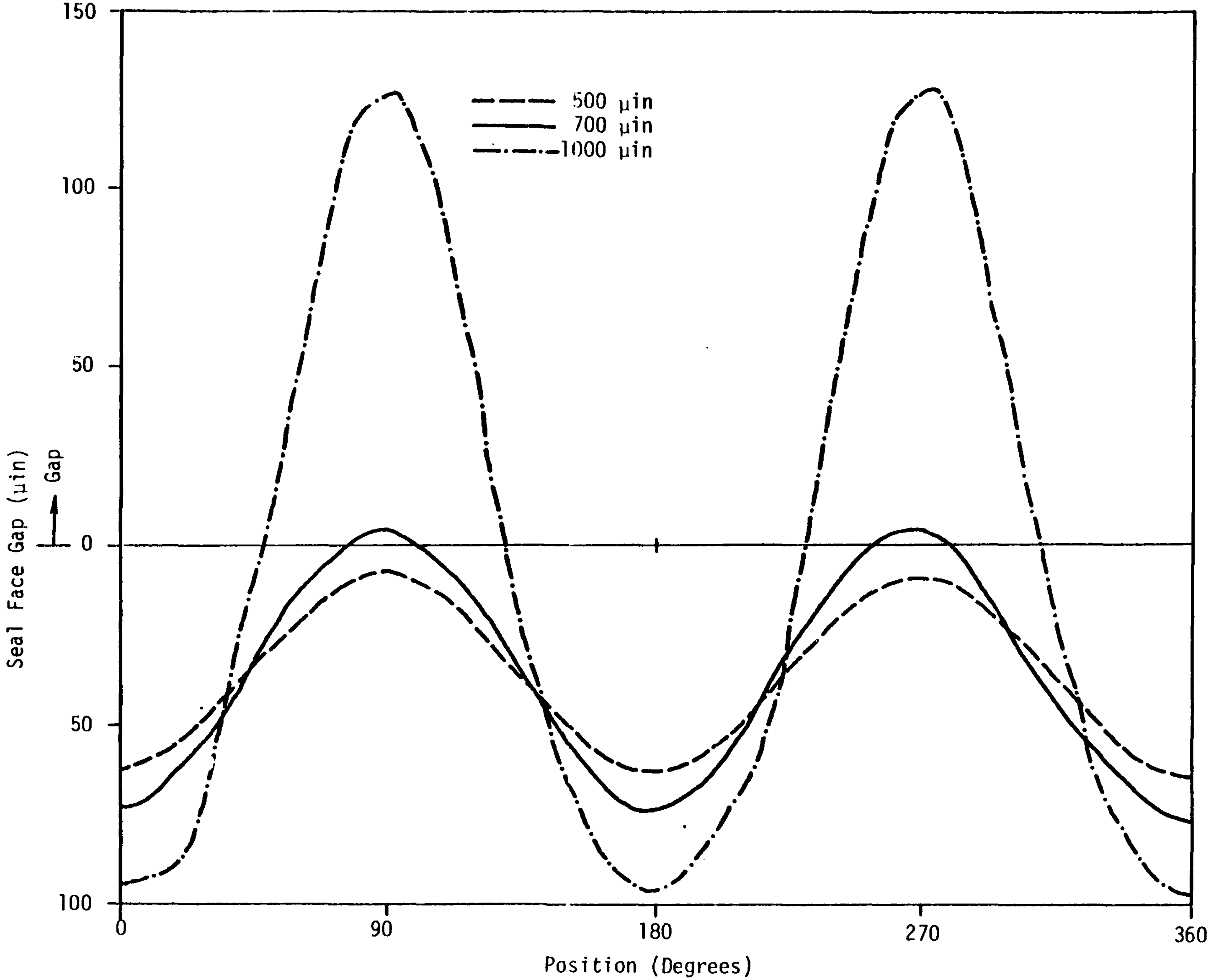

Figure 5-16. Effect of 2nd Harmonic Wave in Lock Ring Groove.

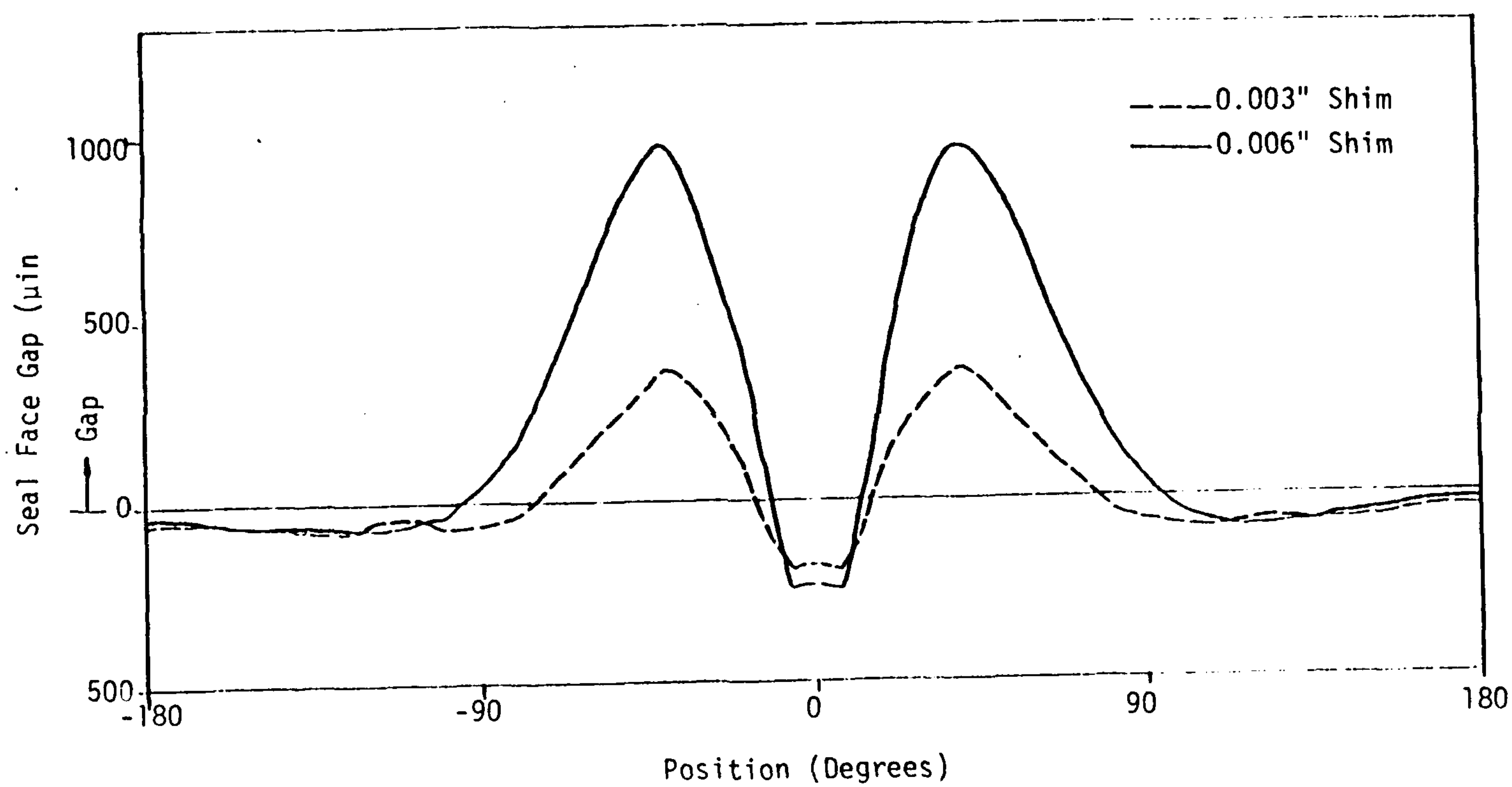

Figure 5-17. Effect of Shim in Lock Ring Groove

on a full scale seal. The measured leakage is shown. The model predicts similar results.

Face Offset

Study 4 shows the effect of an offset in the seal face as might occur if one seal segment shifts relative to the adjacent segment as has been known to occur in some tests. Clearly such a gap cannot be completely closed. Figure 5-18 shows the model's prediction of how the submarine seal will respond to a 0.001 in. face offset. The figure shows that there will be a large deformation of the carbon segment sticking up but about a 0.0005 in. gap will remain. The length of the gap is about 15 degrees before it completely closes. The cube mean gap value shows that a significant leakage will occur.

The solid curve in Figure 5-18 is for a seal design which is many times more compliant than the original design. The cube mean gap remains essentially the same and the length of the gap is reduced to 10 degrees.

The conclusion to be reached here are that submarine face seals cannot readily comply to segment offsets by bending of the rings even if the rings are quite flexible. Offsets such as these must either be minimized by design in the first place or must be complied with by mounting the segments themselves in a compliant manner such that these ends can have a relative movement to eliminate the offset.

The two ring contact model has been shown to be very useful in making such studies. The overall conclusions made from these studies are summarized in Chapter 9.

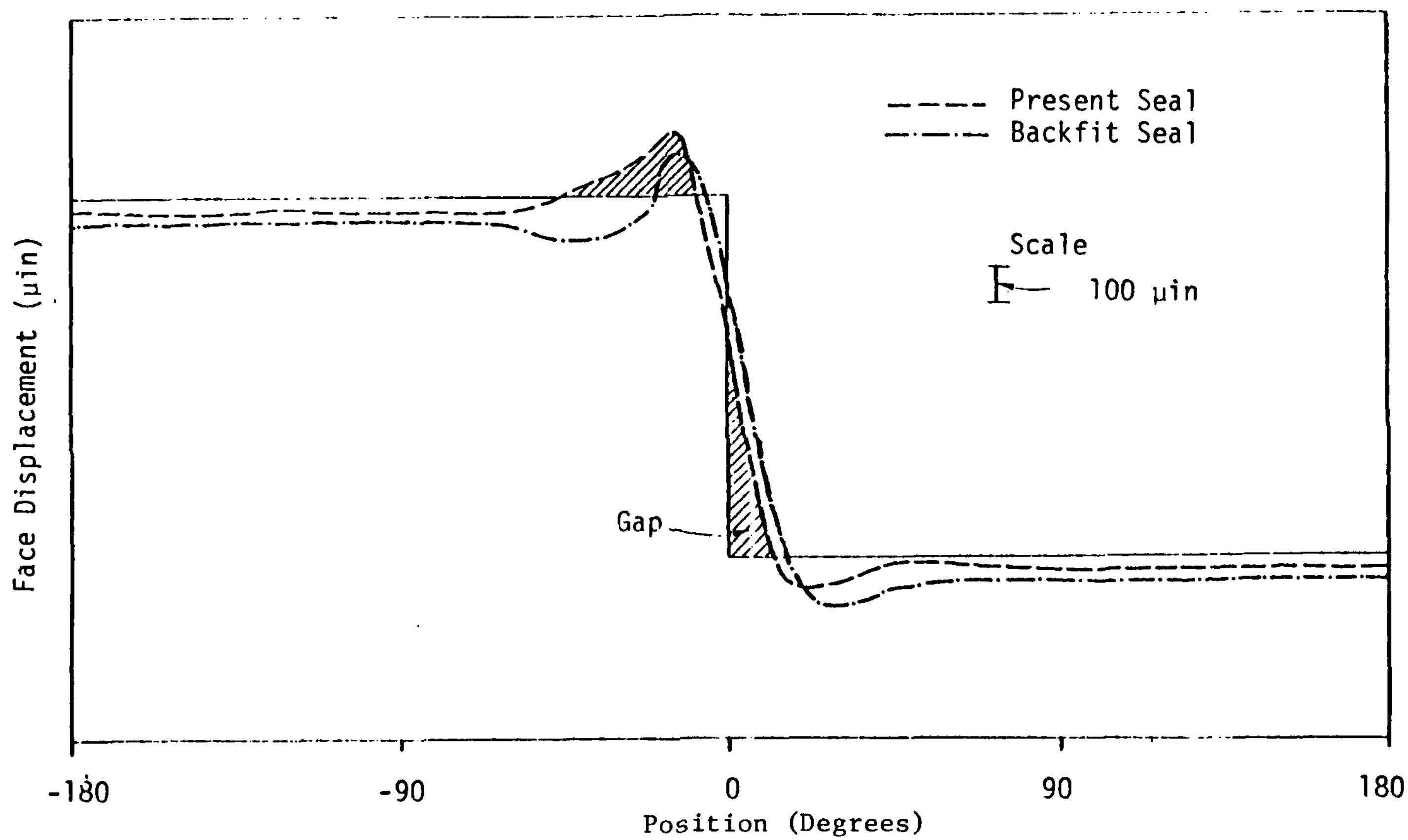

Figure 5-18. Effect of Face Offset.

Two Ring Contact Model-Magnetic Seal

The two ring contact model was also used to help understand leakage problems in some small magnetic seals used in Naval devices. The magnetic seal is shown in Figure 5-19. The magnet attracts the metal holder and pulls the carbon toward it. Waviness measurements of these seals were taken so that seal profiles were known. Leakage measurements as a function of angular positions were also taken. The complete details of this program are reported in Reference [41].

The two ring contact program was applied to the magnetic seal. Details of this application are contained in Appendix C. Figure 5-20 shows a specific example. The original measured profiles are shown. The net gap before deflection is shown. Then after the seal rings are loaded and bend toward each other, the net gap shown by the dashed curve results. Note that considerable flattening out occurs and that there are three regions of contact.

Leakage for the net gap was computed and then the two profiles were rotated relative to each other and the above solutions repeated. A different net gap and profile resulted. This procedure was repeated to establish a leakage versus relative position curve as shown in Figure 5-21. These results are compared to experimental results in the same figure. Agreement is considered to be reasonable since the model totally ignores radial effects (assumes the gap is parallel across the seal). These results show that the two ring contact model is a useful tool for understanding conformability problems in seals. Further details are given in Reference [41].

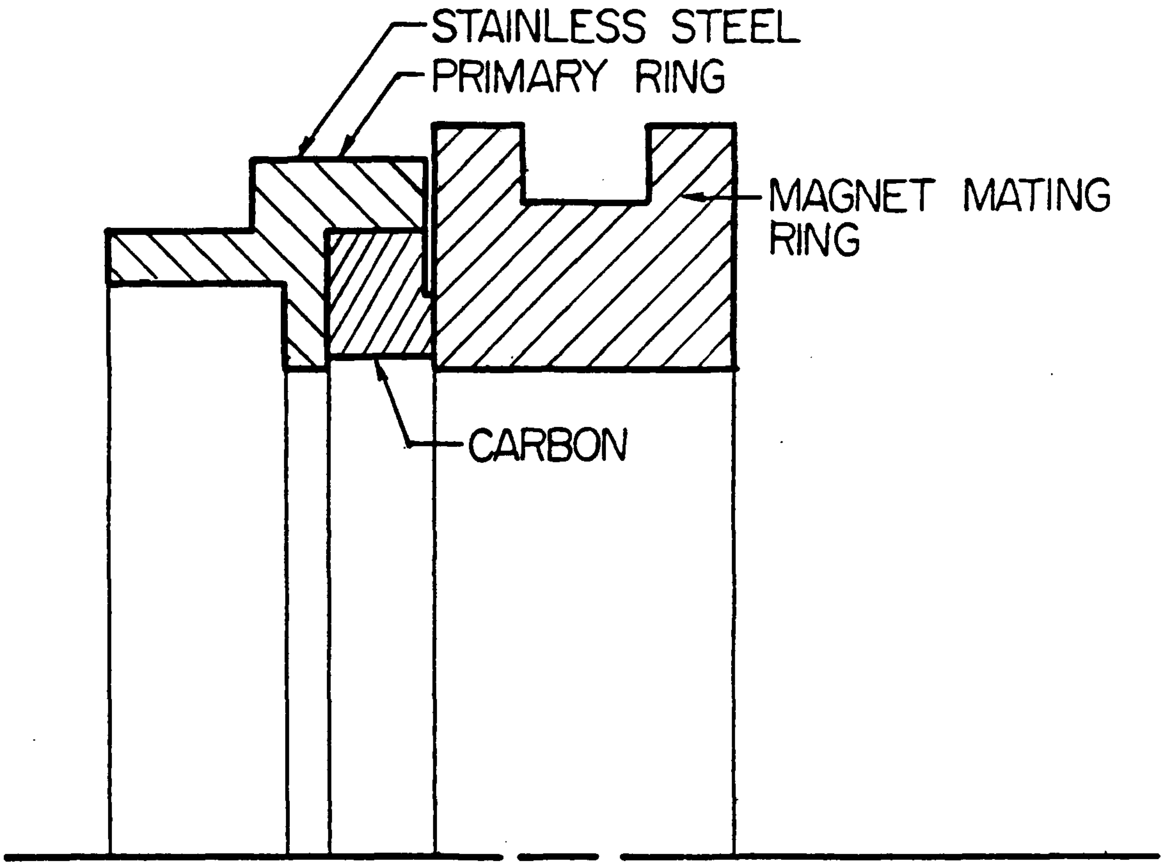

Figure 5-19. Magnetic Seal.

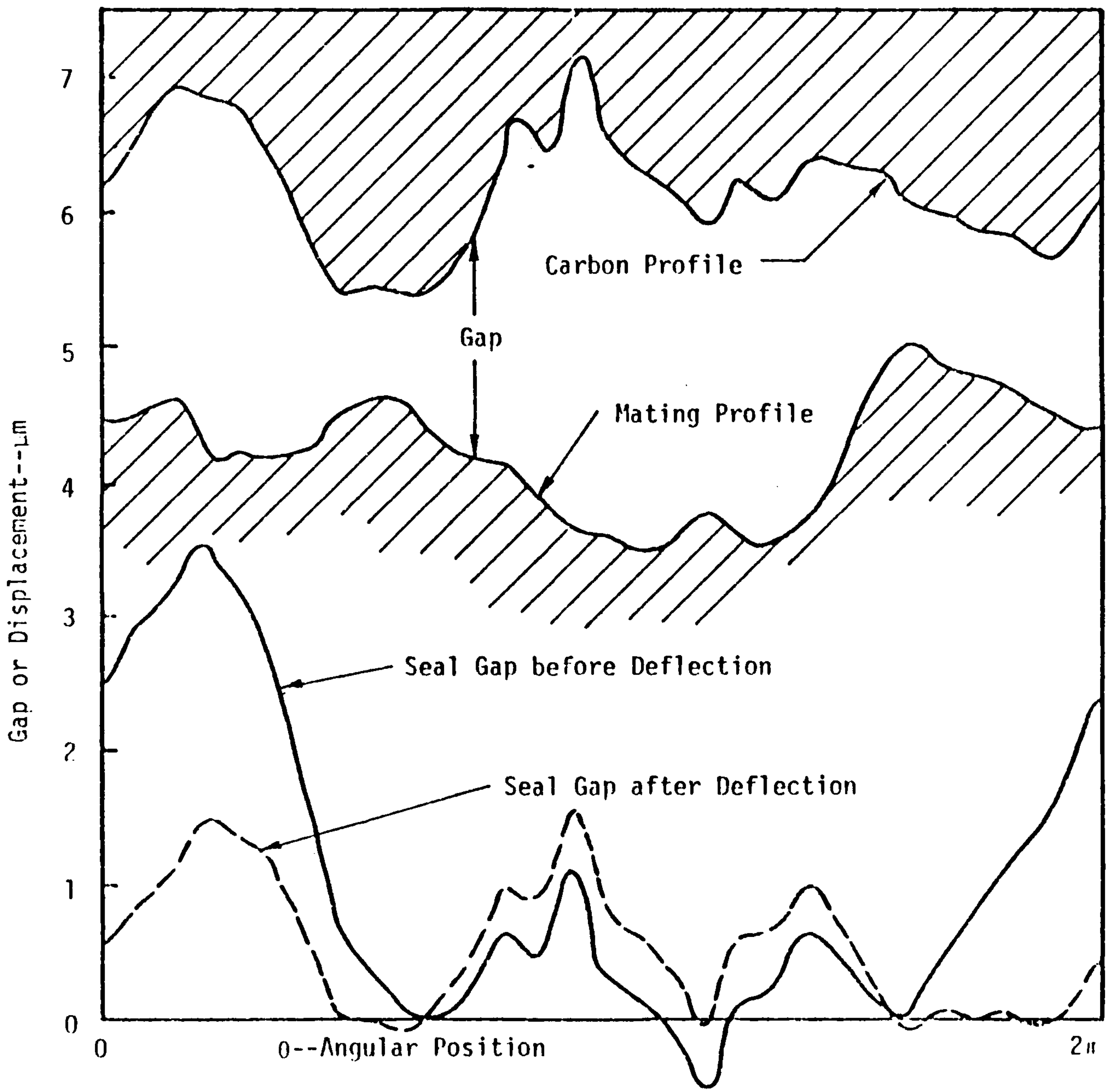

Figure 5-20. Surface Profiles and Seal Gap.

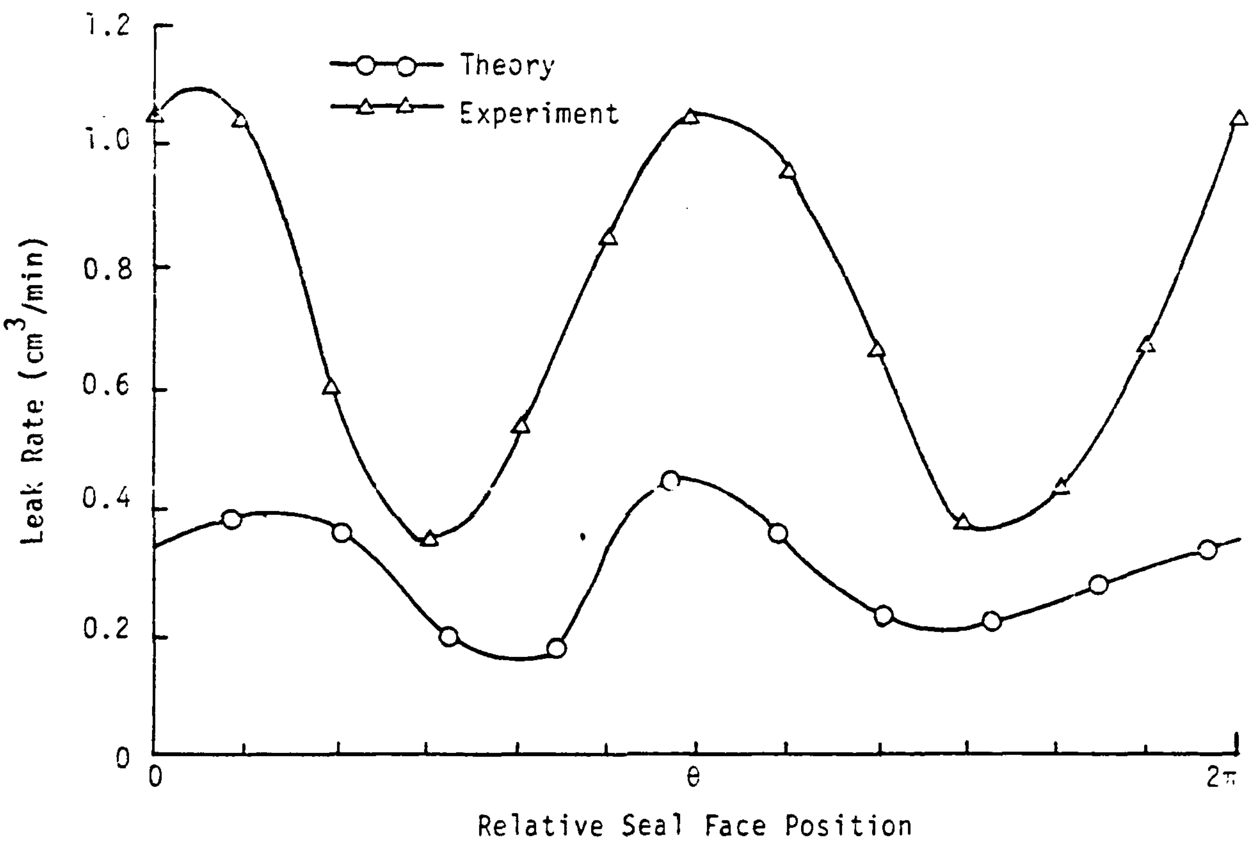

Figure 5-21. Comparison of Experimental to Theoretical Leakage.

Nonlinear Joint Model

As discussed previously, there is some question as to the proper way to model the bolted joints in the rings for the purpose of solving deflection and contact problems. Clearly assuming the joint behaves like the rest of the ring is incorrect. The loose bolt assumption is also incorrect. However, these two approaches represent cases which are readily modeled and have been used accordingly as a starting point.

A more precise definition of joint deflections versus forces is needed. If this relationship is known, it can readily be put into the ring finite element program of interest so that proper joint deflection is accounted for. As a part of this research program, it was decided that some studies should be undertaken to define these relationships so that proper seal ring deflection modeling could be performed.

A literature search revealed that the moment-rotation characteristics of several different types of bolted joints have been investigated. Bose [44] and Krishnamurthy [45] investigated the moment-rotation characteristics of bolted connections commonly used in steel structures. Their work indicates that the response of top-angle, tee-stub, and end-plate connections to moments is nonlinear. Bose [44] reports the results of experiments performed on the three types of connections and shows that the joint stiffnesses decrease with increased loading. Krishnamurthy developed a two-dimensional finite element code to analyze these joints.

Tsutsumi, Ito, and Masuko [46] performed bending experiments on two types of bolted joints used in machine tools. Again, their results show that the joint stiffnesses decrease with increasing moment. Sawa, Maruyama, and Edamoto [47] examined the distribution of contact pressure in a joint with a tap bolt both analytically and experimentally. They showed that the pressure distribution depends on the fastener depth and is not constant across the interface.

These papers suggest that the moment-rotation characteristics of tap bolted joints, as in the seal rings, are nonlinear. They do not, however, provide such a solution to the actual problem of interest.

A preliminary finite element numerical model of bolted joint similar to that in a seal ring has been developed. It consists of two rectangular blocks bolted together. This model is broken into a coarse finite element mesh of 32 elements and 88 nodes (Figure 5-22). The joint itself is modeled using three-dimensional, 8-node brick elements using the finite element code ADINA. The interfaces between the joint halves and between the bolt head and the joint are modeled using truss elements. These elements act as springs and allow contact between the joint halves and the bolt and also simulate the bolt pretension. Initially, their stiffnesses are large compared to the stiffnesses of the brick elements.

A stepwise increasing moment is applied to the joint. As forces in the springs become tensile, the stiffnesses of those particular elements are lowered to simulate the joint opening. The results (Figure 5-23) show that the joint's response is linear until it begins to open. As the load increases past that point, the joint stiffness

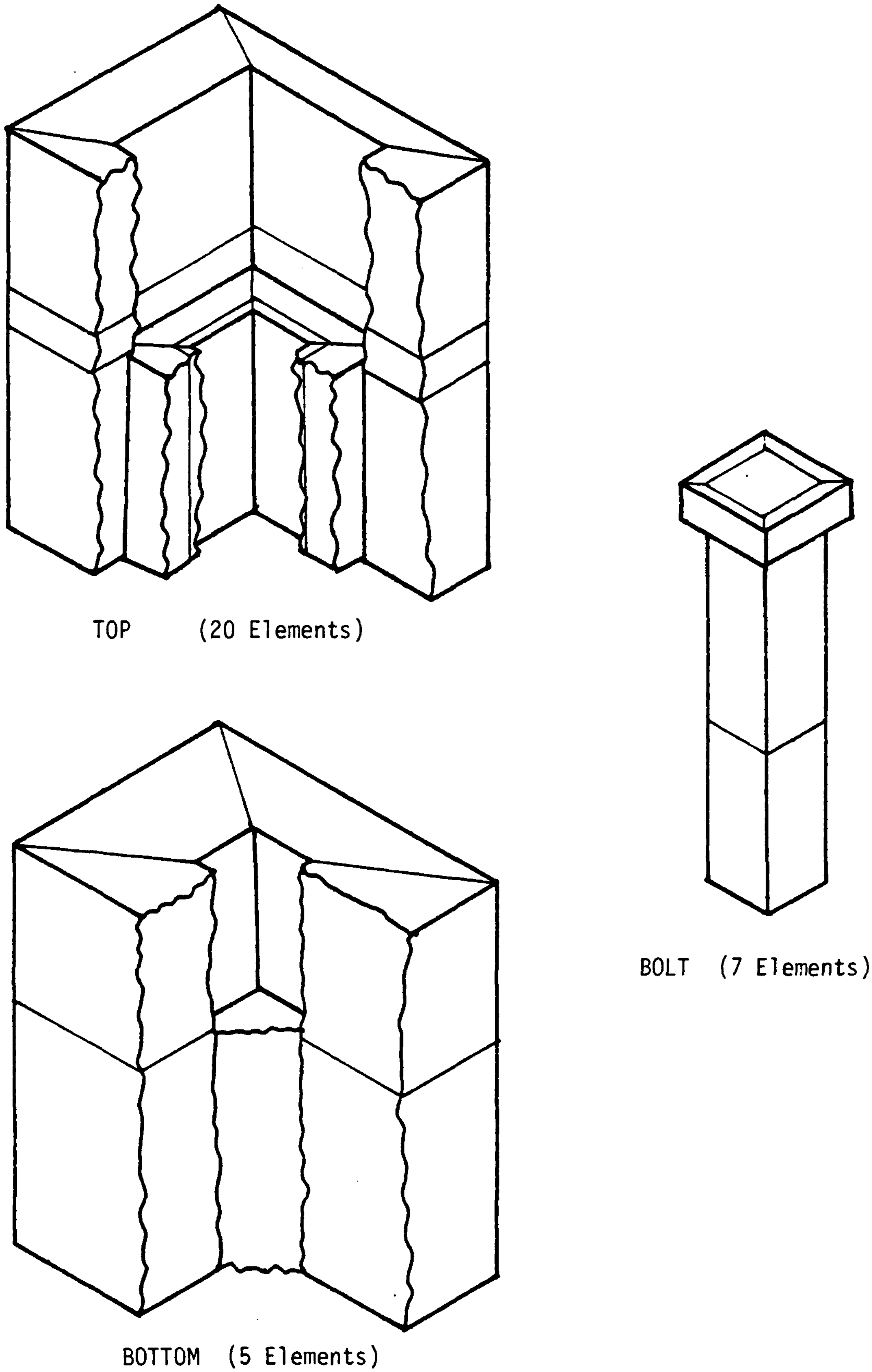

Figure 5-22. Finite Element Mesh.

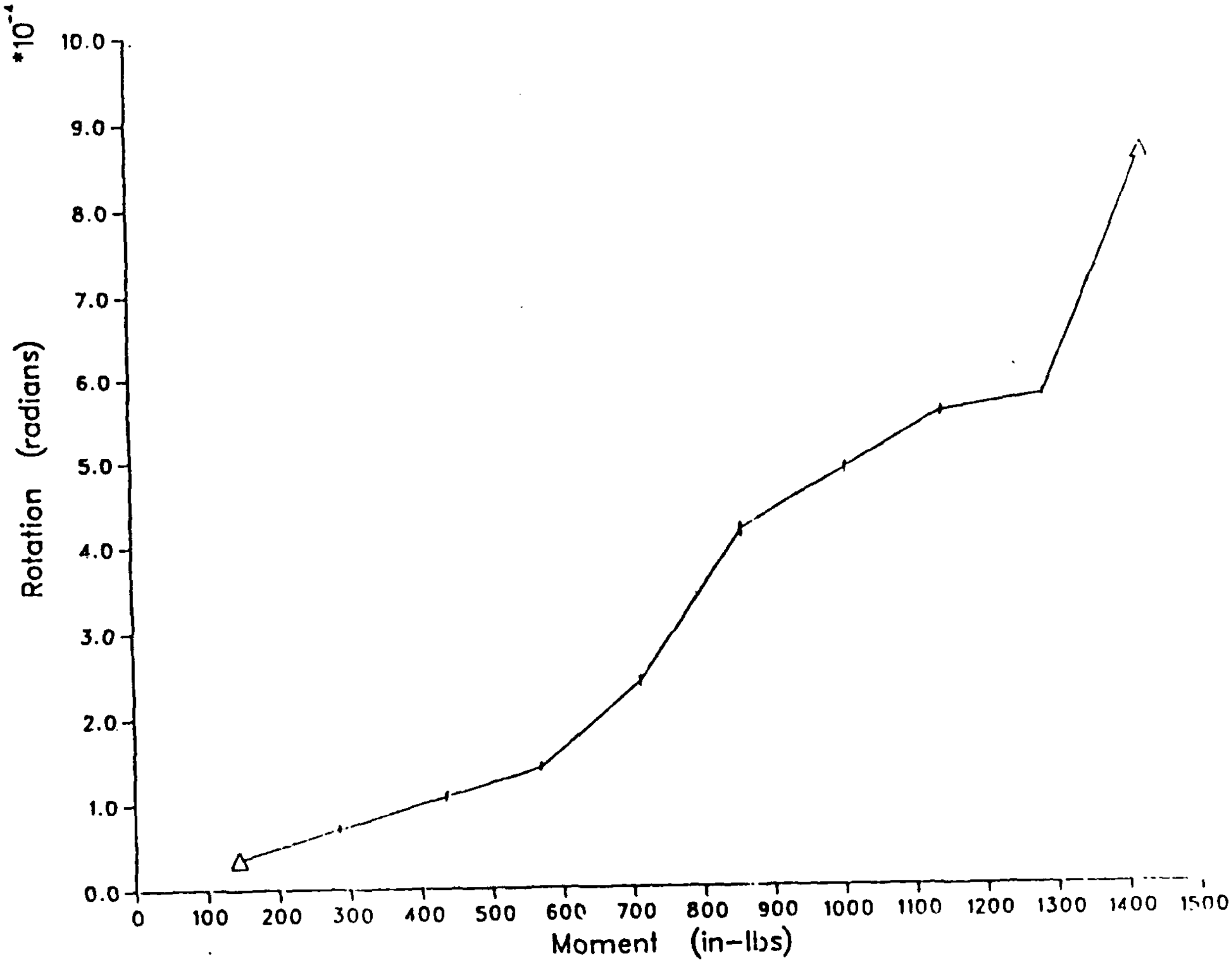

Figure 5-23. Moment-rotation Curve.

decreases giving a nonlinear response. The lack of smoothness in the curve in Figure 5-23 is due to the coarseness of the mesh, the large load increments and/or the placement of the applied loads.

It is proposed to further investigate the moment-rotation characteristics of the joint by greatly refining the mesh. A mesh generating program will be written and used to produce the refined element mesh. It will place the nodes and develop element connectivity. The program will allow the mesh size to be changed easily and will format the node and element data for input to the finite element code used. Using the finite element code, loads will be applied to produce a pure bending moment about the joint. The load will be incremented and springs will be eliminated as they go into tension. Joint rotations will be calculated and plotted against the applied moment to develop a moment-rotation curve.

A joint physical model will be built and tested to provide experimental results to compare with the numerical ones. The test setup will be like that shown in Figure 5-24. The experimental results will be used to verify the finite element model.

Once the technique of estimating joint stiffness using the finite element model has been validated, then a finite element model of this actual joint can be constructed to obtain the actual stiffness to be used in the ring model.

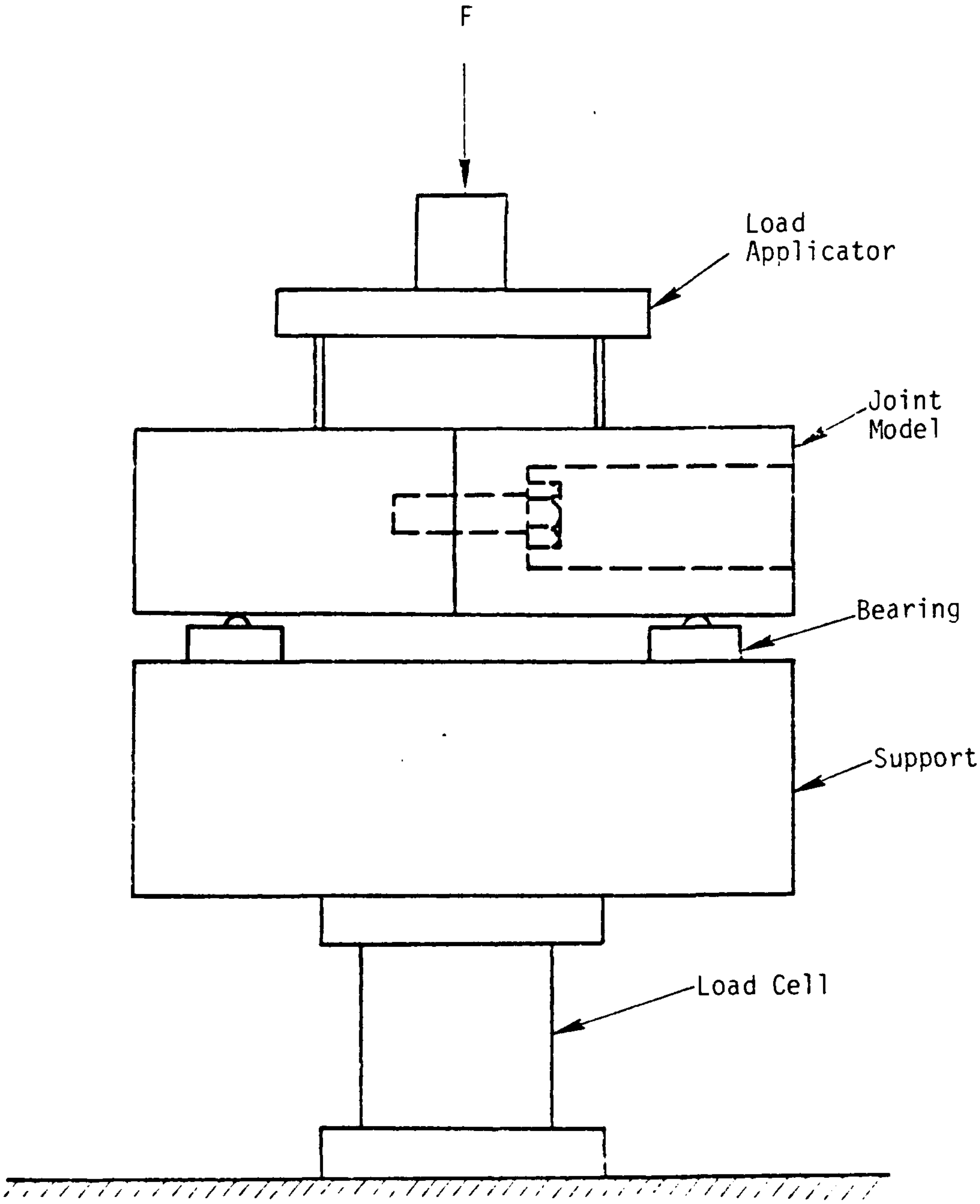

Figure 5-24. Joint Test Apparatus

CHAPTER 6

MICROASPERITY LUBRICATION

Background

Previous work [5] shows that at very low speeds (5-50 mm/sec) seal friction is very high. As the speed increases above this value, friction drops off very rapidly (specific results are shown later). This result is the same for both wavy and flat faced seals. It applies to the case of a carbon graphite sliding against a hard surface with mechanical contact in water.

This behavior is important to seal performance in two ways. First the high friction at low speed must be allowed for in the mechanical design of a seal because it represents the startup condition. Also some seals, such as in submarines, operate at a very low speed for a significant fraction of their life. Since this low speed friction can be as much as ten times the friction at higher speeds, such considerations must be made. The second reason for the importance of friction reduction with speed is that this reduction may in fact make it possible to operate seals of moderate and higher speeds. If the friction did not decrease, the friction power at higher speeds would become prohibitively large, and seals would heat check, wear, and score much quicker than is the actual case. Thus, this friction characteristic is very beneficial.

It was thought in the early part of this investigation that the friction reduction observed is due to hydrodynamic effects caused by

waviness. The flat face variable speed tests reported in the 1981 report [5] refutes this idea. In fact it is to be noted from those results that the experimental reduction in friction is much greater than that predicted by hydrodynamic effects caused by waviness.

After these observations were made it was decided that an investigation of speed caused friction behavior in carbon-hardface-water lubricated sliding systems should be pursued in some detail for the following reasons:

1) Good quantitative speed versus friction and wear data was needed for seal design purposes.
2) The cause of the friction reduction was not understood.
3) If the mechanics of the reduction could be understood, it might be possible to enhance it and reduce seal friction (and wear) even further.
4) If this behavior could be properly quantified, then it would make the task of assessing hydrodynamic effects in water much easier.

To fulfill these objectives, a study was undertaken to better understand sliding friction in carbon-hardface-water systems.

Theory

Approaching the phenomenon from a lubrication standpoint, if one considers theoretically flat parallel surfaces sliding parallel to each other and separated by an isothermal, uniform, steady film of Newtonian fluid, it can be shown using classical lubrication theory that no fluid films pressure is generated which might cause a friction reduction. On

the other hand, considering this phenomenon as being caused by a reduction of mechanical friction between the two materials as caused by the generally accepted adhesion theory of friction, then one must rationalize that adhesive bond shear strength must somehow decrease with increasing speed. No known theory suggests any strong relationship between adhesion bond strength and speed. However, it is widely known in dry sliding that starting friction is higher than moving friction. In the case of lubricated sliding this difference as reported in Reference [48] for many cases is not nearly as pronounced as has been measured in this present work.

Thus while it is possible that some of the observed behavior is caused by changes in the mechanical contact friction; the results show that friction coefficient approaches 0.01 with increasing speed. No known dry friction is this low, so that the reduction in friction cannot simply be a reduction of adhesive bond strength. Thus some type of hydrodynamic mechanism must account for all or a part of this reduction. This notion is supported by the fact that similar observations to the present have been made for parallel surface oil lubricated thrust bearings.

Many explanations have been advanced for the reduction in friction with speed in lubricated parallel sliding systems. Nearly all of the explanations hold that true parallel surfaces cannot be achieved in reality or that nonparallel surface geometries are generated by the process itself. Thus such load support can be explained by temperature induced warpage, unplanned machined waviness, eccentric rotation, seal

wobble and bounce, lubricant density changes, non-Newtonian lubricant effects, and microasperity lubrication.

Microasperity lubrication occurs when surface asperities act as small hydrodynamic thrust bearings. All real surfaces have asperities which can act as microscopic hydrobearings and provide lift. Because carbon has many natural asperities and because most of the other possible causes were minimized in the experiments, it was hypothesized that microasperity lubrication is the mechanism which causes the large friction reduction in the tests cited previously. The remainder of this chapter explains how this hypothesis was tested.

Microasperity Lubrication

The application of classical lubrication theory to a symmetric asperity like the one shown in Figure 6-1 yields a pressure distribution similar to the one depicted. Since the pressure distribution is an odd function, integration over the asperity to obtain load support yields zero. In actuality, the film pressure cannot become negative (fluids cannot support tensile stress) and the liquid cavitates when the pressure drops below the cavitation pressure. This situation is shown in Figure 6-2. Integration of the truncated pressure distribution yields a net positive load support.

Research reported by Hamilton et al. [49] clearly shows the relationship between microasperities and load support in parallel face rotary seals. An experimental seal with an optically transparent rotor was constructed so cavitation steamers could be observed in the oil lubricating film. In Hamilton's first test the torque was initially

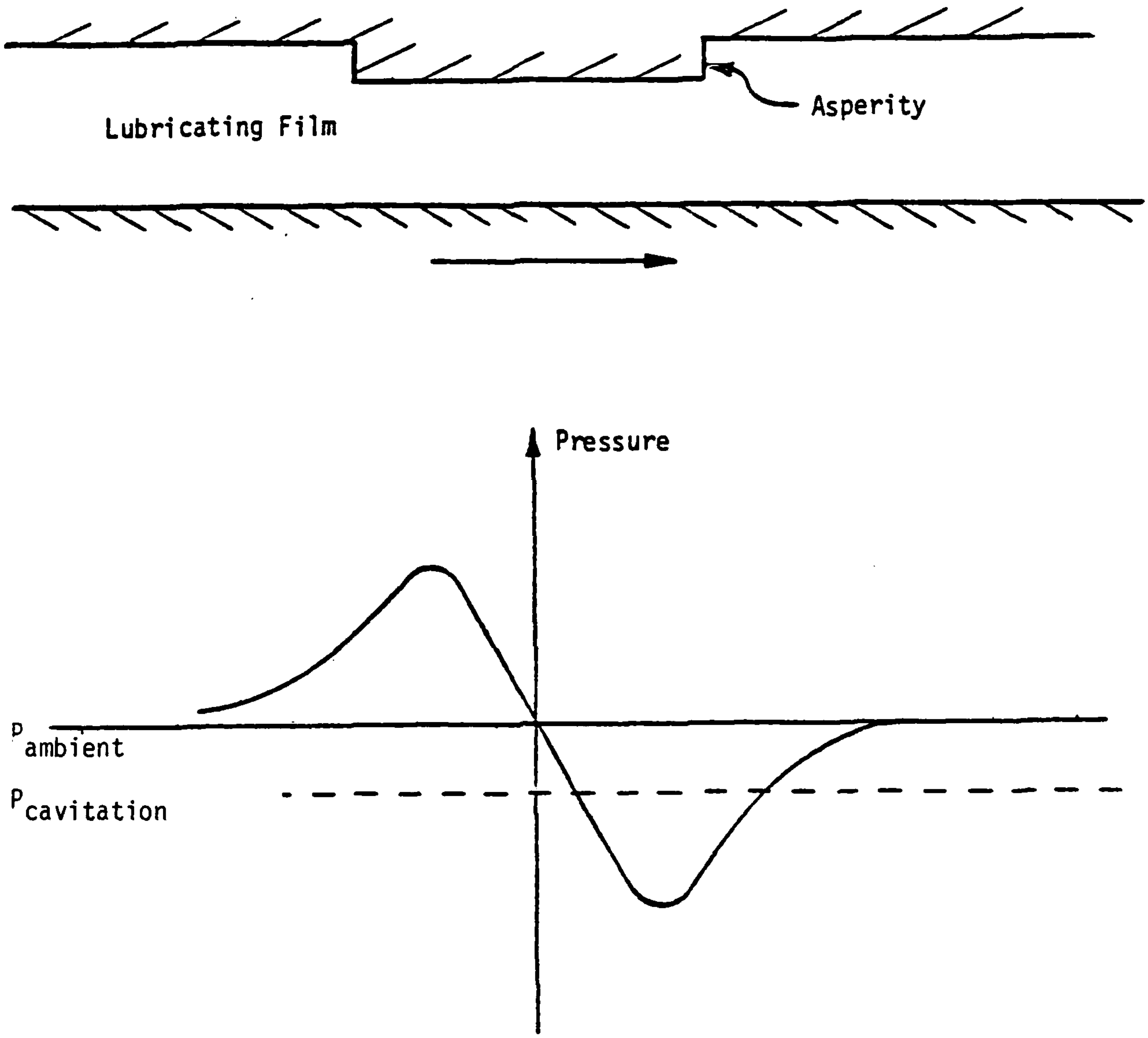

Figure 6-1. Asperity Pressure Distribution Predicted by Classical Lubrication Theory.

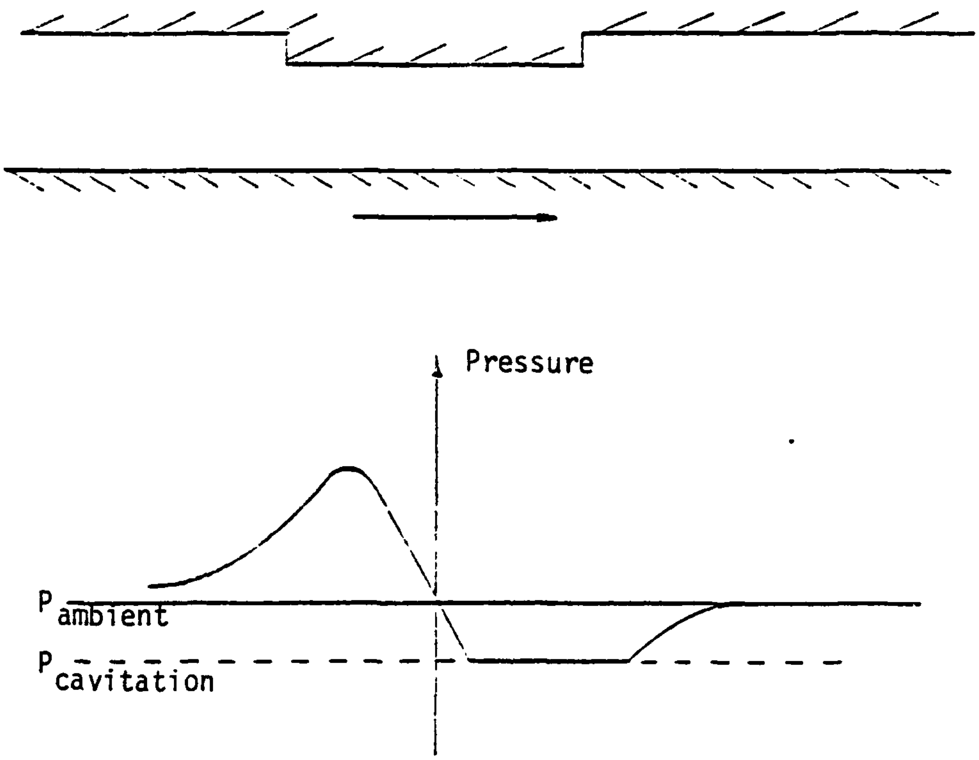

Figure 6-2. Truncated Asperity Pressure Distribution.

high and no cavitation streamers were observed. About one minute after start up the friction torque dropped sharply and cavitation streamers appeared simultaneously. Later it was found that the bands of cavitation occurred in areas where fine scratches or irregularities existed.

Next, asperity patterns were photoetched into the stator and tested using a hardened steel rotor. A known face load was applied and the film thickness measured by passing a very small alternating current of 7 kHz through the film. The face load was increased until a partial or complete destruction of the ac-film voltage drop occurred. At this point the film was considered to be nonexistent and load capacity reached. The test results indicated that there is a relationship between asperity distribution and geometry, speed, and load capacity. These results are shown in Figure 6-3.

Hamilton et al. [49] also presented a theoretical analysis and obtained an approximate solution for the load support generated by a field of asperities. The analysis begins with the Reynolds equation in polar form applied to the asperity shown in Figure 6-4. The result is then applied to the asperity field also shown in Figure 6-4 and then integrated to obtain load support. This model accounts for the existence of cavitation and shows load support to be a function of ambient pressure. This mathematical model is used as a comparison to the experimental results in this work.

The derivation of Hamilton's [49] model begins with the Reynolds equation in polar form. The major assumptions made are:

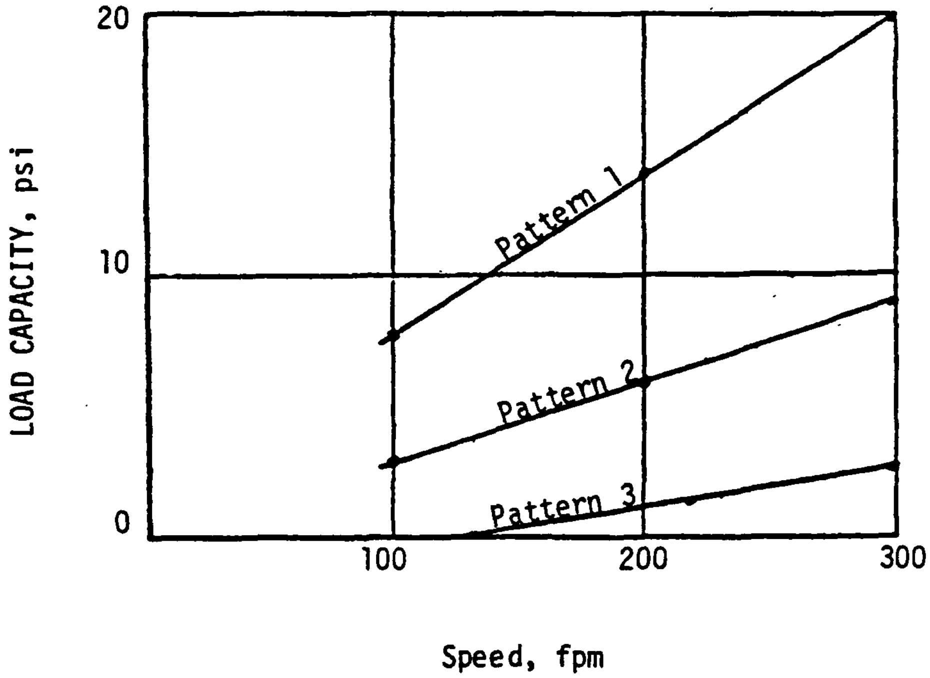

Experimental load capacity. Lubricant: 13.5-centistoke (100°F) mineral oil; stator-surface temperature, 100°F; inside sealed pressure, 5 psig.

Pattern	Asperity diameter, mils	Number of Asperities per sq. in.	Fraction of Area Covered by Asperities	Average Asperity Height, Microin.
1	4.6	12100	0.21	100
2	1.2	22500	0.026	83
3	1.7	22500	0.051	130

Figure 6-3. Experimental Results from Hamilton et al [9].

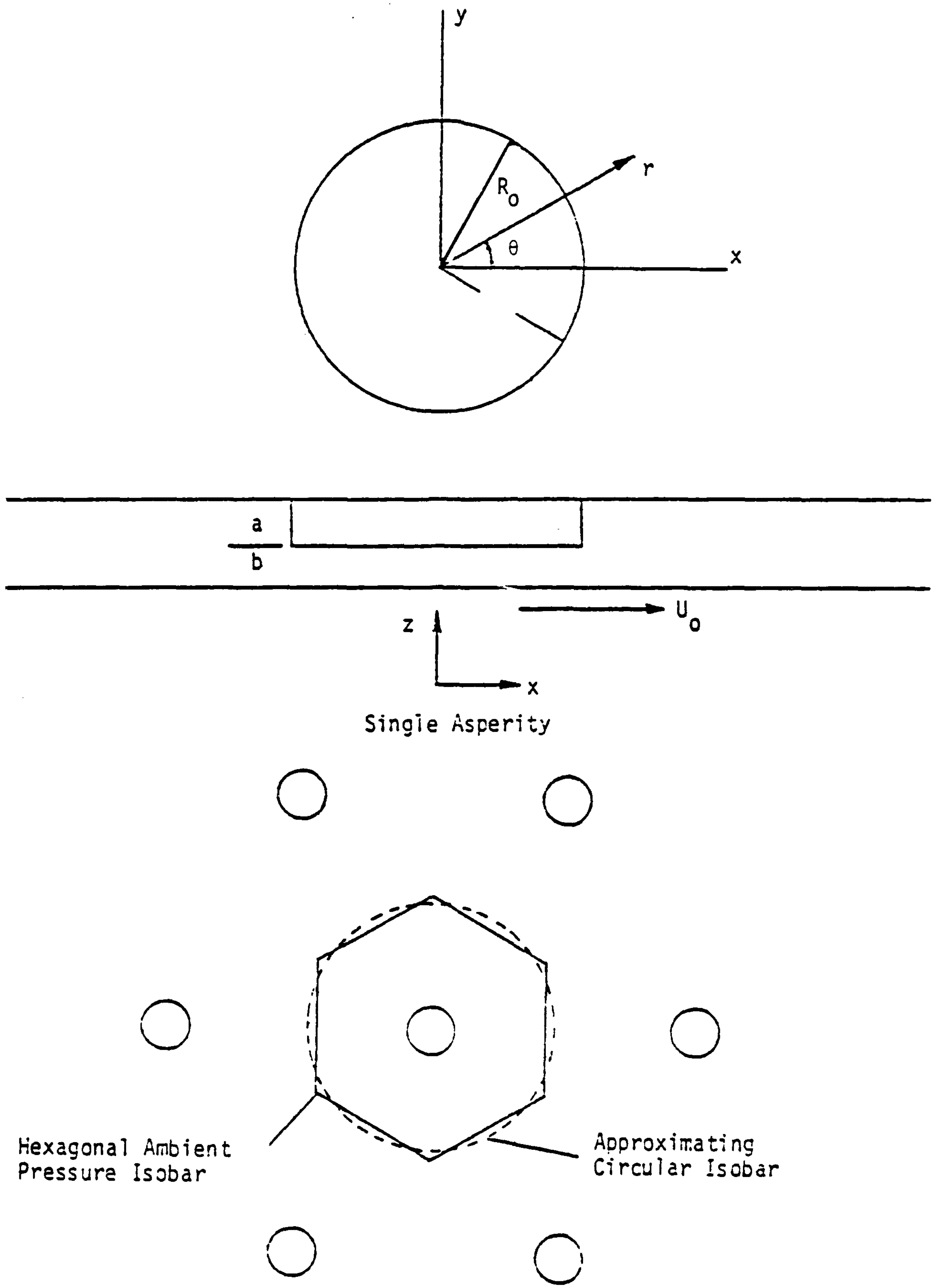

Figure 6-4. Asperity Geometry from Hamilton et al [49].

1) The Reynolds equation and all the assumptions made in its derivation apply.

2) Pressures calculated below the cavitation pressure of the lubricant are replaced by the cavitation pressure.

3) Load support is obtained by integration of the resulting truncated pressure distribution.

With reference to Figure 6-4

P = lubricant pressure

P_∞ = ambient pressure

P_c = cavitation pressure

p = amplitude of P-P

q_θ = tangential volumetric flow rate

q_r = radial volumetric flow rate

μ = absolute viscosity

δ^2 = area fraction occupied by asperities

W = load support

h, a, b, R_o, u_o, r, θ as defined by Figure 5

From Figure 6-4

$$h(r) = \begin{cases} b, \; r < R_o , & \text{Region I} \\ a + b, \; r > R_o , & \text{Region II} \end{cases} \tag{6-2}$$

The final result of Hamilton's work is

$$w = \frac{8 \, \mu \, V_o \, R_o \, a \, \delta}{\pi(b^3 + \gamma(a + b)^3) \, (1 + \delta)} - \frac{1}{2} \, (P_\infty - P_c) \; . \tag{6-3}$$

This equation shows that load support can be readily developed by micro-asperities.

Other investigators have considered microasperity lubrication. Kojabashian and Richardson [50] investigated the surface topography of the mating surfaces in carbon face seals. The experimental results reveal the existence of a micropad structure that develops with wear. This structure consists of flat raised pads highly variable in size. It is shown that these pads can be adequately described by an exponential probability distribution. These micropads are modeled by an equivalent step bearing and used to predict the performance of carbon seals. It was found that using average pad sizes in the analytical model causes hydrodynamic load support to be underestimated by an order of magnitude. It is concluded that more work is necessary before the micropad model can be definitely established or refuted.

Kistler et al. [51] have concentrated on the cavitation phenomenon in face seals. The objective of this work was to experimentally and theoretically study the effects of cavitation in thin lubricating films between rough surfaces. Presented in this work is the concept of a pressure distribution being truncated by cavitation. A model presented by Patir and Cheng [52] that considers the effects of surface roughness is modified to include the effects of cavitation. This model used to generate a pressure distribution between two rough surfaces sliding parallel to each other. The resulting pressure distribution is used to generate a plot of load capacity versus ambient pressure and clearly shows that load capacity is developed by an asperity field.

Test of Hypothesis

Microasperity lubrication has never been investigated in water sliding systems. While in oil systems the work of Hamilton [49] provides a virtual certainty that microasperity effects do exist and provide load support, no such verification exists for water. Of course, previous equations and work both indicate that microasperity lubrication should occur, although its effect will be smaller than for oil because of the reduced viscosity.

To test the existence of microasperity lubrication in a real system is difficult. (Note Hamilton contrived microasperities.) However an unusual approach was found. If the hypothesis that the fluid pressure is an odd function and is truncated by cavitation is true in microasperity lubrication, then ambient pressure should have an effect on load support. For example, if the ambient pressure is raised, less of the pressure distribution will fall below the cavitation pressure, resulting in a lower load support. If the ambient pressure is raised to a high enough level such that the asperity fluid pressure never drops below the cavitation pressure, the load support will be zero (see Figure 6-5). Thus, changing the ambient pressure and observing the resulting load support can be used to experimentally investigate the effects of microasperities on hydrodynamic lubrication. The load support need not be directly measured; instead, a constant load is applied and friction torque is measured. An increase in friction is interpreted as a decrease in hydrodynamic load support.

This approach is supported by Hamilton's equation. Figure 6-6 shows predicted load support as a function of ambient pressure at

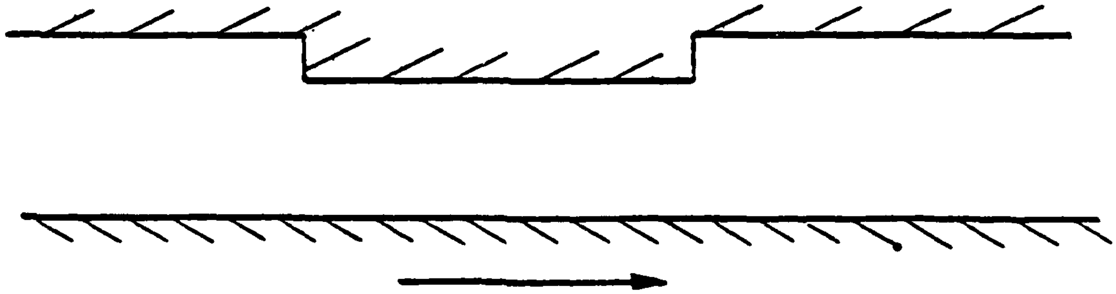

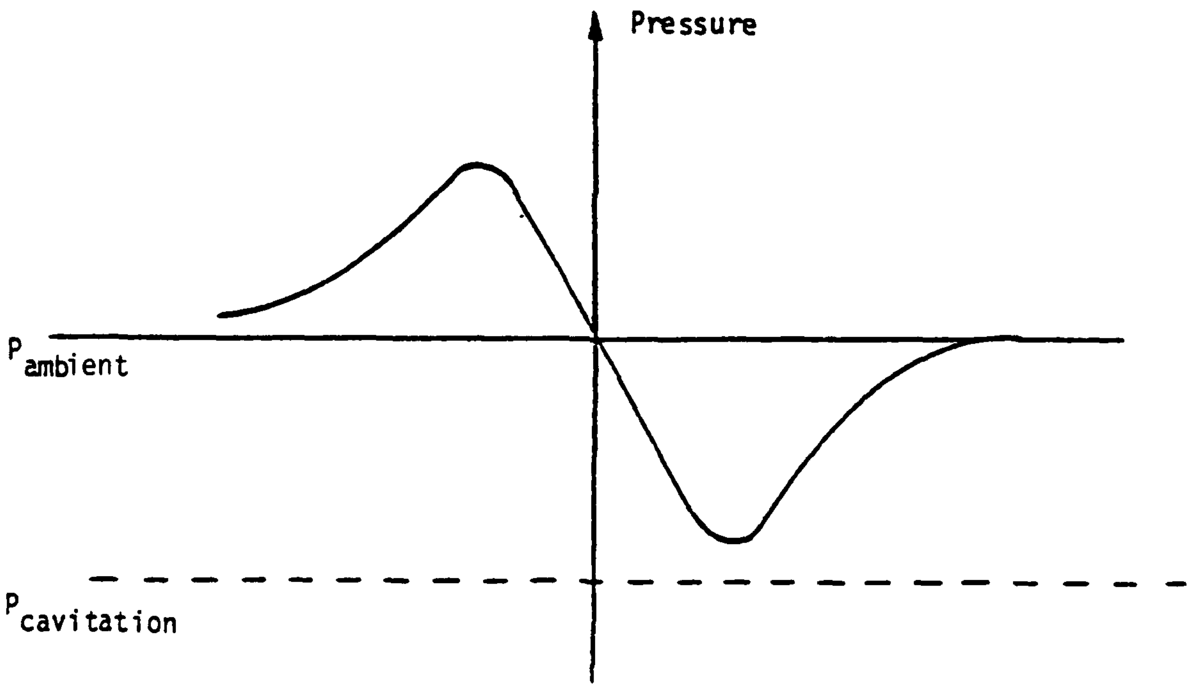

Figure 6-5. Zero Load Support.

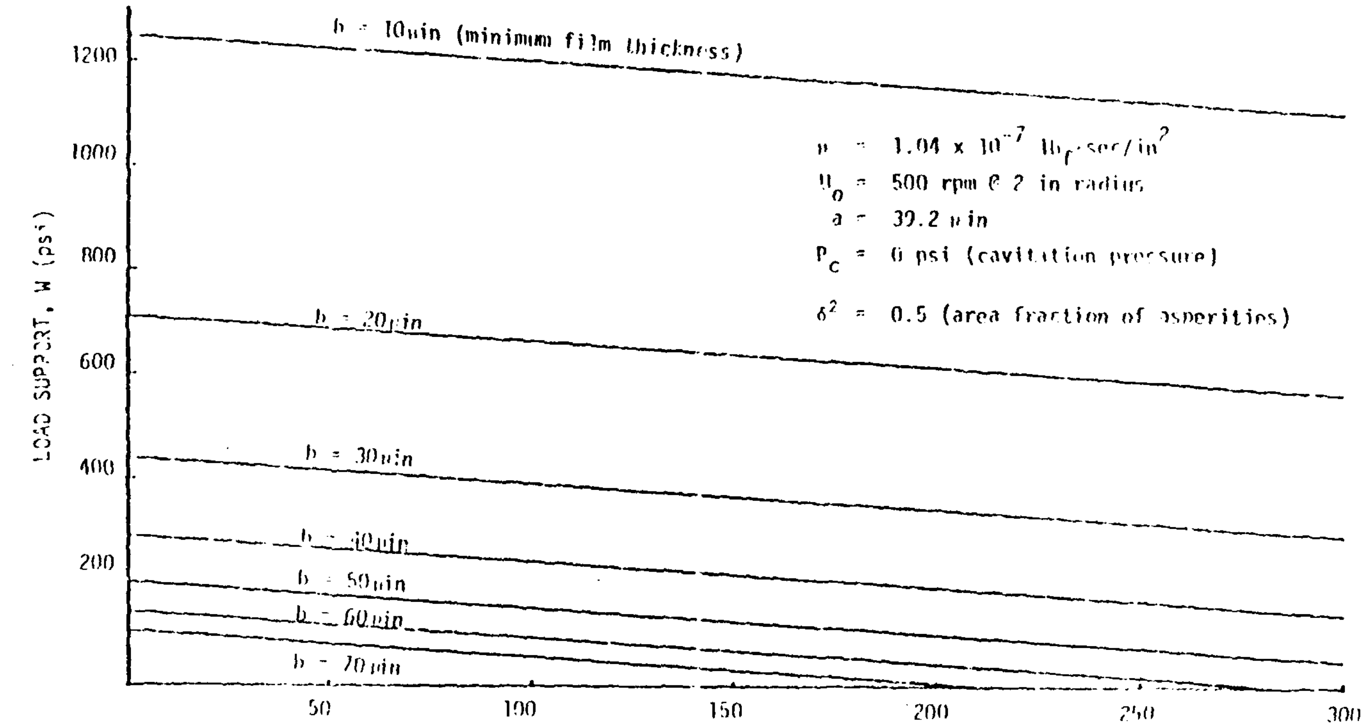

Figure 6-6. Load Support vs Ambient Pressure (from Hamilton) [49].

constant minimum film thickness. As ambient pressure is increased the decreased load support would require that more of the load be supported by mechanical contact and friction would therefore increase. Kistler [51] shows a similar result in Figure 6-7. Thus, experimentally operating a parallel sliding experiment in the presence of a variable ambient pressure should provide an indication of whether or not micro-asperity lubrication is functioning.

Experimental Apparatus

To test the stated hypothesis, an apparatus was designed to measure friction under the following conditions:

1) Parallel sliding in water.

2) Carbon versus hard face material.

3) Tilt of the face and wobble of the rotor to be minimized.

4) Water can be pressurized to 300 psi.

5) Variable speed from 0.5 to 500 in./s.

6) No hydrostatic load support component (unlike in face seals).

An experimental apparatus designed by Summers and Lebeck in 1981 [5] for the purpose of measuring dynamic coefficients of friction of carbon materials rubbing on hard faced materials in water under pressure was used to meet the basic condition and criteria above. This apparatus consists of a rotating support system, stationary support system, pneumatic load unit, strain gage unit, and a pressure vessel (see Figure 6-8).

The rotating support system is driven by a constant torque variable speed DC motor and the rotor (rubbing surface) is a tungsten

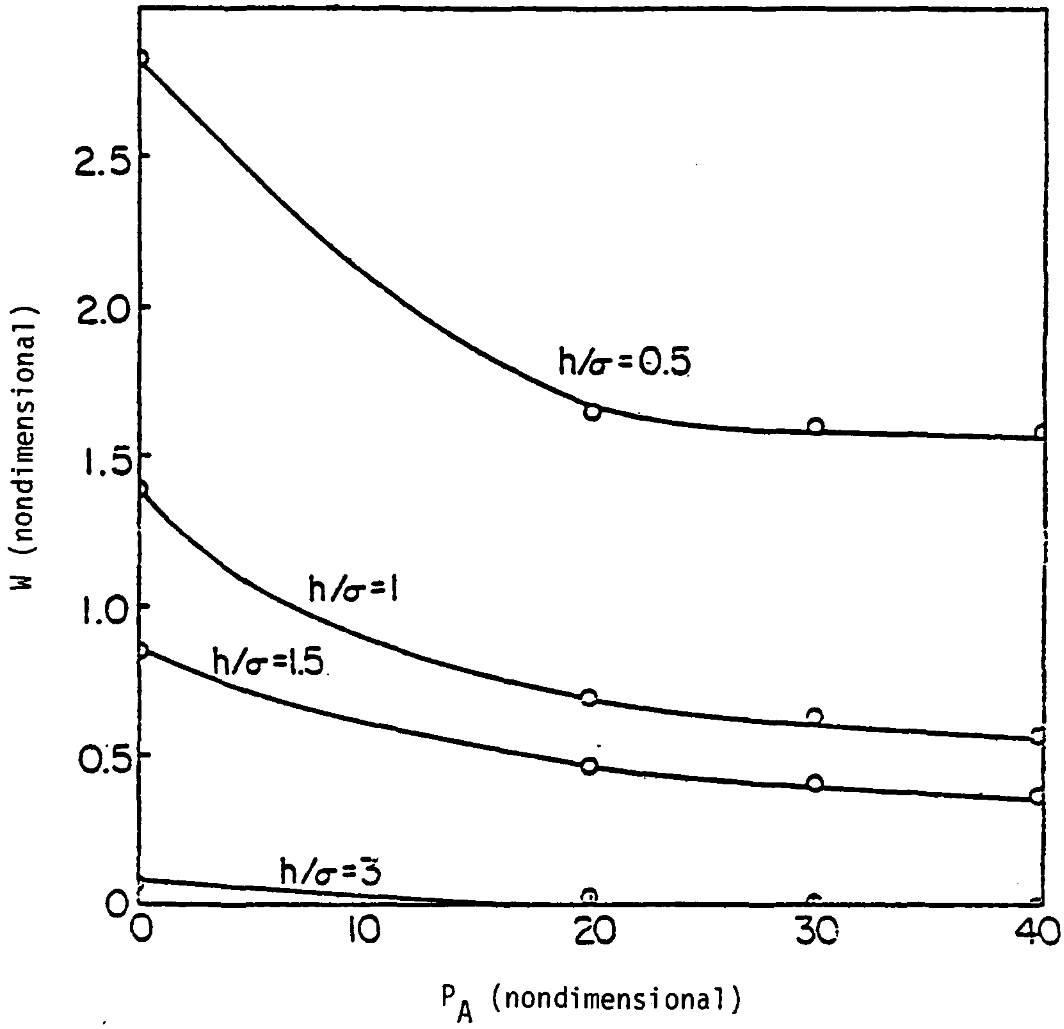

Figure 6-7. Load Support vs Ambient Pressure (from Kistler) [3].

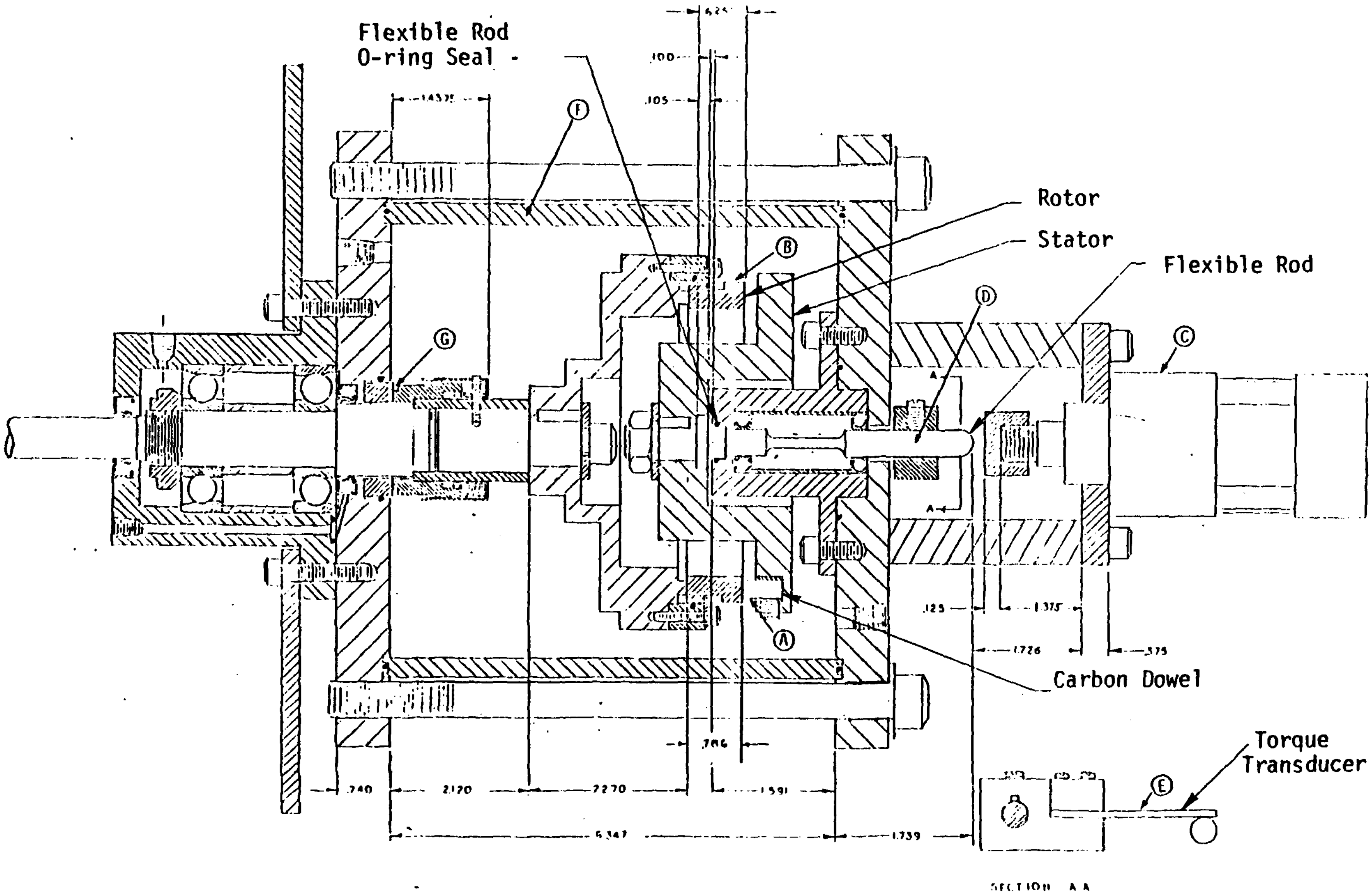

Figure 6-8. Friction and Wear Test Apparatus.

carbide seal ring. The axial runout of the rotor at the rubbing radius was reduced to 0.0002 in. total indicated reading to minimize hydrodynamic load support generated by wobble and bounce. This was accomplished by grinding the rotor supporting mount in the bearings that are used in the tester itself.

The stationary support system holds three carbon dowels on the rotor face. The faces of the carbon dowels are always held parallel to the face of the rotor even after wear occurs, thus eliminating hydrodynamic load support that would be generated if these surfaces were not parallel. This geometry is maintained by supporting the stator (the carbon dowels) with a flexible rod which can deflect to compensate for uneven wear and misalignment. A combination of the three point contact geometry of the carbon dowels and the flexible rod assures that the plane formed by the carbon dowel rubbing surfaces will be parallel to the plane of the rotor rubbing surface when a load is applied to the flexible rod.

The torque measuring and load application parts of this original apparatus were completely redesigned herein because it was discovered early in this investigation that the O-ring over the flexible rod caused indeterminate friction both for the torque measurement and for load application.

Initially two designs were considered. The first reduces O-ring size and separates the stator from the rod through which the load is applied, the objective being to reduce friction at the O-ring seal and make the measured friction torque independent of the vessel pressure (see Figure 6-9). The contact radius between the load rod and the

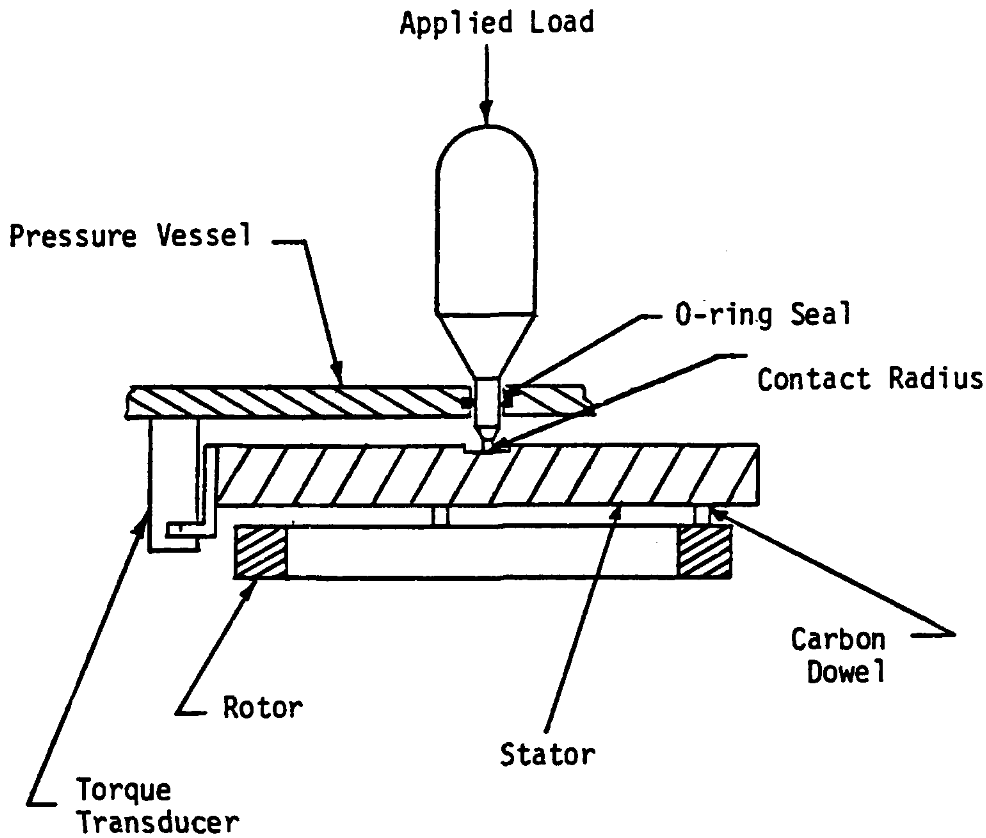

Figure 6-9. Point Load Design

stator is minimized in order to reduce the friction torque generated there. This contact radius is limited by the stress developed in the small diameter rod used to make this contact. Since a small contact radius is desired to minimize the unwanted friction, the stress developed in the small diameter used to make this contact is extremely high. This design would not make the measured friction torque independent of vessel pressure. The friction developed at the O-ring is reduced but still a function of vessel pressure in an unknown way making the applied load an unknown function of vessel pressure. This design would make it necessary to measure friction torque inside the pressure vessel as shown in Figure 6-9.

The second design considered incorporates a hydrostatic bearing in place of the flexible rod and creates a zero friction liquid coupling between the applied load and the stator (see Figure 6-10). The hydrostatic bearing assures that a fluid gap exists between the bearing parts. Since there is zero speed between these parts, there is zero friction. This design requires the torque transducer to be inside the pressure vessel. This configuration makes measured friction torque independent of vessel pressure but the applied load is still made through an O-ring seal and therefore dependent on vessel pressure in an unknown way. However this problem can be avoided by including a means for measuring the applied load inside the pressure vessel. It was decided to use the hydrostatic bearing design because this design totally eliminates torque error caused by unwanted friction.

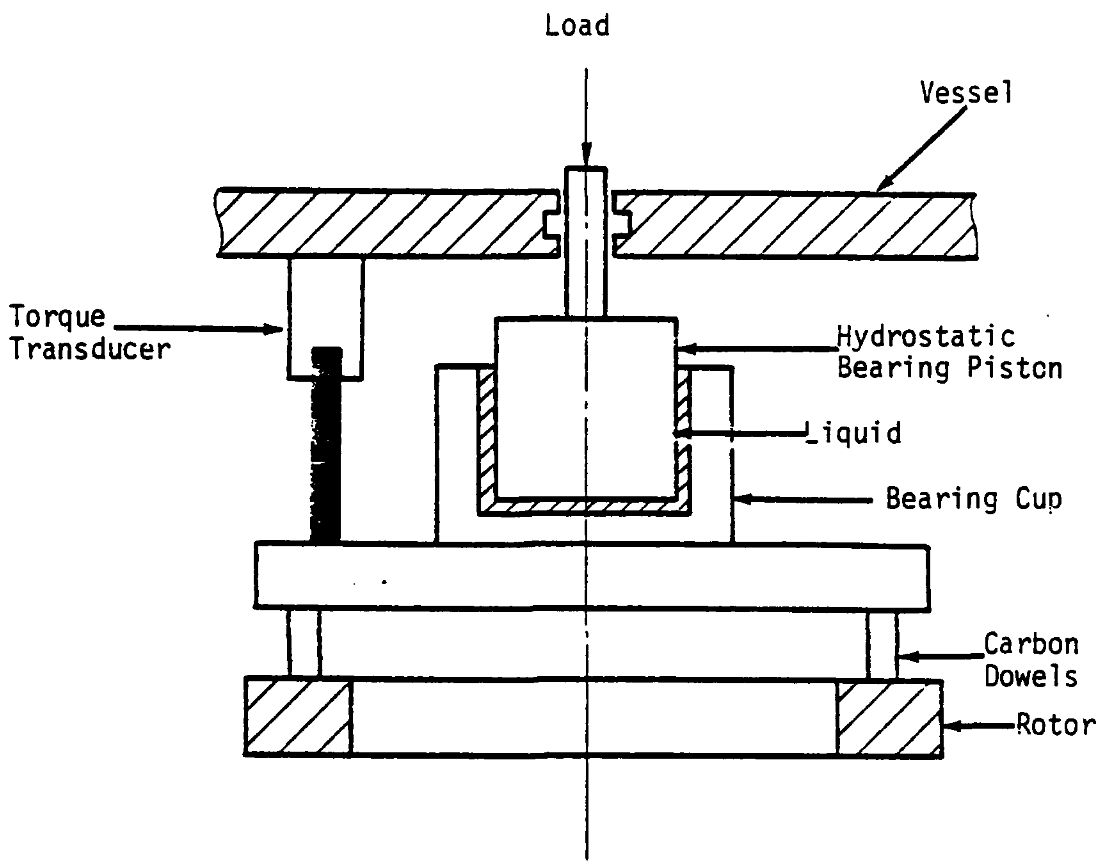

Figure 6-10. Hydrostatic Bearing Support.

Hydrostatic Bearing Design

The hydrostatic bearing designed must be capable of supporting normal and radial loads. The normal load is the applied load. The radial load comes from the torque reaction and unequal friction on the three dowels. A piston shaped bearing with hydrostatic pads on the sides and bottom (see Figure 6-11) is used. The piston fits into a cylindrical bearing cup. This particular bearing design has two s ts of four pads each spaced axially some distance apart. The purpose of the four pads is to provide radial stiffness in all directions as shown in Figure 6-12. The two sets are used to provide angular stiffness (Figure 6-12). The axial load is carried by the one pad at the bottom.

The details of the design procedure are contained in Reference [29]. Many factors were considered:

1) Radial stiffness, angular stiffness, axial stiffness
2) Total flow
3) Minimum clearance
4) Deformation of the bearing parts
5) Effects of misalignment

Capillary compensation was chosen. Each bearing on the side is stiff by itself but always acts opposite to another so that it tends to center the piston. The operating clearance was selected at 0.00075 in. (0.02 mm) to minimize flow yet be large enough to get good separation.

The two essential parts of the design are shown in Figure 6-13 and 6-14. An assembly is shown in Figure 6-17. Capillary tubes are shown in Figure 6-11. In order to assure that the stator dowels are held

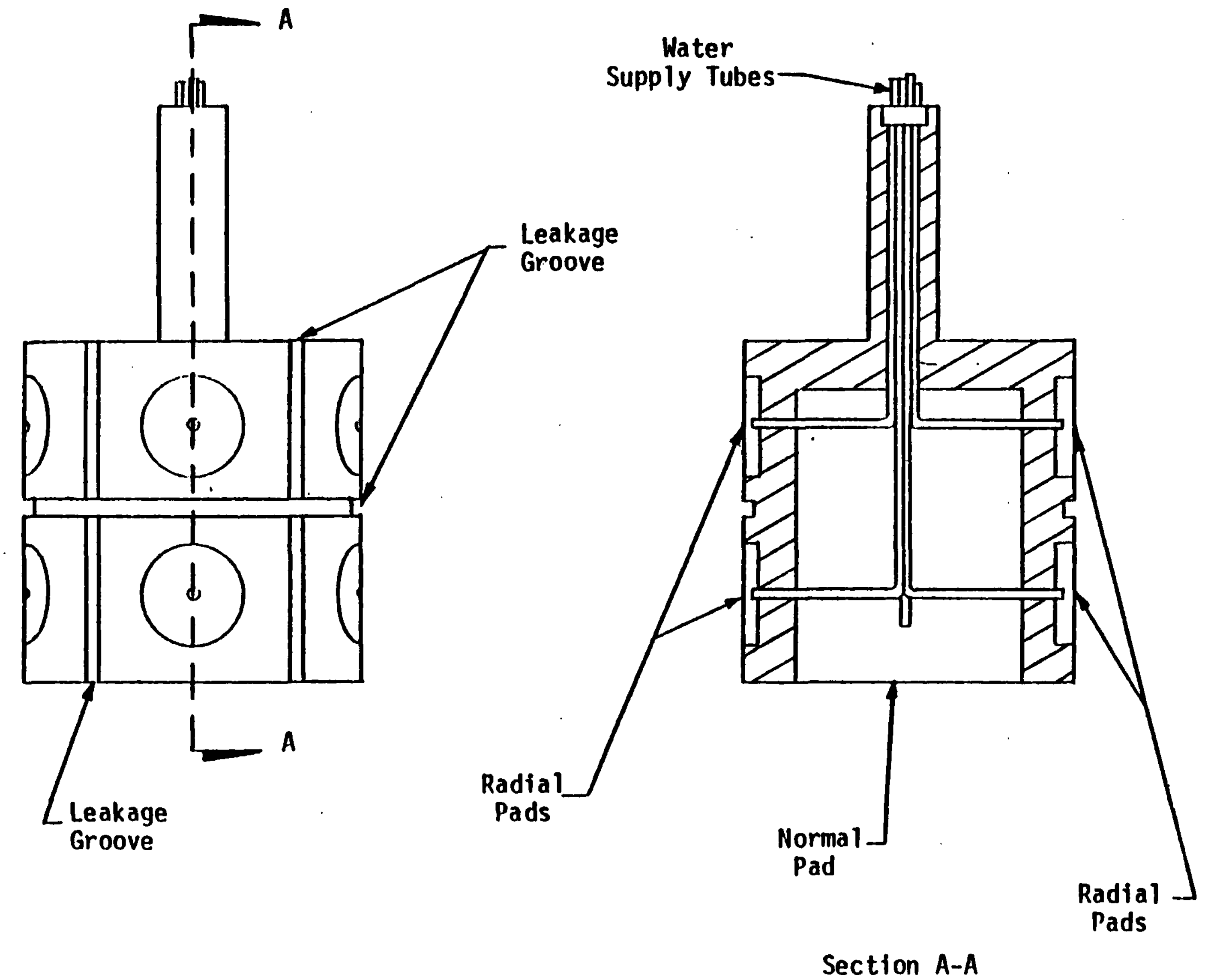

Figure 6-11. Hydrostatic Bearing Piston.

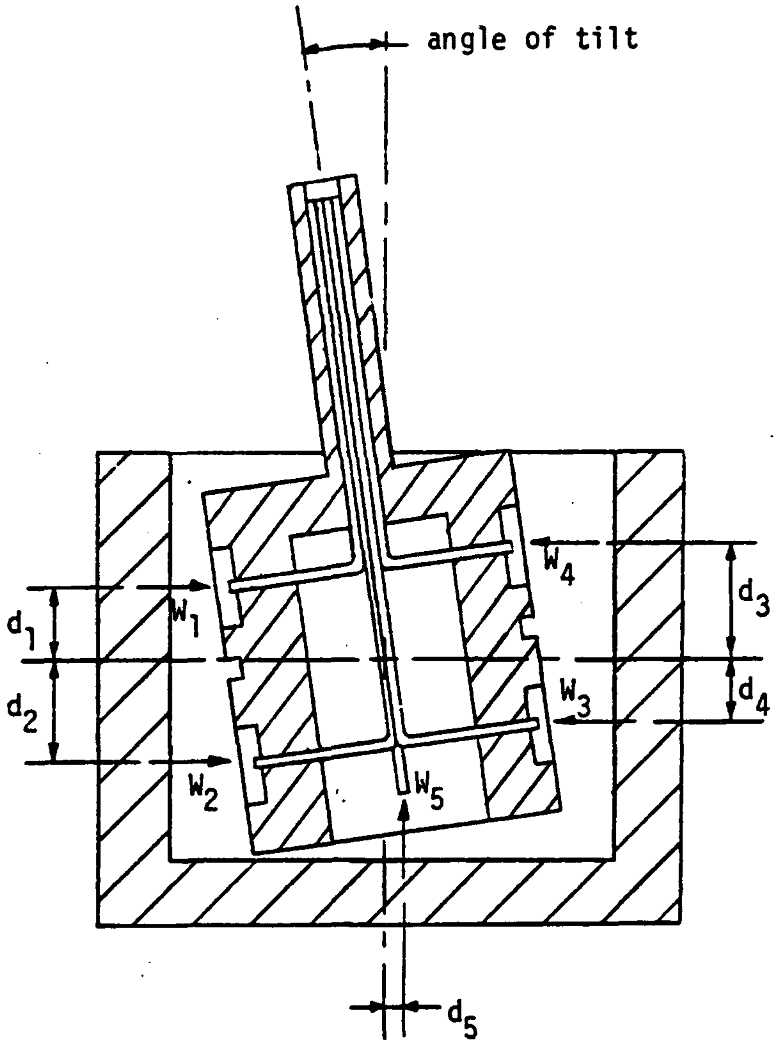

$$\text{Restoring Moment} = W_1 d_1 + W_3 d_3 - W_2 d_2 - W_4 d_4 - W_5 d_5$$

Figure 6-12. Bearing Misalignment and Moment Generated.

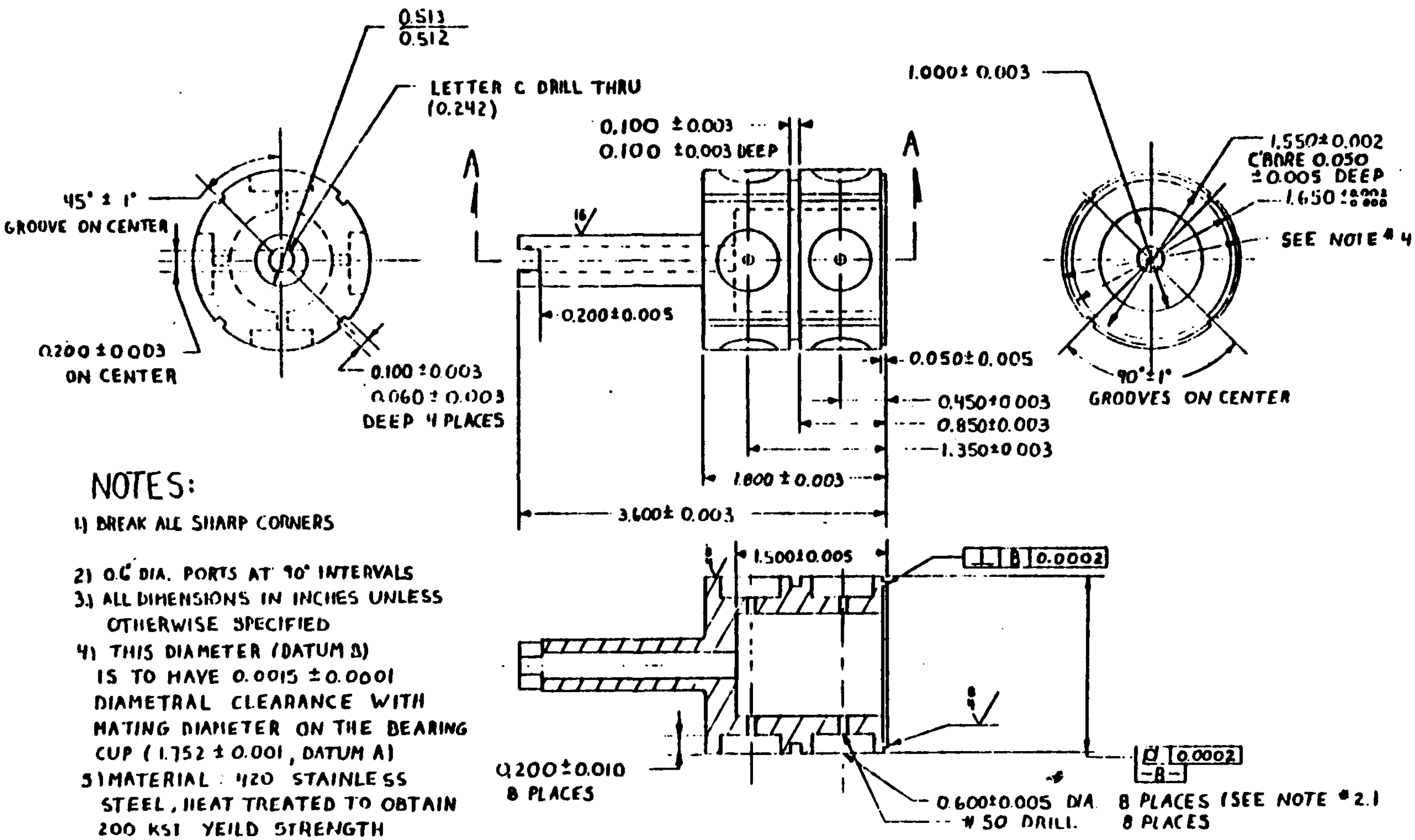

Figure 6-13. Hydrostatic Bearing Piston.

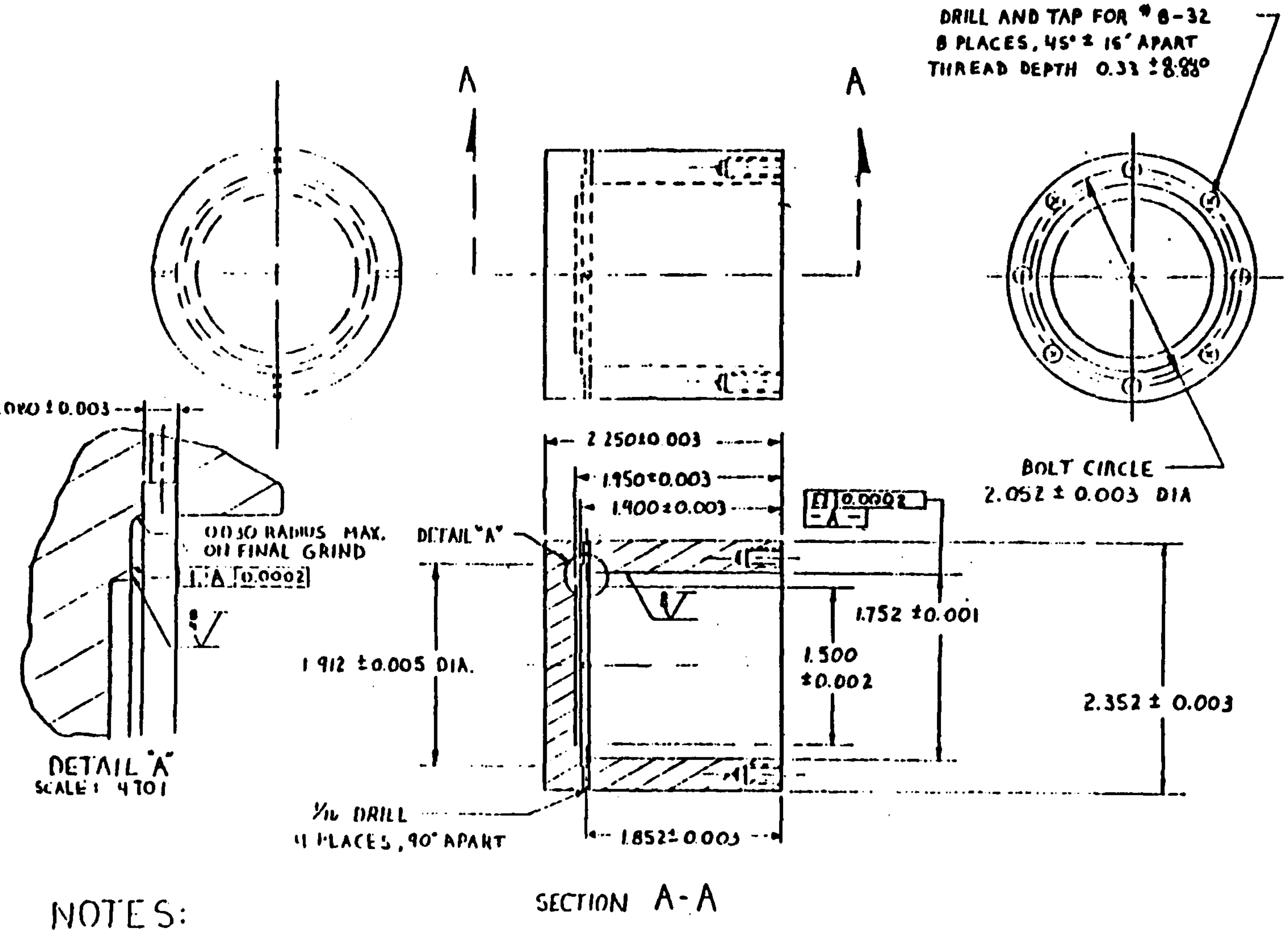

NOTES:

1) BREAK ALL SHARP CORNERS
2) ALL DIMENSIONS IN INCHES UNLESS OTHERWISE SPECIFIED
3) MATERIAL : 420 STAINLESS HEAT TREATED TO OBTAIN 200 KSI YEILD STRENGTH

Figure 6-14. Hydrostatic Bearing Cup.

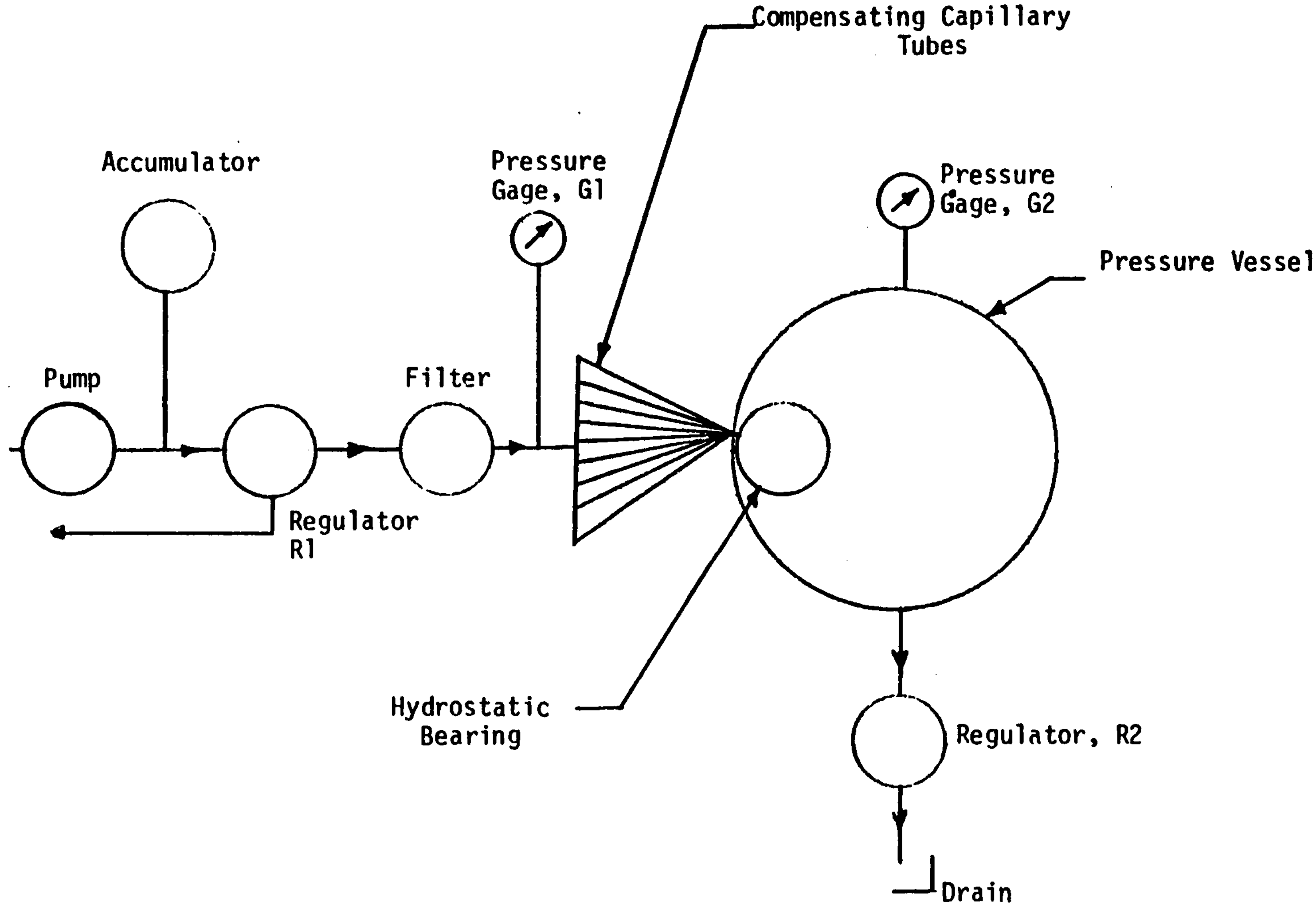

Figure 6-17. Water System Plumbing Duagram.

flat on the rotor, regardless of shaft misalignments through the pressure vessel, it is necessary to couple the hydrostatic bearing with a spring of much smaller stiffness. Figure 6-16 illustrates this configuration schematically. The flexible coupling is accomplished using an annular diaphragm shown in Figure 6-15. This diaphragm must be less stiff than the hydrostatic bearing and resistant to a water environment.

The friction torque reaction generated at the rotor-stator interface is transmitted directly from the stator to a cantilever beam mounted on the pressure vessel bulkhead (see Figure 6-15). This cantilever beam has a strain gage bridge mounted on it to measure bending strain. The cantilever beam is designed to have as much bending strain as possible to maximize the torque transducer output and increase torque resolution.

The piston must pass through the pressure vessel bulkhead where it is externally loaded with a pneumatic load unit. Therefore the piston must pass through an O-ring where vessel pressure dependent axial friction is generated. This is undesirable because it makes the load applied to the stator dependent on vessel pressure in an unknown way. This problem is minimized by reducing this O-ring friction to a minimum without ruining the integrity of the seal. This problem was later completely eliminated by measuring the load independently of the air pressure by placing strain gages on the diaphragm.

To insure that the bearing was working properly, the bearing cup was insulated electrically from the carbon holder ring and a wire was connected to the cup through the vessel. Then, when the cup was not

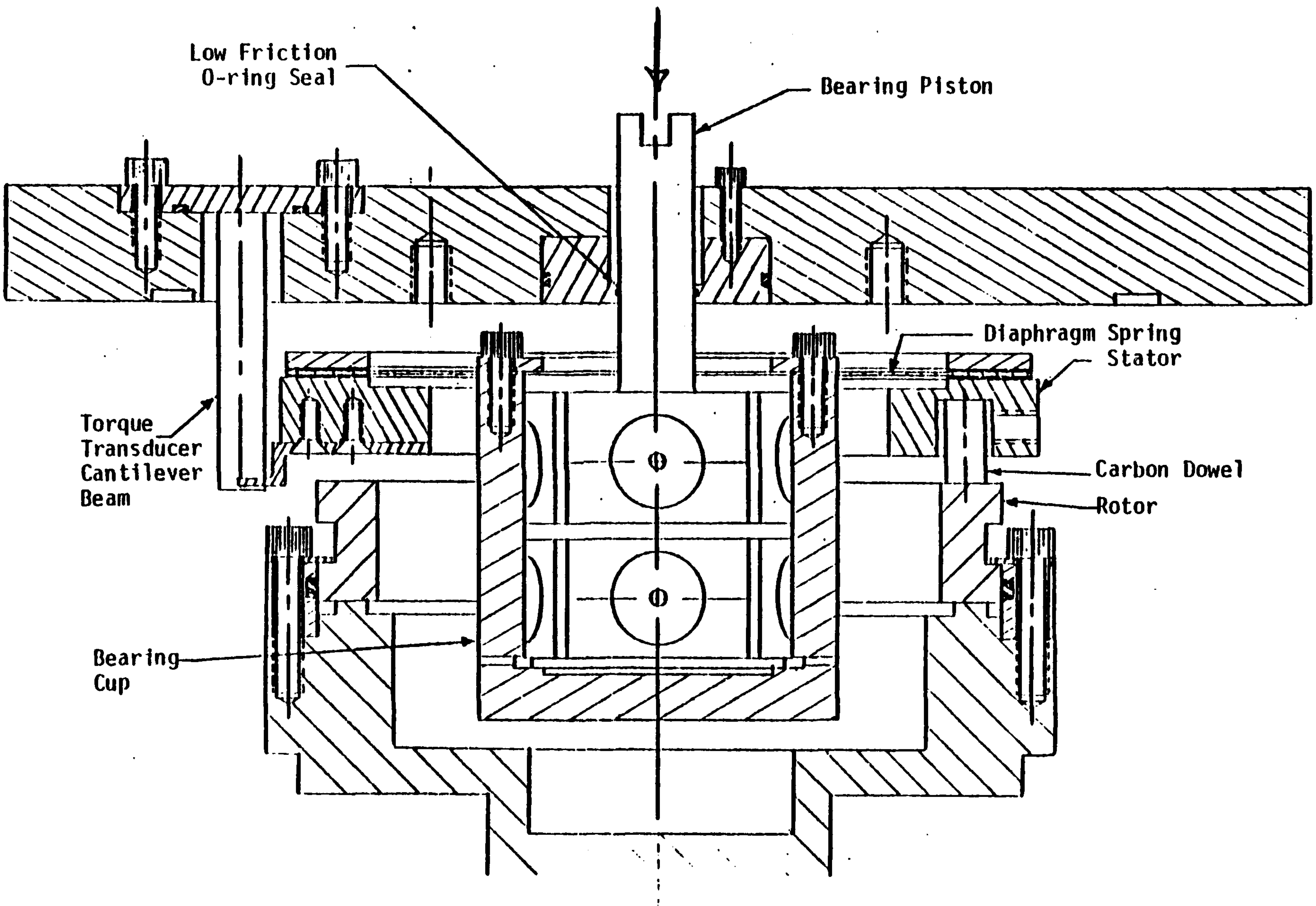

Figure 6-15. Hydrostatic Bearing Assembly.

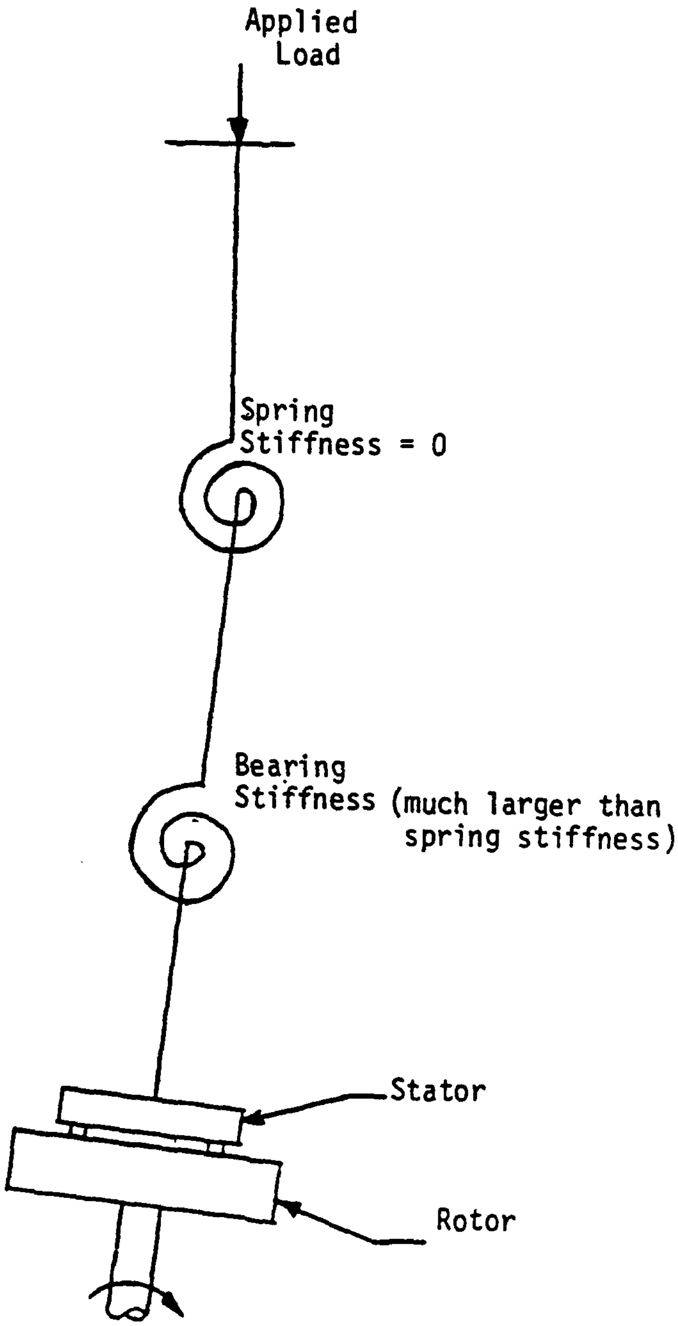

Figure 6-16. Torsional Spring Model.

touching, electrical resistance between the cup and the machine was large. When resistance became essentially zero, touching occurred.

Fabrication of the hydrostatic bearing was difficult because of the heat treating and precision required. Details of this process are contained in Reference [29].

Support System

A flow system was designed as shown in Figure 6-17. This arrangement allows the pressure drop through the capillary tubes and the bearing to be set at the desired level while permitting the vessel pressure (ambient) to be controlled. The need for the filter arises because clearances in the bearing are small (less than 0.00075 in.) and particulates can become jammed in the bearing causing mechanical contact to occur. The pump is a positive displacement triplex pump and delivers about 4 gpm at pressures up to 1200 psi. Pressure surges from the pump are controlled by the accumulator. The pressure on the inlet side of the bearing is controlled by back pressure regulator R1. Water is filtered to 2 μm before entering the bearing. The vessel pressure is controlled by back pressure regulator R2. The pressure drop across the bearing and capillary tube is now the difference between the capillary tubes inlet pressure and the vessel pressure (G1-G2). To minimize the burden on the water filter, distilled water was used and recirculated as shown. Figure 6-18 shows the test apparatus assembly. The support equipment is behind the panel.

Data is collected with HP 9835B computer with internal printer and real time clock, an HP 9872A plotter, and an HP 6940 multiprogrammer

Figure 6-18. Friction Test Support System.

with a low level A/D card. Rotor speed, vessel pressure, flow rate, and applied load are all set manually.

Hydrostatic Bearing Tests and Calibration

The purpose of using a hydrostatic bearing in the friction and wear test apparatus is to create a frictionless fluid coupling between the applied load and the stator. Any friction generated in this interface will influence the friction torque being measured and invalidate the measurement, defeating the purpose of using a hydrostatic bearing. It is therefore necessary to monitor the bearing to be sure touching does not occur. As described, checking for bearing touching is accomplished by measuring the electrical resistance across the lubricating film in the bearing. If touching occurs the resistance will drop to zero. The results of the resistance measurement varied a lot over a period of time. The cause for this fluctuation was determined to be the result of a voltage generated across the film by ions in conjunction with using a DVM. Measurement showed this voltage to be about 1 μV. Since the voltage generated by the digital meter to measure resistance is also about 1 μV, the meter was being fooled by the voltage generated by the migrating ions and the resistance measurement is not correct.

It was discovered when operating the bearing that an analog resistance meter did not have this resistance fluctuation problem because this meter uses a much larger voltage in the measurement of resistance. The analog meter was therefore used for monitoring touching and the technique was considered reliable.

The first performance test consisted of applying a known load to the bearing with a 150 psi pressure differential across the capillary tubes and the bearing. The load was increased until touching occurred. These tests showed that bearing operation was highly dependent on the cleanliness of the water and the bearing surfaces and that the load support of the bearing, indicated by the load at which touching first occurred, was less than predicted. This low load support prompted flow rate experiments to see if the flow rates predicted by the hydrostatic bearing model occurred in fact. It was determined that some redesign of the capillaries was needed [29]. After modifications were made, the bearing supported up to 170 lb normal load without touching. The model predicts that touching will occur with a 300 lb load. Recognizing that the bearing geometry was not perfect, this was considered adequate to start the test.

Calibration was accomplished by hanging weights with known values on the torque transducer cantilever beam and sampling 50 points with the data acquisition system described previously. An average of these points is then taken and a calibration constant (in.-lb/V) calculated. The calibration constant was 1.2 in.-lb/mV giving a least bit resolution of 0.006 in.-lb.

Testing of the force transducer on the diaphragm was performed by assembling the friction and wear test apparatus and applying an incrementally increasing load to the diaphragm. The resulting strain, read from the strain indicator attached to the bridge, was recorded for each load. Once the load reached 170 lb, the load was incrementally decreased and strains recorded. These tests showed the force

transducer's sensitivity to applied load is about 0.177 lb/microstrain. The force transducers sensitivity to tangential strain was shown to be insignificant. When the load was decreased from 170 lb, the strain readings were different from when the load was being increased by as much as 100 microstrain (18 lb). This was caused by the O-ring friction, and this demonstrates why the independent load measuring technique were necessary.

Experimental Procedure

The experimental procedure used to operate the modified friction and wear test apparatus is:

1) The capillary inlet pressure is set 300 psi above the desired vessel pressure (300 to 600 psi) using regulator R1 (see Figure 30).
2) Vessel pressure is set (10 to 300 psi) using regulator R2.
3) The torque transducer zero is obtained by reading the output of this transducer with no load applied.
4) The force transducer is zeroed by lifting the stator off the rotor and zeroing the strain indicator. The stator is separated from the rotor by pulling up on the piston.
5) If the test is the first in a series of tests with constant carbon pressure, the load is applied and the resulting strain on the diaphragm is recorded. For all other tests at this carbon pressure the load is applied by increasing the air pressure on the pneumatic load unit until the same strain

reading as on the first test at this carbon pressure is achieved.

6) When a test is finished the zero of the force transducer is checked to assure that no significant zero shift has occurred.

7) The desired rotor speed is set (50 to 2500 rpm) using a phototachometer.

8) The load applied to the stator (0 to 1000 psi carbon pressure) is adjusted using the air regulator on the pneumatic load unit.

9) Rotor speed is rechecked and readjusted if necessary.

10) The bearing film is monitored for a nonzero film resistance to assure that touching does not occur.

11) The computer program that runs the data acquisition system is run sampling 150 points/minute. Five minute tests are run.

12) Temperature control was achieved by circulating tap water of a constant temperature through a heat exchanger located in the distilled water reservoir.

Test Results

Using the tester as described before the hydrostatic bearing was added, many tests were run. Figure 6-19 shows a typical curve generated for friction as a function of speed. This curve is of questionable accuracy for the reasons mentioned but is included here to illustrate the trend of interest. When lower speeds were attempted friction

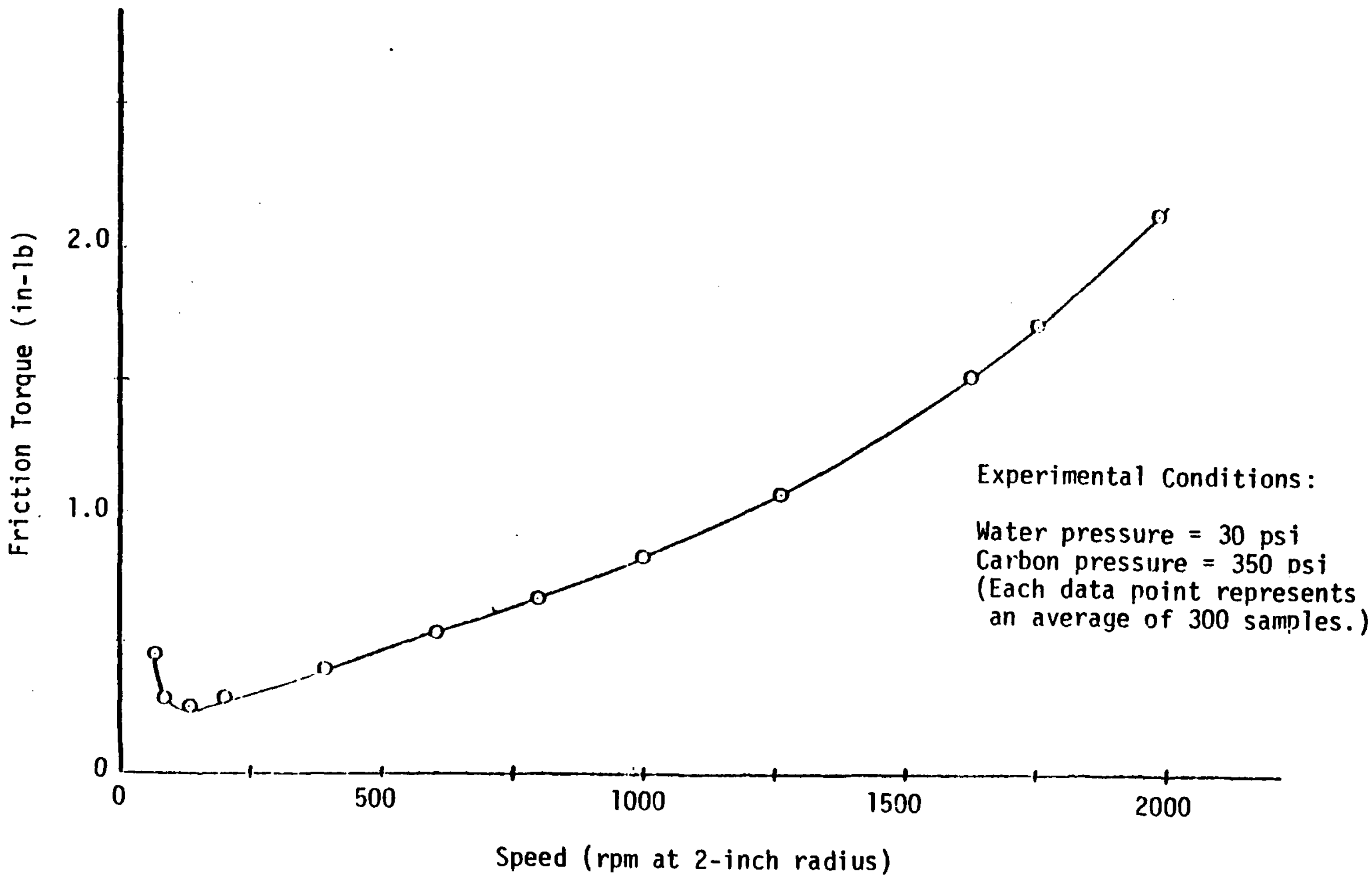

Figure 6-19. Friction Torque vs. Speed (early tests).

was very large, but stable operation could not be achieved so these data were not plotted.

Using the unmodified tester, it was also concluded that ambient pressure had no measurable effect in friction. However it was clear in these early tests that there was some uncertainty in the tests. Thus, it was at that point decided to modify the test apparatus and incorporate the hydrostatic bearing to eliminate the uncertainty caused by O-ring friction effects on the torque measurement.

After the modifications to the test apparatus, Figure 6-20 is representative of a typical test. Each point plotted represents the average of many samples. Typically 450 samples are taken during the two minute period of one test. The tests are not exactly repeatable but the trends established are.

Figure 6-21 shows friction as a function of ambient pressure at 100 and 200 rpm. First, it is to be noted that the friction is very low to start with. Second, the downward trend with increasing ambient pressure is opposite of that hypothesized. The character of the curve shown cannot be explained in terms of known theory.

It was then decided that at the higher speed the hydrodynamic effects (if they do exist) might be so strong that the modest levels of ambient pressure applied may not cause a significant decrease in cavitation. Thus tests at lower speeds were conducted by modifying the test apparatus. Figure 6-22 shows tests at very low speed. Again based on these results the hypothesis must be rejected. If anything the results show decreasing friction with increasing ambient pressure. Figure 6-23 shows the speed effect at these low speeds. It is apparent

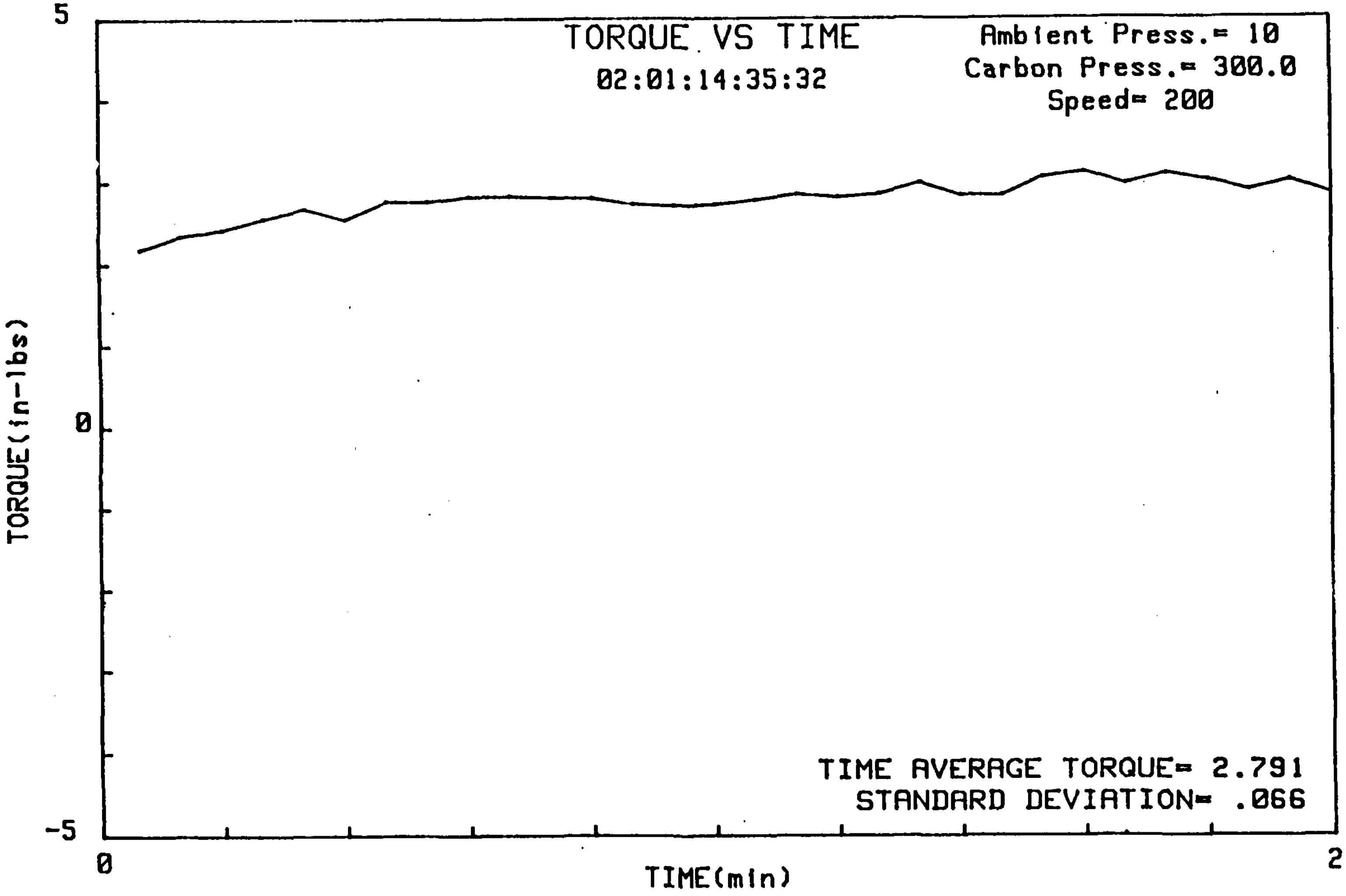

Figure 6-20. Friction Torque vs Time.

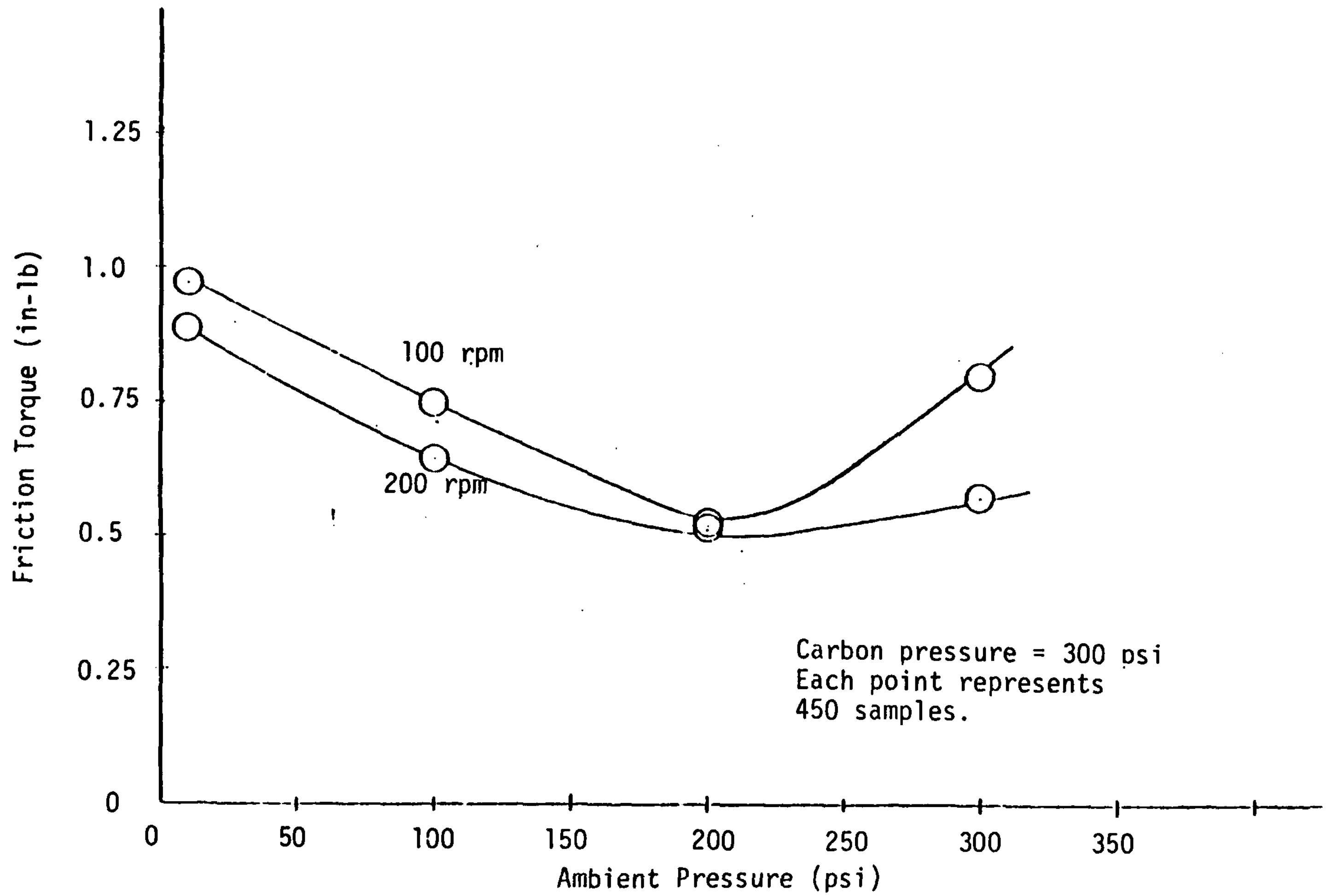

Figure 6-21. Friction Torque vs Ambient Pressure (high speed)

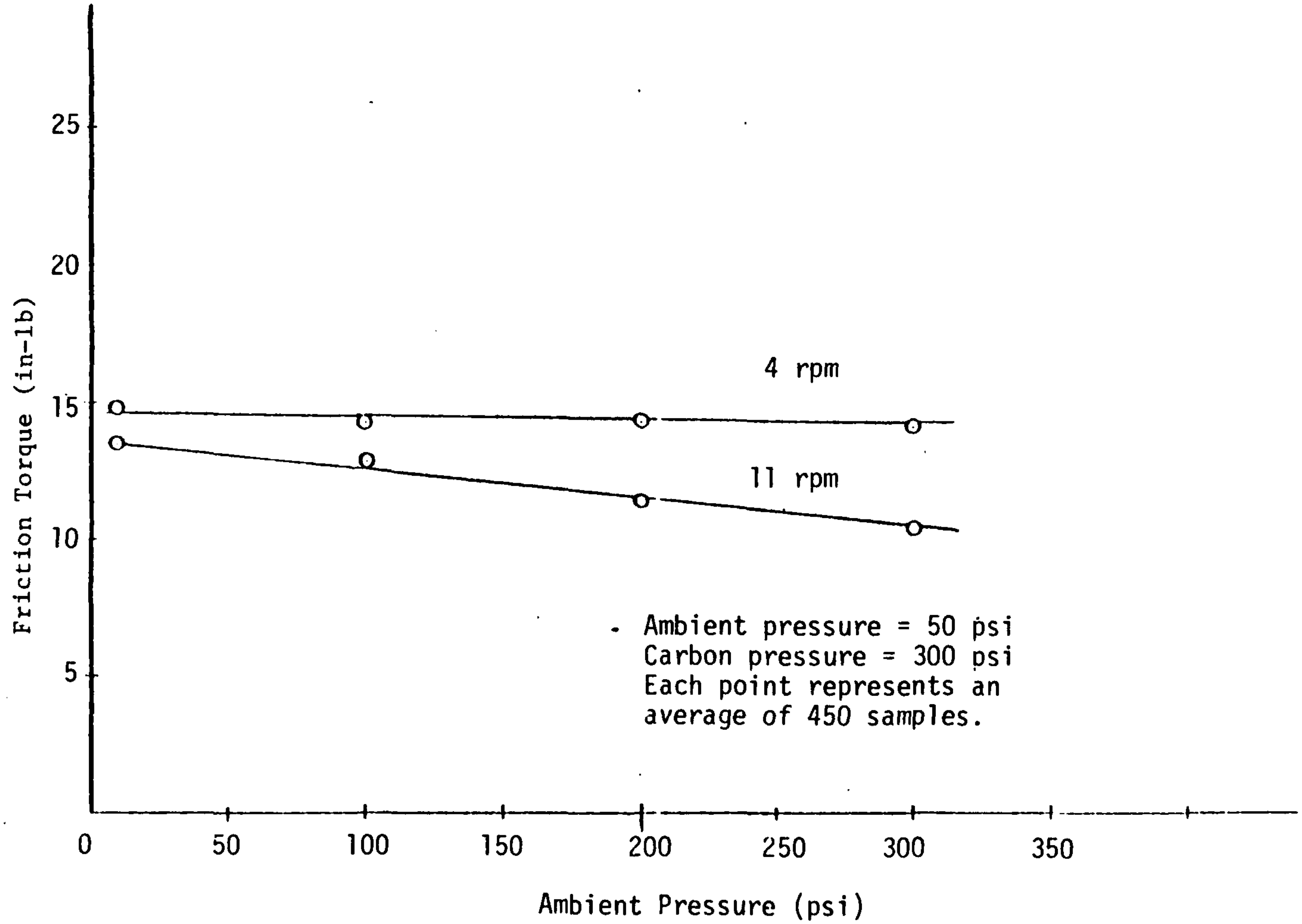

Figure 6-22. Friction Torque vs Ambient Pressure (low pressure).

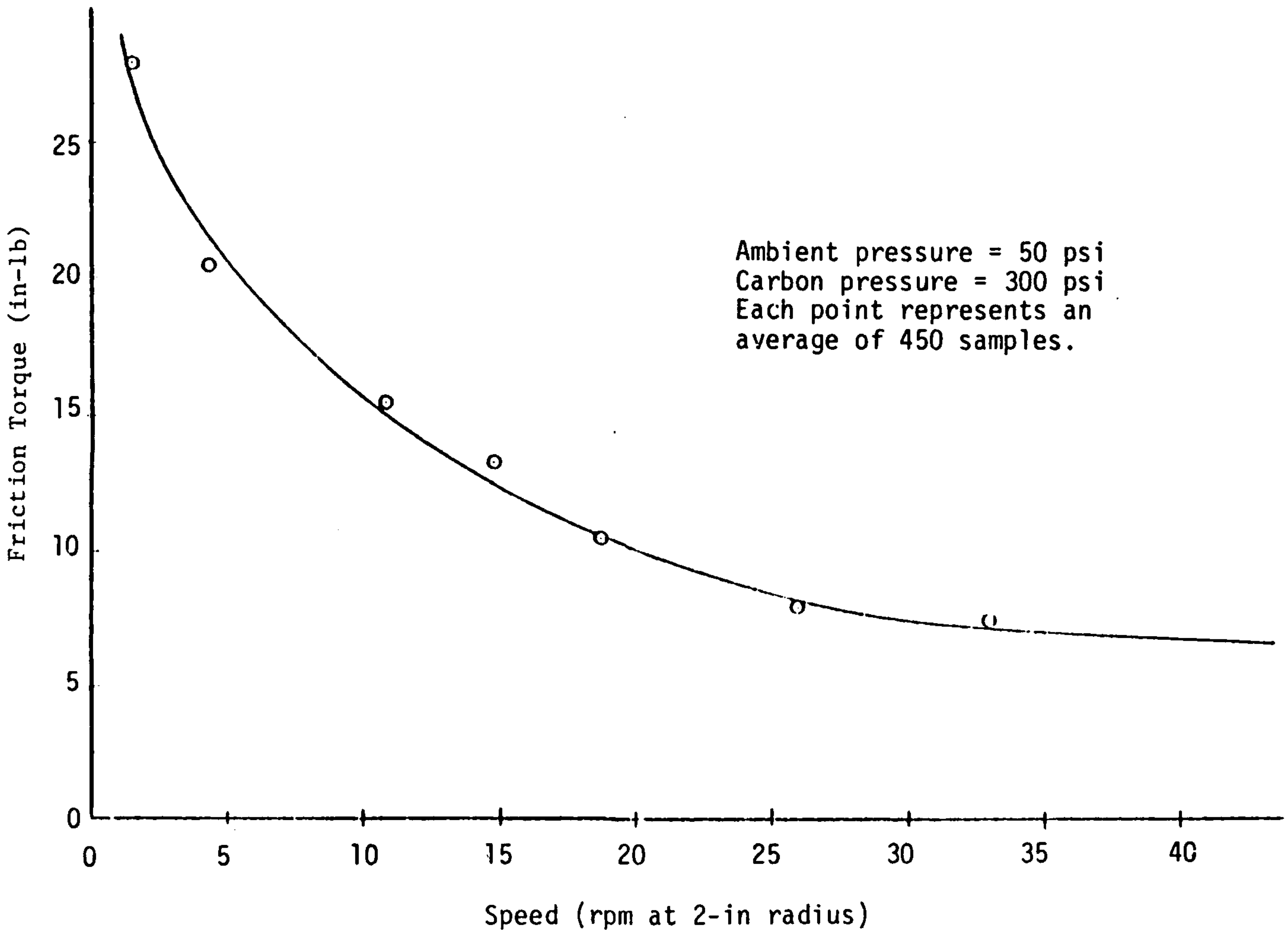

Figure 6-23. Friction Torque vs Speed (low speed).

from this curve that the speed effect was active at the speeds of the two ambient pressure tests of Figure 6-22.

The results contradicting the hypothesis were surprising. Apparently cavitation around asperities is playing no significant role in providing hydrodynamic load support in this carbon-hardface-water sliding system. Further conclusions and comments are made in Chapter 9.

CHAPTER 7

SEAL ANALYSIS

Throughout the seals research and development effort there has been a continual need to perform numerical analysis of seals. Many computer programs have already been described in the past [1-6] which are used to analyze wavy performance and for seal design. Such programs are very specific to these unique applications and hard to generalize for others to use. There are other programs however that have possible wider application and are easie: to set up for general use. These programs are described herein.

Role of Automated Analysis of Seals

Numerical tools are now available which can perform a very precise analysis of mechanical parts under load. While considerable satisfaction is gained from performing a finite element analysis of a seal ring which has already been designed. Such techniques are hard to employ during design because as soon as the smallest change is made, the mesh geometry must be entirely redefined and this is often very time consuming even if a CAD system is used. Thus to be most useful, analysis tools need to be automated as much as possible so that the designer's problem may be redefined in the simplest terms (moving a line on a screen) and the entire analysis is then made automatically.

Such a level of automation is difficult to achieve for general problems even using large software codes. However, for more

specialized problems like seals, automated analysis becomes much easier, and several such automated analysis packages have been developed herein.

Geometrical Considerations

To make it possible to do completely automated analysis for seals, advantage has been taken of certain common geometrical characteristics. Thus for the programs that follow the following restrictions apply:

1) The seals are made of axisymmetric rings.
2) The ring cross section shape must be describable by lines parallel and perpendicular to the axis.

The second condition is the most restrictive, but most seal rings observed are either like this or can be approximated as such.

The geometry definition needed for a ring is shown in Figure 7-1. Only the corner point coordinates in clockwise order need be provided to the programs. For the example shown in the figure, 14 pairs of coordinates are needed. The starting point is arbitrary.

Once these points are input, the analysis becomes automatic. Thus, it can be seen that it is a very simple matter to change geometry and make another analysis.

Method

All of the analysis programs described require that a mesh be imposed on the cross sections for the purpose of making finite difference and finite element calculations. The essentials of this

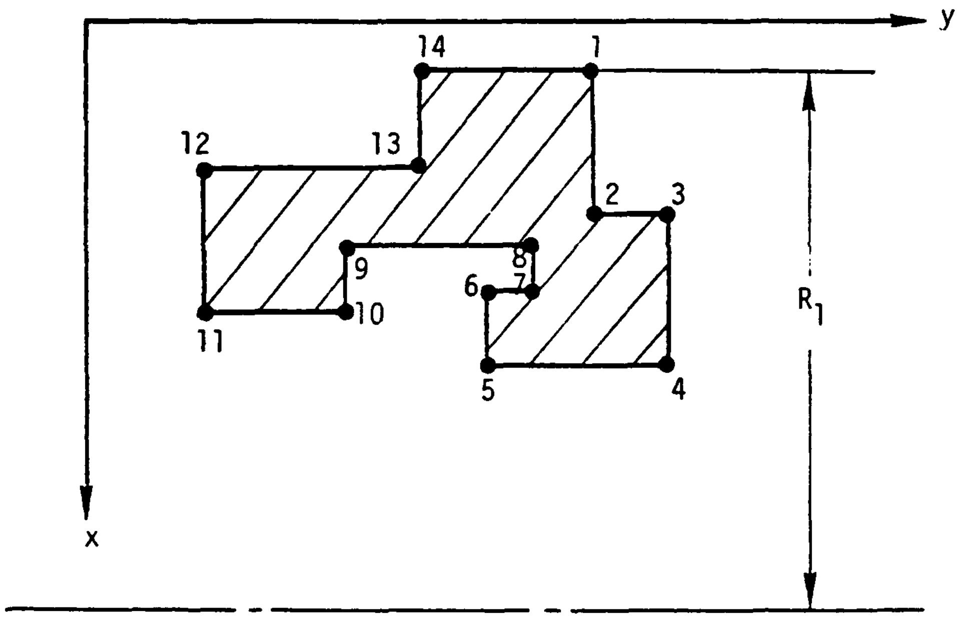

Figure 7-1. Seal Ring Cross Section Definition.

process will be described here so that the user can troubleshoot the program.

First a coarse mesh is generated based upon the sides of the section given. The coarse mesh will appear as in 7-2. The mesh will be of variable size but its boundaries will exactly coincide with the original boundaries of the part. While redundancy is eliminated by the program, having mesh points too close together is not, and the numerical consequences of such an occurrence have not been considered as yet.

After defining the coarse mesh, the program goes on to define the material contained within each rectangle of the mesh as to whether it is solid or a void. The solid-void definition is printed out as shown in the figures and will illustrate the basic shape of the object.

Once this step is completed, some computation can be performed using the coarse mesh. However, finite element, heat transfer, nd torsional stiffness calculations require a refined mesh. Thus, the next step is to introduce additional mesh lines between the ones shown according to a user specified maximum Dx and Dy. Once these lines are put in, then each of the refined rectangles is defined as to solid or void and the result looks the same as Figure 7-2 but the mesh will be more uniform and finer.

At that point computations can be made. Finite difference computations are made using proper derivative approximations for the variable mesh. The finite element mesh setup simply creates rectangular elements of the size discussed. The three programs available herein are now discussed.

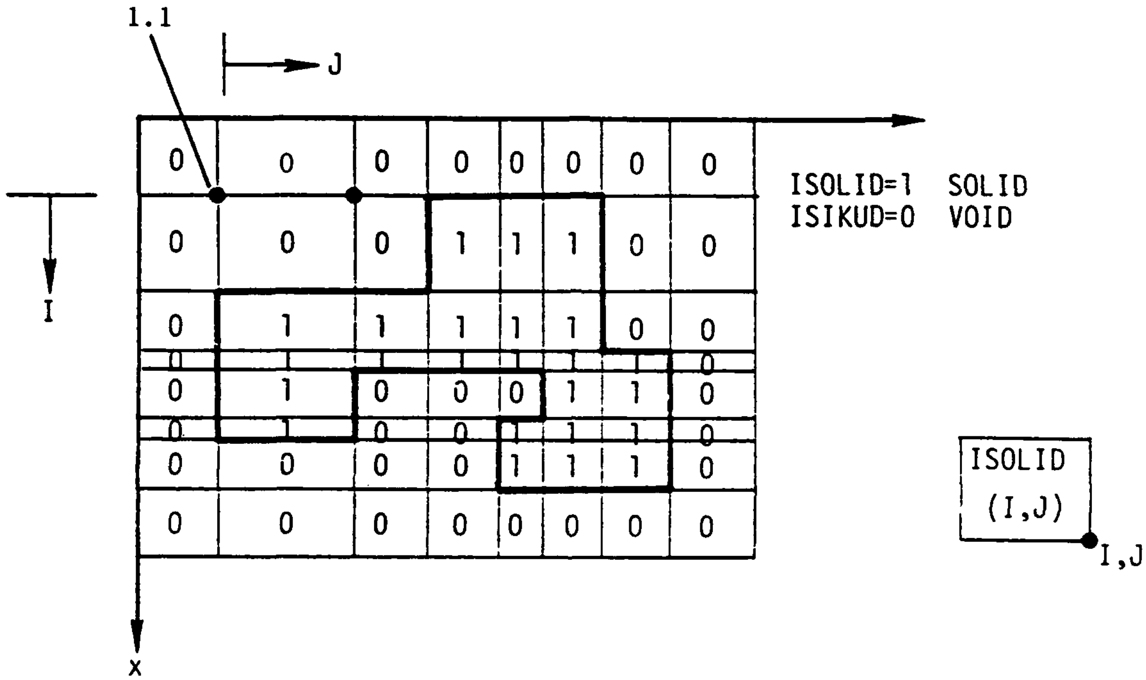

Figure 7-2. Coarse Mesh Generation

Section Properties Program

Appendix D contains the section properties program. It creates a refined mesh as described and calculates section properties.

First the centroid location is computed. Then straight beam theory moments of inertia are calculated first using an exact relationship to give

$$a = \int_A dA \ ,$$

$$I_x = \int_A y^2 \ dA \ ,$$

$$I_y = \int_A x^2 \ dA \ ,$$

$$I^2_{xy} = \int_A xy \ dA \ ,$$

where x and y are in the directions as defined with the origin at the centroid. Next moments of inertia for curved beams are computed by the exact solution of the following integrals:

$$J_x = \int_A \frac{y^2}{1 - \frac{x}{R}} \ dA \ ,$$

$$J_y = \int_A \frac{x^2}{1 - \frac{x}{R}} \ dA \ ,$$

$$J_{xy} = \int_A \frac{xy}{1 - \frac{x}{R}} \ dA \ .$$

While many times the straight beam approximations are sufficiently close in value to the curved beam properties to be used, it is useful to be able to calculate both easily and compare the two. It is also useful to have J_{xy} available because J_{xy} couples in-plane and out-of-plane deflection and loads as discussed in Chapter 5.

The torsional constant is often very difficult to compute for typical seal cross sections using handbook methods. For torsion of a noncircular section, it can be shown that a Poisson's type equation applies [32]

$$\frac{\partial^2 \phi}{\partial x^2} + \frac{\partial^2 \phi}{\partial y^2} = -2 ,$$

where ϕ is a stress function. This equation was solved using a variable spacing finite difference method. Then

$$J_\theta = 2 \int \phi \, dA .$$

Using this program it is readily shown that the approximate formulas often used for cross sections like these are quite inaccurate.

Mesh Generation

Appendix E contains a mesh generation program. The program takes the data generated by the section program and automatically generates finite element coordinates, node numbers, element numbers, and connectivity data for rectangular axisymmetric elements to feed into a finite element program. It then goes on to ask for constraint and load input

which is properly formatted along with the above to create a data set for reading by SAPIV. This program or its equivalent is very useful to have if FEM are needed as a part of the design process.

Heat Transfer

Appendix F contains a heat transfer and thermal rotation analysis program for seal type geometries. The program permits the use of two materials with heat generation at a sliding interface between them. It also permits arbitrary convection boundaries. It solves for the temperature distributions in the two seal rings and the thermal rotation of each ring based on this temperature distribution. It uses the refined mesh generation program described in Appendix D to set up the basic mesh. Several conditions and assumptions were made when developing the program:

1) The program calculates the mechanical pressure at the interface assuming a linear fluid pressure drop. It then assumes that the mechanical load is uniform, that friction created by the mechanical load (per the friction coefficient) is all turned into heat, and that this results in a uniform heat generation at the seal interface.
2) It is assumed that both materials have the same temperature at the interface, i.e., one node is common to both materials. This is reasonable for a first approximation, but it must be recognized that in high heat flux situations contact resistance can cause the two materials to have different temperatures at their faces.

3) Thermal rotation is computed using circular ring theory [9]. It is known that this is an approximation. For more accurate results the temperature computed herein may be passed to a FEM program.

The power of this program is that it solves the arbitrary heat transfer region program by setting up finite difference equations which accommodate the variable mesh size. Boundary conditions are very easy to specify and the program sets up the appropriate heat balance equation on these boundaries as needed. Final solution is obtained very quickly by relaxation methods.

Again while this problem can be elegantly solved using FEM, the program described is completely automatic in providing a heat transfer solution, and the program is relatively small and easy to implement.

Other Programs

A program which calculates moments due to pressure forces would also be useful. The same basic program as above can be used. Pressure boundary conditions can be input similar to convection boundaries above. The program remains to be written.

All of the programs above would be easier to use if data input was done by graphical display. Thus the logical next step would be to write these programs for graphical interactive computers.

CHAPTER 8

SQUEEZE SEALS AND BEARINGS

Introduction

Early in this research program there was motivation to find a simple means of applying waviness to seals to more easily obtain the advantages of waviness. As discussed earlier, while the advantages of using waviness have been clear, a very simple means of applying the wave is essential to make the idea practical.

The squeeze seal concept was born of this motivation. Figure 8-1 shows this concept. Here a wave moves along a stationary (nonsliding) surface on one part at velocity U_2. The second part slides along in a conventional manner (velocity U_1). Of interest is the case where $U_1 = U_2$ because it is easy to conceive how this might be simply implemented.

The next section shows how this problem is solved and how in fact the squeeze seal/bearing is identical to the standard wavy seal/bearing (Figure 8-2). Thus, while the squeeze bearing may provide an advantage in implementation, it does not provide an advantage in performance. The squeeze seal concept then led to the third wavy seal concept described in Chapter 4 where the wave moves with the rotating part of the seal.

While it happens that the above three concepts are identical in performance, there is yet another way of creating a wavy squeeze seal of some interest. The concept is shown in Figure 8-3.

Surface A is a conventional wavy surface if it is used as a seal and may be a multilobed journal if used as a bearing. Surface B is a

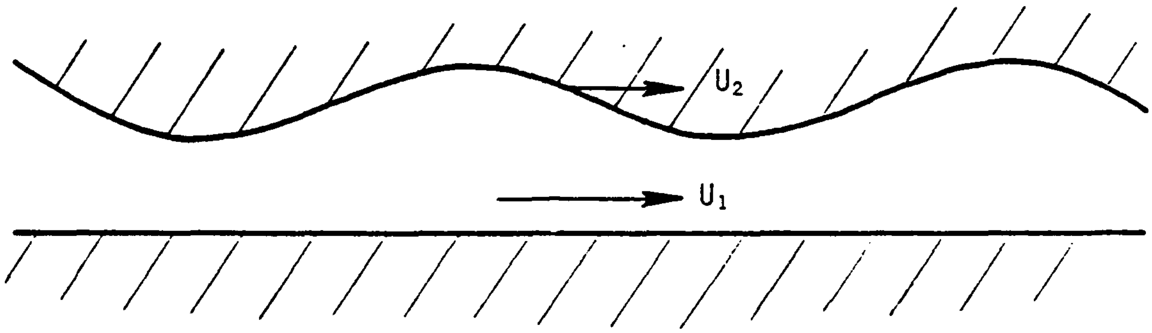

Figure 8-1. Squeeze Seal/Bearing

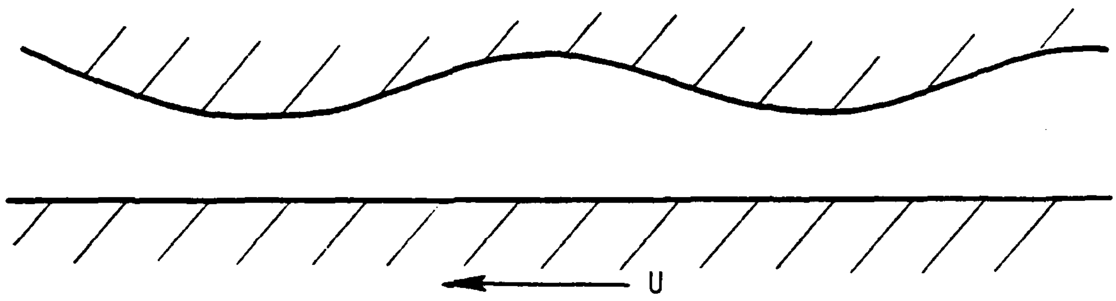

Figure 8-2. Conventional Wavy Seal/Bearing.

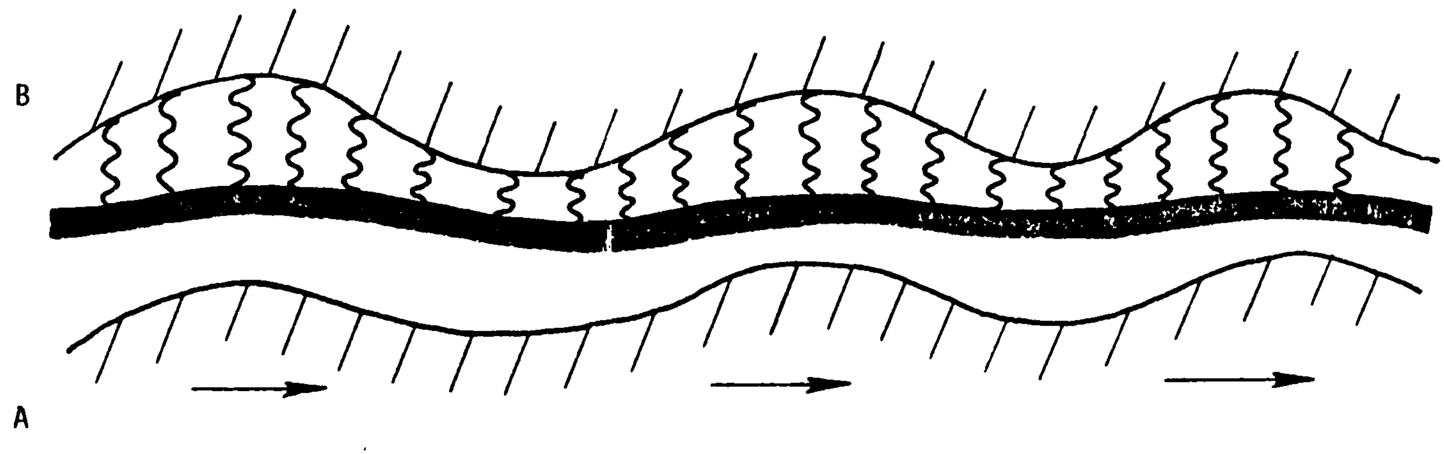

Figure 8-3. Elastic Foundation Squeeze Seal/Bearing.

beam or plate on an elastic foundation which has a variable stiffness support along its length. Thus, as surface A slides along, surface B will react differently at different locations because of the variable stiffness. The analysis and performance of this concept is discussed in a later section.

Rigid Body Squeeze Bearings/Seals

In this section, the governing finite difference equations for both conventional and squeeze bearings/seals are first derived by using Elrod's cavitation algorithm [53]. The techniques for obtaining values of pressure from the governing equation accompanied by the given boundary conditions are presented and discussed. Although the governing equations for both conventional and squeeze bearings are different, it can be proven through analytical methods that performance for both bearings/seals under complete film condition is exactly the same. For conditions in which cavitation occurs, it can also be proven, by using numerical methods, that performance for both bearings/seals is identical.

Governing Equations

Assumptions

The assumptions upon which the present solutions are based are as follows:

1) Lubricant is Newtonian
2) Flow is laminar

3) Fluid film is so thin that the pressure remains constant across its depth.

4) No slip occurs between fluid and bearing/seal surfaces.

5) The viscosity is constant throughout the film.

6) The effects of thermal and elastic distortion are neglected.

7) Inertia and body forces are negligible.

8) The curvature of surfaces is large compared with film thickness.

The justifications for these assumptions have been presented previously and will not be repeated here.

According to Cameron [54], with these assumptions the flow rate in the x direction per unit y width is

$$q_x = -\frac{h^3}{12\mu}\frac{\partial p}{\partial x} + \frac{h}{2}(U_a + U_b) \quad . \tag{8-1}$$

Similarly, in the y direction

$$q_y = -\frac{h^3}{12\mu}\frac{\partial p}{\partial y} + \frac{h}{2}(V_a + V_b) \quad , \tag{8-2}$$

where U_a, U_b are the surface velocities in x direction, V_a, V_b are the surface velocities in the y direction. The continuity equation can be described as

$$\frac{\partial q_x}{\partial x} + \frac{\partial q_y}{\partial y} = \frac{\partial h}{\partial t} \quad . \tag{8-3}$$

Equations (8.1), (8.2), and (8.3) can only be used in a complete film zone. The problem of cavitation must be dealt with. The cavitation phenomenon is caused by negative pressure occurring in a fluid

film lubrication region. It was found by Jacobson et al. [55] that in a cavitation zone, only a certain fraction, θ, of the film gap is occupied by the fluid and the remaining space, $1 - \theta$, is occupied by the intervening gas. The pressure throughout the cavitation zone is constant.

By using Jacobson's theory, Elrod [53] modified the Reynolds equation and proposed a computational method which will be reviewed here. Elrod defines the fractional film content, θ, as

$$\theta = \rho/\rho_c , \tag{8-4}$$

where ρ_c is the liquid density within the cavitated zone and ρ is the average density. The film pressure is

$$p = p_c + \beta(\theta - 1) , \qquad \theta > 1 ,$$

$$p = p_c , \qquad \theta \le 1 , \tag{8-5}$$

where p_c is the cavity pressure and β is the compression factor (for an essentially incompressible problem, a convenient arbitrary value can be used).

A cavitation index g is also defined as

$$g = 0 \quad \text{for} \quad \theta < 1 ,$$

$$g = 1 \quad \text{for} \quad \theta \ge 1 . \tag{8-6}$$

By using the defined variables and finite difference method (nomenclature shown in Figure 8-4), Equation (8-1) was modified as [53]

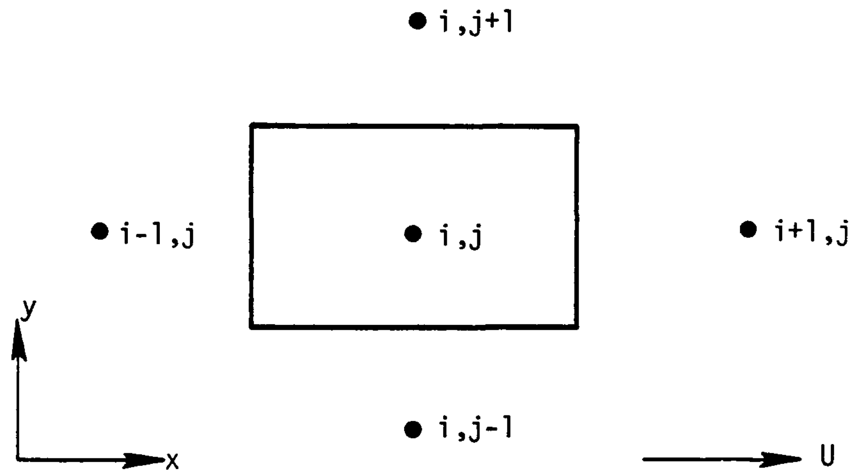

Figure 8-4. Finite Difference Symbol Definition.

$$q_x = \left(\frac{h^3}{12\mu}\right)_{av} \beta\rho_c \left\{\frac{g_{i-1\cdot j}(\theta_{i-1\cdot j} - 1) - g_{i\cdot j}(\theta_{i\cdot j} - 1)}{\Delta x}\right\}$$

$$+ \frac{\rho_c U}{2} \left\{\theta_{i-1\cdot j}\, h_{i-1\cdot j}(1 - g_{i-1\cdot j}) + g_{i-1\cdot j}\, h_{i-1\cdot j}\right.$$

$$\left. + \frac{g_{i\cdot j}\, g_{i-1\cdot j}(h_{i\cdot j} - h_{i-1\cdot j})}{2}\right\} \tag{8-7}$$

where U is the surface velocity in the x direction. Equation (8-2) was modified in a similar way.

Based on the cavitation concept, Equation (8-3) is also modified to

$$\frac{\Delta q_x}{\Delta x} + \frac{\Delta q_y}{\Delta y} = \frac{\partial[h(\theta(1 - g) + g)]}{\partial t} \; . \tag{8-8}$$

Equations for Conventional and Squeeze Wavy Seals With No Cavitation

For the complete film condition, Equation (8-3) can be used. The derivation of the governing equations is as follows (for the present problems, only one of the surfaces of bearing/seal has a constant moving velocity:

$$\frac{\partial q_x}{\partial x} = \frac{\partial}{\partial x}\left(- \frac{h^3}{12\mu}\frac{\partial p}{\partial x} + \frac{h}{2}U\right) = - \frac{1}{12\mu}\frac{\partial}{\partial x}\left(h^3 \frac{\partial p}{\partial x}\right) + \frac{U}{2}\frac{2h}{\partial x} \; , \tag{8-9}$$

$$\frac{\partial q_y}{\partial y} = \frac{\partial}{\partial y}\left(- \frac{h^3}{12\mu}\frac{\partial p}{\partial y}\right) = - \frac{1}{12\mu}\frac{\partial}{\partial y}\left(h^3 \frac{\partial p}{\partial y}\right) . \tag{8-10}$$

Substitute Equations (8-9) and (8-10) into Equation (8-3) and rearrange its terms, Equation (8-3) becomes (for conventional wavy seal)

$$\frac{\partial}{\partial x}\left(h^3 \frac{\partial p}{\partial x}\right) + \frac{\partial}{\partial y}\left(h^3 \frac{\partial p}{\partial y}\right) = 6\mu U \frac{\partial h}{\partial x} \tag{8-11}$$

For squeeze wavy seal:

$$\frac{\partial}{\partial x}\left(h^3 \frac{\partial p}{\partial x}\right) + \frac{\partial}{\partial y}\left(h^3 \frac{\partial p}{\partial y}\right) = 6\mu \left(U \frac{\partial h}{\partial x} - 2 \frac{\partial h}{\partial t}\right) . \tag{8-12}$$

Equations for Conventional and Squeeze Wavy Seals with Cavitation

For conditions in which cavitation occurs, Equation (8-3) alone is not enough to fully represent the fluid film performance and Equation (8-8) is used. By using the Elrod's cavitation algorithm, the governing equations for a rigid squeeze wavy seal with cavitation are obtained:

$$\frac{\Delta q_x}{\Delta x} = \frac{1}{\Delta x}\left[q_{i-1/2\cdot j\cdot t} - q_{i+1/2\cdot j\cdot t}\right]$$

$$= \frac{\beta \rho_c}{12\mu}\left[\left(\frac{h_{i-1\cdot j\cdot t} + h_{i\cdot j\cdot t}}{2}\right)^3 \left(\frac{g_{i-1\cdot t}(\theta_{i-1\cdot j\cdot t} - 1) - g_{i\cdot j\cdot t}(\theta_{i\cdot j\cdot t} - 1)}{(\Delta x)^2}\right)\right.$$

$$\left. - \left(\frac{h_{i\cdot j\cdot t} + h_{i+1\cdot j\cdot t}}{2}\right)^3 \left(\frac{g_{i\cdot j\cdot t}(\theta_{i\cdot j\cdot t} - 1) - g_{i+1\cdot j\cdot t}(\theta_{i+1\cdot j\cdot t} - 1)}{(\Delta x)^2}\right)\right]$$

$$+ \frac{U\rho_c}{2\Delta x}\left[\theta_{i-1\cdot j\cdot t} h_{i-1\cdot j\cdot t}(1 - g_{i-1\cdot j\cdot t}) + g_{i-1\cdot j\cdot t} h_{i-1\cdot j\cdot t}\right.$$

$$\left. + \frac{1}{2}\, q_{i\cdot j\cdot t} q_{i-1\cdot j\cdot t}(h_{i\cdot j\cdot t} - h_{i-1\cdot j\cdot t})\right]$$

$$- \frac{U\rho_c}{2\Delta x}\Big[\theta_{i\cdot j\cdot t}h_{i\cdot j\cdot t}(1 - g_{i\cdot j\cdot t}) + g_{i\cdot j\cdot t}h_{i\cdot j\cdot t}$$

$$+ \frac{1}{2}\, g_{i+1\cdot j\cdot t}g_{i\cdot j\cdot t}(h_{i+1\cdot j\cdot t} - h_{i\cdot j\cdot t})\Big] \,. \qquad (8\text{-}13)$$

$$\frac{\Delta q_y}{\Delta y} = \frac{1}{\Delta y}\,[q_{i\cdot j-1/2,t} - q_{i\cdot j+1/2,t}]$$

$$= \frac{\beta\rho_c}{12\mu}\Bigg[\left(\frac{h_{i\cdot j-1\cdot t} + h_{i\cdot j\cdot t}}{2}\right)^3 \left(\frac{g_{i\cdot j-1\cdot t}(\theta_{i\cdot j-1\cdot t} - 1) - g_{i\cdot j\cdot t}(\theta_{i\cdot j\cdot t} - 1)}{(\Delta y)^2}\right)$$

$$- \left(\frac{h_{i\cdot j\cdot t} + h_{i\cdot j+1\cdot t}}{2}\right)^3 \left(\frac{g_{i\cdot j\cdot t}(\theta_{i\cdot j\cdot t} - 1) - g_{i\cdot j+1\cdot t}(\theta_{i\cdot j+1\cdot t} - 1)}{(\Delta y)^2}\right)\Bigg]$$

$$(8\text{-}14)$$

$$\frac{\partial(h(\theta(1 - g) + g))}{\partial t}$$

$$= \frac{h_{i\cdot j\cdot t}(\theta_{i\cdot j\cdot t}(1 - g_{i\cdot j\cdot t}) + g_{i\cdot j\cdot t})}{\Delta t}$$

$$- \frac{h_{i\cdot j\cdot t-\Delta t}(\theta_{i\cdot j\cdot t-\Delta t}(1 - g_{i\cdot j\cdot t-\Delta t}) + g_{i\cdot j\cdot t-\Delta t})}{\Delta t} \qquad (8\text{-}15)$$

By substituting Equation (8-13), (8-14), and (8-15) into Equation (8-8), the governing equation for a two-dimensional squeeze wavy seal can be obtained.

The governing equation for a one-dimensional squeeze wavy seal is:

$$\theta_{i+1,t}\left[- \frac{\beta\rho_c}{12\mu\Delta x}\left(\frac{h_{i,t} + h_{i+1,t}}{2}\right)^3 g_{i+1,t}\right]$$

$$+ \theta_{i-1,t} \left[- \frac{\beta\rho_c}{12\mu\Delta x} \left(\frac{h_{i,t} + h_{i-1,t}}{2} \right)^3 g_{i-1,t} - \rho_c \frac{U}{2} h_{i-1,t}(1 - g_{i-1,t}) \right]$$

$$+ \theta_{i,t} \left[\frac{\beta\rho_c}{12\mu\Delta x} \left[\left(\frac{h_{i,t} + h_{i+1,t}}{2} \right)^3 g_{i,t} + \left(\frac{h_{i,t} + h_{i-1,t}}{2} \right)^3 g_{i-t} \right] \right.$$

$$\left. + \rho_c \frac{U}{2} h_{i,t}(1 - g_{i,t}) + \rho_c \frac{\Delta x}{\Delta t} h_{i,t}(1 - g_{i,t}) \right]$$

$$= \frac{\beta\rho_c}{12\mu\Delta x} \left[\left(\frac{h_{i,t} + h_{i-1,t}}{2} \right)^3 (g_{i,t} - g_{i-1,t}) \right.$$

$$\left. + \left(\frac{h_{i,t} + h_{i+1,t}}{2} \right)^3 (g_{i,t} - g_{i+1,t}) \right]$$

$$+ \rho_c \frac{U}{2} [g_{i-1,t}h_{i-1,t} - g_{i,t}h_{i,t}$$

$$+ 0.5\, g_{i,t}g_{i-1,t}(h_{i,t} - h_{i-1,t})$$

$$- 0.5\, g_{i+1,t}g_{i,t}(h_{i+1,t} - h_{i,t})]$$

$$+ \rho_c \frac{\Delta x}{\Delta t} [h_{i,t-1}g_{i,t-1} - h_{i,t}g_{i,t}]$$

$$+ \theta_{i,t-1} \left[\rho_c \frac{\Delta x}{\Delta t} h_{i,t-1}(1 - g_{i,t-1}) \right] . \qquad (8\text{-}16)$$

For a conventional wavy seal,

$$\frac{\partial(h(\theta(1 - g) + g))}{2t} \qquad (8\text{-}15)$$

is equal to zero (due to steady state condition). The governing equation can be obtained by combining Equation (8-13) and (8-14).

Comparison Between Conventional and Rigid Squeeze Wavy Bearings/Seals

(a) Complete film condition occurs throughout the bearing.

Under complete film conditions the governing equation for a squeeze wavy bearing/seal is

$$\frac{\partial}{\partial x}\left(h^3 \frac{\partial p}{\partial x}\right) + \frac{\partial}{\partial y}\left(h^3 \frac{\partial p}{\partial y}\right) = 6\mu U \frac{\partial h}{\partial x} - 12\mu \frac{\partial h}{\partial t} \; . \tag{8-12}$$

Due to the fact from Figure 8-1 with

$$U_1 = U_2 = U \; ,$$

$$\frac{\partial h}{\partial t} = -U \frac{\partial h}{\partial x} \; ,$$

the right-hand side terms of Equation (8-12) can be expressed as

$$6\mu U \frac{\partial h}{\partial x} - 12\mu \frac{\partial h}{\partial t} = -6\mu U \frac{\partial h}{\partial x}$$

and Equation (8-12) becomes

$$\frac{\partial}{\partial x}\left(h^3 \frac{\partial p}{\partial x}\right) + \frac{\partial}{\partial y}\left(h^3 \frac{\partial p}{\partial y}\right) = 6\mu(-U) \frac{\partial h}{\partial x} \tag{8-17}$$

Since the governing equation for a conventional wavy seal is

$$\frac{\partial}{\partial x}\left(h^3 \frac{\partial p}{\partial x}\right) + \frac{\partial}{\partial y}\left(h^3 \frac{\partial p}{\partial y}\right) = 6\mu U \frac{\partial h}{\partial x} \; . \tag{8-10}$$

It is obvious that a squeeze wavy seal can be treated as a conventional wavy seal except that now the moving surface is moved in an opposite direction. Actually, this does not effect the performance. Numerical results for Equations (8-10) and (8-17) for a two-dimensional region

with the film thickness shown by Table 8-1 are shown in Tables 8-2 and 8-3. They are identical except for the moving direction.

(b) Cavitation occurs somewhere in the fluid film

If cavitation occurs, the governing equations for both conventional and squeeze wavy seals are tedious. The only way to solve these equations is through iterative computational methods.

The following are two examples; one deals with the one-dimensional case and the other two-dimensional case. The comparison between conventional and squeeze wavy seals/bearings is considered:

(i) One-dimensional Case

In this one-dimensional problem, the governing equation for a squeeze wavy seal is given as Equation (8-16) and the film thickness is

$$h = h_0 + h_1 \cos(n(x - Ut)) \ , \qquad (8\text{-}18)$$

where

h_0 = nominal film thickness

h_1 = amplitude of wave

n = number of waves around seal/bearing face

t = time

The boundary conditions for use here are described as follows:

1) At the beginning of each wave (each wave begins with point where film thickness is a maximum), the pressure is assumed to be zero. This means these points are moved with the wave.

TABLE 8-1

Distribution of Film Thickness over One Wave of a Seal Face

				r				
1	1.23	1.74	2.35	2.97	3.58	4.20	4.82	5.43
2	1.23	1.73	2.33	2.94	3.54	4.15	4.75	5.36
3	1.24	1.70	2.28	2.85	3.43	4.00	4.58	5.15
4	1.25	1.66	2.19	2.71	3.24	3.76	4.29	4.82
5	1.26	1.61	2.07	2.53	3.00	3.46	3.92	4.38
6	1.27	1.55	1.94	2.32	2.71	3.10	3.49	3.87
7	1.29	1.48	1.79	2.10	2.41	2.71	3.02	3.33
8	1.30	1.42	1.65	1.87	2.10	2.33	2.56	2.79
9	1.31	1.36	1.51	1.66	1.82	1.97	2.13	2.28
10	1.32	1.30	1.39	1.48	1.57	1.66	1.76	1.85
11	1.33	1.26	1.31	1.35	1.39	1.43	1.47	1.51
12	1.34	1.24	1.25	1.26	1.27	1.28	1.29	1.30
θ 13	1.34	1.23	1.23	1.23	1.23	1.23	1.23	1.23
14	1.34	1.24	1.25	1.26	1.27	1.28	1.29	1.30
15	1.33	1.26	1.31	1.35	1.39	1.43	1.47	1.51
16	1.32	1.30	1.39	1.48	1.57	1.66	1.76	1.85
17	1.31	1.36	1.51	1.66	1.82	1.97	2.13	2.28
18	1.30	1.42	1.65	1.87	2.10	2.33	2.56	2.79
19	1.29	1.48	1.79	2.10	2.41	2.71	3.02	3.33
20	1.27	1.55	1.94	2.32	2.71	3.10	3.49	3.87
21	1.26	1.61	2.07	2.53	3.00	3.46	3.92	4.38
22	1.25	1.66	2.19	2.71	3.24	3.76	4.29	4.82
23	1.24	1.70	2.28	2.85	3.43	4.00	4.58	5.15
24	1.23	1.73	2.33	2.94	3.54	4.15	4.75	5.36
25	1.23	1.74	2.35	2.97	3.58	4.20	4.82	5.43

TABLE 8-2

Pressure Distribution for a Conventional Wavy Seal
under Full Film Conditions

U = 0.1885E+03   U1 = 0.1885E+03   VO = 0.7200E-05
P2 = 0.4000E+04   CO = 0.2000E-84
HO = 0.2460E-84   FO = 0.2299E-03

r

	1	0	112	155	174	184	190	194	197
	2	0	115	158	177	187	192	195	197
	3	0	116	161	180	189	194	196	197
	4	0	116	163	183	192	196	197	197
	5	0	114	164	186	196	199	199	197
	6	0	111	166	190	200	203	201	197
	7	0	108	167	195	207	209	205	197
	8	0	102	167	200	215	216	210	197
	9	0	94	163	204	223	226	216	197
	10	0	83	153	200	226	233	223	197
	11	0	68	133	182	214	228	222	197
	12	0	49	100	144	177	198	206	197
θ	13	0	30	62	93	121	148	173	197
	14	0	14	30	49	73	103	143	197
	15	0	6	16	31	54	88	134	197
	16	0	8	20	39	65	99	143	197
	17	0	19	38	62	89	120	156	197
	18	0	34	62	88	114	141	168	197
	19	0	50	85	112	135	157	177	197
	20	0	66	105	131	151	168	183	197
	21	0	81	121	145	163	176	187	197
	22	0	92	134	156	171	181	190	197
	23	0	101	143	164	176	185	192	197
	24	0	108	150	169	181	188	193	197
	25	0	112	155	174	184	190	194	197

The load support is 0.7355E+03.

TABLE 8-3

Pressure Distribution for a Squeeze Wavy Seal Seal under Full Film Conditions

r

	1	0	112	155	174	184	190	194	197
	2	0	108	150	169	181	188	193	197
	3	0	101	143	164	176	185	192	197
	4	0	92	134	156	171	181	190	197
	5	0	81	121	145	163	176	187	197
	6	0	66	105	131	151	168	183	197
	7	0	50	85	112	135	157	177	197
	8	0	34	62	88	114	141	168	197
	9	0	19	38	62	89	120	156	197
	10	0	8	20	39	65	99	143	197
	11	0	6	16	31	54	88	134	197
	12	0	14	30	49	73	103	143	197
θ	13	0	30	62	93	121	148	173	197
	14	0	49	100	144	177	198	206	197
	15	0	68	133	182	214	228	222	197
	16	0	83	153	200	226	233	223	197
	17	0	94	163	204	223	226	216	197
	18	0	102	167	200	215	216	210	197
	19	0	108	167	195	207	209	205	197
	20	0	111	166	190	200	203	201	197
	21	0	114	164	186	196	199	199	197
	22	0	116	163	183	192	196	197	197
	23	0	116	161	180	189	194	196	197
	24	0	115	158	177	187	192	195	197
	25	0	112	155	174	184	190	194	197

The load support is 0.7355E+03.

2) For each wave, at a location where cavitation first occurs, the pressure and pressure gradient are equal to zero.

The reason why these two boundary conditions are chosen actually comes from the idea that a lubricant film having converging-diverging geometry (such as a journal bearing) usually increases its pressure from the beginning of its convergent section. At the location where cavitation first occurs, pressure and pressure gradient are equal to zero.

Although these two boundary conditions are actually used to obtain the solution, only the first boundary condition is included directly in the solution procedure. The reason is that the governing equation used here is derived from Elrod's cavitation algorithm and this algorithm itself has the ability to automatically handle the cavitation boundary condition.

To find the solution, the following procedures are used.

(1) All $g_{i \cdot t}(t = 0)$ were set equal to one at the start.

(2) Value of $\theta_{i \cdot t}$ at the beginning of each wave was obtained by Equation (8-5) using an assumed pressure distribution.

(3) By using the Gauss elimination method, the distribution of $\theta_{i \cdot t}(t = 0)$ was obtained.

(4) By using Equation (6), new $g_{i,t}(t = 0)$ were found.

(5) Using new $g_{i,t}(t = 0)$ and repeat procedure (2)-(4), until the solutions of $\theta_{i \cdot t}(t = 0)$ are converged.

(6) Assume the values of all $g_{i \cdot t+t}$ were equal to 1.

(7) Use Gauss elimination method to find $\theta_{i,t+\Delta t}$.

(8) By using Equation (8-6), new $g_{i,t+\Delta t}$ were found.

(9) The new $g_{i,t+\Delta t}$ were used and repeat procedure (7)-(9) until the solution of $\theta_{i,t+\Delta t}$ were converged.

(10) By using Equation (5) and assuming all negative pressures are equal to zero, the pressure distribution was found.

In all the iteration processes, the criterion to decide whether the solution converges is that three successively determined load supports should not differ by more than 0.1 percent.

The method used to solve the governing equation for a conventional wavy seal/bearing is similar to that of a squeeze wavy seal/bearing except that now the film thickness is

$$h = h_0 + h_1 \cos nx \; . \qquad (8\text{-}19)$$

The numerical data used here are

$h_0 = 0.383 \times 10^{-3}$ in.

$h_1 = 0.3 \times 10^{-4}$ in.

$n = 3$

$\beta = 5000$

$U = 377$ in./sec

$\mu = 0.99 \times 10^{-7}$ Reyn.

The numerical results obtained for the conventional and squeeze wavy seals are not exactly the same (see Figure 8-5). However, it was found that by reducing the size of the mesh, the value of the load support for a squeeze wavy seal converges to that of a conventional wavy seal (see Figure 8-6). This proves that if the mesh size is small enough, the results for both conventional and squeeze wavy seals are identical.

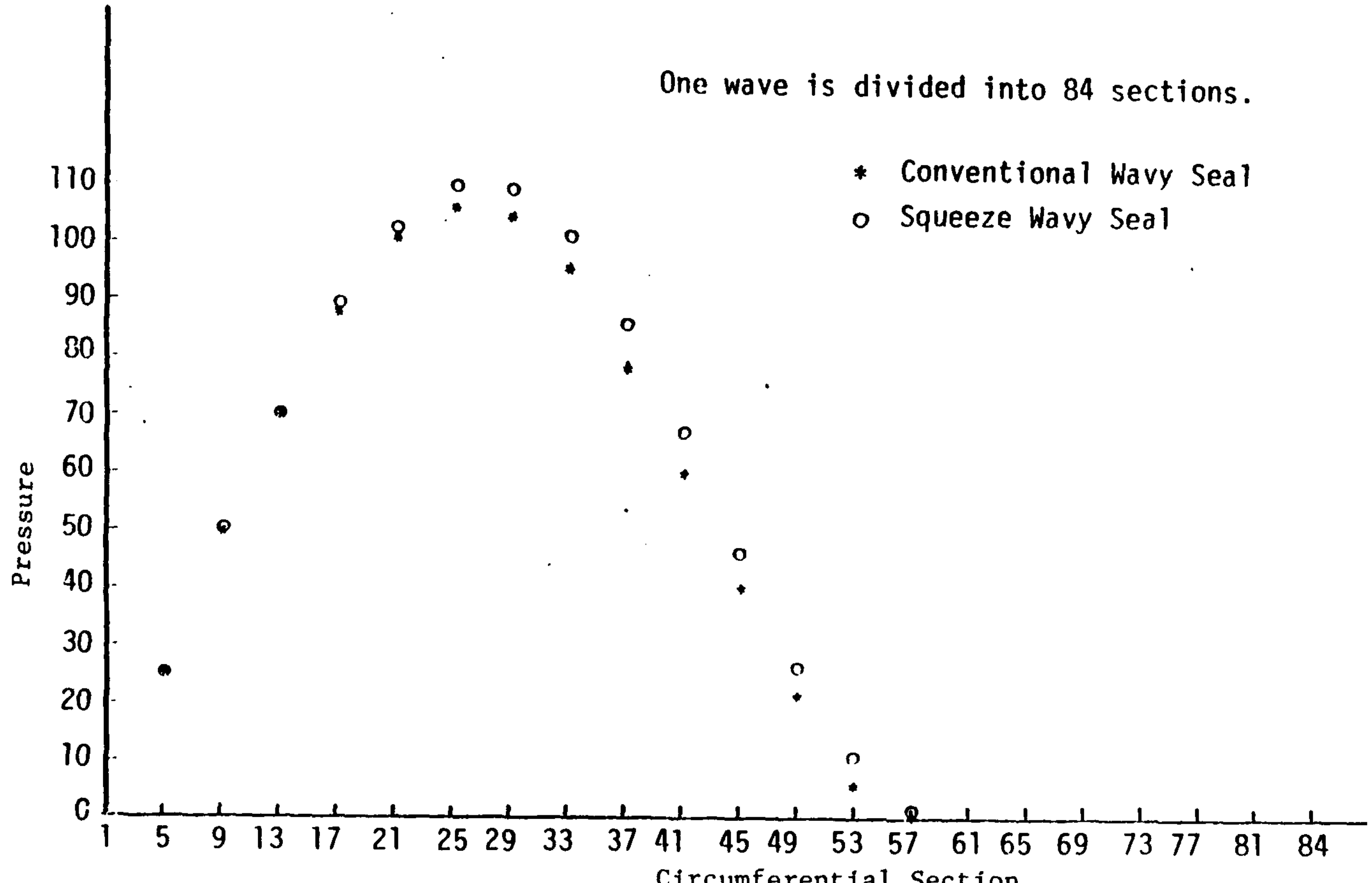

Figure 8-5. Comparison of Pressure with Cavitation.

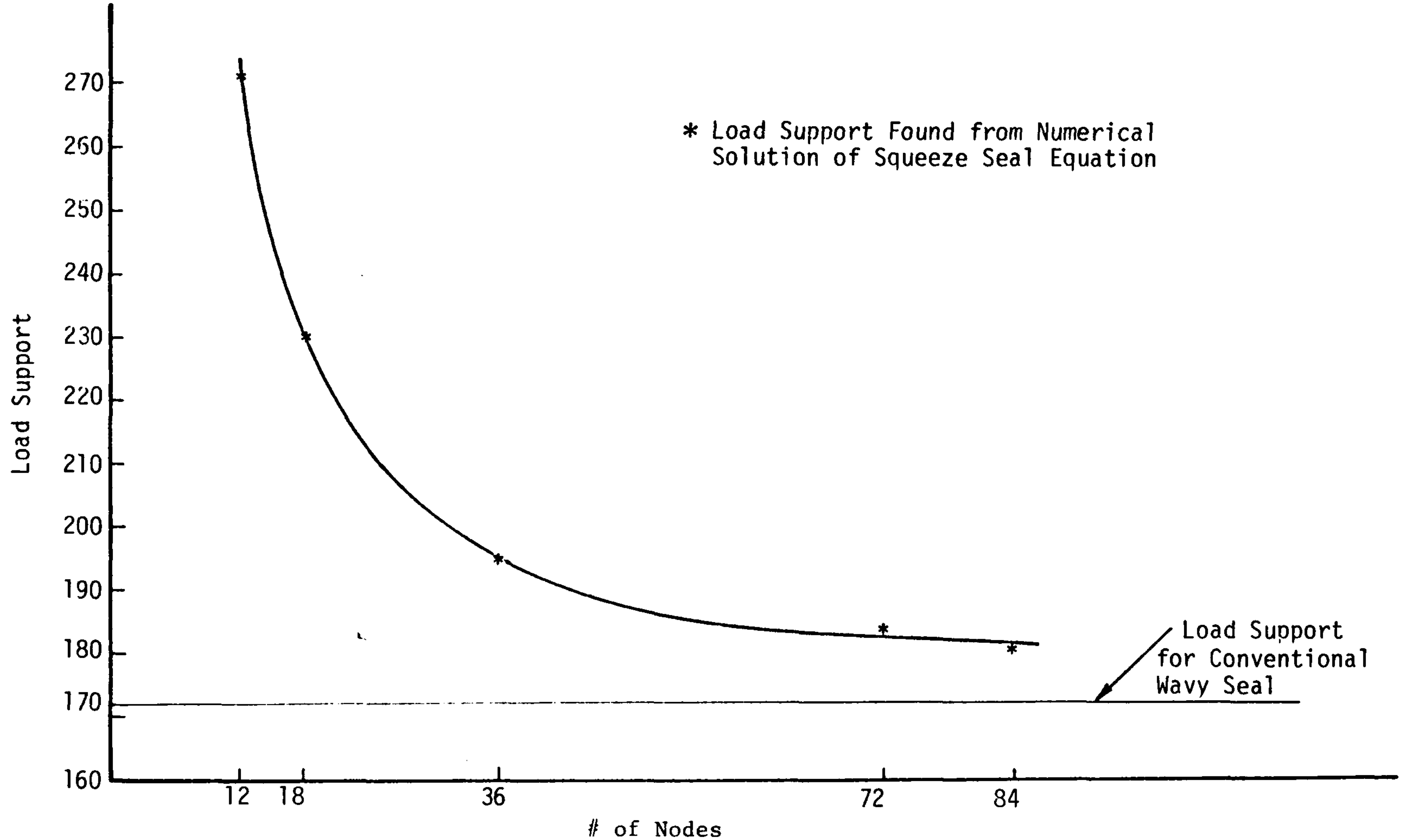

Figure 8-6. Effect of Mesh Size on Squeeze Seal Load Support.

(ii) Two-dimensional Case

Consider a two-dimensional squeeze film flow occurring between two circular rings (seal). The coordinates here are cylindrical. The nomenclature is shown in Figure 8-7.

The derivation procedure of the governing equation for the present problem is similar to that for rectangular coordinates obtained in the previous section. This governing equation is given as

$$\theta_{i+1\cdot j\cdot t}\left[-\frac{\beta\rho_c\Delta r}{12\mu r\Delta\alpha}\left(\frac{h_{i\cdot j\cdot t}+h_{i+1\cdot j\cdot t}}{2}\right)^3 g_{i+1\cdot j\cdot t}\right]$$

$$+\ \theta_{i-1\cdot j\cdot t}\left[-\frac{\beta\rho_c\Delta r}{12\mu r\Delta\alpha}\left(\frac{h_{i-1\cdot j\cdot t}+h_{i\cdot j\cdot t}}{2}\right)^3 g_{i-1\cdot j\cdot t}\right.$$

$$\left.-\ \frac{r\omega\Delta r}{2}\,h_{i-1\cdot j\cdot t}(1-g_{i-1\cdot j\cdot t})\right]$$

$$+\ \theta_{i\cdot j+1\cdot t}\left[-\frac{\beta\rho_c(r+\frac{\Delta r}{2})\,\Delta\alpha}{12\mu\Delta r}\left(\frac{h_{i\cdot j\cdot t}+h_{i\cdot j+1\cdot t}}{2}\right)^3 g_{i\cdot j+1\cdot t}\right]$$

$$+\ \theta_{i\cdot j-1\cdot t}\left[-\frac{\beta\rho_c(r-\frac{\Delta r}{2})\,\Delta\alpha}{12\mu\Delta r}\left(\frac{h_{i\cdot j\cdot t}+h_{i\cdot j-1\cdot t}}{2}\right)^3 g_{i\cdot j-1\cdot t}\right]$$

$$+\ \theta_{i\cdot j\cdot t}\left[\frac{\beta\rho_c\,\Delta r}{12\mu r\Delta\alpha}\left(\frac{h_{i\cdot j\cdot t}+h_{i+1\cdot j\cdot t}}{2}\right)^3 g_{i\cdot j\cdot t}\right.$$

$$+\ \frac{\beta\rho_c\,\Delta r}{12\mu r\Delta\alpha}\left(\frac{h_{i-1\cdot j\cdot t}+h_{i\cdot j\cdot t}}{2}\right)^3 g_{i\cdot j\cdot t}$$

$$+\ \frac{\beta\rho_c(r+\frac{\Delta r}{2})\,\Delta\alpha}{12\mu\Delta r}\left(\frac{h_{i\cdot j\cdot t}+h_{i\cdot j+1\cdot t}}{2}\right)^3 g_{i\cdot j\cdot t}$$

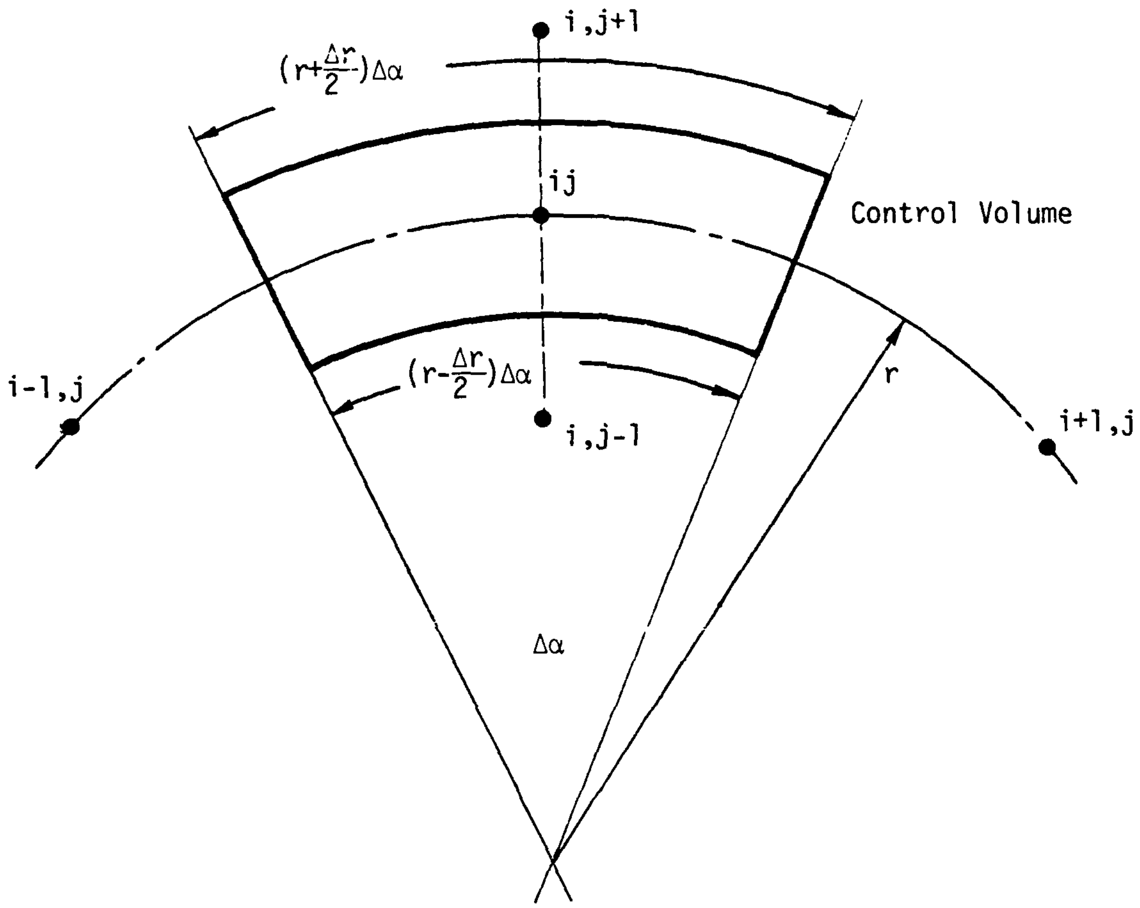

Figure 8-7. Control Volume in Cylindrical Coordinates.

$$+ \frac{\beta\rho_c\,(r - \frac{\Delta r}{2})\,\Delta\alpha}{12\mu\Delta r}\left(\frac{h_{i\cdot j\cdot t} + h_{i\cdot j-1\cdot t}}{2}\right)^3 g_{i\cdot j\cdot t}$$

$$+ \frac{r\omega\Delta r}{2}\, h_{i\cdot j\cdot t}(1 - g_{i\cdot j\cdot t})$$

$$+ r\Delta\theta\Delta r(1 - g_{i\cdot j\cdot t})\,\frac{h_{i\cdot j\cdot t}}{\Delta t}\Bigg]$$

$$= \frac{\beta\rho_c\,\Delta r}{12\mu r\Delta\alpha}\left(\frac{h_{i\cdot j\cdot t} + h_{i+1\cdot j\cdot t}}{2}\right)^3 (g_{i\cdot j\cdot t} - g_{i+1\cdot j\cdot t})$$

$$+ \frac{\beta\rho_c\,\Delta r}{12\mu r\Delta\alpha}\left(\frac{h_{i\cdot j\cdot t} + h_{i-1\cdot j\cdot t}}{2}\right)^3 (g_{i\cdot j\cdot t} - g_{i-1\cdot j\cdot t})$$

$$+ \frac{\beta\rho_c(r + \frac{\Delta r}{2})\,\Delta\alpha}{12\mu\Delta r}\left(\frac{h_{i\cdot j\cdot t} + h_{i\cdot j+1\cdot t}}{2}\right)^3 (g_{i\cdot j\cdot t} - g_{i\cdot j+1\cdot t})$$

$$+ \frac{\beta\rho_c(r - \frac{\Delta r}{2})\,\Delta\alpha}{12\mu\Delta r}\left(\frac{h_{i\cdot j\cdot t} + h_{i\cdot j-1\cdot t}}{2}\right)^3 (g_{i\cdot j\cdot t} - g_{i\cdot j-1\cdot t})$$

$$+ \frac{r\omega\Delta r}{2}\,(g_{i-1\cdot j\cdot t}h_{i-1\cdot j\cdot t} - g_{i\cdot j\cdot t}h_{i\cdot j\cdot t})$$

$$- r\Delta\theta\Delta r\ \theta_{i\cdot j\cdot t-\Delta t}(1 - g_{i\cdot j\cdot t\cdot\Delta t})\,\frac{h_{i\cdot j\cdot t-\Delta t}}{\Delta t}$$

$$+ \frac{r\omega\Delta r}{2}\,[\frac{1}{2}\, g_{i\cdot j\cdot t}g_{i-1\cdot j\cdot t}(h_{i\cdot j\cdot t} - h_{i-1\cdot j\cdot t})$$

$$- \frac{1}{2}\, g_{i\cdot j\cdot t}g_{i+1\cdot j\cdot t}(h_{i+1\cdot j\cdot t} - h_{i\cdot j\cdot t})]\ . \qquad (8\text{-}20)$$

The film thickness for the squeeze wavy seal is described in detail in Reference [6], and is given as

$$h = h_o + w(r) + [v_o + (r - r_c)\ \phi_o]\ \cos(-\ n(\theta - \omega t))\ , \qquad (8\text{-}21)$$

where

$$w(r) = -\min\{[v_o + (r - r_c)\ \phi_o]\ \cos(-n(\theta - \omega t))\}$$

h_o = minimum film thickness

v_o = amplitude

ϕ_o = the maximum tilt of the seal

ω = angular speed

r_c = radius to centroid of seal ring

r = radial coordinate

α = angular coordinate

The boundary conditions are at

$$r = r_i\ , \qquad p = p_i\ ,$$

$$r = r_o\ , \qquad p = p_o\ , \qquad (8\text{-}22)$$

where

r_i = inside radius of circular ring

r_o = outside radius of circular ring

p_i = seal inside pressure

p_o = seal outside pressure

The numerical data used here are

$h_o = 0.246 \times 10^{-4}$ in.

$V_o = 0.72 \times 10^{-5}$ in.

$\phi_o = 0.23 \times 10^{-3}$

$\omega = 1800$ rpm

$r_c = 1.9361$ in.

$r_i = 1.90$ in.

$r_o = 2.0875$ in.

$p_i = 0$

$p_o = 500$ psi

$\mu = 0.99 \times 10^{-7}$ lb·s/in.^{2}

$\beta = 5000$

The solution procedures for both conventional and squeeze wavy seals of 2-D case are similar to that of 1-D case. Again, it is shown that by reducing the size of the mesh, the value of the load support for a squeeze wavy seal approaches that of a standard wavy seal (Figure 8-8).

Deformable Body Squeeze Sliding Bearings/Seals

In the previous section, distortion caused by the pressure forces induced in a fluid film flow was not considered. In actual situations, the distortion does affect the lubrication performance. For example, according to Brighton, Hooke, and O'Donoghue [56], in a journal bearing, the effects of distortion include

(1) reducing the peak pressure for a given load

(2) increasing the eccentricity ratio for a given load

(3) moving the location of minimum film thickness towards the cavitation zone

(4) increasing the cavitation angle

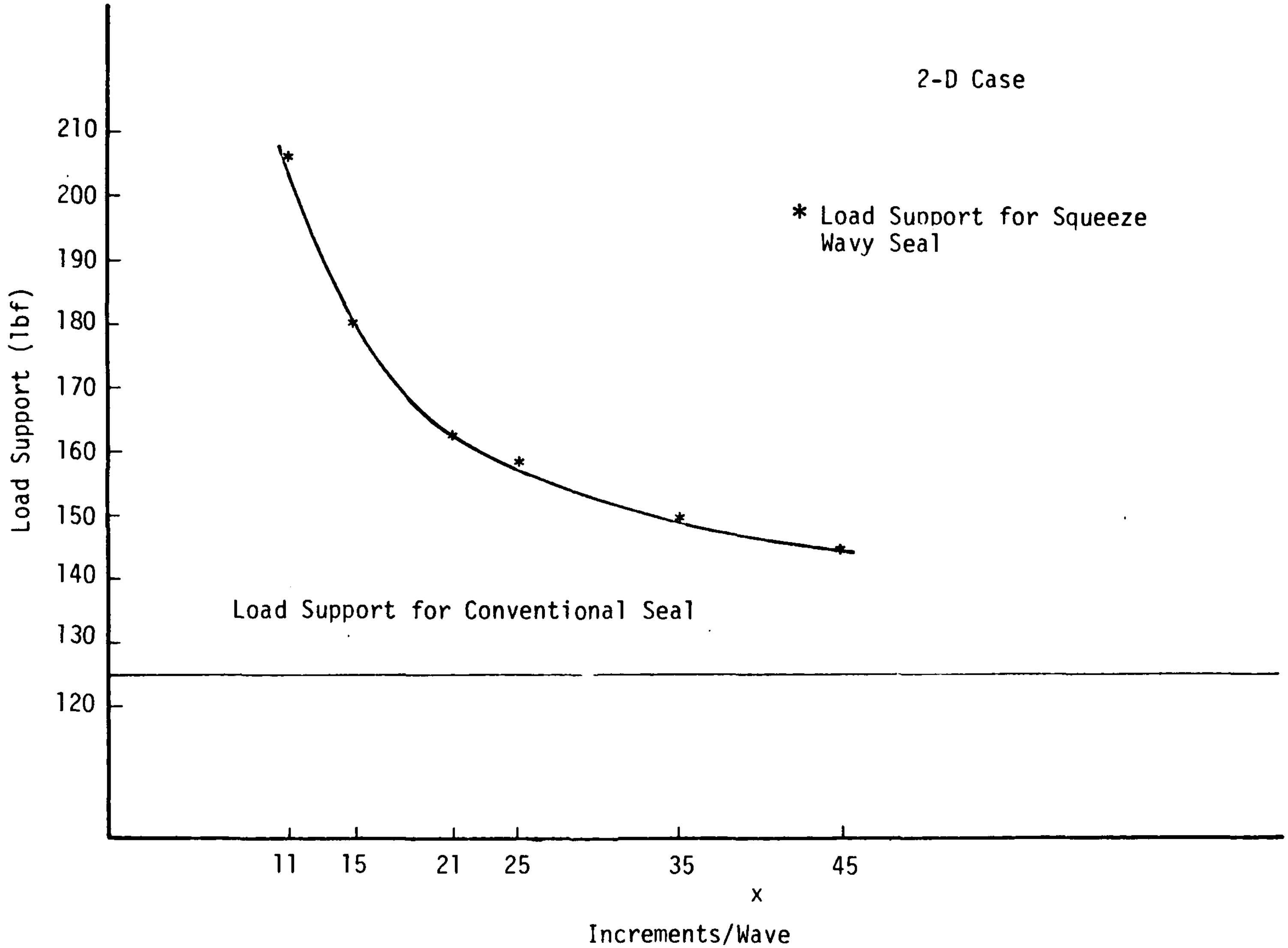

Figure 8-8. Effect of Mesh Size--Two Dimensional Case.

While it has been shown that the performance of rigid body squeeze wavy seals are identical to that of rigid body standard wavy seals, it would be interesting to find out about the performance of a deformable squeeze wavy seal/bearing which could be obtained by having a housing with variable stiffness along its length (as described earlier in this chapter, see Figure 8-3. In fact a new type of journal bearing (Figure 8-9) can be designed according to this concept.

In (Figure 8-9), it is shown that instead of having a circular shaft as that of classical journal bearings, a shaft constructed by n wavy surfaces (only three are shown in Figure 8-9) is placed and eccentrically rotated inside the bearing. The bearing is surrounded by an elastic housing having variable stiffness.

The bearing may be thought of as an infinite plate resting on a so-called Winkler foundation [57]. The foundation can be modeled as a series of closely spaced springs, each of which can deflect independently of its neighbors.

For simplicity, it is assumed that the length of the bearing is long as compared to its diameter and thus enabling us to first consider this problem as a one-dimensional case.

In Figure 8-10 it is shown that the bearing is represented by an infinite plate resting on an elastic foundation having variable stiffness, while the shaft with wavy surfaces is made to move at a velocity U_2.

To find the solution of this problem, the deflection caused by pressure force must be first found.

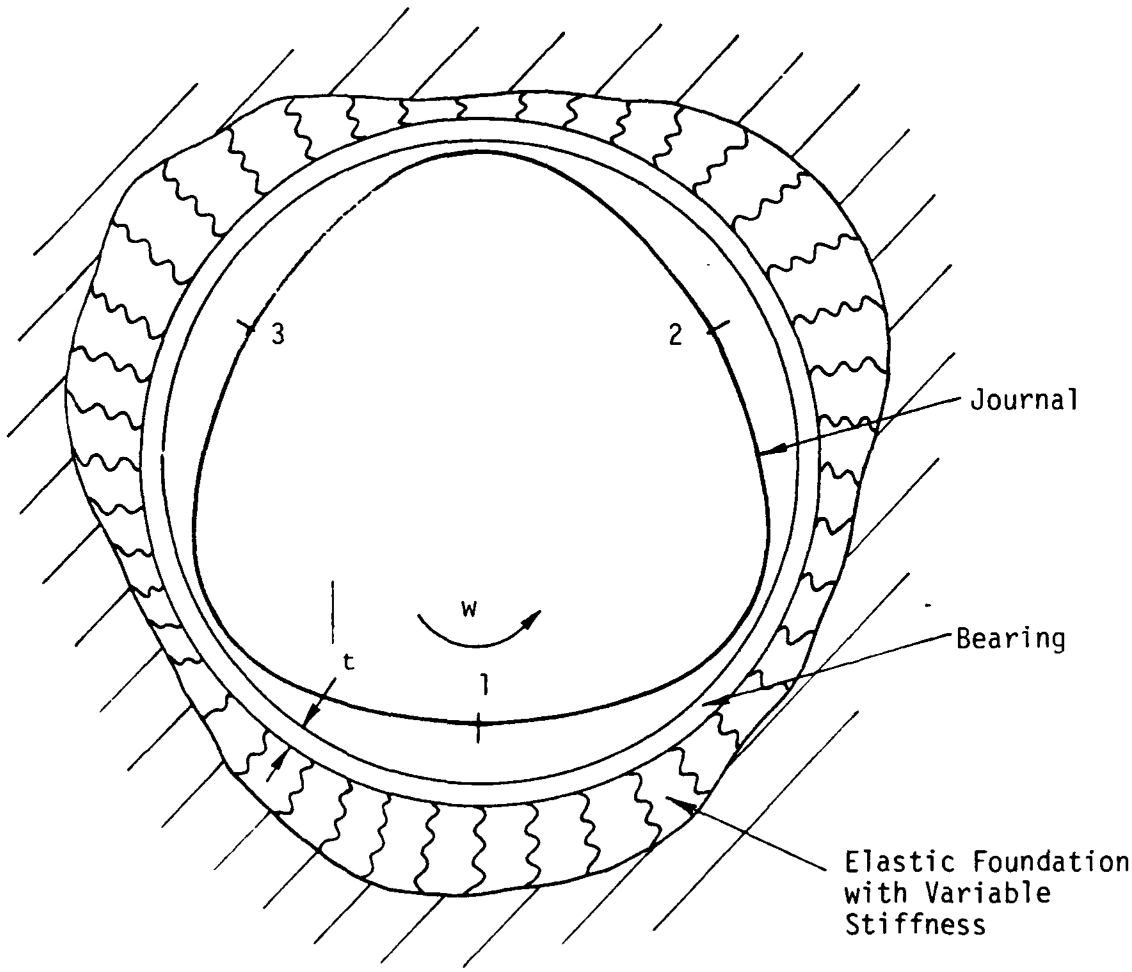

Figure 8-9. Wavy-Squeeze-Deformable Journal Bearing.

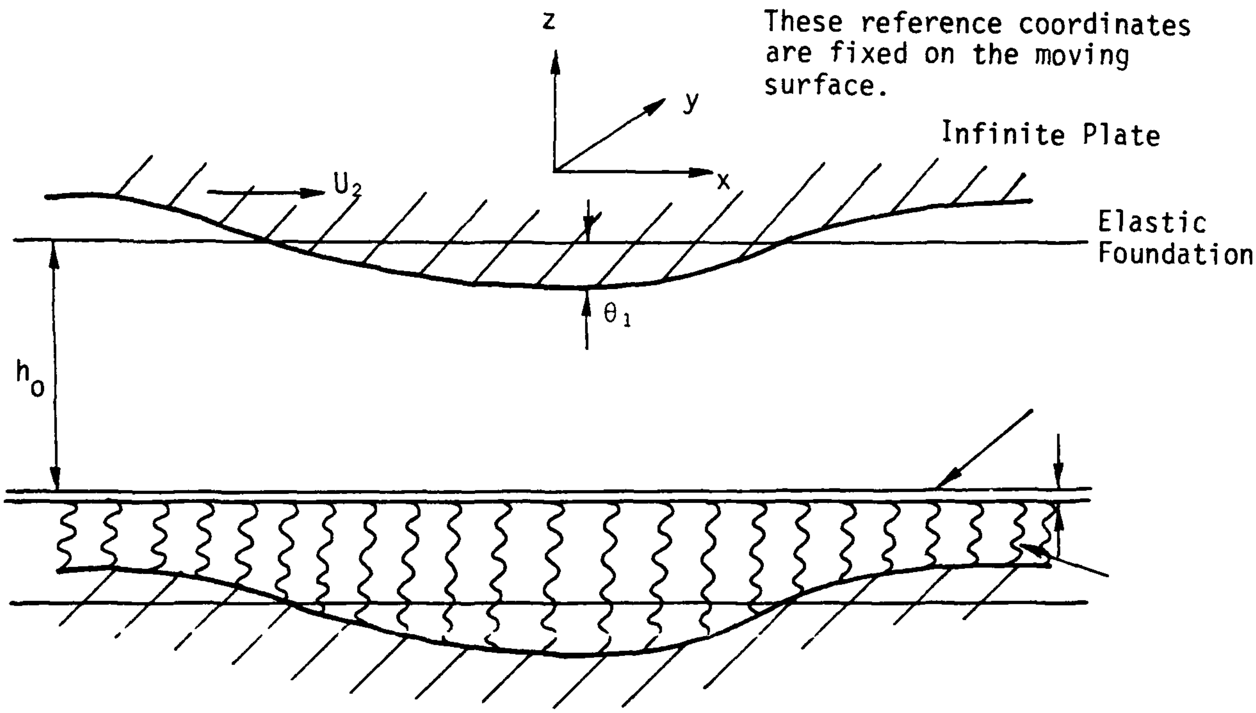

Figure 8-10. Wavy-Squeeze-Deformable Problem.

Deflection of An Infinite Plate Resting on an Elastic Foundation

Consider an infinitely long rectangular plate with uniform thickness t subjected to a uniformly distributed pressure force along its center line (Figure 8-11). The governing deflection equation for this plate can be represented by

$$D\left(\frac{\partial^4 W}{\partial x^4} + \frac{\partial^4 W}{\partial x^2 \partial y^2} + \frac{\partial^4 W}{\partial y^4}\right) = D - kW \ , \tag{8-23}$$

where

$$D = \frac{Et^3}{12(1 - \mu^2)}$$

W = deflection

k = foundation modulus

p = given pressure force

L = axial length of the bearing

If the axial length of the bearing is long enough, the variation of deflection along the y direction can be ignored, i.e., $W \neq W(y)$. In such a case, Equation (8-23) becomes

$$D \frac{d^4 W}{dx^4} = P - kW \ . \tag{8-24}$$

The value of k is assumed as

$$k(x) = C_1 + C_2 \sin(nx) \ , \tag{8-25}$$

where

C_1, C_2 = constant

n = number of wave .

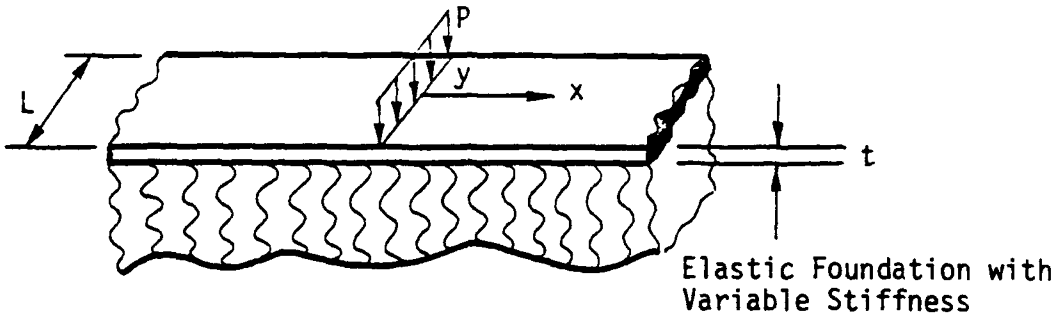

Figure 8-11. Plastic Foundation.

The reason why k is chosen as a sine wave is based on the fact that the original undeformed film thickness is chosen as a cosine wave. Under this condition, the effects of this variable stiffness can be clearly expressed.

The boundary conditions to be used here with Equation (8-24) are

$$x \to \infty \qquad W = 0 , \tag{8-26}$$

$$M = D \frac{d^2W}{dx^2} = 0 , \tag{8-27}$$

$$x \to -\infty \qquad W = 0 , \tag{8-28}$$

$$M = D \frac{d^2W}{dx^2} = 0 , \tag{8-29}$$

where M is moment.

An approximate solution can be obtained by changing Equation (8-20) into a finite difference equation, using the above boundary conditions, and solving with Gauss elimination method.

Since the value of k is changed from point to point along this infinite plate, it is necessary to find the deflection curves caused by a unit pressure force acting on each location.

By using the data for these deflection curves and the superposition method, one can easily obtain a deflection curve caused by any kind of pressure distribution.

Governing Equation of the Squeeze Wavy Bearing with Variable Stiffness

The assumptions upon which the present solution is based are similar to those discussed earlier except that elastic distortion is

The film thickness is now given as

$$h = h_i + \delta \ , \tag{8-30}$$

where

h_i = original film thickness under no deformation condition

δ = deformation caused by pressure force

Here h_i is expressed as (see Figure 8-10)

$$h_i = h_o + \varepsilon_1 \cos(-n(Ut - x)) \ . \tag{8-31}$$

To solve Equation (8-16), the boundary conditions are the same as that described previously, that is, pressure is zero at the point of maximum film thickness and cavitation occurs where it needs to. To solve for a one-dimensional undeformed squeeze wavy seal, the solution procedure is described as follows:

(1) At each time instant the pressure distribution under which no deformation is considered is first obtained by using over-relaxation method (relaxation factor = 1.7).

(2) This pressure distribution is then used to determine the distortion. The distortion alters the film shape and consequently a new pressure distribution is developed. This iteration process is continued until a final solution which satisfies both the hydrodynamic and elastic deformation requirements of the system is reached.

(3) The pressure distribution and film thickness obtained from the present time instant are substituted into Equation

(8-16). A new pressure distribution for the next time instant is generated.

For all the iteration processes, an effective way to speed up the convergence is by adjusting the pressure distribution at each iteration. In other words, instead of only using the pressure distribution obtained by the previous iteration, a weighted mean of those pressures obtained from the previous iteration is also applied to the next iteration, i.e.,

$$p(j) = p(j - 1) * \mathrm{CONV} + (1 - \mathrm{CONV}) * p_m \, , \tag{8-32}$$

where

j = iteration number

CONV = convergent factor (0.58 is used)

p_m = weighted mean of pressure

Numerical Results

The numerical data used here are

$h_o = 4.5 \times 10^{-4}$ in.

$\varepsilon_1 = 5.0 \times 10^{-5}$ in.

$n = 3$

$E = 3 \times 10^6$ lb/in.^{2}

$\mu = 0.99 \times 10^{-7}$ Reyn.

$\nu = 0.3$

$\omega = 1800$ rpm

$k = 3 \times 10^6 + 1 \times 10^6 \sin nx$ lb/in.

$\beta = 500$

$\Delta t = 0.3175 \times 10^{-3}$ sec

The numerical result for the present problem is shown in Figure 8-12. Since the reference coordinates are fixed on the shaft (or moving surface), the stiffness curves of the elastic foundation are different for each time instant. In order to compare the load support to a conventional bearing, a minimum film thickness is held as constant all the time ($h_{min} = 4.3 \times 10^{-4}$ in.). It is shown that the values of the load support vary within the range of 82.7 ~ 120 lb. Maximum load support occurs at time $t = (28 - 1) * \Delta t$ and minimum load support occurs at time $t = (11 - 1) * \Delta t$. The stiffness curves for both maximum and minimum load support are shown in Figure 8-13. It is found that minimum load support occurs at location where the stiffness curves has the same shape as that of the film thickness. The maximum load occurs at a location where the stiffness curve is just opposite to the shape of the film thickness. Since the deformation is small as compared to the original undeformed film thickness, the shape of the film thickness can be roughly described as Figure 8-13(c).

Conclusion

Due to the convergence difficulty encountered in the iteration process, only small elastic deformation (at the order of 10^{-6} in.) is considered here. The difference in load support found so far is small. Further investigation is still necessary to fully understand the performance of the squeeze wavy seal/bearing.

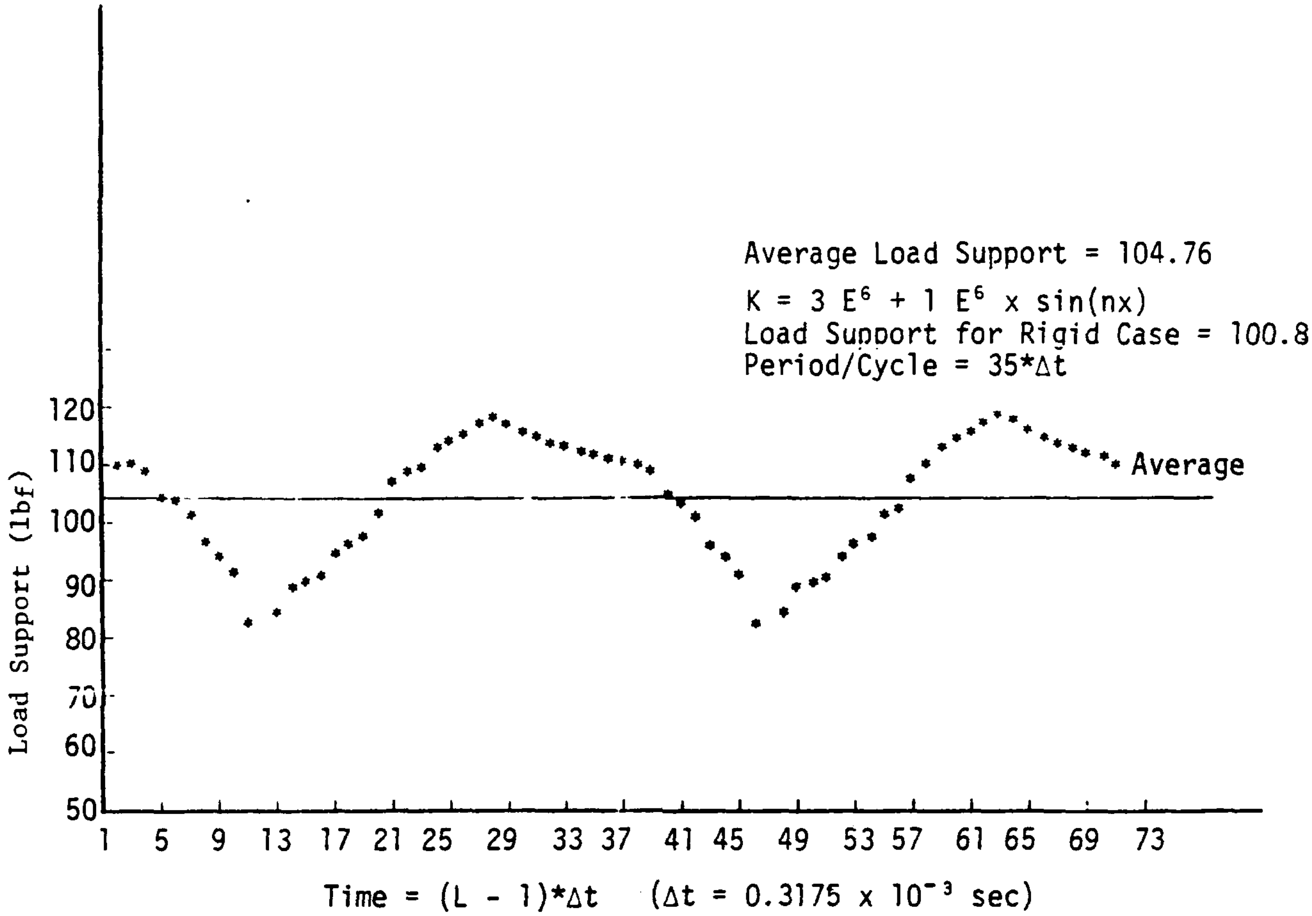

Figure 8-12. Wavy-Squeeze-Deformable Seal Load Support.

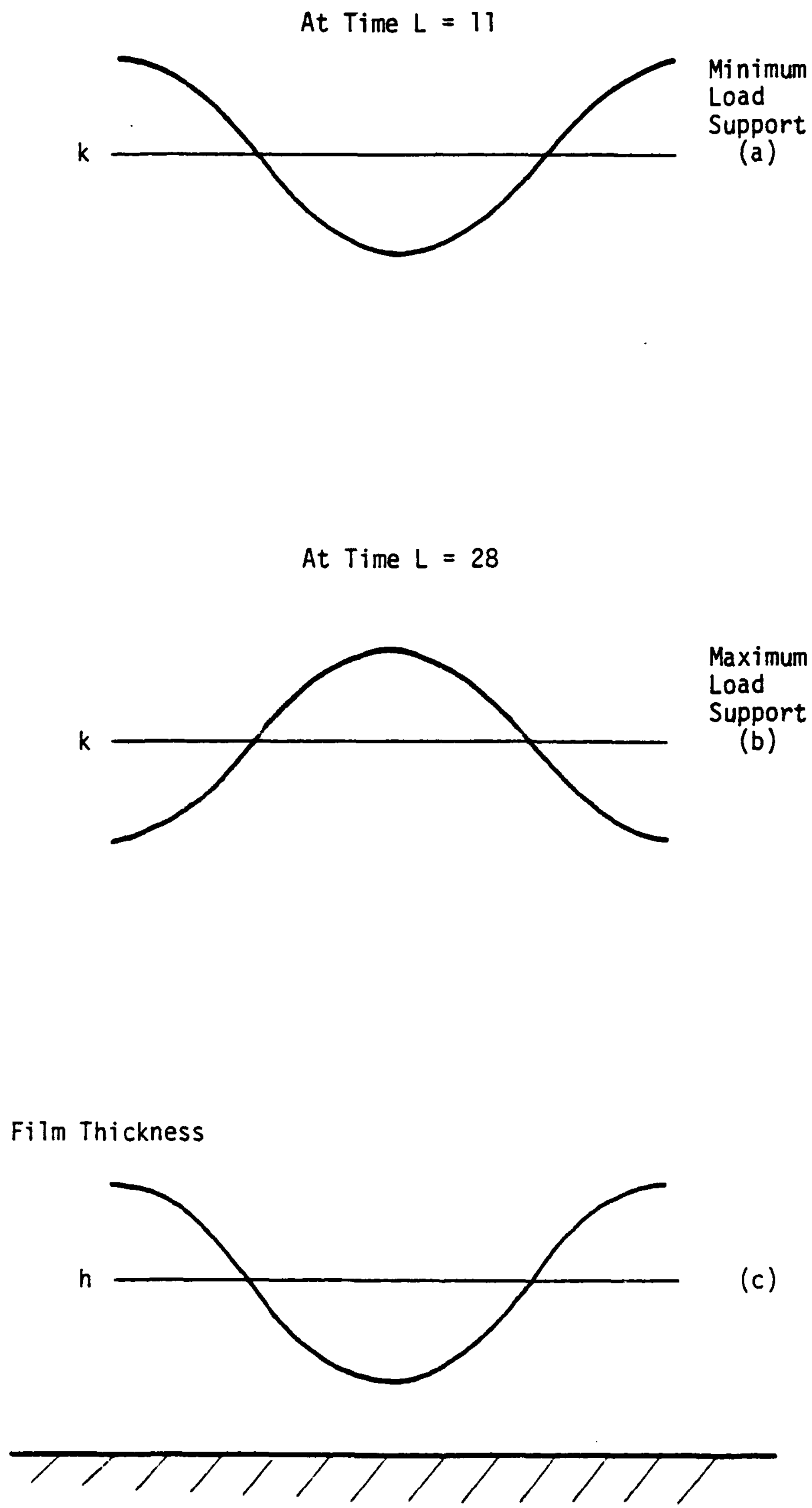

Figure 8-13. Condition of Maximum and Minimum Load Support.

CHAPTER 9

SUMMARY AND CONCLUSIONS

Nine Wave Seal--Design 1

After initial design problems were overcome, this seal ran for the 2000 hour test successfully. Face wear was very low (530 μin.) and would be expected to provide more than adequate wear life for 150000 hours of operation. Torque was somewhat higher and leakage somewhat lower than predicted indicating that not as much wave as desired was actually present on the seal faces.

It was concluded that even though this seal design operated successfully, it is too complex to manufacture for practical applications because of the many small flow passages and machined pads. A simpler type of design was sought.

Nine Wave Seal--Design 2

A much simpler and easier to fabricate design was created. This design uses an all carbon seal ring with no cut pads. Fifty-four O-ring seal pistons are used on the inside of the seal. This part is manifolded using soldered tubing. These parts were machined from brass and protected by being incapsulated in epoxy.

This seal design was fabricated and ran for 2000 hours with no significant problems. Wear was 355 μin. average, lower than for design one (0.026 in. wear in 150000 hours). Torque was slightly higher and leakage lower than predicted.

Even though this design was successful and relatively simple to fabricate, it was decided that the uncertainty in reliability brought about by the pressure pads and O-ring system plus the complexity of the essential auxiliary pressure system were still significant disadvantages to the practical application of the wavy seal. Thus, an even simpler design and waviness drive system were sought.

<u>Nine Wave Seal--Design 3</u>

After many different approaches were considered and discarded, it was decided that placing the unique wave shape permanently on the hard face produced, a wavy seal with the greatest possible advantage in that no auxiliary support or pressure system is needed at all. The design has the same low leakage--low torque characteristics as the previous design. There is only one potential limitation and that is that the high spots may wear off of the hard face. Unlike the previous designs, both faces are not wiped everywhere. There are many reasons to believe that the wave will not wear off during the practical lifetime of the seal, but only testing will tell for sure. Short term tests run to date look very promising.

This idea represents a compromise between having the ultimate in wearing faces with the uncertainty of auxiliary systems and having possibly a somewhat shorter lifetime with near absolute reliability. Given the excellent wear resistance of SiC, there is a high probability that the hard face will perform adequately.

A new type of grinding fixture was designed to grind the nine wave tilted face. The fixture is based on a flexure mount so that it can be made of only moderately precision parts.

500 Hour Parallel Face Test

A 500 hour variable condition test was run using the flat faced version of the first nine wave seal. The wear on the seal was surprisingly low and torque was very high (many times exceeding the capacity of the test machine). It was concluded that while the wear is low the high friction of this type of seal will make long term operation somewhat uncertain because of possible material damage due to high interface temperature.

Force Transducer Design

A new type of integral force transducer was designed in an attempt to find a better force applyer than the O-ring systems. This system was based on using a porous medium and an epoxy diaphragm. Several experiments were run. The device worked but was judged too unreliable for the intended purpose.

Torsion of Composite Section

Some unique work was performed to develop a method to evaluate the torsional stiffness of cross sections made up of two materials.

Warping Evaluation

For nine wave seal design 2, warp again (as in design 1) turned out to add significantly to the stiffness in the torsional deformation required to produce the wave. Three-dimensional finite element modeling was performed to evaluate the warping function. In this design, measured waviness is reasonably close to predicted waviness in a large part because warping was properly accounted for.

Two Ring Contact Model

The two ring contact model was analyzed, checked experimentally, and proved to be very useful in evaluating stiffness effects in actual submarine seals. In particular, studies show

1) Submarine seal leakage is readily caused by lock ring groove out of flatness.
2) Submarine seals cannot close up gaps of the size found in typical leakers--they are very stiff.
3) The model successfully predicted the effects placing a shim in the lock ring groove.
4) The variation of stiffness at the seal joint in conjunction with the large moment in the ring causes the seal to just separate.
5) Even a highly compliant seal will not close off an opening caused by a 0.001 in. segment shift.

Magnetic Seals

The two ring contact model was used to predict leakage caused by waviness in small magnetic seals caused by waviness.

Nonlinear Joint Model

It became clear in using the two ring contact model that a better model of the seal bolted joint is needed. Some preliminary FEM modeling of the joint has been made. More extensive modeling and experiments are planned.

Seal Conformability

Various stiffness studies and the design of the wavy seal show how tangential stiffness must be carefully considered in seal design. In the case of the wavy seal, nine waves are needed so that they do not flatten out and cause the wavy effect to be diminished. In the case of submarine seals and the magnetic seals evaluated herein, they are too stiff to properly close to minimize leakage. With the various stiffness models tools are now in hand to carefully make these evaluations.

Friction and Wear Tester

A new hydrostatic bearing support was designed and fabricated for the friction and wear test machine. The design reduced the influence of friction on measurements to zero and allows accurate application of the load. The bearing is designed to operate on a 0.00075 in. film of water.

Microasperity Lubrication

Using the above apparatus extensive measurements were made of carbon-WC friction in water independent of hydrostatic and conventional hydrodynamic effects. It was found that friction is greatly reduced with increasing speed suggesting hydrodynamic effects. By varying ambient water pressure, experiments were run to reduce the effectiveness of microasperity cavitation--the hypothesized mechanism. There was no effect. Thus it appears that microasperity lubrication is not causing this beneficial lubrication. Given the importance of this unknown mechanism (in that it might be even more effectively and widely applied if understood), more work is being conducted to begin to understand this strong speed effect.

Seal Analysis

Several automated computer programs have been developed for the purpose of expediting design and analysis of seals. The first program creates a refined finite difference mesh for a completely arbitrary cross section and calculates the circular ring section properties and the torsional stiffness by solving the Poisson equation. Input is very simple and the program does all of the work automatically.

A second program creates a mesh for FEM input automatically. A third program solves the heat transfer equations to find the temperature distributions in a two ring seal (with interface) and the thermal rotation. Arbitrary convective boundaries can be easily input. The analysis is completely automatic and serves as a very powerful design tool to look at the effect of thermal rotation on design.

Squeeze Seal/Bearings

It has been shown that certain squeeze seal concepts are hydrodynamically identical to the present wavy seal but may be simpler to implement.

A new type of wavy squeeze/seal bearing which uses an elastic foundation of variable stiffness is being evaluated.

General

A great deal has been learned and written about in terms of the proper design considerations for wavy seals as well as conventional seals. The role of stiffness, deflection, hydrodynamic and hydrostatic lubrication and thermal rotation have been much better understood. Many mechanic's problems have been solved to obtain this understanding.

Yet there remain uncertainties in seal design and related lubrication problems where more attention would be most worthwhile. In particular a better understanding of the fundamental lubrication mechanisms in carbon-hard face sliding system is sorely needed. Identification of the existence and content of cavitation in water hydrodynamics has never been done. Work on the role of microasperities in lubrication remains unfinished. Finally obtaining an understanding of a whole new type of bearing/seal--the squeeze seal/bearing has just begun. There remain many challenges in these areas of tribology.

REFERENCES

1. Lebeck, A. O., Teale, J. L., and Pierce,R. E., "Elastohydrodynamic Lubrication with Wear and Asperity Contact in Mechanical Face Seals," Annual Report ME-76(77)ONR-414-1, ONR Contract N-00014-76-C-0071, Bureau of Engineering Research, The University of New Mexico, Albuquerque, New Mexico, January 1977.

2. Lebeck, A. O., Teale, J. L., and Pierce, R. E., "Hydrodynamic Lubrication with Wear and Asperity Contact in Mechanical Face Seals," Annual Report ME-86(78)ONR-414-1, prepared for the Office of Naval Research under Contract No. ONRN-00014-76-C-0071, Bureau of Engineering Research, The University of New Mexico, Albuquerque, New Mexico, January 1978.

3. Lebeck, A. O., Teale, J. L., and Pierce, R. E., "Hydrodynamic Lubrication with Wear and Asperity Contact in Mechanical Face Seals," Annual Report ME-95(79)ONR-414444-1, prepared for the Office of Naval Research under Contract No. ONR-N-00014-76-C-0071, Bureau of Engineering Research, The University of New Mexico, Albuquerque, New Mexico, January 1979.

4. Lebeck, A. O. and Young, L. A., "The Wavy Mechanical Face Seal--Theoretical and Experimental Results," Annual Report ME-105(80)ONR-414-1, prepared for the Office of Naval Research under Contract ONR-N-00014-76-C-0071, Bureau of Engineering Research, The University of New Mexico, Albuquerque, New Mexico, January 1980.

5. Lebeck, A. O. and Young, L. A., "The Wavy Mechanical Face Seal--Theoretical and Experimental Results," Annual Report ME-111(81)ONR-414-1, prepared for the Office of Naval Research under Contract ONR-N-00014-76-C-0071, Bureau of Engineering Research, The University of New Mexico, Albuquerque, New Mexico, January 1981.

6. Lebeck, A. O., Young, L. A., Wong, K. L., and Knowlton, J., "Application of the Wavy Mechanical Face Seal to Submarine Seal Design," Summary of Report ME-117(82) ONR-414-1, prepared for the Office of Naval Research under Contract ONR-N-00014-76-C-0071, Bureau of Engineering Research, The University of New Mexico, Albuquerque, New Mexico, July 1982.

7. Lebeck, A. O., Teale, J. L., and Pierce, R. E.,"Hydrodynamic Lubrication and Wear in Wavy Contacting face Seals, Journal of Lubrication Technology, Vol. 100, January 1978, pp. 81-91.

8. Lebeck, A. O., "A Study of Mixed Lubrication in Contacting Mechanical Face Seals," presented at the 4th Leeds-Lyon Symposium on Lubrication, Lyon, France, September 13-16, 1977, published in "Surface Roughness Effects in Lubrication," proceedings of the 4th Leeds-Lyon Symposium on Tribology. Published by Mechanical Engineering Publications Limited for the Institute of Tribology, Leeds University and the Institut National Des Sciences Appliquées de Lyon, 1978.

9. Lebeck, A. O., "A Mixed Friction Hydrostatic Face Seal Model with Thermal Rotation and Wear," ASLE Transactions, Vol. 23, No. 4, October 1980, pp. 375-387.

10. Lebeck, A. O., "The Effect of Ring Deflection and Heat Transfer on the Thermoelastic Instability of Rotating Face Seals," presented at the ONR Thermal Deformation Workshop, June 1979, published in Thermal Deformation in Frictionally Heated Systems, R. A. Burton, Editor, Elsevier, The Netherlands, 1980.

11. Lebeck, A. O., "A Mixed Friction Hydrostatic Face Seal Model with Phase Change," Journal of Lubrication Technology, Vol. 102, No. 2,April 1980, pp. 133-138.

12. Teale, J. L. and Lebeck, A. O., "An Evaluation of the Average Flow Model [1] for Surface Roughness Effects in Lubrication," Journal of Lubrication Technology, Vol. 102, No. 3, July 1980, pp. 360-367.

13. Lebeck, A. O., "Hydrodynamic Lubrication in Wavy Contacting Face Seals--A Two-dimensional Model," Journal of Lubrication Technology, Vol. 103, No. 4, October 1981, pp. 578-586.

14. Lebeck, A. O., "A Test Apparatus for Measuring the Effects of Waviness in Mechanical Face Seals," ASLE Transactions, Vol. 24, No. 3, July 1981, pp. 371-378.

15. Lebeck, A. O. and Young, L. A., "Design of an Optimum Moving Wave and Tilt Mechanical Face Seal for Liquid Applications," 9th International Conference on Fluid Sealing, sponsored by the BHRA, The Netherlands, April 1-3, 1981.

16. Young, L. A. and Lebeck, A. O., "Experimental Evaluation of a Mixed Friction Hydrostatic Mechanical Face Seal Model Considering Radial Taper, Thermal Taper, and Wear," Journal of Lubrication Technology, 1982.

17. Lebeck, A. O. and Chiou, B. C., "Two Phase Mechanical Face Seal Operation: Experimental and Theoretical Observations," Proceedings, 11th Annual Turbomachinery Syumposium, Turbomachinery Laboratories, Department of Mechanical Engineering, Texas A&M University, December 1982.

18. Lebeck, A. O. and Wong, K. L., "Moving Wave Gas Seal," ASLE Transactions, v. 27, no. 1, January 1984, pp. 53-60.

19. Lebeck, A. O. and Knowlton, J. A., "A Finite Element for the Three-Dimensional Deformation of a Circular Ring for Arbitrary Cross Section," accepted for publication in International Journal of Numerical Methods in Engineering, submitted November 1982.

20. Granzow, G. D. and Lebeck, A. O., "An Improved One Dimensional Foil Bearing Solution," accepted for presentation at ASLE/ASME Joint Lubrication Conference, October 1984 (Related paper).

21. Lebeck, A. O., "Prediction of Leakage Gap in Non-axisymmetric Geometry Face Seals," Journal of Tribology, July 1984, pp. 329-337.

22. Lebeck, A. O., "Face Seal Waviness--Measurement, Prediction, Causes, and Effects," published and presented at the 10th International Conference on Fluid Sealing, BHRA, Innsbruck, April 1984.

23. Teale, J. L., "Surface Roughness Effects in Hydrodynamic Lubrication," MS Thesis, Mechanical Engineering Department, University of New Mexico, August 1978.

24. Pierce, R. E.,. "A Design Study for a Wavy Hydrodynamic Mechanical Face seal," MS Thesis, Mechanical Engineering Depaitment, University of New Mexico, May 1978.

25. Young, L. A., "Experimental Evaluation of a Mixed Friction Hydrostatic Mechanical Face Seal Model," MS Thesis, Mechanical Engineering Department, University of New Mexico, December 1980.

26. Chiou, B. C., "The Effect of Two-phase Operation on Seal Performance," MS Thesis, Mechanical Engineering Department, University of New Mexico, December 1980.

27. Wong, K. L., "Moving Wave Gas Seal," MS Thesis, Mechanical Engineering Department, University of New Mexico, January 1982.

28. Knowlton, J. S., "A Finite Element for the Three-Dimensional Deformation of a Circular Ring of Arbitrary Cross Section," MS Thesis, Mechanical Engineering Department, University of New Mexico, December 1982.

29. Kanas, P., "Microasperity Lubrication," MS Thesis, Mechanical Engineering Department, University of New Mexico, (in progress, expected December 1984).

30. Williams, H. E., "The Stability of Circular Rings under a Uniformly Distributed Radial Load," California Institute of Technology, Pasadena, California, January 1970, NTIS N70-17318.

31. Timoshenko, S. P. and Goodler, J. NM., Theory of Elasticity, Third Edition, McGraw-Hill, 1970, pp. 291-297.

32. Oden, J. T., Mechanics of Elastic Structures, McGraw-Hill, 1967, pp. 203-205.

33. Vlasov, V. Z., "Thin Walled Elastic Beams," translated from Russian, NTIS TT-61-11400, 1961.

34. Lebeck, A. O., "Causes and Effects of Waviness in Mechanical Face Seals," Final Report, Technical Report ME-68(76)NSF-271-1, The University of New Mexico Bureau of Engineering Research, Albuquerque, New Mexico, January 1976.

35. Paxton, R. Manufactured Carbon: A Self-lubricating Material for Mechanical Devices, CRC Press, 1979, pp. 124-126.

36. Iny, E. H., "The Design of Hydrodynamically Lubricated Seals with Predictable Operating Characteristics," 5th International Conference on Fluid Sealing, BHRA, April 1971.

37. Snapp, R. B. and Sasdelli, K. R., "Performance Characteristics of High Pressure Face Seal with Radially Converging Interface Shapes," Paper E4, 6th International Conference on Fluid Sealing, February 1973, BHRA, Munich.

38. Roark, R. J. and Young, W. C., Formulas for Stress and Strain, New York, McGraw-Hill, 1975, p. 260.

39. Lebeck, A. O., "Mechanical Loading--A Primary Source of Waviness in Mechanical Face Seals," presented at the 31st Annual ASLE Meeting, Philadelphia, PA, May 1976, ASLE Trans., 20(3), pp. 195-208.

40. Meck,H. R., "Three-Dimensional Deformation and Buckling of a Circular Ring of Arbitrary Section," Transactions of the ASME Journal of Engineering for Industry, February 1969, pp. 266-272.

41. Lebeck, A. O. and Reyna, S., "Leakage in Magnetic Seals," Report ME-126(84)NAVY-249-1, work performed under contract Nos. N000140-83-C-5574 and N000140-82-C-0673 for Naval Air Propulsion Center, Trenton, NJ by The Bureau of Engineering Research, University of New Mexico, Albuquerque, NM, March 1984.

42. Lebeck, A. O., "Preliminary Engineering Evaluation of DTNSROC Conformable Submarine Seal Design (Trident Backfit), work performed under ONR Contract NC001483-K-0304 by The Bureau of Engineering Research, The University of New Mexico, Albuquerque, NM, August 1983.

43. Harbage, A. B., "Mechanical Design of Submarine Propeller Shaft Seals, Progress Report and Position Paper for Fiscal Year 1982," October 1982, DTNSRDC, TM-27-82-77.

44. Bose, B., "Moment-Rotation Characteristics of Semi-rigid Joints," J. Inst. Eng., India, Part CI, v. 62, September 1981, pp. 128-132.

45. Krishnamurthy, N., "Modeling and Prediction of Bolted Connection Behavior," Comp. and Struct. v. 11-1/2, pp. 75-82.

46. Tsutsumi, M., Ito, Y., Masuko, M., "Deformation Mechanism of Bolted joint in Machine Tools," Bull. of JSME, v. 22, n. 67, June 1979, pp. 885-892.

47. Sawa, T., Maruyama, K., Edamoto, K., "On Characteristics of a Bolted Joint with a Tap Bolt," Bull. of JSME, v. 24, n. 197, November 1981, pp. 2027-2035.

48. Baumeister, T., Avalloni, A. A., Marks' Standard Handbook for Mechanical Engineers, McGraw Hill, 8th edition, 1978.

49. Hamilton, D. B., Walowit, J. A., Allen, C. M., "A Theory of Lubrication by Microirregularities," ASME Journal of Basic Engineering, March 1966, pp. 177-185.

50. Kojobashian, C. and Richardson, H. H., "A Micropad Model for the Hydrodynamic Performance of Carbon Face Seals," Third International Conference on Fluid Sealing Proceedings, Cambridge, 1967.

51. Kistler, A. L., Cheng, H. S., Nivatvongs, K. and Ozakat, I., "Cavitation Phenomena in Face Seals," prepared for ONR Contract N00014-79-C-0007, Department of Mechanical and Nuclear Engineering, Northwestern University, Evanston, Illinois, July 1981.

52. Patir, N. and Cheng, H. S., "An Average Flow Model for Determining Effects of Three Dimensional Roughness on Partial Hydrodynamic Lubrication," Journal of Lubrication Technology, Vol. 100, Jan. 1978, p. 2.

53. Elrod, H. B., "A Cavitation Algorithm," presented at the Century 2 ASME-ASLE International Lubrication Conference (San Francisco: Aug. 1980) ASME Paper 80-C2/LUB-54.

54. A. Cameron, "Basic Lubrication Theory," John Wiley & Sons, 1976, page 26.

55. Jakobsson, B. and Floberg, F., "The Finite Journal Bearing Considering Vaporization," Report No. 3, 1957, Institute of Machine Elements, Chalmers University, Gothenburg, Sweden.

56. J. O'Donoghue, D. K. Brighton, C.J.K. Hooke, "The Effects of Elastic Distortion on Journal Bearing Performance," Journal of Lubrication Technology, Oct. 1967, pp. 409-417.

57. Enrico Volterra and J. H. Gaines, "Advanced Strength of Materials," Prentice-Hall, Inc., 1971.

Distribution List

Recipient	Number of Copies
Office of Naval Research 800 N. Quincy Street Arlington, Virginia 22217 Attn: M. Keith Ellingsworth, Code 473	(3)
Defense Documentation Center Building 5 Cameron Station Alexandria, Virginia 22314	(12)
Naval Research Laboratory 4555 Overlook Avenue Washington, DC 20390 Attn: Technical Information Division	
Code 2627	(6)
Dr. Ravner, Code 6170	(1)
U.S. Naval Postgraduate School Monterey, California 93940 Attn: Dept. of Mechanical Engineering	(1)
U.S. Naval Academy Annapolis, Maryland 21402 Attn: Dept. of Mechanical Engineering	(1)
Naval Air Systems Command Jefferson Plaza Washington, DC 20360 Attn: B. Poppert, Code 204E	(1)
Naval Sea Systems Command Crystal City, National Center #3 Washington, DC 20360 Attn: Frank Ventriglio, Code OSR14	(1)
DTNSRDC Annapolis, Maryland 21402 Attn: Fuels & Tribology Branch J. F. Dray	(1)
Naval Air Engineering Center Lakehurst, New Jersey 08733 Attn: Mr. P. Senholzi	(1)

Distribution List (continued)

Recipient	Number of Copies
Naval Air Propulsion Test Center Trenton, New Jersey 08628 Attn: Mr. R. Valori	(1)
Naval Air Development Center Warminster, Pennsylvania 18974 Attn: Mr. A. Conte	(1)
National Science Foundation 1800 G Street, NW Washington, DC 20550 Attn: Dr. C. J. Astill	(1)
National Bureau of Standards Washington, DC 20234 Attn: Dr. W. Ruff	(1)
NASA Lewis Research Center 21000 Brookpark Road Cleveland, Ohio 44135 Attn: R. L. Johnson	(1)
Air Force Office of Scientific Research Washington, DC 20333 Attn: Directorate of Engineering Sciences	(1)
Air Force Aeropropulsion Laboratory Wright-Patterson Air Force Base, Ohio 45433 Attn: AFAPL/POD-1, Dick Quigley, Jr.	(1)
Army Research Office Durham, North Carolina 27706 Attn: Dr. E. A. Saibel	(1)
Office of Naval Research Branch Office 1030 East Green Street Pasadena, California 91106	(1)
Assistant Chief for Technology Office of Naval Research, Code 200 Arlington, Virginia	(1)
Prof. H. S. Cheng Department of Mechanical Engineering Northwestern University Evanston, Illinois	(1)

Distribution List (continued)

Recipient	Number of Copies
Crane Packing Company 6400 Oakton Street Morton Grove, Illinois 60053 Attn: Art Zobens	(1)
Sealol, Inc. Box 2158 Providence, Rhode Island 02905 Attn: H. F. Greiner	(1)
Pure Carbon Company St. Marys, Pennsylvania 15857 Attn: R. R. Paxton	(1)
Franklin Research Institute 20th and Race Streets Philadelphia, Pennsylvania 19103 Attn: Harry C. Rippel	(1)
Naval Sea Systems Command Crystal City, National Center #4 Washington, DC 20360 Attn: Dick Graham, Code 56X43	(1)
DTNSRDC Annapolis, Maryland 21402 Attn: Al Harbage	(1)
Prof. Francis E. Kennedy, Jr. Thayer School of Engineering Dartmouth College Hanover, New Hampshire 03755	(1)
Mr. Cliff Mussen PMS 396-223 Trident Submarine Ship Acquisition Project Naval Sea Systems Command Department of Navy Washington, DC 20362	(1)

APPENDIX A

FINITE DIFFERENCE SOLUTION TO THE TORSION PROBLEM OF A COMPOSITE CROSS SECTION

Considering the rectangular cross section as shown in Figure A1 where the boundaries align with the x and y axis, the free boundary condition from Chapter 3 is

$$\left(\frac{\partial\psi}{\partial x} - y\right)\frac{dy}{ds} - \left(\frac{\partial\psi}{\partial y} + x\right)\frac{dx}{ds} = 0 \tag{1}$$

For corner #1, $\frac{dy}{ds} = 1$ and $\frac{dx}{ds} = 1$. So the finite difference formulation gives

$$\psi_{(I,J)} = \left[\frac{(x(I+1) - x(I))\ (y(J+1) - y(J))}{(x(I+1) - x(I)) + (y(J+1) - y(J))}\right] x$$

$$\left[\frac{\psi_{(I+1,J)}}{x(I+1) - x(I)} + \frac{\psi_{(I,J+1)}}{y(J+1) - y(J)} - y(J) - x(I)\right] \tag{2}$$

For the boundary between corners #1 and #2, we have that $\frac{dy}{ds} = 1$ and $\frac{dx}{ds} = 0$, so this gives

$$\psi_{(I,J)} = \psi_{(I+1,J)} - \Big(x(I+1) - x(J)\Big)\ y(J) \tag{3}$$

Corner #2 has $\frac{dy}{ds} = 1$ and $\frac{dx}{ds} = 1$ so

$$\psi_{(I,J)} = \left[\frac{(x(I+1) - x(I))\ (y(J) - y(J-1))}{(x(I+1) - x(I))\ (y(J) - y(J-1))}\right] x$$

$$\left[\frac{\psi_{(I+1,J)}}{x(I+1) - x(I)} + \frac{\psi_{(I,J-1)}}{y(J) - y(J-1)} - y(J) - x(I)\right] \tag{4}$$

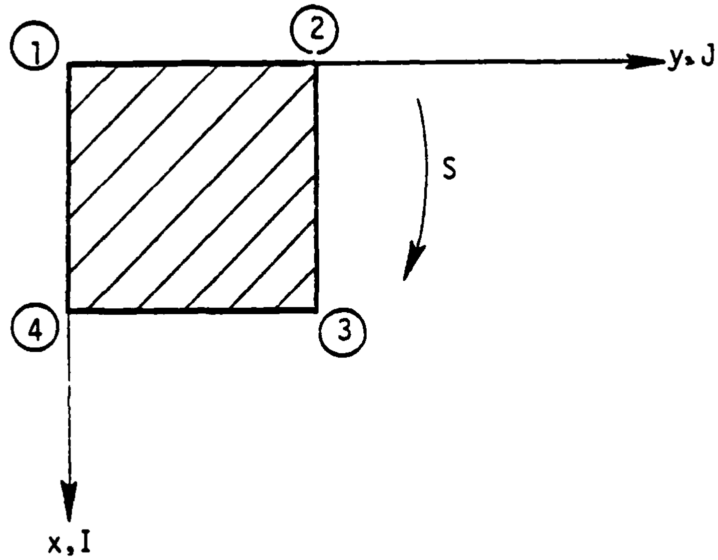

Figure A1. Simple Cross Section for Boundary Derivations.

For the boundary between corners 2 and #3 we have $\frac{dy}{ds} = 0$ and $\frac{dx}{ds} = 1$; so

$$\psi_{(I,J)} = \psi_{(I,J-1)} - (y(J) - y(J-1)\; x(I) \qquad (5)$$

Corner #3 has $\frac{dy}{ds} = -1$ and $\frac{dx}{ds} = 1$ which gives

$$\psi_{(I,J)} = \left[\frac{(\;x(I) - x(I-1))\;(\;(y(J) - y(J-1))}{(x(I) - x(I-1)) + ((y(J) - y(J-1))}\right] x$$

$$\left[\frac{\psi_{(I-1,J)}}{x(I) - x(I-1)} + \frac{\psi_{(I,J-1)}}{y(J) - y(J-1)} + y(J) - x(I)\right] \qquad (6)$$

The boundary 3 - 4 has $\frac{dy}{ds} = -1$ and $\frac{dx}{ds} = 0$; so

$$\psi_{(I,J)} = \psi_{(I-1,J)} + (x(I)) - x(I-1))y(J) \qquad (7)$$

For corner #4, $\frac{dy}{ds} = -1$ and $\frac{dx}{ds} = -1$ which gives

$$\psi_{(I,J)} = \left[\frac{(x(I) - x(I-1))\;(y(J+1) - y(J))}{(x(I) - x(I-1)) + (y(J+1) - y(J))}\right] x$$

$$\left[\frac{\psi_{(I-1,J)}}{x(I) - x(I-1)} + \frac{\psi_{(I,J+1)}}{y(J+1) - y(J)} + y(J) + x(I)\right] \qquad (8)$$

And finally for the boundary 4 - 1 , we have $\frac{dy}{ds} = 0$ and $\frac{dx}{ds} = -1$

which gives

$$\psi_{(I,J)} = \psi_{(I,J+1)} + (y(J+1) - y(J))\, x(I) \tag{9}$$

For all internal nodes we have

$$\psi(I,J) = AIM1(I,J)\psi(I-1,J) + AIP1(I,J)\psi(I+1,J) + AJM1(I,J)\psi(I,J-1) + AJP1(I,J)\psi(I,J+1) \tag{10}$$

where

$$AIJ = \frac{-2}{(x(I-1) - x(I))(x(I+1) - x(I)} - \frac{2}{(y(J-1) - y(J))(y(J+1) - y(J))}$$

$$\begin{aligned}
AIM1(I,J) &= \frac{2}{(AIJ)(x(I-1) - x(I))(x(I-1) - x(I+1))} \\
AIP1(I,J) &= \frac{-2}{(AIJ)(x(I+1) - x(I))(x(I-1) - x(I+1))} \qquad (11) \\
AJM1(I,J) &= \frac{2}{(AIJ)(y(J-1) - y(J))(y(J-1) - y(J+1))} \\
AJP1(I,J) &= \frac{-2}{(AIJ)(y(J+1) - y(J))(y(J-1) - y(J+1))}
\end{aligned}$$

Now, taking the analysis one step further and considering a cross section of two different materials as shown in Figure A2, all boundary conditions are the same as previously derived. The only additional boundary condition is that across 2 - 5 . For this boundary $\frac{dy}{ds} = 0$ and $\frac{dx}{ds} = 1$ and $\psi_1 = \psi_2 = \psi$ at the boundary. This gives

$$G_1 \left(\frac{\partial\psi}{\partial y} + x\right) = G_2 \left(\frac{\partial\psi}{\partial y} + x\right) \tag{12}$$

Finite differencing gives

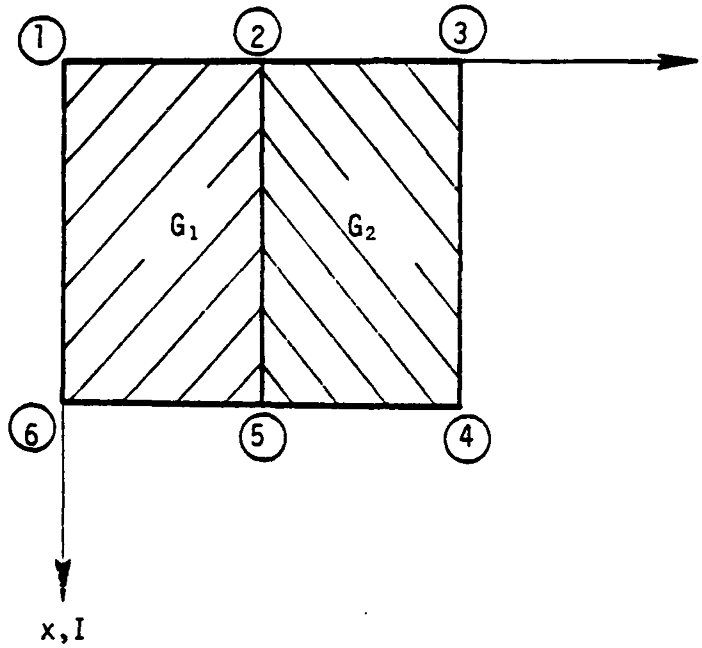

Figure A2. Composite Cross Section.

$$\psi_{(I,J)} = \frac{1}{1 + A(J)} \left[A(J) \left(\psi_{(I,J+1)} + (y(J+1) - y(J))x(I) \right) \right.$$

$$\left. + \psi_{(I,J-1)} - (y(J) \; y(J-1))x(I) \right] \qquad (13)$$

where

$$A(J) = \frac{G_2}{G_1} \frac{y(J) - y(J-1)}{y(J+1) - y(J)} \qquad (14)$$

A computer program was written using the derived boundary conditions. Results for the cross section of Figure A2 are given in Table A1. The results for G^*J_θ are those for the composite cross section method of solution and for the method not considering a composite section, i.e., the section has only one G value. These runs were made to check the consistency of G^*J_θ when the type of mesh and size were changed. The results show that for a non-uniform mesh in both x and y, the mesh must be refined. For the 29 x 29 matrix, there is only an 8% difference between a uniform and non-uniform mesh. However, for a 9 x 9 mesh, the error using a non-uniform mesh is large.

TABLE A-1

Run #	Modulus of Rigidity	Type Mesh	Size of Mesh	$G^* J_\theta$ w/ Composite Crossection	$G^* J_\theta$ w/o Composite Crossection
1	$G_1 = 11.5 \times 10^6$ $G_2 = 11.5 \times 10^6$	Uniform in both x and y	9 x 9	2427	2460
2	$G_1 = 11.5 \times 10^6$ $G_2 = 1.25 \times 10^6$	Uniform in both x and y	9 x 9	811	2460
3	$G_1 = 11.5 \times 10^6$ $G_2 = 1.25 \times 10^6$	Non-uniform in y only	9 x 9	588	2416
4	$G_1 = 11.5 \times 10^6$ $G_2 = 11.5 \times 10^6$	Non-uniform in y only	9 x 9	2145	2416
5	$G_1 = 11.5 \times 10^6$ $G_2 = 11.5 \times 10^6$	Uniform in both x and y	29 x 29	2567	2566
6	$G_1 = 11.5 \times 10^6$ $G_2 = 1.25 \times 10^6$	Uniform in both x and y	29 x 29	866*	2566
7	$G_1 = 11.5 \times 10^6$ $C_2 = 1.25 \times 10^6$	Non-uniform in y only	29 x 29	820	2560
8	$G_1 = 11.5 \times 10^6$ $G_2 = 1.25 \times 10^6$	Non-uniform in both x and y	29 x 29	800	2553

*Reference Solution.

11/2/82

```
  LOA COMPO3
READY
LIS
 10 C     STIFFNESS CONSTANT (G*JO) CALCULATED USING A FINITE DIFFERENCE
 20 C     METHOD AND CONSIDERING A COMPOSITE CROSSECTION
 25 C
 30          DIMENSION X(40),Y(40),AIM1(40,40),AIP1(40,40),AJM1(40,40)
 40          DIMENSION AJP1(40,40),BRHS(40,40),P(40,40),PSI(40,40),A(40)
 50          ERR=1.E-06
 55          G1=11.5E+06
 56          G2=1.25E+06
 60          BB1=.08
 70          BB2=.1
 80          BB3=.2
 90          AA1=.08
100          AA2=.1
105          AA3=.15
106          AA4=.2
110          I1=8
120          I2=15
130          I3=29
140          J1=8
150          J2=15
155          J3=22
156          J4=29
160          XX=0.0
170          X(1)=XX
180          DX=BB1/(I1-1)
190          DO 10 I=2,I3
200             IF(I.GT.I1) DX=(BB2-BB1)/(I2-I1)
210             IF(I.GT.I2) DX=(BB3-BB2)/(I3-I2)
220              XX=XX+DX
230              X(I)=XX
240       10 CONTINUE
250          YY=0.0
260          Y(1)=YY
270          DY=AA1/(J1-1)
280          DO 20 J=2,J4
290             IF(J.GT.J1) DY=(AA2-AA1)/(J2-J1)
295             IF(J.GT.J2) DY=(AA3-AA2)/(J3-J2)
296             IF(J.GT.J3) DY=(AA4-AA3)/(J4-J3)
300              YY=YY+DY
310              Y(J)=YY
320       20 CONTINUE
330          IMAX=I3-1
340          JMAX=J4-1
350          DO 30 I=2,IMAX
360          DO 30 J=2,JMAX
370             AIJ=-2./(X(I-1)-X(I))/(X(I+1)-X(I))
380             AIJ=AIJ-2./(Y(J-1)-Y(J))/(Y(J+1)-Y(J))
390             AIM1(I,J)=2./(X(I-1)-X(I))/(X(I-1)-X(I+1))/AIJ
400             AIP1(I,J)=-2./(X(I+1)-X(I))/(X(I-1)-X(I+1))/AIJ
410             AJM1(I,J)=2./(Y(J-1)-Y(J))/(Y(J-1)-Y(J+1))/AIJ
420             AJP1(I,J)=-2./(Y(J+1)-Y(J))/(Y(J-1)-Y(J+1))/AIJ
430             BRHS(I,J)=2./AIJ
440       30 CONTINUE
450          DO 40 I=1,I3
460          DO 40 J=1,J4
470             P(I,J)=0.0
480       40 CONTINUE
490          OMEG=1.5
500          OMO=1.-OMEG
```

```
            AMAX=0.0
      DO 50 I=2,IMAX
            JMAX=J4-1
            JMIN=2
C           IF(I.GT.I1) JMAX=J1-1
C           IF(I.GT.I2) JMAX=J2-1
       DO 50 J=JMIN,JMAX
            POLD=P(I,J)
            PNEW=AIM1(I,J)*P(I-1,J)+AIP1(I,J)*P(I+1,J)
            PNEW=PNEW+AJM1(I,J)*P(I,J-1)+AJP1(I,J)*P(I,J+1)+BRHS(I,J)
            P(I,J)=PNEW*OMEG+OMO*POLD
            VAL=ABS((P(I,J)-POLD))
            IF(VAL.GT.AMAX) AMAX=VAL
   50  CONTINUE
       IF(AMAX.LT.ERR) GO TO 80
   60  CONTINUE
       WRITE(6,70)
   70  FORMAT(2X,'EXCEEDS ITERATIONS')
   80  JMAX=J4-1
       IMAX=I3-1
       AJ=0.0
       DO 90 I=1,IMAX
       DO 90 J=1,JMAX
            Z=P(I,J)+P(I+1,J)+P(I+1,J+1)+P(I,J+1)
            AJ=AJ+.25*Z*(X(I+1)-X(I))*(Y(J+1)-Y(J))
   90  CONTINUE
       AJ=2.*AJ
       AJO=AJ*G1
C
C      ADDITION TO AJO TO APPROXIMATE TOTAL STIFFNESS
C
       WRITE(6,100) AJO,IT
  100  FORMAT(5X,'G*JO=',E10.5,3X,'ITERATIONS=',I4,/)
       DO 105 I=1,I3
       DO 105 J=1,J4
            PSI(I,J)=0.0
  105  CONTINUE
       JMAX=J4
       JMID=(JMAX+1)/2
       DO 130 IT=1,2000
           AMAX=0.0
       DO 120 I=1,I3
           JMAX=J4
           JMIN=1
       DO 120 J=JMIN,JMAX
           A(J)=(Y(J)-Y(J-1))/(Y(J+1)-Y(J))*G2/G1
           PSIOLD=PSI(I,J)
           IF(I.EQ.1) GO TO 111
           IF(I.EQ.I3) GO TO 114
           IF(J.EQ.JMIN.OR.J.EQ.JMAX) GO TO 112
           IF(J.EQ.JMID) GO TO 110
           PSINEW=AIM1(I,J)*PSI(I-1,J)-AIP1(I,J)*PSI(I+1,J)
           PSINEW=PSINEW+AJM1(I,J)*PSI(I,J-1)+AJP1(I,J)*PSI(I,J+1)
           GO TO 119
  110      PSINEW=1./(1.+A(J))*(A(J)*(PSI(I,J+1)+(Y(J+1)
     *      -Y(J))*X(I))+PSI(I,J-1)-(Y(J)-Y(J-1))*X(I))
           GO TO 119
  111      IF(J.EQ.JMIN.OR.J.EQ.JMAX) GO TO 112
           IF(J.EQ.JMID) PSINEW=1./(1.+A(J))*(A(J)*(PSI(I,J+1)+(Y(J+1)
     *      -Y(J))*X(I))+PSI(I,J-1)-(Y(J)-Y(J-1))*X(I))
           IF(J.NE.JMID) PSINEW=PSI(I+1,J)-(X(I+1)-X(I))*Y(J)
           GOTO 119
  112      IF(J.EQ.JMIN) PSINEW=((X(I+1)-X(I))*(Y(J+1)-Y(J)))/
     *       ((X(I+1)-X(I))+(Y(J+1)-Y(J)))*(PSI(I+1,J)/(X(I+1)-X(I))
     *        +PSI(I,J+1)/(Y(J+1)-Y(J))-Y(J)+X(I))
```

```
          IF(J.EQ.JMAX) PSINEW=((X(I-1)-X(I))*(Y(J)-Y(J-1)))/
     *      ((X(I+1)-X(I))+(Y(J)-Y(J-1)))*(PSI(I+1,J)/(X(I+1)-X(I))
     *      +PSI(I,J-1)/(Y(J)-Y(J-1))-Y(J)-X(I))
          GO TO 119
 113      IF(J.EQ.JMIN) PSINEW=PSI(I,J+1)+(Y(J+1)-Y(J))*X(I)
          IF(J.EQ.JMAX) PSINEW=PSI(I,J-1)-(Y(J)-Y(J-1))*X(I)
          GO TO 119
 114      IF(J.EQ.JMIN.OR.J.EQ.JMAX) GO TO 115
          IF(J.EQ.JMID) PSINEW=1./(1.+A(J))*(A(J)*(PSI(I,J+1)+(Y(J+1)
     *     -Y(J))*X(I))+PSI(I,J-1)-(Y(J)-Y(J-1))*X(I))
          IF(J.NE.JMID) PSINEW=PSI(I-1,J)+(X(I)-X(I-1))*Y(J)
          GO TO 119
 115      IF(J.EQ.JMIN) PSINEW=((X(I)-X(I-1))*(Y(J+1)-Y(J)))/
     *      ((X(I)-X(I-1))+(Y(J+1)-Y(J)))*(PSI(I-1,J)/(X(I)-X(I-1))
     *      +PSI(I,J+1)/(Y(J-1)-Y(J))+Y(J)+X(I))
          IF(J.EQ.JMAX) PSINEW=((X(I)-X(I-1))*(Y(J)-Y(J-1)))/
     *      ((X(I)-X(I-1))+(Y(J)-Y(J-1)))*(PSI(I-1,J)/(X(I)-X(I-1))
     *      +PSI(I,J-1)/(Y(J)-Y(J-1))+Y(J)-X(I))
          GO TO 119
 119      PSI(I,J)=PSINEW*OMEG+OMO*PSIOLD
          VAL=ABS(PSI(I,J)-PSIOLD)
          IF(VAL.GT.AMAX) AMAX=VAL
 120      CONTINUE
 121 IF(AMAX.LT.ERR) GO TO 140
 130 CONTINUE
     WRITE(6,70)
 140 CONTINUE
     DO 1000 I=1,I3,7
     WRITE(6,2000) (PSI(I,J),J=1,J4,7)
1000 CONTINUE
2000 FORMAT(1X,5F8.5,/)
C
C          INTEGRATION ROUTINE
C
 145 JMAX=J4-1
     IMAX=I3-1
     ATHETA=0.0
     DO 160 I=1,IMAX
     DO 160 J=1,JMAX
          DX=X(I+1)-X(I)
          DY=Y(J+1)-Y(J)
          IF(J.LT.JMID) G=G1
          IF(J.GE.JMID) G=G2
          DPSIDY=(PSI(I,J+1)-PSI(I,J)+PSI(I+1,J+1)-PSI(I+1,J))
     *               /2./DY
          DPSIDX=(PSI(I+1,J)-PSI(I,J)+PSI(I+1,J+1)-PSI(I,J-1))
     *               /2./DX
          XMID=X(I)+DX/2.
          YMID=Y(J)+DY/2.
          ATHETA=ATHETA-G*(XMID*DPSIDY+XMID**2)*DX*DY-
     *                   G*(YMID*DPSIDX-YMID**2)*DX*DY
 160 CONTINUE
     WRITE(6,170) ATHETA,IT
 170 FORMAT(/,5X,'G*JTHETA=',E11.5,5X,'ITERATIONS=',I4,/)
     STOP
     END
```

APPENDIX B

SINGLE RING DEFLECTION PROGRAM

APPENDIX B

Single Ring Deflection Program

Program Description

The ring deflection program calculates the response of a single ring to given arbitrary loads and boundary conditions using the ring finite element discussed in Chapter 5. It models the ring with an even number of nodes and beam elements. Six degrees of freedom are allowed at each node. Concentrated and distributed loads can be applied in all six degrees. The program computes the deflection at each node in all six degrees of freedom, the Fourier coefficients of the deflections in the x- and y-directions and the twist about the θ-axis, the forces at the ends of each element, and the reaction forces at the supports.

Program Input

There must be an even number of nodes. The program is set for thirty nodes. They are numbered clockwise looking in the positive y-direction (Fig. B1).

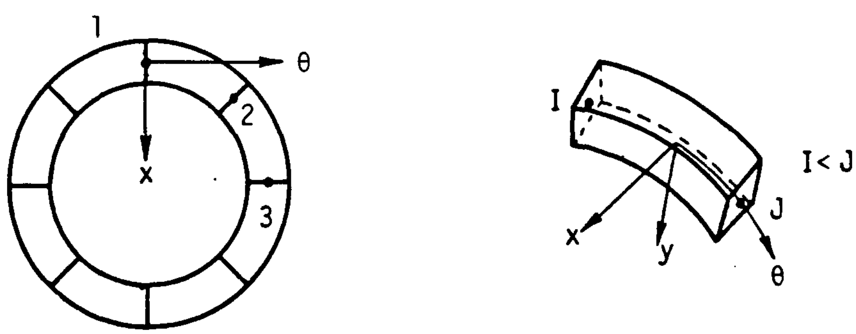

Figure B1. Node Numbering.

The program reads the input data from a data file which must have the following format:

I CONTROL CARD (2I5)

columns	entry
1-5	Number of Nodes (setup is for 30) Must be even number of nodes evenly spaced.
6-10	Number of Fourier coefficients to be calculated (LE.8)

II ELEMENT PROPERTIES (6F 10.0)

columns	entry
1-10	Radius at cross section centroid
11-20	a-cross sectional area
21-30	J_x--Moment of inertia for a circular beam about x-axis
31-40	J_y--Moment of inertia for a circular beam about y-axis
41-50	J_{xy}--Product of inertia for a circular beam
51-60	J_θ --Section torsional constant

III MATERIAL PROPERTIES (2F10.0)

columns	entry
1-10	Young's modulus
11-20	Poisson's ratio

IV LOAD AND CONSTRAINT INFORMATION (2I5)

columns	entry
1-5	Number of nodes where concentrated loads are applied
6-10	Number of constrained nodes

V CONCENTRATED LOADS (I5, 6F10.0)

Input one card for each node where concentrated loads are applied.

columns	entry
1-5	Node number
6-15	Applied load in x-direction
16-25	Applied load in y-direction
26-35	Applied load in θ-direction
36-45	Applied moment about x-axis
46-45	Applied moment about y-axis
56-65	Applied moment about θ-axis

VI DISTRIBUTED LOADS (6F10.0)

This card must be input. If there are no distributed loads, enter all 0.0's.

columns	entry
1-10	Load in x-direction (total load)
11-20	Load in y-direction (total load)
21-30	Load in θ-direction (total load)
31-40	Moment about x-axis (total load)
41-50	Moment about y-axis (total load)
51-60	Moment about θ-axis (total load)

VII BOUNDARY CONDITIONS (CONSTRAINTS) (I5, 6F10.0)

Input one card for each node where boundary conditions are specified.

columns	entry
1-5	Node number
6-15	Constraint in x-direction Eq. 0.0 no constraint Eq. 1.0 no displacement allowed
16-25	Constraint in y-direction
26-35	Constraint in θ-direction
36-45	Constraint about x-axis
46-55	Constraint about y-axis
56-65	Constraint about θ-axis

Sample Problem

The program is used to model a ring with a one square inch cross section and a 10-inch radius. The section properties are:

$$J_x = 0.0833 \text{ in}^4$$

$$J_y = 0.0833 \text{ in}^4$$

$$J_{xy} = 0.050 \text{ in}^4$$

$$J_\theta = 0.0982 \text{ in}^4$$

The ring is broken into a mesh of 30 nodes and elements. Concentrated loads of 50 lbs each were applied in the x-direction at nodes 8 and 23. A distributed load of 100 lbs total was applied in the y-direction (Fig. B2). Node 1 was constrained in the x-, y-, and θ-directions and node 16 was constrained in the y-direction. The data file, output, and program follow.

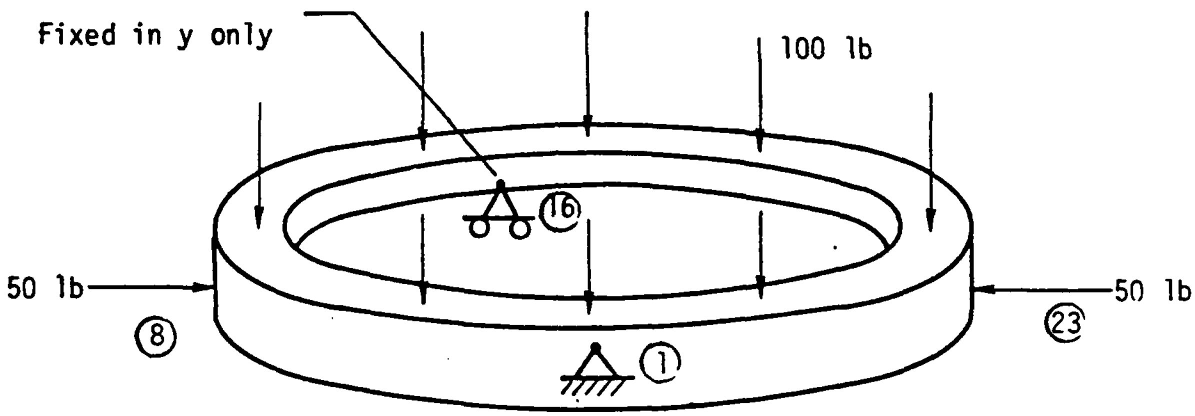

Figure B2. Applied Loads.

```
 10     30     8
 20       10.0         1.0     0.0833     0.0833       0.05     0.0982
 30     30.0E06        0.3
 40      2     2
 50      8       50.0
 60     23       50.0
 70                  100.0
 80      1        1.0         1.0         1.0         0.0         0.0         0.0
 90     16        0.0         1.0         0.0         0.0         0.0         0.0
100
```

LINKR 05/21/84 15.48.30
0
WARNING- AT NODE 1 BOTH LOAD AND BC ARE SPECIFIED
WARNING- AT NODE 15 BOTH LOAD AND BC ARE SPECIFIED

DISPLACEMENTS

N	U	V	W	DVDT	PSI	PHI
1	0.0	0.0	0.0	-0.9623D-05	0.6715D-04	0.4355D-03
2	0.1424D-03	0.1966D-03	0.1361D-04	0.1858D-03	0.7193D-04	0.3835D-03
3	0.3152D-03	0.7273D-03	0.5965D-04	0.3086D-03	0.9961D-04	0.2664D-03
4	0.5342D-03	0.1413D-02	0.1467D-03	0.3592D-03	0.1286D-03	0.1039D-03
5	0.7800D-03	0.2188D-02	0.2831D-03	0.3465D-03	0.1450D-03	-0.6735D-04
6	0.9998D-03	0.2857D-02	0.4695D-03	0.2868D-03	0.1335D-03	-0.2206D-03
7	0.1111D-02	0.3371D-02	0.6912D-03	0.2020D-03	0.8014D-04	-0.3354D-03
8	0.1007D-02	0.3703D-02	0.9176D-03	0.1169D-03	-0.2740D-04	-0.4039D-03
9	0.6182D-03	0.3850D-02	0.1091D-02	0.1595D-04	-0.1307D-03	-0.4135D-03
10	0.5401D-04	0.3749D-02	0.1162D-02	-0.1149D-03	-0.1714D-03	-0.3741D-03
11	-0.5429D-03	0.3368D-02	0.1109D-02	-0.2467D-03	-0.1633D-03	-0.2717D-03
12	-0.1058D-02	0.2735D-02	0.9184D-03	-0.3508D-03	-0.1184D-03	-0.1221D-03
13	-0.1413D-02	0.1935D-02	0.6753D-03	-0.4021D-03	-0.5633D-04	0.5413D-04
14	-0.1572D-02	0.1101D-02	0.3581D-03	-0.3812D-03	0.6311D-05	0.2293D-03
15	-0.1545D-02	0.3963D-03	0.2770D-04	-0.2771D-03	0.5157D-04	0.3684D-03
16	-0.1384D-02	0.0	-0.2817D-03	-0.9814D-04	0.6735D-04	0.4355D-03
17	-0.1153D-02	0.3336D-04	-0.5497D-03	0.1090D-03	0.7398D-04	0.4048D-03
18	-0.8344D-03	0.4079D-03	-0.7636D-03	0.2269D-03	0.9961D-04	0.2993D-03
19	-0.4198D-03	0.9771D-03	-0.8946D-03	0.2957D-03	0.1236D-03	0.1503D-03
20	0.6343D-04	0.1604D-02	-0.9338D-03	0.2939D-03	0.1450D-03	-0.9907D-05
21	0.5518D-03	0.2177D-02	-0.8698D-03	0.2475D-03	0.1335D-03	-0.1526D-03
22	0.9518D-03	0.2625D-02	-0.7118D-03	0.1777D-03	0.8014D-04	-0.2517D-03
23	[illegible]	[illegible]	[illegible]	[illegible]	[illegible]	[illegible]
24	0.1043D-02	0.3039D-02	-0.2557D-03	0.2416D-04	-0.1307D-03	-0.3404D-03
25	0.7496D-03	0.3002D-02	-0.6686D-04	-0.9063D-04	-0.1714D-03	-0.2995D-03
26	0.3930D-03	0.2688D-02	0.5179D-04	-0.2074D-03	-0.1623D-03	-0.2037D-03
27	0.7750D-04	0.2151D-02	0.9850D-04	-0.2993D-03	-0.1194D-03	-0.6374D-04
28	-0.1276D-03	0.1474D-02	0.8983D-04	-0.3385D-03	-0.5630D-04	0.1003D-03
29	-0.1933D-03	0.7819D-03	0.5263D-04	-0.3095D-03	0.6813D-05	0.2629D-03
30	-0.1326D-03	0.2336D-03	0.1557D-04	-0.2003D-03	0.5157D-04	0.3848D-03

FOURIER COEFFICIENTS

N	U	V	PHI
1	0.7061E-03	0.3926E-03	0.3926E-04
2	0.9543E-03	0.1716E-02	0.4044E-03
3	0.2694E-08	0.1949E-08	0.1309E-08
4	0.1388E-03	0.1465E-03	0.2629E-04
5	0.5887E-09	0.1797E-08	0.1673E-08
6	0.1013E-04	0.1372E-04	0.3195E-05
7	0.1537E-08	0.1741E-08	0.9777E-09
8	0.7526E-05	0.7631E-05	0.1455E-05

FORCES AND MOMENTS

N	VX	VY	NT	MX	MY	MT
1	-0.2613D+01	-0.3333D-02	0.2486D-02	-0.1536D-03	-0.3955D-02	0.1333D-05
2	0.7725D+01	0.3333D+02	-0.3373D+02	0.1066D+03	0.7369D+02	-0.3737D+02
2	-0.7725D+01	-0.3000D+02	0.3373D+02	-0.1066D+03	-0.7369D+02	0.3737D+02
3	0.1250D+02	0.3000D+02	-0.1165D+02	0.5619D+02	0.5744D+02	-0.4065D+02

3	-0.1250D+02	-0.1667D-02	0.2165D+02	-0.5689D-02	-0.5744D+02	0.4505D+02
4	0.1673D-02	0.1667D+02	-0.1858D+02	0.1163D-02	0.2672D-02	-0.5225D-01
4	-0.1673D+02	-0.1333D+02	0.1858D+02	-0.1163D+02	-0.2672D+02	0.5225D+02
5	0.2023D+02	0.1333D+02	-0.1469D+02	-0.2721D-02	-0.1212D-02	-0.5062D+02
5	-0.2023D+02	-0.1000D+02	0.1469D+02	0.2721D-02	0.1212D+02	0.5062D-02
6	0.2284D+02	0.1000D+02	-0.1017D+02	-0.5793D+02	-0.5719D+02	-0.4167D-02
6	-0.2284D+02	-0.6667D+01	0.1017D+02	0.5793D-02	0.5719D-02	0.4167D-02
7	0.2445D+02	0.6667D-01	-0.5198D+01	-0.7919D-02	-0.1071D-02	-0.2725D-02
7	-0.2445D+02	-0.3333D+01	0.5198D-01	0.7919D+02	0.1071D+03	0.2725D+02
8	0.2500D+02	0.3333D+01	-0.1005D-04	-0.9006D+02	-0.1591D+03	-0.9465D+01
8	0.2500D+02	0.3162D-12	0.1005D-04	0.9006D+02	0.1591D+03	0.9465D+01
9	-0.2445D+02	-0.3162D-12	-0.5198D+01	-0.9006D+02	-0.1071D+03	0.9465D+01
9	0.2445D+02	0.3333D+01	0.5198D+01	0.9006D+02	0.1071D+03	-0.9465D+01
10	-0.2284D+02	-0.3333D+01	-0.1017D+02	-0.7919D+02	-0.5719D+02	0.2725D+02
10	0.2284D+02	0.6667D+01	0.1017D+02	0.7919D+02	0.5719D+02	-0.2725D+02
11	-0.2023D+02	-0.6667D+01	-0.1469D+02	-0.5793D+02	-0.1212D+03	0.4167D+02
11	0.2023D+02	0.1000D+02	0.1469D+02	0.5793D+02	0.1212D+02	-0.4167D-02
12	-0.1673D+02	-0.1000D+02	-0.1858D+02	-0.2721D-02	0.2672D-02	0.5062D+02
12	0.1673D+02	0.1333D+02	0.1858D+02	0.2721D+02	-0.2672D+02	-0.5062D+02
13	-0.1250D+02	-0.1333D+02	-0.2165D+02	0.1163D-02	0.5744D+02	0.5225D+02
13	0.1250D+02	0.1667D+02	0.2165D+02	-0.1163D+02	-0.5744D+02	-0.5225D+02
14	-0.7725D+01	-0.1667D+02	-0.2273D+02	0.5689D+02	0.7869D+02	0.4505D+02
14	0.7725D+01	0.2000D+02	0.2273D+02	-0.5689D+02	-0.7869D+02	-0.4505D+02
15	-0.2613D+01	-0.2000D+02	-0.2486D+02	0.1066D+03	0.9956D-01	0.2737D+02
15	0.2613D+01	0.2333D+02	0.2486D+02	-0.1066D+03	-0.9956D+02	-0.2737D-02
16	0.2613D+01	-0.2333D-02	-0.2486D-02	0.1516D+03	0.9956D+02	0.1222D-05
16	-0.2613D+01	-0.2333D+02	0.2486D+02	-0.1516D+03	-0.9956D+02	-0.1222D-05
17	0.7725D-01	0.2333D+02	-0.2273D+02	0.1066D-03	0.7869D-02	-0.2737D-02
17	-0.7725D+01	-0.2000D+02	0.2273D+02	-0.1066D+03	-0.7869D+02	0.2737D+02
18	0.1250D+01	0.2000D+02	-0.2165D+02	0.5689D+02	0.5744D+02	-0.4505D+02
18	-0.1250D+02	-0.1667D+02	0.2165D-02	-0.5689D+02	-0.5744D-02	0.4505D+01
19	0.1673D+02	0.1667D+02	-0.1858D+02	0.1163D+02	0.2672D+02	-0.5225D-02

19	-0.1673D+02	-0.1333D+02	0.1858D+02	-0.1151D+02	-0.2672D+02	0.5225D-01
20	0.2023D+02	0.1333D+02	-0.1469D+02	-0.2721D+01	-0.1212D+02	-0.5062D+02
20	-0.2023D+02	-0.1000D+02	0.1469D+02	0.2721D+01	0.1212D+02	0.5062D+02
21	0.2284D+02	0.1000D+02	-0.1017D+02	-0.5793D+02	-0.5739D+02	-0.4167D+01
21	-0.2284D+02	-0.6667D+01	0.1017D+02	0.5793D+02	0.5739D+02	0.4167D+02
22	0.2445D+02	0.6667D+01	-0.5198D+01	-0.7919D+02	-0.1071D+03	-0.2725D+02
22	-0.2445D+02	-0.3333D+01	0.5198D+01	0.7919D+02	0.1071D+03	0.2725D-01
23	0.2500D+02	0.3333D+01	-0.1011D-04	-0.9006D+02	-0.1591D+03	-0.9465D+01
23	0.2500D+02	-0.4484D-11	0.1011D-04	0.9006D+02	0.1591D+03	0.9465D+01
24	-0.2445D+02	0.4484D-11	-0.5198D+01	-0.9006D+02	-0.1071D+03	0.9465D+01
24	0.2445D+02	0.3333D+01	0.5198D+01	0.9006D+02	0.1071D+03	-0.9465D+01
25	-0.2284D+02	-0.3333D+01	-0.1017D+02	-0.7919D+02	-0.5739D+02	0.2725D+02
25	0.2284D+02	0.6667D+01	0.1017D+02	0.7919D+02	0.5739D+02	-0.2725D+02
26	-0.2023D+02	-0.6667D+01	-0.1469D+02	-0.5793D+02	-0.1212D+02	0.4167D+02
26	0.2023D+02	0.1000D+02	0.1469D+02	0.5793D+02	0.1212D+02	-0.4167D+02
27	-0.1673D+02	-0.1000D+02	-0.1858D+02	-0.2721D+02	0.2672D+02	0.5062D+02
27	0.1673D+02	0.1333D+02	0.1858D+02	0.2721D+01	-0.2672D+02	-0.5062D+02
28	-0.1250D+02	-0.1333D+02	-0.2165D+02	0.1151D+02	0.5744D+02	0.5225D+02
28	0.1250D+02	0.1667D-02	0.2165D+02	-0.1151D+02	-0.5744D+02	-0.5225D+02
29	-0.7725D+01	-0.1667D-02	-0.2273D+02	0.5639D+02	0.7869D+02	0.4505D+02
29	0.7725D+01	0.2000D+02	0.2273D+02	-0.5639D+02	-0.7869D+02	-0.4505D+02
30	-0.2613D+01	-0.2000D+02	-0.2486D+02	0.1066D+03	0.8956D+02	0.2787D+02
30	0.2613D+01	0.2333D+02	0.2486D+02	-0.1066D+03	-0.8956D+02	-0.2787D+02
1	0.2613D-01	-0.2333D+02	-0.2486D+02	0.1586D+03	0.8956D+02	-0.1233D-05

REACTIONS AT CONSTRAINED NODES

N	RX	RY	RZ	RMX	RMY	RMZ
1	0.1314E-06	-0.5000E-01	-0.3677E-05	0.1343E-05	0.7533E-05	-0.7411E-12
16	-0.2767E-06	-0.5000E-02	0.1101E-04	-0.5274E-05	-0.5603E-05	-0.2558E-11

STOP
TIME 0.4 SECS

```
C SINGLE RING DEFLECTION PROGRAM
C   THIS PROGRAM DETERMINES THE REACTIONS OF A SINGLE RING
C   SUBJECTED TO GIVEN LOADS AND BOUNDARY CONDITIONS.  THE
C   LOADS CAN BE NONAXISYMMETRIC.  THERE MUST BE AN EVEN
C   NUMBER OF NODES AND THEY MUST BE SPACED EVENLY.  THEY
C   ARE NUMBERED CLOCKWISE LOOKING IN THE POSITIVE Y-DIREC-
C   TION.  THIS PROGRAM COMPUTES THE DEFLECTIONS, THE
C   FOURIER COEFFICIENTS OF THE DEFLECTIONS, THE FORCES IN
C   THE RING, AND THE REACTION FORCES AT THE SUPPORTS.
C
      DOUBLE PRECISION KP,AMAT,IMAT,IIMAT,IIIMAT,IVMAT,BMAT
      DOUBLE PRECISION PIE,SUM(6,6),DELTAP(12),FORCE(12)
      REAL*4 JX,JY,JXY,JT,NT,MX,MY,MT,MXDL,MYDL,MTDL
      DIMENSION CVX(30),CVY(30),CNT(30),CMX(30),CMY(30),CMT(30)
      DIMENSION AMAT(180,35),IMAT(6,6),IIMAT(6,6),IIIMAT(6,6)
      DIMENSION KP(12,12),IVMAT(6,6),BMAT(180)
      DIMENSION VX(30),VY(30),NT(30),MX(30),MY(30),MT(30)
      DIMENSION III(30),ICOMP(30),ICC(30),ICCOLD(30)
      DIMENSION DDX(30),DDY(30),DDT(30),DDDX(30),DDDY(30)
      DIMENSION DDDT(30),CDD(30,6)
      DIMENSION UGC(8,30),UGS(8,30),U(8),VGC(8,30),VGS(8,30)
      DIMENSION V(8),PGC(8,30),PGS(8,30),P(8)
      DIMENSION REAC(30,5),OFOR(6),OFOR1(6),IFLAG(30),JFLAG(30)
      CALL OPSYS ('ALLOC','RDATA',9)
C
C   READ PARAMETERS AND INITIALIZE VARIABLES
      READ (9,2000) N,NCOEF
      READ (9,2010) RC,A,JX,JY,JXY,JT
      READ (9,2020) E,PR
      DO 100 I=1,N
         VX(I)=0.0
         VY(I)=0.0
         NT(I)=0.0
         MX(I)=0.0
         MY(I)=0.0
         MT(I)=0.0
         DDX(I)=0.0
         DDY(I)=0.0
         DDT(I)=0.0
         DDDX(I)=0.0
         DDDY(I)=0.0
         DDDT(I)=0.0
         IFLAG(I)=0
         JFLAG(I)=0
  100 CONTINUE
      READ (9,2000) NCL,NEC
      IF (NCL.EQ.0) GO TO 109
      DO 105 I=1,NCL
         READ (9,2040) IN,VX(IN),VY(IN),NT(IN),MX(IN),MY(IN),MT(IN)
  105 CONTINUE
  109 READ (9,2010) XDL,YDL,TDL,MXDL,MYDL,MTDL
      DO 106 I=1,N
         VX(I)=VX(I)+XDL/N
         VY(I)=VY(I)+YDL/N
         NT(I)=NT(I)+TDL/N
         MX(I)=MX(I)+MXDL/N
         MY(I)=MY(I)+MYDL/N
         MT(I)=MT(I)+MTDL/N
  106 CONTINUE
      DO 107 I=1,NEC
         READ (9,2040) IN,DDX(IN),DDY(IN),DDT(IN),DDDX(IN),DDDY(IN)...
```

```
      *                       IDDT(IX)
           IFLAG(I)=IX
           JFLAG(IX)=I
  107 CONTINUE
  106 CONTINUE
 2000 FORMAT (2I5)
 2010 FORMAT (6F10.0)
 2020 FORMAT (2F10.0)
 2040 FORMAT (I5,6F10.0)
C
      PIE=4.*DATAN(1.D+00)
      PIES=PIE
      DT=2.*PIE/N
      G=E/2.0/(1.0+PR)
C
C CALCULATE INDEX RELATIONSHIPS - RENUMBERS NODES FOR COMPUTATIONAL
C EFFICIENCY
      III(1)=1
      III(2)=2
      DO 110 I=3,N
         AI=I
         BI=I/2
         AI=AI/2.-BI
         IF(AI.GT.0.1) GO TO 120
         III(I)=(I+2)/2
         GO TO 110
  120    III(I)=(2*N+3-I)/2
  110 CONTINUE
      DO 133 I=1,N
         IIN=III(I)
  133    ICOMP(IIN)=I
C
C REASSIGN COMPUTATIONAL SUBSCRIPTS TO LOADS AND BOUNDARY CONDITIONS
      DO 150 I=1,N
         II=III(I)
         CVX(I)=VX(II)
         CVY(I)=VY(II)
         CNT(I)=NT(II)
         CMX(I)=MX(II)
         CMY(I)=MY(II)
         CMT(I)=MT(II)
         CDD(I,1)=DDX(II)
         CDD(I,2)=DDY(II)
         CDD(I,3)=DDT(II)
         CDD(I,4)=DDDX(II)
         CDD(I,5)=DDDY(II)
         CDD(I,6)=DDDT(II)
  150 CONTINUE
C
C CONSTRUCT THE STIFFNESS MATRIX
      CALL ADDSTF(R0,A,JX,JY,JXY,JT,E,G,DT,KP
      NEQ=6*N
      MBAND=17
      DO 250 I=1,NEQ
         EMAT(I)=0
         DO 250 J=1,15
  250    AMAT(I,J)=0.
      DO 125 I=1,6
         DO 125 J=1,6
            IMAT(I,J)=0
            IIMAT(I,J)=0.
            IIIMAT(I,J)=0.
            IVMAT(I,J)=0.
  125 CONTINUE
      CALL ISUB(KP,IMAT)
      CALL IVSUB(KP,IVMAT)
```

```
      CALL ADD(IMAT,IVMAT,SUM)
      CALL IISUB(KF,IIMAT)
      CALL IIISUB(KF,IIIMAT)
      J1=19
      DO 300 I=1,6
         J1=J1-1
         J2=J1+5
         JJ=0
         DO 300 J=J1,J2
            JJ=JJ+1
            AMAT(I,J)=SUM(I,JJ)
            AMAT(I,J-6)=IIMAT(I,JJ)
            IF((J+12).GT.35) GO TO 301
            AMAT(I,J+12)=IIIMAT(I,JJ)
            GO TO 300
  301       WRITE(6,302)
  300 CONTINUE
  302 FORMAT (1X,'LINE 302 - CHECK COUNTERS J1 & J2')
      J1=19
      DO 400 I=7,12
         II=I-6
         J1=J1-1
         J2=J1+5
         JJ=0
         DO 400 J=J1,J2
            JJ=JJ+1
            AMAT(I,J)=SUM(II,JJ)
            AMAT(I,J+12)=IIMAT(II,JJ)
  400       AMAT(I,J-6)=IIIMAT(II,JJ)
      NM2=N-2
      NODD=1
      DO 1000 NN=3,NM2
         IST=(NN-1)*6+1
         ISTOP=IST+5
         IF(NODD.EQ.1) GO TO 1050
         GO TO 1060
 1050    CONTINUE
 1060    J1=19
         II=0
         DO 1070 I=IST,ISTOP
            II=II+1
            J1=J1-1
            J2=J1+5
            JJ=0
            DO 1070 J=J1,J2
               JJ=JJ+1
               AMAT(I,J)=SUM(II,JJ)
               GO TO (1080,1090),NODD
 1080          IF((J-12).LT.1) GO TO 1081
               AMAT(I,J-12)=IIMAT(II,JJ)
 1081          IF((J+12).GT.35) GO TO 1071
               AMAT(I,J+12)=IIIMAT(II,JJ)
               GO TO 1070
 1090          IF((J-12).LT.1) GO TO 1091
               AMAT(I,J-12)=IIIMAT(II,JJ)
 1091          IF((J+12).GT.35) GO TO 1071
               AMAT(I,J+12)=IIMAT(II,JJ)
 1070    CONTINUE
         GO TO 1072
 1071    WRITE(6,1073)
 1073    FORMAT (1X,'LINE 1073 - CHECK COUNTERS J1 & J2')
 1072    CONTINUE
         IF(NODD.EQ.1) GO TO 1095
         NODD=1
         GO TO 1000
 1095    NODD=2
```

```
 1000 CONTINUE
      NM1=N-1
      IST=NM2*6+1
      ISTOP=IST+5
      J1=19
      II=0
      DO 500 I=IST,ISTOP
         II=II+1
         J1=J1-1
         J2=J1+5
         JJ=0
         DO 500 J=J1,J2
            JJ=JJ+1
            AMAT(I,J)=SUM(II,JJ)
            IF((J-12).LT.1) GO TO 500
            AMAT(I,J-12)=IIMAT(II,JJ)
  500       AMAT(I,J+6)=IIIMAT(II,JJ)
      IST=NM1*6+1
      ISTOP=IST+5
      J1=19
      II=0
      DO 600 I=IST,ISTOP
         II=II+1
         J1=J1-1
         J2=J1+5
         JJ=0
         DO 600 J=J1,J2
            JJ=JJ+1
            AMAT(I,J)=SUM(II,JJ)
            IF((J-12).LT.1) GO TO 600
            AMAT(I,J-12)=IIIMAT(II,JJ)
  600       AMAT(I,J-6)=IIMAT(II,JJ)
C
C CONSTRUCT THE FORCE MATRIX
      DO 700 NN=1,N
         NC=(NN-1)*6+1
         BMAT(NC)=BMAT(NC)+CVX(NN)
         BMAT(NC+1)=BMAT(NC+1)+CVY(NN)
         BMAT(NC+2)=BMAT(NC+2)+CNT(NN)
         BMAT(NC+3)=BMAT(NC+3)+CMX(NN)
         BMAT(NC+4)=BMAT(NC+4)+CMY(NN)
         BMAT(NC+5)=BMAT(NC+5)+CMT(NN)
  700 CONTINUE
C
C INCLUDE BOUNDARY CONDITIONS IN STIFFNESS MATRIX AND
C CHECK FOR NODES WITH BOTH LOAD AND BOUNDARY CONDITION SPECIFIED
      DO 750 I=1,N
         NA=III(I)
         DO 751 II=1,6
            IF(CDD(I,II).EQ.0.) GO TO 751
            JJJ=6*(I-1)+II
            DO 752 J=1,35
  752          AMAT(JJJ,J)=0.
            AMAT(JJJ,18)=1.
            IF(BMAT(JJJ).EQ.0.) GO TO 751
            NR=JFLAG(NA)
            REAC(NR,II)=REAC(NR,II)-BMAT(JJJ)
            BMAT(JJJ)=0.0
            WRITE(6,754) NA
  754       FORMAT (1X,'WARNING- AT NODE ',I4,' BOTH LOAD AND BC ARE
     *              ' SPECIFIED')
  751    CONTINUE
  750 CONTINUE
C
C SOLVE FOR DISPLACEMENTS
      CALL GAUSS(AMAT,BMAT,MBAND,NEQ)
```

```
C
C PRINT DISPLACEMENTS
      WRITE(6,7)
    7 FORMAT(//1X,'DISPLACEMENTS'//,3X,'N',6X,'U',11X,'V',11X,'W',10X,
     *       'DVDT',8X,'PSI',9X,'PHI')
      DO 800 NN=1,N
         IC=ICOMP(NN)
         IC=(IC-1)*6
         WRITE(6,5) NN,(BMAT(IC+J),J=1,6)
    5    FORMAT(1X,I3,6E12.4)
  800 CONTINUE
C
C COMPUTE AND WRITE FOURIER COEFFICIENTS OF DEFLECTIONS
      THETA=0.0
      DO 802 NN=1,N
         IC=ICOMP(NN)
         IC=(IC-1)*6
         DO 801 INT=1,NCOEF
            UGC(INT,NN)=BMAT(IC+1)*COS(INT*THETA)
            UGS(INT,NN)=BMAT(IC+1)*SIN(INT*THETA)
            VGC(INT,NN)=BMAT(IC+2)*COS(INT*THETA)
            VGS(INT,NN)=BMAT(IC+2)*SIN(INT*THETA)
            PGC(INT,NN)=BMAT(IC+6)*COS(INT*THETA)
            PGS(INT,NN)=BMAT(IC+6)*SIN(INT*THETA)
  801    CONTINUE
         THETA=THETA+DT
  802 CONTINUE
      CALL FOUR(UGC,UGS,U,N,NCOEF)
      CALL FOUR(VGC,VGS,V,N,NCOEF)
      CALL FOUR(PGC,PGS,P,N,NCOEF)
      WRITE (6,202)
  202 FORMAT(//1X,'FOURIER COEFFICIENTS'//3X,'N',8X,'U',11X,'V',
     *       10X,'PHI')
      DO 204 I=1,NCOEF
         WRITE (6,203) I,U(I),V(I),P(I)
  203    FORMAT (1X,I3,3E12.4)
  204 CONTINUE
C
C WRITE FORCES AND MOMENTS
      WRITE(6,11)
   11 FORMAT(//1X,'FORCES AND MOMENTS')
      WRITE(6,12)
   12 FORMAT(/3X,'N',6X,'VX',10X,'VY',10X,'NT',10X,'MX',10X,'MY',10X,
     *       'MT')
      DO 6000 I1=1,N
         I2=I1+1
         IF(I2.GT.N) I2=1
         II1=(ICOMP(I1)-1)*6
         II2=(ICOMP(I2)-1)*6
         DO 6001 I=1,6
            DELTAP(I)=BMAT(II1+I)
            DELTAP(I+6)=BMAT(II2+I)
 6001    CONTINUE
         DO 6002 I=1,12
            FORCE(I)=0.
            DO 6002 J=1,12
 6002       FORCE(I)=FORCE(I)+KP(I,J)*DELTAP(J)
         WRITE(6,13) I1,(FORCE(J),J=1,6)
         WRITE(6,13) I2,(FORCE(J),J=7,12)
   13    FORMAT(1X,I3,6E12.4)
         WRITE(6,14)
   14    FORMAT(/)
         IF(I1.NE.1) GO TO 6006
         IF(JFLAG(1).EQ.0) GO TO 6020
         DO 6005 IT=1,6
            OFOR1(IT)=FORCE(IT)
```

```
 6005    CONTINUE
         GO TO 6020
 6006    IF(JFLAG(I1).EQ.0) GO TO 6020
         NR=JFLAG(I1)
         DO 6010 IT=1,6
            REAC(NR,IT)=REAC(NR,IT)+OFOR(IT)+FORCE(IT)
 6010    CONTINUE
 6020    IF(JFLAG(I2).EQ.0) GO TO 6040
         DO 6030 IT=1,6
            OFOR(IT)=FORCE(IT+6)
 6030    CONTINUE
 6040    IF(I2.EQ.1.AND.JFLAG(1).NE.0) GO TO 6050
         GO TO 6000
 6050    NR=JFLAG(1)
         DO 6060 IT=1,6
            REAC(NR,IT)=REAC(NR,IT)+OFOR1(IT)+FORCE(IT+6)
 6060    CONTINUE
 6000 CONTINUE
      WRITE (6,6080)
      DO 6070 I=1,NBC
         WRITE (6,6090) IFLAG(I),(REAC(I,J),J=1,6)
 6070 CONTINUE
 6080 FORMAT(//1X,'REACTIONS AT CONSTRAINED NODES'//3X,'N',
     *         6X,'RX',10X,'RY',10X,'RT',9X,'RMX',9X,'RMY',
     *         9X,'RMT')
 6090 FORMAT(1X,I3,6E12.4)
      STOP
      END
C
C
      SUBROUTINE ISUB(KP,IMAT)
      DOUBLE PRECISION KP(12,12),IMAT(6,6)
      DO 10 I=1,6
         DO 10 J=1,6
   10       IMAT(I,J)=KP(I,J)
      RETURN
      END
C
C
      SUBROUTINE IVSUB(KP,IVMAT)
      DOUBLE PRECISION KP(12,12),IVMAT(6,6)
      DO 10 I=1,6
         DO 10 J=1,6
            II=I+6
            JJ=J+6
   10       IVMAT(I,J)=KP(II,JJ)
      RETURN
      END
C
C
      SUBROUTINE IISUB(KP,IIMAT)
      DOUBLE PRECISION KP(12,12),IIMAT(6,6)
      DO 10 I=1,6
         DO 10 J=1,6
            JJ=J+6
   10       IIMAT(I,J)=KP(I,JJ)
      RETURN
      END
C
C
      SUBROUTINE IIISUB(KP,IIIMAT)
      DOUBLE PRECISION KP(12,12),IIIMAT(6,6)
      DO 10 I=1,6
         DO 10 J=1,6
            II=I+6
   10       IIIMAT(I,J)=KP(II,J)
```

```
      RETURN
      END
C
C
      SUBROUTINE ADD(MATA,MATB,MATSUM)
      DOUBLE PRECISION MATA(6,6),MATB(6,6),MATSUM(6,6)
      DO 10 I=1,6
         DO 10 J=1,6
   10       MATSUM(I,J)=MATA(I,J)+MATB(I,J)
      RETURN
      END
C
C
      SUBROUTINE FOUR(GRANDC,GRANDS,V,N,NCOEF)
      DIMENSION GRANDC(NCOEF,N),GRANDS(NCOEF,N),V(NCOEF)
      DIMENSION A(8),B(8)
      PI=4.0*ATAN(1.0)
      DT=2*PI/N
      DO 20 I=1,NCOEF
         A(I)=0.0
         B(I)=0.0
         DO 10 J=1,N
            A(I)=A(I)+GRANDC(I,J)*DT/PI
            B(I)=B(I)+GRANDS(I,J)*DT/PI
   10    CONTINUE
         V(I)=(A(I)**2+B(I)**2)**0.5
   20 CONTINUE
      RETURN
      END
C
C
      SUBROUTINE ADLCOP(RC,AREA,JX,JY,JXY,JT,E,G,DT,K)
      [illegible]
      DOUBLE PRECISION A(12,12),K(12,12),WORK(12),DET(2),D(12,12)
      DOUBLE PRECISION T(2),PIE,R,AA,JYOAR2,JXYOJX,JXYOJY,P,Q,SS
      DOUBLE PRECISION U,V,S,C,TH,F
      DIMENSION IPVT(12)
      PIE=4.*DATAN(1.D+00)
      T(1)=1
      T(2)=T(1)+DT
      R=RC
      AA=E*JX/G/JT
      JYOAR2=JY/AREA/R/R
      JXYOJX=JXY/JX
      JXYOJY=JXY/JY
      P=1./JXYOJX
      Q=0.5+(1.+1./AA)/JXYOJX
      SS=(1.+JYOAR2)/JXYOJX-JYOAR2*JXYOJY
      U=1./JXYOJY-JXYOJX
      V=(1.+1./AA)/JXYOJY-JXYOJX
      DO 10 I=1,12
         DO 10 J=1,12
            A(I,J)=0
            K(I,J)=0
   10       D(I,J)=0.
      F=1.
      DO 20 II=1,2
         TH=T(II)
         C=DCOS(TH)
         S=DSIN(TH)
         I=1+(II-1)*6
         A(I,3)=-Q*TH*C
         A(I,4)=Q*TH*S
         A(I,5)=-P*TH*S
```

```
4560  A(I,6)=-P*TH*C
4570  A(I,7)=P
4580  A(I,8)=-Q*TH*C
4590  A(I,9)=Q*TH*S
4600  A(I,10)=P*S
4610  A(I,11)=P*C
4620  I=I+1
4630  A(I,1)=1.
4640  A(I,2)=TH
4650  A(I,3)=S
4660  A(I,4)=C
4670  A(I,5)=TH*S
4680  A(I,6)=TH*C
4690  I=I+1
4700  A(I,3)=-Q*(C+TH*S)
4710  A(I,4)=Q*(S-TH*C)
4720  A(I,5)=-P*(S-TH*C)
4730  A(I,6)=-P*(C+TH*S)
4740  A(I,7)=SS*TH
4750  A(I,8)=-Q*(C+TH*S)
4760  A(I,9)=Q*(S-TH*C)
4770  A(I,11)=P*S
4780  A(I,10)=-P*C
4790  A(I,12)=1.
4800  I=I+1
4810  A(I,2)=1./R
4820  A(I,3)=C/R
4830  A(I,4)=-S/R
4840  A(I,5)=(TH*C+S)/R
4850  A(I,6)=(-TH*S+C)/R
4860  I=I+1
4870  A(I,3)=-2.*Q*C/R
4880  A(I,4)=2.*Q*S/R
4890  A(I,5)=-2.*P*S/R
4900  A(I,6)=-2.*P*C/R
4910  A(I,7)=SS*TH/R
4920  A(I,8)=-2.*Q*C/R
4930  A(I,9)=2.*Q*S/R
4940  A(I,12)=1./R
4950  I=I+1
4960  A(I,5)=-TH*S/R
4970  A(I,6)=-TH*C/R
4980  A(I,7)=1./R
4990  A(I,8)=S/R
5000  A(I,9)=C/R
5010  I=1+(II-1)*6
5020  D(I,3)=V*C*F/R
5030  D(I,4)=-V*S*F/R
5040  D(I,5)=2.*U*S*F/R
5050  D(I,6)=2.*U*C*F/R
5060  D(I,8)=V*C*F/R
5070  D(I,9)=-V*S*F/R
5080  I=I+1
5090  D(I,3)=-1.*F/R/AA
5100  I=I+1
5110  D(I,3)=V*S*F/R
5120  D(I,4)=V*C*F/R
5130  D(I,5)=-2.*U*C*F/R
5140  D(I,6)=2.*U*S*F/R
5150  D(I,8)=V*S*F/R
5160  D(I,9)=V*C*F/R
5170  I=I+1
5180  D(I,3)=-S*F/AA
5190  D(I,4)=-C*F/AA
5200  D(I,8)=-S*F/AA
5210  D(I,9)=-C*F/AA
```

```
          I=I+1
          D(I,3)=-V*S*F
          D(I,4)=-V*C*F
          D(I,5)=2.*U*C*F
          D(I,6)=-2.*U*S*F
          D(I,7)=-U*F
          D(I,8)=-V*S*F
          D(I,9)=-V*C*F
          I=I+1
          D(I,2)=-F/AA
          D(I,3)=-C*F/AA
          D(I,4)=S*F/AA
          D(I,8)=-C*F/AA
          D(I,9)=S*F/AA
          F=-1.
   20 CONTINUE
      CALL DGEFA(A,12,12,IPVT,INFO)
      WRITE(6,1) INFO
    1 FORMAT(1H ,I5)
      JOB=1
      CALL DGEDI(A,12,12,IPVT,DET,WORK,JOB)
      DO 30 I=1,12
          DO 30 J=1,12
              DO 40 JJ=1,12
   40             K(I,J)=K(I,J)+D(I,JJ)*A(JJ,J)
              K(I,J)=K(I,J)*E*JX/R**2
   30 CONTINUE
 2    FORMAT(1H ,6E12.4)
      RETURN
      END
C
C
      SUBROUTINE DAXPY(N,DA,DX,INCX,DY,INCY)
      DOUBLE PRECISION DX(1),DY(1),DA
      INTEGER I,INCX,INCY,IXIY,M,MP1,N
      IF(N.LE.0)RETURN
      IF (DA .EQ. 0.0D0) RETURN
      IF(INCX.EQ.1.AND.INCY.EQ.1)GO TO 20
      IX = 1
      IY = 1
      IF(INCX.LT.0)IX = (-N+1)*INCX + 1
      IF(INCY.LT.0)IY = (-N+1)*INCY + 1
      DO 10 I = 1,N
          DY(IY) = DY(IY) + DA*DX(IX)
          IX = IX + INCX
          IY = IY + INCY
   10 CONTINUE
      RETURN
   20 M = MOD(N,4)
      IF( M .EQ. 0 ) GO TO 40
      DO 30 I = 1,M
          DY(I) = DY(I) + DA*DX(I)
   30 CONTINUE
      IF( N .LT. 4 ) RETURN
   40 MP1 = M + 1
      DO 50 I = MP1,N,4
          DY(I) = DY(I) + DA*DX(I)
          DY(I + 1) = DY(I + 1) + DA*DX(I + 1)
          DY(I + 2) = DY(I + 2) + DA*DX(I + 2)
          DY(I + 3) = DY(I + 3) + DA*DX(I + 3)
   50 CONTINUE
      RETURN
      END
C
C
      INTEGER FUNCTION IDAMAX(N,DX,INCX)
```

```
      DOUBLE PRECISION DX(1),DMAX
      INTEGER I,INCX,IX,N
      IDAMAX = 0
      IF( N .LT. 1 ) RETURN
      IDAMAX = 1
      IF(N.EQ.1)RETURN
      IF(INCX.EQ.1)GO TO 20
      IX = 1
      DMAX = DABS(DX(1))
      IX = IX + INCX
      DO 10 I = 2,N
         IF(DABS(DX(IX)).LE.DMAX) GO TO 5
         IDAMAX = I
         DMAX = DABS(DX(IX))
    5    IX = IX + INCX
   10 CONTINUE
      RETURN
   20 DMAX = DABS(DX(1))
      DO 30 I = 2,N
         IF(DABS(DX(I)).LE.DMAX) GO TO 30
         IDAMAX = I
         DMAX = DABS(DX(I))
   30 CONTINUE
      RETURN
      END
C
C
      SUBROUTINE  DSCAL(N,DA,DX,INCX)
      DOUBLE PRECISION DA,DX(1)
      INTEGER I,INCX,M,MP1,N,NINCX
      IF(N.LE.0)RETURN
      IF(INCX.EQ.1)GO TO 20
      NINCX = N*INCX
      DO 10 I = 1,NINCX,INCX
         DX(I) = DA*DX(I)
   10 CONTINUE
      RETURN
   20 M = MOD(N,5)
      IF( M .EQ. 0 ) GO TO 40
      DO 30 I = 1,M
         DX(I) = DA*DX(I)
   30 CONTINUE
      IF( N .LT. 5 ) RETURN
   40 MP1 = M + 1
      DO 50 I = MP1,N,5
         DX(I) = DA*DX(I)
         DX(I + 1) = DA*DX(I + 1)
         DX(I + 2) = DA*DX(I + 2)
         DX(I + 3) = DA*DX(I + 3)
         DX(I + 4) = DA*DX(I + 4)
   50 CONTINUE
      RETURN
      END
C
C
      SUBROUTINE  DSWAP (N,DX,INCX,DY,INCY)
      DOUBLE PRECISION DX(1),DY(1),DTEMP
      INTEGER I,INCX,INCY,IX,IY,M,MP1,N
      IF(N.LE.0)RETURN
      IF(INCX.EQ.1.AND.INCY.EQ.1)GO TO 20
      IX = 1
      IY = 1
      IF(INCX.LT.0)IX = (-N+1)*INCX + 1
      IF(INCY.LT.0)IY = (-N+1)*INCY + 1
      DO 10 I = 1,N
         DTEMP = DX(IX)
```

```
         DX(IX) = DY(IY)
         DY(IY) = DTEMP
         IX = IX + INCX
         IY = IY + INCY
   10 CONTINUE
      RETURN
   20 M = MOD(N,3)
      IF( M .EQ. 0 ) GO TO 40
      DO 30 I = 1,M
         DTEMP = DX(I)
         DX(I) = DY(I)
         DY(I) = DTEMP
   30 CONTINUE
      IF( N .LT. 3 ) RETURN
   40 MP1 = M + 1
      DO 50 I = MP1,N,3
         DTEMP = DX(I)
         DX(I) = DY(I)
         DY(I) = DTEMP
         DTEMP = DX(I + 1)
         DX(I + 1) = DY(I + 1)
         DY(I + 1) = DTEMP
         DTEMP = DX(I + 2)
         DX(I + 2) = DY(I + 2)
         DY(I + 2) = DTEMP
   50 CONTINUE
      RETURN
      END
C
C
      SUBROUTINE DGEFA(A,LDA,N,IPVT,INFO)
      INTEGER LDA,N,IPVT(1),INFO
      DOUBLE PRECISION A(LDA,1)
      DOUBLE PRECISION T
      INTEGER IDAMAX,J,K,KP1,L,NM1
      INFO = 0
      NM1 = N - 1
      IF (NM1 .LT. 1) GO TO 70
      DO 60 K = 1, NM1
         KP1 = K + 1
         L = IDAMAX(N-K+1,A(K,K),1) + K - 1
         IPVT(K) = L
         IF (A(L,K) .EQ. 0.0D0) GO TO 40
         IF (L .EQ. K) GO TO 10
         T = A(L,K)
         A(L,K) = A(K,K)
         A(K,K) = T
   10    CONTINUE
         T = -1.0D0/A(K,K)
         CALL DSCAL(N-K,T,A(K+1,K),1)
         DO 30 J = KP1, N
            T = A(L,J)
            IF (L .EQ. K) GO TO 20
            A(L,J) = A(K,J)
            A(K,J) = T
   20       CONTINUE
            CALL DAXPY(N-K,T,A(K+1,K),1,A(K+1,J),1)
   30    CONTINUE
         GO TO 50
   40    CONTINUE
         INFO = K
   50    CONTINUE
   60 CONTINUE
   70 CONTINUE
      IPVT(N) = N
      IF (A(N,N) .EQ. 0.0D0) INFO = N
```

```
      RETURN
      END
C
C
      SUBROUTINE DGEDI(A,LDA,N,IPVT,DET,WORK,JOB)
      INTEGER LDA,N,IPVT(1),JOB
      DOUBLE PRECISION A(LDA,1),DET(2),WORK(1)
      DOUBLE PRECISION T
      DOUBLE PRECISION TEN
      INTEGER I,J,K,KB,KP1,L,NM1
      IF (JOB/10 .EQ. 0) GO TO 70
      DET(1) = 1.0D0
      DET(2) = 0.0D0
      TEN = 10.0D0
      DO 50 I = 1, N
         IF (IPVT(I) .NE. I) DET(1) = -DET(1)
         DET(1) = A(I,I)*DET(1)
         IF (DET(1) .EQ. 0.0D0) GO TO 60
   10    IF (DABS(DET(1)) .GE. 1.0D0) GO TO 20
         DET(1) = TEN*DET(1)
         DET(2) = DET(2) - 1.0D0
         GO TO 10
   20    CONTINUE
   30    IF (DABS(DET(1)) .LT. TEN) GO TO 40
         DET(1) = DET(1)/TEN
         DET(2) = DET(2) + 1.0D0
         GO TO 30
   40    CONTINUE
   50 CONTINUE
   60 CONTINUE
   70 CONTINUE
      IF (MOD(JOB,10) .EQ. 0) GO TO 150
      DO 100 K = 1, N
         A(K,K) = 1.0D0/A(K,K)
         T = -A(K,K)
         CALL DSCAL(K-1,T,A(1,K),1)
         KP1 = K + 1
         IF (N .LT. KP1) GO TO 90
         DO 80 J = KP1, N
            T = A(K,J)
            A(K,J) = 0.0D0
            CALL DAXPY(K,T,A(1,K),1,A(1,J),1)
   80    CONTINUE
   90    CONTINUE
  100 CONTINUE
      NM1 = N - 1
      IF (NM1 .LT. 1) GO TO 140
      DO 130 KB = 1, NM1
         K = N - KB
         KP1 = K + 1
         DO 110 I = KP1, N
            WORK(I) = A(I,K)
            A(I,K) = 0.0D0
  110    CONTINUE
         DO 120 J = KP1, N
            T = WORK(J)
            CALL DAXPY(N,T,A(1,J),1,A(1,K),1)
  120    CONTINUE
         L = IPVT(K)
         IF (L .NE. K) CALL DSWAP(N,A(1,K),1,A(1,L),1)
  130 CONTINUE
  140 CONTINUE
  150 CONTINUE
      RETURN
      END
C
```

```
C
      SUBROUTINE GAUSS(A,B,MBAND,NEQ)
C THIS SUBPROGRAM PERFORMS GAUSSIAN ELIMINATION
C ON A NON SYMMETRICAL BANDED MATRIX
      DOUBLE PRECISION A(6300),B(130),C,S
      NQ1=NEQ-1
      DO 10 I=1,NQ1
         I1=I+1
         I2=I+MBAND
         DO 20 II=I1,I2
            J=I
            K=(J-II+MBAND)*NEQ+II
            IF(A(K).EQ.0.) GO TO 20
            KK=(J-I+MBAND)*NEQ+I
            C=A(K)/A(KK)
            J1=J
            J2=J+MBAND
            IF(J2.GT.NEQ) J2=NEQ
            DO 40 JJ=J1,J2
               KKK=(JJ-II+MBAND)*NEQ+II
               KKKK=(JJ-I+MBAND)*NEQ+I
   40          A(KKK)=A(KKK)-C*A(KKKK)
            B(II)=B(II)-C*B(I)
   20    CONTINUE
   10 CONTINUE
      K=MBAND*NEQ+NEQ
      B(NEQ)=B(NEQ)/A(K)
      DO 50 II=1,NQ1
         I=NEQ-II
         J1=I+1
         J2=I+MBAND
         S=0.
         IF(J2.GT.NEQ) J2=NEQ
         DO 60 J=J1,J2
            K=(J-I+MBAND)*NEQ+I
   60       S=S+A(K)*B(J)
         KK=MBAND*NEQ+I
   50    B(I)=(B(I)-S)/A(KK)
      RETURN
      END
```

APPENDIX C

TWO RING DEFLECTION PROGRAM

APPENDIX C

Two Ring Deflection Program

Program Description

The two ring deflection program calculates the face deflections and forces developed in a two ring face seal subjected to operating loads. It uses the finite element method to model the seal with beam and spring elements.

The program models the rings with an even number of nodes and beam elements. As presented here, it assumes even spacing of the nodes so each element is $2\pi R/(\#$ of nodes) long. Variable element size can also be used.

Spring elements connect the nodes on the primary ring to corresponding nodes on the mating ring. These model the face contact. Where the ring faces touch, the springs' stiffness is set equal to the stiffness of the carbon insert. The springs have zero stiffness where there is no contact. As the load is applied and the rings deform, springs are given the face stiffness or zero stiffness as they come into or go out of contact.

Both rings may have an initial face profile. The datum from which the profiles are measured is arbitrary since the program subtracts out the first harmonic tilt between the two rings. The program calculates a likely initial-face contact pattern after tilting the seal faces.

To avoid instability in the solution, the program applies the loads incrementally. After the total loads are applied, the program

iterates up to two more times to see that the contact pattern is constant. It prints a message confirming convergence if the solution is consistent. When the total loads have been applied, the deflections and forces are calculated and printed. The average gap and the cube mean gap are computed at the end.

Program Input

The two ring deflection program requires information about the ring geometries, ring materials, and applied forces. Some data is read from a file and some is input by changing program lines.

The program lines that contain input information are:

Line 310: N--Number of nodes (set up for 30)

Line 320: RCP--Radius to the centroid of the primary ring

Line 360: AP--Cross section area of the primary ring

Line 370: JXP--Moment of inertia about the x-axis of primary ring

$$\left(JXP = \int_A \frac{y^2}{1 - x/R} \, dA \right)$$

Line 380: JYP--Moment of inertia about the y-axis of primary ring

Line 390: JXYP--Product of inertia of primary ring

Line 400: JTP--Torsional constant of primary ring cross section

Line 410: EP--Young's modulus of primary ring material

Line 420: GP--Shear modulus of primary ring material

Lines 430-500: RCM, AM, JXM, JYM, JXYM, JTM, EM, GM--Same as above for mating ring

Line 510: RF--Radius to seal face

Line 520: RS--Radius to support of mating ring

Line 580: VXP(I)--Applied force in x-direction at node I on primary ring

Line 590: VYP(I)--Applied force in y-direction at node I on primary ring

Line 600: MTP(I)--Applied moment about θ-axis at node I on primary ring

Lines 610-630: VXM(I), VYM(I), MTM(I)--Same as above for mating ring

Line 640: KS(I)--Support stiffness at node I

Line 650: KF(I)--Face stiffness at node I

Line 660: DELSI(I)--Initial support profile at node I

The initial ring face profiles are read from a data file in 6F10.0 format.

Sample Problem

The modified (reduced section) magnetic face seal shown in Figure C-1 is considered as a sample problem. (See Chapter 5 and Ref. [41]). The primary ring cross section properties are:

$RCP = 0.6414$ in

$AP = 0.01603$ in^2

$JXP = 4.44 \times 10^{-5}$ in^4

$JYP = 3.5366 \times 10^{-5}$ in^4

$JXYP = 2.019 \times 10^{-5}$ in^4

$JTP = 2.074 \times 10^{-5}$ in^4

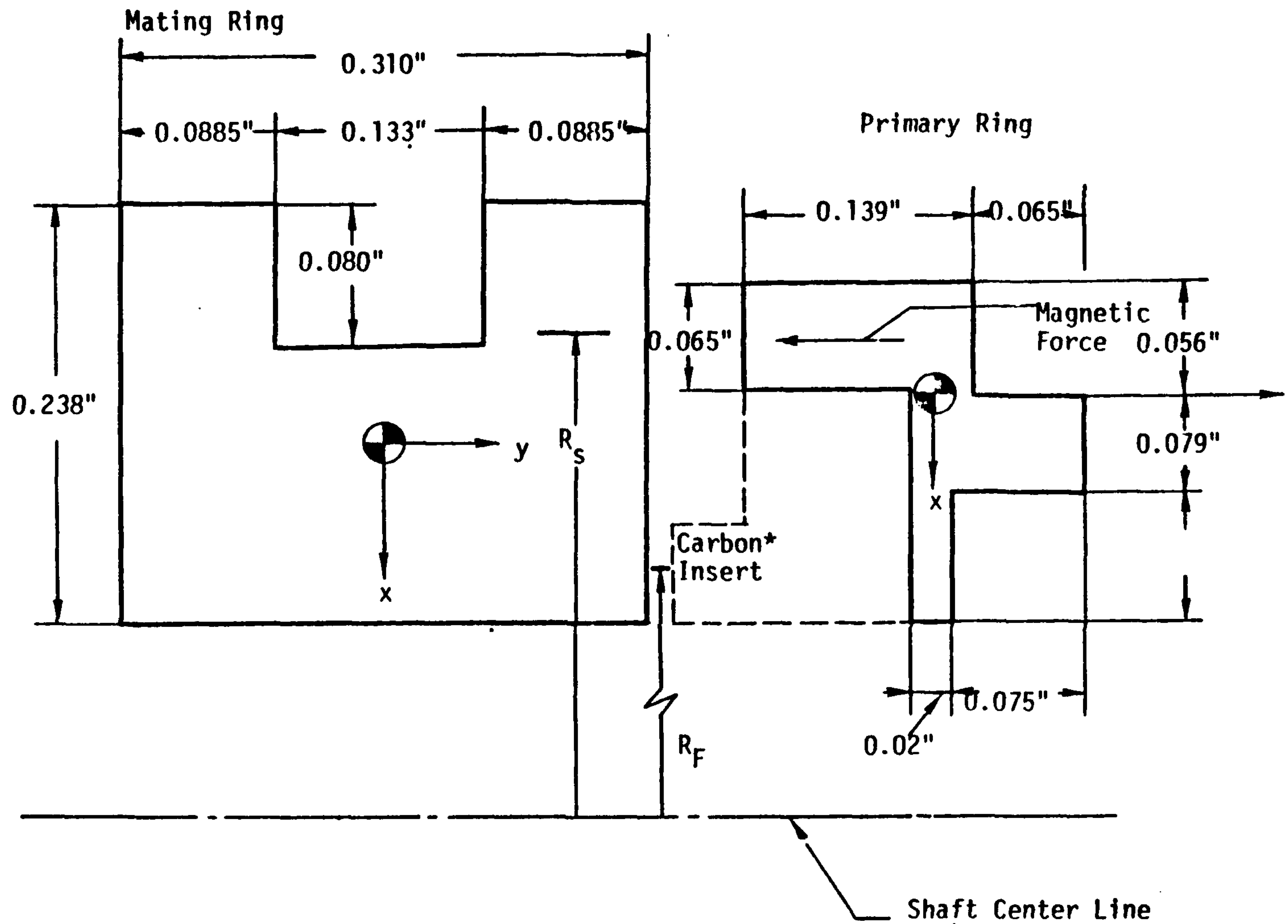

*Note: The carbon insert is not included in calculation of primary ring properties.

Figure C-1. Reduced Seal Cross Section used for Sample Problem.

The mating ring cross section properties are:

RCM = 0.613 in

AM = 0.06314 in^2

JXM = 5.752×10^{-4} in^4

JYM = 2.650×10^{-4} in^4

JXYM = 0.0

JTM = 4.73×10^{-4} in^4

The support and face radii are:

RS = 0.675 (the radius at which the magnet acts)

RF = 0.553

The ring material properties are:

EP = 27×10^6 psi

GP = 10.6×10^6 psi

EM = 20×10^6 psi

GP = 8.33×10^6 psi

The applied loads come from magnetic force of the mating ring acting on the primary ring. The total magnetic force is 1.92 lbs acting in the negative y-direction. It is assumed to act at a .675 radius so it also creates a moment about the θ-axis. The applied forces are:

VXP(I) = 0.0

VYP(I) = -1.92/30

$MTP(I) = -1.92\ (0.675 - 0.632^{1})/30$

$VXM(I) = 0.0$

$VYM(I) = 0.0$

$MTM(I) = 0.0$

The stiffness of the carbon insert is the face stiffness:

$$KF(I) = \frac{AE}{L}$$

$$= \frac{2\pi(.553)(0.06)(3 \times 10^6)}{0.1156/30}$$

$$= 5.4 \times 10^6/30$$

The total support stiffness is chosen to be 5.4×10^4 lb/in, 100 times lower to simulate the high conformability of the magnet. Thus

$KS(I) = 5.4 \times 10^4/30$

The data file of the initial face profiles is shown in the example. The program input and output are shown. A plot of the output shows that the gap in the face lessens when the force is applied as expected but does not completely close.

---

[1] Should have been 0.6441.

```
     AV             SAV             CAV
 0.1576E-03 -0.4757E-05 -0.2041E-04

CONTACTING NODES . . .
   10 11 25

PLANE EQUATION COEFFICIENTS . . .
 0.4093E-04  0.2340E-04  0.4685E-04


INITIAL FACE DEFLECTIONS

 0.9955E-04  0.1182E-03  0.1282E-03  0.1415E-03  0.1290E-03  0.1065E-03
 0.7175E-04  0.3325E-04  0.1692E-04 -0.1091E-10  0.0          0.8534E-05
 0.2493E-04  0.1897E-04  0.4407E-04  0.1273E-04  0.5426E-05 -0.4919E-05
-0.2116E-04  0.6266E-05  0.9311E-05  0.2495E-04  0.1964E-04  0.7082E-05
 0.2638E-10  0.1718E-04  0.3073E-04  0.4515E-04  0.5631E-04  0.7762E-04


INITIAL FACE CONTACT PATTERN

0 0 0 0 0 0 1 1 1 1 1 1 0 0 0 0 0 1 1 0 0 0 0 1 1 1 1 1 1
   0
   0


FACE CONTACT PATTERN AFTER FORCES ARE APPLIED

0 0 0 0 0 0 0 0 1 1 0 0 0 0 0 0 0 0 1 0 0 0 0 0 1 0 0 0 1 0


FACE DEFLECTIONS AFTER FORCES ARE APPLIED

-0.2002E-04 -0.3338E-04 -0.4259E-04 -0.5970E-04 -0.5526E-04 -0.4431E-04
-0.2353E-04 -0.2131E-06  0.7986E-06  0.4152E-05 -0.4053E-05 -0.1673E-04
-0.3927E-04 -0.3582E-04 -0.6229E-04 -0.3168E-04 -0.2484E-04 -0.1487E-04
 0.1073E-05 -0.2541E-04 -0.2684E-04 -0.3974E-04 -0.3015E-04 -0.1144E-04
 0.3694E-05 -0.5580E-06 -0.8344E-07 -0.3211E-06  0.1566E-05 -0.7368E-05


FACE FORCES

 0.0         0.0          0.0          0.0          0.0          0.0
 0.0        -0.3836E-01   0.1437E 00   0.7473E 00   0.0          0.0
 0.0         0.0          0.0          0.0          0.0          0.0
 0.1932E 00  0.0          0.0          0.0          0.0          0.0
 0.6650E 00  0.0         -0.1502E-01  -0.5730E-01   0.2819E 00   0.0
Repeats
FACE CONTACT PATTERN AFTER FORCES ARE APPLIED

0 0 0 0 0 0 0 0 1 1 0 0 0 0 0 0 0 0 1 0 0 0 0 0 1 0 0 0 1 0


FACE DEFLECTIONS AFTER FORCES ARE APPLIED

-0.2049E-04 -0.3391E-04 -0.4318E-04 -0.6033E-04 -0.5590E-04 -0.4493E-04
-0.2409E-04 -0.6833E-06  0.6242E-06  0.4126E-05 -0.3964E-05 -0.1855E-04
-0.3904E-04 -0.3557E-04 -0.6205E-04 -0.3148E-04 -0.2468E-04 -0.1478E-04
 0.1111E-05 -0.2539E-04 -0.2685E-04 -0.3978E-04 -0.3021E-04 -0.1154E-04
```

0.3559E-05 -0.8495E-06 -0.5279E-06 -0.8440E-06 0.1247E-05 -0.7759E-05

FACE FORCES

0.0	0.0	0.0	0.0	0.0	0.0
0.0	0.0	0.1124E 00	0.7426E 00	0.0	0.0
0.0	0.0	0.0	0.0	0.0	0.0
0.2000E 00	0.0	0.0	0.0	0.0	0.0
0.6406E 00	0.0	0.0	0.0	0.2245E 00	0.0

CONVERGENCE IS OK

AVG. GAP	CUBE MEAN
0.2191E 02	0.3376E 02

```
C TWO RING DEFLECTION PROGRAM
C   THIS PROGRAM CALCULATES THE DEFLECTIONS AND FORCES DEVELOPED
C   IN A TWO RING FACE SEAL SUBJECTED TO OPERATING FORCES.  IT
C   USES THE FINITE ELEMENT METHOD TO MODEL THE SEAL.  THE RINGS
C   ARE MODELED WITH BEAM ELEMENTS AND THE FACE CONTACT IS MODELED
C   WITH SPRINGS.  THE INITIAL AND FINAL FACE DEFLECTIONS AND
C   FORCES ARE CALCULATED AND THE AVERAGE GAP AND CUBE MEAN OF
C   THE GAP ARE DETERMINED.
C
      DOUBLE PRECISION KP,KM,AMAT,IMAT,IIMAT,IIIMAT,IVMAT,RHA,RHB,BMAT
      COMMON CVXP(30),CVXM(30),CVYM(30),CVYP(30),CMTM(30),CMTP(30)
      COMMON CDELFI(30),CDELSI(30),CKS(30),CKF(30),KP(12,12),KM(12,12)
      COMMON AMAT(360,59),IMAT(12,12),IIMAT(12,12),IIIMAT(12,12)
      COMMON IVMAT(12,12),BMAT(360),RHA(12),RHB(12)
      COMMON RCP,RCM,RF,RS
      REAL*4 MTM,MTP,JXP,JYP,JXYP,JTP,JXM,JYM,JXYM,JTM
      REAL*4 KS,KF
      DIMENSION VXP(30),VXM(30),VYM(30),VYP(30),MTM(30),MTP(30)
      DIMENSION DELSI(30),DELF(30),KS(30),KF(30),DEF(30)
      DIMENSION III(30),ICOMP(30),ICC(30),ICCOLD(30)
      DIMENSION UOUT(30),VOUT(30),PHIOUT(30)
      DOUBLE PRECISION PIE,SUM(12,12)
      DIMENSION DELP(30),DELM(30),FORC(30),DELNET(30),DELMTP(30)
      DIMENSION DELTAP(12),DELTAM(12),FORCE(12)
C
      PIE=4.*DATAN(1.D+00)
      PIES=PIE
C
C INPUT NUMBER OF NODES, INITIAL WAVINESS AND RINGS' SECTION
C PROPERTIES
      N=30
      READ(5,18) DELP
      READ(5,18) DELMTP
18    FORMAT(6F10.0)
      RCP=0.6414
      AP=0.016035
      JXP=4.44E-5
      JYP=3.536E-5
      JXYP=2.019E-5
      JTP=2.0738E-5
      EP=27.E+06
      GP=10.6E+06
      RCM=0.613
      AM=0.06314
      JXM=5.752E-04
      JYM=2.65E-04
      JXYM=1.E-06
      JTM=4.729E-04
      EM=20.E+06
      GM=6.333E+06
      RF=0.553
      RS=0.675
C
C INPUT THE RING LOADS VX,VY,MT HERE.  OTHER LOADS ARE ASSUMED ZERO.
C THESE ARE ACTUAL LOADS AT THE NODES
      ALOAD=-1.92
      DO 100 I=1,N
         VXP(I)=0.
         VYP(I)=ALOAD/N
         MTP(I)=-VYP(I)*(.675-.632)
         VXM(I)=0.
         VYM(I)=0.
         MTM(I)=0.
```

```
         KS(I)=5.4E+04/N
         KF(I)=5.4E+06/N
         DELSI(I)=0.
  100 CONTINUE
      DT=2.*PIE/N
      DO 8000 IROT=1,1
      IMOV=IROT-1
C
C ELIMINATE FIRST HARMONIC FROM GAP
      DO 22 I=1,N
         II=I+IMOV
         IF(II.GT.N) II=II-N
22       DELM(I)=DELMTP(II)
      DO 20 I=1,N
20       DELF(I)=(-DELP(I)-DELM(I))*1.E-06
      SAV=0.
      CAV=0.
      AV=0.
      NP1=N+1
         DO 25 I=1,NP1
         FAC=2.
         J=I-1
         IF(I.EQ.1) FAC=1.
         IF(I.EQ.NP1) FAC=1.
         II=I
         IF(I.EQ.NP1) II=1
         AV=AV+DELF(II)*FAC*.5
         SAV=SAV+DELF(II)*FAC*SIN(2.*PIES*J/N)
   25    CAV=CAV+DELF(II)*FAC*COS(2.*PIES*J/N)
      AV=AV/N
      SAV=SAV/N
      CAV=CAV/N
      WRITE (6,27)
   27 FORMAT(//6X,'AV',10X,'SAV',10X,'CAV')
      WRITE(6,3) AV,SAV,CAV
      DO 30 I=1,N
         J=I-1
         DELF(I)=DELF(I)-AV-CAV*COS(2.*PIES*J/N)-SAV*SIN(2.*PIES*J/N)
   30 CONTINUE
3     FORMAT(1H ,6E12.4)
C TRY PICKING THREE SMALLEST IN THREE SEGMENTS
      AMIN=1.E+06
      N1=N/3
      DO 35 I=1,N1
         IF(DELF(I).GT.AMIN) GO TO 35
         AMIN=DELF(I)
         IA=I
35    CONTINUE
      BMIN=1.E+06
      N1=N1+1
      N2=N1+N/3
      DO 36 I=N1,N2
         IF(DELF(I).GT BMIN) GO TO 36
         BMIN=DELF(I)
         IB=I
36    CONTINUE
      N1=N2+1
      CMIN=1.E+06
      DO 37 I=N1,N
         IF(DELF(I).GT.CMIN) GO TO 37
         CMIN=DELF(I)
         IC=I
37    CONTINUE
4     FORMAT(1H ,3012)
      WRITE (6,6)
    6 FORMAT(/1X,'CONTACTING NODES      .')
```

```
      WRITE(6,7) IA,IB,IC
    7 FORMAT(3X,3I3)
      TA=(IA-1)*DT
      TB=(IB-1)*DT
      TC=(IC-1)*DT
      DET=(SIN(TA)-SIN(TB))*(COS(TA)-COS(TC))
      DET=DET-(COS(TA)-COS(TB))*(SIN(TA)-SIN(TC))
      DC2=(DELF(IB)-DELF(IA))*(COS(TA)-COS(TC))
      DC2=DC2-(DELF(IC)-DELF(IA))*(COS(TA)-COS(TB))
      C2=DC2/DET
      C3=DELF(IB)-DELF(IA)-C2*(SIN(TA)-SIN(TB))
      C3=C3/(COS(TA)-COS(TB))
      C1=-DELF(IA)-C2*SIN(TA)-C3*COS(TA)
      WRITE (6,8)
    8 FORMAT(/1X,'PLANE EQUATION COEFFICIENTS . . .')
      WRITE(6,3) C1,C2,C3
      DO 39 I=1,N
         TT=(I-1)*DT
         ICC(I)=0
         IF(DELF(I).LE.0.) ICC(I)=1
         DELF(I)=DELF(I)+C1+C2*SIN(TT)+C3*COS(TT)
         IF(DELF(I).LT.1.E-06) ICC(I)=1
 39   CONTINUE
      WRITE (6,40)
   40 FORMAT(//1X,'INITIAL FACE DEFLECTIONS'/)
      WRITE(6,3) DELF
      WRITE (6,41)
   41 FORMAT(//1X,'INITIAL FACE CONTACT PATTERN'/)
      WRITE(6,4) ICC
C
C REARRANGE SUBSCRIPTS FOR COMPUTATIONAL EFFICIENCY
      III(1)=1
      III(2)=2
      DO 110 I=3,N
         AI=I
         BI=I/2
         AI=AI/2.-BI
         IF(AI.GT.0.1) GO TO 120
         III(I)=(I+2)/2
         GO TO 110
  120    III(I)=(2*N+3-I)/2
  110 CONTINUE
      DO 133 I=1,N
         IIN=III(I)
  133    ICOMP(IIN)=I
    9 FORMAT(1H ,3I5)
C
C COMPUTE ELEMENT STIFFNESSES
      CALL AOLCOP(RCP,AP,JXP,JYP,JXYP,JTP,EP,GP,DT,KP)
      CALL AOLCOP(RCM,AM,JXM,JYM,JXYM,JTM,EM,GM,DT,KM)
      DO 135 I=1,12
         RHA(I)=0.
         RHB(I)=0.
         DO 135 J=1,12
            IMAT(I,J)=0.
            IIMAT(I,J)=0.
            IIIMAT(I,J)=0.
            IVMAT(I,J)=0.
  135 CONTINUE
      DO 140 I=1,N
         II=III(I)
         CDELSI(I)=-DELSI(II)
 140     CDELFI(I)=-DELF(II)
      FRAC=0.
      NFRAC=8
      NITMAX=NFRAC+2
```

```
      DO 5000 NIT=1,NITMAX
         FRAC=FRAC+1./NFRAC
         IF(FRAC.GT.1.0) FRAC=1.
         DO 150 I=1,N
            II=III(I)
            CVXP(I)=FRAC*VXP(II)
            CVXM(I)=FRAC*VXM(II)
            CVYM(I)=FRAC*VYM(II)
            CVYP(I)=FRAC*VYP(II)
            CMTM(I)=FRAC*MTM(II)
            CMTP(I)=FRAC*MTP(II)
            CKS(I)=KS(II)
  150       CKF(I)=KF(II)*ICC(II)
         NEQ=12*N
         MBAND=29
C
C ASSEMBLE GLOBAL STIFFNESS AND FORCE MATRICES
         DO 250 I=1,NEQ
            BMAT(I)=0.
            DO 250 J=1,59
  250          AMAT(I,J)=0.
         CALL ISUB(1,2)
         CALL IVSUB(3,1)
         CALL ADD(IMAT,IVMAT,SUM)
         CALL IISUB
         CALL IIISUB
         J1=31
         DO 300 I=1,12
            BMAT(I)=RHA(I)+RHB(I)
            J1=J1-1
            J2=J1+11
            JJ=0
            DO 300 J=J1,J2
               JJ=JJ+1
               AMAT(I,J)=SUM(I,JJ)
               AMAT(I,J+12)=IIMAT(I,JJ)
               IF((J+24).GT.59) GO TO 300
               AMAT(I,J+24)=IIIMAT(I,JJ)
  300    CONTINUE
         CALL ISUB(2,4)
         CALL IVSUB(1,2)
         CALL ADD(IMAT,IVMAT,SUM)
         J1=31
         DO 400 I=13,24
            II=I-12
            BMAT(I)=RHA(II)+RHB(II)
            J1=J1-1
            J2=J1+11
            JJ=0
            DO 400 J=J1,J2
               JJ=JJ+1
               AMAT(I,J)=SUM(II,JJ)
               IF((J+24).GT.59) GO TO 400
               AMAT(I,J+24)=IIMAT(II,JJ)
  400          AMAT(I,J-12)=IIIMAT(II,JJ)
         NM2=N-2
         NODD=1
         DO 1000 NN=3,NM2
            IST=(NN-1)*12+1
            ISTOP=IST+11
            IF(NODD.EQ.2) GO TO 1050
            CALL ISUB(NN,NN-2)
            CALL IVSUB(NN+2,NN)
            CALL ADD(IMAT,IVMAT,SUM)
            GO TO 1060
 1050       CONTINUE
```

```
                 CALL ISUB(NN,NN+2)
                 CALL IVSUB(NN-2,NN)
                 CALL ADD(IMAT,IVMAT,SUM)
      1060       J1=31
                 II=0
                 DO 1070 I=IST,ISTOP
                    II=II+1
                    BMAT(I)=RHA(II)+RHB(II)
                    J1=J1-1
                    J2=J1+11
                    JJ=0
                    DO 1070 J=J1,J2
                       JJ=JJ+1
                       AMAT(I,J)=SUM(II,JJ)
                       GO TO (1080,1090),NODD
      1080             IF((J-24).LT.1) GO TO 1081
                       AMAT(I,J-24)=IIMAT(II,JJ)
      1081             IF((J+24).GT.59) GO TO 1070
                       AMAT(I,J+24)=IIIMAT(II,JJ)
                       GO TO 1070
      1090             IF((J-24).LT.1) GO TO 1091
                       AMAT(I,J-24)=IIIMAT(II,JJ)
      1091             IF((J+24).GT.59) GO TO 1070
                       AMAT(I,J+24)=IIMAT(II,JJ)
      1070       CONTINUE
                 IF(NODD.EQ.1) GO TO 1095
                 NODD=1
                 GO TO 1000
      1095       NODD=2
      1000    CONTINUE
              NM1=N-1
              CALL ISUB(NM1,NM1-2)
              CALL IVSUB(N,N-1)
              CALL ADD(IMAT,IVMAT,SUM)
              IST=NM2*12+1
              ISTOP=IST+11
              J1=31
              II=0
              DO 500 I=IST,ISTOP
                 II=II+1
                 BMAT(I)=RHA(II)+RHB(II)
                 J1=J1-1
                 J2=J1+11
                 JJ=0
                 DO 500 J=J1,J2
                    JJ=JJ+1
                    AMAT(I,J)=SUM(II,JJ)
                    IF((J-24).LT.1) GO TO 500
                    AMAT(I,J-24)=IIMAT(II,JJ)
       500          AMAT(I,J+12)=IIIMAT(II,JJ)
              CALL ISUB(N,N-1)
              CALL IVSUB(N-2,N)
              CALL ADD(IMAT,IVMAT,SUM)
              IST=NM1*12+1
              ISTOP=IST+11
              J1=31
              II=0
              DO 600 I=IST,ISTOP
                 II=II+1
                 BMAT(I)=RHA(II)+RHB(II)
                 J1=J1-1
                 J2=J1+11
                 JJ=0
                 DO 600 J=J1,J2
                    JJ=JJ+1
                    AMAT(I,J)=SUM(II,JJ)
```

```
                  IF((J-24).LT.1) GO TO 600
                  AMAT(I,J-24)=IIIMAT(II,JJ)
      600         AMAT(I,J-12)=IIMAT(II,JJ)
            DO 700 NN=1,N
               NC=(NN-1)*12+1
               BMAT(NC)=BMAT(NC)+CVXP(NN)
               BMAT(NC+1)=BMAT(NC+1)+CVYP(NN)
               BMAT(NC+5)=BMAT(NC+5)+CMTP(NN)
               BMAT(NC+6)=BMAT(NC+6)+CVXM(NN)
               BMAT(NC+7)=BMAT(NC+7)+CVYM(NN)
      700      BMAT(NC+11)=BMAT(NC+11)+CMTM(NN)
C
C ENFORCE ZERO DISPLACEMENT BOUNDARY CONDITIONS:
C UP1,UM1,WP1,WM1,WPN,WMN=0
            II=12*NM1
            DO 750 J=1,59
               AMAT(1,J)=0.
               AMAT(7,J)=0.
               AMAT(3,J)=0.
               AMAT(9,J)=0.
               AMAT(II+3,J)=0.
      750      AMAT(II+9,J)=0.
            AMAT(1,30)=1.
            AMAT(7,30)=1.
            AMAT(3,30)=1.
            AMAT(9,30)=1.
            AMAT(II+3,30)=1.
            AMAT(II+9,30)=1.
            BMAT(1)=0.
            BMAT(3)=0.
            BMAT(7)=0.
            BMAT(9)=0.
            BMAT(II+3)=0.
            BMAT(II+9)=0.
C
C SOLVE FOR DEFLECTIONS
            CALL GAUSS(AMAT,BMAT,MBAND,NEQ)
C
C CALCULATE AND PRINT DEFLECTIONS AND FORCES
            ICCSUM=0
            DO 900 I=1,N
               II=(ICOMP(I)-1)*12
               DEF(I)=BMAT(II+8)-BMAT(II+2)-BMAT(II+12)*(RF-RCM)
               DEF(I)=DEF(I)+BMAT(II+6)*(RF-RCP)
               FORC(I)=(DEF(I)-DELF(I))*KF(I)*ICC(I)
               DELNET(I)=DEF(I)-DELF(I)
               ICCOLD(I)=ICC(I)
               ICC(I)=0
               IF(DEF(I).GE.DELF(I)) ICC(I)=1
               ICCSUM=ICCSUM+(ICC(I)-ICCOLD(I))**2
  900       CONTINUE
            IF(FRAC.NE.1.) GO TO 5000
            WRITE (6,905)
      905   FORMAT(//1X,'FACE CONTACT PATTERN AFTER FORCES ARE APPLIED'/)
            WRITE(6,4) ICC
            WRITE (6,906)
      906   FORMAT(//1X,'FACE DEFLECTIONS AFTER FORCES ARE APPLIED'/)
            WRITE(6,3) DELNET
            WRITE (6,907)
      907   FORMAT(//1X,'FACE FORCES'/)
            WRITE(6,3) FORC
            IF(ICCSUM.EQ.0) GO TO 6000
 5000    CONTINUE
         GO TO 6001
 6000    WRITE(6,17)
 17      FORMAT(//1X,'CONVERGENCE IS OK')
```

```
C
C COMPUTE AVERAGE GAP AND CUBE MEAN OF THE GAP
6001   HAV=0.
       HAV3=0.
       DO 8002 I=1,N
       IF(DELNET(I).GT.0.) GO TO 8002
       HAV=HAV-DELNET(I)
       HAV3=HAV3-DELNET(I)**3
8002    CONTINUE
       HAV=HAV*1.E+06/N
       HAV3=(HAV3/N)**0.333333333333*1.E+06
       WRITE (6,8003)
 8003  FORMAT(//3X,'AVG.  GAP      CUBE MEAN')
       WRITE(6,8004) HAV,HAV3
8004   FORMAT(1X,E12.4,E12.4)
8000   CONTINUE
       STOP
       END
C SUBROUTINES USED BY THE PROGRAM
       SUBROUTINE ISUB(IA,IB)
       DOUBLE PRECISION KP,KM,AMAT,IMAT,IIMAT,IIIMAT,IVMAT,RHA,RHB,BMAT
       COMMON CVXP(30),CVXM(30),CVYM(30),CVYP(30),CMTM(30),CMTP(30)
       COMMON CDELFI(30),CDELSI(30),CKS(30),CKF(30),KP(12,12),KM(12,12)
       COMMON AMAT(360,59),IMAT(12,12),IIMAT(12,12),IIIMAT(12,12)
       COMMON IVMAT(12,12),BMAT(360),RHA(12),RHB(12)
       COMMON RCP,RCM,RF,RS
       DO 10 I=1,6
          DO 10 J=1,6
   10        IMAT(I,J)=KP(I,J)
       DO 20 I=7,12
          DO 20 J=7,12
             II=I-6
             JJ=J-6
   20        IMAT(I,J)=KM(II,JJ)
       IMAT(2,2)=IMAT(2,2)+CKF(IA)*.5
       IMAT(2,6)=IMAT(2,6)-CKF(IA)*.5*(RF-RCP)
       IMAT(2,8)=-CKF(IA)*.5
       IMAT(2,12)=CKF(IA)*.5*(RF-RCM)
       IMAT(6,2)=IMAT(6,2)-CKF(IA)*.5*(RF-RCP)
       IMAT(6,6)=IMAT(6,6)+CKF(IA)*.5*(RF-RCP)**2
       IMAT(6,8)=CKF(IA)*.5*(RF-RCP)
       IMAT(6,12)=-CKF(IA)*.5*(RF-RCM)*(RF-RCP)
       IMAT(8,2)=-CKF(IA)*.5
       IMAT(8,6)=CKF(IA)*.5*(RF-RCP)
       IMAT(8,8)=IMAT(8,8)+CKF(IA)*.5+CKS(IA)*.5
       IMAT(8,12)=IMAT(8,12)-CKF(IA)*.5*(RF-RCM)+CKS(IA)*.5*(RCM-RS)
       IMAT(12,2)=CKF(IA)*.5*(RF-RCM)
       IMAT(12,6)=-CKF(IA)*.5*(RF-RCM)*(RF-RCP)
       IMAT(12,8)=IMAT(12,8)-CKF(IA)*.5*(RF-RCM)+CKS(IA)*.5*(RCM-RS)
       IMAT(12,12)=IMAT(12,12)+CKF(IA)*.5*(RF-RCM)**2+CKS(IA)*.5*(RCM-RS)
      ***2
       RHA(2)=CKF(IA)*.5*CDELFI(IA)
       RHA(6)=-CKF(IA)*.5*CDELFI(IA)*(RF-RCP)
       RHA(8)=-CKF(IA)*.5*CDELFI(IA)+CKS(IA)*.5*CDELSI(IA)
       RHA(12)=CKF(IA)*.5*CDELFI(IA)*(RF-RCM)+CKS(IA)*.5*CDELSI(IA)*(RCM-
      *RS)
       RETURN
       END
C
C
       SUBROUTINE IVSUB(IA,IB)
       DOUBLE PRECISION KP,KM,AMAT,IMAT,IIMAT,IIIMAT,IVMAT,RHA,RHB,BMAT
       COMMON CVXP(30),CVXM(30),CVYM(30),CVYP(30),CMTM(30),CMTP(30)
       COMMON CDELFI(30),CDELSI(30),CKS(30),CKF(30),KP(12,12),KM(12,12)
       COMMON AMAT(360,59),IMAT(12,12),IIMAT(12,12),IIIMAT(12,12)
       COMMON IVMAT(12,12),BMAT(360),RHA(12),RHB(12)
```

```
      COMMON RCP,RCM,RF,RS
      DO 10 I=1,6
         DO 10 J=1,6
            II=I+6
            JJ=J+6
   10       IVMAT(I,J)=KP(II,JJ)
      DO 20 I=7,12
         DO 20 J=7,12
   20       IVMAT(I,J)=KM(I,J)
      IVMAT(2,2)=IVMAT(2,2)+CKF(IB)*.5
      IVMAT(2,6)=IVMAT(2,6)-CKF(IB)*.5*(RF-RCP)
      IVMAT(2,8)=-CKF(IB)*.5
      IVMAT(2,12)=CKF(IB)*.5*(RF-RCM)
      IVMAT(6,2)=-CKF(IB)*.5*(RF-RCP)+IVMAT(6,2)
      IVMAT(6,6)=IVMAT(6,6)+CKF(IB)*.5*(RF-RCP)**2
      IVMAT(6,8)=CKF(IB)*.5*(RF-RCP)
      IVMAT(6,12)=-CKF(IB)*.5*(RF-RCM)*(RF-RCP)
      IVMAT(8,2)=-CKF(IB)*.5
      IVMAT(8,6)=CKF(IB)*.5*(RF-RCP)
      IVMAT(8,8)=IVMAT(8,8)+CKF(IB)*.5+CKS(IB)*.5
      IVMAT(8,12)=IVMAT(8,12)-CKF(IB)*.5*(RF-RCM)+CKS(IB)*.5*(RCM-RS)
      IVMAT(12,2)=CKF(IB) *.5*(RF-RCM)
      IVMAT(12,6)=-CKF(IB)*.5*(RF-RCM)*(RF-RCP)
      IVMAT(12,8)=-CKF(IB)*.5*(RF-RCM)+CKS(IB)*.5*(RCM-RS)+IVMAT(12,8)
      IVMAT(12,12)=IVMAT(12,12)+CKF(IB)*.5*(RF-RCM)**2+CKS(IB)*.5*(RCM-R
     *S)**2
      RHB(2)=CKF(IB)*.5*CDELFI(IB)
      RHB(6)=-CKF(IB)*.5*CDELFI(IB)*(RF-RCP)
      RHB(8)=-CKF(IB)*.5*CDELFI(IB)+CKS(IB)*.5*CDELSI(IB)
      RHB(12)=CKF(IB)*.5*CDELFI(IB)*(RF-RCM)+CKS(IB)*.5*CDELSI(IB)*(RCM-
     *RS)
      RETURN
      END
C
C
      SUBROUTINE IISUB
      DOUBLE PRECISION KP,KM,AMAT,IMAT,IIMAT,IIIMAT,IVMAT,RHA,RHB,BMAT
      COMMON CVXP(30),CVXM(30),CVYM(30),CVYP(30),CMTM(30),CMTP(30)
      COMMON CDELFI(30),CDELSI(30),CKS(30),CKF(30),KP(12,12),KM(12,12)
      COMMON AMAT(360,59),IMAT(12,12),IIMAT(12,12),IIIMAT(12,12)
      COMMON IVMAT(12,12),BMAT(360),RHA(12),RHB(12)
      COMMON RCP,RCM,RF,RS
      DO 10 I=1,6
         DO 10 J=1,6
            JJ=J+6
   10       IIMAT(I,J)=KP(I,JJ)
      DO 20 I=7,12
         DO 20 J=7,12
            II=I-6
   20       IIMAT(I,J)=KM(II,J)
      RETURN
      END
C
C
      SUBROUTINE IIISUB
      DOUBLE PRECISION KP,KM,AMAT,IMAT,IIMAT,IIIMAT,IVMAT,RHA,RHB,BMAT
      COMMON CVXP(30),CVXM(30),CVYM(30),CVYP(30),CMTM(30),CMTP(30)
      COMMON CDELFI(30),CDELSI(30),CKS(30),CKF(30),KP(12,12),KM(12,12)
      COMMON AMAT(360,59),IMAT(12,12),IIMAT(12,12),IIIMAT(12,12)
      COMMON IVMAT(12,12),BMAT(360),RHA(12),RHB(12)
      COMMON RCP,RCM,RF,RS
      DO 10 I=1,6
         DO 10 J=1,6
            II=I+6
   10       IIIMAT(I,J)=KP(II,J)
      DO 20 I=7,12
```

```
          DO 20 J=7,12
             JJ=J-6
   20        IIIMAT(I,J)=KM(I,JJ)
       RETURN
       END
C
C
       SUBROUTINE ADD(MATA,MATB,MATSUM)
       DOUBLE PRECISION MATA(12,12),MATB(12,12),MATSUM(12 ,12)
       DO 10 I=1,12
          DO 10 J=1,12
   10        MATSUM(I,J)=MATA(I,J)+MATB(I,J)
       RETURN
       END

C
C AOLCOP - ELEMENT STIFFNESS MATRIX FOR COUPLED RING
       SUBROUTINE AOLCOP(RC,AREA,JX,JY,JXY,JT,E,G,DT,K)
       REAL*4 JX,JY,JXY,JT
       DOUBLE PRECISION A(12,12),K(12,12),WORK(12),DET(2),D(12,12)
       DOUBLE PRECISION T(2),PIE,R,AA,JYOAR2,JXYOJX,JXYOJY,P,Q,SS
       DOUBLE PRECISION U,V,S,C,TH,F
       DIMENSION IPVT(12)
       PIE=4.*DATAN(1.D+00)
       T(1)=1.
       T(2)=T(1)+DT
       R=RC
       AA=E*JX/G/JT
       JYOAR2=JY/AREA/R/R
       JXYOJX=JXY/JX
       JXYOJY=JXY/JY
       P=1./JXYOJX
       Q=0.5*(1.+1./AA)/JXYOJX
       SS=(1.+JYOAR2)/JXYOJX-JYOAR2*JXYOJY
       U=1./JXYOJY-JXYOJX
       V=(1.+1./AA)/JXYOJY-JXYOJX
       DO 10 I=1,12
          DO 10 J=1,12
             A(I,J)=0.
             K(I,J)=0.
   10        D(I,J)=0.
       F=1.
       DO 20 II=1,2
          TH=T(II)
          C=DCOS(TH)
          S=DSIN(TH)
          I=1+(II-1)*6
          A(I,3)=-Q*TH*C
          A(I,4)=Q*TH*S
          A(I,5)=-P*TH*S
          A(I,6)=-P*TH*C
          A(I,7)=P
          A(I,8)=-Q*TH*C
          A(I,9)=Q*TH*S
          A(I,10)=P*S
          A(I,11)=P*C
          I=I+1
          A(I,1)=1.
          A(I,2)=TH
          A(I,3)=S
          A(I,4)=C
          A(I,5)=TH*S
          A(I,6)=TH*C
          I=I+1
          A(I,3)=-Q*(C+TH*S)
          A(I,4)=Q*(S-TH*C)
```

```
          A(I,5)=-P*(S-TH*C)
          A(I,6)=-P*(C+TH*S)
          A(I,7)=SS*TH
          A(I,8)=-Q*(C+TH*S)
          A(I,9)=Q*(S-TH*C)
          A(I,11)=P*S
          A(I,10)=-P*C
          A(I,12)=1.
          I=I+1
          A(I,2)=1./R
          A(I,3)=C/R
          A(I,4)=-S/R
          A(I,5)=(TH*C+S)/R
          A(I,6)=(-TH*S+C)/R
          I=I+1
          A(I,3)=-2.*Q*C/R
          A(I,4)=2.*Q*S/R
          A(I,5)=-2.*P*S/R
          A(I,6)=-2.*P*C/R
          A(I,7)=SS*TH/R
          A(I,8)=-2.*Q*C/R
          A(I,9)=2.*Q*S/R
          A(I,12)=1./R
          I=I+1
          A(I,5)=-TH*S/R
          A(I,6)=-TH*C/R
          A(I,7)=1./R
          A(I,8)=S/R
          A(I,9)=C/R
          I=1+(II-1)*6
          D(I,3)=V*C*F/R
          D(I,4)=-V*S*F/R
          D(I,5)=2.*U*S*F/R
          D(I,6)=2.*U*C*F/R
          D(I,8)=V*C*F/R
          D(I,9)=-V*S*F/R
          I=I+1
          D(I,2)=-1.*F/R/AA
          I=I+1
          D(I,3)=V*S*F/R
          D(I,4)=V*C*F/R
          D(I,5)=-2.*U*C*F/R
          D(I,6)=2.*U*S*F/R
          D(I,8)=V*S*F/R
          D(I,9)=V*C*F/R
          I=I+1
          D(I,3)=-S*F/AA
          D(I,4)=-C*F/AA
          D(I,8)=-S*F/AA
          D(I,9)=-C*F/AA
          I=I+1
          D(I,3)=-V*S*F
          D(I,4)=-V*C*F
          D(I,5)=2.*U*C*F
          D(I,6)=-2.*U*S*F
          D(I,7)=-U*F
          D(I,8)=-V*S*F
          D(I,9)=-V*C*F
          I=I+1
          D(I,2)=-F/AA
          D(I,3)=-C*F/AA
          D(I,4)=S*F/AA
          D(I,8)=-C*F/AA
          D(I,9)=S*F/AA
          F=-1.
   20 CONTINUE
```

```
      CALL DGEFA(A,12,12,IPVT,INFO)
      WRITE(6,1) INFO
    1 FORMAT(1H ,I5)
      JOB=1
      CALL DGEDI(A,12,12,IPVT,DET,WORK,JOB)
      DO 30 I=1,12
         DO 30 J=1,12
            DO 40 JJ=1,12
   40          K(I,J)=K(I,J)+D(I,JJ)*A(JJ,J)
            K(I,J)=K(I,J)*E*JX/R**2
   30 CONTINUE
    2 FORMAT(1H ,6E12.4)
      RETURN
      END
C
C
      SUBROUTINE DAXPY(N,DA,DX,INCX,DY,INCY)
      DOUBLE PRECISION DX(1),DY(1),DA
      INTEGER I,INCX,INCY,IXIY,M,MP1,N
      IF(N.LE.0)RETURN
      IF (DA .EQ. 0.0D0) RETURN
      IF(INCX.EQ.1.AND.INCY.EQ.1)GO TO 20
      IX = 1
      IY = 1
      IF(INCX.LT.0)IX = (-N+1)*INCX + 1
      IF(INCY.LT.0)IY = (-N+1)*INCY + 1
      DO 10 I = 1,N
         DY(IY) = DY(IY) + DA*DX(IX)
         IX = IX + INCX
         IY = IY + INCY
   10 CONTINUE
      RETURN
   20 M = MOD(N,4)
      IF( M .EQ. 0 ) GO TO 40
      DO 30 I = 1,M
         DY(I) = DY(I) + DA*DX(I)
   30 CONTINUE
      IF( N .LT. 4 ) RETURN
   40 MP1 = M + 1
      DO 50 I = MP1,N,4
         DY(I) = DY(I) + DA*DX(I)
         DY(I + 1) = DY(I + 1) + DA*DX(I + 1)
         DY(I + 2) = DY(I + 2) + DA*DX(I + 2)
         DY(I + 3) = DY(I + 3) + DA*DX(I + 3)
   50 CONTINUE
      RETURN
      END
C
C
      INTEGER FUNCTION IDAMAX(N,DX,INCX)
      DOUBLE PRECISION DX(1),DMAX
      INTEGER I,INCX,IX,N
      IDAMAX = 0
      IF( N .LT. 1 ) RETURN
      IDAMAX = 1
      IF(N.EQ.1)RETURN
      IF(INCX.EQ.1)GO TO 20
      IX = 1
      DMAX = DABS(DX(1))
      IX = IX + INCX
      DO 10 I = 2,N
         IF(DABS(DX(IX)).LE.DMAX) GO TO 5
         IDAMAX = I
         DMAX = DABS(DX(IX))
    5    IX = IX + INCX
   10 CONTINUE
```

```
      RETURN
   20 DMAX = DABS(DX(1))
      DO 30 I = 2,N
         IF(DABS(DX(I)).LE.DMAX) GO TO 30
         IDAMAX = I
         DMAX = DABS(DX(I))
   30 CONTINUE
      RETURN
      END
C
C
      SUBROUTINE  DSCAL(N,DA,DX,INCX)
      DOUBLE PRECISION DA,DX(1)
      INTEGER I,INCX,M,MP1,N,NINCX
      IF(N.LE.0)RETURN
      IF(INCX.EQ.1)GO TO 20
      NINCX = N*INCX
      DO 10 I = 1,NINCX,INCX
         DX(I) = DA*DX(I)
   10 CONTINUE
      RETURN
   20 M = MOD(N,5)
      IF( M .EQ.  0 ) GO TO 40
      DO 30 I = 1,M
         DX(I) = DA*DX(I)
   30 CONTINUE
      IF( N .LT.  5 ) RETURN
   40 MP1 = M + 1
      DO 50 I = MP1,N,5
         DX(I) = DA*DX(I)
         DX(I + 1) = DA*DX(I + 1)
         DX(I + 2) = DA*DX(I + 2)
         DX(I + 3) = DA*DX(I + 3)
         DX(I + 4) = DA*DX(I + 4)
   50 CONTINUE
      RETURN
      END
C
C
      SUBROUTINE  DSWAP (N,DX,INCX,DY,INCY)
      DOUBLE PRECISION DX(1),DY(1),DTEMP
      INTEGER I,INCX,INCY,IX,IY,M,MP1,N
      IF(N.LE.0)RETURN
      IF(INCX.EQ.1.AND.INCY.EQ.1)GO TO 20
      IX = 1
      IY = 1
      IF(INCX.LT.0)IX = (-N+1)*INCX + 1
      IF(INCY.LT.0)IY = (-N+1)*INCY + 1
      DO 10 I = 1,N
         DTEMP = DX(IX)
         DX(IX) = DY(IY)
         DY(IY) = DTEMP
         IX = IX + INCX
         IY = IY + INCY
   10 CONTINUE
      RETURN
   20 M = MOD(N,3)
      IF( M .EQ.  0 ) GO TO 40
      DO 30 I = 1,M
         DTEMP = DX(I)
         DX(I) = DY(I)
         DY(I) = DTEMP
   30 CONTINUE
      IF( N .LT.  3 ) RETURN
   40 MP1 = M + 1
      DO 50 I = MP1,N,3
```

```
         DTEMP = DX(I)
         DX(I) = DY(I)
         DY(I) = DTEMP
         DTEMP = DX(I + 1)
         DX(I + 1) = DY(I + 1)
         DY(I + 1) = DTEMP
         DTEMP = DX(I + 2)
         DX(I + 2) = DY(I + 2)
         DY(I + 2) = DTEMP
   50 CONTINUE
      RETURN
      END
C
C
      SUBROUTINE DGEFA(A,LDA,N,IPVT,INFO)
      INTEGER LDA,N,IPVT(1),INFO
      DOUBLE PRECISION A(LDA,1)
      DOUBLE PRECISION T
      INTEGER IDAMAX,J,K,KP1,L,NM1
      INFO = 0
      NM1 = N - 1
      IF (NM1 .LT. 1) GO TO 70
      DO 60 K = 1, NM1
         KP1 = K + 1
         L = IDAMAX(N-K+1,A(K,K),1) + K - 1
         IPVT(K) = L
         IF (A(L,K) .EQ. 0.0D0) GO TO 40
         IF (L .EQ. K) GO TO 10
         T = A(L,K)
         A(L,K) = A(K,K)
         A(K,K) = T
   10    CONTINUE
         T = -1.0D0/A(K,K)
         CALL DSCAL(N-K,T,A(K+1,K),1)
         DO 30 J = KP1, N
            T = A(L,J)
            IF (L .EQ. K) GO TO 20
            A(L,J) = A(K,J)
            A(K,J) = T
   20       CONTINUE
            CALL DAXPY(N-K,T,A(K+1,K),1,A(K+1,J),1)
   30    CONTINUE
         GO TO 50
   40    CONTINUE
         INFO = K
   50    CONTINUE
   60 CONTINUE
   70 CONTINUE
      IPVT(N) = N
      IF (A(N,N) .EQ. 0.0D0) INFO = N
      RETURN
      END
C
C
      SUBROUTINE DGEDI(A,LDA,N,IPVT,DET,WORK,JOB)
      INTEGER LDA,N,IPVT(1),JOB
      DOUBLE PRECISION A(LDA,1),DET(2),WORK(1)
      DOUBLE PRECISION T
      DOUBLE PRECISION TEN
      INTEGER I,J,K,KB,KP1,L,NM1
      IF (JOB/10 .EQ. 0) GO TO 70
      DET(1) = 1.0D0
      DET(2) = 0.0D0
      TEN = 10.0D0
      DO 50 I = 1, N
         IF (IPVT(I) .NE. I) DET(1) = -DET(1)
```

```
            DET(1) = A(I,I)*DET(1)
            IF (DET(1) .EQ. 0.0D0) GO TO 60
   10       IF (DABS(DET(1)) .GE. 1.0D0) GO TO 20
            DET(1) = TEN*DET(1)
            DET(2) = DET(2) - 1.0D0
            GO TO 10
   20       CONTINUE
   30       IF (DABS(DET(1)) .LT. TEN) GO TO 40
            DET(1) = DET(1)/TEN
            DET(2) = DET(2) + 1.0D0
            GO TO 30
   40       CONTINUE
   50    CONTINUE
   60    CONTINUE
   70    CONTINUE
         IF (MOD(JOB,10) .EQ. 0) GO TO 150
         DO 100 K = 1, N
            A(K,K) = 1.0D0/A(K,K)
            T = -A(K,K)
            CALL DSCAL(K-1,T,A(1,K),1)
            KP1 = K + 1
            IF (N .LT. KP1) GO TO 90
            DO 80 J = KP1, N
               T = A(K,J)
               A(K,J) = 0.0D0
               CALL DAXPY(K,T,A(1,K),1,A(1,J),1)
   80       CONTINUE
   90       CONTINUE
  100    CONTINUE
         NM1 = N - 1
         IF (NM1 .LT. 1) GO TO 140
         DO 130 KB = 1, NM1
            K = N - KB
            KP1 = K + 1
            DO 110 I = KP1, N
               WORK(I) = A(I,K)
               A(I,K) = 0.0D0
  110       CONTINUE
            DO 120 J = KP1, N
               T = WORK(J)
               CALL DAXPY(N,T,A(1,J),1,A(1,K),1)
  120       CONTINUE
            L = IPVT(K)
            IF (L .NE. K) CALL DSWAP(N,A(1,K),1,A(1,L),1)
  130    CONTINUE
  140    CONTINUE
  150    CONTINUE
         RETURN
         END
C
C
         SUBROUTINE GAUSS(A,B,MBAND,NEQ)
C THIS SUBPROGRAM PERFORMS A GAUSS ELIMINATION
C ON A NON SYMMETRICAL BANDED MATRIX
         DOUBLE PRECISION A(6300),B(180),C,S
         NQ1=NEQ-1
         DO 10 I=1,NQ1
            I1=I+1
            I2=I+MBAND
            DO 20 II=I1,I2
               J=I
               K=(J-II+MBAND)*NEQ+II
               IF(A(K).EQ.0.) GO TO 20
               KK=(J-I+MBAND)*NEQ+I
               C=A(K)/A(KK)
               J1=J
```

```
            J2=J+MBAND
            IF(J2.GT.NEQ) J2=NEQ
            DO 40 JJ=J1,J2
               KKK=(JJ-II+MBAND)*NEQ+II
               KKKK=(JJ-I+MBAND)*NEQ+I
40             A(KKK)=A(KKK)-C*A(KKKK)
            B(II)=B(II)-C*B(I)
20       CONTINUE
10    CONTINUE
      K=MBAND*NEQ+NEQ
      B(NEQ)=B(NEQ)/A(K)
      DO 50 II=1,NQ1
         I=NEQ-II
         J1=I+1
         J2=I+MBAND
         S=0.
         IF(J2.GT.NEQ) J2=NEQ
         DO 60 J=J1,J2
            K=(J-I+MBAND)*NEQ+I
60          S=S+A(K)*B(J)
         KK=MBAND*NEQ+I
50       B(I)=(B(I)-S)/A(KK)
      RETURN
      END
```

Face Profiles

10	2.27	-13.95	-27.26	-24.34	-19.47	-3.57
20	18.17	34.40	31.48	34.07	29.21	12.98
30	-15.90	-8.44	-38.29	-11.68	-3.57	3.57
40	12.01	-1.30	5.52	-9.41	-7.14	-4.54
50	5.84	9.74	14.28	16.23	23.69	18.17
60	-151.22	-149.27	-144.73	-162.90	-160.30	-161.60
70	-159.01	-149.27	-144.08	-144.73	-155.11	-162.25
80	-163.55	-177.18	-182.37	-184.97	-190.16	-188.21
90	-178.48	-187.56	-189.51	-179.77	-164.20	-140.18
100	-128.50	-134.34	-137.59	-140.18	-146.67	-152.52

APPENDIX D

SECTION PROPERTIES PROGRAM

APPENDIX D

Section Properties Program

Program Description

The section properties program calculates the area, centroid, radius to centroid, section moments and torsional constant of ring cross sections. Line segments parallel to the x- and y-axes define the cross section.

To compute the area, centroid, and section moments, the program divides the cross section into a coarse mesh. The section corner points determine the element edges. The area is then found by summing the elemental areas and the centroid is computed from the area weighted average of the x and y values of the element centroids. The moments for the straight beam theory are:

$$I_x = \int y^2 \, dA$$

$$I_y = \int x^2 \, dA \qquad (1)$$

$$I_{xy} = \int_A xy \, dA$$

These are computed exactly by the program using the parallel axis theorem. The moments of inertia for curved beam theory are:

$$J_x = \int_A \frac{y^2}{1 - x/R} \, dA$$

$$J_y = \int_A \frac{x^2}{1 - x/R}\, dA \tag{2}$$

$$J_{xy} = \int_A \frac{xy}{1 - x/R}\, dA$$

These are also computed exactly.

To calculate the torsional constant, the program refines the mesh and then uses a finite difference scheme to solve the Poisson equation.

Program Input

The program requires that the cross section be oriented in an x-y coordinate system shown in the text. The x-coordinate is in the radial direction towards the center of curvature and the y-coordinate is in the axial direction. The following variables are input to the program:

XC--x-coordinates of the corner points. These must be input in clockwise order around the section.

YC--y-coordinates of the corner points. Their order must correspond to the x-coordinates.

RX1--Radius at first corner point

NC--Number of corner points

DXMAX--Maximum grid spacing desired in the x-direction for the refined mesh. The number of points along the x-direction must be 40 or less as the program is set up.

DYMAX--Maximum grid spacing desired in the y-direction

Sample Problem 1

The first sample problem is to find the section properties of the cross section shown in Figure D-1 using the program. The cross section is oriented in an x-y coordinate system as shown in Figure D-2. The corner point coordinates are

N	XC	YC
1	0.0	0.0
2	0.0	0.75
3	0.75	0.75
4	0.75	1.0
5	2.0	1.0
6	2.0	0.5
7	1.5	0.5
8	1.5	0.0
9	0.5	0.0
10	0.5	0.2
11	0.25	0.2
12	0.25	0.0

The radius at point 1 is 3.0 in and the chosen grid size is 0.2 in; so R x 1 = 3.0, NC = 12, DXMAX = 0.2, and DYMAX = 0.2.

The results are shown in the program output. The section properties matrix and the torsional properties matrix are representations of the element meshes. Each "1" identifies a solid element of the section.

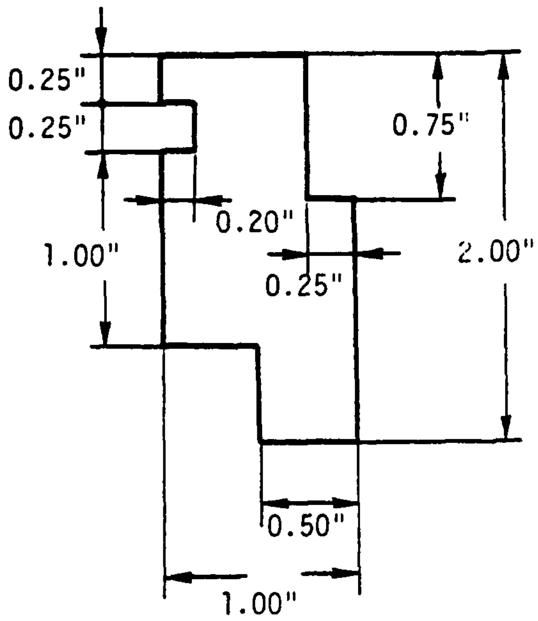

Figure D-1. Cross Section for First Sample Problem

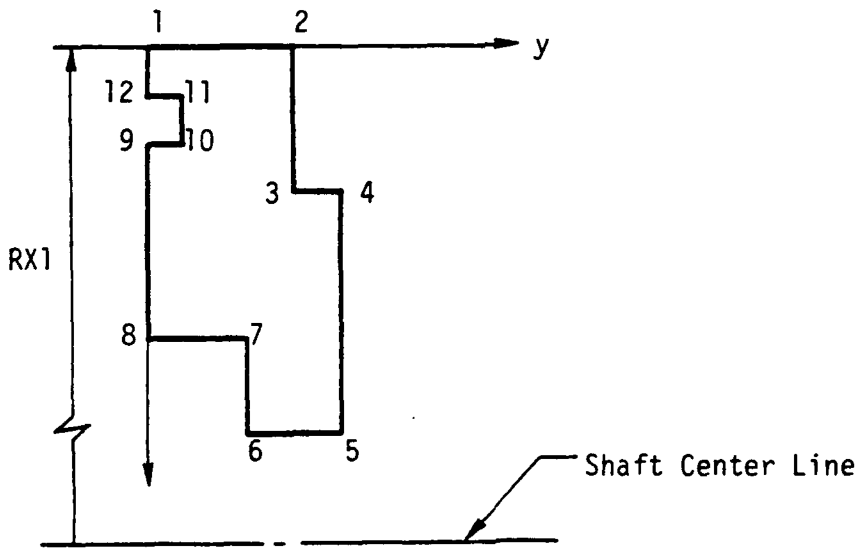

Figure D-2. Cross Section in Coordinate System.

Sample Problem 2

The second sample problem allows a comparison between the numerical and theoretical section property values. A rectangular section was used (Fig.D-3). The preparation of the program input is similar to the first problem.

The output is shown in the printout. The closed form solutions of equations (2) are obtained by integration. The section moments of inertia are:

$$J = - R \frac{\left(y_2^{\,3} - y_1^{\,3}\right)}{3} \quad \ln\left(\frac{R - x_2}{R - x_1}\right)$$

$$J_y = - (R^2)(y_2 - y_1) \left[\frac{1}{2}\frac{\left(x_2^{\,2} - x_1^2\right)}{R} + (x_2 - x_1) + R \ln\left(\frac{R - x_2}{R - x_1}\right)\right]$$

$$J_{xy} = - R\left(\frac{y_2^{\,2} - y_1^{\,2}}{2}\right)\left[(x_2 - x_1) + R \ln\left(\frac{R - x_2}{R - x_1}\right)\right]$$

Substituting in

$x_1 = -0.25$

$x_2 = 0.25$

$y_1 = -0.5$

$y_2 = 0.5$

$R = 2.5$

The moments of inertia are:

$J_x = 0.04181 \text{ in}^4$

$J_y = 0.01048 \text{ in}^4$

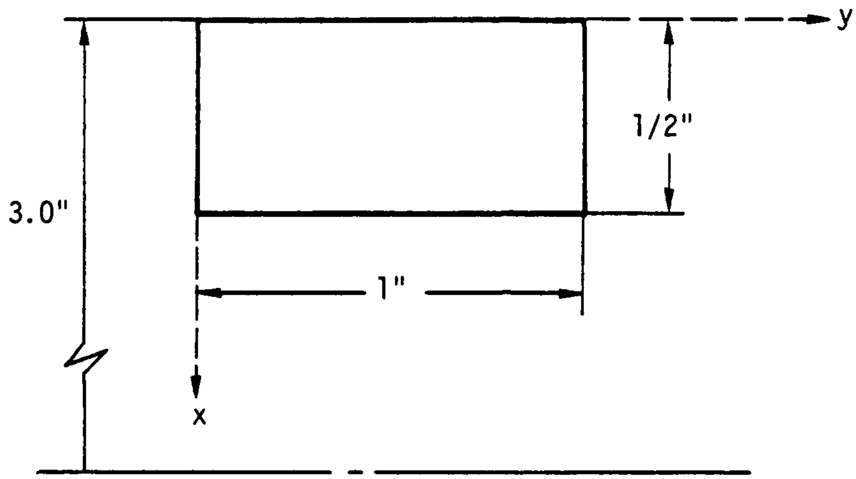

Figure D-3. Cross Section used for Comparing Numerical and Theoretical Section Moments.

$$J_{xy} = 0.0 \text{ in}^4$$

The expression for the torsion constant for a rectangular cross section is [38]

$$J = ab^3 \left[\frac{16}{3} - 3.36 \frac{b}{a} \left(1 - \frac{b^4}{12a^4} \right) \right]$$

where a and b are respectively half the length of the long and short sides of the rectangle. Substituting in

$$a = 0.5$$

$$b = 0.25$$

the torsion constant is

$$J = 0.02861 \text{ in}^4.$$

The numerical section moments of inertia are

$$J_x = 0.04178 \text{ in}^4$$

$$J_y = 0.01047 \text{ in}^4$$

$$J_{xy} = 0.0 \text{ in}^4$$

These agree to three significant figures with the theoretical results. The numerical torsion constant is 0.02776 in^4 which differs by approximately 3% from the theoretical result.

```
SECTION 07/10/84 14.12 41

SAMPLE PROBLEM 2


    INPUT GRID LOCATIONS
    XC
         0         0.        0.5000 0.5000 0.        0.        0.        0.        0.
         0         0.        0.        0.        0.        0.        0.        0.        0.
         0         0.        0.        0.
    YC
         0         1.0000 1.0000 0.        0.        0.        0.        0.        0.
         0         0.        0.        0.        0.        0.        0.        0.        0.
         0         0.        0.        0.

    ADJUSTED GRID LOCATIONS
    XG
         0.        0.5000
    YG
         0.        1.0000

    SECTION PROPERTIES MATRIX

     0 0 0
     0 1 0
     0 0 0

    [illegible]
    I = 0.4167E-01      I = 0.1042E-01     I = 0.0
    I = 0.4167E-01      I = 0.1047E-01     I = 0.0

    FINER MESH ADJUSTMENT
    XGP
         0         0.0455 0.0909 0.1364 0.1818 0.2273 0.2727 0.3182 0.3636
         0.4091 0.4545 0.5000
    YGP
         0.        0.0909 0.1818 0.2727 0.3636 0.4545 0.5455 0.6364 0.7273
         0.8182 0.9091 1.0000

    TORSIONAL PROPERTIES MATRIX

     0 0 0 0 0 0 0 0 0 0 0 0 0
     0 1 1 1 1 1 1 1 1 1 1 1 0
     0 1 1 1 1 1 1 1 1 1 1 1 0
     0 1 1 1 1 1 1 1 1 1 1 1 0
     0 1 1 1 1 1 1 1 1 1 1 1 0
     0 1 1 1 1 1 1 1 1 1 1 1 0
     0 1 1 1 1 1 1 1 1 1 1 1 0
     0 1 1 1 1 1 1 1 1 1 1 1 0
     0 1 1 1 1 1 1 1 1 1 1 1 0
     0 1 1 1 1 1 1 1 1 1 1 1 0
     0 1 1 1 1 1 1 1 1 1 1 1 0
     0 1 1 1 1 1 1 1 1 1 1 1 0
     0 0 0 0 0 0 0 0 0 0 0 0 0

    DIFFERENCE IN AREAS= 0.1103E-05

    JTHETA= 0.2778E-01
```

```
SECTION 07/20/84 14 24 43

SAMPLE PROBLEM 1


     INPUT GRID LOCATIONS
     XC.
          0.        0.        0.7500 0.7500 2.0000 2.0000 1.5000 1.5000 0.5000
          0.5000 0.2500 0.2500 0.        0.        0.        0.        0        0
          0.        0.        0.        0.
     YC.
          0.        0.7500 0.7500 1.0000 1.0000 0.5000 0.5000 0        0.
          0.2000 0.2000 0.        0.        0.        0.        0.        0.        0.
          0.        0.        0.        0.


     ADJUSTED GRID LOCATIONS
     XG.
          0.        0.2500 0.5000 0.7500 1.5000 2.0000
     YG.
          0.        0.2000 0.5000 0.7500 1.0000

     SECTION PROPERTIES MATRIX

      0 0 0 0 0 0
      0 1 1 1 0 0
      0 0 1 1 0 0
      0 1 1 1 0 0
      0 1 1 1 1 0
      0 0 0 1 1 0
      0 0 0 0 0 0

     AREA= 0.1512E+01    XBAR= 0.8742E+00    YBAR= 0.5081E+00    PI= 0.1026E+01
     IX= 0.1102E+00      IY= 0.4180E+00      IXY= 0.[illegible]E-01
     JX= 0.1123E+00      J = 0.4846E+00      JX = 0.1020E-0[illegible]

     FINER MESH ADJUSTMENT
     XGF:
          0.        0.1250 0.2500 0.3750 0.5000 0.6250 0.7500 0.9000 1.0500
          1.2000 1.3500 1.5000 1.6250 1.7500 1.8750 2.0000
     YGF:
          0.        0.1000 0.2000 0.3000 0.4000 0.5000 0.6250 0.7500 0.8750
          1.0000

     TORSIONAL PROPERTIES MATRIX

      0 0 0 0 0 0 0 0 0 0 0
      0 1 1 1 1 1 1 1 0 0 0
      0 1 1 1 1 1 1 1 0 0 0
      0 0 0 1 1 1 1 1 0 0 0
      0 0 0 1 1 1 1 1 0 0 0
      0 1 1 1 1 1 1 1 0 0 0
      0 1 1 1 1 1 1 1 0 0 0
      0 1 1 1 1 1 1 1 1 1 0
      0 1 1 1 1 1 1 1 1 1 0
      0 1 1 1 1 1 1 1 1 1 0
      0 1 1 1 1 1 1 1 1 1 0
      0 1 1 1 1 1 1 1 1 1 0
      0 0 0 0 0 0 1 1 1 1 0
      0 0 0 0 0 0 1 1 1 1 0
      0 0 0 0 0 0 1 1 1 1 0
      0 0 0 0 0 0 1 1 1 1 0
      0 0 0 0 0 0 0 0 0 0 0

     DIFFERENCE IN AREAS= 0.1144E-04

     JTHETA= 0.1754E+00


  STOP
  TIME 0.5 SECS
```

```
C SECTION PROPERTIES PROGRAM
C    THIS PROGRAM CALCULATES THE SECTION PROPERTIES OF
C    CROSS SECTIONS MADE UP OF ANY NUMBER OF LINE SEG-
C    MENTS PARALLEL TO THE X AND Y AXES.  (THE X-AXIS IS
C    IN THE RADIAL DIRECTION TOWARDS THE CENTER OF CURVA-
C    TURE AND THE Y-AXIS IS IN THE AXIAL DIRECTION.
C    THIS PROGRAM COMPUTES THE CROSS SECTIONAL AREA, THE
C    SECTION CENTROID AND THE RADIUS AT THE CENTROID.   IT
C    COMPUTES THE SECTION MOMENTS USING BOTH STRAIGHT BEAM
C    AND CURVED BEAM THEORY.   IT ALSO CALCULATES THE TOR-
C    SIONAL CONSTANT.
C
      DOUBLE PRECISION XG(22),YG(22),XGP(40),YGP(40),XC(22),YC(22)
      DOUBLE PRECISION AIM1(40,40),AIP1(40,40),AJM1(40,40),AJP1(40,40)
      DOUBLE PRECISION P(40,40),BRHS(40,40),POLD,VAL
      DIMENSION IEO(22),IGXC(22),JGYC(22),ISOLID(22,22),IGN(40)
      DIMENSION JGN(40),IPSOLI(40,40)
      DIMENSION  IFE(80),YFE(80)
      CALL OPSYS('ALLOC','FEDATA',7)
C
C INPUT THE COORDINATES OF THE CORNER POINTS IN CLOCKWISE
C ORDER.   THE STARTING POINT IS ARBITRARY.
      DATA XC/0.0,0.0,0.75,0.75,2.0,2.0,1.5,1.5,.5,.5,.25,.25/
      DATA YC/0.0,0.75,0.75,1.0,1.0,0.5,0.5,0.0,0.0,0.2,0.2,0.0/
C
C INPUT RADIUS AT X1 AND NUMBER OF CORNER POINTS
      RX1=3.0
      NC=12
      NSM=1
C
C INPUT GRID SIZE FOR FINER MESH
      [illegible]
      [illegible]
C
C SET UP THE GRID POINTS
      NG=NC/2
      DO 10 I=1,NG
         XG(I)=XC(2*I)
   10    YG(I)=YC(2*I)
C
C ARRANGE THE GRID POINTS IN INCREASING ORDER
      DO 20 II=1,NG
         IST=II
         AMIN=1.E+06
         DO 22 I=IST,NG
            IF (XG(I).GT.AMIN) GO TO 22
            AMIN=XG(I)
            J=I
   22    CONTINUE
         XTMP=XG(II)
         XG(II)=XG(J)
   20    XG(J)=XTMP
      DO 25 II=1,NG
         IST=II
         AMIN=1.E+06
         DO 27 I=IST,NG
            IF(YG(I).GT.AMIN) GO TO 27
            AMIN=YG(I)
            J=I
   27    CONTINUE
         YTMP=YG(II)
         YG(II)=YG(J)
   25    YG(J)=YTMP
C
```

```
C ELIMINATE EQUAL XG AND YG VALUES
      NGM1=NG-1
      IIEQ=0
      DO 30 I=1,NGM1
         IF(XG(I).NE.XG(I+1)) GO TO 30
         IIEQ=IIEQ+1
         IEQ(IIEQ)=I
   30 CONTINUE
      NGX=NG
      IF(IIEQ.EQ.0) GO TO 100
      DO 40 I=1,IIEQ
         NGX=NGX-1
         IST=IEQ(I)
         DO 50 II=IST,NGX
   50       XG(II)=XG(II+1)
   40 CONTINUE
  100 IIEQ=0
      DO 60 I=1,NGM1
         IF(YG(I).NE.YG(I+1)) GO TO 60
         IIEQ=IIEQ+1
         IEQ(IIEQ)=I
   60 CONTINUE
      NGY=NG
      IF(IIEQ.EQ.0) GO TO 200
      DO 70 I=1,IIEQ
         NGY=NGY-1
         IST=IEQ(I)
         DO 80 II=IST,NGY
   80       YG(II)=YG(II+1)
   70 CONTINUE
C
C MATCH CORNER POINTS WITH GRID POINTS
C IGXC(IC) IS GRID POINT CORRESPONDING TO CORNER POINT IC
  200 DO 90 IC=1,NC
         DO 90 IG=1,NGX
            IF(XC(IC).EQ.XG(IG)) IGXC(IC)=IG
   90 CONTINUE
      DO 95 JC=1,NC
         DO 95 JG=1,NGY
            IF(YC(JC).EQ.YG(JG)) JGYC(JC)=JG
   95 CONTINUE
C
C IDENTIFY THE VOID AND SOLID REGIONS
C I,J REFERS TO REGION WHICH IS ABOVE AND TO THE LEFT OF POINT I,J
C CODE: VOID-0, SOLID-1, UNASSIGNED-2
      NGXP1=NGX+1
      NGYP1=NGY+1
      DO 101 I=1,NGXP1
         DO 101 J=1,NGYP1
  101       ISOLID(I,J)=2
      DO 1000 M=1,NC
         N=M+1
         IF(M.EQ.NC) N=1
         IC=0
         IF(YC(N).GT.YC(M)) IC=1
         IF(XC(N).GT.XC(M)) IC=2
         IF(YC(N).LT.YC(M)) IC=3
         IF(XC(N).LT.XC(M)) IC=4
         GO TO (110,120,130,140),IC
  110    IN=IGXC(N)
         JN=JGYC(N)
         JM=JGYC(M)
         JM=JM+1
         DO 112 J=JM,JN
            ISOLID(IN,J)=0
  112       ISOLID(IN+1,J)=1
```

```
            GO TO 1000
  120       IM=IGXC(M)
            IM=IM+1
            JM=JGYC(M)
            IN=IGXC(N)
            DO 122 I=IM,IN
               ISOLID(I,JM)=1
  122          ISOLID(I,JM+1)=0
            GO TO 1000
  130       IN=IGXC(N)
            JN=JGYC(N)
            JN=JN+1
            JM=JGYC(M)
            DO 132 J=JN,JM
               ISOLID(IN,J)=1
  132          ISOLID(IN+1,J)=0
            GO TO 1000
  140       IN=IGXC(N)
            IN=IN+1
            JN=JGYC(N)
            IM=IGXC(M)
            DO 142 I=IN,IM
               ISOLID(I,JN)=0
  142          ISOLID(I,JN+1)=1
 1000 CONTINUE
C
C SET BOUNDARIES TO VOID
      DO 310 J=1,NGYP1
         ISOLID(1,J)=0
  310    ISOLID(NGXP1,J)=0
      DO 320 I=1,NGXP1
         ISOLID(I,1)=0
  320    ISOLID(I,NGYP1)=0
C
C USE Y SWEEP TO SET ALL OTHERS
      DO 400 I=2,NGX
         DO 410 J=1,NGYP1
            IF(ISOLID(I,J).NE.2) GO TO 410
            J1=J
            DO 420 JJ=J1,NGYP1
               IF(ISOLID(I,JJ).EQ.2) GO TO 420
               J2=JJ-1
               GO TO 430
  420       CONTINUE
            WRITE(6,31)
   31       FORMAT(1H ,'TROUBLE1')
  430       DO 415 JJ=J1,J2
  415          ISOLID(I,JJ)=ISOLID(I,J1-1)
  410    CONTINUE
  400 CONTINUE
C
C DETERMINE CENTROID LOCATION
      SMY=0.
      SMX=0.
      AREA=0
      DO 500 I=2,NGX
         DO 500 J=2,NGY
            ISOL=ISOLID(I,J)
            DA=(XG(I)-XG(I-1))*(YG(J)-YG(J-1))*ISOL
            AREA=AREA+DA
            X=(XG(I)+XG(I-1))*.5
            Y=(YG(J)+YG(J-1))*.5
            SMY=SMY+DA*X
  500       SMX=SMX+DA*Y
      XBAR=SMY/AREA
      YBAR=SMX/AREA
```

```
C
C DETERMINE SECTION MOMENTS
      AIX=0.0
      AIY=0.0
      AIXY=0.0
      AJX=0.0
      AJY=0.0
      AJXY=0.0
      RC=RX1+XC(1)-XBAR
      DO 510 I=2,NGX
         DO 510 J=2,NGY
            ISOL=ISOLID(I,J)
            DX=XG(I)-XG(I-1)
            DY=YG(J)-YG(J-1)
            DA=DX*DY
            X=(XG(I)+XG(I-1))*.5
            Y=(YG(J)+YG(J-1))*.5
            X=X-XBAR
            Y=Y-YBAR
            X1=X-DX*0.5
            X2=X+DX*0.5
            Y1=Y-DY*0.5
            Y2=Y+DY*0.5
            AIX=AIX+(DX*DY**3/12.+DA*Y*Y)*ISOL
            AIY=AIY+(DY*DX**3/12.+DA*X*X)*ISOL
            AIXY=AIXY+X*Y*DA*ISOL
            FACT=ALOG((RC-X2)/(RC-X1))
            AJX=AJX-RC*(Y2**3-Y1**3)/3.0*FACT*ISOL
            TERM1=0.5*(X2**2-X1**2)/RC
            TERM2=X2-X1+RC*ALOG((RC-X2)/(RC-X1))
            AJY=AJY-RC**2*(Y2-Y1)*(TERM1+TERM2)*ISOL
            TERM1=X2-X1+RC*ALOG((RC-X2)/(RC-X1))
            AJXY=AJXY-RC*(Y2**2-Y1**2)/2*TERM1*ISOL
  510 CONTINUE
C
C REFINE THE MESH
      JY=0
      IX=0
      NGXM1=NGX-1
      DO 540 I=1,NGXM1
         IGN(I)=(XG(I+1)-XG(I))/DXMAX+1.5
         DXUSED=(XG(I+1)-XG(I))/IGN(I)
         IGNI=IGN(I)
         IF(I.EQ.NGXM1) IGNI=IGNI+1
         DO 520 II=1,IGNI
            IX=IX+1
            XGR(IX)=XG(I)+DXUSED*(II-1)
  520    CONTINUE
  540 CONTINUE
      NGYM1=NGY-1
      DO 550 I=1,NGYM1
         JGN(I)=(YG(I+1)-YG(I))/DYMAX+1.5
         DYUSED=(YG(I+1)-YG(I))/JGN(I)
         JGNI=JGN(I)
         IF(I.EQ.NGYM1) JGNI=JGNI+1
         DO 530 JJ=1,JGNI
            JY=JY+1
            YGR(JY)=YG(I)+DYUSED*(JJ-1)
  530    CONTINUE
  550 CONTINUE
C
C SET ADDITIONAL MESH AREAS TO SOLID OR VOID.
      IXMAX=IX
      JYMAX=JY
      JBEG=1
      IBEG=1
```

```
      NFGXP1=IXMAX-1
      NFGYP1=JYMAX+1
      DO 560 II=1,NFGXP1
         DO 560 JJ=1,NFGYP1
560         IPSOLI(II,JJ)=0.
      DO 595 I=2,NGX
         JBEG=1
         DO 590 J=2,NGY
            IEND=IBEG+IGN(I-1)
            JEND=JBEG+JGN(J-1)
            IBEGP1=IBEG+1
            JBEGP1=JBEG+1
            IF(ISOLID(I,J).EQ.1) GO TO 570
            GO TO 590
570         CONTINUE
            DO 580 II=IBEGP1,IEND
               DO 580 JJ=JBEGP1,JEND
580               IPSOLI(II,JJ)=1
590         JBEG=JGN(J-1)+JBEG
595      IBEG=IGN(I-1)+IBEG
C
C CHECK TO SEE IF TOTAL AREA IS THE SAME.
      AREA2=0
      DO 700 I=2,IXMAX
         DO 700 J=2,JYMAX
            IPSOL=IPSOLI(I,J)
            DA=(XGP(I)-XGP(I-1))*(YGP(J)-YGP(J-1))*IPSOL
            AREA2=AREA2+DA
700 CONTINUE
      DIFF=AREA-AREA2
C
C PRINT OUT RESULTS
      WRITE (6,18)
   [illegible] FORMAT( [illegible] SAMPLE [illegible]
      WRITE(6,1)
    1 FORMAT( [illegible] INPUT GRID LOCATIONS [illegible]
      WRITE(6,2) XC
    2 FORMAT(9X,8F7.4)
      WRITE(6,3)
    3 FORMAT(5X,'YC')
      WRITE(6,2) YC
      WRITE(6,4)
    4 FORMAT(/,5X,'ADJUSTED GRID LOCATIONS',/,5X,'XG')
      WRITE(6,2) (XG(I),I=1,NGX)
      WRITE(6,5)
    5 FORMAT(5X,'YG')
      WRITE(6,2) (YG(I),I=1,NGY)
      WRITE(6,6)
    6 FORMAT(/,5X,'SECTION PROPERTIES MATRIX' [illegible]
      DO 7 I=1,NGXP1
    7 WRITE(6,8) (ISOLID(I,J),J=1,NGYP1)
    8 FORMAT(5X,40I2)
      WRITE(6,9) AREA,XBAR,YBAR, [illegible]
    9 FORMAT( [illegible] AREA=',E11.4, [illegible] XBAR=',E11.4,3X,'YBAR=
     *E11.4,3X,'RC=',E11.4,/,5X,'IX=',E11.4,5X,'IY=',E11.4,
     *5X,'IXY=',E11.4)
      WRITE (6,16) AJX,AJY,AJXY
   16 FORMAT (5X,'JX=',E11.4,5X,'JY=',E11.4,5X,'JXY=',E11.4)
      WRITE(6,11)
   11 FORMAT(/,5X,'FINER MESH ADJUSTMENT',/,5X,'XGP')
      WRITE(6,2) (XGP(I),I=1,IXMAX)
      WRITE(6,12)
   12 FORMAT(5X,'YGP')
      WRITE(6,2) (YGP(I),I=1,JYMAX)
      IF(NFGXP1.GT.40) GO TO 705
      WRITE(6,13)
```

```
   13 FORMAT(/,5X,'TORSIONAL PROPERTIES MATRIX',/)
      DO 14 I=1,NPGXP1
   14 WRITE(6,8) (IPSOLI(I,J),J=1,NPGYP1)
  705 CONTINUE
      WRITE(6,15) DIFF
   15 FORMAT(/,5X,'DIFFERENCE IN AREAS=',E11.4)
      WRITE(7,17)NDM,IXMAX,JYMAX,NPGXP1,NPGYP1,PX1,XC(1)
      WRITE(7,2) (XGP(I),I=1,IXMAX)
      WRITE(7,2) (YGP(J),J=1,JYMAX)
      DO 707 I=1,NPGXP1
         WRITE(7,8) (IPSOLI(I,J),J=1,NPGYP1)
  707 CONTINUE
   17 FORMAT(5I3,2F8.4)
C
C TORSIONAL CONSTANT CALCULATION USING FINITE DIFFERENCE
      ERR=.000001
      IMAXM1=IXMAX-1
      JMAXM1=JYMAX-1
      DO 710 I=2,IMAXM1
         DO 710 J=2,JMAXM1
               IPSOL=1
               IF(IPSOLI(I,J).EQ.0.OR.IPSOLI(I+1,J).EQ.0.OR.
     *            IPSOLI(I+1,J+1).EQ.0.OR.IPSOLI(I,J+1).EQ.0) IPSOL=0
            AIJ=-2./(XGP(I-1)-XGP(I))/(XGP(I+1)-XGP(I))
            AIJ=AIJ-2./(YGP(J-1)-YGP(J))/(YGP(J+1)-YGP(J))
            AIM1(I,J)=2./(XGP(I-1)-XGP(I))/(XGP(I-1)-XGP(I+1))/AIJ
     *               *IPSOL
            AIP1(I,J)=-2./(XGP(I+1)-XGP(I))/(XGP(I-1)-XGP(I+1))/AIJ
     *               *IPSOL
            AJM1(I,J)=2./(YGP(J-1)-YGP(J))/(YGP(J-1)-YGP(J+1))/AIJ
     *               *IPSOL
            AJP1(I,J)=-2./(YGP(J+1)-YGP(J))/(YGP(J-1)-YGP(J+1))/AIJ
     *               *IPSOL
            BRHS(I,J)=2./AIJ*IPSOL
  710 CONTINUE
      DO 720 I=1,IXMAX
         DO 720 J=1,JYMAX
  720       F(I,J)=0.
      OMEG=1.7
      OMO=1.-OMEG
      DO 740 IT=1,300
         AMAX=0.0
         DO 730 I=2,IXMAX
            DO 730 J=2,JYMAX
               POLD=F(I,J)
               PNEW=AIM1(I,J)*F(I-1,J)+AIP1(I,J)*F(I+1,J)
               PNEW=PNEW+AJM1(I,J)*F(I,J-1)+AJP1(I,J)*F(I,J+1)+BRHS(I,J)
               F(I,J)=PNEW*OMEG+OMO*POLD
               VAL=DABS((F(I,J)-POLD))
               IF(VAL.GT.AMAX) AMAX=VAL
  730    CONTINUE
         IF(AMAX.LT.ERR) GO TO 750
  740 CONTINUE
      WRITE(6,745) IT
  745 FORMAT(5X,'EXCEEDS ITERATIONS, IT=',I4)
  750 CONTINUE
C
C INTEGRATION ROUTINE
      AJ=0
      DO 760 I=1,IMAXM1
         DO 760 J=1,JMAXM1
            Z=F(I,J)+F(I+1,J)+F(I+1,J+1)+F(I,J+1)
            AJ=AJ+.25*Z*(XGP(I+1)-XGP(I))*(YGP(J+1)-YGP(J))
  760 CONTINUE
      AJ=2.*AJ
      AJO=AJ
      WRITE(6,770) AJO
  770 FORMAT(/,5X,'JTHETA=',E11.4//)
      STOP
      END
```

APPENDIX E

MESH GENERATING PROGRAM

APPENDIX E

Mesh Generating Program

Program Description

The mesh generating program develops a two-dimensional, finite element mesh for circular ring cross sections of the type just discussed. It reads the nodal locations from a data file, assigns node numbers, determines element connectivity, computes applied forces and outputs a data file which can be used with the finite element code SAPIV (or other codes with modification).

The input data file is created by the section properties program (Appendix D). It contains information about the number of nodes in the x- and y- directions and the nodal coordinates. The cross section geometry is also in the data file. Thus, the mesh generating program reads the nodal coordinates and assigns node numbers to the nodes. It numbers in the shortest direction to minimize the stiffness matrix bandwidth. SAPIV requires the y-coordinates to be in the radial direction and the z-coordinate to be in the axial direction, so the program transforms the x-y-coordinates to the y-z-coordinate system.

Using the cross section geometry information, the program next develops the element connectivity. The node and element information is written to the output file.

Next, the applied loads data are input interactively. The program gives the choice of inputting loads at individual nodes or applying pressure loads on surfaces.

The program properly formats this information and writes it to the output file.

Program Input

Much of the program input is created by the section properties program and instructions for that program should be followed. After the mesh generating program reads the input file and assigns node and element numbers, it prints out node and element maps. These maps are then used for the following interactive input:

Constrained nodes: The program asks for the number of constrained nodes, the node numbers, and the directions in which they are constrained (y-z coordinates).

Applied loads: The program asks whether loads will be applied as concentrated loads to individual nodes (manual input) or as pressure loads to surfaces. For manual input, the program asks for the number of loaded nodes, the node numbers, the magnitude of the force and the direction (radial or axial) of the force. For pressure loading, the program asks for the applied pressure and the number of surfaces to which the pressure is applied. Then, for each surface, the program asks for the number of nodes on the surface, the direction in which the pressure acts and the node numbers on the surface.

A face pressure may also be calculated. This is the pressure on the sealing face and is assumed to vary linearly from the applied pressure to zero across the width of the face. Again,

the program asks for the number of nodes on the face, the direction in which the pressure acts, and the node numbers.

Sample Problem

The cross section shown in Figure E-1 is considered as a sample problem. It is a segment from an infinitely long cylinder which has an external pressure of 300 psi applied to it. This problem allows comparison between the numerical and theoretical stress distributions. The input file created by the section properties program is shown and the program run with interactive input underlined is shown next. The data file created by the program and the program listing are shown after that.

Results

The theoretical stress distribution of a pressurized thick-walled pressure vessel is [1]

$$\sigma_r = \frac{r_o^2 r_i^2}{r_o^2 - r_i^2}(p_o - p_i)\frac{1}{r^2} + \frac{p_i r_i^2 - p_o r_o^2}{r_o^2 - r_i^2}$$

$$\sigma_\theta = -\frac{r_o r_i^2}{r_o^2 - r_i^2}(p_o + p_i)\frac{1}{r^2} + \frac{p_i r_i^2 - p_o r_o^2}{r_o^2 - r_i^2}$$

where

σ_r = radial stress distribution

σ_θ = hoop (tangential) stress distribution

---

1 Oden, J. T., Ripperrrger, E. A. Mechanics of Elastic Structures. McGraw-Hill, 1981, p. 91.

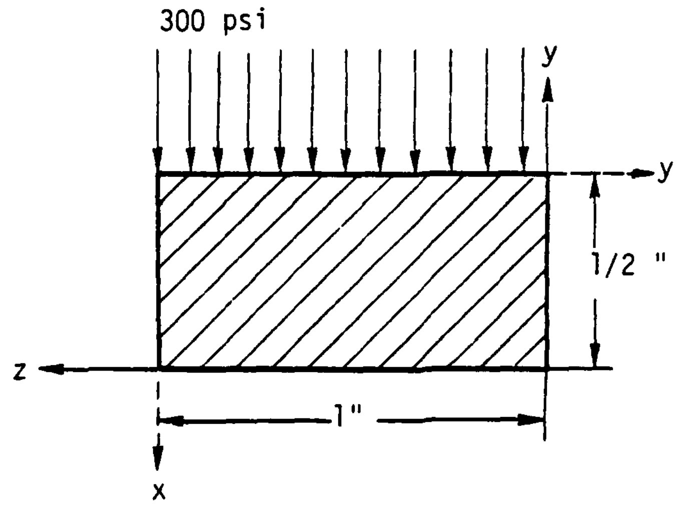

Figure E-1. Sample Cross Section.

r_o = outside radius (3.0 in)

r_i = inside radius (2.5 in)

r = radial distance

p_o = outside pressure (300 psi)

p_i = inside pressure (0. psi)

Using the data set created, the SAPIV program was run and comparisons of the theoretical and numerical stress distributions are shown in Figures E-2 and E-3.

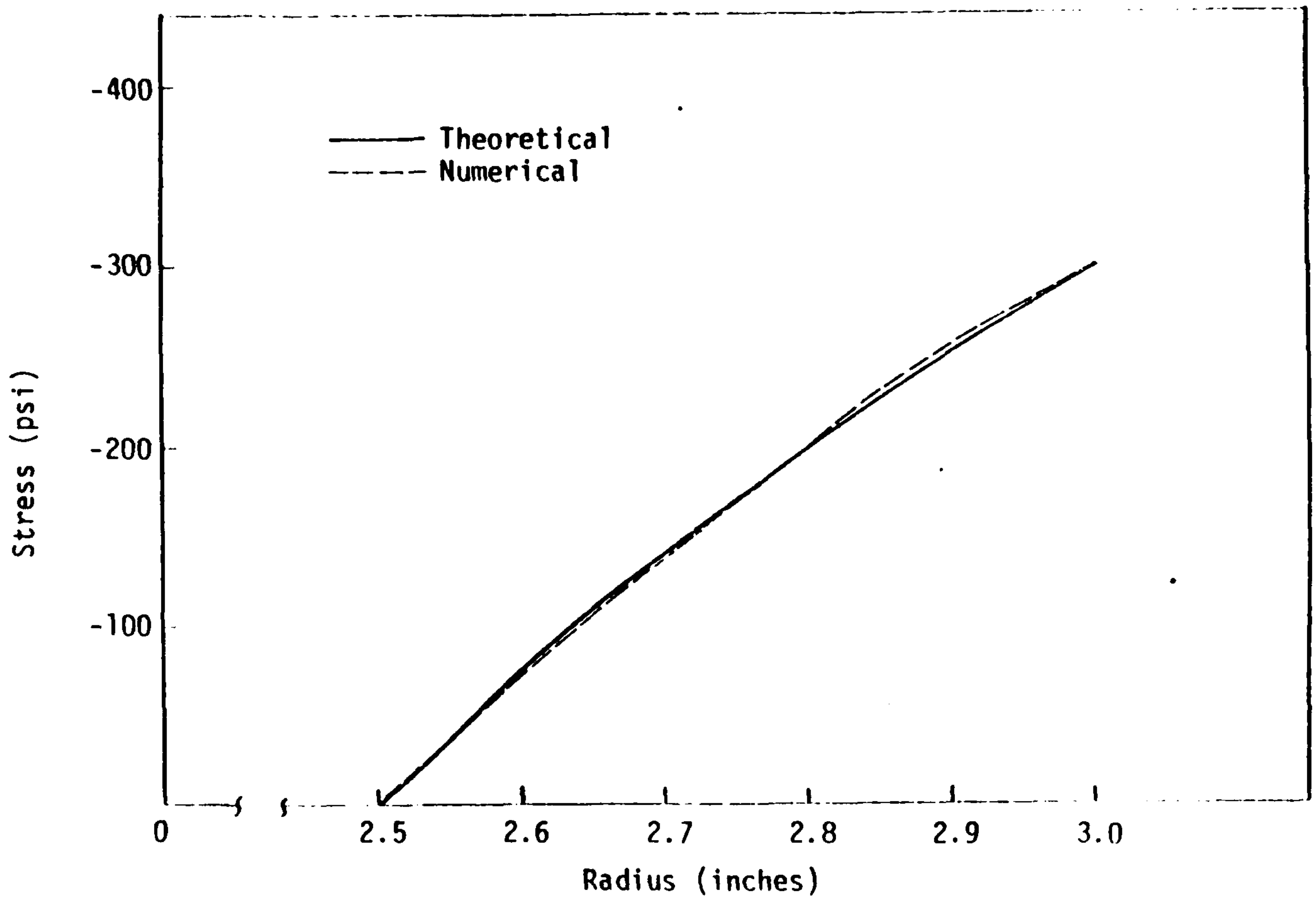

Figure E-2. Radial Stress Distribution (σ_r, S11)

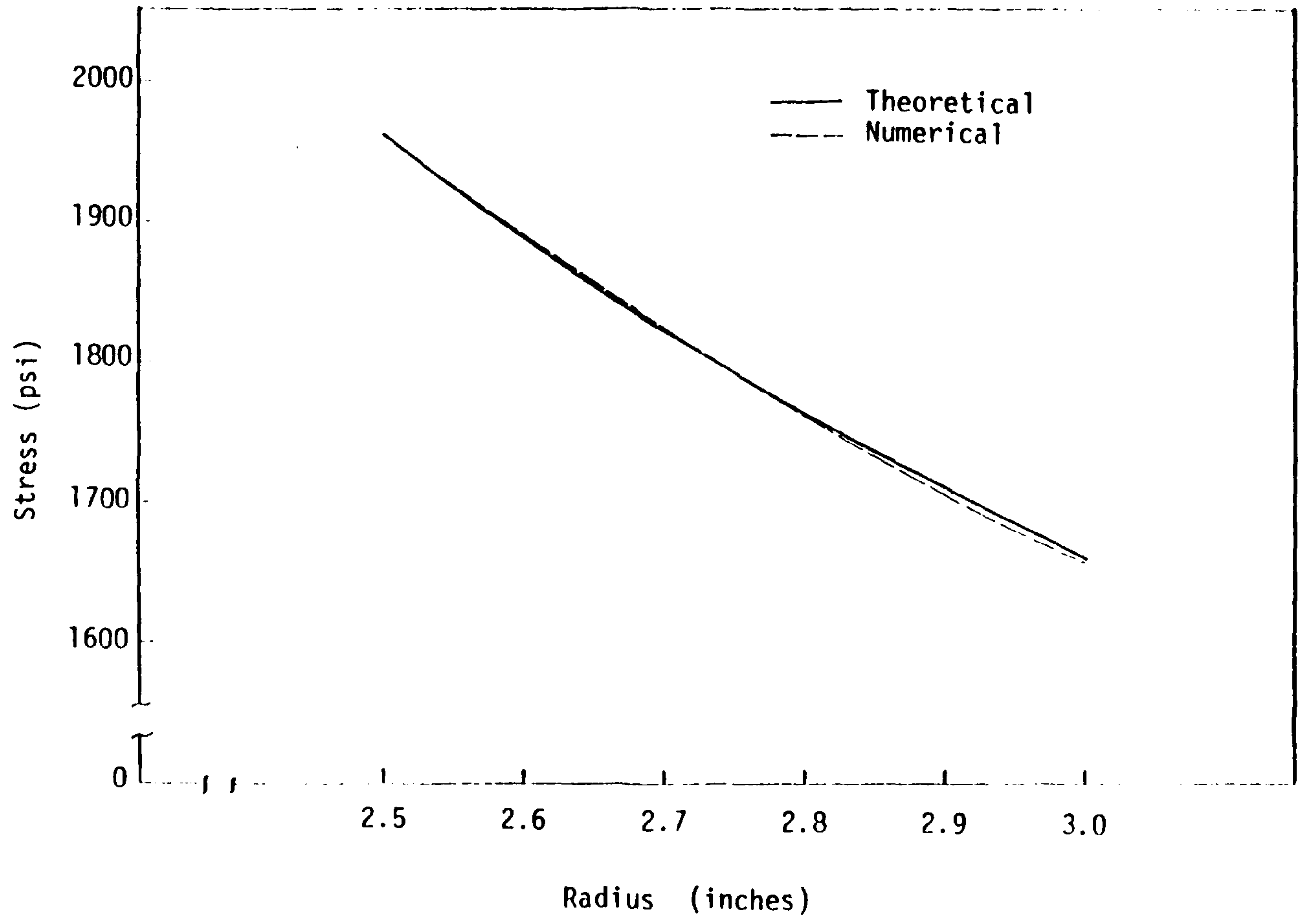

Figure E-3. Hoop Stress Distribution (σ_θ, 533)

Input File Created by the Section Properties Program

```
 1 12 12 13 13   3.0000   0.
          0.       0.0455 0.0909 0.1364 0.1818 0.2273 0.2727 0.3182 0.3636
          0.4091   0.4545 0.5000
          0.       0.0909 0.1818 0.2727 0.3636 0.4545 0.5455 0.6364 0.7273
          0.8182   0.9091 1.0000
      0 0 0 0 0 0 0 0 0 0 0 0 0
      0 1 1 1 1 1 1 1 1 1 1 1 0
      0 1 1 1 1 1 1 1 1 1 1 1 0
      0 1 1 1 1 1 1 1 1 1 1 1 0
      0 1 1 1 1 1 1 1 1 1 1 1 0
      0 1 1 1 1 1 1 1 1 1 1 1 0
      0 1 1 1 1 1 1 1 1 1 1 1 0
      0 1 1 1 1 1 1 1 1 1 1 1 0
      0 1 1 1 1 1 1 1 1 1 1 1 0
      0 1 1 1 1 1 1 1 1 1 1 1 0
      0 1 1 1 1 1 1 1 1 1 1 1 0
      0 1 1 1 1 1 1 1 1 1 1 1 0
      0 0 0 0 0 0 0 0 0 0 0 0 0
```

Program Run with Interactive Input

```
FEMESH 07/20/84 11.11.20

    NODE MAP:

  1  13  25  37  49  61  73  85  97 109 121 133
  2  14  26  38  50  62  74  86  98 110 122 134
  3  15  27  39  51  63  75  87  99 111 123 135
  4  16  28  40  52  64  76  88 100 112 124 136
  5  17  29  41  53  65  77  89 101 113 125 137
  6  18  30  42  54  66  78  90 102 114 126 138
  7  19  31  43  55  67  79  91 103 115 127 139
  8  20  32  44' 56  68  80  92 104 116 128 140
  9  21  33  45  57  69  81  93 105 117 129 141
 10  22  34  46  58  70  82  94 106 118 130 142
 11  23  35  47  59  71  83  95 107 119 131 143
 12  24  36  48  60  72  84  96 108 120 132 144

    ELEMENT MAP:

  1  12  23  34  45  56  67  78  89 100 111
  2  13  24  35  46  57  68  79  90 101 112
  3  14  25  36  47  58  69  80  91 102 113
  4  15  26  37  48  59  70  81  92 103 114
  5  16  27  38  49  60  71  82  93 104 115
  6  17  28  39  50  61  72  83  94 105 116
  7  18  29  40  51  62  73  84  95 106 117
  8  19  30  41  52  63  74  85  96 107 118
  9  20  31  42  53  64  75  86  97 108 119
 10  21  32  43  54  65  76  87  98 109 120
 11  22  33  44  55  66  77  88  99 110 121

    HOW MANY NODES ARE CONSTRAINED?
?1

    INPUT FIXED NODES IN ASCENDING ORDER  .  AND DIRECTION. X=1, Y=2 BOTH=3
[illegible]

    DO YOU WANT TO MANUALLY INPUT LOADS? YES=1, NO=0
?0

    WHAT IS THE PRESSURE?
?100.0

    HOW MANY SURFACES HAVE PRESSURE? EXCLUDE SEALING FACE
?1

    SURFACE # 1

    HOW MANY NODES IN THIS SURFACE?
?11

    WHICH DIRECTION IS PRESSURE ACTING?
    +X=1, +Y=2, -X=3, -Y=4
?1

    INPUT NODES (ONE AT A TIME IN ORDER)
[illegible]

    IS A FACE PRESSURE TO BE CALCULATED? YES=1,NO=0
?0
STOP
TIME 0.3 SECS
```

Card Image Format Data File for SAPIV

```
 **** HOOP STRESS CALCULATION ****
 144    1    1    0    0    0    0    0
   1    1    0    1    1    1    1    0.          3.0000     1.0000     0   0.
   2    1    0    1    1    1    1    0.          2.9545     1.0000     0   0.
   3    1    0    1    1    1    1    0.          2.9091     1.0000     0   0.
   4    1    0    1    1    1    1    0.          2.8636     1.0000     0   0.
   5    1    0    1    1    1    1    0.          2.8182     1.0000     0   0
   6    1    0    1    1    1    1    0.          2.7727     1.0000     0   0.
   7    1    0    1    1    1    1    0.          2.7273     1.0000     0   0.
   8    1    0    1    1    1    1    0.          2.6818     1.0000     0   0
   9    1    0    1    1    1    1    0.          2.6364     1.0000     0   0.
  10    1    0    1    1    1    1    0.          2.5909     1.0000     0   0.
  11    1    0    1    1    1    1    0.          2.5455     1.0000     0   0.
  12    1    0    1    1    1    1    0.          2.5000     1.0000     0   0
  13    1    0    0    1    1    1    0.          3.0000     0.9091     0   0.
  14    1    0    0    1    1    1    0.          2.9545     0.9091     0   0.
  15    1    0    0    1    1    1    0.          2.9091     0.9091     0   0.
  16    1    0    0    1    1    1    0.          2.8636     0.9091     0   0.
  17    1    0    0    1    1    1    0.          2.8182     0.9091     0   0.
  18    1    0    0    1    1    1    0.          2.7727     0.9091     0   0.
  19    1    0    0    1    1    1    0.          2.7273     0.9091     0   0.
  20    1    0    0    1    1    1    0.          2.6818     0.9091     0   0.
  21    1    0    0    1    1    1    0.          2.6364     0.9091     0   0.
  22    1    0    0    1    1    1    0.          2.5909     0.9091     0   0.
  23    1    0    0    1    1    1    0.          2.5455     0.9091     0   0.
  24    1    0    0    1    1    1    0.          2.5000     0.9091     0   0.
  25    1    0    0    1    1    1    0.          3.0000     0.8182     0   0.
  26    1    0    0    1    1    1    0.          2.9545     0.8182     0   0.
  27    1    0    0    1    1    1    0.          2.9091     0.8182     0   0.
  28    1    0    0    1    1    1    0.          2.8636     0.8182     0   0
  29    1    0    0    1    1    1    0.          2.8182     0.8182     0   0.
  30    1    0    0    1    1    1    0.          2.7727     0.8182     0   0.
  31    1    0    0    1    1    1    0.          2.7273     0.8182     0   0.
  32    1    0    0    1    1    1    0.          2.6818     0.8182     0   0.
  33    1    0    0    1    1    1    0.          2.6364     0.8182     0   0.
  34    1    0    0    1    1    1    0.          2.5909     0.8182     0   0
  35    1    0    0    1    1    1    0.          2.5455     0.8182     0   0.
  36    1    0    0    1    1    1    0.          2.5000     0.8182     0   0.
  37    1    0    0    1    1    1    0.          3.0000     0.7273     0   0.
  38    1    0    0    1    1    1    0.          2.9545     0.7273     0   0.
  39    1    0    0    1    1    1    0.          2.9091     0.7273     0   0.
  40    1    0    0    1    1    1    0.          2.8636     0.7273     0   0
  41    1    0    0    1    1    1    0.          2.8182     0.7273     0   0
  42    1    0    0    1    1    1    0           2.7727     0.7273     0   0.
  43    1    0    0    1    1    1    0.          2.7273     0.7273     0   0
  44    1    0    0    1    1    1    0.          2.6818     0.7273     0   0
  45    1    0    0    1    1    1    0           2.6364     0.7273     0   0
  46    1    0    0    1    1    1    0.          2.5909     0.7273     0   0
  47    1    0    0    1    1    1    0.          2.5455     0.7273     0   0
  48    1    0    0    1    1    1    0.          2.5000     0.7273     0   0
  49    1    0    0    1    1    1    0.          3.0000     0.6364     0   0.
  50    1    0    0    1    1    1    0.          2.9545     0.6364     0   0.
  51    1    0    0    1    1    1    0.          2.9091     0.6364     0   0.
  52    1    0    0    1    1    1    0.          2.8636     0.6364     0   0
  53    1    0    0    1    1    1    0.          2.8182     0.6364     0   0.
  54    1    0    0    1    1    1    0.          2.7727     0.6364     0   0.
  55    1    0    0    1    1    1    0           2.7273     0.6364     0   0.
  56    1    0    0    1    1    1    0.          2.6818     0.6364     0   0.
  57    1    0    0    1    1    1    0.          2.6364     0.6364     0   0
  58    1    0    0    1    1    1    0.          2.5909     0.6364     0   0.
  59    1    0    0    1    1    1    0.          2.5455     0.6364     0   0.
  60    1    0    0    1    1    1    0.          2.5000     0.6364     0   0
  61    1    0    0    1    1    1    0           3.0000     0.5455     0   0.
```

64	62	1	0	0	1	1	1	0.	2.9545	0.5455	0	0.
65	63	1	0	0	1	1	1	0.	2.9091	0.5455	0	0.
66	64	1	0	0	1	1	1	0.	2.8636	0.5455	0	0.
67	65	1	0	0	1	1	1	0.	2.8182	0.5455	0	0.
68	66	1	0	0	1	1	1	0.	2.7727	0.5455	0	0.
69	67	1	0	0	1	1	1	0.	2.7273	0.5455	0	0.
70	68	1	0	0	1	1	1	0.	2.6818	0.5455	0	0.
71	69	1	0	0	1	1	1	0.	2.6364	0.5455	0	0.
72	70	1	0	0	1	1	1	0.	2.5909	0.5455	0	0.
73	71	1	0	0	1	1	1	0.	2.5455	0.5455	0	0.
74	72	1	0	0	1	1	1	0.	2.5000	0.5455	0	0.
75	73	1	0	0	1	1	1	0.	3.0000	0.4545	0	0.
76	74	1	0	0	1	1	1	0.	2.9545	0.4545	0	0.
77	75	1	0	0	1	1	1	0.	2.9091	0.4545	0	0.
78	76	1	0	0	1	1	1	0.	2.8636	0.4545	0	0.
79	77	1	0	0	1	1	1	0.	2.8182	0.4545	0	0.
80	78	1	0	0	1	1	1	0.	2.7727	0.4545	0	0.
81	79	1	0	0	1	1	1	0.	2.7273	0.4545	0	0.
82	80	1	0	0	1	1	1	0.	2.6818	0.4545	0	0.
83	81	1	0	0	1	1	1	0.	2.6364	0.4545	0	0.
84	82	1	0	0	1	1	1	0.	2.5909	0.4545	0	0.
85	83	1	0	0	1	1	1	0.	2.5455	0.4545	0	0.
86	84	1	0	0	1	1	1	0.	2.5000	0.4545	0	0.
87	85	1	0	0	1	1	1	0.	3.0000	0.3636	0	0.
88	86	1	0	0	1	1	1	0.	2.9545	0.3636	0	0.
89	87	1	0	0	1	1	1	0.	2.9091	0.3636	0	0.
90	88	1	0	0	1	1	1	0.	2.8636	0.3636	0	0.
91	89	1	0	0	1	1	1	0.	2.8182	0.3636	0	0.
92	90	1	0	0	1	1	1	0.	2.7727	0.3636	0	0.
93	91	1	0	0	1	1	1	0.	2.7273	0.3636	0	0.
94	92	1	0	0	1	1	1	0.	2.6818	0.3636	0	0.
95	93	1	0	0	1	1	1	0.	2.6364	0.3636	0	0.
96	94	1	0	0	1	1	1	0.	2.5909	0.3636	0	0.
[illegible]	[illegible]	1	[illegible]	[illegible]	1	1	1	[illegible]	[illegible]	[illegible]	[illegible]	[illegible]
[illegible]	[illegible]	1	0	0	1	1	1	[illegible]	[illegible]	[illegible]	[illegible]	[illegible]
[illegible]	[illegible]	1	[illegible]	[illegible]	1	1	1	[illegible]	[illegible]	[illegible]	[illegible]	[illegible]
100	98	1	0	0	1	1	1	0.	2.9545	0.2727	[illegible]	0.
101	99	1	0	0	1	1	1	0.	2.9091	0.2727	[illegible]	[illegible]
102	100	1	0	0	1	1	1	0.	2.8636	0.2727	0	0.
103	101	1	0	0	1	1	1	0.	2.8182	0.2727	0	0.
104	102	1	0	0	1	1	1	0.	2.7727	0.2727	0	0.
105	103	1	0	0	1	1	1	0.	2.7273	0.2727	0	0.
106	104	1	0	0	1	1	1	0.	2.6818	0.2727	0	0.
107	105	1	0	0	1	1	1	0.	2.6364	0.2727	0	0.
108	106	1	0	0	1	1	1	0.	2.5909	0.2727	[illegible]	[illegible]
109	107	1	0	0	1	1	1	0.	2.5455	0.2727	[illegible]	[illegible]
110	108	1	0	[illegible]	1	1	1	[illegible]	2.5000	0.2727	[illegible]	[illegible]
[illegible]	[illegible]	1	[illegible]	[illegible]	1	1	1	[illegible]	[illegible]	[illegible]	[illegible]	[illegible]
[illegible]	[illegible]	1	[illegible]	[illegible]	1	1	1	[illegible]	[illegible]	[illegible]	[illegible]	[illegible]
[illegible]	[illegible]	1	[illegible]	[illegible]	1	1	1	[illegible]	[illegible]	[illegible]	[illegible]	[illegible]
[illegible]	[illegible]	1	[illegible]	[illegible]	1	1	1	[illegible]	[illegible]	[illegible]	[illegible]	[illegible]
[illegible]	[illegible]	1	[illegible]	[illegible]	1	1	1	[illegible]	[illegible]	[illegible]	[illegible]	[illegible]
[illegible]	[illegible]	1	[illegible]	[illegible]	1	1	1	[illegible]	[illegible]	[illegible]	[illegible]	[illegible]
[illegible]	[illegible]	1	[illegible]	[illegible]	1	1	1	[illegible]	[illegible]	[illegible]	[illegible]	[illegible]
[illegible]	[illegible]	1	[illegible]	[illegible]	1	1	1	[illegible]	[illegible]	[illegible]	[illegible]	[illegible]
[illegible]	[illegible]	1	[illegible]	[illegible]	1	1	1	[illegible]	[illegible]	[illegible]	[illegible]	[illegible]
[illegible]	[illegible]	1	[illegible]	[illegible]	1	1	1	[illegible]	[illegible]	[illegible]	[illegible]	[illegible]
[illegible]	[illegible]	1	[illegible]	[illegible]	1	1	1	[illegible]	[illegible]	[illegible]	[illegible]	[illegible]
[illegible]	[illegible]	1	[illegible]	[illegible]	1	1	1	[illegible]	[illegible]	[illegible]	[illegible]	[illegible]
[illegible]	[illegible]	1	[illegible]	[illegible]	1	1	1	[illegible]	[illegible]	0.0909	[illegible]	[illegible]
[illegible]	[illegible]	1	[illegible]	[illegible]	1	1	1	[illegible]	[illegible]	[illegible]	[illegible]	[illegible]
[illegible]	[illegible]	1	[illegible]	[illegible]	1	1	1	[illegible]	[illegible]	[illegible]	[illegible]	[illegible]
[illegible]	[illegible]	1	[illegible]	[illegible]	1	1	1	[illegible]	[illegible]	[illegible]	[illegible]	[illegible]
[illegible]	[illegible]	1	[illegible]	[illegible]	1	1	1	[illegible]	[illegible]	[illegible]	[illegible]	[illegible]
[illegible]	[illegible]	1	[illegible]	[illegible]	1	1	1	[illegible]	[illegible]	[illegible]	[illegible]	[illegible]
[illegible]	[illegible]	1	[illegible]	[illegible]	1	1	1	[illegible]	[illegible]	[illegible]	[illegible]	[illegible]

[illegible]	[illegible]	[illegible]	[illegible]	[illegible]	[illegible]	[illegible]	[illegible]	[illegible]	[illegible]	[illegible]	[illegible]	[illegible]	[illegible]
[illegible]	[illegible]	[illegible]	[illegible]	[illegible]	[illegible]	[illegible]	[illegible]	[illegible]	[illegible]	[illegible]	[illegible]	[illegible]	[illegible]
[illegible]	[illegible]	1	[illegible]	[illegible]	[illegible]	[illegible]	[illegible]	0.	2.[illegible]	[illegible]	[illegible]	[illegible]	[illegible]
[illegible]	[illegible]	1	[illegible]	[illegible]	[illegible]	[illegible]	[illegible]	0.	1.5455	0.	[illegible]	[illegible]	[illegible]
134	[illegible]	1	0	0	1	1	1	0.	[illegible]	0.	0909	[illegible]	[illegible]
135	133	1	0	0	1	1	1	0.	3.0000	0.		[illegible]	0.
136	134	1	0	0	1	1	1	0.	2.9545	0.		0	[illegible]
137	135	1	0	0	1	1	1	[illegible]	2.[illegible]	0.		0	[illegible]
[illegible]	136	1	0	0	[illegible]	1	1	0.	2.[illegible]	0.		[illegible]	[illegible]
139	[illegible]	1	[illegible]	0	1	1	1	0.	2.[illegible]	0.		[illegible]	[illegible]
140	[illegible]	1	[illegible]	[illegible]	1	1	1	0.	[illegible]	[illegible]		[illegible]	[illegible]
141	[illegible]	1	[illegible]	[illegible]	1	1	1	[illegible]	[illegible]	[illegible]		[illegible]	[illegible]
[illegible]	[illegible]	1	[illegible]	[illegible]	1	1	1	[illegible]	[illegible]	[illegible]		[illegible]	[illegible]
[illegible]	[illegible]	1	[illegible]	[illegible]	1	1	1	[illegible]	[illegible]	[illegible]		[illegible]	[illegible]
144	[illegible]	1	[illegible]	[illegible]	1	1	1	[illegible]	[illegible]	[illegible]		[illegible]	[illegible]
[illegible]	[illegible]	1	[illegible]	[illegible]	1	1	1	[illegible]	[illegible]	[illegible]		[illegible]	[illegible]
[illegible]	[illegible]	1	[illegible]	[illegible]	1	1	1	0.	1.5000	0.		[illegible]	[illegible]

[illegible]

88.8

[illegible]

E13

195	41	57	56	44	45	1	0.	0.	20	1	1.0
196	42	58	57	45	46	1	0.	0.	20	1	1.0
197	43	59	58	46	47	1	0.	0.	20	1	1.0
198	44	60	59	47	48	1	0.	0.	20	1	1.0
199	45	62	61	49	50	1	0.	0.	20	1	1.0
200	46	63	62	50	51	1	0.	0.	20	1	1.0
201	47	64	63	51	52	1	0.	0.	20	1	1.0
202	48	65	64	52	53	1	0.	0.	20	1	1.0
203	49	66	65	53	54	1	0.	0.	20	1	1.0
204	50	67	66	54	55	1	0.	0.	20	1	1.0
205	51	68	67	55	56	1	0.	0.	20	1	1.0
206	52	69	68	56	57	1	0.	0.	20	1	1.0
207	53	70	69	57	58	1	0.	0.	20	1	1.0
208	54	71	70	58	59	1	0.	0.	20	1	1.0
209	55	72	71	59	60	1	0.	0.	20	1	1.0
210	56	74	73	61	62	1	0.	0.	20	1	1.0
211	57	75	74	62	63	1	0.	0.	20	1	1.0
212	58	76	75	63	64	1	0.	0.	20	1	1.0
213	59	77	76	64	65	1	0.	0.	20	1	1.0
214	60	78	77	65	66	1	0.	0.	20	1	1.0
215	61	79	78	66	67	1	0.	0.	20	1	1.0
216	62	80	79	67	68	1	0.	0.	20	1	1.0
217	63	81	80	68	69	1	0.	0.	20	1	1.0
218	64	82	81	69	70	1	0.	0.	20	1	1.0
219	65	83	82	70	71	1	0.	0.	20	1	1.0
220	66	84	83	71	72	1	0.	0.	20	1	1.0
221	67	86	85	73	74	1	0.	0.	20	1	1.0
222	68	87	86	74	75	1	0.	0.	20	1	1.0
223	69	88	87	75	76	1	0.	0.	20	1	1.0
224	70	89	88	76	77	1	0.	0.	20	1	1.0
225	71	90	89	77	78	1	0.	0.	20	1	1.0
226	72	91	90	78	79	1	0.	0.	20	1	1.0
227	73	92	91	79	80	1	0.	0.	20	1	1.0
228	74	93	92	80	81	1	0.	0.	20	1	1.0
229	75	94	93	81	82	1	0.	0.	20	1	1.0
230	76	95	94	82	83	1	0.	0.	20	1	1.0
231	77	96	95	83	84	1	0.	0.	20	1	1.0
232	78	98	97	85	86	1	0.	0.	20	1	1.0
233	79	99	98	86	87	1	0.	0.	20	1	1.0
234	80	100	99	87	88	1	0.	0.	20	1	1.0
235	81	101	100	88	89	1	0.	0.	20	1	1.0
236	82	102	101	89	90	1	0.	0.	20	1	1.0
237	83	103	102	90	91	1	0.	0.	20	1	1.0
238	84	104	103	91	92	1	0.	0.	20	1	1.0
239	85	105	104	92	93	1	0.	0.	20	1	1.0
240	86	106	105	93	94	1	0.	0.	20	1	1.0
241	87	107	106	94	95	1	0.	0.	20	1	1.0
242	88	108	107	95	96	1	0.	0.	20	1	1.0
243	89	110	109	97	98	1	0.	0.	20	1	1.0
244	90	111	110	98	99	1	0.	0.	20	1	1.0
245	91	112	111	99	100	1	0.	0.	20	1	1.0
246	92	113	112	100	101	1	0.	0.	20	1	1.0
247	93	114	113	101	102	1	0.	0.	20	1	1.0
248	94	115	114	102	103	1	0.	0.	20	1	1.0
249	95	116	115	103	104	1	0.	0.	20	1	1.0
250	96	117	116	104	105	1	0.	0.	20	1	1.0
251	97	118	117	105	106	1	0.	0.	20	1	1.0
252	98	119	118	106	107	1	0.	0.	20	1	1.0
253	99	120	119	107	108	1	0.	0.	20	1	1.0
254	100	122	121	109	110	1	0.	0.	20	1	1.0
255	101	123	122	110	111	1	0.	0.	20	1	1.0
256	102	124	123	111	112	1	0.	0.	20	1	1.0
257	103	125	124	112	113	1	0.	0.	20	1	1.0
258	104	126	125	113	114	1	0.	0.	20	1	1.0
259	105	127	126	114	115	1	0.	0.	20	1	1.0
260	106	128	127	115	116	1	0.	0.	20	1	1.0

```
261   107  129  128  116  117     1       0.        0    20    1     1.0
262   108  130  129  117  118     1       0         0.   20    1     1.0
263   109  131  130  118  119     1       0.        0.   20    1     1.0
264   110  132  131  119  120     1       0.        0    20    1     1.0
265   111  134  133  121  122     1       0.        0.   20    1     1.0
266   112  135  134  122  123     1       0.        0.   20    1     1.0
267   113  136  135  123  124     1       0.        0.   20    1     1.0
268   114  137  136  124  125     1       0.        0.   20    1     1.0
269   115  138  137  125  126     1       0.        0.   20    1     1.0
270   116  139  138  126  127     1       0.        0.   20    1     1.0
271   117  140  139  127  128     1       0.        0.   20    1     1.0
272   118  141  140  128  129     1       0.        0.   20    1     1.0
273   119  142  141  129  130     1       0.        0.   20    1     1.0
274   120  143  142  130  131     1       0.        0.   20    1     1.0
275   121  144  143  131  132     1       0.        0.   20    1     1.0
276     1    1    0.       -40.9050    0.        0.        0.        0.
277    13    1    0.       -81.8100    0         0.        0.        0
278    25    1    0.       -81.8100    0.        0.        0.        0.
279    37    1    0.       -81.8100    0.        0.        0.        0.
280    49    1    0.       -81.8100    0.        0.        0.        0.
281    61    1    0.       -81.8550    0.        0.        0.        0.
282    73    1    0.       -81.8550    0.        0.        0.        0
283    85    1    0.       -81.8100    0.        0.        0.        0.
284    97    1    0.       -81.8100    0.        0.        0.        0.
285   109    1    0.       -81.8100    0.        0.        0.        0.
286   121    1    0.       -81.8100    0.        0.        0.        0.
287   133    1    0.       -40.9050    0.        0.        0.        0.
288
289        1.0       1.0       1.0       1.0
290
291
292 /*
```

```
C MESH GENERATING PROGRAM
C
C THIS PROGRAM GENERATES A 2-D FINITE ELEMENT MESH FOR A
C GIVEN CROSS SECTION.  THE SECTION GEOMETRY IS READ FROM
C AN INPUT FILE CREATED BY THE "SECTION" PROGRAM.  LOAD AND
C CONSTRAINT INFORMATION IS INPUT INTERACTIVELY.  THE PROGRAM
C OUTPUT IS A CARD IMAGE FORMAT DATA FILE WHICH CAN BE USED
C WITH THE FINITE ELEMENT CODE "SAPIV."
C
      DIMENSION IP(40,40),ZFE(200),YFE(200),XGP(40),YGP(42)
      DIMENSION IPSOLI(40,40),IELEM(40,40),NFIXED(20),IFD(20)
      DIMENSION IN(200),FY(200),FZ(200)
      CALL OPSYS('ALLOC','FEDATA',7)
    1 FORMAT(5I3,2F8.4)
    2 FORMAT(5X,9F7.4)
    3 FORMAT(5X,40I2)
    4 FORMAT(20I4)
    5 FORMAT(5X,I3,5X,F7.4,5X,F7.4)
    6 FORMAT(/,5X,'NODE MAP:',/)
    7 FORMAT(//,5X,'ELEMENT MAP:',/)
    8 FORMAT(/,5X,'ELEMENT NUMBER',5X,'I',5X,'J',5X,'K',5X,'L'
    9 FORMAT(6I5,2F10.2,2I5,F10.1)
C
C READ SECTION GEOMETRY FROM INPUT FILE 'FEDATA'
      READ(7,1) NDM,IXMAX,JYMAX,NPGXP1,NPGYP1,RM1,XC1
      DO 775 I=1,IXMAX
         DO 775 J=1,JYMAX
  775       IP(I,J)=0
      READ(7,2) (XGP(I),I=1,IXMAX)
      READ(7,2) (YGP(J),J=1,JYMAX)
      DO 777 I=2,NPGXP1
  777    READ(7,3) (IPSOLI(I,J),J=2,NPGYP1)
C
C NUMBER NODES - NUMBER IN SHORTEST DIRECTION TO MINIMIZE
C BANDWIDTH
      YTOT=YGP(JYMAX)-YGP(1)
      XTOT=XGP(IXMAX)-XGP(1)
      IF(XTOT.LT.YTOT) GO TO 900
      DO 800 I=2,NPGXP1
         DO 800 J=2,NPGYP1
            IF(IPSOLI(I,J).EQ.1) NEL=NEL+1
            NEMAX=NEL
            IF(IPSOLI(I,J).EQ.1) IELEM(I,J)=NEL
            IF(IPSOLI(I,J).EQ.1.OR.IPSOLI(I,J-1).EQ.1.OR.IPSOLI(I-1,J-1)
     *         .EQ.1.OR.IPSOLI(I-1,J).EQ.1) GO TO 790
            GO TO 800
  790       INODE=INODE+1
            IP(I-1,J-1)=INODE
            ZFE(INODE)=YTOT-YGP(J-1)
            YFE(INODE)=RM1+XC1-XGP(I-1)
            MNODE=INODE
  800 CONTINUE
      GO TO 930
  900 DO 920 J=2,NPGYP1
         DO 920 I=2,NPGXP1
            IF(IPSOLI(I,J).EQ.1) NEL=NEL+1
            NEMAX=NEL
            IF(IPSOLI(I,J).EQ.1) IELEM(I,J)=NEL
            IF(IPSOLI(I,J).EQ.1.OR.IPSOLI(I,J-1).EQ.1.OR.IPSILI(I-1,J-1)
     *         .EQ.1.OR.IPSOLI(I-1,J).EQ.1) GO TO 910
            GO TO 920
```

```
 910         INODE=INODE-1
             IF(I-1,J-1)=INODE
             ZFE(INODE)=YTOT-YGP(J-1)
             YFE(INODE)=RXL+XCL-XGP(I-1)
             MNODE=INODE
 920 CONTINUE
 910 CONTINUE
C
C PRINT NODE AND ELEMENT MAPS
      WRITE(6,6)
      DO 950 I=1,IXMAX
 950     WRITE(6,4) (IF(I,J),J=1,JYMAX)
      WRITE(6,7)
      DO 955 I=2,IXMAX
 955     WRITE(6,4) (IELEM(I,J),J=2,JYMAX)
C
C DEVELOP OUTPUT FILE
      CALL OPSYS('ALLOC','DATA1',7)
C HEADING CARD
      WRITE(7,20)
  20 FORMAT(1X,'**** HOOF STRESS CALCULATION ****')
C MASTER CONTROL CARD
      NUMNP=MNODE
      NELTYP=1
      LL=1
      NF=0
      NDYN=0
      MODEX=0
      NAD=0
      KEQB=0
      WRITE(7,30) NUMNP,NELTYP,LL,NF,NDYN,MODEX,NAD,KEQB
  30 FORMAT(8I5)
C NODAL POINT DATA
      WRITE(6,33)
  33 FORMAT(/,5X,'HOW MANY NODES ARE CONSTRAINED?')
      READ(5,*) NCON
      WRITE(6,31)
  31 FORMAT(/,5X,'INPUT FIXED NODES IN ASCENDING ORDER ...AND '
     *,'DIRECTION..Z=1,Y=2,BOTH=3')
      DO 37 I=1,NCON
  37     READ(5,*) NFIXED(I),IFD(I)
      IXT=1
      IYT=0
      IZT=0
      IXR=1
      IYR=1
      IZR=1
      KN=0
      T=0.0
      X=0.0
      DO 36 INODE=1,MNODE
         NGO=0
         DO 38 I=1,NCON
            IF(INODE.EQ.NFIXED(I)) NFN=I
  38        IF(INODE.EQ.NFIXED(I)) NGO=1
         IF(NGO.EQ.1) GO TO 34
         WRITE(7,32) INODE,IXT,IYT,IZT,IXR,IYR,IZR,X,YFE(INODE)
     *                 ,ZFE(INODE),KN,T
  32     FORMAT(1X,I4,6I5,3F10.4,I5,F5.1)
         GO TO 36
  34     IZT=1
         IYT=1
         IF(IFD(NFN).EQ.3) GO TO 35
         IF(IFD(NFN).NE.1) IZT=0
         IF(IFD(NFN).NE.2) IYT=0
  35     WRITE(7,32) INODE,IXT,IYT,IZT,IXR,IYR,IZR,X,YFE(INODE)
```

```
                         ,IFE(INODE),KN,T
          IZT=0
          IYT=0
   35 CONTINUE
C ELEMENT DATA
      NELT=4
      MNTC=1
      NTYA=0
      WRITE(7,40) NELT,NEMAX,NDM,MNTC,NTYA
   40 FORMAT(6I5)
C MATERIAL PROPERTY INFORMATION
C EACH MATERIAL MUST BE CONSIDERED
C MATERIAL #1
      MIDN=1
      NDT=1
      WD=0.0
      AMD=0.0
      BETA=0.0
      WRITE(7,42) MIDN,NDT,WD,AMD,BETA
   42 FORMAT(2I5,3F10.1)
      TEMP=0.0
      E=3.1E+06
      ANUS=.2
      G=E/2/(1+ANUS)
      WRITE(7,45) TEMP,E,E,E,ANUS,ANUS,ANUS,G
   45 FORMAT(8F10.1)
      CTE=0.000003
      WRITE(7,46) CTE,CTE,CTE
   46 FORMAT(3F10.6)
      IF (NDM.EQ.1) GO TO 70
C MATERIAL #2
      MIDN=2
      WRITE(7,42) MIDN,NDT,WD,AMD,BETA
      E=3.1E+06
      ANUS=.2
      G=E/2/(1+ANUS)
      WRITE(7,45) TEMP,E,E,E,ANUS,ANUS,ANUS,G
      WRITE(7,46) CTE,CTE,CTE
   70 CONTINUE
C ELEMENT LOAD FACTORS (FOUR CARDS)
      FTL=1
      FPL=1
      FG=0
      WRITE(7,47) FTL,FPL,FG,FG,FG
   47 FORMAT(5F10.1)
      WRITE(7,47) FG,FG,FG,FG,FG
      WRITE(7,47) FG,FG,FG,FG,FG
      WRITE(7,47) FG,FG,FG,FG,FG
C ELEMENT NUMBER INFORMATION
      NEL=0
      RT=0.0
      FN=0.0
      NSO=20
      K=1
      ET=1.
      IF(YTOT.LT.XTOT) GO TO 50
      DO 957 J=1,JYMAX
         DO 957 I=1,IXMAX
            IF(IELEM(I,J).EQ.0) GO TO 957
            NEL=NEL+1
            II=IP(I,J)
            JJ=IP(I-1,J)
            KK=IP(I-1,J-1)
            LL=IP(I,J-1)
            WRITE(7,9) NEL,II,JJ,KK,LL,IPSOLI(I,J)),RT,FN,NSO,K,ET
  957 CONTINUE
```

```
      GOTO 60
   50 DO 55 I=1,IXMAX
        DO 55 J=1,JYMAX
          IF(IELEM(I,J).EQ.0) GO TO 55
          NEL=NEL+1
          II=IP(I,J)
          JJ=IP(I-1,J)
          KK=IP(I-1,J-1)
          LL=IP(I,J-1)
          WRITE(7,9) NEL,II,JJ,KK,LL,IPSOLI(I,J),RT,PN,NSO,K,ET
   55 CONTINUE
   60 CONTINUE
C CONCENTRATED LOAD/MASS DATA
      DO 62 I=1,MNODE
        FY(I)=0.0
        FZ(I)=0.0
   62 CONTINUE
      WRITE(6,61)
   61 FORMAT(/,5X,'DO YOU WANT TO MANUALLY INPUT LOADS? YES=1,'
     *,' NO=0')
      READ(5,*) NA
      IF(NA.EQ.1) GO TO 126
      WRITE(6,79)
   79 FORMAT(/,5X,'WHAT IS THE PRESSURE?')
      READ(5,*) PW
      WRITE(6,80)
   80 FORMAT(/,5X,'HOW MANY SURFACES HAVE PRESSURE? EXCLUDE '
     *,'SEALING FACE')
      READ(5,*) NSURF
      DO 100 NS=1,NSURF
   81   WRITE(6,83) NS
   83   FORMAT(/,5X,'SURFACE #',I2)
        WRITE(6,85)
   85   FORMAT(/,5X,'HOW MANY NODES ON THIS SURFACE?')
        READ(5,*) NNSF
        WRITE(6,87)
   87   FORMAT(/,5X,'WHICH DIRECTION IS PRESSURE ACTING?',/,5X,
     *  '-Y=1,  +Y=2,  -Z=3,  +Z=4')
        READ(5,*) IDIR
        WRITE(6,88)
   88   FORMAT(/,5X,'INPUT NODES (ONE AT A TIME IN ORDER) ')
        IF(IDIR.EQ.3.OR.IDIR.EQ.4) GO TO 95
C SURFACE FORCES IN THE RADIAL DIRECTION
        DO 89 I=1,NNSF
   89     READ(5,*) IN(I)
        NM1=NNSF-1
        FAC=1.
        IF(IDIR.EQ.1) FAC=-1.
        DO 90 I=1,NM1
          DZ=ABS(ZFE(IN(I+1))-ZFE(IN(I)))
          ALOAD=PW*DZ*YFE(IN(I))
          FY(IN(I))=FY(IN(I))+ALOAD/2.0*FAC
          FY(IN(I+1))=FY(IN(I+1))-ALOAD/2.0*FAC
   90   CONTINUE
        GO TO 100
C SURFACE FORCES IN THE AXIAL DIRECTION
   95   DO 96 I=1,NNSF
   96     READ(5,*) IN(I)
        NM1=NNSF-1
        FAC=1.
        IF(IDIR.EQ.3) FAC=-1.
        DO 97 I=1,NM1
          ALOAD=PW*ABS(YFE(IN(I+1))**2-YFE(IN(I))**2)/2.0
          FZ(IN(I))=FZ(IN(I))+ALOAD/2.0*FAC
          FZ(IN(I+1))=FZ(IN(I+1))+ALOAD/2.0*FAC
   97   CONTINUE
```

```
  100 CONTINUE
C FACE LOADS
      WRITE(6,110)
  110 FORMAT(/,5X,'IS A FACE PRESSURE TO BE CALCULATED? YES=1'
     *,',NO=0')
      READ(5,*) NA
      IF(NA.EQ.0) GO TO 130
      WRITE(6,85)
      READ(5,*) NNSF
      WRITE(6,87)
      READ(5,*) IDIR
      WRITE(6,115)
  115 FORMAT(/,5X,'INPUT NODES FROM INSIDE RADIUS TO OUTSIDE')
      DO 120 I=1,NNSF
  120    READ(5,*) IN(I)
      NM1=NNSF-1
      FAC=1.
      IF(IDIR.EQ.3) FAC=-1.
      SLOPE=PW/(YFE(IN(NNSF))-YFE(1))
      B=PW-SLOPE*YFE(IN(NNSF))
      DO 125 I=1,NM1
         PRESS=SLOPE*(YFE(IN(I))+YFE(IN(I+1)))/2.0+B
         ALOAD=PRESS*(YFE(IN(I+1))**2-YFE(IN(I))**2)/2.0
         FZ(IN(I))=FZ(IN(I))+ALOAD/2.0*FAC
         FZ(IN(I+1))=FZ(IN(I+1))+ALOAD/2.0*FAC
  125 CONTINUE
      GO TO 130
C MANUAL LOAD INPUT
  126 WRITE(6,127)
  127 FORMAT(/,5X,'HOW MANY NODES?')
      READ(5,*) INOD
      WRITE(6,128)
  128 FORMAT(/,5X,'INPUT NODE,LOAD,AND IS IT RADIAL(1) OR '
     *,'AXIAL(2)?')
      DO 129 I=1,INOD
         READ(5,*) N,F,IFA
         IF(IFA.EQ.1) FY(N)=F
         IF(IFA.EQ.2) FZ(N)=F
  129 CONTINUE
  130 CONTINUE
      NSLC=1
      FX=0.0
      AMX=0.0
      AMY=0.0
      AMZ=0.0
      DO 140 I=1,MNODE
         IF(FY(I).EQ.0..AND.FZ(I).EQ.0.) GO TO 140
         WRITE(7,135) I,NSLC,FX,FY(I),FZ(I),AMX,AMY,AMZ
  135    FORMAT(2I5,6F10.4)
  140 CONTINUE
      WRITE(7,*)
C ELEMENT LOAD MULTIPLIERS
      EM=1.
      WRITE(7,145) EM,EM,EM,EM
  145 FORMAT(4F10.1)
      WRITE(7,150)
  150 FORMAT(//,'//')
      STOP
      END
```

APPENDIX F

HEAT TRANSFER ANALYSIS

APPENDIX F

Heat Transfer Analysis

Program Description

The heat transfer analysis program solves for the temperature distribution and thermal rotation for two materials rubbing together in a seal configuration. Data similar to that for the Section Properties program is needed as input to define the seal. Heat generation at the sliding interface arises from friction due to the mechanical contact. Boundary conditions around the seal are convective having an arbitrary convection coefficient. Once the temperature field is established, thermal rotation of the two rings is computed.

Data Input

With reference to the example problem shown in Figure F-1 and the following program listing, the following data input is needed:

XC, YC	x and y coordinates of the corner points input clockwise
RX1	Radius at corner point 1
NC	Number of corner points
DXMAX, DYMAX	Maximum grid spacing in x and y directions
XMIN1, YMIN1	Minimum coordinates of material 2
XMAX1, YMAX1	Maximum coordinates of material 2
	Material 2 must be a rectangular solid contained with the original boundary
COND (1 & 2)	Thermal conductivity of materials 1 and 2

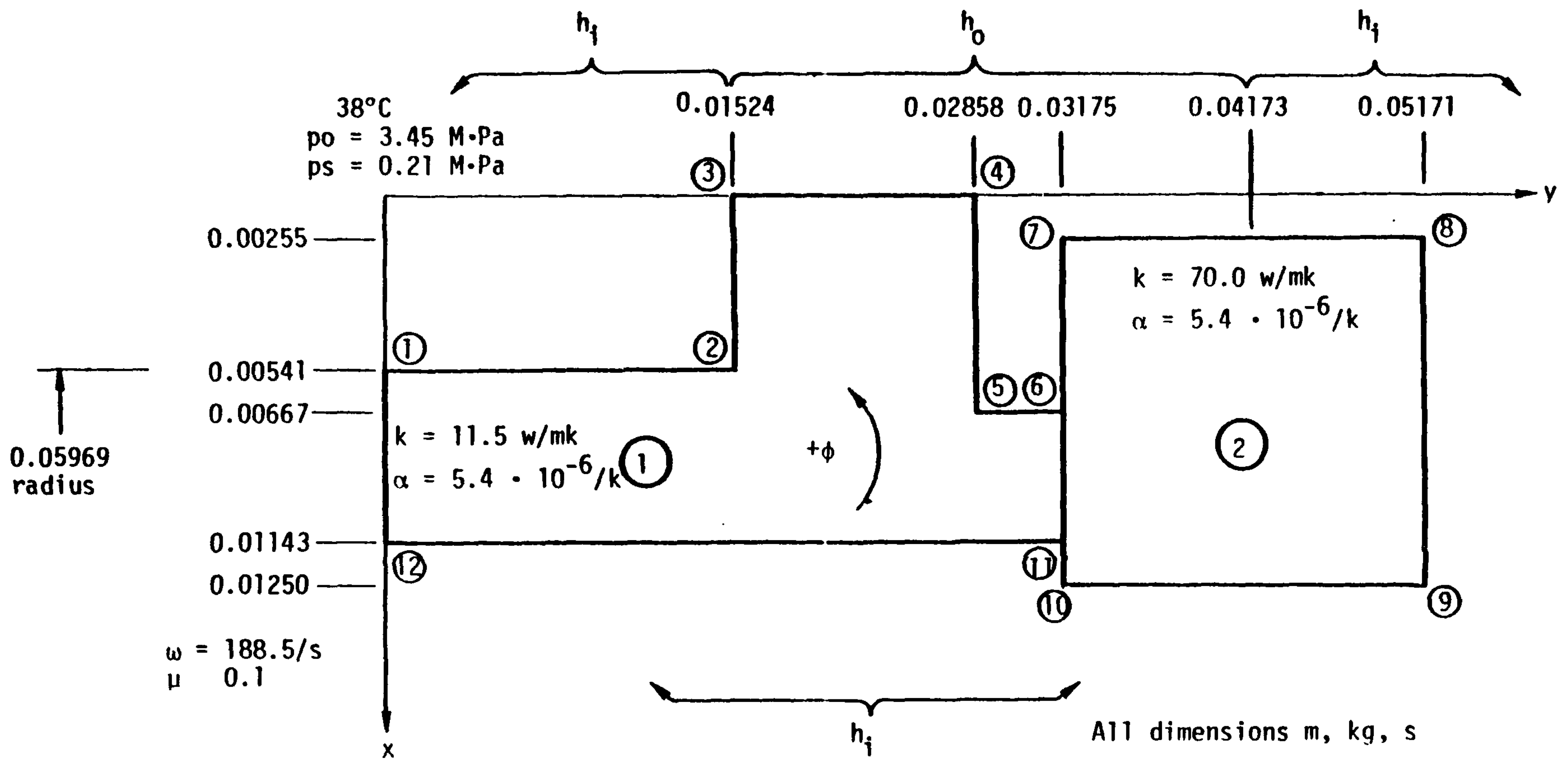

$h_b = 17700\ w/m^2k$
$h_i = 5900$

Figure F-1. Sample heat Transfer Problem.

ALPHA1 & ALPHA2	Thermal coefficient of expansion of materials 1 and 2
OMEG	angular velocity
RO	Outside radius of seal face contact
RI	Inside radius of seal face contact
BAL	Balance ratio of seal
PSP	Spring load on face
PO	Sealed pressure (outside pressure)
AMU	Friction coefficient associated with mechanical contact pressure only
Q	Computed heat flow into seal faces
TINF	Seal environment temperature
HCM(I) HCP(I)	Convection coefficient just behind and just ahead of corner point I. If the convection coefficient does not change at the corner point, then HCM = HCP. A change may be introduced as well. (See later example.)
XCHG(I) YCHGII)	If there is to be a change in convection coefficient along the boundary between XC(I) and XC(I+1) or YC(I) and YC(I+1), then either XCHG(I) or YCHG(I) (as necessary) must be specified. The program knows when to expect such a change because there will be a difference between HCP(I) and HCM(I+1) in such cases. The program introduces a step change in convection coefficient at XCHG or

YCHG according to the values HCP(I) and HCM(I+1). Proper interpolation between element spaces is done.

Example

Figure F-1 shows a seal used as an example. The data is input into the program as described. The output follows the program listing. In the example, material 1 is carbon and material 2 is WC. The seal used for this example is the first wavy seal used for early research on waves in water [4]. Note how material 2 is included in the original boundary. The convection coefficient is changed along the 7 - 8 boundary.

The output from this program is shown. The refined mesh suggests the shape of the problem. Finally, the temperature distribution is shown. The direction of printing was changed 90° here to accommodate the longer than thick seal geometry. The -0 temperature values are meaningless temperature values at locations where there is no material. The -0 represents a roundoff for zero from the negative side. Thermal rotations are also shown using the sign conventions shown in Figure F-1.

Figure F-1 will be provided later.

```
C PROGRAM TO CALCULATE SECTION PROPERTIES, HEAT TRANSFER, AND
C THERMAL ROTATION FOR ARBITRARY CROSS SECTIONS MADE UP OF ANY
C NUMBER OF STRAIGHT LINE SEGMENTS PARALLEL TO THE X AND Y AXES.
C
C INPUT NUMBER OF POINTS NC AND THE POINTS X(I), Y(I) IN
C CLOCKWISE DIRECTION AROUND THE PART.  STARTING POINT IS
C ARBITRARY.  EACH POINT BY DEFINITION MUST BE A CORNER.
C THIS PROGRAM ACCEPTS A MATERIAL #1 IN A RECTANGULAR SHAPE ONLY.
C THE XMIN,YMIN AND XMAX,YMAX CORNERS OF THE MATERIAL MUST BE
C SPECIFIED.  MATERIAL #2 MUST BE WITHIN THE ORIGINAL BOUNDARY.
C THIS PROGRAM CONSIDERS THE VERTICAL (Y=CONST) INTERFACE BETWEEN
C THE TWO MATERIALS TO BE A UNIFORM HEAT SOURCE Q W/M**2 TO SIMULATE
C A SEAL INTERFACE.
C SI UNITS M,KG,S ARE USE
C MATERIAL 1 IS CARBON, MATERIAL 2 IS WC
      DIMENSION XG(22),YG(22),XGF(40),YGF(40),XC(22),YC(22)
      DIMENSION AIM1(40,40),AIP1(40,40),AJM1(40,40),AJP1(40,40)
      DIMENSION T(40,40),BIJ(40,40),HCM(22),HCP(22),RGF(40)
      DIMENSION ISO(22),IGXC(22),JGYC(22),ISOLID(22,22),IGN(40)
      DIMENSION JGN(40),IFSOLI(40,40),IS(4)
      DIMENSION YCHG(22),XCHG(22),COND(2)
      DIMENSION TTT(50)
      CALL OPSYS('ALLOC','DATA2',T)
      REAL*4 JX1,JX2,JY1,JY2,JXY1,JXY2
      REAL*4 KIP1,KIM1,KJP1,KJM1
      DATA XC/.00541,.00541,0.,0.,.00657,.00657,.00255,.00255
     1.01250,.01250,.01140,.01140/
      DATA YC/0.,.01524,.01524,.02858,.02858,.00175,.00175,
     1.05171,.05171,.00175,.00175,0./
C INPUT MATERIAL #2 COORDINATES XMIN,YMIN,XMAX,YMAX
C [illegible]
      XMIN1=0.00255
      YMIN1=0.00175
      XMAX1=0.01250
      YMAX1=0.05171
C INPUT RADIUS AT X1
      RX1=0.05965
      NC=12
      NG=NC/2
C INPUT GRID SIZE FOR FINER MESH
      DXMAX=0.0015
      DYMAX=0.0015
      PIE=3.14159265
      W=17750.
      H=40./3.
      COND(1)=11.7
      COND(2)=73.0
      ALPHA1=5.4E-06
      ALPHA2=5.4E-06
      TMED=100.0
      RO=0.05082
      RI=0.04826
      BAL=1.0
      PSF=0.21E+06
      PO=0.45E+06
      AMU=0.1
      PNET=PO*BAL+PSF-0.5*PI
      VAV=(RO+RI)*.5*OMEG
      Q=PNET*VAV*AMU
      QTOT=Q*PIE*(RO**2-RI**2)
      WRITE(6,1488) QTOT
 1488 FORMAT(1H ,'QTOT=',E11.4)
      DTA1=.5*(RO-RI)
```

```
      TINF=38.
C ENTER THE POINTS ALONG THE BOUNDARY WHERE CONVECTION COEFFICIENT
C CHANGES
      DO 31 I=1,NC
      YCHG(I)=0.
31     XCHG(I)=0.
C ENTER THE CONVECTION COEFFICIENTS
      HCM(1)=HI
      HCP(1)=HI
      HCM(2)=HI
      HCP(2)=HI
      HCM(3)=HI
      HCP(3)=HO
      HCM(4)=HO
      HCP(4)=HO
      HCM(5)=HO
      HCP(5)=HO
      HCM(6)=HO
      HCP(6)=HO
      HCM(7)=HO
      HCP(7)=HO
      HCM(8)=HI
      HCP(8)=HI
      HCM(9)=HI
      HCP(9)=HI
      HCM(10)=HI
      HCP(10)=HI
      HCM(11)=HI
      HCP(11)=HI
      HCM(12)=HI
      HCP(12)=HI
      YCHG(7)=0.04173
C SET UP THE GRID POINTS
      DO 10 I=1,NG
      XG(I)=XC(2*I)
   10 YG(I)=YC(2*I)
C ARRANGE THE GRID POINTS IN INCREASING ORDER
      DO 20 II=1,NG
      IST=II
      AMIN=1.E+06
      DO 22 I=IST,NG
      IF(XG(I).GT.AMIN) GO TO 22
      AMIN=XG(I)
      J=I
   22 CONTINUE
      XTMP=XG(II)
      XG(II)=XG(J)
   20 XG(J)=XTMP
      DO 25 II=1,NG
      IST=II
      AMIN=1.E+06
      DO 27 I=IST,NG
      IF(YG(I).GT.AMIN) GO TO 27
      AMIN=YG(I)
      J=I
   27 CONTINUE
      YTMP=YG(II)
      YG(II)=YG(J)
   25 YG(J)=YTMP
C ELIMINATE EQUAL XG AND YG VALUES.
      NGM1=NG-1
      IIEQ=0
      DO 30 I=1,NGM1
      IF(XG(I).NE.XG(I+1)) GO TO 30
      IIEQ=IIEQ+1
      IEQ(IIEQ)=I
```

```
   30 CONTINUE
      NGX=NG
      IF(IIEQ.EQ.0) GO TO 100
      DO 40 I=1,IIEQ
      NGX=NGX-1
      IST=IEQ(I)
      DO 50 II=IST,NGX
   50 XG(II)=XG(II+1)
   40 CONTINUE
  100 IIEQ=0
      DO 60 I=1,NGM1
      IF(YG(I).NE.YG(I+1)) GO TO 60
      IIEQ=IIEQ+1
      IEQ(IIEQ)=I
   60 CONTINUE
      NGY=NG
      IF(IIEQ.EQ.0) GO TO 200
      DO 70 I=1,IIEQ
      NGY=NGY-1
      IST=IEQ(I)
      DO 80 II=IST,NGY
   80 YG(II)=YG(II+1)
   70 CONTINUE
C MATCH CORNER POINTS WITH GRID POINTS
C IGXC(IC) IS GRID POINT CORRESPONDING TO CORNER POINT IC
  200 DO 90 IC=1,NC
      DO 90 IG=1,NGX
      IF(XC(IC).EQ.XG(IG)) IGXC(IC)=IG
   90 CONTINUE
      DO 95 JC=1,NC
      DO 95 JG=1,NGY
      IF(YC(JC).EQ.YG(JG)) JGYC(JC)=JG
   95 CONTINUE
C IDENTIFY THE VOID AND SOLID REGIONS.
C I,J REFERS TO REGION WHICH IS ABOVE AND TO THE LEFT OF POINT I,J
C CODE: VOID-0, SOLID-1, SOLID-2, UNASSIGNED-3.
      NGXP1=NGX+1
      NGYP1=NGY+1
      DO 101 I=1,NGXP1
      DO 101 J=1,NGYP1
  101 ISOLID(I,J)=3
      DO 999 M=1,NC
      N=M+1
      IF(M.EQ.NC) N=1
      IC=0
      IF(YC(N).GT.YC(M)) IC=1
      IF(XC(N).GT.XC(M)) IC=2
      IF(YC(N).LT.YC(M)) IC=3
      IF(XC(N).LT.XC(M)) IC=4
      GO TO (110,120,130,140),IC
  110 IN=IGXC(N)
      JN=JGYC(N)
      JM=JGYC(M)
      JM=JM+1
      DO 112 J=JM,JN
      ISOLID(IN,J)=0
  112 ISOLID(IN+1,J)=1
      GO TO 999
  120 IM=IGXC(M)
      IM=IM+1
      JM=JGYC(M)
      IN=IGXC(N)
      DO 122 I=IM,IN
      ISOLID(I,JM)=1
  122 ISOLID(I,JM+1)=0
      GO TO 999
```

```
  130 IN=IGXC(N)
      JN=JGYC(N)
      JN=JN+1
      JM=JGYC(M)
      DO 132 J=JN,JM
      ISOLID(IN,J)=1
  132 ISOLID(IN+1,J)=0
      GO TO 999
  140 IN=IGXC(N)
      IN=IN+1
      JN=JGYC(N)
      IM=IGXC(M)
      DO 142 I=IN,IM
      ISOLID(I,JN)=0
  142 ISOLID(I,JN+1)=1
999   CONTINUE
C SET BOUNDARIES TO VOID
      DO 310 J=1,NGYP1
      ISOLID(1,J)=0
  310 ISOLID(NGXP1,J)=0
      DO 320 I=1,NGXP1
      ISOLID(I,1)=0
  320 ISOLID(I,NGYP1)=0
C USE Y SWEEP TO SET ALL OTHERS
      DO 400 I=2,NGX
      DO 410 J=1,NGYP1
      IF(ISOLID(I,J).NE.9) GO TO 410
      J1=J
      DO 420 JJ=J1,NGYP1
      IF(ISOLID(I,JJ).EQ.9) GO TO 420
      J2=JJ-1
      GO TO 430
  420 CONTINUE
      WRITE(6,319)
  [illegible]
  430 DO 425 JJ=J1,J2
  425 ISOLID(I,JJ)=ISOLID(I,J1-1)
  410 CONTINUE
  400 CONTINUE
C REDEFINE: ISOLID(I,J)=2 IS MATERIAL 2
      DO 405 I=2,NGX
      DO 405 J=2,NGY
      XMID=(XG(I)+XG(I-1))*.5
      YMID=(YG(J)+YG(J-1))*.5
      IF((XMID.GT.XMIN1).AND.(XMID.LT.XMAX1)) GO TO 406
      GO TO 405
406   IF((YMID.GT.YMIN1).AND.(YMID.LT.YMAX1)) ISOLID(I,J)=2
  405 CONTINUE
      SMY=0.
      SMX=0.
      AREA1=0.
      DO 500 I=2,NGX
      DO 500 J=2,NGY
      ISOL=ISOLID(I,J)
      IF(ISOL.EQ.2) ISOL=0
      DA=(XG(I)-XG(I-1))*(YG(J)-YG(J-1))*ISOL
      AREA1=AREA1+DA
      X=(XG(I)+XG(I-1))*.5
      Y=(YG(J)+YG(J-1))*.5
      SMY=SMY+DA*X
  500 SMX=SMX+DA*Y
      XBAR1=SMY/AREA1
      YBAR1=SMX/AREA1
      AIX1=0.
      AIY1=0.
      AIXY1=0.
```

```
      RC1=RX1+XC(1)-XBAR1
      DO 510 I=2,NGX
      DO 510 J=2,NGY
      ISOL=ISOLID(I,J)
      IF(ISOL.EQ.2) ISOL=0
      DX=XG(I)-XG(I-1)
      DY=YG(J)-YG(J-1)
      DA=DX*DY
      X=(XG(I)+XG(I-1))*.5
      Y=(YG(J)+YG(J-1))*.5
      X=X-XBAR1
      Y=Y-YBAR1
      AIX1=AIX1+(DX*DY**3/12.+DA*Y*Y)*ISOL
      AIY1=AIY1+(DY*DX**3/12.+DA*X*X)*ISOL
  510 AIXY1=AIXY1+X*Y*DA*ISOL
      SMY=0.
      SMX=0.
      AREA2=0.
      DO 501 I=2,NGX
      DO 501 J=2,NGY
      ISOL=ISOLID(I,J)
      IF(ISOL.EQ.1) ISOL=0
      IF(ISOL.EQ.2) ISOL=1
      DA=(XG(I)-XG(I-1))*(YG(J)-YG(J-1))*ISOL
      AREA2=AREA2+DA
      X=(XG(I)+XG(I-1))*.5
      Y=(YG(J)+YG(J-1))*.5
      SMY=SMY+DA*X
501   SMX=SMX+DA*Y
      XBAR2=SMY/AREA2
      YBAR2=SMX/AREA2
      AIX2=0.
      AIY2=0.
      AIXY2=0.
      RC2=RX1+XC(1)-XBAR2
      DO 511 I=2,NGX
      DO 511 J=2,NGY
      ISOL=ISOLID(I,J)
      IF(ISOL.EQ.1) ISOL=0
      IF(ISOL.EQ.2) ISOL=1
      DX=XG(I)-XG(I-1)
      DY=YG(J)-YG(J-1)
      DA=DY*DX
      X=(XG(I)+XG(I-1))*.5
      Y=(YG(J)+YG(J-1))*.5
      X=X-XBAR2
      Y=Y-YBAR2
      AIX2=AIX2+(DX*DY**3/12.+DA*Y*Y)*ISOL
      AIY2=AIY2+(DY*DX**3/12.+DA*X*X)*ISOL
511   AIXY2=AIXY2+X*Y*DA*ISOL
C REFINE THE MESH
      JY=0.
      IX=0.
      NGXM1=NGX-1
      DO 540 I=1,NGXM1
      IGN(I)=(XG(I+1)-XG(I))/DXMAX+.999
      DXUSED=(XG(I+1)-XG(I))/IGN(I)
      IGNI=IGN(I)
      DO 520 II=1,IGNI
      IX=IX+1
      XGP(IX)=XG(I)+DXUSED*(II-1)
  520 CONTINUE
      IF(I.EQ.NGXM1) XGP(IX+1)=XG(I+1)
  540 CONTINUE
      NGYM1=NGY-1
      DO 550 I=1,NGYM1
```

```
      JGN(I)=(YG(I+1)-YG(I))/DYMAX+.999
      DYUSED=(YG(I+1)-YG(I))/JGN(I)
      JGNI=JGN(I)
      DO 530 JJ=1,JGNI
      JY=JY+1
      YGP(JY)=YG(I)+DYUSED*(JJ-1)
  530 CONTINUE
      IF(I.EQ.NGYM1) YGP(JY+1)=YG(I+1)
  550 CONTINUE
C SET ADDITIONAL MESH AREAS TO SOLID OR VOID.
      IXMAX=IX+1
      JYMAX=JY+1
      JBEG=1
      IBEG=1
      NPGXP1=IXMAX+1
      NPGYP1=JYMAX+1
C     WRITE(7,*) IXMAX,JYMAX,NPGXP1,NPGYP1,RX1,XC(1)
      DO 560 II=1,NPGXP1
      DO 560 JJ=1,NPGYP1
  560 IPSOLI(II,JJ)=0.
      DO 595 I=2,NGX
      JBEG=1
      DO 590 J=2,NGY
      IEND=IBEG+IGN(I-1)
      JEND=JBEG+JGN(J-1)
      IBEGP1=IBEG+1
      JBEGP1=JBEG+1
      IF(ISOLID(I,J).NE.0) GO TO 570
      GO TO 590
  570 CONTINUE
      DO 580 II=IBEGP1,IEND
      DO 580 JJ=JBEGP1,JEND
  580 IPSOLI(II,JJ)=1
  590 JBEG=JGN(J-1)+JBEG
  595 IBEG=IGN(I-1)+IBEG
C REDEFINE: IPSOLI(I,J)=2 IS THE CARBON
      DO 600 I=2,IXMAX
      DO 600 J=2,JYMAX
      XMID=(XGP(I)+XGP(I-1))*.5
      YMID=(YGP(J)+YGP(J-1))*.5
      IF((XMID.GT.XMIN1).AND.(XMID.LT.XMAX1)) GO TO 601
      GO TO 600
601   IF((YMID.GT.YMIN1).AND.(YMID.LT.YMAX1)) IPSOLI(I,J)=2
  600 CONTINUE
C CHECK TO SEE IF TOTAL AREA IS THE SAME.
      AREA=0.
      DO 700 I=2,IXMAX
      DO 700 J=2,JYMAX
      IPSOL=IPSOLI(I,J)
      IF(IPSOL.EQ.2) IPSOL=1
      DA=(XGP(I)-XGP(I-1))*(YGP(J)-YGP(J-1))*IPSOL
      AREA=AREA+DA
  700 CONTINUE
      DO 702 I=1,IXMAX
702   RGP(I)=RX1-XGP(I)
      DIFF=AREA1+AREA2-AREA
C
      WRITE(6,1)
    1 FORMAT(///,5X,'INPUT GRID LOCATIONS',/,5X,'XC:')
      WRITE(6,2) XC
    2 FORMAT(9X,9F7.4)
      WRITE(6,3)
    3 FORMAT(5X,'YC:')
      WRITE(6,2) YC
      WRITE(6,4)
    4 FORMAT(//,5X,'ADJUSTED GRID LOCATIONS',/,5X,'XG:')
```

```
      WRITE(6,2) (XG(I),I=1,NGX)
      WRITE(6,5)
    5 FORMAT(5X,'YG:')
      WRITE(6,2) (YG(I),I=1,NGY)
      WRITE(6,6)
    6 FORMAT(/,5X,'SECTION PROPERTIES MATRIX',/)
      DO 7 I=1,NGXP1
    7 WRITE(6,8) (ISOLID(I,J),J=1,NGYP1)
    8 FORMAT(2X,40I2)
      WRITE(6,9) AREA1,XBAR1,YBAR1,RC1,AIX1,AIY1,AIXY1
    9 FORMAT(/,5X,'AREA1=',E11.4,3X,'XBAR1=',E11.4,3X,'YBAR1=',
     *E11.4,3X,'RC1=',E11.4,/,5X,'IX1=',E11.4,3X,'IY1=',E11.4,
     *3X,'IXY1=',E11.4)
      WRITE(6,17) AREA2,XBAR2,YBAR2,RC2,AIX2,AIY2,AIXY2
17    FORMAT(/,5X,'AREA2=',E11.4,3X,'XBAR2=',E11.4,3X,'YBAR2=',
     1E11.4,3X,'RC2=',E11.4,/,5X,'IX2=',E11.4,3X,'IY2=',E11.4,
     23X,'IXY2=',E11.4)
      WRITE(6,11)
   11 FORMAT(/,5X,'FINER MESH ADJUSTMENT',/,5X,'XGP:')
      WRITE(6,2) (XGP(I),I=1,IXMAX)
      WRITE(7,2) (XGP(I),I=1,IXMAX)
      WRITE(6,12)
   12 FORMAT(5X,'YGP:')
      WRITE(6,2) (YGP(I),I=1,JYMAX)
      WRITE(7,2) (YGP(I),I=1,JYMAX)
      IF(NPGXP1.GT.40) GO TO 705
      WRITE(6,13)
  13  FORMAT(/,5X,'REFINED MESH',/)
      DO 14 I=1,NPGXP1
       WRITE(7,8) (IPSOLI(I,J),J=1,NPGYP1)
   14 WRITE(6,8) (IPSOLI(I,J),J=1,NPGYP1)
  705 CONTINUE
      WRITE(6,15) DIFF
   15 FORMAT(/,5X,'DIFFERENCE IN AREAS=',E11.4)
      ERR=0.01
      IMAXM1=IXMAX-1
      JMAXM1=JYMAX-1
C HEAT TRANSFER EQUATION SETUP
C FIND THE NUMBER OF ZEROS
      DO 710 I=1,IXMAX
      DO 710 J=1,JYMAX
      QS=0.
      H=0.
      IS(2)=IPSOLI(I,J)
      IS(1)=IPSOLI(I,J+1)
      IS(3)=IPSOLI(I+1,J)
      IS(4)=IPSOLI(I+1,J+1)
      NZGO=0
      DO 800 K=1,4
      IF(IS(K).EQ.0) NZGO=NZGO+1
  800 CONTINUE
C FIND WHICH ORIGINAL BOUNDARY YOU ARE ON
      IC=0
      DO 810 K=1,NC
      KP1=K+1
      IF(KP1.GT.NC) KP1=1
      IF(XC(K).EQ.XGP(I)) GO TO 812
      IF(YC(K).EQ.YGP(J)) GO TO 814
      GO TO 810
  812 IF(YC(K).EQ.YGP(J)) GO TO 820
      IF((YGP(J).GT.YC(K)).AND.(YGP(J).LT.YC(KP1))) GO TO 825
      IF((YGP(J).LT.YC(K)).AND.(YGP(J).GT.YC(KP1))) GO TO 825
      GO TO 810
  814 IF((XGP(I).GT.XC(K)).AND.(XGP(I).LT.XC(KP1))) GO TO 830
      IF((XGP(I).LT.XC(K)).AND.(XGP(I).GT.XC(KP1))) GO TO 830
C NOT A BOUNDARY POINT
```

```
  810 CONTINUE
      GO TO 900
C THIS IS A CORNER POINT
  820 IC=K
      GO TO 900
C POINT IS ON X=CONST LINE BETWEEN ICX AND ICX+1
  825 IC=K
      GO TO 900
C POINT IS ON Y=CONST LINE BETWEEN ICY AND ICY+1
  830 IC=K
C WATCH OUT - EITHER WAY ALGEBRAICALLY
C CALCULATE CONDUCTIVE COEFFICIENTS
C NOTE - SOME QUANTITIES BELOW ARE UNDEFINED
  900 ICP1=IC+1
      IF(ICP1.GT.NC) ICP1=1
      DYJP1=YGP(J+1)-YGP(J)
      DYJM1=YGP(J)-YGP(J-1)
      DXIP1=XGP(I+1)-XGP(I)
      DXIM1=XGP(I)-XGP(I-1)
      IF(DYJP1.EQ.0.) DYJP1=2.
      IF(DYJM1.EQ.0.) DYJM1=2.
      IF(DXIP1.EQ.0.) DXIP1=2.
      IF(DXIM1.EQ.0.) DXIM1=2.
C NOTE - COND(0) IS UNDEFINED
      COND1=COND(IS(1))
      COND2=COND(IS(2))
      COND3=COND(IS(3))
      COND4=COND(IS(4))
      IF(IS(1).EQ.0) COND1=0.
      IF(IS(2).EQ.0) COND2=0.
      IF(IS(3).EQ.0) COND3=0.
      IF(IS(4).EQ.0) COND4=0.
C THESE ARE ZERO FOR COND ZERO
      KIM1=0.5*(COND1*DYJP1+COND2*DYJM1)*2.*PIE*(RGP(I)+.5*DXIM1)/DXIM1
      KIP1=0.5*(COND4*DYJP1+COND3*DYJM1)*2.*PIE*(RGP(I)-0.5*DXIP1)/DXIP1
      KJM1=COND2*.5*DXIM1*2.*PIE*(RGP(I)+.25*DXIM1)
      KJM1=(KJM1+COND3*.5*DXIP1*2.*PIE*(RGP(I)-.25*DXIP1))/DYJM1
      KJP1=COND1*.5*DXIM1*2.*PIE*(RGP(I)+.25*DXIM1)
      KJP1=(KJP1+COND4*.5*DXIP1*2.*PIE*(RGP(I)-DXIP1*.25))/DYJP1
C GO TO THE SELECTED CASE
      NZGO=NZGO+1
      GO TO (1000,1100,1200,1300,1400),NZGO
C CLL SOLID - CASE 14
C WILL ASSUME HEAT INPUT ON Y=CONST LINE IF MATLS ARE DIFFERENT
C ON EACH SIDE - IE - SLIDING INTERFACE
C Q MUST BE HEAT GENERATED PER AREA
 1000 QS=0.
      IF(IS(1).EQ.IS(2)) GO TO 1010
      AREA=2.*PIE*(RGP(I)+.25*DXIM1)*DXIM1*.5+2.*PIE*(RGP(I)-.25*DXIP1)*
     *DXIP1*.5
      QS=Q*AREA
 1010 AJ=KIP1+KIM1+KJP1+KJM1
      AIP1(I,J)=KIP1/AJ
      AIM1(I,J)=KIM1/AJ
      AJP1(I,J)=KJP1/AJ
      AJM1(I,J)=KJM1/AJ
      BIJ(I,J)=QS/AJ
      GO TO 710
C ONE ZERO
 1100 IF(IS(1).EQ.0) GO TO 1110
      IF(IS(2).EQ.0) GO TO 1120
      IF(IS(3).EQ.0) GO TO 1130
      IF(IS(4).EQ.0) GO TO 1140
      WRITE(6,1111)
 1111 FORMAT(' WHOOPS')
C CASE 10
```

```
 1110 QS=0.
      IF(IS(3).EQ.IS(4)) GO TO 1115
      AREA=2.*PIE*(RGP(I)-.25*DXIP1)*.5*DXIP1
      QS=Q*AREA
 1115 H=2.*PIE*RGP(I)*.5*DYJP1*HCP(IC)
      H=H+2.*PIE*(RGP(I)+DXIM1*.25)*.5*DXIM1*HCM(IC)
      GO TO 1150
C CASE 9
 1120 QS=0.
      IF(IS(3).EQ.IS(4)) GO TO 1125
      AREA=2.*PIE*(RGP(I)-.25*DXIP1)*.5*DXIP1
      QS=Q*AREA
 1125 H=2.*PIE*RGP(I)*.5*DYJM1*HCM(IC)
      H=H+2.*PIE*(RGP(I)+DXIM1*.25)*.5*DXIM1*HCP(IC)
      GO TO 1150
C CASE 12
 1130 QS=0.
      IF(IS(2).EQ.IS(1)) GO TO 1135
      AREA=2.*PIE*(RGP(I)+.25*DXIM1)*.5*DXIM1
      QS=Q*AREA
 1135 H=2.*PIE*RGP(I)*.5*DYIM1*HCP(IC)
      H=H+1.*PIE*(RGP(I)-.25*DXIP1) *.5*DXIP1*HCM(IC)
      GO TO 1150
C CASE 11
 1140 QS=0.
      IF(IS(2).EQ.IS(1)) GO TO 1145
      AREA=2.*PIE*(RGP(I)+.25*DXIM1)*DXIM1*.5
      QS=Q*AREA
 1145 H=2.*PIE*RGP(I)*.5*DYJP1*HCM(IC)
      H=H+2.*PIE*(RGP(I)-.25*DXIP1)*.5*DXIP1*HCP(IC)
 1150 AJ=KIP1+KIM1+KJP1+KJM1+H
      AIP1(I,J)=KIP1/AJ
      AIM1(I,J)=KIM1/AJ
      AJP1(I,J)=KJP1/AJ
      AJM1(I,J)=KJM1/AJ
      BIJ(I,J)=(QS+H*TINF)/AJ
      GO TO 710
C TWO ZEROS
 1200 DO 1201 II=1,4
      IP1=II+1
      IF(IP1.EQ.5) IP1=1
      IF((IS(II)*IS(IP1)).NE.0) NGO=II
 1201 CONTINUE
      GO TO (1230,1240,1210,1220),NGO
C CASE 1
 1210 QS=0.
      IF(IS(3).NE.IS(4)) QS=2.*PIE*(RGP(I)-.25*DXIP1)*.5*DXIP1*Q
      YM=YGP(J)-DYJM1*.5
      YP=YGP(J)+DYJP1*.5
      IF(YCHG(IC).NE.0.) GO TO 1211
      H=2.*PIE*RGP(I)*(YP-YM)*HCP(IC)
      GO TO 1250
 1211 FRAC=(YCHG(IC)-YM)/(YP-YM)
      IF(FRAC.LT.0.) FRAC=0.
      IF(FRAC.GT.1.) FRAC=1.
      H=(FRAC*HCP(IC)+(1.-FRAC)*HCM(ICP1))*2.*PIE*RGP(I)*(YP-YM)
      GO TO 1250
C CASE 2
 1220 XP=XGP(I)+DXIP1*.5
      XM=XGP(I)-DXIM1*.5
      RAV=RX1-(XP+XM)*.5
      IF(XCHG(IC).NE.0.) GO TO 1221
      H=2.*PIE*RAV*(XP-XM)*HCP(IC)
      GO TO 1250
 1221 FRAC=(XCHG(IC)-XM)/(XP-XM)
      IF(FRAC.LT.0.) FRAC=0.
```

```
      IF(FRAC.GT.1.) FRAC=1.
      H=(FRAC*HCM(ICP1)+(1.-FRAC)*HCP(IC))*2.*PIE*RAV*(XP-XM)
      GO TO 1250
C CASE 3
 1230 QS=0.
      IF(IS(2).NE.IS(1)) QS=2.*PIE*(RGP(I)+.25*DXIM1)*.5*DXIM1*Q
      YM=YGP(J)-DYJM1*.5
      YP=YGP(J)+DYJP1*.5
      IF(YCHG(IC).NE.0.) GO TO 1231
      H=2.*PIE*RGP(I)*(YP-YM)*HCP(IC)
      GO TO 1250
1231   FRAC=(YCHG(IC)-YM)/(YP-YM)
      IF(FRAC.LT.0.) FRAC=0.
      IF(FRAC.GT.1.) FRAC=1.
      H=(FRAC*HCM(ICP1)+(1.-FRAC)*HCP(IC))*2.*PIE*RGP(I)*(YP-YM)
      GO TO 1250
C CASE 4
 1240 XP=XGP(I)+DXIP1*.5
      XM=XGP(I)-DXIM1*.5
      RAV=RX1-(XP+XM)*.5
      IF(XCHG(IC).NE.0.) GO TO 1241
      H=2.*PIE*RAV*(XP-XM)*HCP(IC)
      GO TO 1250
 1241 FRAC=(XCHG(IC)-XM)/(XP-XM)
      IF(FRAC.LT.0.) FRAC=0.
      IF(FRAC.GT.1.) FRAC=1.
      H=(FRAC*HCP(IC)+(1.-FRAC)*HCM(ICP1))*2.*PIE*RAV*(XP-XM)
 1250 AJ=KIP1+KIM1+KJP1+KJM1+H
      AIP1(I,J)=KIP1/AJ
      AIM1(I,J)=KIM1/AJ
      AJP1(I,J)=KJP1/AJ
      AJM1(I,J)=KJM1/AJ
      BIJ(I,J)=(QS+H*TINF)/AJ
      GO TO 710
C THREE ZEROS
 1300 DO 1301 II=1,4
      IF(IS(II).NE.0) NGO=II
 1301 CONTINUE
      GO TO (1310,1320,1330,1340),NGO
C CASE 5
 1310 RAV=RGP(I)+DXIM1*.25
      H=2.*PIE*(RAV*DXIM1*.5*HCP(IC)+RGP(I)*DYJP1*.5*HCM(IC))
      GO TO 1350
C CASE 6
 1320 RAV=RGP(I)+DXIM1*.25
      H=2.*PIE*(RAV*DXIM1*.5*HCM(IC)+RGP(I)*DYJM1*.5*HCP(IC))
      GO TO 1350
C CASE 7
 1330 RAV=RGP(I)-DXIP1*.25
      H=2.*PIE*(RAV*DXIP1*.5*HCP(IC)+RGP(I)*DYJM1*.5*HCM(IC))
      GO TO 1350
C CASE 8
 1340 RAV=RGP(I)-DXIP1*.25
      H=2.*PIE*(RAV*DXIP1*.5*HCM(IC)+RGP(I)*DYJP1*.5*HCP(IC))
 1350 AJ=KIP1+KIM1+KJP1+KJM1+H
      AIP1(I,J)=KIP1/AJ
      AIM1(I,J)=KIM1/AJ
      AJP1(I,J)=KJP1/AJ
      AJM1(I,J)=KJM1/AJ
      BIJ(I,J)=(QS+H*TINF)/AJ
      GO TO 710
C FOUR ZEROS - VOID - CASE 13
 1400 AIP1(I,J)=0.
      AIM1(I,J)=0.
      AJP1(I,J)=0.
      AJM1(I,J)=0.
```

```
      BIJ(I,J)=0.
710    CONTINUE
1947   FORMAT(1H ,2I3,6E12.4)
      DO 720 I=1,IXMAX
      DO 720 J=1,JYMAX
720   T(I,J)=TINF
      OMEG=1.7
      OMO=1.-OMEG
      DO 740 IT=1,100
      AMAX=0.0
      DO 730 I=1,IXMAX
      DO 730 J=1,JYMAX
      TOLD=T(I,J)
      TNEW=AIM1(I,J)*T(I-1,J)+AIP1(I,J)*T(I+1,J)+AJM1(I,J)*T(I,J-1)
      TNEW=TNEW+AJP1(I,J)*T(I,J+1)+BIJ(I,J)
      T(I,J)=TNEW*OMEG+OMO*TOLD
      VAL=ABS(T(I,J)-TOLD)
      IF(VAL.GT.AMAX) AMAX=VAL
  730 CONTINUE
      IF(AMAX.LT.ERR) GO TO 750
  740 CONTINUE
      WRITE(6,745) IT
  745 FORMAT(5X,'EXCEEDS ITERATIONS..IT=',I4)
  750 CONTINUE
      DO 610 J=1,JYMAX
      DO 611 I=1,IXMAX
      II=IXMAX+1-I
611   TTT(II)=T(I,J)
610   WRITE(6,612) (TTT(II),II=1,IXMAX)
612   FORMAT(1H ,12F5.0)
C EXACT SECTION PROPERTIES AND THERMAL ROTATION
      JX1=0.
      JX2=0.
      JY1=0.
      JY2=0.
      JXY1=0.
      JXY2=0.
      YT1=0.
      YT2=0.
      T1=0.
      T2=0.
      DO 2000 I=1,IXMAX
      DO 2000 J=2,JYMAX
      S1=0.
      S2=0.
      IF(IPSOLI(I,J).EQ.1) S1=1.
      IF(IPSOLI(I,J).EQ.2) S2=1.
      DA=(XGP(I)-XGP(I-1))*(YGP(J)-YGP(J-1))
      YY=(YGP(J)+YGP(J-1))*.5
      XX=(XGP(I)+XGP(I-1))*.5
      XX1=XX-XBAR1
      YY1=YY-YBAR1
      XX2=XX-XBAR2
      YY2=YY-YBAR2
      TT=(T(I,J)+T(I-1,J)+T(I,J-1)+T(I-1,J-1))*.25
C DEFLECTION IS BASED ON TEMP RISE RELATIVE TO TINF
      TT=TT-TINF
      DEN1=1.-XX1/RC1
      DEN2=1.-XX2/RC2
      JX1=JX1+YY1*YY1*DA*S1/DEN1
      JY1=JY1+XX1*XX1*DA*S1/DEN1
      JXY1=JXY1+XX1*YY1*DA*S1/DEN1
      T1=T1+TT*DA*S1
      YT1=YT1+TT*YY1*DA*S1
      JX2=JX2+YY2*YY2*DA*S2/DEN2
      JY2=JY2+XX2*XX2*DA*S2/DEN2
```

```
      JXY2=JXY2+XX2*YY2*DA*S2/DEN2
      T2=T2+TT*DA*S2
      YT2=YT2+TT*YY2*DA*S2
 2000 CONTINUE
      Q1=AREA1*RC1*RC1+JY1
      PHI1=RC1*(Q1*YT1-RC1*JXY1*T1)/(JX1*Q1-JXY1**2)
      PHI1=PHI1*ALPHA1
      Q2=AREA2*RC2*RC2+JY2
      PHI2=RC2*(Q2*YT2-RC2*JXY2*T2)/(JX2*Q2-JXY2**2)
      PHI2=PHI2*ALPHA2
      PHI=PHI1-PHI2
      WRITE(6,2005) JX1,JY1,JXY1,PHI1
      WRITE(6,2010) JX2,JY2,JXY2,PHI2
 2005 FORMAT(1H ,'JX1=',E12.4,' JY1=',E12.4,' JXY1=',E12.4,' PHI1=',E12.
     *4)
 2010 FORMAT(1H ,'JX2=',E12.4,' JY2=',E12.4,' JXY2=',E12.4,' PHI2=',E12.
     *4)
      AKTHRM=PHI/(QTOT/(2.*PIE*RFAVG))
      WRITE(6,2015) PHI,AKTHRM
 2015 FORMAT(' PHI=',E12.4,' KTHERMAL=',E12.4)
      STOP
      END
```

```
HTSEAL 07/17/84 13:03:25
QTOT=  0.2797E+04


    INPUT GRID LOCATIONS
    XC:
          0.0054 0.0054 0.     0.     0.0067 0.0067 0.0026 0.0026 0.0125
          0.0125 0.0114 0.0114 0.     0.     0.     0.     0.     0.
          0.     0.     0.     0.
    YC:
          0.     0.0152 0.0152 0.0286 0.0286 0.0318 0.0318 0.0517 0.0517
          0.0318 0.0318 0.     0.     0.     0.     0.     0.     0.
          0.     0.     0.     0.


    ADJUSTED GRID LOCATIONS
    XG:
          0.     0.0026 0.0054 0.0067 0.0114 0.0125
    YG:
          0.     0.0152 0.0286 0.0318 0.0517

    SECTION PROPERTIES MATRIX

  0 0 0 0 0 0
  0 0 1 0 0 0
  0 0 1 0 2 0
  0 1 1 0 2 0
  0 1 1 1 2 0
  0 0 0 0 2 0
  0 0 0 0 0 0

    AREA1= [illegible]   XBAR1= [illegible]   YBAR1= [illegible]   RC1= [illegible]
    IX1= 0.1828E-07   IY1= 0.2461E-08   IXY1=-0.1765E-08

    AREA2= 0.1986E-03   XBAR2= 0.7525E-02   YBAR2= 0.4173E-01   RC2= 0.5757E-0
    IX2= 0.6594E-08   IY2= 0.1639E-08   IXY2= 0.1334E-19

    FINER MESH ADJUSTMENT
    XGP:
          0.     0.0013 0.0026 0.0040 0.0054 0.0067 0.0079 0.0090 0.0102
          0.0114 0.0125
    YGP:
          0.     0.0014 0.0028 0.0042 0.0055 0.0069 0.0083 0.0097 0.0111
          0.0125 0.0139 0.0152 0.0167 0.0182 0.0197 0.0212 0.0227 0.0241
          0.0256 0.0271 0.0286 0.0296 0.0307 0.0318 0.0332 0.0346 0.0360
          0.0375 0.0389 0.0403 0.0417 0.0432 0.0446 0.0460 0.0474 0.0489
          0.0503 0.0517

    REFINED MESH

  0 0 0 0 0 0 0 0 0 0 0 0 0 0 0 0 0 0 0 0 0 0 0 0 0 0 0 0 0 0 0 0 0 0 0 0 0 0
  0 0 0 0 0 0 0 0 0 0 0 0 1 1 1 1 1 1 1 1 1 0 0 0 0 0 0 0 0 0 0 0 0 0 0 0 0 0
  0 0 0 0 0 0 0 0 0 0 0 0 1 1 1 1 1 1 1 1 1 0 0 0 0 0 0 0 0 0 0 0 0 0 0 0 0 0
  0 0 0 0 0 0 0 0 0 0 0 0 1 1 1 1 1 1 1 1 1 0 0 0 2 2 2 2 2 2 2 2 2 2 2 2 2 2
  0 0 0 0 0 0 0 0 0 0 0 0 1 1 1 1 1 1 1 1 1 0 0 0 2 2 2 2 2 2 2 2 2 2 2 2 2 2
  0 1 1 1 1 1 1 1 1 1 1 1 1 1 1 1 1 1 1 1 1 0 0 0 2 2 2 2 2 2 2 2 2 2 2 2 2 2
  0 1 1 1 1 1 1 1 1 1 1 1 1 1 1 1 1 1 1 1 1 1 1 1 2 2 2 2 2 2 2 2 2 2 2 2 2 2
  0 1 1 1 1 1 1 1 1 1 1 1 1 1 1 1 1 1 1 1 1 1 1 1 2 2 2 2 2 2 2 2 2 2 2 2 2 2
  0 1 1 1 1 1 1 1 1 1 1 1 1 1 1 1 1 1 1 1 1 1 1 1 2 2 2 2 2 2 2 2 2 2 2 2 2 2
  0 1 1 1 1 1 1 1 1 1 1 1 1 1 1 1 1 1 1 1 1 1 1 1 2 2 2 2 2 2 2 2 2 2 2 2 2 2
  0 0 0 0 0 0 0 0 0 0 0 0 0 0 0 0 0 0 0 0 0 0 0 0 2 2 2 2 2 2 2 2 2 2 2 2 2 2
  0 0 0 0 0 0 0 0 0 0 0 0 0 0 0 0 0 0 0 0 0 0 0 0 0 0 0 0 0 0 0 0 0 0 0 0 0 0
```

```
   DIFFERENCE IN AREAS=  0.1537E-07
  -0.   38.   38.   38.   38.   38    38.   -0.   -0.   -0.   -0
  -0.   38.   38.   38.   38.   38.   38.   -0.   -0.   -0.   -0.
  -0.   38.   38.   38.   38.   38.   38.   -0.   -0.   -0.   -0.
  -0.   38.   38.   38.   38.   38.   38.   -0.   -0.   -0.   -0.
  -0.   38.   38.   38.   38.   38.   38.   -0.   -0.   -0.   -0.
  -0.   38.   38.   38.   38.   38.   38.   -0.   -0.   -0.   -0.
  -0.   38.   38.   38.   38.   38.   38.   -0.   -0.   -0.   -0.
  -0.   38.   38.   38.   38.   38.   38.   -0.   -0.   -0.   -0.
  -0.   38.   38.   38.   38.   38.   38.   -0.   -0.   -0.   -0.
  -0.   38.   38.   38.   38.   38.   38.   -0.   -0.   -0.   -0.
  -0.   38.   38.   38.   38.   38.   38.   -0.   -0.   -0.   -0.
  -0.   38.   38.   38.   38.   38.   38.   38.   38.   38.   38.
  -0.   38.   38.   39.   39.   39.   39.   38.   38.   38.   38.
  -0.   38.   39.   39.   39.   39.   39.   39.   38.   38.   38.
  -0.   39.   39.   39.   39.   39.   39.   39.   39.   38.   38.
  -0.   39.   40.   40.   40.   40.   40.   39.   39.   39.   38
  -0.   40.   40.   41.   41.   41.   40.   40.   39.   39.   38.
  -0.   41.   42.   43.   42.   42.   41.   40.   39.   39.   38.
  -0.   42.   45.   45.   45.   43.   41.   40.   39.   39.   38.
  -0.   46.   49.   50.   48.   44.   41.   40.   39.   38.   38.
  -0.   52.   59.   60.   54.   44.   40.   39.   38.   38.   38.
  -0.   61.   71.   72.   64.   48.   -0.   -0.   -0.   -0.   -0.
  -0.   76.   90.   91.   81.   57.   -0.   -0    -0.   -0.   -0.
  94.  107.  119.  119.  106.   83.   63.   53.   48.   -0.   -0.
  88.   93.   97.   96.   89.   77.   65.   56.   51.   -0.   -0.
  78.   81.   83.   82.   77.   71.   63.   56.   51.   -0.   -0.
  69.   72.   73.   72.   69.   65.   60.   55.   50.   -0.   -0.
  63.   64.   65.   65.   63.   60.   57.   53.   49.   -0.   -0.
  58.   59.   60.   59.   58.   56.   54.   51.   47.   -0.   -0.
  54.   55.   55.   55.   55.   53.   52.   49.   46.   -0.   -0.
  51.   52.   52.   52.   52.   51.   50.   48.   46.   -0.   -0.
  48.   49.   50.   50.   49.   49.   48.   47.   46.   -0.   -0.
  46.   47.   48.   48.   48.   47.   47.   46.   45.   -0.   -0.
  45.   46.   46.   46.   46.   46.   45.   45.   44.   -0.   -0.
  44.   44.   45.   45.   45.   45.   44.   44.   43.   -0.   -0.
  43.   43.   44.   44.   44.   44.   44.   43.   43.   -0.   -0.
  42.   43.   43.   43.   43.   43.   43.   43.   42.   -0.   -0.
  42.   42.   42.   43.   43.   42.   42.   42.   42.   -0.   -0.
JX1=   0.1864E-07 JY1=   0.2374E-08 JXY1= -0.1691E-08 PHI1=   0.1772E-03
JX2=   0.6576E-08 JY2=   0.1620E-08 JXY2=   0.1388E-15 PHI2= -0.6259E-03
PHI=   0.6031E-03 KTHERMAL=   0.9134E-07
STOP
TIME 1.3 SECS
```